



Evaluation of LNAPL Distribution and Mobility in Heterogeneous Porous Media under Water Table Fluctuations

by

Evangelos Gatsios

A Dissertation

Submitted in fulfilment for the degree of

DOCTOR OF PHILOSOPHY

In

Faculty of Engineering and Information Technology

Principal supervisor:

Dr. Robert McLaughlan (UTS)

Co-supervisor:

Mr. John Rayner (CSIRO Land and Water)

University of Technology Sydney

New South Wales, Australia

2018

CERTIFICATE OF ORIGINAL AUTHORSHIP

I certify that the work in this thesis has not previously been submitted for a degree nor has it been submitted as part of requirements for a degree except as part of the collaborative doctoral degree and/or fully acknowledged within the text.

I also certify that the thesis has been written by me. Any help that I have received in my research work and the preparation of the thesis itself has been acknowledged. In addition, I certify that all information sources and literature used are indicated in the thesis.

Signature of Student:

Production Note:
Signature removed prior to publication.

Evangelos Gatsios

Date: 1 May 2018

DEDICATION

*This work is dedicated to my wonderful parents, Ioanni & Athena,
to my brother Michali, to my grandmother Kalomoira and
to my cousins Konstantino and Michali.*

BIOGRAPHY

Evangelos Gatsios was born in Athens, Greece on July 10, 1988. Evangelos is a MSc, MEng Environmental Engineer. In 2014 he started his PhD at University of Technology Sydney (UTS). The years 2014-2017, he conducted his research at the Commonwealth Scientific and Industrial Research Organisation (CSIRO) in Perth, W. Australia. His Thesis was part of the project between CRC CARE and CSIRO, titled: "Endpoints for petroleum LNAPL remediation-technology performance and risk reduction".

During the period of 2006-2013, he completed his M. Eng. and MSc. degrees at Technical University of Crete in Greece, achieving the highest GPA in the School of Environmental Engineering. Evangelos is a scholar of A. S. Onassis Foundation, University of Technology Sydney and the CRC CARE Australia. Also, he has been a scholar of State Scholar Foundation of Greece (ISF) and Technical University of Crete.

ACKNOWLEDGMENTS

I would like to express my sincere thanks to University of Technology Sydney, CRC for Contamination Assessment and Remediation of the Environment (CRC CARE), A. S. Onassis Foundation and CSIRO for their financial support of my PhD studies. The research was conducted under the CRC CARE Project: Endpoints for Petroleum LNAPL Remediation – Technology Performance and Risk Reduction (7.1.02.11/12).

I would like to express my sincere gratitude to my supervisor Dr. Robert McLaughlan. I have learnt a lot from him and this piece of work would be impossible for me without his help and support. As my principal supervisor, Dr McLaughlan has been guiding me since the first days of my arrival in Australia providing his knowledge and I consider myself fortunate having worked under his supervision. In addition I would like to express my sincere thanks to my co-supervisor Mr John Rayner. I worked under the supervision of John at CSIRO in Perth for 3 and a half years, feeling grateful for the knowledge I obtained these years close to him. I would like to thank him as his comments, his guidance and his knowledge were crucial for my PhD thesis. John was a great companion especially in the field work trips to our contaminated site, as these three years we had a daily contact collecting and interpreting the field data.

I would like to thank Mr Colin Johnston who gave me the opportunity to work on this wonderful research topic, as I was under his supervision at CSIRO during my first 1.5 years in Australia until his retirement. Colin was always helpful and supportive having a great knowledge on NAPL contamination concepts.

I would like to thank my colleagues and mentors at CSIRO Land and Water. Many thanks to Dr Greg Davis, Dr Bob Lenhard and Dr Elise Bekele for their valuable comments during my PhD journey. In addition, Elise assisted in field data collection, building and maintaining the project database and drafting the borelogs.

I would also like to thank Dr Trevor Bastow and Mrs Geste Yasuko for conducting all of the laboratory petroleum analysis of LNAPL, soil, water and vapour samples.

Many thanks also to Mr Robert Woodbury for his support. Rob assisted in data collection and sampling during my field trials and his assistance was appreciated in teaching me how to operate the LNAPL density and viscosity instruments at CSIRO labs.

The support and assistance of the research field site owners (John and Tom Sheehan) is also greatly appreciated. They provided support in terms of services and sustenance during the project.

I would also like to thank my two colleagues and friends Mr Gabriel Paiva-Lago and Mr Jonas Garcia Rincon for their precious friendship and support since the start of my PhD studies. I spent 3.5 wonderful years at CSIRO with these two wonderful guys and PhD

candidates, working all together in the same project as part of our PhD theses. I will always remember our great times in our field trips, the problems we faced during our studies and the solutions we were trying to find together. Without their help and their support this work would be more difficult to finish. Gabriel and Jonas assisted in conducting the LNAPL hydraulic tests and sampling and describing soil cores.

Wayne Hick from edrill completed all the subsurface installations and Numac drilling conducted the High Resolution Vertical Profiling (HRVP) testing.

Last but not least, I could not have reached this point in my life without the support and care of my family and of my friends. Grateful thanks to my parents and to my brother for their love and encouragement.

“Knowledge is the food of the soul”

*Plato, Greek philosopher, student of Socrates
and teacher of Aristotle, 427-347 B.C.*

TABLE OF CONTENTS

CERTIFICATE OF ORIGINAL AUTHORSHIP	I
DEDICATION	II
BIOGRAPHY	III
ACKNOWLEDGMENTS.....	IV
TABLE OF CONTENTS	VII
TABLE OF FIGURES	XI
LIST OF TABLES	XVIII
ACRONYMS.....	XX
TERMINOLOGY.....	XXI
ABSTRACT	XXIII
1. Introduction.....	1
1.1. Research background.....	1
1.2. Research objectives and contribution to knowledge.....	2
1.2.1. Research objectives	2
1.2.2 Approach	3
1.2.3. Contribution to knowledge	4
2. Literature Review	5
2.1. Conceptual models of LNAPLs in subsurface.....	5
2.1.1. Types of LNAPL and their properties.....	6
2.1.2. LNAPL transport and distribution.....	7
2.2. Water table fluctuations and LNAPL redistribution	23
2.3. LNAPL confinement conditions and apparent LNAPL thickness	24
2.3.1. NAPL Diagnostic Gauge Plots.....	26
2.3.2. Gauge thickness plots	26
2.3.3. Hydrostratigraphs	29
2.3.4. Discharge versus Drawdown Graphs	30
2.3.5. Graphical Analysis of LNAPL Baildown Test Data	31

2.3.6.	Related Research Work.....	32
2.4.	LNAPL Transmissivity.....	34
2.4.1.	Introduction.....	34
2.4.2.	Complexity of LNAPL transmissivity.....	36
2.4.3.	LNAPL Transmissivity Test Methods.....	37
2.4.4.	LNAPL Transmissivity Analysis.....	39
2.4.5.	Related research work.....	40
2.5.	In-Situ LNAPL Remediation Technologies.....	43
2.5.1.	Classification of in-situ LNAPL remedial techniques.....	44
2.5.2.	LNAPL mass recovery technologies.....	45
2.5.3.	Remediation performance of mass recovery techniques.....	50
3.	Materials and Methods.....	52
3.1.	Monitoring installations.....	53
3.2.	LNAPL characterisation.....	53
3.3.	Fluid level monitoring.....	56
3.4.	Direct push profiling tools.....	57
3.5.	LNAPL bail-down testing analysis.....	59
3.6.	Long term recovery system data.....	65
3.7.	LDRM (LNAPL Liquids Distribution and Recovery Model).....	67
3.8.	Experimental procedure.....	71
3.8.1.	Study area.....	71
3.8.2.	Mass recovery experiments.....	72
4.	Overview of the Site Setting.....	76
4.1.	Site and hydrogeological characteristics.....	76
4.2.	LNAPL occurrence, characterization and distribution.....	78
4.2.1.	LNAPL characterization and properties.....	78
4.2.2.	LNAPL distribution.....	79
5.	Assessment of LNAPL Distribution and Hydrogeological Conditions.....	81

5.1. Critical In-Well Test Application for Evaluation of LNAPL Hydrogeological Conditions	81
5.2. Spatial Variability of LNAPL Saturation.....	100
5.3. LDRM Simulation and Theoretical T_n Estimation	104
5.4. Conclusions	125
6. Assessment of LNAPL Mobility and Recoverability	127
6.1. Spatial Variability of LNAPL Transmissivity	127
6.2. In-Well Thickness: An Indicator of LNAPL Transmissivity	130
6.3. Variability in LNAPL Transmissivity under Natural Water Table Fluctuations.....	133
6.4. Estimation of LNAPL Drawdown during Mass Recovery Trials	134
6.5. Variability in LNAPL Transmissivity during Skimming.....	137
6.6. Variability in LNAPL Transmissivity during Induced Water Table Drawdown	147
6.7. Comparison between LNAPL Transmissivity Estimated from Bail-down and Mass Recovery Methods.....	150
6.8. Effect of Induced Vacuum on LNAPL transmissivity	151
6.9. The Impact of Physical Properties Changes and Mobile Interval on T_n	153
6.10. Uncertainty in Estimation of LNAPL Transmissivity	158
6.10.1 Sensitivity and error analysis	158
6.10.2 Effect of product amount removal on LNAPL transmissivity estimation	161
6.10.3 Effect of radius of capture on T_n estimation	163
6.11. Conclusions	164
7. Conclusions and Recommendations.....	168
7.1. Summary of Research	168
7.2. Conclusions	168
7.3. Recommendations for Future Work	171
8. References	173
Appendices.....	188
Appendix A. Materials and Methods	188
Appendix B. Site Characterization	195
Appendix C. Bail-down Testing.....	225

Appendix D. Formation Fluid Levels	232
Appendix E. T_n Estimations During Applied Mass Recovery Techniques	236
Appendix F. Physicochemical Properties	247
Appendix G. LDRM Simulation	254
Appendix H. Performance Assessment of Selected Mass Recovery Technologies	258
Appendix I. Publications	265
Appendix J. NAPL Baildown Testing at the Donnybrook Site (W.A.), 2015 – 2016	265
Appendix K. Manuscript entitled “LNAPL transmissivity as a remediation metric in complex sites under water table fluctuations”	265

TABLE OF FIGURES

Figure 2. 1. Illustration of an LNAPL release in subsurface (CL:AIRE 2014).....	5
Figure 2. 2. The four physical phases of petroleum hydrocarbons in the unsaturated zone after (Rivett et al. 2011).	8
Figure 2. 3. Residual and entrapped LNAPL in a porous media. Unsaturated zone i) LNAPL is isolated as a thin immobile film. Saturated zone and ii) LNAPL is entrapped as blobs or ganglia after (Johnston 2010).	10
Figure 2. 4. Influence of the density of LNAPL on the potential for LNAPL recovery for certain LNAPL specific volumes (Awar 2008). Where D refers to specific volume of NAPLs.	12
Figure 2. 5. Influence of the viscosity of LNAPL on the recovery of LNAPL thickness in the well after bailing (Ahmed 2014).	13
Figure 2. 6. Cartoon depicting non-wetting (LNAPL) and its contact angle with solid surface in the presence of wetting phase (water).	15
Figure 2. 7. Schematic of the distribution of fluids in a porous media showing the radius of curvature of the interfaces as a result of fluid pressure differences (Johnston 2010).	16
Figure 2. 8. Schematic of the saturation-capillary pressure relationship for two fluids in a porous media. Where, P_d is the fluid displacement pressure, S_r the residual saturation and S_e the entrapped saturation. $S_e = (1 - S_m)$, where S_m is the critical saturation. At this point (S_m) the capillary pressure is zero and the non-wetting fluid (LNAPL) will not flow into a recovery well (Johnston 2010).	19
Figure 2. 9. Schematic showing hypothetical relative permeability relationships for LNAPL and water in a saturated porous media. Where S_r : residual saturation, S_m : critical saturation and S_w : saturation of wetting fluid.....	20
Figure 2. 10. Schematic showing an LNAPL monitoring well with fluid elevations.....	21
Figure 2. 11. Schematic showing the distribution of capillary pressure in the presence of LNAPL (Charbeneau 2007b). Where p_n : NAPL pressure, p_w : water pressure, $P_{c,an}$: air-LNAPL capillary pressure and $P_{c,nw}$: LNAPL water capillary pressure.....	22
Figure 2. 12. Schematic showing the vertical distribution of LNAPL saturation with the equivalent fluid levels after (Johnston 2010).	23
Figure 2. 13. Schematic showing in-well thickness (b_n) in unconfined, confined and perched LNAPL conditions (Hawthorne 2010).	25
Figure 2. 14. A diagnostic gauge plot illustrating unconfined and confined LNAPL conditions. The graph presents air-LNAPL and LNAPL-water referenced interface elevations and the potentiometric surface elevation versus the gauged b_n	29

Figure 2. 15. Hydrostratigraph included a hydrograph soil lithology, gamma-ray data, and LIF response data (Kirkman, Adamski & Hawthorne 2013).	30
Figure 2. 16. Schematic showing the measured LNAPL discharge versus calculated LNAPL drawdown, during a bail-down test (API 2012).....	31
Figure 2. 17. Schematic showing baildown test results versus LNAPL discharge (Kirkman, Adamski & Hawthorne 2013).....	32
Figure 2. 18. Diagnostic gauge plot presenting LNAPL unconfined conditions in RW54 well (Kahraman 2013). Where AN: is the air-NAPL interface elevation, NW: is the NAPL-water elevation and CGWS: is the potentiometric surface elevation.	33
Figure 2. 19. Diagnostic gauge plot presenting LNAPL confined conditions (Hartsock 2014).	33
Figure 2. 20. Schematic diagram showing the relationship of LNAPL transmissivity to saturation (CL:AIRE 2014).	36
Figure 2. 21. Schematic showing groundwater elevation and LNAPL thickness along with T_n values (m^2/day) (Beckett & Huntley 2015).....	37
Figure 2. 22. Schematic showing T_n values during short-term baildown and long-term skimming testing in Area 1 (Nagaiah, Law & Ueland 2015).	41
Figure 2. 23. Schematic showing T_n values during short-term baildown and long-term skimming testing in Area 2 (Nagaiah, Law & Ueland 2015).	41
Figure 2. 24. Illustration showing T_n values and statistics for t_0 , t_1 and t_2 (Palmier, Dodt & Atteia 2016).	42
Figure 2. 25. Overview of common applied in-situ LNAPL remediation technologies (after Johnston, 2010).....	45
Figure 2. 26. Measured NAPL recovery rate (Q_n) over the course of the sequential recovery trial in 2001 (Johnston et al. 2002).	51
Figure 3. 1. Schematic diagram of the construction of NAPL recovery well PB (100 mm), (not to scale).	53
Figure 3. 2. LNAPL drawdown- discharge relation (API 2012).....	60
Figure 3. 3. Selection of NAPL conditions in home worksheet (API 2012).	61
Figure 3. 4. Entered and calculated parameters in Data sheet.	61
Figure 3. 5. Entered fluid levels data during bail-down testing at a remediation well in the site of research.	62
Figure 3. 6. Example of bail-down test data analysis using Bouwer and Rice method.	64
Figure 3. 7. Bouwer and Rice worksheet.	65
Figure 3. 8. Project set up window.	69

Figure 3. 9. Data input screen.	69
Figure 3. 10. Initial output screen.	70
Figure 3. 11. LDRM graphical output: saturation and NAPL relative permeability profiles....	70
Figure 3. 12. Input field data by the user.	70
Figure 3. 13. Site layout showing the three research areas A (PB29 recovery well), B (PB27 recovery well) and C (PB40 recovery well), the monitoring wells (09, 58, 50, 11, 44), the LIF (51, 52, 53, 43, 47, 57, 68) and HPT points (59, 60, 62, 73, 74).	72
Figure 3. 14. The specific gravity skimmer pump.	74
Figure 3. 15. Arrangement of well head for water and vacuum enhanced recovery at well PB40.	74
Figure 4. 1. Monitoring network at the site of research and location of areas A, B, C and spill location at UST (scale: 15x15 m).	77
Figure 4. 2. Time series of potentiometric surface elevation and in-well thicknesses in the whole research site.	79
Figure 5. 1. Hydrograph plot of the potentiometric surface elevations versus gauged LNAPL thickness for well PB29 (17/12/2014 - 28/4/2016). The arrows show the general trend of Z_{aw} changes with time.	82
Figure 5. 2. Gauge thickness plot of the air-NAPL interface, LNAPL-water interface, and potentiometric surface elevations versus gauged LNAPL thickness for well PB29 (17/12/2014 – 28/4/2016).	82
Figure 5. 3. Gauge thickness plot of the air-NAPL interface, LNAPL-water interface, and potentiometric surface elevations versus gauged LNAPL thickness for well PB29 (17/12/2014 - 7/7/2015). The arrow shows the trend of Z_{aw} with time.	83
Figure 5. 4. Gauge thickness plot of the air-NAPL interface, LNAPL-water interface, and potentiometric surface elevations versus gauged LNAPL thickness for well PB29 (3/8/2014- 8/10/2015). The arrows show the trend of Z_{aw} with time.	84
Figure 5. 5. Gauge thickness plot of the air-NAPL interface, LNAPL-water interface, and potentiometric surface elevations versus gauged LNAPL thickness for well PB29 (10/11/2015- 28/4/2016). The arrows show the trend of Z_{aw} with time.	84
Figure 5. 6. A hydrostratigraph illustrating the in-well air-NAPL interface, LNAPL-water interface, the potentiometric surface elevation and the gauged LNAPL thickness in time including the stratigraphic description for well PB29 (17/12/2014- 28/4/2016).	85
Figure 5. 7. NAPL saturations (MP50 location: 18/05/2016) along with in-well fluid elevations (well PB29: 17/05/2016) and HPT 73 (20/05/2016) profile at research area A, indicating the	

smear zone and the stratigraphic transition point at site of research. MP50 and HPT73 were installed 1.5 and 1.15 m respectively away from the presented well PB29..... 86

Figure 5. 8. Baildown test results presenting the gauged referenced air-LNAPL (Z_{an}) and LNAPL-water interfaces (Z_{nw}), the potentiometric surface elevation (Z_{aw}), the apparent thickness (ANT) and the static elevations for Z_{an} , Z_{nw} and ANT vs. LNAPL discharge for well PB29..... 88

Figure 5. 9. LNAPL drawdown- discharge relation during baildown testing. 88

Figure 5. 10. Gauge thickness plot of the air-NAPL interface, LNAPL-water interface, and potentiometric surface elevations versus gauged LNAPL thickness for well PB27 (25/11/2014 - 24/4/2016). 90

Figure 5. 11. Gauge thickness plot of the air-NAPL interface, LNAPL-water interface, and potentiometric surface elevations versus gauged LNAPL thickness for well PB27 (25/11/2014 - 14/ 7/2015). The arrows show the trend of Z_{aw} with time. 90

Figure 5. 12. Gauge thickness plot of the air-NAPL interface, LNAPL-water interface, and potentiometric surface elevations versus gauged LNAPL thickness for well PB27 (14/7/2015 - 8/10/2015). The arrows show the trend of Z_{aw} with time. 91

Figure 5. 13. Gauge thickness plot of the air-NAPL interface, LNAPL-water interface, and potentiometric surface elevations versus gauged LNAPL thickness for well PB27 (8/10/2015 - 28/4/2016). The arrows show the trend of Z_{aw} with time..... 91

Figure 5. 14. A hydrostratigraph illustrating the in-well air-NAPL interface, LNAPL-water interface, the potentiometric surface elevation and the gauged LNAPL thickness in time including the stratigraphic description for site DK, well PB27 (5/11/2014- 28/4/2016)..... 92

Figure 5. 15. NAPL saturations (MP58 well location: 18/05/2016) along with in-well fluid elevations (well PB27:18/05/2016) and HPT 74 (20/05/2016) profile at research area B, indicating the smear zone and the stratigraphic transition point at site of research. MP58 and HPT74 were installed 1.5 and 1.4 m respectively away from the presented well PB27..... 93

Figure 5. 16. Baildown test results presenting the gauged referenced air-LNAPL (Z_{an}) and LNAPL-water interfaces (Z_{nw}), the potentiometric surface elevation (Z_{aw}), the apparent thickness (ANT) and the static elevations for Z_{an} , Z_{nw} and ANT vs. LNAPL discharge for well PB27..... 95

Figure 5. 17. LNAPL drawdown- discharge relation during baildown testing. After a drawdown adjustment of 0.0043 m..... 95

Figure 5. 18. Gauge thickness plot of the air-NAPL interface, LNAPL-water interface, and potentiometric surface elevations versus gauged LNAPL thickness for well PB40 (8/10/2015- 28/4/2016). The arrows show the Z_{aw} elevation with time..... 96

Figure 5. 19. Hydrograph plot of the potentiometric surface elevations versus gauged LNAPL thickness for well PB40 (8/10/2015-28/4/2016). The arrow shows how Z_{aw} changes with time.	97
Figure 5. 20. A hydrostratigraph illustrating the air-NAPL interface, LNAPL-water interface, the potentiometric surface elevation and the gauged LNAPL thickness in time including the stratigraphic description for well PB40 (8/10/2015- 28/4/2016).....	98
Figure 5. 21. NAPL saturations (MP44 location: 18/05/2016) along with in-well fluid elevations (well PB40: 18/05/2016) and HPT 60, HPT62 (20/05/2016) profiles at research area C, indicating the smear zone and the stratigraphic transition point at site of research. MP44, HPT60 and HPT62 were installed 1.3, 1.85 and 2.0 m respectively away from the presented well PB40.	98
Figure 5. 22. LNAPL drawdown- discharge relation during baildown testing depicting unconfined NAPL conditions (06/04/2016).	99
Figure 5. 23. NAPL saturations at well locations MP50 (Area A), MP58 (Area B) and MP44 (Area C) along with in-well thicknesses (wells: PB29, PB27 and PB40) at the site of research (17-18/05/2016).	101
Figure 5. 24. Correlation between geological material and NAPL saturation.	102
Figure 5. 25. The three simulated layers at area B.	110
Figure 5. 26. NAPL saturation and NAPL relative permeability profiles.	111
Figure 5. 27. Layers with mobile NAPL.	112
Figure 5. 28. The three simulated layers at area C.	113
Figure 5. 29. NAPL saturation and NAPL relative permeability profiles.	114
Figure 5. 30. Layers with mobile NAPL.	115
Figure 5. 31. NAPL saturation and NAPL relative permeability profiles.	116
Figure 5. 32. NAPL saturation and NAPL relative permeability profiles.	118
Figure 5. 33. Profile of T_n along with $vG\alpha$ for different vGN values.	119
Figure 5. 34. Profile of T_n along with vGN for different $vG\alpha$ values.	120
Figure 5. 35. NAPL saturation and NAPL relative permeability profiles.	123
Figure 5. 36. Layers with mobile NAPL.	124
Figure 6. 1. Spatial variability of LNAPL transmissivity at the site of research.	128
Figure 6. 2. Illustration of T_n -distance from release relationship (date 5-6/4/2016, $Z_{aw} = 56.20$ m AHD).	130
Figure 6. 3. T_n versus in-well thickness profile in the whole contaminated site.	131
Figure 6. 4. T_n versus in-well thickness profile at PB29 well.	132
Figure 6. 5. T_n versus in-well thickness profile at PB27 well.	132

Figure 6. 6. Correlation between the T_n and Z_{aw} at the three areas of research (years: 2015-2016).	133
Figure 6. 7. Contaminated site hydrograph along with bail-down T_n values at the three research areas. Gray columns indicate the time periods of recovery applications in 2015 and 2016.	134
Figure 6. 8. DTP correlation between the wells PB27 - PB09 (monitoring period: 5/11/2014-21/07/2015).	135
Figure 6. 9. Z_{an} correlation between the wells PB27-PB09 (monitoring period: 19/03/2015-15/06/2016).	136
Figure 6. 10. Z_{an} correlation between the wells PB29-MP50 (monitoring period: 20/05/2016-5/10/2016).	136
Figure 6. 11. DTP correlation between the wells PB40-PB11 (monitoring period: 5/04/2016-14/06/2016).	137
Figure 6. 12. Site layout showing the three research areas A, B and C. Tested and monitoring wells, LIF and HPT points are illustrated.	138
Figure 6. 13. HPT73 – LIF43 profiles along with NAPL saturations (MP50) and in-well thicknesses, b_n (PB29 well), at research area A. Four different fluid elevations are illustrated: I refers to fluid levels the day of core sampling (late May 2016), II shows the fluid levels the day before the 4-week sequential free recovery trial (mid-June 2016), III presents fluid levels just after the end of the recovery trial (early July 2016) and, finally, IV refers to the fluid levels just before the 2015 trial (early July 2015).	139
Figure 6. 14. HPT74 profile along with NAPL saturations (MP58) and in-well thicknesses, b_n (PB27 well) at research area B. Four different fluid elevations are illustrated: I refers to fluid levels the day of core sampling (late May 2016), II shows the fluid levels the day before the 4-week sequential free recovery trial (mid-June 2016), III presents fluid levels just after the end of the recovery trial (early July 2016) and, finally, IV refers to the fluid levels just before the 2015 trial (early July 2015).	140
Figure 6. 15. HPT59, HPT60 HPT62 profiles along with NAPL saturations (MP44) and in-well thicknesses, b_n (PB40 well), at research area C. Three different fluid elevations are illustrated: I refers to fluid levels the day of core sampling (late May 2016), II shows the fluid levels the day before the 4-week sequential free recovery trial (mid-June 2016) and III presents fluid levels just after the end of the recovery trial (early July 2016).	140
Figure 6. 16. Time series of LNAPL transmissivity and potentiometric surface elevation during bail-down testing and skimming processes, at research area A, well PB29, in 2015.	142
Figure 6. 17. Time series of LNAPL transmissivity and potentiometric surface elevation during bail-down testing and skimming processes, at research area B, well PB27, in 2015.	142

Figure 6. 18. Profiles of T_n and Z_{aw} during bail-down testing and hydraulic free recovery processes, at research area A, well PB29.	143
Figure 6. 19. Profiles of T_n and Z_{aw} during bail-down testing and hydraulic free recovery processes, at research area B, well PB27.	144
Figure 6. 20. Profiles of T_n and Z_{aw} during bail-down testing and hydraulic free recovery processes, at research area C, well PB40.	145
Figure 6. 21. Profiles of $T_{n,SK}$ and Z_{aw} at areas A, B, and C during the first week of the 2016 skimming trials.....	146
Figure 6. 22. $T_{n,BD}$ values before and during the 2016 skimming trial at area A.	147
Figure 6. 23. Comparison of T_n values between bail-down testing, skimming and water enhanced skimming along with fluid elevations at area A (2015 and 2016 trials).	148
Figure 6. 24. Comparison of T_n values between bail-down testing, skimming and water enhanced skimming along with fluid elevations at area B (2015 and 2016 trials).	148
Figure 6. 25. Comparison of T_n values between bail-down testing, skimming and water enhanced skimming along with fluid elevations at area C (2015 and 2016 trials).	149
Figure 6. 26. Profile of Z_{aw} values along with $T_{n,SK} / T_{n,BD}$ ratio values at areas A, B and C during the skimming and water-enhanced skimming trials in 2016.	150
Figure 6. 27. Profile of T_n and b_n at PB29 well (yrs: 2015, 2016).	155
Figure 6. 28. Profile of T_n and b_n at PB27 well (yrs: 2015, 2016).	155
Figure 6. 29. Profile of T_n and b_n at PB40 well (yrs: 2016).	156
Figure 6. 30. Fluid levels along with abs. piezometric pressures at PB29 well location.....	157
Figure 6. 31. Fluid levels along with abs. piezometric pressures at PB27 well location.....	157
Figure 6. 32. Fluid levels along with abs. piezometric pressures at PB40 well location.....	157
Figure 6. 33. A schematic illustrating the apparent thicknesses (cases 1 – 3) after bailing of the conducted experiments at area A (i) and B (ii) and NAPL saturations along with potentiometric surface elevations. Case I refers to the initial apparent thickness before bailing.	162
Figure 6. 34. Effect of R_{oi} on $T_{n,SK} / T_{n,BD}$ at well locations PB29, PB27 and PB40 (16-17/06/2016).	163
Figure 6. 35. Conceptual understanding of the research site.....	166

LIST OF TABLES

Table 2. 1. Typical density, viscosity, interfacial tension (LNAPL-water) and, surface tension (air-LNAPL) of typical fuel LNAPLs along with the temperature of measurement (CL:AIRE 2014; Johnston 2010; Newell 1995).....	6
Table 2. 2. Dynamics and illustrations to diagnostic gauge plot trend analysis (Hawthorne 2011b).	27
Table 3. 1. Parameters required to estimate LNAPL distribution and recovery.	68
Table 3. 2. Monitoring network and NAPL hydrogeological conditions during the pilot-scale mass recovery trials at the three research areas.	72
Table 3. 3. Chronology of events during field trial of NAPL recovery at area A, PB29 well. .	75
Table 3. 4. Chronology of events during field trial of NAPL recovery at area B, PB27 well. .	75
Table 3. 5. Chronology of events during field trial of NAPL recovery at area C, PB40 well. .	75
Table 4. 1. Site Coordinates.	76
Table 4. 2. LNAPL product characterisation.	78
Table 4. 3. Minimum and maximum in-well thickness and potentiometric surface elevation across the whole contaminated site.	80
Table 5. 1. Input parameters for area A.	104
Table 5. 2. Input parameters for area B.	105
Table 5. 3. Input parameters for area C.	107
Table 5. 4. Theoretical T_n estimation.	112
Table 5. 5. Theoretical T_n estimation.	115
Table 5. 6. Input parameters for scenario A.	117
Table 5. 7. Input parameters for scenario B.	121
Table 5. 8. Theoretical T_n estimation for scenario A.	124
Table 5. 9. Theoretical T_n estimation for scenario B.	124
Table 6. 1. LNAPL hydrogeological conditions during the pilot-scale trials.	137
Table 6. 2. Effect of applied vacuum on T_n at PB29 well, area A.	152
Table 6. 3. Errors in $T_{n,BD}$ estimation if drawdown correction and cut-off time are not applied.	158
Table 6. 4. Effect of DTP values to T_n estimates.	159
Table 6. 5. Effect of increasing initial values by 20% on T_n estimates.	160

Table 6. 6. Sensitivity and relationship to T_n for parameters related to bail-down testing. .. 160

Table 6. 7. LNAPL transmissivity values and NAPL conditions for different extracted NAPL volumes at research areas A (PB29 well) and B (PB27 well) during baildown testing..... 161

ACRONYMS

AHD	Australian Height Datum
ANT	Apparent NAPL thickness
ASTM	American Society for Testing and Materials
BGL	Below ground level elevation
BTOC	Below top of casing
CRC CARE	Cooperative Research Centre for Contamination Assessment and Remediation of the Environment
CSIRO	Commonwealth Scientific and Industrial Research Organisation
DGP	Diagnostic gauge plots
DNAPL	Dense non-aqueous phase liquid
DTP	Depth to Product
DTW	Depth to Water
HPT	Hydraulic Profiling Tool
ITRC	Interstate Technology & Regulatory Council
LDRM	LNAPL Liquids Distribution and Recovery Model
LCSM	LNAPL conceptual site model
LIF	Laser-Induced Fluorescence
LNAPL	Light non-aqueous phase liquid
NAPL	Non-aqueous phase liquid
PAH	Polycyclic aromatic hydrocarbon
TPH	Total petroleum hydrocarbons
UST	Underground store tank
UTS	University of Technology Sydney
VOC	Volatile organic compounds

TERMINOLOGY

Symbol	Definition	Dimensions
b_a	screen length open to the portion of the vadose zone representative of the saturated hydraulic conductivity value used	L
b_n	in-well NAPL thickness	L
d	density	M/L ³
H	fluid heads	L
J	Kirkman J-ratio	Dimensionless
K	hydraulic conductivity	L/T
k^*	intrinsic permeability	L ²
K_n	LNAPL conductivity	L/T
k_n	LNAPL relative permeability	Dimensionless
k_r	relative permeability	Dimensionless
k_{ra}	relative permeability of open screen length in the vadose zone to air	Dimensionless
K_w	saturated hydraulic conductivity value for corresponding to the soil type existing in the vadose zone immediately above the mobile LNAPL interval	L/T
M	Van Genuchten parameter	Dimensionless
N	Van Genuchten parameter	Dimensionless
P_c	capillary pressure	L
P_{nw}	non-wetting fluid pressure	L
P_w	wetting fluids pressure	L
Q_α	air discharge rate in terms of standard air pressure and temperature	L ³ /T
Q_n	the LNAPL discharge	L ³ /T
Q_w	water discharge rate in terms of standard air pressure and temperature	L ³ /T
R_{oi}	radius of capture	L
r_w	well borehole radius	L
S_e	entrapped saturation	Dimensionless
$S_{e[t]}$	<i>total liquid effective saturation</i>	Dimensionless
$S_{e[w]}$	<i>water effective saturation</i>	Dimensionless
S_m	critical saturation	Dimensionless
S_n	NAPL saturation	Dimensionless
s_n	LNAPL drawdown	L
S_e	residual saturation	Dimensionless
s_{skim}	the maximum skimming drawdown	L
S_w	<i>water saturation</i>	Dimensionless
s_w	water extraction induced drawdown	L
t	time	T
T_n	LNAPL transmissivity	L ² /T
$T_{n,BD}$	LNAPL transmissivity via bail-down testing	L ² /T

$T_{n,SK}$	LNAPL transmissivity during the skimming operations	L^2/T
T_w	aquifer transmissivity	L^2/T
Z_{an}	air-LNAPL interface	L (AHD)
Z_{aw}	potentiometric groundwater surface elevation	L (AHD)
Z_{nw}	LNAPL-water interface	L (AHD)
α	Van Genuchten parameter	L^{-1}
Θ	total soil porosity	Dimensionless
μ	viscosity	$M*L^{-1}*T^{-1}$
μ_{ar}	relative viscosity of air to water	Dimensionless
ρ	fluid mass density	M/L^3
ρ_{fb}	soil bulk density	Dimensionless
ρ_r	the relative LNAPL to water density	Dimensionless

ABSTRACT

This research is focused on examining LNAPL distribution and mobility in heterogeneous porous media under the effect of water table fluctuations. Although it has been recognised that the potentiometric surface (Z_{aw}) changes may play a crucial role on LNAPL transmissivity (T_n), the related field based published work that has directly address it is limited and provides little insight regarding the impact of geological heterogeneity and complex NAPL distributions. This research work encompasses field studies in a heterogeneous gasoline contaminated site that presents seasonal water table fluctuations of 2 - 3 m.

LNAPL distribution and hydrogeological conditions were evaluated using diagnostic gauge plots, hydrostratigraphs, contaminant concentrations in cores, high resolution characterisation methods, LDRM simulations and baildown testing. T_n was evaluated using bail-down testing during both seasonal water table fluctuations and during induced hydraulic conditions (skimming, water-enhanced skimming, vacuum-enhanced skimming and water- and vacuum-enhanced skimming).

Collectively these tools and approaches have given useful insight into NAPL distribution and mobility under both natural and induced hydraulic conditions during seasonal changes and mass recovery applications. Results indicated that the NAPL hydrogeological conditions were related to the behavior of Z_{aw} and both confined and unconfined conditions can be found in the same well seasonally. Additionally, in heterogeneous settings the stratigraphy may override typical smearing patterns related to homogeneous systems. T_n ranged from 0.03 m²/day to 2.13 m²/day under unconfined LNAPL conditions, exhibiting a strong spatial variability. An inverse relationship between the Z_{aw} and T_n was found under natural conditions. The area with a wider NAPL distribution and higher NAPL saturations was less sensitive to changes in Z_{aw} during the skimming trials. The calculated T_n values from bail-down and skimming testing were in a close agreement and showed similar trends in most of the situations (less than a factor of 2 difference). However, in areas with narrow NAPL distribution and low NAPL saturations the discrepancy between both methods presented clearly higher differences (by a factor up to 7.3) and was related to Z_{aw} . Under stable Z_{aw} , T_n was found to be a relatively reliable metric for LNAPL recoverability. In contrast, variable water table conditions affected the evolution of T_n . Consequently, remediation practitioners, researchers and regulators should account for the nexus between T_n , LNAPL distribution, geological setting and temporal effects for a more efficient management of NAPL contaminated sites.

1. Introduction

1.1. Research background

Petroleum hydrocarbons such as gasoline, diesel and jet fuel are the most common and widespread contaminants in urban and industrial environments. Due to their relatively low density and solubility in water, these substances are found as light non-aqueous phase liquids (LNAPLs) in the subsurface and pose potential risks to human health and the environment because of their toxicity. LNAPL mobility depends on properties of the fluids and the geological medium at different scales. Immobile LNAPL is found in the saturated and unsaturated zones as entrapped and residual LNAPL respectively (White, Oostrom & Lenhard 2004). Mass transfer processes such as dissolution and volatilization increase the mobility of these chemicals in other phases.

LNAPL remediation efforts usually start with the application of mass recovery technologies. Such technologies allow the control of the source zone mobility if necessary. However, the limited radius of capture, the complexity of multiphase physics and the heterogeneity of geological media make impractical the total recovery of NAPL mass and the risk reduction is not necessarily effective (Alexandra, Gerhard & Kueper 2012; Huntley & Beckett 2002). Even though, the achieved mass reduction can still enhance natural depletion processes and improve the performance of posterior in-situ technologies focused on the immobile fraction and the dissolved phase. Thus, the combination of different technologies is the best way to optimally reduce risks and source zone longevity (Rao et al. 2002) and it is fundamental to assess the performance of mass recovery systems. Furthermore, removal of an entire LNAPL mass from the subsurface is quite difficult therefore the desired “natural” endpoints (removal to degree practicable) of remediation technologies at a specific contaminated site need to be carefully matched to be achievable remediation objectives.

The transport of LNAPL in the subsurface is a multi-phase flow problem. Many parameters give complexity to this problem affecting the transport, distribution and remediation process of these contaminants. The mobility of the LNAPL is influenced by the size of the release and the fluid’s properties. Physicochemical properties such as density, viscosity, interfacial tension, composition, aqueous solubility, vapor pressure and wetting behavior as well biodegradation control their environmental fate (CL:AIRE 2014; Newell 1995). As a result, a process understanding of the way LNAPL is distributed and its fate and transport in relation to the various remediation technologies is crucial especially in fine texture materials where there is a poor understanding of LNAPL behaviour.

The subsurface heterogeneity gives more complexity to the contaminated system and makes the remediation approach strategy more difficult and challenging (Adamski et al. 2005; Beckett & Huntley 1998; Illangasekare et al. 1995; Johnston & Trefry 2009). Moreover, other factors such as water table fluctuations (Dobson, Schroth & Zeyer 2007; McElroy, Drinkwater & Kanzler 1992; Wang et al. 2014) and NAPL confining conditions (CL:AIRE 2014; Kirkman, Adamski & Hawthorne 2013) provide more uncertainty to the existing problem. So far, free phase mass recovery techniques and concepts (Charbeneau et al. 2000; Delin & Herkelrath 2014; Gabr, Sharmin & Quaranta 2013; Gidarakos & Aivalioti 2007) have been tested successfully in field scale trials even though the documented research work is limited as regards more complex geologies such as fracture rock sites and fine grained systems (Johnston 2010).

The meaning of LNAPL transmissivity (T_n), is the capacity of a porous medium to transmit LNAPLs through the connected voids in the matrix structure filled with this fluid. T_n is a function of LNAPL conductivity (K_n) and LNAPL thickness in the formation (Nagaiah, Law & Ueland 2015). It is also an accurate proportional metric for LNAPL recoverability (ASTM 2013; Kirkman 2013) that can be applied as a start-up and shutdown (API 2012; ASTM 2013; ITRC 2009a) indicator for LNAPL recovery. Moreover, T_n is useful for the estimation of LNAPL removal rate for different remedial techniques as well as for trends identification in recoverability. Although LNAPL transmissivity is an accurate metric for LNAPL recoverability, it can also be a complex parameter because is not constant and changes with time, test conditions and water table fluctuations. Moreover, it includes subsurface parameters responsible for this variability such as soil permeability, LNAPL saturation and other physical characteristics of the plume (density and viscosity) (Beckett & Huntley 2015).

There are major deficiencies to predicting the fate of LNAPL in complex, heterogeneous and dynamic subsurface environments. The goal of this study is to address these deficiencies by field testing of LNAPL remediation technologies and characterization tools and to establish the practicability of T_n as a performance metric or endpoint criterion. More specifically, the focus of this research work is to examine LNAPL distribution and transmissivity in a heterogeneous gasoline contaminated site under water table fluctuations. A process of understanding the way LNAPL is distributed and its fate and transport is crucial.

1.2. Research objectives and contribution to knowledge

1.2.1. Research objectives

This dissertation study has two major objectives:

- I. To evaluate the impact of water table fluctuations on LNAPL distribution and hydrogeological conditions within the heterogeneous subsurface
- II. To evaluate the impact of the nexus between water table fluctuations and geological heterogeneity on LNAPL transmissivity.

1.2.2 Approach

The approach to the study was field-based using a gasoline contaminated site. A unique feature of the site was the very recent nature of the spill, the seasonally variable water table conditions and heterogeneous geology. These challenging conditions required a broad suite of tools to gain insight into the research objectives. In-well measurements on NAPL thickness and fluids elevations over a period of 3 years were undertaken at 23 wells. During this time there was typically a seasonal 2-3 m water table fluctuation leading to both unconfined and confined NAPL conditions in the research site. NAPL hydrogeological conditions were evaluated using diagnostic gauge plots comprising in-well NAPL thickness and fluids elevations, and by other lines of evidence such as hydrostratigraphs, NAPL saturations and baildown testing. NAPL distributions at various locations across the site were measured using contaminant concentration analysis in cores and LIF probing. In addition, NAPL distributions were evaluated by LDRM simulations. Subsurface physical properties were evaluated using logging of core samples and HPT probing. LNAPL transmissivity was evaluated using bail-down tests during both seasonal water table fluctuations and during induced hydraulic conditions (skimming, water enhanced skimming, vacuum enhanced skimming and skimming with vacuum and water enhancement). By examining NAPL transmissivity under these different hydraulic conditions, insight was gained into controls on NAPL transmissivity. Apart from NAPL transmissivity, the performance of the tested mass recovery techniques was evaluated by measuring NAPL recovery rates in both liquid and gas phase. Collectively these tools and approaches have given useful insight into NAPL distribution, transmissivity, mobility and recoverability under both natural flow conditions and induced conditions during remediation trials.

1.2.3. Contribution to knowledge

Within the research literature, the majority of the available remedial techniques have so far been tested in a limited set of geological environments. Primarily these trials have been carried out in sandy aquifers under stable water table conditions where the multi-phase physics of LNAPL behaviour is less complex. The need of pilot-scale remediation applications in fine texture materials has been stated in the literature (Johnston, 2010). This study takes place in heterogeneous subsurface settings. Moreover, this research will help in assessing the impact that water table fluctuations may have on NAPL distribution and on T_n in heterogeneous contaminated sites and how the validity of T_n as a leading and lagging metric is affected. Although it has been stated that the water table fluctuations may play a crucial role on T_n (Beckett & Huntley 2015; Kirkman & Hawthorne 2014), the existing field based research papers (Nagaiah, Law & Ueland 2015; Palmier, Dodt & Atteia 2016; Pennington et al. 2016) do not directly address it. Furthermore, the nexus between water table fluctuations, geological heterogeneity and complex NAPL distributions is investigated. Thus, the outcomes of this research could have an important impact on regulatory frameworks and contaminated site management strategies.

2. Literature Review

2.1. Conceptual models of LNAPLs in subsurface

The development of a LNAPL conceptual site model (LCSM) depends on an understanding of the behavior of LNAPL petroleum liquids in subsurface. The physicochemical properties and the setting of the LNAPL body are described in detail in a LCSM. The LNAPL conceptual site model provides the basis from which assessments of flux, risk, and appropriate remediation action can be generated (ASTM 2014). Altering conditions in the contaminated site as well as more new knowledge is gained, make the LCSM a dynamic model that changes through time.

A number of important sources in the literature elucidate the behavior of LNAPL in the subsurface (Adamski et al. 2005; Charbeneau et al. 2000; Huntley & Beckett 2002; Jeong & Charbeneau 2014; Johnston & Adamski 2005; Johnston & Trefry 2009; Kirkman, Adamski & Hawthorne 2013; Lenhard & Parker 1990; Mercer & Cohen 1990; Newell 1995; Soga, Page & Illangasekare 2004). Figure 2.1 depicts a simple LNAPL release concept even though, heterogeneity (especially fine textured materials) and other complicating factors such as multi-phase partitioning to soil, water and air phases, water table fluctuations and changes of LNAPL characteristics make the understanding of LNAPL behavior more complicated and uncertain.

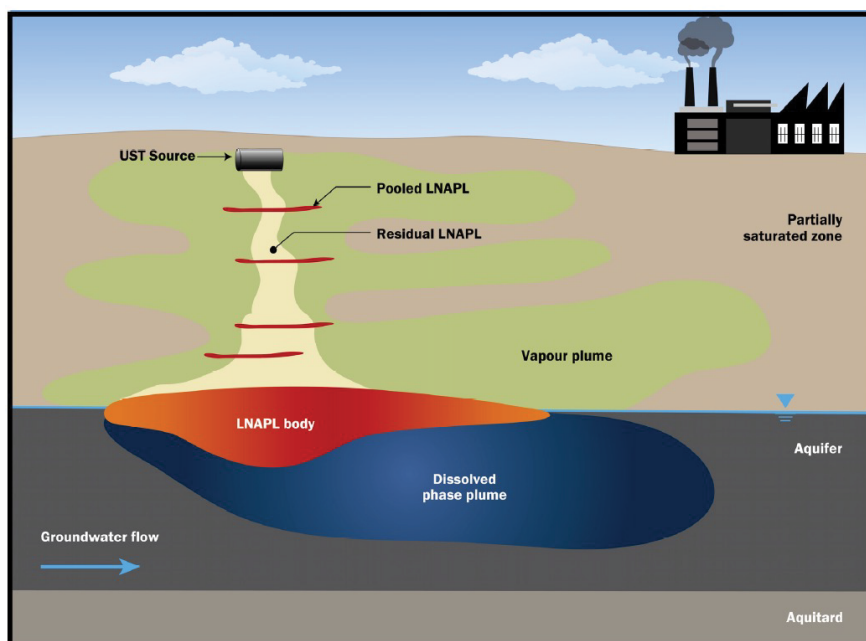


Figure 2. 1. Illustration of an LNAPL release in subsurface (CL:AIRE 2014).

2.1.1. Types of LNAPL and their properties

The term NAPL (non-aqueous phase liquid) describes any immiscible liquid that maintains a stable interface with water (Huling & Weaver 1991). This capacity includes a well-defined interfacial tension. LNAPL (light non-aqueous phase liquid) is a NAPL that is relatively immiscible with water (hydrophobic) and has density less than that of water. These characteristics affect their behavior in the geological settings after they released as petroleum products.

LNAPLs can be multicomponent mixtures of thousands of organic compounds. Petroleum hydrocarbon fuels are complex in composition containing aliphatic (such as alkanes and alkenes) and aromatic organic compounds. A variety of additives for enhancing and extending the performance of fuels can also be found in these hydrocarbon mixtures. Hydrocarbon fuel types have different carbon number (molecular weight) ranges and as a result differences in their physical-chemical properties. These characteristics affect their fate and transport in the subsurface. Representative properties of some typical LNAPLs are presented in Table 2.1.

Table 2. 1. Typical density, viscosity, interfacial tension (LNAPL-water) and, surface tension (air-LNAPL) of typical fuel LNAPLs along with the temperature of measurement (CL:AIRE 2014; Johnston 2010; Newell 1995).

	Density (g/cm³)	Viscosity (cP)	Interfacial tension (LNAPL-water) (mN/m)	Surface tension (air-LNAPL) (mN/m)	Temperature (°C)
Kerosene	0.809	1.73	38.6	26.8	22-24
Petrol	0.733	0.48	22.9	20.5	22-24
Jet A-1	0.811	2.0	25.5	29.1	25
JP-4	0.75	1.0/ 0.83	50	-	15/ 21
JP-5	0.82	2.0	-	-	15
JP-8	0.78-0.84	2.0	-	-	15
Water	0.998	1.14	-	67.1	15

Generally, hydrocarbons have low aqueous solubility that decreases with increasing molecular mass. Aromatic compounds are more soluble than the alkanes, also with decreasing solubility as molecular weight increases. The hydrophobicity of the petroleum hydrocarbon constituents is correlated with the octanol-water partitioning coefficient, K_{ow} (CL:AIRE 2014). There is also partition of the constituent compounds of LNAPL into an air/gas phase. The partitioning of LNAPL constituents between the dissolved and gaseous phases

can be described by the Henry's coefficient, k_H and, the vapour pressure of the NAPL compounds is a measure of the potential for partitioning into air.

After the contaminant release, the individual compounds of LNAPL may become sorbed, volatilized, dissolved in the water phase and degraded by biological processes. Thus, the physical properties of the contaminant change over time a process that is referred as weathering of the LNAPL (Lekmine et al. 2014). As a result of all the mentioned processes above is a potential reduce to the LNAPL mass and changes to LNAPL chemical composition.

2.1.2. LNAPL transport and distribution

The LNAPL transport and distribution processes at pore and field scale rely on NAPL and porous media characteristics. At the pore scale, transport and fate parameters such as, density, viscosity, interfacial tension, wettability, relative permeability, capillary pressure, saturation and residual saturation play a dominant role on LNAPL behavior. Heterogeneous subsurface settings and contaminant release history also make LNAPL transport prediction difficult at the field scale.

Contaminant phase distribution

LNAPL constituents may exist in the subsurface in four different phases: i) an immiscible liquid phase (LNAPL), ii) dissolved in groundwater as the aqueous phase iii) volatilised into soil gas as the vapour phase and iv) adsorbed to soil particles in the solid phase (sorbed). All four phases may be present in the vadose (unsaturated) zone whereas, in the saturated zone, contaminants will not be present in the vapour phase as water has displaced air from pore spaces. Compounds may also partition between the various non-liquid phases (vapour–dissolved, dissolved–sorbed).

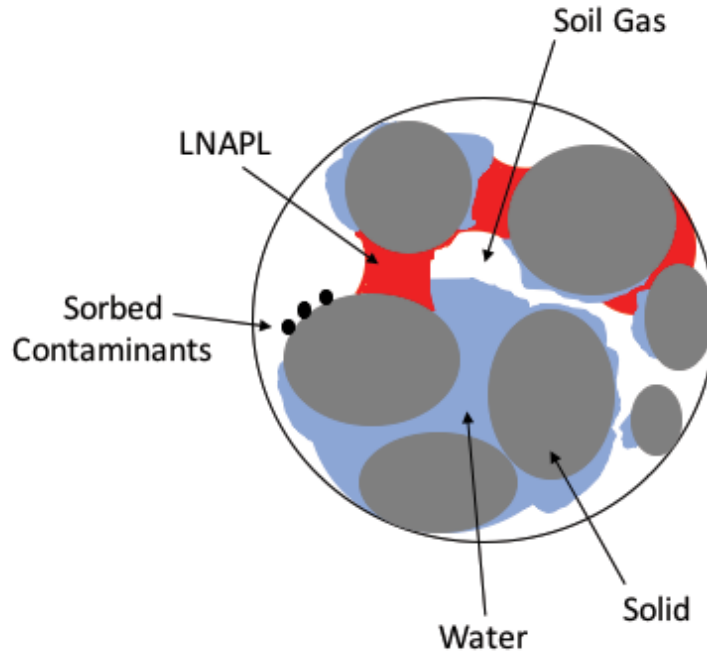


Figure 2. 2. The four physical phases of petroleum hydrocarbons in the unsaturated zone after (Rivett et al. 2011).

Partitioning equations can estimate the concentration of LNAPL components in the different phases when a multi-component LNAPL is in contact with water and air. Partitioning between the LNAPL and air phases under equilibrium conditions can be estimated by Raoult's Law giving the concentration of the i -th compound in air, $C_{i,a}$ as (Corapcioglu & Baehr 1987):

$$C_{i,a} = \frac{\omega_i p_i^* x_i \gamma_{i,n}}{RT} \quad [\text{Equation 1}]$$

where ω_i is molecular weight, p_i^* is vapor pressure of the pure compound, x_i is mole fraction in the NAPL phase, $\gamma_{i,n}$ is activity coefficient in the LNAPL, R is the universal gas constant and T is temperature.

As regards partitioning of volatile organics between the water and gas phases, the partial pressure of a dissolved compound in water in equilibrium with the water phase is governed by Henry's Law via (Johnston 2010):

$$p_i = k_{H,i} C_{i,w} \quad [\text{Equation 2}]$$

where $k_{H,i}$ is the Henry's coefficient and $C_{i,w}$ is concentration in water. Equation 3 follows the previous equations as:

$$C_{i,a} = \frac{\omega_i k_{H,i} C_{i,w}}{RT} \quad [\text{Equation 3}]$$

2.1.2.1. LNAPL behavior in porous media

2.1.2.1.1 Fluid migration and distribution at field scale

Several processes govern the LNAPL movement in the subsurface settings. Once the hydrocarbon fuel is released, NAPL will redistribute under the influence of gravity and capillary forces (Huling & Weaver 1991).

Initially, the downward infiltration of LNAPL in the vadose zone is driven under the force of gravity where air can be displaced. The ultimate depth reached by infiltrating LNAPL is influenced by many factors such as, the volume of the NAPL release, the loss mechanisms affecting on the LNAPL, the heterogeneity of the subsurface materials, and the location of the water table. Upon the downward migrated NAPL reaches the capillary fringe, then a lateral movement of the LNAPL takes place as a free-phase continuous layer due to capillary forces and gravity (Newell 1995).

2.1.2.1.2 LNAPL mobility

At the pore scale, LNAPL exists as mobile or immobile LNAPL. A mobile LNAPL has the ability to move under applied pressure gradients being in a continuous, connected body of fluid in the porous material. Immobile LNAPL is not able to move under normal pressure gradients and exists as isolated ganglia of liquid and/or spread as thin films (Johnston 2010). The terminology above refers to LNAPL behaviour in the prevailing conditions even though changing conditions such as water table fluctuations can cause LNAPL to become mobile or immobile (Newell 1995).

The immobile LNAPL may be subdivided into: i) residual LNAPL, or ii) entrapped LNAPL (White, Oostrom & Lenhard 2004). A residual LNAPL exists above the capillary fringe in a multiphase (three-fluid phase) system and is not able to move further under an applied pressure gradient, being thinly spread within the pore network, or isolated within the pores (Figure 2.3). Entrapped LNAPL is defined as 2 phase system (water / LNAPL) which exists as isolated blobs or ganglia within a pore network (Figure 2.3). The snap-off mechanisms at pore throats and fluid by-passing are responsible for the isolation of discrete blobs or ganglia.

Macroscopic entrapment may also take place (Wilson et al. 1990). The initial saturation and the type of soil in which the LNAPL release occurred affect the residual saturation (CL:AIRE 2014).

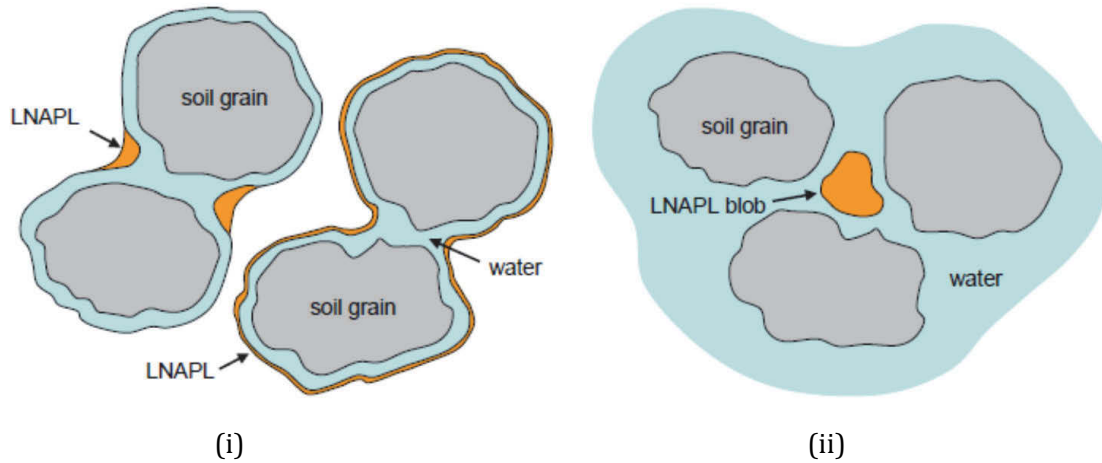


Figure 2. 3. Residual and entrapped LNAPL in a porous media. Unsaturated zone i) LNAPL is isolated as a thin immobile film. Saturated zone and ii) LNAPL is entrapped as blobs or ganglia after (Johnston 2010).

NAPL saturation characterizes the potential for NAPL to be mobile. It should be noticed that, there is a TPH threshold (known as soil saturation limit for the NAPL mixture or $C_{sat,soil}$) for NAPL occurrence (Brost & DeVaul, 2000; Rivett, Dearden & Wealthall 2014). The $C_{sat,soil}$ calculation of a mixture, takes into account the partitioning coefficients (to other phases such as: air, water and sorbed) of its individual chemicals. When LNAPL is present at saturations exceeding residual saturation, then it is mobile (ASTM 2014; ITRC 2009a). Ignoring partitioning to other phases (water, air, sorbed), the following equation converts total petroleum hydrocarbon (TPH) soil concentrations to LNAPL saturations as fraction of pore space (ASTM 2014; Parker, Waddill & Johnson 1994):

$$S_n = \frac{[TPH]}{10^{-6}} \cdot \frac{\rho_{fb}}{\rho_o} \cdot \Theta^{-1} \quad [Equation 4]$$

Where:

S_n = NAPL saturation (fraction of pore space filled with NAPL)

[TPH]= Total petroleum hydrocarbon soil concentration (mg/kg)

ρ_{fb} = Soil bulk density

ρ_o = NAPL/ oil density

Θ = Total soil porosity

An outcome of the presented variable in Equation 4 is that NAPL saturations are dependent on both the type of LNAPL and the type of soil impacted.

2.1.2.2. Influences on LNAPL transport and distribution

The basic principles affecting LNAPL transport and distribution are the same after a LNAPL release. The type of the LNAPL, release mode and subsurface variations manage transport at both the pore scale and field scale. At the pore scale, the following documented factors govern LNAPL migration and distribution whereas at the field scale, complex parameters such as release history and subsurface heterogeneity make LNAPL migration more difficult to predict. The following presented principles are crucial to understanding better the contamination issue and to evaluate the remediation process.

Density

The definition of density is the mass of a substance per unit volume. Density is expressed as the specific gravity which is the ratio of the mass of a given volume of substance at a specified temperature to the mass of the same volume of water at the same temperature (Mercer & Cohen 1990). If a NAPL has a specific gravity value less than water (< 1.0) then it is less dense than water (LNAPL) and will float on water. If it has a specific gravity value greater than water, (> 1.0) then it is denser than water (DNAPL). The NAPL movement in the subsurface can be affected by density differences of 1% (Mackay, Roberts & Cherry 1985). Density also affects the subsurface mobility of NAPLs. In a porous medium, the NAPL conductivity is a function of the density and viscosity of the fluid (Equation 5) as well as of other parameters. Thus, the NAPL conductivity increases as the density increases (with respect to the liquid). As can be seen in Figure 2.4, the change in the potential for LNAPL recovery was found to be smaller than 20% for different LNAPL changes in a homogeneous soil environment with $K=3\text{ft/day}$ (Awar 2008). Temperature is a parameter that affects density. More specifically, the density of NAPLs decreases as temperature rises. Remediation processes may decrease the density of DNAPLs converting them to LNAPLs (Newell 1995).

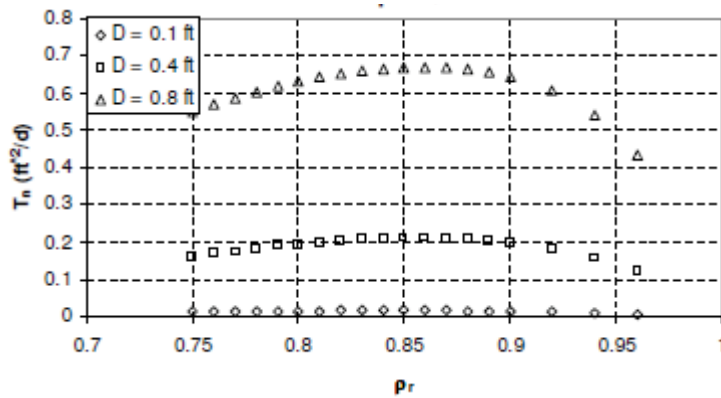


Figure 2. 4. Influence of the density of LNAPL on the potential for LNAPL recovery for certain LNAPL specific volumes (Awar 2008). Where D refers to specific volume of NAPLs.

Viscosity

Viscosity (dynamic, or absolute) is defined as the resistance of a fluid to flow, expressed in units of mass per unit length per unit time. Molecular cohesion is the leading cause of viscosity (Huling & Weaver 1991). Viscosity is temperature dependent, which decreases as the temperature rises. The lower the viscosity, the easier a fluid flows in a porous medium (Ahmed 2014). Figure 2.5 presents the influence of different viscosity values to in-well thickness recovery after bailing product. The NAPL conductivity decreases (Equation 5) as the fluid viscosity increases leading to slower LNAPL migration and increased timeframes for contaminants to reach hydrostatic equilibrium (CL:AIRE 2014). In a rising water table period, a viscous LNAPL might not rise as fast as the water table and can be fully entrapped (bypassed) by the less viscous water (Oostrom, Hofstee & Wietsma 2006).

$$K = \frac{k_n \cdot k^* \cdot \rho_n \cdot g}{\mu_n} \quad [Equation 5]$$

Where:

K_n = NAPL conductivity (m/s)

k^* = intrinsic permeability (m^2)

ρ_n = NAPL mass density (kg/m^3)

g = gravity (m/s^2)

μ_n = NAPL dynamic (absolute) viscosity ($kg/m \cdot s$)

k_n = is the NAPL relative permeability for the given conditions.

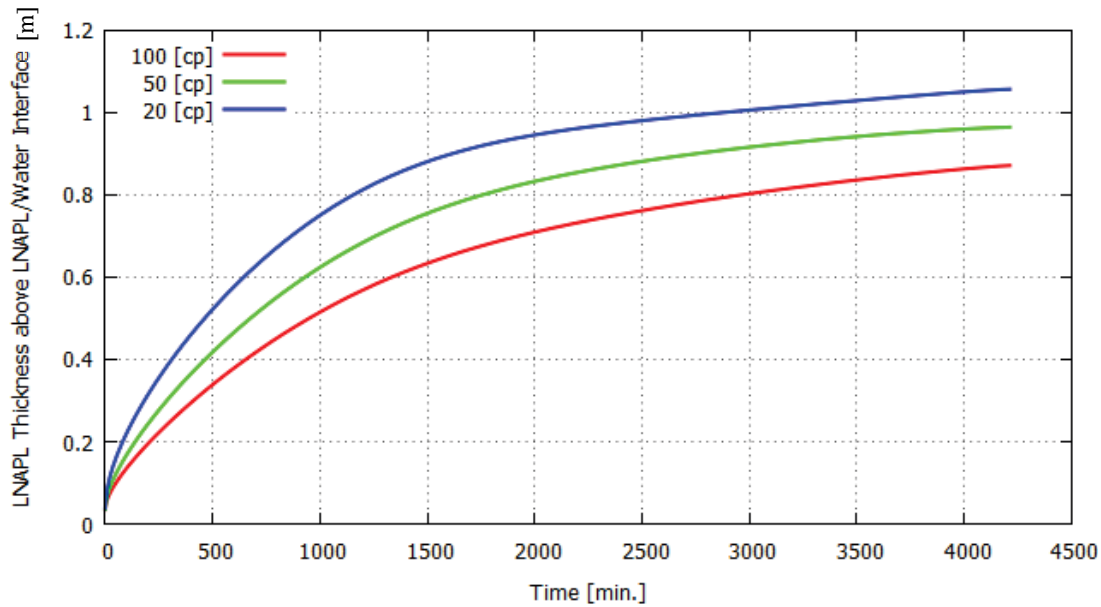


Figure 2. 5. Influence of the viscosity of LNAPL on the recovery of LNAPL thickness in the well after bailing (Ahmed 2014).

The Energy (Head) Gradient

NAPL pressures are often presented as equivalent water heads (height of a water column supported by the fluid pressure). If there is a pressure head difference, then the energy gradient causes LNAPL flow movement whereas, if there is no pressure head difference then no NAPL flow will occur in the subsurface. LNAPL and groundwater contour maps can determine the flow direction in the media, with NAPL and groundwater flowing from high to lower head regions. Fluid heads, H , are scaled from the pressures according to:

$$H = \frac{P}{\rho_w \cdot g} \text{ [Equation 6]}$$

where: ρ_w is the density of water, P is the pressure and g is the acceleration due to gravity.

More details about the importance of LNAPL and water pressures on LNAPL mobility are presented later in the section of Capillary Pressure.

Solids Nature and Porosity

The nature of the solids and the interstitial pore spaces are the main properties of porous materials that affect the distribution and movement of LNAPL. The size, morphology and interconnections of the pore space control usually the distribution of LNAPL in geological media even though the physicochemical interactions of the solids with fluids are important (Johnston 2010). The geometry of the pore space is asymmetrical and complex. The

heterogeneity of the subsurface affects the distribution of the capillary pressures along the interfaces between the water and NAPL phases (Huling & Weaver 1991). Fine grained media exhibit lower LNAPL saturations than coarser materials for the same observed thickness in a monitoring well (Beckett & Huntley 1998) and present lower NAPL recovery potential compared to coarser materials (Ahmed 2014). Saturated column experiments showed that NAPL preferentially travelled through strings of macropores, by-passing the water saturated micropores (U.S. EPA 1990). Moreover, the organic fluid preferentially moved through the coarse lens material rather than through the fine porous material in a heterogeneous environment simulation. Macropores were indicated to control the saturation, distribution and mobility of LNAPL in fine grained systems (Adamski et al. 2005). The particle grain size governs the residual saturation of a gasoline hydrocarbon (Hinchee & Reisinger 1987). The residual saturation has been found to be greater in dry fine sands (55%) compared to dry coarse sands (14%).

Interfacial Tension

When two or more immiscible fluids are in contact in a pore space of a porous medium, an interfacial energy exists between the liquids, resulting in a physical interface which acts as a membrane under tension (Charbeneau 2007b). Interfacial tension is the surface energy at the interface that results from differences in the attractive forces between molecules within the liquid phase (Newell 1995). The units for interfacial tension expression are energy per unit area. The greater the interfacial tension, the greater the stability of the interface between the liquids. Temperature (Davis & Lien 1993) and pH changes, surfactants and dissolved gases affect the interfacial tension. It is an important parameter that affects wettability (Mercer & Cohen 1990) and a decrease in value can mobilize trapped ganglia (Ryan & Dhir 1996).

Wettability

Wettability is one of the complex subsurface parameters that affect the remediation of non-aqueous phase liquids (Drake, O'Carroll & Gerhard 2013). Wettability is generally defined as the preferential spreading of one fluid over a solid surface in the presence of another fluid with which it is immiscible. Wettability describes fluid distribution at the pore scale and depends on interfacial tension. In a multiphase system, the wetting fluid will tend to coat the solid surfaces occupying smaller pore spaces in porous media, whereas the non-wetting fluid will generally be restricted to the largest interconnected openings (Mercer & Cohen 1990). In

the unsaturated zone, where air, water, and LNAPL are present, water preferentially wets solid surfaces however, under conditions where only LNAPL and air are present (semi-arid climates), LNAPL will preferentially coat the solid surfaces and displace air from pores. In the saturated zone, with water and LNAPL present, water will generally be the wetting fluid and will displace LNAPL from pore spaces (Newell 1995). The contact angle is the angle between tangential line to the NAPL-water interface starting from the three phase contact line and solid surface and can be used to characterise wetting behaviour (CL:AIRE 2014). NAPL and aqueous phase composition, presence of organic matter, surfactants and mineralogy are parameters that affect wettability (Mercer & Cohen 1990).

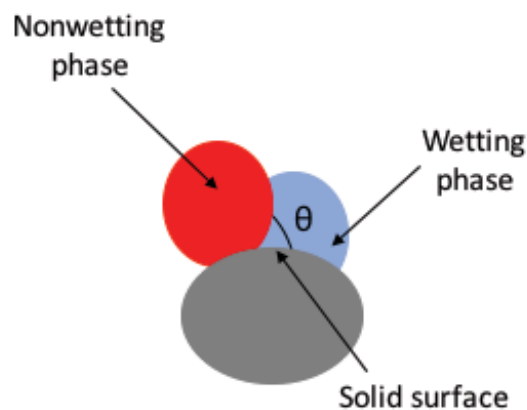


Figure 2. 6. Cartoon depicting non-wetting (LNAPL) and its contact angle with solid surface in the presence of wetting phase (water).

Capillary pressure

Fluid pressure is a critical parameter for mobile LNAPL. LNAPL are held in the pores by capillary forces. Capillary pressure is the pressure difference across the interface between the wetting (typically water) and non-wetting (typically LNAPL) phases often expressed as the height of an equivalent water column. Within a geological porous media the LNAPL pressure in relation to the other fluids govern its distribution (Newell 1995). A stable interface exists between the fluids therefore the interfacial forces act on the curved interface between the fluids maintaining the difference in fluid pressures. For a two-fluid phase system, capillary pressure, P_c is defined as the difference in pressure between the non-wetting and wetting fluids (Johnston 2010):

$$P_c = P_{nw} - P_w \text{ [Equation 7]}$$

Where, P_{nw} is the non-wetting fluid pressure and P_w and refers to the wetting fluids pressure. In a water-wet, two-fluid phase system, water is the wetting phase and either air or

LNAPL is the non-wetting phase. $P_{c,aw}$ refers to air-water capillary pressure and $P_{c,nw}$ refers to LNAPL-water capillary pressure. For a three-fluid phase system, the capillary pressure is the pressure difference between any two fluid pairs with due regard to the hierarchy of wetting (water>LNAPL>air). Thus, $P_{c,an}$ refers to air-LNAPL capillary pressure.

The capillary pressure must be exceeded before the non-wetting fluid (typically NAPL) can enter the media. The minimum pressure required for the NAPL to enter the porous medium is termed the entry pressure. The entry pressure is directly proportional to the interfacial tension (σ_{nw}) between the LNAPL and water and cosine of the contact angle (θ) (Figures 2.6 and 2.7) and inversely proportional to the pore throat radius (r).

$$P_{c,mw} = P_n - P_w = \frac{2 \cdot \sigma_{mw} \cdot \cos(\theta)}{r_1} \quad [\text{Equation 8}]$$

$$P_{c,an} = P_a - P_n = \frac{2 \cdot \sigma_{an} \cdot \cos(\theta)}{r_2} \quad [\text{Equation 9}]$$

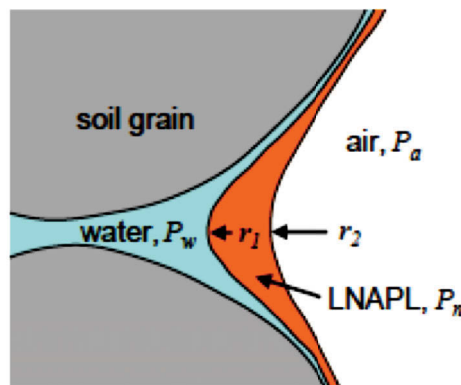


Figure 2. 7. Schematic of the distribution of fluids in a porous media showing the radius of curvature of the interfaces as a result of fluid pressure differences (Johnston 2010).

Capillary pressure increases with decreasing pore size, decreasing initial moisture content, and increasing interfacial tension. Capillary conditions control the configuration and amount of trapped and residual NAPL. Preferential LNAPL movement through coarse-grained materials rather than fine-grained media is an effect of capillary pressure according to field observations (Adamski et al. 2005; Newell 1995).

Capillary Pressure - Saturation Models

A quantitative analysis of capillary pressure – saturation curve measurements can be provided via mathematical models. Two popular formulations developed originally for water-

soil applications are the van Genuchten (Van Genuchten 1980) and Brooks-Corey (Brooks & Corey 1964) relationships. The van Genuchten (vG) model has been considered as an appropriate approach for soils that have already been affected by LNAPLs (Charbeneau 2007b; Jeong & Charbeneau 2014; Lenhard et al. 2017; Lenhard et al. 2018). The mathematical form for the vG model is:

$$S_{ef} = \left(1 + (\alpha * h_c)^N\right)^{-M} \quad [Equation 10]$$

Where S_{ef} is the effective wetting-phase saturation that is scaled from 0 to 1 and h_c is the capillary pressure head (Van Genuchten 1980). α , N and M are vG parameters. The parameters α and N are used for the characterization of soil textures. The parameters M and N are independent of α and are based on one of two permeability models: Burdine (Burdine 1953) and Mualem (Mualem 1976). The mathematical form between N and M parameters is:

If $N > 2$, then $M = 1 - 2/N$ (Burdine 1953)

If $N > 1$, then $M = 1 - 1/N$ (Mualem 1976)

Saturation and Residual Saturation

Fluid saturation (S) is the relative fraction of total pore space occupied by particular fluid (for instance NAPL) in a porous media. Equation 11 illustrates the fluid saturation, S , as the ratio of the volume fraction of the fluid to the porosity of the porous medium.

$$S = \frac{\theta_v}{\Theta} \quad [Equation 11]$$

where θ_v is the volumetric content of the fluid.

The relationship between saturation and relative permeability determines the mobility of LNAPLs. Residual saturation (S_r) is the saturation level where a continuous NAPL becomes immobile by capillary forces (White, Oostrom & Lenhard 2004). Residual saturation is a percentage of the NAPL saturation and varies based upon the maximum saturation and the soil type (Kueper et al. 1993; Steffy, Barry & Johnston 1997). A linear relationship between residual and initial LNAPL saturation even for fine texture materials has been documented (Johnston & Adamski 2005). Residual saturation of LNAPL is an important concern for the environment representing a continuous source for ground water contamination. S_r is quite variable affected by the heterogeneity of the subsurface taking into consideration parameters

such as properties of the fluids and soil solids, hydraulic gradients, flow rates and pore size distribution (Demond & Roberts 1991).

Typical NAPL residual saturations in different soil types in saturated zone is provided by the Interstate Technology and Regulatory Council (ITRC 2009b), where sands have the highest residual saturation values of 25% (of pore space), sandy clay 10% and silty clay 6%. According to Mercer and Cohen research (Mercer & Cohen 1990), the NAPL residual saturation in the vadose zone ranged from about 10% to 20% and about 15% to 50% of the total pore volume in the saturated zone. Interestingly, Adamski et al (Adamski et al. 2005) documented maximum measured LNAPL saturations <2% for a fine grained system. Several factors are responsible for higher retention of NAPLs in the saturated zone than in the vadose zone such as i) in the vadose zone potential the NAPL exist as the wetting fluid relative to air resulting in NAPL spreading to adjacent pores with residual remained in small pore throats, 2) in the saturated zone the NAPL is presented as the non-wetting fluid resulting in NAPL exist as blobs in larger pore spaces.

The saturation-capillary pressure ($S - P_c$) relationship is a characteristic of the porous material and fluids (Johnston & Adamski 2005). The $S-P_c$ relationship is complex taking into consideration the hysteresis and the history of fluid saturation changes in the porous materials. Figure 2.8 illustrates the primary drainage and imbibition curves (referenced to the wetting fluid) for a two-fluid phase system along with secondary curves. The drainage curve depicts the displacement of the wetting fluid (water) by the non-wetting fluid (NAPL) and the imbibition curve shows the displacement of the non-wetting fluid by the wetting fluid (Charbeneau 2007b).

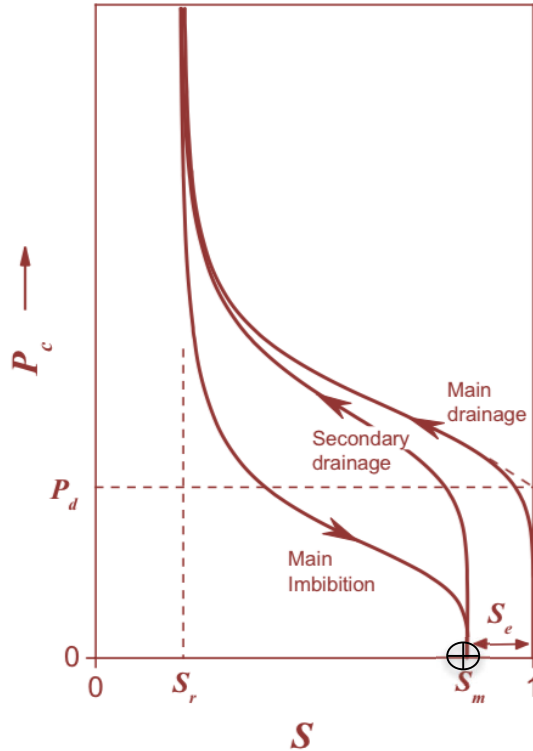


Figure 2. 8. Schematic of the saturation-capillary pressure relationship for two fluids in a porous media. Where, P_d is the fluid displacement pressure, S_r the residual saturation and S_e the entrapped saturation. $S_e = (1 - S_m)$, where S_m is the critical saturation. At this point (S_m) the capillary pressure is zero and the non-wetting fluid (NAPL) will not flow into a recovery well (Johnston 2010).

Relative Permeability

In multiphase flow in porous medium, relative permeability (k_r) is defined (Equation 12) as the ratio of the effective permeability of the media to a fluid at a fixed saturation and the permeability of the medium to the fluid at 100% saturation (intrinsic permeability). Values for relative permeability vary between 0 and 1 (Mercer & Cohen 1990; Newell 1995).

$$k_r = \frac{k}{k^*} \text{ [Equation 12]}$$

where k is the fluid permeability for the given conditions and k^* is the intrinsic permeability of the porous medium.

Figure 2.9 illustrates hypothetical relative permeability relationships for LNAPL and water in a fully saturated porous medium. The mobility is reduced for both LNAPL and water. In the unsaturated zone where air, NAPL and water exist, more complex relationships may occur (Ferrand, Milly & Pinder 1989).

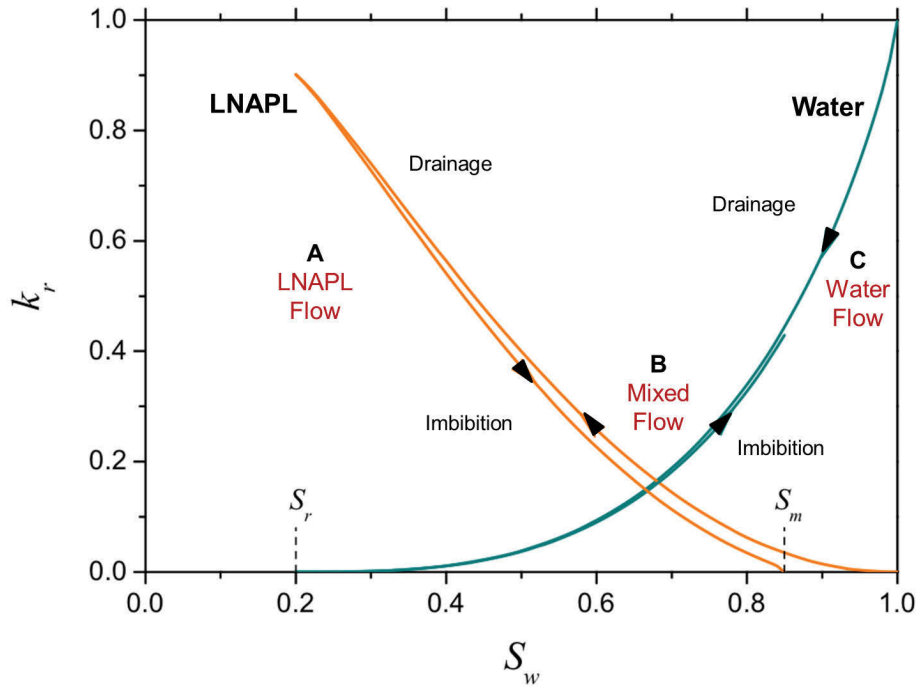


Figure 2. 9. Schematic showing hypothetical relative permeability relationships for LNAPL and water in a saturated porous media. Where S_r : residual saturation, S_m : critical saturation and S_w : saturation of wetting fluid.

Zone A: LNAPL exists at high saturation as a potentially mobile, whereas water is restricted to small pores with low relative permeability.

Zone B: Both LNAPL and water exist. The relative permeability of each fluid is significantly reduced by the saturation of the other fluid.

Zone C: LNAPL is discontinuous and entrapped as blobs or ganglia. LNAPL is immobile and the flow is only the movement of water.

Equations 13 and 14 are the van Genuchten-Burdine and van Genuchten Mualem relative permeability functions respectively (Charbeneau 2007b):

$$k_n(S_w, S_n) = (S_{e[t]} - S_{e[w]})^2 * ((1 - S_{e[w]}^{1/M})^M - (1 - S_{e[t]}^{1/M})^M) \quad [\text{Equation 13}]$$

$$k_n(S_w, S_n) = \sqrt{(S_{e[t]} - S_{e[w]})} * ((1 - S_{e[w]}^{1/M})^M - (1 - S_{e[t]}^{1/M})^M)^2 \quad [\text{Equation 14}]$$

where k_n is the NAPL relative permeability, S_w is the water saturation, S_n the NAPL saturation, $S_{e[t]}$ is the total liquid effective saturation and $S_{e[w]}$ is the water effective saturation.

2.1.2.3. Distribution of LNAPL in the vicinity of the water table

The levels of fluids in a well are in equilibrium with those in the formation and are determined by the formation LNAPL distribution. The pressure difference between the well and the formation cause liquid flow into or out of the well until the equilibrium is reached (Charbeneau 2007b). The following schematic (Figure 2.8) illustrates fluid elevations in a monitoring well. Air-LNAPL interface (Z_{an}), LNAPL-water interface (Z_{nw}) and potentiometric groundwater surface (Z_{aw}) elevations can be seen. The elevation Z_{gs} depicts the ground surface elevation and b_n is the apparent LNAPL thickness (ANT) in the monitoring well.

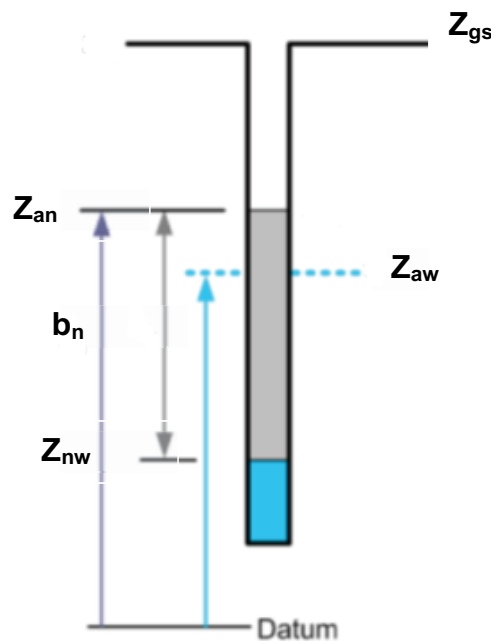


Figure 2. 10. Schematic showing an LNAPL monitoring well with fluid elevations.

The first concept of understanding the LNAPL migration in a porous medium presented the LNAPL body as a continuous separate “pancake” layer floating on the water table, developing a continuous fully saturated NAPL layer. This concept did not recognise the significance of capillary forces over-predicting both the amount of LNAPL in the formation, in addition to the amount of recoverable LNAPL (Huntley & Beckett 2002) . Later concepts (Farr, Houghtalen & McWhorter 1990; Lenhard & Parker 1990) related liquid contents of the porous media to capillary pressures. Considering the capillary pressure forces, the LNAPL saturation profile is assumed to have the shape of a shark fin within a homogeneous unconfined aquifer under equilibrium conditions. A heterogeneous subsurface may affect the NAPL saturation profile giving less characteristics of the shark fin profile (Huntley, Hawk & Corley 1994).

The following figure (Figure 2.11) illustrates the distribution of capillary pressure in the presence of LNAPL. The water pressure is zero at the water table. The LNAPL pressure is

zero at the elevation Z_{an} . The LNAPL and water pressures are the same at Z_{nw} where the LNAPL-water capillary pressure is zero. Figure 2.12 presents an idealised vertical distribution of LNAPL saturation with the equivalent fluid levels after a period of water table fluctuations.

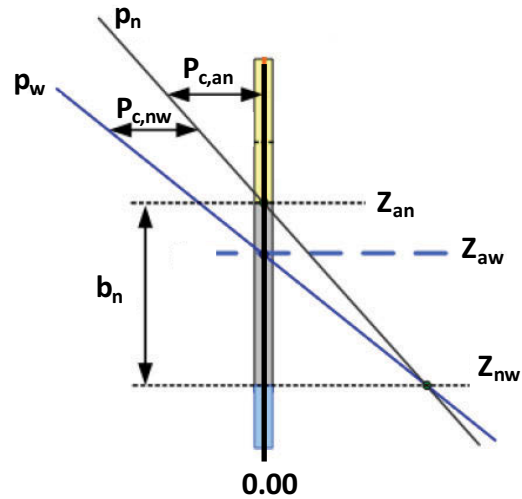


Figure 2. 11. Schematic showing the distribution of capillary pressure in the presence of LNAPL (Charbeneau 2007b). Where p_n : NAPL pressure, p_w : water pressure, $P_{c,an}$: air-LNAPL capillary pressure and $P_{c,nw}$: LNAPL water capillary pressure.

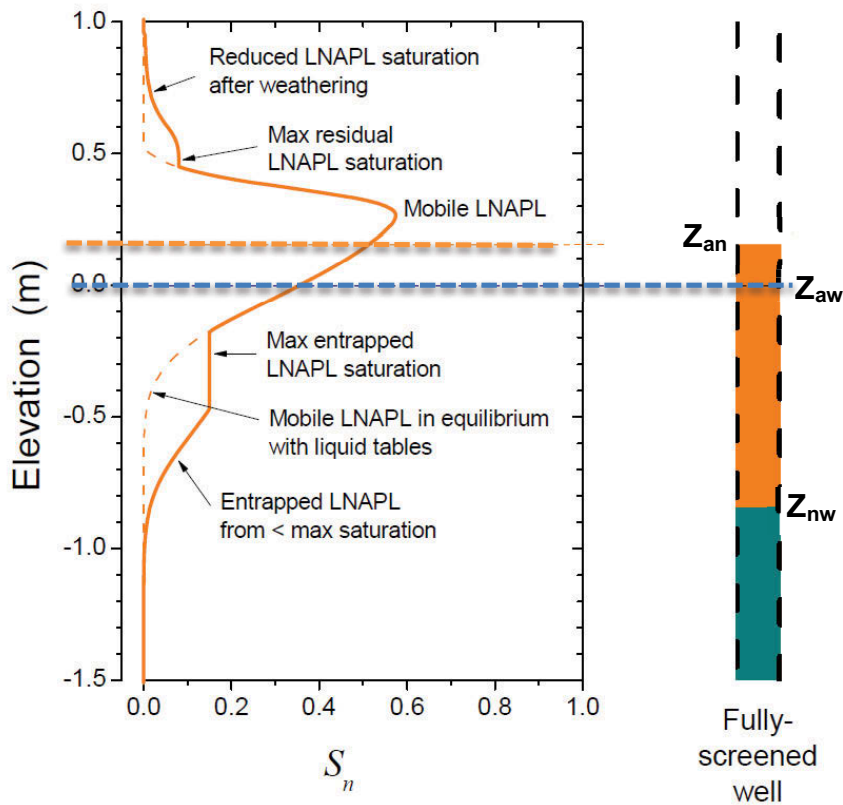


Figure 2. 12. Schematic showing the vertical distribution of LNAPL saturation with the equivalent fluid levels after (Johnston 2010).

Figures 2.11 and 2.12 depict different interfaces in the monitoring well as an outcome of the fluid pressures within the aquifer. The air-LNAPL interface shows where the LNAPL pressure ($P_{c,an}$) is zero (equals to air pressure). The LNAPL-water interface presents where the LNAPL pressure and the water pressure are equal ($P_{c,nw}=0$).

2.2. Water table fluctuations and LNAPL redistribution

Water table fluctuations may influence the distribution of LNAPL in the monitoring wells and formation (Kemblowski & Chiang 1990). Water table conditions may play a crucial role on LNAPL redistribution, its mobility and the partitioning into other phases and can affect the value of T_n by orders of magnitude (Beckett & Huntley 2015). Formation of residual and entrapped LNAPL from vertical displacement affects mass recovery under variable water table conditions and has been observed in contaminated field sites (Kuo et al. 2016; Steffy, Johnston & Barry 1995; Teramoto & Chang 2017) and laboratory studies. The laboratory experiments included the monotonic increase of water pressure in a sand column to avoid hysteretic behaviour (Lenhard et al. 1988) and the applications of fluctuations in the water level (Chompusri, Rivett & Mackay 2002; Dobson, Schroth & Zeyer 2007; Lenhard, Johnson

& Parker 1993; Oostrom, Hofstee & Wietsma 2006; Steffy, Johnston & Barry 1998; Van Geel & Sykes 1997; Yimsiri et al. 2016). Hysteresis has been proved to be a relevant aspect at field scale (Essaid, Herkelrath & Hess 1993; Sookhak Lari, Davis & Johnston 2016), although the water table fluctuations were not found to be as important for the modelling of LNAPL distributions in some cases (Dillard, Essaid & Herkelrath 1997).

Hydrographs obtained from field sites usually show that the water table elevation and T_n follow opposite trends (Beckett & Huntley 2015). In-well LNAPL thickness also changes with time and especially with water table fluctuations. The followed behaviour is a line of evidence to identify NAPL unconfined, confined and perched conditions (Kirkman, Adamski & Hawthorne 2013). However, as it has been widely recognized in the past, caution should be exercised when b_n is applied as a metric of potential LNAPL recoverability or LNAPL volume in the formation. Equilibrium in-well fluid levels should be representative of the fluid pressures in the formation and their analysis should be performed through the application of proper models (Kemblowski & Chiang 1990; Lenhard & Parker 1990; Marinelli & Durnford 1996; Sleep, Sehayek & Chien 2000). For instance, current and historic fluid levels in wells have been used to predict the LNAPL distribution in the formation and T_n in homogenous scenarios (Lenhard, Rayner & Davis 2017).

For unconfined aquifers, LNAPL thickness in wells decreases when the water table rises up and increases when the water table elevation decreases. The different NAPL hydrogeological conditions are presented in detail in section 2.3. When the water table falls, the LNAPL body drains because of gravity forces and smears forming a residual LNAPL saturation via imbibition process. When water level increases, the buoyant LNAPL rises however, some proportion of LNAPL will be entrapped due to capillary forces. When the water table falls again, some of the entrapped LNAPL will drain again (CL:AIRE 2014). Heterogeneity is an important parameter that may cause variation from this ideal conceptualisation presented above. For confined aquifers, LNAPL thickness in wells follows the same trend with the water table elevation (Marinelli & Durnford 1996). In fact, water table fluctuations is a parameter probably undesirable (Dobson, Schroth & Zeyer 2007). In periods of increased water table levels, the compression of the capillary fringe may reduce the apparent thickness (measured LNAPL thickness in a monitoring well) (Newell 1995).

2.3. LNAPL confinement conditions and apparent LNAPL thickness

LNAPL exist in subsurface as unconfined, confined or perched (API 2012; Johnston 2010; Kirkman, Adamski & Hawthorne 2013). In confined LNAPL conditions the capillary LNAPL pressure is less than the pore entry pressure in the upper finer texture soil layer, thus the porous media doesn't allow the LNAPL to migrate through the upper parts (Adamski et al.

2005; Hawthorne 2011a). Under perched LNAPL conditions, LNAPL is accumulated in the vadose zone above a layer that exhibits a pore entry pressure greater than the LNAPL pressure, impeding the downward movement of LNAPL (Hawthorne 2011c). In unconfined LNAPL conditions, LNAPL may migrate with limited capillary force restrictions.

LNAPL in a well is only a reflection of, but not necessarily equate to, the free LNAPL in the formation and does not reflect the residual and entrapped saturations of LNAPL (Johnston 2010). The thickness of the subsurface where NAPL exist above residual saturation can be presented as the mobile NAPL interval (MNI) (Reyenga & Hawthorne 2011). A wrong estimation of MNI brings errors to the analysis and prediction of LNAPL distribution, mass, mobility, and recovery. NAPL conditions must be known for correct calculations of LNAPL drawdown under perched and confined conditions (ASTM 2013; Hawthorne 2014a; Kirkman, Adamski & Hawthorne 2013). The remediation process may not target the right interval of the subsurface if the MNI is unknown. The vertical NAPL migration through the medium because of water table fluctuations, may change the location and thickness of the MNI. In unconfined NAPL conditions, the apparent (in-well) NAPL thickness b_n is a good indicator of the MNI (Kirkman, Adamski & Hawthorne 2013). In confined and perched LNAPL conditions, even though the MNI thickness and location are constant during water table fluctuations the b_n will change as the water table varies becoming larger than the MNI during higher water tables. More specifically, under confined NAPL conditions the mobile interval is between the transition point and the depth to water interface (Kirkman, Adamski & Hawthorne 2013). It should be noticed that, the well screened intervals have to be carefully chosen for the proper measurement of representative in-well fluid levels. Figure 2.13 illustrates unconfined, confined and perched LNAPL and b_n effect on a porous media.

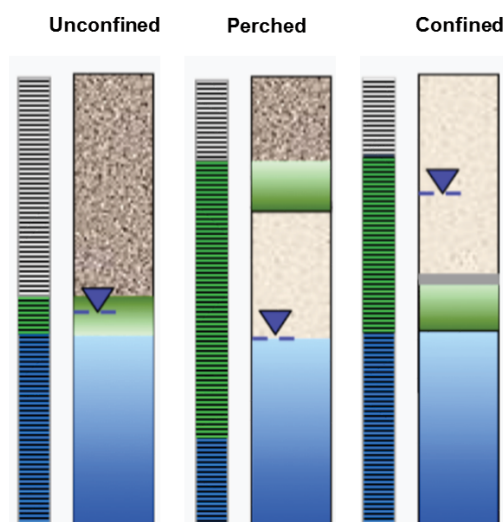


Figure 2. 13. Schematic showing *in-well thickness* (b_n) in unconfined, confined and perched LNAPL conditions (Hawthorne 2010).

In-well thickness causes an exaggeration problem for confined and perched LNAPL conditions. It causes a logarithmic exaggeration on recovery estimates, which will result in an unsuccessful remediation process and extra costs. Therefore, the LNAPL hydrogeological condition it is crucial to be known in order to estimate the MNI. For the determination of LNAPL conditions NAPL diagnostic gauge plots can be used.

2.3.1. NAPL Diagnostic Gauge Plots

For a detailed site wide analysis of LNAPL distribution and hydrogeological conditions, plume scale diagnostic gauge plots can be successfully used. A Diagnostic Gauge Plot (DGP) is a graph of the air-LNAPL interface (Z_{an}), LNAPL-water interface (Z_{nw}) and potentiometric groundwater surface (Z_{aw}) elevations versus the thickness of LNAPL observed in a well over time. NAPL diagnostic gauge plots (for individual wells) are valuable tools for light non-aqueous phase liquid analysis and LNAPL conceptual site modelling (LCSM) that can be used to: i) Identify the NAPL hydrogeological condition for a well (unconfined, confined, perched), ii) Estimate the mobile NAPL interval (mobile NAPL thickness) in the formation, iii) Estimate confining or perching elevations and iv) Calculate effective LNAPL density (Kirkman, Adamski & Hawthorne 2013). These gauge plots may also be utilized to obtain a general understanding of an entire site's NAPL distribution and hydrogeological conditions (for instance, identification of separate transmissive zones with NAPL). Hydrostratigraphs, gauge thickness plots, discharge versus drawdown graphs and baildown test data are part of these tools and are presented in this document.

The presented tools above were initially created to evaluate individual wells. However they could also be applied to achieve a general understanding of a whole site's NAPL distribution and hydrogeological conditions. Thus, a diagnostic gauge plot analysis can be used to: i) Identify separate NAPL transmissive zones, ii) Identify NAPL hydrogeological condition for each transmissive zone and iii) Estimate the range of NAPL thicknesses related to each transmissive zone (Hawthorne 2014b).

2.3.2. Gauge thickness plots

Diagnostic Gauge Plots are one tool that can be used to determine if LNAPL is unconfined, confined or perched, and to estimate the formation mobile LNAPL thickness (Hawthorne 2011b). Fluctuating elevations trends can be used to identify periods of unconfined, confined or perched LNAPL conditions (see Table 2.2). More specifically:

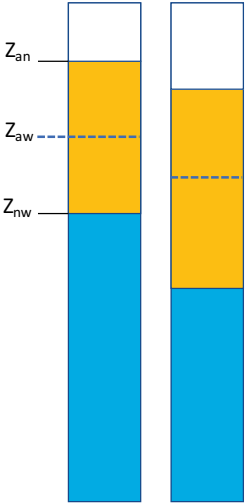
a) Unconfined LNAPL: during unconfined LNAPL conditions, all three interfaces and the LNAPL thickness will typically fluctuate. The apparent LNAPL thickness will fluctuate in the opposite direction of the three interfaces.

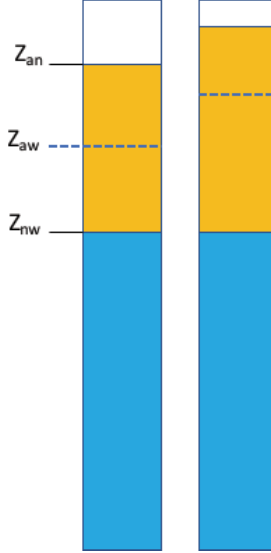
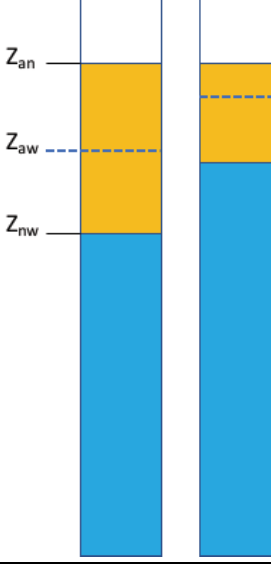
b) Confined LNAPL: during confined LNAPL conditions, the Z_{nw} elevation will typically be stable, and the other three measurements (Z_{an} , Z_{aw} and b_n) will fluctuate, all in the same direction.

c) Perched LNAPL: During perched LNAPL conditions, the Z_{an} elevation is theoretically stable and the other three measurements (Z_{nw} , Z_{aw} and b_n) fluctuate. The apparent b_n trend will be opposite to the Z_{nw} and Z_{aw} trends (Kirkman, Adamski & Hawthorne 2013).

Figure 2.14 depicts a diagnostic gauge thickness plot showing LNAPL confined conditions. Z_{aw} values are obtained by measuring the Z_{an} , Z_{aw} elevations in the tested well and by using the Equations presented in section 3.3.

Table 2. 2. Dynamics and illustrations to diagnostic gauge plot trend analysis (Hawthorne 2011b).

Hydrogeological Conditions	Stable Surface (in equilibrium)	Dynamics	Illustrations
Unconfined	None	b_n increases as Z_{an} , Z_{nw} and Z_{aw} decrease, and vice versa	

<p>Confined</p>	<p>Z_{nw}</p>	<p>b_n increases as Z_{an} and Z_{aw} increase, and vice versa</p>	
<p>Perched</p>	<p>Z_{an}</p>	<p>b_n decreases as Z_{nw} and Z_{aw} increase, and vice versa</p>	

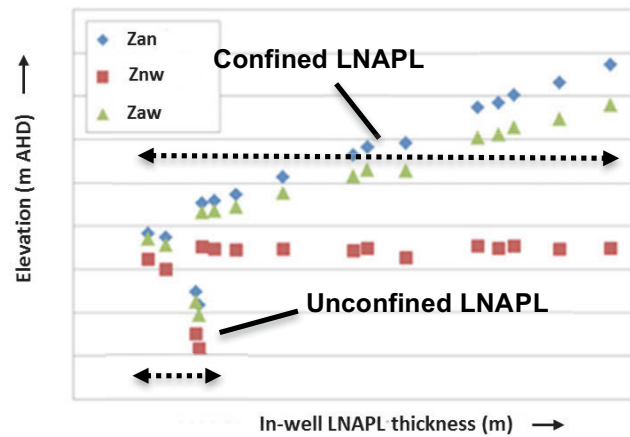


Figure 2. 14. A diagnostic gauge plot illustrating unconfined and confined LNAPL conditions. The graph presents air-LNAPL and LNAPL-water referenced interface elevations and the potentiometric surface elevation versus the gauged b_n .

2.3.3. Hydrostratigraphs

Hydrostratigraphs describe graphs created by combining hydrograph elevations over time with stratigraphic contact elevations to graphically depict and evaluate the distribution and mobility of LNAPL over vertically varying piezometric conditions. Hydrograph diagrams include three data sets that define them:

- i) Elevation versus Time: Elevation-related data such as LNAPL hydrograph and well screen elevations are graphed on the primary horizontal (time) and primary vertical (elevation) axes.
- ii) Thickness versus Time: With the addition of a second vertical axis, b_n at a vertical scale sufficient to identify trends over time is plotted on the primary horizontal time axis.
- iii) Stratigraphy versus Elevation: Lithologic contacts are plotted on the primary horizontal (time) and vertical (elevation) axes.

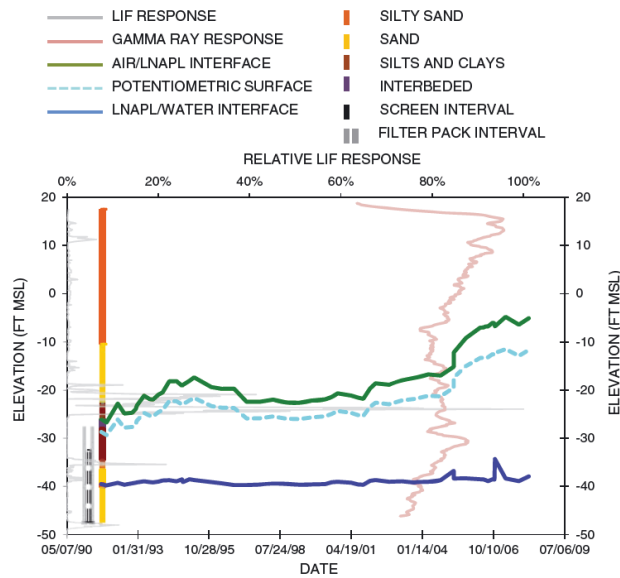


Figure 2. 15. Hydrostratigraph included a hydrograph soil lithology, gamma-ray data, and LIF response data (Kirkman, Adamski & Hawthorne 2013).

2.3.4. Discharge versus Drawdown Graphs

Discharge versus Drawdown Graphs are used in conjunction with LNAPL baildown tests to graphically confirm ideal unconfined LNAPL discharge conditions (Hawthorne & Kirkman 2011). The theory of aquifer slug testing is similar and applicable to the measurement of LNAPL transmissivity (T_n) via baildown testing. The baildown testing procedure consists of removing instantaneously the entire LNAPL volume from the well casing and filter pack, and gauging the fluid levels during recovery induced by the existed head differential (more details are presented later in section 2.4.3). Bouwer and Rice (Bouwer & Rice 1976) showed that under ideal conditions discharge during a slug test is directly proportional to drawdown. A Discharge versus Drawdown Graph is a scatter plot of LNAPL recharge (Q_n) into a well (recharge into a well includes any initial filter pack drainage and the discharge from the formation) during a baildown test versus the LNAPL drawdown (s_n). It is an important diagnostic tool used to determine Drawdown Adjustment to account for initial non-equilibrium between formation and well fluids. Typically LNAPL drawdown is calculated as either i) change in air/NAPL interface or ii) change in apparent NAPL thickness times the quantity one minus the LNAPL specific gravity (Kirkman 2013). Both methods assume unconfined conditions, but the b_n method also assumes a constant potentiometric surface (Charbeneau, Kirkman & Muthu 2012). Constant discharge periods indicate confined or perched LNAPL (API 2012).

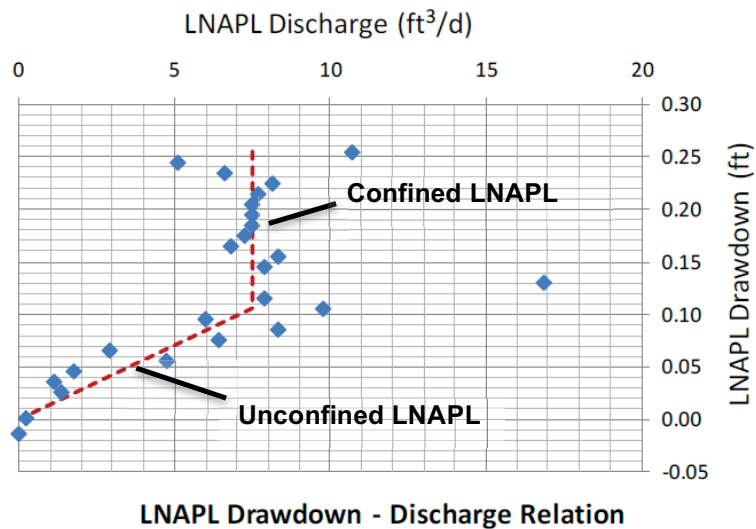


Figure 2. 16. Schematic showing the measured LNAPL discharge versus calculated LNAPL drawdown, during a bail-down test (API 2012).

2.3.5. Graphical Analysis of LNAPL Baildown Test Data

Baildown tests provide the data to construct discharge versus drawdown diagrams and are conducted to calculate LNAPL transmissivity (T_n) values from individual wells. Baildown test data is an additional method of assessing whether or not LNAPL is confined (Kirkman, Adamski & Hawthorne 2013). The fluid level elevations and the b_n during the baildown tests are plotted versus the corresponding discharge rate of LNAPL into the well. This is another way of illustrating discharge versus drawdown graphs using the fluid elevation during the NAPL recovery instead of drawdown. At the beginning of the recovery during the tests the thickness is lowest and the discharge is high. Moreover, the Z_{aw} and Z_{an} were both recovering because LNAPL and water were removed at the beginning of the test. When the potentiometric surface is equilibrated the LNAPL-water interface (Z_{nw}) would be expected to decrease (in elevation) and the air-LNAPL interface to increase as NAPL recharges into the tested well. LNAPL drawdown is calculated based on the change in the air-LNAPL interface (Huntley 2000) for unconfined conditions. Therefore, the rise in the air-LNAPL interface would be expected to result in a decrease in LNAPL drawdown and discharge. When modified for LNAPL baildown tests, the Bouwer-Rice slug test method implies that discharge should be directly related to drawdown, whether drawdown is based on the change in either LNAPL thickness or air-LNAPL interface (Bouwer & Rice 1976; Huntley 2000).

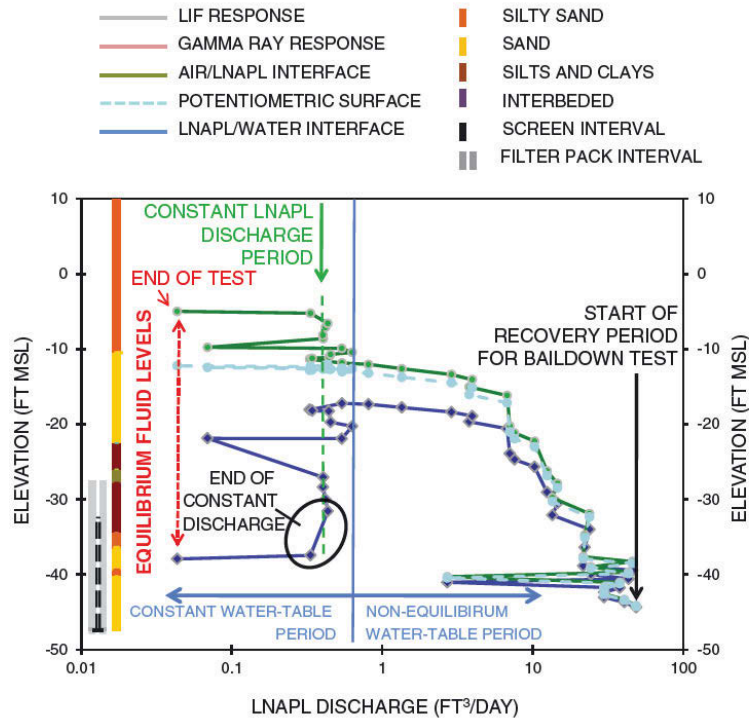


Figure 2. 17. Schematic showing baildown test results versus LNAPL discharge (Kirkman, Adamski & Hawthorne 2013).

2.3.6. Related Research Work

In 2013, Kahraman (Kahraman 2013) determined the LNAPL hydrogeologic conditions in a LNAPL contaminated site of South Texas. Stratigraphic descriptions, ROST (rapid optical screening tool), CPT (cone penetration testing) and DGPs were used for the evaluation of LNAPL conditions. The outcome of his research was that both confined and unconfined conditions were presented in the site of interest even though, in some well locations the collected data was insufficient for analysis. The issue in this work was that the R-squared values in the diagnostic gauge plots were low, indicating poorly correlated parameters and as a result more sufficient data for conclusions was required. Figure 2.18 illustrates unconfined LNAPL conditions in one of the testing wells during the aforementioned research. Hartsock (Hartsock 2014) enhanced the LNAPL hydrogeologic condition outcomes of his research using diagnostic gauge plots, hydrostratigraphs, stratigraphic descriptions and PID values together, however poor correlations between b_n and fluid levels were illustrated in the diagnostic gauge plots. The outcome of his study was that confined, unconfined and perched conditions were presented in the research site, even though in some well locations the DGPs and hydrostratigraphs were not consistent with the stratigraphic descriptions. DGPs and hydrostratigraphs in some cases were described as unreliable. Figure 2.19 depicts confined

LNAPL conditions in one of the research sites of his scientific work.

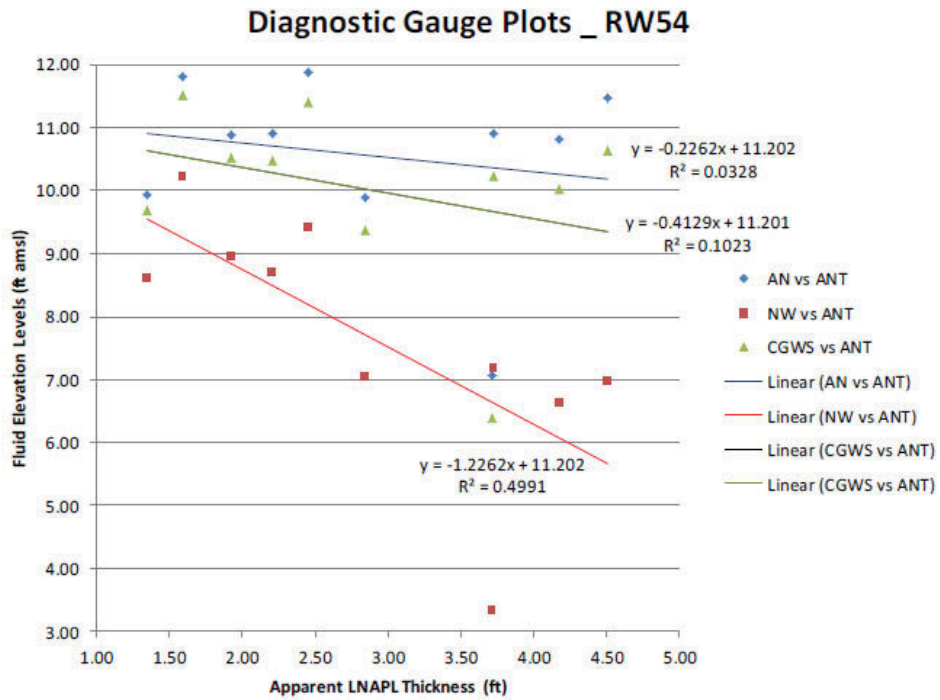


Figure 2. 18. Diagnostic gauge plot presenting LNAPL unconfined conditions in RW54 well (Kahraman 2013). Where AN: is the air-NAPL interface elevation, NW: is the NAPL-water elevation and CGWS: is the potentiometric surface elevation.

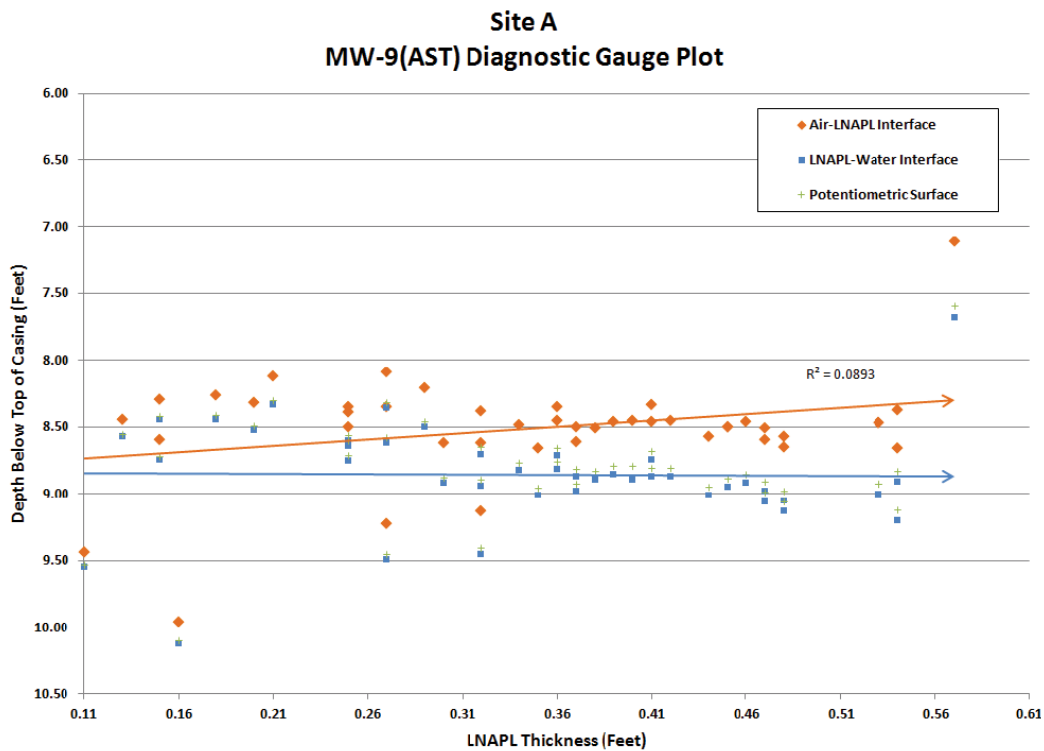


Figure 2. 19. Diagnostic gauge plot presenting LNAPL confined conditions (Hartssock 2014).

2.4. LNAPL Transmissivity

2.4.1. Introduction

LNAPL transmissivity (T_n) is a useful metric for predicting LNAPL recoverability. T_n represents the volume of LNAPL that flows through a unit width of a medium per unit time for a unit drawdown, in an analogous way to groundwater transmissivity (Kirkman 2013). T_n is useful for the estimation of LNAPL removal rates for different recovery techniques as well as for identifying trends in recoverability (Nagaiah, Law & Ueland 2015). In addition, it has been stated that T_n is a consistent metric across soil types, LNAPL types and LNAPL confined, unconfined and perched conditions. Moreover, T_n is applied in the design, implementation and evaluation of remediation systems as both a leading and lagging metric (Kirkman, 2013). A leading metric is an indicator of the potential future performance of a system. For instance, T_n is used to determine the start-up of a LNAPL mass recovery system or to gain insight into the expected LNAPL recovery rates. On the other hand, a lagging metric is an indicator of the past and current performance of a system. For instance, T_n is used to assess the progress of LNAPL mass recovery techniques and it is also used as an endpoint criterion to determine the shutdown of the system. A T_n value of 0.009 to 0.07 m²/day has been suggested as a lower limit value for hydraulic LNAPL recovery (ITRC 2009a), based on closed sites in United States. Further study and experience may refine this T_n range (ITRC 2009a). A solid knowledge of the site conditions and the underlying multiphase physics is essential to properly assess the system since T_n is a complex parameter. It depends on the applied methodology and test conditions, the water table fluctuations and fluid and geological properties (Beckett & Huntley 2015; Kirkman & Hawthorne 2014).

The NAPL relative permeability (conductivity) k_n is a function of NAPL saturation $k_n(S_n)$. The relative permeability of the hydrocarbon phase decreases exponentially as hydrocarbon saturation decreases (see Figure 2.9). T_n (Equation 15 and 16) is given by the summed product of NAPL conductivity, K_n and b_n (Figure 2.20). In a homogeneous setting, the predominant transmissive zone of the LNAPL body will be at the peak of the measured S_n in the aquifer (Figure 2.12), whereas in a heterogeneous subsurface, the more geologically permeable zones contribute more LNAPL especially if they contain also high S_n (CL:AIRE 2014). The estimation of LNAPL conductivity from baildown testing is quite uncertain without having knowledge about the LNAPL saturation (Beckett & Huntley 2015). Low saturation leads to a low value of relative permeability and LNAPL flows slowly to the well, being less mobile (Ahmed 2014). Furthermore, Ahmed (Ahmed 2014) concluded that more permeable soils and less viscous NAPLs affect positively the T_n values. The influence of the LNAPL density on T_n

is not significant compared to soil parameters (Awar 2008). Equations for the calculation of T_n are presented below.

$$T_n = \sum K_n \cdot b_n \text{ [Equation 15]}$$

$$T_n = \int_{Z_{nw}}^{Z_{an}} k_n \cdot k^* \cdot \frac{\rho_n \cdot g}{\mu_n} dz \text{ [Equation 16]}$$

where k_n is the NAPL relative permeability for the given conditions, k^* is the intrinsic permeability of the porous medium, ρ_n is the density of the hydrocarbon, g is the acceleration due to gravity, μ_n is the viscosity of the hydrocarbon, Z_{an} is the elevation of the oil/air interface and Z_{nw} is the elevation of the oil/water interface.

LNAPL transmissivity is a useful and directly proportional metric for interpreting the LNAPL recoverability and more accurate than the gauged LNAPL thickness in the well (ASTM 2013; Huntley 2000). T_n is suitable for estimating recovery rates from multiple hydraulic remediation technologies especially by pumping. The common methodologies for the estimation of T_n include i) short term testing methods such as LNAPL baildown testing and manual skimming testing and ii) long term methods such as LNAPL recovery system performance analysis and LNAPL tracer testing (ASTM 2013; Simon 2012).

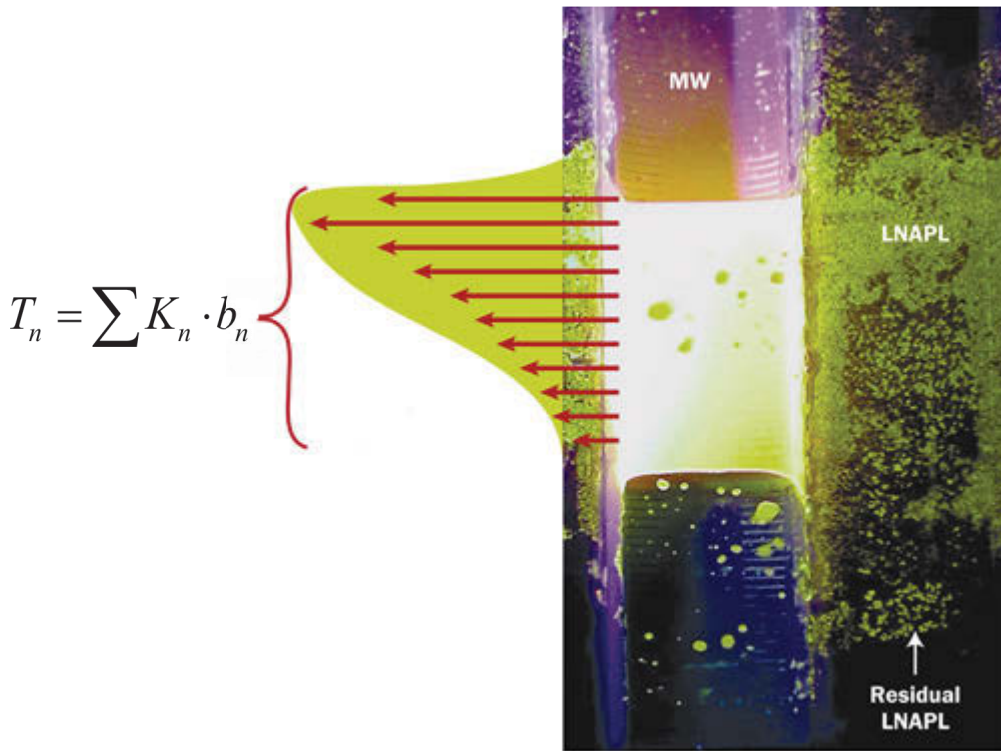


Figure 2. 20. Schematic diagram showing the relationship of LNAPL transmissivity to saturation (CL:AIRE 2014).

2.4.2. Complexity of LNAPL transmissivity

T_n has been proposed as an accurate remediation metric however, it can also be a quite complex parameter because is not constant and changes with time, test conditions and water table fluctuations. Moreover, it includes subsurface parameters responsible for this variability such as soil permeability, LNAPL saturation and other physical characteristics of the plume (density and viscosity) (Ahmed 2014; ASTM 2013). Beckett and Huntley (Beckett & Huntley 2015) referred to transmissivity's complexity mentioning how LNAPL saturations, water table fluctuations and boundary conditions of testing methods could affect the value and accuracy of transmissivity. The transience of T_n is another important parameter. T_n differs in time and spatially. In addition, sedimentation, biofouling and other physical factors affect the LNAPL flow due to PVC well screen (Hampton 2003).

Water table fluctuations are phenomena (Dobson, Schroth & Zeyer 2007) that affect LNAPL redistribution, its mobility and the partitioning into other phases (Chatzis, Morrow & Lim 1983; Dobson, Schroth & Zeyer 2007; Kuo et al. 2016; Steffy, Johnston & Barry 1998; Steffy, Johnston & Barry 1995; Teramoto & Chang 2017; Wang et al. 2014) and can affect the value of LNAPL transmissivity by orders of magnitude (Beckett & Huntley 2015). Two main mechanisms are behind this relationship between the potentiometric surface elevation and T_n .

Firstly, the induced vertical displacement of LNAPL mass to zones with different intrinsic permeability. Secondly, the generation of immobile LNAPL, in particular the entrapment of LNAPL when Z_{aw} increases (Chompusri, Rivett & Mackay 2002; Lenhard, Johnson & Parker 1993; Steffy, Johnston & Barry 1995). Hydrographs obtained from field sites usually show that Z_{aw} and T_n follow opposite trends (Beckett & Huntley, 2015), thus indicating the importance of entrapment phenomena in unconsolidated porous media. Recently, a model to predict subsurface LNAPL volumes and T_n after consideration of immobile LNAPL resulting from water table fluctuations in homogenous scenarios was presented (Lenhard, Rayner & Davis 2017).

Figure 2.21 shows a hydrograph showing that for higher water table elevations seasonally the LNAPL transmissivity follows the behavior of LNAPL thickness approaching the value zero. Actually, in periods of increased water table levels, the compression of the capillary fringe may reduce the apparent thickness (measured LNAPL thickness in a monitoring well) (Marinelli & Durnford 1996; Newell 1995). Sometimes a confined response can be depicted where the LNAPL thickness in well increases with water table rise and decreases as the water table falls (CL:AIRE 2014).

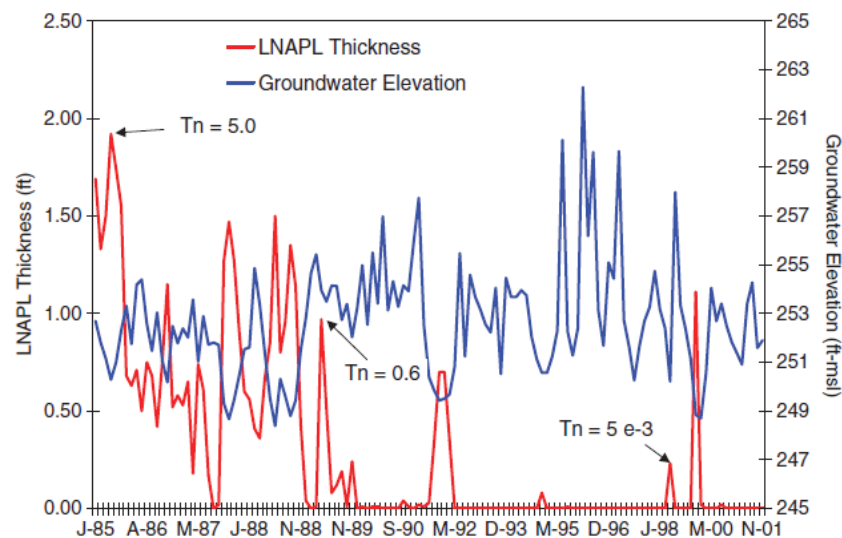


Figure 2. 21. Schematic showing groundwater elevation and LNAPL thickness along with T_n values (m^2/day) (Beckett & Huntley 2015).

2.4.3. LNAPL Transmissivity Test Methods

Regarding the existing field procedures for the estimation of T_n , short-term methods such as bail-down testing or manual skimming and long-term methods such as recovery system analysis or tracer tests have been proposed (ASTM 2013; Pennington et al. 2016; Sale et al. 2007). Short-term methods apply instantaneous stress to LNAPL product, while

long-term testing involves application of continuous stress to the LNAPL. Tracer testing measures average T_n value over a long period of testing thereby incorporating the impact of water table fluctuations while, bail-down tests represent T_n values over the short term in conditions local to the testing well (Pennington et al. 2016). Baildown testing requires less resources than mass recovery applications and it has also been used as a way to determine LNAPL thickness in the formation (Aral & Liao 2000) as well as van Genuchten capillary parameters and hydraulic conductivities by using numerical models (Zhu, Lundy & Zimmerman 1993). However, the estimated T_n values obtained after applying an instantaneous stress to the LNAPL product may not compare identically with the results from recovery systems because of the different mathematical representations of the problem and the scale of evaluation dissimilarities (because of the discrepancy between the radius of capture of both methods). The radius of capture depends on the geological material being larger for coarser sediment textures (Beckett & Huntley 1998). In the case of groundwater systems, it has been documented that borehole effects and other artifacts may have an impact as well (Butler & Healey 1998). The importance of these dissimilarities is also related to the LNAPL distribution and geological variability within the radius of capture of each method. In spite of these differences, similar increasing and decreasing trends can be observed in both methods (ASTM 2013; Nagaiah, Law & Ueland 2015). T_n differences within one order of magnitude between bail-down and tracer testing have been documented. These differences could have been caused by slow NAPL recovery and groundwater fluctuations (Pennington et al. 2016).

Baildown testing has been proposed as a field method for the estimation of LNAPL transmissivity (Hampton 2003) at wells exhibiting sufficient LNAPL thickness (> 15.2 cm) (Kirkman 2013; Kolhatkar et al. 1999) and cannot be used for the calculation of the formation hydrocarbon thickness (Aral & Liao 2000; Huntley 2000). The testing procedure consists of removing the entire LNAPL volume from the well casing (via bailers or peristaltic pumps) and filter pack, and gauging the fluid levels during recovery induced by the existed head differential.

Manual LNAPL skimming test is another short-term testing method for T_n calculation. Manual skimming tests are useful for wells exhibiting LNAPL thickness less than 15.2 cm and their advantage is that they have more accuracy of recovery volumes estimates representing larger areas of the formation as they run for longer time periods. Long-term testing involves application of continuous stress to the product via recovery methods or tracer tests. LNAPL fluxes and T_n estimates can be derived through tracer testing under conditions of natural or imposed gradient. Hydrophobic fluorescent tracers are used. Measurements of tracer concentration through time are taken via a spectrometer. The test duration of natural gradient tests is weeks or months and the duration of imposed gradient tests is hours to days (ASTM 2013). The ASTM guide E2856-13 (ASTM 2013) provides analytical equations for T_n

calculation using LNAPL recovery data from i) skimming, ii) vacuum enhanced skimming, iii) total fluids pumping, single or dual pump and iv) multiphase fluid extraction (Charbeneau 2007b; Lundy & Zimmerman 1996).

2.4.4. LNAPL Transmissivity Analysis

The obtained data during LNAPL recovery is used for the calculation of LNAPL transmissivity by using analytical solutions (Bouwer & Rice 1976; Cooper, Bredehoeft & Papadopoulos 1967; Skibitzke 1958). Bouwer-Rice method can be used for constant potentiometric surface (Z_{aw}) conditions whereas Cooper method for varying Z_{aw} (Huntley 2000). Two methods (Huntley 2000; Lundy & Zimmerman 1996) were developed to adapt the Bouwer and Rice approach for slug test analysis under unconfined conditions (Bouwer & Rice 1976). It should be taken into account that some of the theoretical assumptions in the Bouwer and Rice approach are not necessarily met in the case of multiphase systems and T_n analysis (Batu 2012). However, several authors have defended this methodology claiming that is robust enough under field conditions (Charbeneau, Kirkman & Adamski 2013). The two aforementioned methods assume radial flow towards the well (Bouwer & Rice 1976; Charbeneau et al. 2000) that could be affected by complex and anisotropic NAPL distributions. They also assume a constant change in LNAPL drawdown to change of in-well LNAPL thickness, requiring a constant potentiometric surface or depth to the water-NAPL interface. To overcome this limitation, an adapted methodology that reduces the errors related to variations in the potentiometric surface was introduced (Kirkman 2013), resulting in the Bouwer and Rice method being applicable to broader conditions of bail-down tests. However, in the case of groundwater slug tests, it has been seen that the Bouwer and Rice solution may introduce significant errors mainly derived of the presence of a low-permeability skin or anisotropic conditions (Hyder & Butler 1995).

A relatively good correlation between the modified Bouwer and Rice approaches (Huntley 2000; Kirkman 2013), the modified Jacob and Lohman solution (Huntley 2000) and the modified Cooper solution (Beckett & Lyverse 2002) has been found at the field scale under unconfined conditions (Palmier, Dodt & Atteia 2016). These methods also presented a good correlation with NAPL hydraulic conductivity estimations from the Parker and Lenhard constitutive model (Parker, Lenhard & Kuppasamy 1987) at the laboratory scale (Palmier, Cazals & Atteia 2017).

A detailed understanding of LNAPL hydrogeological conditions is crucial for the calculation of LNAPL drawdown during the baildown testing because unconfined, confined and perched LNAPL require different approach regarding the drawdown calculation (Kirkman, Adamski & Hawthorne 2013).

The Bouwer and Rice (Bouwer & Rice 1976) method for slug test analysis combines a simple representation for flow to the well from the Thiem equation and continuity of fluids within the well. The flow equation is:

$$Q_n = \frac{2\pi T_n s_n}{\ln(R/r_w)} \text{ [Equation 17]}$$

With the effective well radius determined and with use of the Kirkman J-ratio, the generalized Bouwer and Rice formula for determining the LNAPL transmissivity ($T_{n,BD}$) takes the form (API 2012; Kirkman 2013):

$$T_{n,BD} = \frac{r_e^2 \ln(R/r_w) \ln(s_n(0)/s_n(t))}{2(-J)t} \text{ [Equation 18]}$$

Where: Q_n is the LNAPL discharge, $T_{n,BD}$ is the LNAPL transmissivity via bail-down testing, R is the radius of capture, r_w is the well borehole radius, r_e is the effective well radius, s_n is the LNAPL drawdown, J is the Kirkman J-ratio and t is the time.

2.4.5. Related research work

LNAPL baildown and manual skimming testing reflect conditions near the well representing a limited radius of capture. T_n values from short-term testing may not compare well with estimated T_n values from recovery based data even though, increasing and decreasing trends in T_n can be seen in both short and long term testing procedures (ASTM 2013). Nagaiah et al (Nagaiah, Law & Ueland 2015) compared short-term baildown tests with long-term skimming trials in two areas with initial T_n values 2.74 and 2.52 m²/day, respectively. LNAPL bearing zones were in sand and gravel lithology (Area 2 had some silt) under unconfined conditions. The results of their research are presented in Figures 2.22 and 2.23.

The outcome of this research was that short-term T_n obtained by bail-down testing agreed well with T_n values of long-term skimming, both depicting decreasing trends with slope differences. As it can be inferred also from these graphs, Area 2 which contains also some silty material, presented lower slope values in LNAPL transmissivity equations, in contrast with Area 1 where only sand and gravels exist. Area 1 presented a greater decrease in T_n values, as well higher T_n values compared to Area 2.

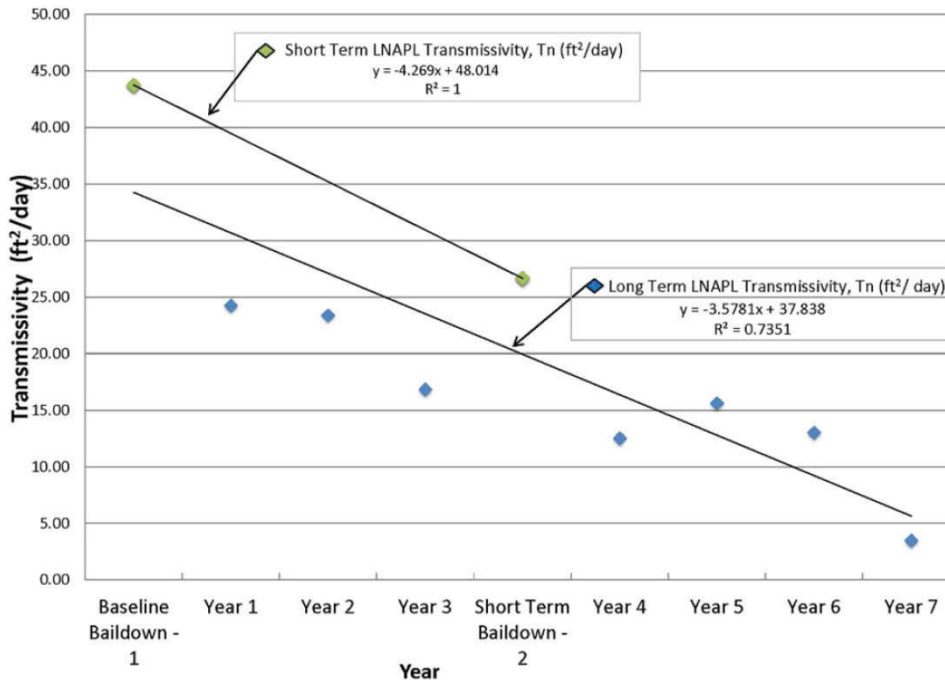


Figure 2. 22. Schematic showing T_n values during short-term baildown and long-term skimming testing in Area 1 (Nagaiah, Law & Ueland 2015).

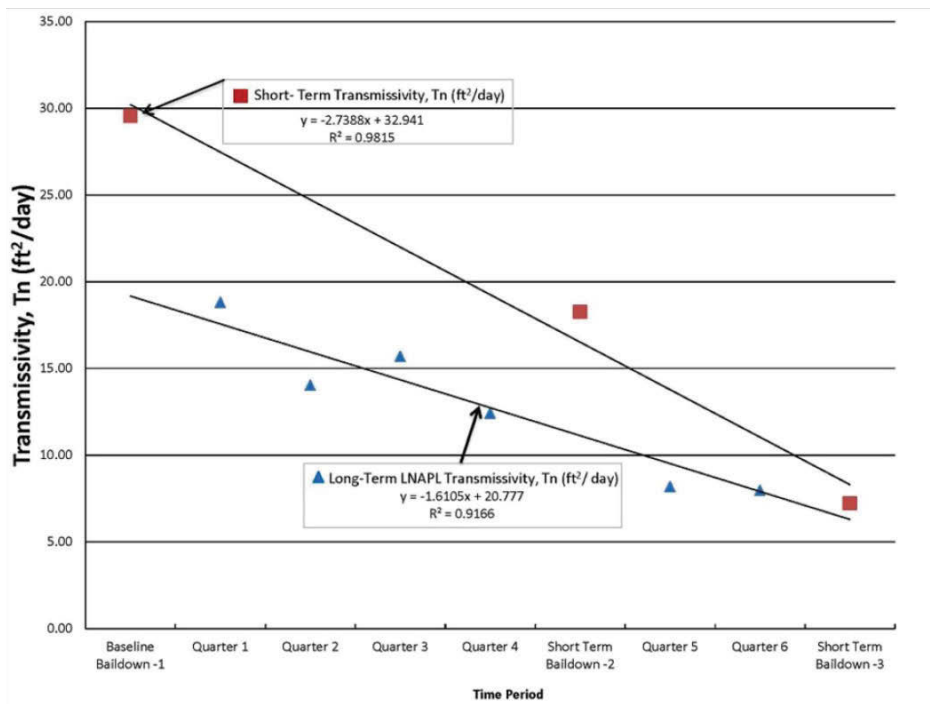


Figure 2. 23. Schematic showing T_n values during short-term baildown and long-term skimming testing in Area 2 (Nagaiah, Law & Ueland 2015).

In 2016, Pennington et al (Pennington et al. 2016) compared T_n values obtained by tracer testing, bail-down testing and recovery system applications in low permeability soils contaminated by heavy range LNAPLs. The overall outcome was that T_n values from tracer testing were comparable with the estimations from the other methods, usually within one order of magnitude. Differences were more obvious at areas where ambient water table fluctuations and slow NAPL recovery affected negatively the accuracy of the methods.

Figure 2.24 (Palmier, Dodt & Atteia 2016) depicts T_n values before (t_0), six months after (t_1), and 18 months (t_2) after start of remediation. The contaminant was degraded viscous lubricant oil (viscosity: 90-115 cP) and the aquifer material was sand and coarse sands with some interbedded silt layers. Water enhanced skimming was applied as remediation approach. Groundwater was unconfined with a seasonal fluctuation of 1.5 m.

The results refer to the whole contaminated site and they revealed that, no correlation between oil thickness and T_n exists at the research site. T_n was more related to the texture of the material than the apparent thickness. In addition, it was noted a decrease in both apparent thickness and T_n 18 months after start of remediation. T_n value decreased by 52%. Interestingly, T_n increased slightly during the six first months of extraction (13%), but then reduced significantly (-45%). It was concluded that the remediation system efficiently decreased the oil saturation by the decrease of the apparent thickness and T_n for an equivalent total Z_{aw} .

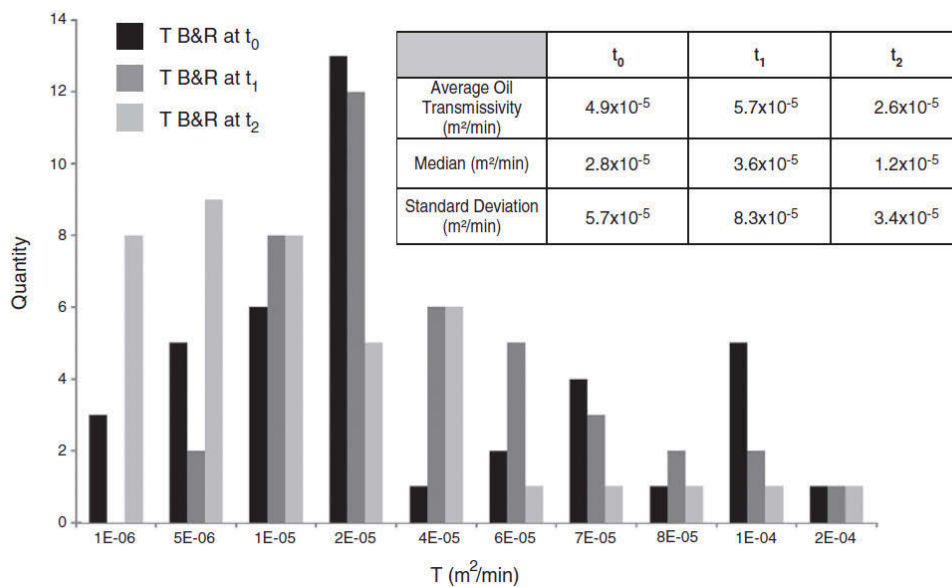


Figure 2. 24. Illustration showing T_n values and statistics for t_0 , t_1 and t_2 (Palmier, Dodt & Atteia 2016).

Discussion

The two of the three presented research works (Nagaiah, Law & Ueland 2015; Palmier, Dodt & Atteia 2016) were conducted mainly in sandy materials and none of them took into account the effect of water table fluctuations. The first related research (Nagaiah, Law & Ueland 2015) presents limited T_n data obtained by bail-down tests, thus conclusions were based on a few points, taking into consideration the long period of remediation efforts. Palmier et al (Palmier, Dodt & Atteia 2016) concluded that water-enhanced skimming was the reason that T_n reduced during the research period, however a T_n decrease may also reflect natural losses, mass migration within the NAPL body and also hysteresis in the relationship between capillary pressure and saturation. Furthermore, information about spatial NAPL distribution could elucidate the outcomes of these works. Finally, Pennington et al (Pennington et al. 2016) conducted their research in fine grained settings, acknowledging the importance of groundwater fluctuations. However, they have presented cases of recovery tests that took place 6 weeks after the baildown testing, thus the comparison of T_n values between short and long term testing includes possibly some errors, as 6 weeks is a long time period where T_n may have been changed even under natural conditions.

2.5. In-Situ LNAPL Remediation Technologies

Removal of an entire LNAPL mass from the subsurface is rarely possible. Persisting with ongoing remediation with diminishing efficiency is increasingly questioned because of practicability and sustainability issues. The primary challenge is to determine the extent of LNAPL mass removal that will match goals for reduction in risk factors associated with vapour inhalation, groundwater ingestion and irrigation, ecosystem impact, and other concerns over the mobility and presence of the LNAPL. Different regulatory policy responses have been demonstrated due to the difficulty of remediating LNAPLs such as: technical impracticability, clean up to the extent practicable (EPA Victoria 2002) and remediation to the extent necessary (EPA SA 2009). These include technical, logistical, financial and sustainability (CL:AIRE 2010) considerations.

To address technical issues, research has focused on remediation techniques targeting LNAPL in the subsurface - for instance, US National Research Council (NRC 1997), US EPA (US EPA 2005), Interstate Technology & Regulatory Council (ITRC 2009a), (Ostrom et al. 2005), TCEQ (TCEQ 2008). However, the endpoints achievable through remediation have been difficult to quantify given the wide range of subsurface environments encountered as well as the new and continual development of remediation strategies. Thus, there is a need to

expand the field evaluation of LNAPL remediation technologies to a wider range of heterogeneous geologies, adapting the complexity of LNAPL and its interactions with the subsurface.

The greatest range of LNAPL remediation options is available for sandy media (Johnston 2010). The existing literature about LNAPL remediation through mass recovery systems in fine grained soils is limited, even though valuable information can be found in the literature (Abdul 1992; Adamski et al. 2005; Andrews 2000; Baker & Bierschenk 1995; Beckett & Huntley 1998; Delin & Herkelrath 2014; Gabr, Sharmin & Quaranta 2013; Gidarakos & Aivalioti 2007; Heffron, Blanchard & Dogrul 2003; Kirshner, Pressly & Roth 1996; Kittel, R.E. Hinchee, et al. 1994; Lesson et al. 1997; Lundy, Li & Katyal 2002; Peargin & Wickland 1999; Ponsin et al. 2015; Prince-Larson & Markley 1994; Purtill 1998; USEPA 2005; Westerby 1992). Common performance metrics that were used in the presented researches include: NAPL drawdown in the pumping well, water levels in observation wells, water pumping rate, soil gas extraction and injection flow rates, volatile hydrocarbon concentrations, oxygen and carbon dioxide concentration in soil gas and induced pressure influence on all wells. It should be mentioned also that unsuccessful remediation efforts may occur due to weak hydraulic connection between the LNAPL pool and the saturated zone (Kramer et al. 1997; Zilliox, Razakarisoa & Rinck 1992).

2.5.1. Classification of in-situ LNAPL remedial techniques

There are many applicable LNAPL remediation techniques, each with different applicability and capability (Gavrilesco 2006; ITRC 2009a; Khan, Husain & Hejazi 2004). Remediation technologies may focus on recovering mobile LNAPL, treating residual LNAPL, managing dissolved-phase and/or vapour-phase plumes (CL:AIRE 2014). It is crucial that, the selected technology should align with the particular LNAPL remedial objective and LNAPL remediation goal. Figure 2.25 shows the classification of common applied in-situ LNAPL remediation technologies (ITRC 2009a) with purpose to provide context to the basic processes through which the LNAPL remediation is achieved. The remedial techniques are assigned to a technology group based on the main mechanism by which they address LNAPL. The divided groups are: i) LNAPL mass recovery technology (LNAPL recovery via physical removal or hydraulic recovery), ii) LNAPL mass-control technology (stabilization of migrating LNAPL by reducing the LNAPL saturation) and iii) LNAPL phase change technology (LNAPL partition to other phases).

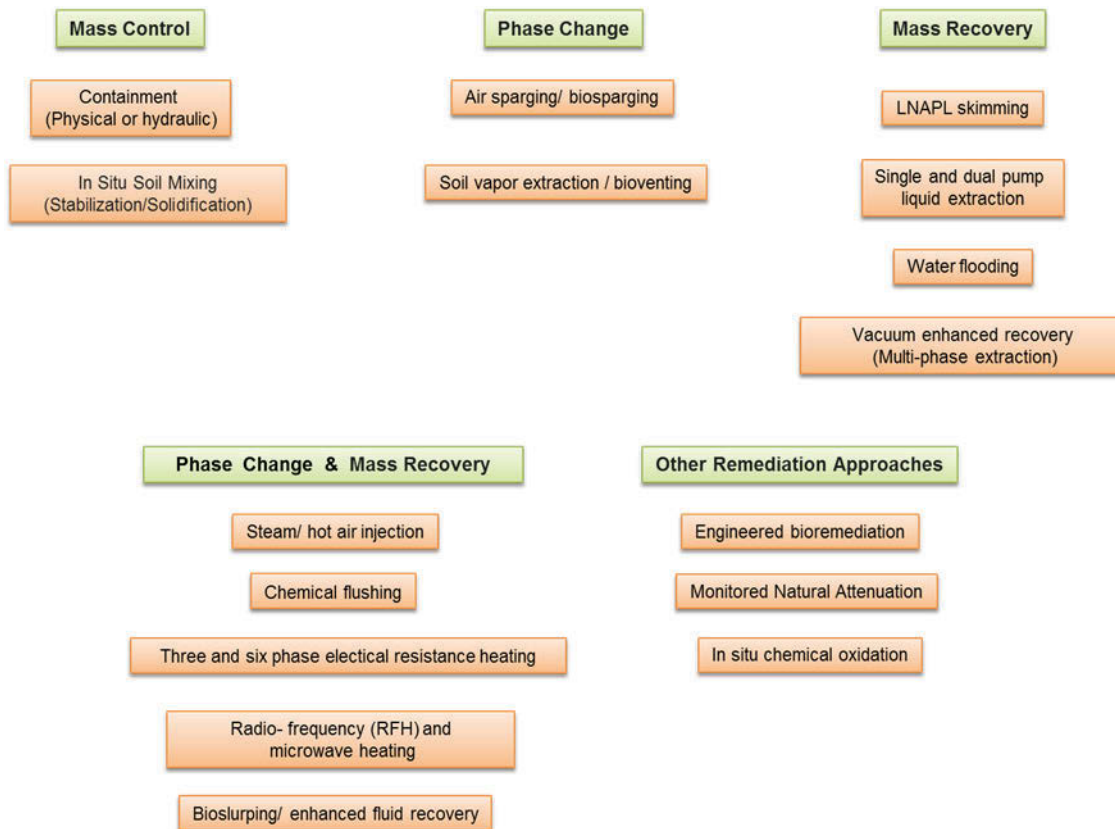


Figure 2. 25. Overview of common applied in-situ LNAPL remediation technologies (after Johnston, 2010).

2.5.2. LNAPL mass recovery technologies

The LNAPL mass recovery group includes remediation technologies such as LNAPL skimming, single/dual pump liquid extraction, water flooding and vacuum-enhanced recovery. The LNAPL recovery is achieved through physical removal or hydraulic recovery. As demonstrated by Huntley and Beckett (Beckett & Huntley 2015) hydraulic recovery is one of the least effective strategies for LNAPL remediation, with limited exceptions. In 2002 (Huntley & Beckett 2002), the same authors presented an analysis of the effect of source LNAPL mass reduction via hydraulic recovery on risk from dissolved constituents. Their outcome was that the initial concentrations and the immediate risk were not reduced even though, the risk longevity was reduced. This research was based on homogeneous aquifers not taking into consideration heterogeneities that affect the LNAPL saturation and ground water flow velocity.

2.5.2.1. LNAPL Skimming

Skimming is a mass recovery technology which uses a single pump or hydrophobic belt to remove LNAPL from a well under natural pressure gradients (EPA 1996). More specifically, the intake to the pump floats at the LNAPL-water interface and penetrates via a hydrophobic filter located just above the interface. The recovery of the free product takes place through a pneumatic collection and discharge pump connected to the intake. Skimmer pumps recover free LNAPL that drains into the well. This remediation method is applicable to all LNAPL types, even though lower viscosity LNAPL is much more recoverable than high viscosity LNAPL (ITRC 2009a).

Skimming may be applicable to any hydrogeological setting that allows free drainage of LNAPL into a well. Thus, this technology is not applicable to LNAPL in the unsaturated zone. Highly permeable aquifers present higher LNAPL recovery and saturation reduction, although, skimmer pumps are also applied to situations where the induced LNAPL inflow to the well is slow and recovery is expected over a reasonably long time period (Charbeneau et al. 2000; EPA 1996; Johnston 2010). In general, skimming is a relatively low intensity technology and can be a slow recovery process.

In 1994, Prince Larson and Markley (Prince-Larson & Markley 1994) evaluated four methods for recovering LNAPL from groundwater at a natural gas processing facility in Texas, without pumping groundwater to the surface. Alternative methods of LNAPL recovery, using a variety of skimming pumps, included: i) LNAPL recovery from large-diameter wells, ii) LNAPL recovery from trenches, iii) LNAPL recovery from small-diameter wells and iv) vacuum-enhanced recovery of LNAPL while skimming with a belt skimmer. The perching layer was dense solid limestone. Their outcome was that, for the recovery of LNAPL only, the belt skimmer is recommended when the LNAPL thickness is not great (less than 1.5 feet) and the formation has low productivity.

2.5.2.2. Single and dual pump liquid extraction

Single or total liquids and dual-pump systems use the depression of the water table for the enhancement of the lateral movement during the recovery of LNAPL from a well. The single pump system is set in a well below the water table elevation so as free LNAPL and water can enter the well and be recovered by the pump. Single pump systems utilize a single pump. The dual-pump systems use two pumps in one well, that is a water-only pump established low in the well to recover groundwater at the same time that a skimmer or other

type of hydrocarbon pump is set above the water pump only for the recovery of LNAPL (Charbeneau & Chiang 1995; Charbeneau et al. 2000; Johnston 2010).

T_n and oil recovery increases during pumping processes with significant drawdown (Beckett & Huntley 2015). Single and dual pump systems are applicable to all LNAPL types however, lower-viscosity LNAPL is much more recoverable than high-viscosity LNAPL (ITRC 2009a). This remediation technology targets LNAPL from the capillary fringe/near water table zone and is designed to transform mobile LNAPL into free LNAPL. These systems are most appropriately applied to hydrogeological settings where the hydraulic conductivity is not too high so as to avoid the treatment of large volumes of water. Although in high permeability settings drawdowns may be small, the relative permeability of the LNAPL would be high allowing LNAPL recovery rates to be proportionately raised. However, situations where the LNAPL-contaminated interval has lower permeability than the underlying aquifer should be avoided (Johnston 2010). According to USEPA's report (USEPA 2005), dual-pump recovery seems to be continually effective at recovering LNAPL from sand, but it is not expected to be a technology for LNAPL recovery in silts and clays.

Dual pump liquid extraction field based applications have been demonstrated successfully in the literature (Delin & Herkelrath 2014; Koll, Palmerton & Kunzel 1994). USEPA published a cost and performance report for LNAPL characterization and remediation (USEPA 2005). The report included a case study with the recovery summary of light non-aqueous phase liquid (LNAPL) at two locations at the BP Products of North America, Inc. Former Amoco Refinery in Sugar Creek, Missouri. The cost and performance were evaluated for two remediation systems: high-vacuum multi-phase extraction and dual-pump LNAPL and groundwater recovery. As regards the dual-pump system, dual-pump recovery has been applied at the lower refinery area consisted of silty to fine sand. The outcomes from this study were that LNAPL recovery is more effective at higher-permeability sands than low-permeability silts and clays. Although dual-pump recovery seems to be continually effective at recovering LNAPL from sand, it is not expected to be a suitable technology for LNAPL recovery in silts and clays. In 2014, a remediation effort was published about the removal of crude-oil via dual pump recovery (Delin & Herkelrath 2014). Although the dual pump recovery system decreased oil thicknesses in the vicinity of the remediation wells, average oil thicknesses were unaffected. The existence of a secondary plume was indicated, thus the recovery at this contaminated site was shown to be quite challenging.

2.5.2.3. Vacuum enhanced recovery

During vacuum-enhanced recovery a partial vacuum is applied to a recovery sealed well. The partial vacuum is applied in either of two ways: i) a partial vacuum is created by an air suction pump connected to the sealed well ii) a connected drop tube is used to an air suction pump with the end placed such that the liquids in the sealed well are drawn up by the air flow and recovered. This application is known as slurping or bioslurping. The pressure gradients are also transferred to the LNAPL, enhancing its movement towards the recovery well. Also, a greater fraction of the LNAPL may transform free to drain into the well by reducing air pressure in the aquifer. Moreover, the elevation of the LNAPL may be raised and water tables causing LNAPL and water to move upwards in the profile (Johnston 2010). Vacuum-enhanced recovery is normally used with skimmer pumps or single- pump systems (Charbeneau et al. 2000).

Vacuum-enhanced recovery systems could be applicable to all those hydrogeological settings suitable for skimmer well, single- and dual-pump systems even though, they have further advantages in lower permeability settings because of the development of large air pressure gradients. The main target of this technique is the LNAPL from the capillary fringe/near water table zone as well as the vadose zone. In general, the processes of this technology are designed to transform mobile LNAPL into free LNAPL by lowering air pressures as well as water pressures (Johnston 2010). Vacuum-enhanced NAPL recovery, sometimes referred to as dual-phase extraction/ Multi-phase extraction (MPE) or bioslurping (Baker & Bierschenk 1995). According to USACE (USACE 1999), the terminology presented by EPA (USEPA 1997) distinguishes between dual-phase and two-phase extraction technologies.

The remediation technology of vacuum enhanced recovery for the removal of LNAPL has been used successfully so far in many case studies (Air Force Center for Environmental Excellence 2000; Andrews 2000; Newell 1995; Purtil 1998; U.S. Department of Energy 2006, 2007). In 2002, Lundy et al. (Lundy, Li & Katyal 2002), evaluated the use of vacuum to skimming wells at a 10-acre jet fuel free product plume at the Holloman Air Force Base in New Mexico. They concluded that vacuum-enhancement seems to accelerate the rate of recovery and moves towards the end point faster, but regarding the long-term it will recover a smaller volume of free-phase product because more of the free phase is transferred to a residual phase. The vacuum-enhanced skimming technology was used also in a pilot scale study by Heffron et al. (Heffron, Blanchard & Dogrul 2003). The results of the pilot test showed that skimming would be the best available technology for the full-scale remediation of the site. In favour of this conclusion was the silt layer between the LNAPL and the ground surface as well as the volatile nature of the LNAPL.

2.5.2.4. LNAPL recovery

Recovery potential for mobile LNAPL is controlled by factors such as LNAPL viscosity, density and relative permeability (Testa & Paczkowski 1989). Liquids trapped by capillary forces are not recoverable using conventional well systems. High LNAPL viscosity, high residual water saturation, and low permeability reduce LNAPL recovery rates (Sale et al. 2007). In a two-phase system the LNAPL flux is given by a modified form of Darcy's law (Huntley 2000):

$$q = k_n k^* \frac{\rho_n g}{\mu_n} i \quad [\text{Equation 19}]$$

where k_n is the NAPL relative permeability, k^* is the intrinsic permeability of the porous medium, ρ_n is the density of the hydrocarbon, g is the acceleration due to gravity, μ_n is the viscosity of the hydrocarbon and i is the hydraulic gradient.

Charbeneau with other co-authors have developed LNAPL recovery rate equations for: (i) skimming (Johns et al. 2003), (ii) water-enhanced skimming (Charbeneau 2007b) and (iii) vacuum-enhanced skimming (Charbeneau 2007b) applications. The development of these equations is presented in detail in the aforementioned references. These equations are an extension of the previous set of equations on NAPL saturation, relative permeability and transmissivity presented in sections 2.1.2, 2.4.1 and 2.4.4. More specifically, the recovery rate equation for a skimmer well in a small radius of capture is:

$$Q_{n,skimmer} = \frac{\pi(1-\rho_r)T_n(b_n)}{\ln(R_c / R_w)} \quad [\text{Equation 20}]$$

where ρ_r is the LNAPL/water density ratio, T_n is the LNAPL transmissivity, b_n is the LNAPL-layer thickness, R_c is the radius of capture of the skimmer well, and R_w is the radius of the skimmer well.

Under water table depression where the LNAPL recovery rate is determined by water production the LNAPL recovery rate can be estimated by:

$$Q_{n,WER} = \frac{T_n(b_n)}{\rho_r T_w(b_w)} Q_w \quad [\text{Equation 21}]$$

where Q_w is the water pumping rate, b_w is the vertical depth of groundwater beneath the water table, and T_w is the transmissivity of the aquifer over the screen length b_w .

The air and LNAPL discharge relationship under vacuum-enhanced recovery (VER) system is described by the equation:

$$Q_{n,VER} = \frac{\mu_{ar} T_n(b_n)}{\rho_r k_{ra} T_w(b_a)} Q_a \quad [\text{Equation 22}]$$

Where Q_a is the volumetric air discharge, μ_{ar} is the air-to-water dynamic viscosity ratio, \bar{k}_{ra} is the average relative permeability of air in the vadose zone, and T_w is the transmissivity of the unsaturated zone over screen length b_a above the water table.

2.5.3. Remediation performance of mass recovery techniques

There many gaps in the understanding of LNAPL remediation performance in fine grained systems with a lack of case studies documenting the performance of LNAPL mass recovery systems especially in complicated hydrogeological systems (Johnston 2010). In developing a LNAPL remedial strategy, the application of multiple technologies either as a system or as a sequentially applied treatment train should be considered. It is likely that several remediation techniques, used in series and/or parallel applications, will be required for maximum contaminant removal. This collaborative effort may be referred to as a treatment train approach. Optimum sequencing of remedial actions in a treatment train will be site specific and will depend on such factors as LNAPL migration rates and distribution, remedial objectives, and applicable remedial technologies. Removal of LNAPL to the extent practicable will be an objective during early stages of remediation at many sites. A deep understanding of the hydrogeological and geochemical characteristics of the site is an essential requirement for a successful treatment. Detailed site characterization efforts and an in-depth understanding of the processes which affect the transport and fate of LNAPLs in the subsurface will permit the optimization of all possible remedial actions, maximize predictability of remediation effectiveness, minimize remediation costs, and make cost estimates more reliable.

Simulation results of an analytical model (Jeong & Charbeneau 2014) for predicting LNAPL distribution and recovery from multi-layered soils showed that LNAPL distribution and recovery are highly affected by soil properties. Sandy media demonstrate high NAPL mobility and recoverability in contrast with fine grained systems where even at high saturations the NAPL mobility is low (Beckett & Huntley 1998; Jeong & Charbeneau 2014). Furthermore, heterogeneity and anisotropy of intrinsic permeability have a negative impact on LNAPL recovery (Kaluarachchi 1996). The year 2000 and 2001 Johnston (Johnston et al. 2005; Johnston, Fisher & Rayner 2002; Johnston et al. 2002; Johnston 2010) conducted pilot tests of mass LNAPL recovery technologies (skimming, vacuum enhanced skimming, slurping, vacuum enhanced recovery plus drawdown) under different water table elevations in the same sandy contaminated site (weathered gasoline/kerosene). The NAPL recovery rates in 2001 were higher compared to 2000 because of the lower water table conditions resulting higher

mobility. The vacuum-enhanced recovery plus drawdown gave the greatest NAPL recovery rates (4-16 times skimming alone) while vacuum-enhanced recovery on its own produced as much as 2.5-10 times the rate for skimming. Moreover, the rates for vacuum-enhanced recovery were better than those for drawdown on its own which also trapped significant residual NAPL below the water table. Figure 2.26 shows the measured LNAPL recovery rate (Q_n) over the course trial (year 2001). Similar results showed by Hernandez-Espriu et al (Hernández-Espriú et al. 2012) in a low conductivity volcanic aquifer using the API/Charbeneau analytical model. Bioslurping, multi-phase and dual-phase extraction found to be more efficient in NAPL recovery compared to skimming process. Lundy et al, (Lundy, Li & Katyal 2002) concluded that vacuum increased skimming rates, however, more free product become entrapped and the higher recovery rates are not expected to be sustainable for the long-term. The research was conducted in a fine grained system and the outcome was that vacuum-enhancement appears to speed up the NAPL recovery rate and moves one towards the end point faster, but over the long-term it will recover a smaller NAPL volume because more of the free phase is becoming entrapped.

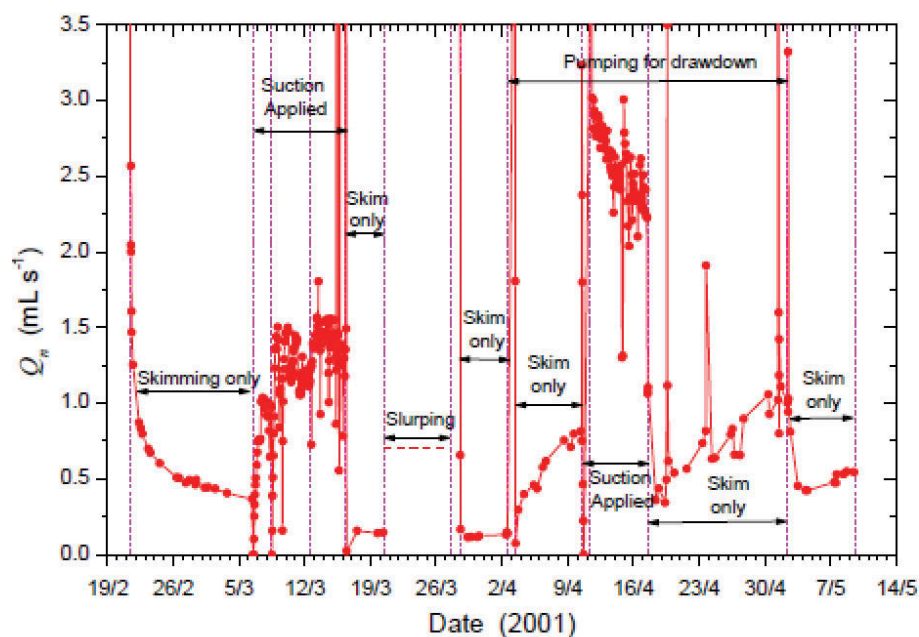


Figure 2. 26. Measured NAPL recovery rate (Q_n) over the course of the sequential recovery trial in 2001 (Johnston et al. 2002).

3. Materials and Methods

The objective of this thesis is the assessment of LNAPL distribution and mobility in heterogeneous aquifers under water table fluctuations. Consequently, a field site consisting of a multi-layered aquifer with 2-3 m of seasonal water table fluctuations was chosen as the area of study. The research focused only on this site for clarity purposes and because of time and resources limitations. The aquifer is unconsolidated and contaminated with gasoline. Such frequently found characteristics make easier to extrapolate the obtained results and conclusions to other sites and though enhance the significance of this work.

The experiments took place in several areas to account for different LNAPL distributions and stratigraphic profiles. High resolution characterisation methods, core descriptions, chemical analyses and analytical simulations were applied to define the subsurface conditions at each area. Thus, multiple lines of evidence were used when possible to reduce the existing uncertainties.

Because of the multilayered nature of the site, it was also necessary to assess the LNAPL confinement conditions. This is a crucial step to choose an appropriate method to estimate LNAPL mobility. Diagnostic gauge plots, hydrostratigraphs and other lines of evidence were critically applied for this purpose.

The contribution value of this research to the field of study is enhanced by assessing LNAPL mobility in terms of LNAPL transmissivity (T_n), since T_n is being increasingly adopted as a remediation metric by many researchers, regulatory agencies and other professionals. T_n was evaluated using bail-down testing and mass recovery methods. Bail-down testing is the most commonly used methodology because of the low resources required and it is less time consuming than others. Bail-down testing was applied before, during and after mass recovery techniques (skimming, water-enhanced skimming, vacuum-enhanced skimming and water-and vacuum-enhanced skimming) to assess the effects of induced hydraulic conditions and be able to compare different methodologies. The experiments were conducted under constant and variable water table conditions to incorporate the effects of water table fluctuations.

A more detailed description of the aforementioned methods is presented in the following sections.

3.1. Monitoring installations

In the contaminated research site 85 monitoring points have been installed since 2014. These installations include: monitoring wells (codes: MB and MP; diameter: 50 mm), production wells (code: PB; diameter: 100 mm), multi-levels (code: ML; slotted intervals every meter, 9 slotted intervals at each well location) and vapour points (usually in pairs, one deep point at 1 m and one shallow point at 0.5 m). All the wells were screened over the entire mobile interval of LNAPL during the experimental periods. The well screens along with fluid elevations during bail-down testing are presented in section 3.2 in Appendix J. The 100 mm production wells were used as remediation wells during the remedial research trial. More details about the installation of the wells can be seen in the Table A.1, Appendix A.

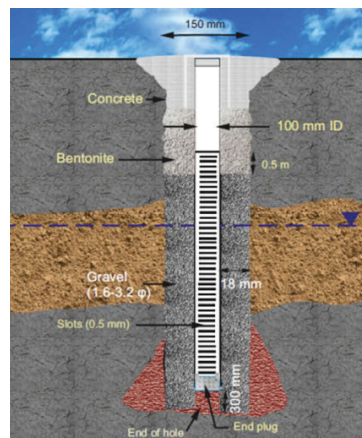


Figure 3. 1. Schematic diagram of the construction of NAPL recovery well PB (100 mm), (not to scale).

3.2. LNAPL characterisation

NAPLs

NAPL samples were collected before, during and after the conducted research LNAPL samples were collected from the field site by one of three methods:

- i) bailed directly from a well and sampled directly into a vial
- ii) sampled directly into a vial lowered into a well (to avoid any cross-contamination and volatile losses during LNAPL sampling. Avoids the need to use a new bailer for every well)
- iii) directly from the effluent stream from a skimmer pump.

The density, viscosity and compositions of the LNAPL samples were determined by laboratory measurement. Density was determined from the measured weight of a sample of known volume. Viscosity was measured with a Cambridge VISLAB 4000 viscometer at a temperature of approximately 20°C. This temperature was chosen for the viscosity analysis as the NAPL during the research trials were located at elevations 4-5 *m b.g.l.*, where the value of temperature was approximately 20°C (see Figure A.1, Appendix A).

Gas chromatography-flame ionising detector (GC-FID) analysis was performed to determine chemical concentrations and molecular weights of the components in the LNAPL phase using a HP 6890 gas chromatograph fitted with a vaporising injector (operating in split mode 100:1 split ratio at 320 °C), helium carrier gas (flow 1.0 mL/min), an auto sampler (0.05 to 0.2 µL of neat NAPL) and a flame ionising detector. The GC was equipped with a 60 m × 0.25 mm internal diameter column coated with a 0.25 µm thick film of dimethyl polysiloxane (DB-1 UI, J&W) and the oven temperature programmed to initiate at 35 °C (3 min) and ramped to 330 °C (20 min) at 10 °C/min. In addition, Gas chromatography-mass spectrometry (GC-MS) was performed to determine the NAPL composition.

Soil sampling and coring

Cores were collected from the research site to determine the NAPL concentration and its components in the soil profile. The cores were collected via a 4" hollow stem auger with a wireline retrieval system for withdrawing the core barrel from the lead auger. The core barrel contained a 5 cm external diameter, polycarbonate tube that was immediately capped and kept cooled in an insulated box with ice. The tube containing the core was then cut into 5 cm sections in the field immediately after the collection. Each 5 cm soil section was placed in tared steel cans and a subsample of ~5 g was taken out of each section (using a small coring device) for the determination of NAPL contents. This subsample was placed immediately into 5 mL of solvent (DCM/methanol) to reduce volatile losses. The remained soil sections were transported to the laboratory for bulk density measurement, the mass fraction of soil organic carbon content (f_{oc}) measurement and calculation of the pore space relationship within 2 days. The concentrations of TPH, TPH fractions and molecular weight were determined by GC-FID. The remained of the soil cores were characterized in the laboratory, according to the standards of ASTM (ASTM 2009). The core sample was dried at 105 °C to determine the total liquid contents and dry bulk density. For volumetric concentrations, the dimensions of each sleeve were measured. An assumed mineral density of 2.65 g/cm³ was used.

A conversion of TPHs in the extracted soils cores to NAPL saturations took place via calculation using Equation 4 (Parker, Waddill & Johnson 1994). The concentration of TPHs in

Equation 4, should be higher than the soil saturation limit for the LNAPL mixture ($C_{sat,soil}$) (Brost & DeVaul, 2000). Equation 4 includes the total TPH value (in liquid, dissolved and sorbed phase) ignoring partitioning.

In the saturated zone the mathematical form for the $C_{sat,i}$ calculation of the component i in the mixture in the saturated zone is (Brost & DeVaul, 2000):

$$C_{sat,i} = \frac{S_{w,i} * X_i}{\rho_{fb}} * (\theta_w + K_{s,i} * \rho_{fb}) \quad [Equation 23]$$

where:

$C_{sat,i}$: chemical concentration of the component i in soil at which sorption limits of soil particles and solubility limits of soil pore water have been reached;

$S_{w,i}$: water solubility of i compound;

X_i : mole fraction of component i in mixture;

ρ_{fb} : soil bulk density;

θ_w : volumetric water content;

$K_{s,i}$: soil-water partition coefficient of component i .

The chemical concentration of component i in dissolved and sorbed phase is calculated by the next equations respectively (Brost & DeVaul, 2000):

$$C_{dissolved,i} = \frac{S_{w,i} * X_i}{\rho_{fb}} * \theta_w \quad [Equation 24]$$

$$C_{sorbed,i} = S_{w,i} * X_i * K_{s,i} \quad [Equation 25]$$

The mathematical form for the $K_{s,i}$ calculation is:

$$K_{s,i} = f_{oc} * K_{oc} \quad [Equation 26]$$

where:

f_{oc} : fraction organic carbon;

K_{oc} : organic matter-water partition coefficient.

As regards the representativeness of the analysed soil samples, it should be noticed that, only one subsample (5g) from each section (5cm core section of ~150g weight) was analysed as this sample size is based on providing the best concentration range for the GC instrument. This approach is quite common due to cost and time issues, even though there are always limitations and uncertainties. We tried to replicate results by extracting cores in

close distances and comparing the results with the profiles obtained by the Laser Induced Fluorescence tool". It should also be noted that the cores were sectioned based on judgmental sampling to give representative samples in areas of interest within the profile. This was intended to give indicative values in a cost-effective manner. Since the sampling was not systematic some TPH peaks in the profile may have been missed, especially in heterogeneous profiles.

3.3. Fluid level monitoring

Fluid elevations were a crucial parameter for this research as they were used in the diagnostic gauge plots section, as well in T_n estimations. Fluid levels in the monitoring wells were measured using an interface probe (H. oil, Heron instruments, Canada) to determine the depth of the air-LNAPL and LNAPL-water interfaces below the top of the well casing or the air-water interface where LNAPL was absent. These measurements were used to calculate the elevation of the air-LNAPL interface (the LNAPL table), z_{an} , and the elevation of the LNAPL-water interface, z_{nw} , from the surveyed elevation of the reference point of the measurement (usually the top of the well casing). The elevation of the air-water interface (water table), z_{aw} , was calculated similarly in the case that LNAPL was absent from the well. Where LNAPL was present in the well, and based on knowledge of water and LNAPL densities, z_{aw} , was calculated (based on hydrostatic conditions within the well) as (Johnston 2010):

$$z_{aw} = z_{nw} + \rho_n b_n \quad [\text{Equation 27}]$$

Where, ρ_n is the density of the LNAPL and b_n is the in-well LNAPL thickness. Here, b_n is calculated simply as:

$$b_n = z_{an} - z_{nw} \quad [\text{Equation 28}]$$

The average NAPL density value across the contaminated site of 0.739 g/cm^3 was used in Equation 27 (see Table B.1, Appendix B). Duplicate monitoring of fluid levels was conducted on each of the tested wells at the same time. The measurement difference was less than 2 mm. Moreover, after fluid monitoring of different wells in the vicinity, fluid levels were measured again in wells that had already been monitored. As a result, fluid levels were measured for 5 times at each well location in a time period of 30 minutes. Again, the

measurement difference in fluid levels was less than 2 mm. These trials indicated the reliable measurement difference of 2 mm. Furthermore, before the start of the bail-down testing, fluid elevations were monitored three times in a time frame of 10 minutes. It should be noted that, the bail-down testing analysis was quite sensitive to the LNAPL drawdown measurements. Sometimes even 1-2 mm could affect the LNAPL transmissivity value, as it will be discussed in Chapters 6.4 and 6.10.1. We tried to use reliable measurements of fluid levels and that is the reason we repeated the depth measurements so as to know the measurer errors.

3.4. Direct push profiling tools

Direct push profiling tools are important methods for subsurface investigations. In this research work, a Hydraulic Profile Tool (HPT) and a Laser Induced Fluorescence – Ultra-Violet Optical Scanning Tool (LIF-UVOST) were used for the characterization of the subsurface contamination. 6 HPT (HPT59- HPT64) and 20 LIF (LIF43 –LIF71) profiles were measured in the research site between 17th and 20th of May 2016 (see Table A.2 and Figure A.2, Appendix A).

Hydraulic Profile Tool (HPT)

The hydraulic profiling tool is a direct push probe which can assess hydrostratigraphy and the permeability of the formation at a centimeter scale for unconsolidated subsurface materials (McCall 2011). HPT continuously measures the hydraulic conductivity of the soil by injecting the constant flow of water through a small stainless steel screen into the soil formation and measuring the hydraulic pressure at both the pump source and the injection port vs. depth. The flow rate of the water into the soil formation is also measured and recorded versus depth. Static formation hydraulic pressure measurements (dissipation tests) can also be made by stopping at discrete intervals to determine the static water level. Empirical relationships developed for the HPT tool, can be used for the estimation of formation hydraulic conductivity.

HPT logs are applicable to (McCall 2011):

- Produce a detailed hydrostratigraphic log
- Define formation permeability (qualitatively)
- Locate contaminant transport zones
- Estimate hydraulic conductivity in the saturated zone

Laser Induced Fluorescence – Ultra-Violet Optical Scanning Tool (LIF-UVOST)

Ultra-violet OPTICAL scanning tool (UVOST) is a laser induced fluorescence technology (LIF) (Germain et al. 2014). The purpose of this technique is the identification of the contaminated subsurface area and the assessment of the NAPL type. In case that LIF logs are established before the installation of monitoring and remediation wells, the number of the wells can be reduced, decreasing in parallel the cost of the project. LIF is a technique that uses laser light to stimulate fluorescent molecules that exist in NAPLs such as petroleum fuels. More specifically, a high- energy laser is used to produce an ultraviolet light source for the detection of polycyclic aromatic hydrocarbons (PAHs). The LIF/ UVOST system employs a excitation beam of light from a laser at 308 nm light pulsed at 50 megahertz. Any residual phase PAHs present in the soil grains will absorb this photon energy in the form of fluorescence. This fluorescence is returned to the optical detection system via a second silica fiber optic line, measured, and recorded in real time across four specific wavelengths, namely 350, 400, 450, and 500 nm. Individual LIF/UVOST logs consist of a primary graph of total fluorescence as a percentage of a Reference Emitter (RE) test standard versus depth, an information box and up to five waveform callouts. These callouts present the fluorescence intensity of each of the monitored wavelengths on the Y-axis (in microvolts (uV)). The four peaks are due to the fluorescence at the four monitored wavelengths called channels. Each channel is assigned a color. Various NAPLs will have a unique waveform signature based on the relative amplitude of the four channels and/or the broadening of one or more of the channels. Performance Testing: All detector systems are tested before and after each survey location to verify proper system response to known reference values.

Advantages of LIF technology:

- ongoing data logging (no data gaps)
- differentiation of NAPLs according to waveforms and color-fill logs
- equal NAPL detection in both the vadose and saturated zones

Disadvantages of LIF technology:

- does not detect BTEX as excitation wavelength for BTEX is incompatible with fiber optics
- soil matrix affects fluorescence – sands and gravels may have as much as 10 times higher response than finer materials (such as clays and silts) (Germain 2014)
- does not work well with gasoline as it contains low amount of PAHs (Germain 2014)
- potential false positives because of non-hydrocarbon products such as natural organic materials (Bujewski & Rutherford 1997).

3.5. LNAPL bail-down testing analysis

Bail-down tests were conducted in the whole contaminated site, since 2015 for the characterization of LNAPL mobility in terms of $T_{n,BD}$. The conducted tests were used also for the identification of NAPL hydrogeologic conditions. The subsurface LNAPL conditions should be known for the calculation of NAPL transmissivity. Testing involved removing a slug of LNAPL using either three bailers tied together or a single bailer depending on the well diameter. A single bailer was used in the monitoring wells of 50 mm diameter. The volume of recovered fluids (LNAPL and water), was measured and the fluid levels monitored in the well to assess recovery. The field procedure entailed the rapid removal of as much LNAPL as possible while minimising the removal of water from the well. Measurements of fluid levels (DTP and DTW) in the well were made manually with an interface probe (H. oil, Heron), initially every 30 seconds to 1 minute, with the interval between measurements subsequently increasing as the rate of recovery in the well decreased.

This procedure mainly followed the Beckett and Lyverse protocol (Beckett & Lyverse 2002) and the ASTM standard (ASTM, 2013). However, some remarks should be mentioned regarding a few recommendations made in these documents:

- The accuracy of bail-down testing is related to the initial in-well thickness among other factors. For thicknesses smaller than 15 cm ASTM recommends to use the manual skimming method instead (ASTM, 2013). In this study, the bail-down testing procedure was found to be more reliable than the manual skimming method even at low in-well thicknesses. This was related to the equipment used in the field site and the NAPL properties (gasoline with low viscosity that could be easily detected by the interface probe).
- It is recommended to maximize the initial NAPL drawdown to improve the data analysis. In some cases, as much NAPL as possible was removed, even if the removal time and the water removed amount were slightly increased. The effects of water removal are taken into account during the data analysis.
- The gauging frequency was sometimes higher than that proposed by ASTM (b_n changes of not less than 1.5 cm) (ASTM, 2013). The issues related to these high frequency measurements were corrected through the filtering data process that is discussed later in this section.

The bail-down testing field data was analyzed by using the modified Bouwer and Rice method (Kirkman 2013) implemented in the API LNAPL Transmissivity Workbook (API 2012). During bail-down testing, the LNAPL drawdown (s_n) is related proportionally to the NAPL discharge rate (Q_n) towards the well. Q_n is assessed by the in-well NAPL thickness (b_n) and

effective well radius (r_e). More specifically, Equation 29 presents the calculation of NAPL drawdown corresponding to time t_i , where DTP_0 is the initial depth to product (pre-test) and Δs_n is a possible applied drawdown correction. The Q_n is calculated by the usage of effective well radius and changes in fluid elevations over time (see Equation 30).

$$s_{n,i} = DTP_i - DTP_0 - \Delta s_n \quad [\text{Equation 29}]$$

$$Q_{ni} = \pi * r_{e(i)}^2 * (DTP_i - DTP_{i+1} + DTW_{i+1} - DTW_i) / (t_{i+1} - t_i) \quad [\text{Equation 30}]$$

For NAPL unconfined conditions, both parameters (s_n , Q_n) present a linear relationship and are expected to decrease until they reach zero values at the same time. If the discharge rate remains constant as drawdown decreases, then there is an indication for confined or perched LNAPL conditions. Figure 3.2 illustrates the confined or perched LNAPL conditions.

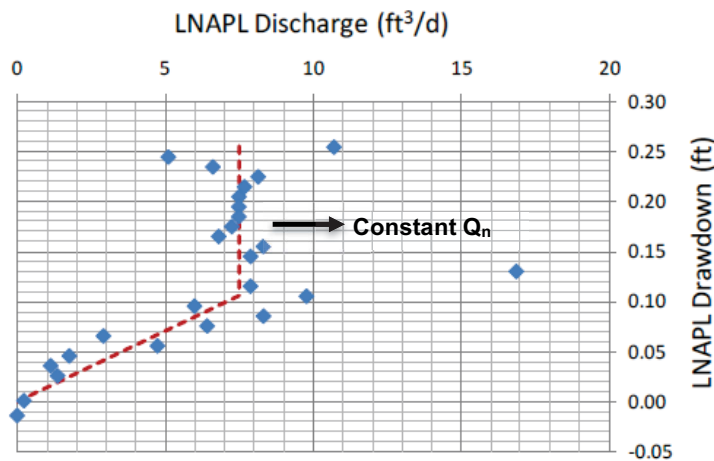


Figure 3. 2. LNAPL drawdown- discharge relation (API 2012).

The first step in the API workbook is to select the NAPL conditions in the tested well. This action refers to home worksheet (see Figure 3.3).

STEP 1: RESET OUTPUT SUMMARY

RESET

STEP 2: ENTER DATA & VIEW FIGURES

STEP 3: CHOOSE WELL CONDITIONS

Unconfined

Confined

Perched

STEP 4: LNAPL TRANSMISSIVITY SUMMARY

Output Summary

Mean LNAPL Transmissivity (ft²/d)

0.00

Standard Deviation (ft²/d)

0.00

Coefficient of Variation

NA

Figure 3. 3. Selection of NAPL conditions in home worksheet (API 2012).

Next step is to enter well configuration data in the data worksheet (see Figure 3.4). Values for parameters in the yellow box should be entered. For the top of casing elevation, data from Table A.1 in Appendix A, was used. Well casing and well radius were also known, as for the remediation wells of 100mm diameter the well radius was 0.075 m and the well casing 0.05 m. A default value 0.175 was used as LNAPL specific yield, S_y , as is recommended (API 2012). The LNAPL Density Ratio (ρ_r) was estimated in the laboratory as 0.74. Figure 3.3 illustrates the place in the workbook where the data was entered for a remediation well in the site of interest.

Ground Surface Elev (m msl)	0.000	<div style="color: red; font-weight: bold; margin-bottom: 5px;">Enter These Data</div> <div style="margin-bottom: 5px;">r_{e1}</div>
Top of Casing Elev (m msl)	0.000	
Well Casing Radius, r _c (m):	0.050	
Well Radius, r _w (m):	0.075	
LNAPL Specific Yield, S _y :	0.175	
LNAPL Density Ratio, ρ _r :	0.740	
Top of Screen (m bgs):	2.150	
Bottom of Screen (m bgs):	8.150	
LNAPL Baidown Vol. (liter):	3.9	
Effective Radius, r _{e3} (m):	0.055	<div style="color: blue; font-weight: bold; margin-bottom: 5px;">Calculated Parameters</div>
Effective Radius, r _{e2} (m):	0.054	
Initial Casing LNAPL Vol. (liter):	1.82	
Initial Filter LNAPL Vol. (liter):	0.40	

Figure 3. 4. Entered and calculated parameters in Data sheet.

Fluid levels data obtained from bail-down testing is then entered for the estimation of T_n . Figure 3.5 presents the part of the worksheet where time, DTP and DTW are entered during the product recovery.

	Enter Data Here		
	Time (min)	DTP (m btoc)	DTW (m btoc)
Initial Fluid Levels:	0	4.739	4.971
Enter Test Data:	0.60	4.765	4.927385593
	1.18	4.756	4.925384615
	1.53	4.754	4.931318182
	1.93	4.752	4.937222222
	3.15	4.748	4.946820513
	8.12	4.742	4.961671233
	12.17	4.74	4.964875519
	23.40	4.739	4.966025641

Figure 3. 5. Entered fluid levels data during bail-down testing at a remediation well in the site of research.

After the entered data of fluid levels recovery and well configuration, the API workbook draws automatically ten figures, which illustrate:

- Figure 1: Fluid interfaces (DTW, DTP, and potentiometric surface) vs Time (arithmetic time scale).
- Figure 2: DTW, DTP, and potentiometric surface vs Time (log time scale).
- Figure 3: LNAPL Drawdown vs Discharge Relationship.
- Figure 4: LNAPL Drawdown vs Thickness Relationship.
- Figure 5: DTP vs LNAPL Discharge.
- Figure 6: DTW vs Discharge.
- Figure 7: LNAPL In-Well Thickness vs Time.
- Figure 8: LNAPL Discharge vs Time.
- Figure 9: LNAPL Well Inflow Volume vs Time.
- Figure 10: LNAPL Drawdown vs Time.

$T_{n,BD}$ estimation

For a precise estimation of T_n value the cut-off time, J-ratio, drawdown adjustment and data filtering should be taken into consideration.

Cut-off time

Filter pack drainage or other effects may impact particularly at the beginning of the bail-down testing process. The specific early time data of fluids elevations may affect the value of LNAPL transmissivity. This collected inappropriate data should be eliminated by using a cut-off time ignoring the well effects. The cut-off time was used in the Bouwer and Rice model for more accurate T_n estimations.

J-ratio

J-ratio is defined as $\Delta S_n/\Delta b_n$ and it can be calculated by the slope of LNAPL drawdown and LNAPL in-well thickness (Kirkman 2013). Figure 4 in the API Transmissivity Workbook is used for the estimation of this parameter. As NAPL drawdown decreases and in-well thickness increases, the estimated *j*-ratio should be negative. On the other hand, positive *j*-ratio estimates depict product leaving the well as drawdown decreases.

Drawdown adjustment

In case that the curve at Figure 1 in the API Transmissivity Workbook does not approach zero drawdown at zero NAPL discharge, it is an evidence that there was not equilibrium between the formation and the in-well fluids the time of the conducted test. For a precise T_n estimation, a drawdown adjustment should be applied to the data before the analysis.

Data filtering

Figure 3.6 shows three different distinct areas noted A, B and C. Interval A refers to early stage collected data that represents the filter pack drainage and it is excluded from the analysis through the cut-off time. Interval B corresponds to the NAPL flow from the adjacent formation and interval C represents the end of the test (return to pre-testing conditions). Thus, data filtering is necessary to keep only the representative points of interval B for the calculation of T_n (fitting the straight line). For the data analysis process, the interval C and anomalous points from interval B have to be identified and filtered. The anomalous data points are usually those associated to negative or negligible discharges generally linked to small changes in b_n or measurement errors under other circumstances.

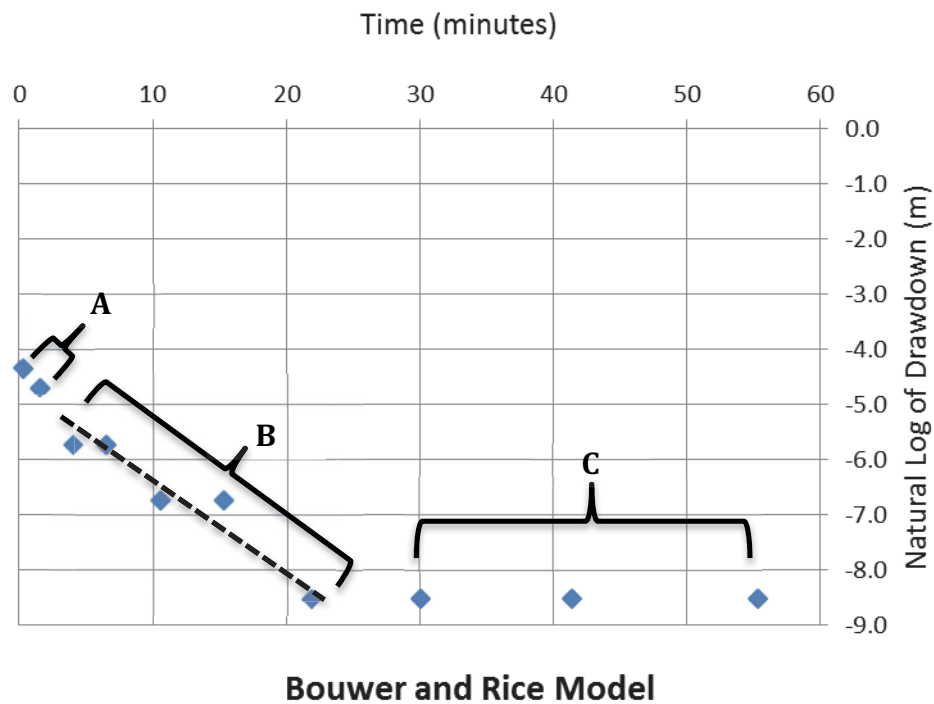


Figure 3. 6. Example of bail-down test data analysis using Bouwer and Rice method.

Bouwer and Rice worksheet

The $T_{n,BD}$ values of this research work were calculated using the B&R worksheet. The B&R method presents the logarithm of the s_n varies as a function of time. The T_n value is determined by a slope of a fitted straight line to the $\log-S_n$ versus time data. The T_n standard deviation is estimated also by the variance of the slope of the line. Figure 3.7 presents an example worksheet of a remediation well in the research site.

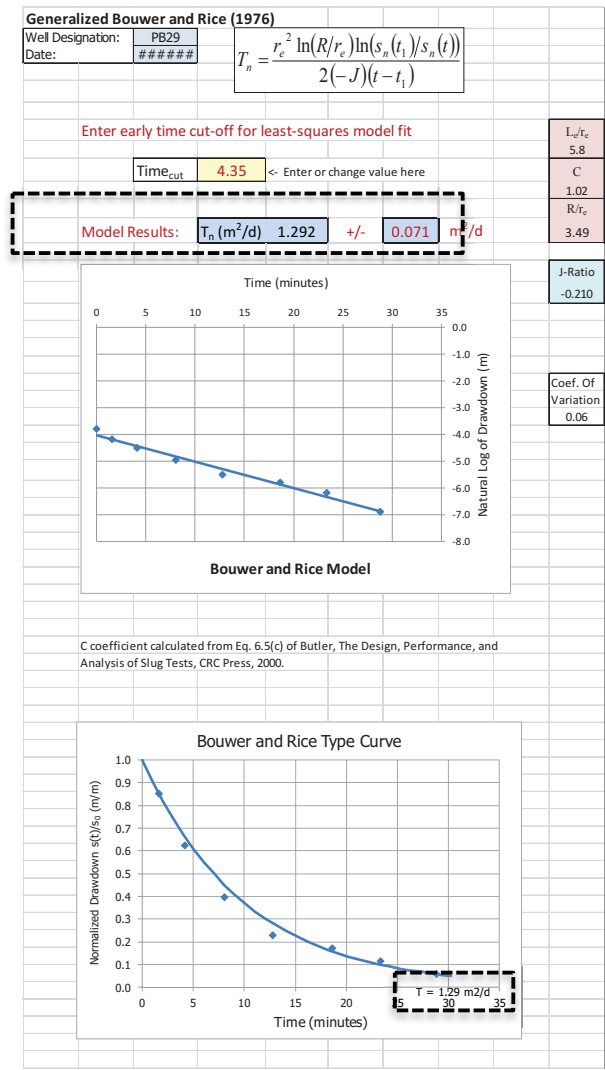


Figure 3. 7. Bouwer and Rice worksheet.

As regards unconfined NAPL conditions, the T_n value is estimated by the Equation 16 in Chapter 2. For confined NAPL conditions, the Confined NAPL worksheet is used, where a constant NAPL discharge value and depth to base of confining bed, should be inserted. The unconfined worksheet can be used also for the time period of the unconfined response (Kirkman 2013).

3.6. Long term recovery system data

Pilot-scale mass recovery techniques such as skimming, water enhanced (water table drawdown) skimming (dual pump), vacuum enhanced skimming and water and vacuum enhanced recovery took place in this research. T_n is calculated from the skimming trials using the modified Thiem equation (Charbeneau 2007b). Relationships of air/ LNAPL interfaces and

in well thicknesses among remediation and monitoring wells were used for the calculation of the formation air/ LNAPL interface in equilibrium. Thus, the LNAPL drawdown (s_n) in the remediation wells was calculated and the LNAPL recovery rates (Q_n) were measured. The following equations are the equations 20-22 re-expressed in the form of T_n . The recovery data for the T_n calculation, was analyzed according to the: *Standard guide for estimation of LNAPL transmissivity* (ASTM 2013). The following equation was used for the estimation of T_n during LNAPL skimming (Charbeneau 2007b):

$$T_{n,SK} = \frac{Q_n \ln\left(\frac{R_{oi}}{r_w}\right)}{2\pi s_n} \quad [\text{Equation 31}]$$

where

Q_n = measured LNAPL recovery rate (L^3/t);

R_{oi} = radius of capture (L);

r_w = well radius (L);

s_n = LNAPL drawdown at time t (L).

The time weighted mean of LNAPL recovery rate (Q_n) and the geometric mean of drawdown (s_n) were used in the equation above for the calculation of LNAPL transmissivity during the skimming operations. Finally, the value $\ln(R_{oi}/r_w)$ was assumed to be equal to 4.6 introducing little error (ASTM 2013).

During the water-enhanced LNAPL recovery (dual phase) the LNAPL transmissivity was calculated using LNAPL and water discharge data. The aquifer transmissivity (T_w) was calculated by the HPT obtained data. The following equation was used for the estimation of T_n during LNAPL water enhanced skimming, where skimming drawdown was greater than 1/10 of the water extraction induced drawdown (Charbeneau 2007b):

$$T_n = \frac{Q_n T_w}{Q_w} \frac{1}{\left(\frac{1}{\rho_r} + \frac{S_{skim}}{S_w}\right)} \quad [\text{Equation 32}]$$

where

T_w = aquifer transmissivity (L^2/t);

Q_w = water discharge rate in terms of standard air pressure and temperature (L^3/t);

S_w = water extraction induced drawdown;

S_{skim} = the maximum skimming drawdown (for unconfined conditions = $b_n(1-p_r)$);

ρ_r = the relative LNAPL to water density

T_n was determined during the vacuum enhanced skimming using air and LNAPL discharge data, formation air permeability and air-water viscosity ratio, and formation hydraulic conductivity across the screened interval above the NAPL. Equation 33 was used for the T_n calculation (Charbeneau 2007b):

$$T_n = \frac{Q_n k_{ra} K_w b_a \rho_r}{\mu_{ar} Q_a} \quad [\text{Equation 33}]$$

where

Q_a = air discharge rate in terms of standard air pressure and temperature (L^3/t);

k_{ra} = relative permeability of open screen length in the vadose zone to air (unit less);

K_w = saturated hydraulic conductivity value for corresponding to the soil type existing in the vadose zone immediately above the mobile LNAPL interval (L/t);

b_a = screen length open to the portion of the vadose zone representative of the saturated hydraulic conductivity value used (L);

μ_{ar} = relative viscosity of air to water (unit less).

The value for relative viscosity, μ_{ar} , was assumed to be 0.018 and relative permeability to air, k_{ra} , was assumed to be 0.9 (ASTM 2013). For the T_n calculation during the water and vacuum enhanced skimming processes, Equation 34 was used (ASTM 2013):

$$T_n = \frac{Q_n \rho_r}{\frac{\mu_{ar} Q_a}{k_{ra} K_w b_a} + \frac{Q_w}{T_w}} \quad [\text{Equation 34}]$$

3.7. LDRM (LNAPL Liquids Distribution and Recovery Model)

LDRM is a Window based modelling program that predicts LNAPL saturation, distribution and recovery in the subsurface (Charbeneau 2007b). Up to three homogenous layers can be expressed defining the soil parameters for each layer separately with a distinct transition point among them. Table 3.1 presents the parameters required for the estimation of LNAPL distribution and mobility. Some basic assumptions that LDRM uses are (Charbeneau

2007a; Jeong & Charbeneau 2014): LNAPL is unconfined and at vertical equilibrium. Moreover, there is a uniform radial distribution of LNAPL adjacent to a recovery well. In addition, all LNAPL within the radius of capture will be captured by the remediation well. Finally, LNAPL recovery is estimated with radial flow equations and Hysteresis is not explicitly considered.

Table 3. 1. Parameters required to estimate LNAPL distribution and recovery.

Thickness, Elevations, Vertical Gradient	Fluid Characteristics	Soil Characteristics
Maximum monitoring well LNAPL thickness (m)	LNAPL density (gm/cc)	Porosity
Ground surface elevation (m)	LNAPL viscosity (cp)	Hydraulic conductivity (m/d)
Water table elevation (m)	Air/water surface tension (dyne/cm)	Van Genuchten N
Water vertical gradient	Air/LNAPL surface tension (dyne/cm)	Van Genuchten α (m ⁻¹)
	LNAPL/water interfacial tension (dyne/cm)	Irreducible water saturation
		Residual LNAPL saturation

After the installation of the program, the user can choose between starting a new simulation or opening an existing simulation. The Project Setup screen is the first window in the beginning of the LDRM (see Figure 3.8). This screen displays options of units, soil heterogeneity (number of soil layers), elevation reference, NAPL smear correction and NAPL residual saturation.

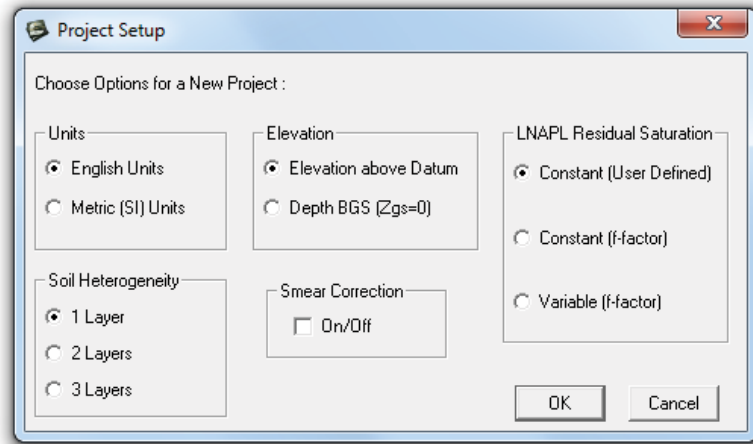


Figure 3. 8. Project set up window.

After the project set up window the Data input screen is opened, as shown in Figure 3.9. This screen requires three categories of parameters for the model simulation (see Table 3.1), which are:

- LNAPL thickness and elevations
- NAPL characteristics
- Soil properties

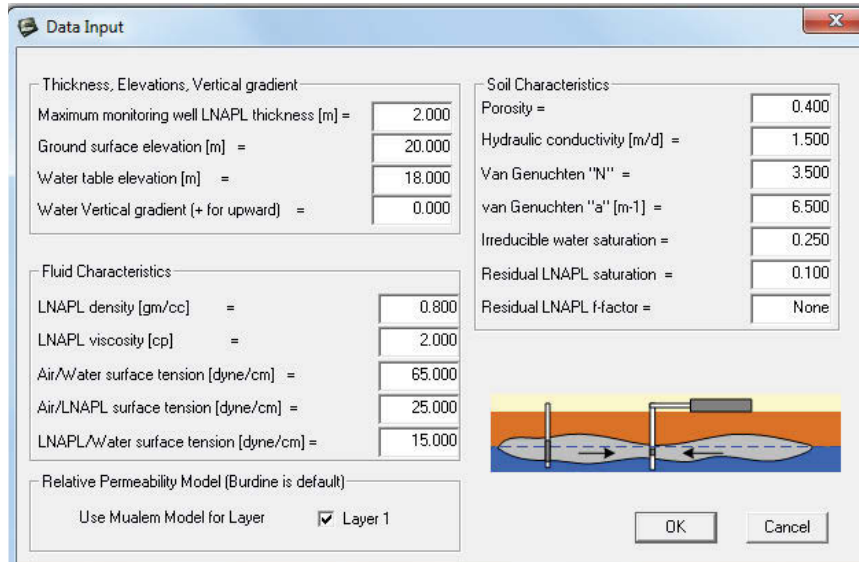


Figure 3. 9. Data input screen.

After the population of data input screen, the user presses “OK”, which results in the screen with the initial outputs of the model including the value of T_n , as shown in Figure 3.10. LDRM provides also graphical output options (based on the provide data in the .txt file) as it can be seen in the graph 3.11. In addition, under the data menu (see Fig. 3.12), the user has the opportunity to add measured field data which can be visualized with the graphs.

LNAPL Distribution and Recovery Model (LDRM)	
File Data Recovery Graphs Options Help Exit	
VARIABLE	INITIAL CONDITIONS FOR RUN
LNAPL Thickness [m]	2.00
Total LNAPL [m]	0.62
Mobile LNAPL [m]	0.62
Recoverable LNAPL [m]	0.48
Residual LNAPL [m]	0.00
LNAPL Transmissivity [m ² /d]	0.92
LNAPL Discharge [lpd]	0.00

Figure 3. 10. Initial output screen.

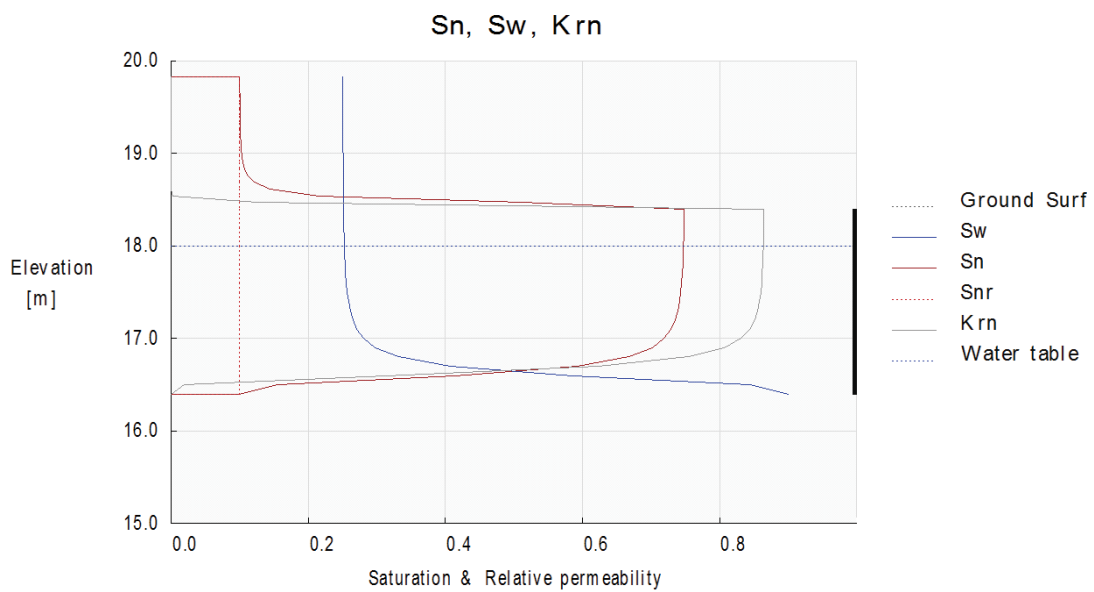


Figure 3. 11. LDRM graphical output: saturation and NAPL relative permeability profiles.

The "Input Field Data" dialog box contains the following options and instructions:

- Enter the Saturation data
- Monitoring Well LNAPL Thickness [m]
- LNAPL Recovery Volume [Liter]
- LNAPL Recovery Rate [L/d]

Instructions: Select an option to enter the field data and click on OK button. Then "field_data.csv" will be generated at the same folder where the program file is located. Open the file and enter field data using Excel Spreadsheet.

OK

Figure 3. 12. Input field data by the user.

3.8. Experimental procedure

3.8.1. Study area

The study area of this research comprises the facilities of a petrol station in Western Australia. Three different areas were chosen for the scope of this research work. The three research areas shown in Fig. 3.13 were chosen to investigate the effect of water table fluctuations in sites with different NAPL distribution and geological material. The tested wells (as regards bail-down and LNAPL recovery testing) were PB29 (research area A), PB27 (research area B) and PB40 (research area C). The distance between the tested wells in area A and B is 12 m, with area C located 30 m away from the other two areas. The areas of interest exhibited differences in the vertical NAPL distribution and the stratigraphic profile. The material at research area C was generally finer than that found at the other two areas. Research area A revealed unconfined LNAPL conditions during the years of research (2014 - 2016). On the other hand, research areas B and C presented both confined and unconfined LNAPL conditions since 2014. The transition point between confined and unconfined NAPL was in the range of 56.7 - 56.8 m AHD (Australian Height Datum) according to different lines of evidence such as diagnostic gauge plots, core logging, HPT profiles, bail-down testing and hydrostratigraphs (Kirkman, Adamski & Hawthorne 2013). Table 3.2 presents the monitoring network and the NAPL hydrogeological conditions (unconfined LNAPL) at the three research areas during the mass recovery trials.

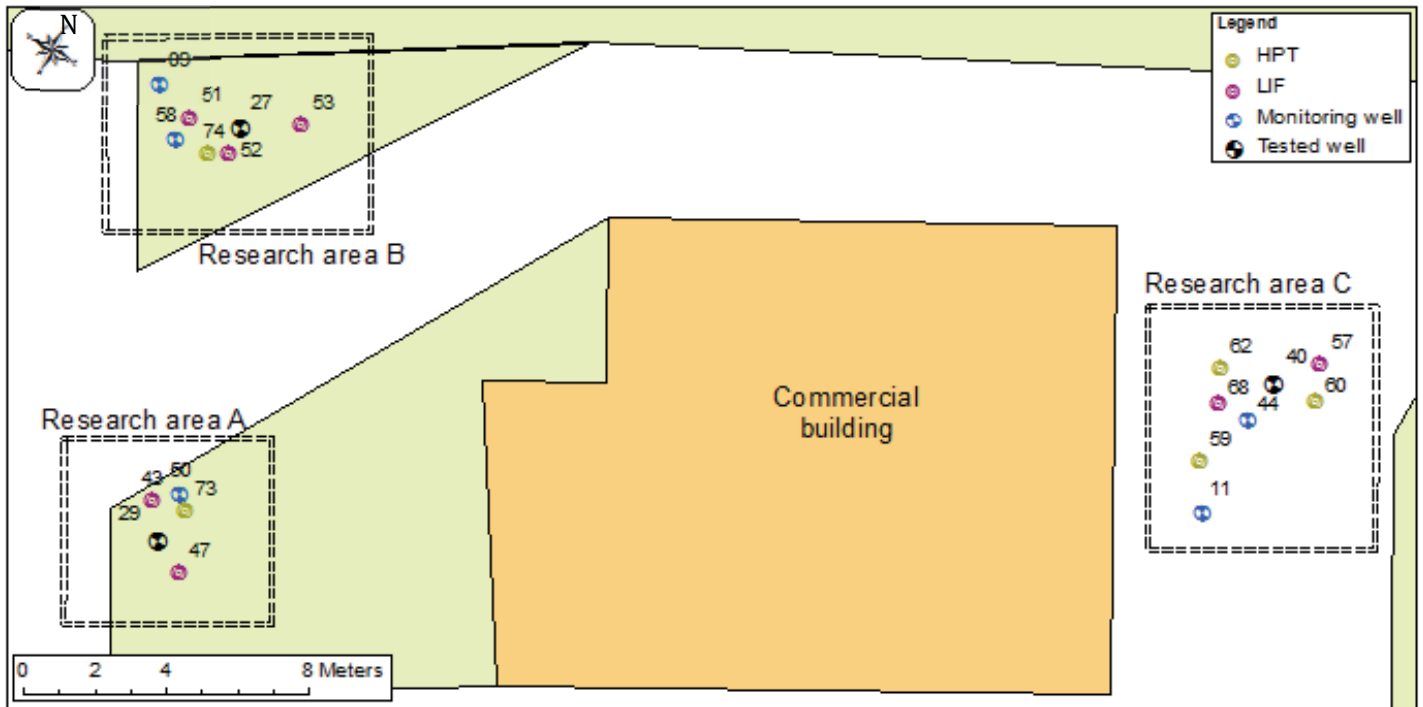


Figure 3. 13. Site layout showing the three research areas A (PB29 recovery well), B (PB27 recovery well) and C (PB40 recovery well), the monitoring wells (09, 58, 50, 11, 44), the LIF (51, 52, 53, 43, 47, 57, 68) and HPT points (59, 60, 62, 73, 74).

Table 3. 2. Monitoring network and NAPL hydrogeological conditions during the pilot-scale mass recovery trials at the three research areas.

Research Area	Recovery Well	Observation Wells	LIF Profiles	HPT Profiles	NAPL Conditions
A	PB29	MP50	LIF43, LIF47	HPT73	Unconfined
B	PB27	PB09	LIF 51, LIF52, LIF53	HPT74	Unconfined
C	PB40	PB11	LIF57, LIF68	HPT60, HPT62	Unconfined

3.8.2. Mass recovery experiments

Periodic measurements of $T_{n,BD}$ (LNAPL transmissivity via bail-down testing) were obtained across the whole field site between 2015 and 2016. Bail-down tests took place before, during and after the mass recovery trials. The areas of interest showed similar initial $T_{n,BD}$ values at the beginning of the remediation trials (areas A and B had an initial $T_{n,BD}$ value of 1.40 m²/d at the beginning of the 2015 mass recovery trial, and areas A,B and C had an

initial $T_{n,BD}$ value of 0.2 - 0.37 m²/d in 2016 trial). The 2015 trials were conducted sequentially in areas A and B under relatively constant water table conditions in the case of area A (water table elevation increased at a rate of +1 cm/week) and a rising potentiometric surface in the case of area B (water table elevation increased at a rate of: +5 cm/week). On the other hand, the 2016 trials were conducted in parallel in the three research areas, so the influence of the rising water table (water table elevation increased at a rate of +7.5 cm/week at the beginning of the trial) could be examined under similar initial conditions ($T_{n,BD}$ and Z_{aw}).

In 2015, the **skimming** operation in areas A and B lasted two weeks. In 2016, the skimming operation at research area B lasted four weeks. A 4-week sequential free recovery trial took place at research areas A and C. The applied techniques were: (i) skimming; (ii) water-enhanced skimming (dual pump inducing water table drawdown); (iii) vacuum-enhanced skimming and (iv) water- and vacuum-enhanced skimming. Continuous soil cores were extracted before the start of the 2016 trials (cored wells: MP44, MP50 and MP58, 20th of May 2016). In addition, LIF and HPT profiles were obtained during the time period of soil coring. The equilibrium fluid levels used in the T_n analysis at areas A, B and C were estimated from the monitoring wells MP50, MP09 and PB11 respectively.

Water-enhanced skimming experiments were conducted under two different removal rates of water (DD1: 4.5 L/min, DD2: 8 L/min in the case of area A and DD1: 2.5 L/min, DD2: 6.2 L/min in the case of area C). When the induced water table drawdown reached steady state conditions, bail-down tests were performed. Afterwards, the skimming pump was introduced into the well. It should be noticed that, regarding the bail-down testing analysis, the horizontal flow assumption is not met potentially causing additional errors.

Vacuum (-3 to -16 kPa) was applied unsuccessfully at well PB29 on 30th of June, as both mud and NAPL were recovered. Vacuum (-1 to -4 kPa) was applied again on 5th of July. Finally, vacuum (-1.5 to -2.5 kPa) and water table drawdown (DD: 4 L/min) were applied on 6th of July. At well PB40, vacuum (-1 to -4 kPa) and water table drawdown (DD: 3.6-3.8 L/min) were applied in parallel on 7th of July. Figures 3.13 and 3.14 depict the specific gravity skimmer pump and the arrangement of water and vacuum enhanced recovery at area C.



Figure 3. 14. The specific gravity skimmer pump.



Figure 3. 15. Arrangement of well head for water and vacuum enhanced recovery at well PB40.

The impact of different NAPL amount removals on the calculation of T_n value, was investigated at research areas A and B via bail-down testing. At PB29 well location (area A), three different experiments were conducted. At PB27 well location (Area B), the research took place conducting four experiments in two different dates under different water table elevations.

Bail-down testing was conducted before, during and after the pilot-scale remediation processes the years 2015 and 2016. Furthermore, several bail-down tests took place since 2015 in the whole contaminated site of research for the determination of NAPL mobility.

Tables 3.3-3.5 present the chronology of events at research areas A, B and C. More detail on the mass recovery testing and on sampling can be seen at Tables A.3 - 6, Appendix A.

Table 3. 3. Chronology of events during field trial of NAPL recovery at area A, PB29 well.

Event	June 2016															July 2016							
	15	16	17	18	19	20	21	22	23	24	25	26	27	28	29	30	1	2	3	4	5	6	7
BD	█	█					█		█	█				█	█	█						█	█
SK	█	█	█	█	█	█	█	█	█								█	█	█	█			█
SK+DD									█	█				█	█								
SK+VCM																	█					█	
SK+VCM+DD																						█	
NAPL Sampling	█								█	█			█		█					█	█	█	█
Vapour Sampling																█						█	█

Where: BD: Bail-down testing, SK+DD: Water enhanced skimming, SK+VCM: Vacuum enhanced skimming, SK+VCM+DD: Vacuum and water enhanced skimming.

Table 3. 4. Chronology of events during field trial of NAPL recovery at area B, PB27 well.

Event	June 2016																July 2016									
	14	15	16	17	18	19	20	21	22	23	24	25	26	27	28	29	30	1	2	3	4	5	6	7	8	
BD	█		█	█																	█				█	
SK			█	█	█	█	█	█	█	█	█	█	█	█	█	█	█						█	█	█	█
NAPL Sampling			█								█	█					█						█	█	█	

Table 3. 5. Chronology of events during field trial of NAPL recovery at area C, PB40 well.

Event	June 2016																July 2016								
	14	15	16	17	18	19	20	21	22	23	24	25	26	27	28	29	30	1	2	3	4	5	6	7	8
BD	█			█				█	█	█					█	█					█			█	
SK		█	█	█	█	█	█	█	█									█	█	█	█	█	█	█	█
SK+DD										█	█						█	█							
SK+VCM																									
SK+VCM+DD																								█	
NAPL Sampling		█							█	█	█				█		█				█			█	█
Vapour Sampling																									█

4. Overview of the Site Setting

Chapter 4 contains information about the characterization of the site of research. More specifically, information regarding site location, history of contamination, site geology and hydrogeology, LNAPL properties and distribution is provided.

4.1. Site and hydrogeological characteristics

The study area comprises an operating petrol station in Western Australia, in an area of 2750 m² which is located within a residential-commercial zone. The site is located at 7 South Western Highway, Donnybrook, WA. The Preston River is approximately 250 m north east of the site and both residential and commercial areas are located northerly, easterly and southerly of the site. Table 4.1 presents the site coordinates and Figure 4.1 the monitoring network at the contaminated site.

Table 4. 1. Site Coordinates.

Site Corner	Easting (m)	Northing (m)
North Corner	390656.896	6285021.370
East Corner	390628.514	6284976.750
South Corner	390652.081	6284958.305
West Corner	390606.452	6284997.882

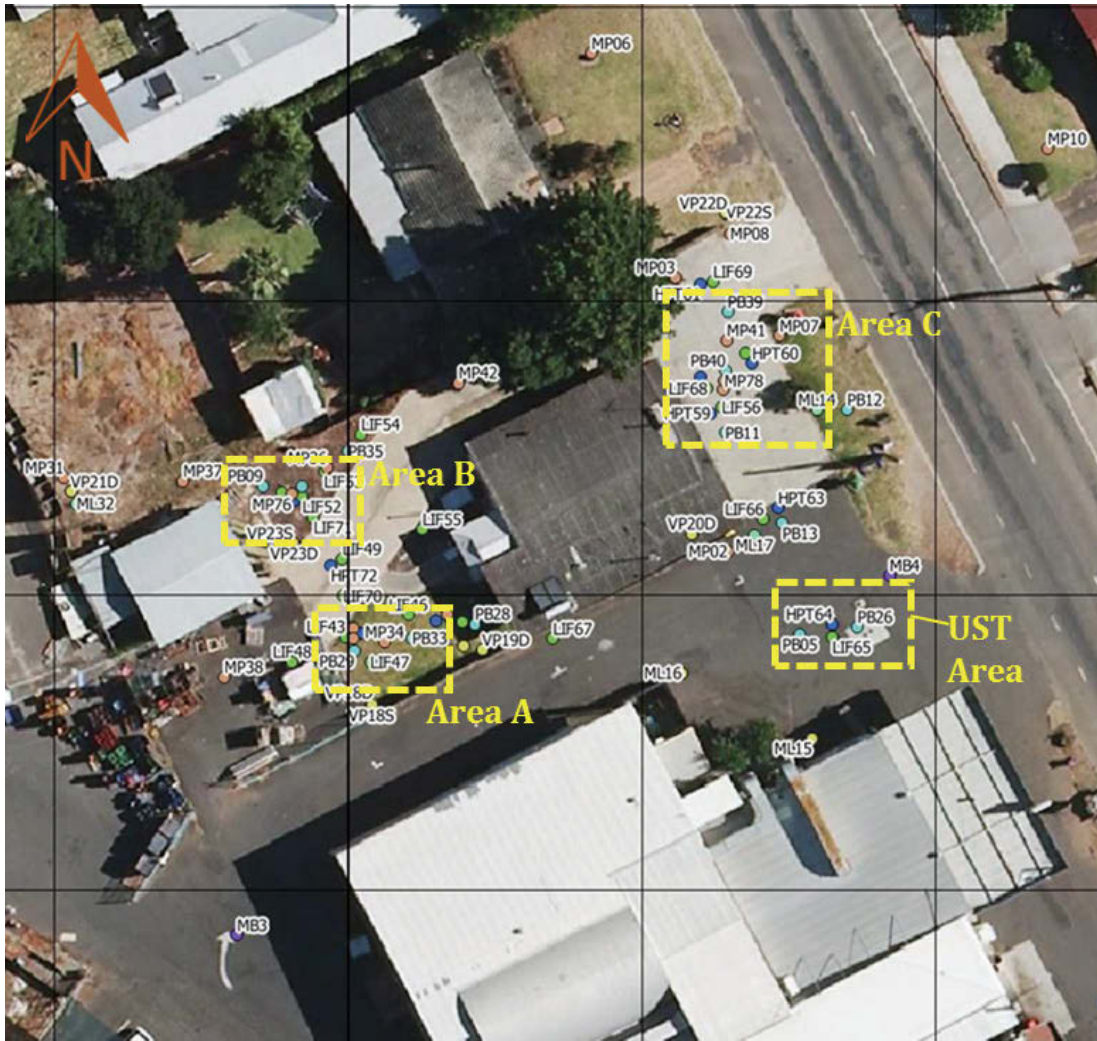


Figure 4. 1. Monitoring network at the site of research and location of areas A, B, C and spill location at UST (scale: 15x15 m).

Since 2014, 85 monitoring points have been installed including production (100 mm) and monitoring wells (50 mm), multi-level strings and vapor point wells. The characterization works included soil coring and direct-push profiling methods such as HPT and LIF at distances of less than 2 m away from the tested wells. Stratigraphic core descriptions (wells: PB27, PB33, PB35 and PB39) and HPT profiles (HPT59, 60, 62, HPT73 and HPT74) were used for the geological characterization of the tested areas (see Figures B.1- B.9, in Appendix B).

The analysis showed that the local hydrogeology consists of a multi-layered unconsolidated aquifer system formed in a fluvial depositional environment. It presents discontinuous interbedded sands, silts and clays. In general, the stratigraphic profile consists of 3 main strata. A clayey silt layer (CL-ML) from 0 to approximately 4.5 m below ground, underlain by a sandy layer (fine and coarse sand with up to 30% of silt and clay) from approximately 4.5 m to 8 m and then heavy clays from approximately 8 m and below. A fining-

upward sequence was observed in the core logs within the sandy unit. The research area recorded water table fluctuations of 2 - 3 m and the topography is relatively flat. The direction of groundwater flow is West, North-West (see Figure B.19, in Appendix B). The hydraulic gradient is also relatively flat (see Figure B.20, in Appendix B).

Soil core descriptions were found in a good agreement with the HPT profiles, as HPT pressure was higher in silty and clayey materials. Moreover, the transition point between sandy to clayey material in the stratigraphic logs agreed with the transition from low to high pressures in the HPT profiles. More details in the agreement between the stratigraphic log descriptions and the HPT profiles are presented in Chapter 5, regarding the design of hydrostratigraphs.

4.2. LNAPL occurrence, characterization and distribution

4.2.1. LNAPL characterization and properties

An underground storage tank (UST) containing unleaded petrol ruptured in 2013, releasing unleaded petrol. The amount of released product is unknown. The type of the contaminant is confirmed by the chemical analysis of the collected product from 10 monitoring wells in the site of interest. Table 4.2 presents the LNAPL characterization of the contaminated site. The depicted results are in a good agreement with fresh gasoline product as was presented by Lekmine (Lekmine et al. 2014). The viscosity of the product (as measured at PB27, PB29 and PB40 wells) is 0.41- 0.48 cP and the average measured density (between samples of 10 wells) is 0.739 g/cm³ with standard deviation of 0.017 g/cm³ (see Table B.1, Appendix B). The measured physical properties are in agreement with the gasoline properties as they were documented by Wilson (Wilson et al. 1990).

Table 4. 2. LNAPL product characterisation.

Compounds	Mean	Standard deviation
Benzene	0.84%	0.28%
Toluene	13.03%	1.22%
EthylBenzene	1.95%	0.45%
m/p-Xylene	6.34%	1.32%
o-Xylene	2.59%	0.68%

135-trimethylbenzene	0.71%	0.23%
124-trimethylbenzene	2.71%	0.88%
123-trimethylbenzene	0.61%	0.22%
Naphthalene	0.10%	0.05%
2-methylnaphthalene	0.04%	0.02%
1-methylnaphthalene	0.02%	0.01%

4.2.2. LNAPL distribution

Figure 4.2 illustrates the times series of in-well measured Z_{aw} versus b_n over the whole contaminated site since 2014. NAPLs were mainly found in the sandy material under different hydrogeological conditions depending on the position of Z_{aw} . NAPL distribution through hydrostratigraphs, NAPL saturations in soil cores and LIF profiles is presented in detail in chapters 5 and 6. LIF profiles in Appendix B (Figures B.10- B.17) depict information about the spatial and vertical NAPL distribution in the three research areas. Area A presented the highest LIF signal among the three areas (LIF43 profile, Figure B.10, Appendix B). Interestingly, differences in LIF signals can be seen in LIF locations which are close to each other (LIF 43-47, LIF 51-52, LIF 56-57-68), around the recovery wells PB29, PB27 and PB40. An extension of LNAPL plume according to fluid levels in the monitoring network can be seen in Figure B.21 in Appendix B.

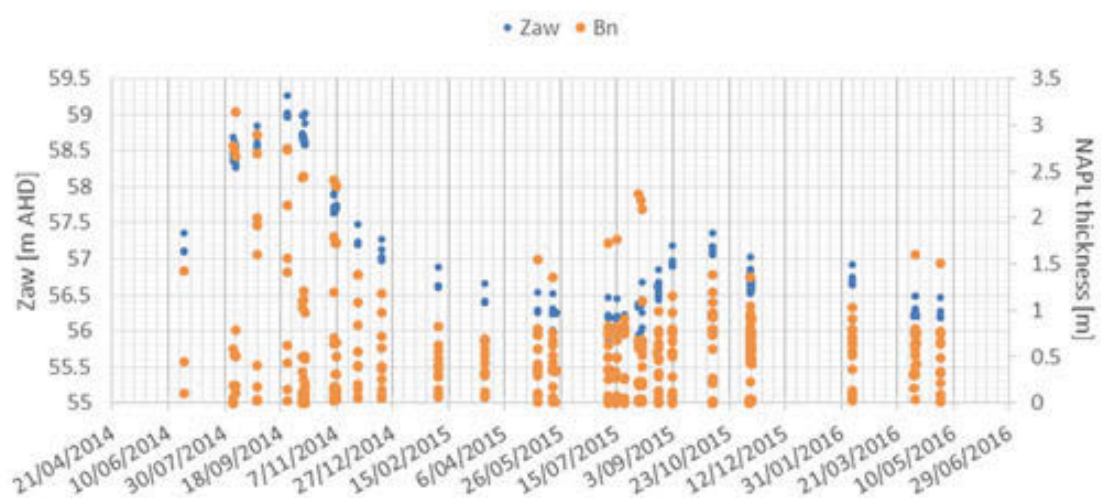


Figure 4. 2. Time series of potentiometric surface elevation and in-well thicknesses in the whole research site.

Table 4.3 presents the minimum and maximum b_n in wells where product exists, presenting the spatial distribution of mobile NAPL contamination at the research site. Higher b_n was found in the vicinity of research area C. Furthermore, high b_n values for high potentiometric surface elevations may depict confined or perched NAPL conditions in the tested wells (see Table 2.2).

Table 4. 3. Minimum and maximum in-well thickness and potentiometric surface elevation across the whole contaminated site.

Well	Date	Z_{aw} (m AHD)	Minimum b_n (m)	Date	Z_{aw} (m AHD)	Maximum b_n (m)
MP01	1/06/2016	56.30	0.062	24/09/2014	59.01	2.745
MP02	28/04/2016	56.46	0.333	3/09/2014	59.87	2.118
MP03	17/12/2014	56.99	0.05	21/07/2015	56.20	0.826
MP07	20/12/2016	56.97	0.029	3/08/2015	55.94	2.253
MP08	18/05/2015	56.24	0.17	1/06/2016	56.48	0.906
MP34	20/12/2016	56.94	0.001	14/06/2016	56.41	0.011
MP36	5/10/2016	58.63	0.032	20/12/2016	56.93	0.265
MP41	8/07/2016	56.57	0.145	8/10/2015	57.11	0.973
MP42	20/12/2016	56.93	0.004	6/04/2016	56.20	0.627
MP44	26/07/2016	58.35	0.444	20/12/2016	56.95	0.896
MP50	20/12/2016	56.93	0.105	20/05/2016	56.17	0.264
MP58	20/12/2016	56.93	0.05	20/05/2016	56.15	0.304
PB05	17/12/2014	57.12	0.26	28/08/2014	58.61	2.899
PB11	7/10/2014	58.70	0.076	16/08/2016	58.88	2.542
PB12	20/06/2016	56.52	0.001	19/03/2015	56.40	0.113
PB13	9/10/2014	60.56	0.001	26/07/2016	57.60	3.098
PB26	5/02/2015	60.05	0.065	9/02/2016	59.17	1.027
PB27	9/02/2016	59.81	0.056	5/10/2016	58.29	2.238
PB28	20/08/2015	56.60	0.001	18/05/2015	56.25	0.007
PB29	5/10/2016	58.61	0.002	7/07/2015	56.20	0.356
PB33	20/12/2016	56.94	0.002	5/04/2016	56.21	0.306
PB39	26/07/2016	58.45	0.287	11/11/2015	55.28	1.359
PB40	21/08/2015	56.63	0.322	5/10/2016	58.63	1.319

5. Assessment of LNAPL Distribution and Hydrogeological Conditions

In this chapter, a detailed analysis of LNAPL distribution and hydrogeological conditions in the three research areas (see Figure 3.12) is presented. The analysis included: (i) plume scale diagnostic gauge plots, (ii) LDRM simulations, (iii) stratigraphic log descriptions, (iv) NAPL saturations (soil coring), (v) hydrostratigraphs, (vi) direct-push profiling methods such as HPT and LIF and (vii) LNAPL drawdown-discharge relations during bail-down testing. The usefulness of Diagnostic Gauge Plots (DGP) for evaluation of the LNAPL hydrogeological conditions is elucidated by using the other aforementioned lines of evidence. LDRM simulations are used to provide further insight regarding the NAPL distribution and geological heterogeneity in the present areas.

5.1. Critical In-Well Test Application for Evaluation of LNAPL Hydrogeological Conditions

Section 5.1 presents the analysis for the identification of NAPL hydrogeological conditions in the three research areas. These LNAPL conditions are related to the Z_{aw} behavior. The identification of NAPL hydrogeologic conditions is crucial for an accurate calculation of LNAPL transmissivity, because NAPL drawdown is calculated differently depending upon whether the NAPL is confined, perched, or unconfined (API 2012; ASTM 2013; Hawthorne 2014a; Kirkman, Adamski & Hawthorne 2013). DGPs are useful tools also for the identification of NAPL conditions in the monitoring wells in the vicinity of the tested recovery well, as the monitoring points can be used only if they present similar NAPL conditions with the remediation well.

5.1.1. LNAPL hydrogeological conditions in area A

Figure 5.1 depicts the hydrograph for the well PB29. Three trends (**A** - **C**) in the potentiometric surface can be observed in this graph. The first period (**A**) exhibits a constantly decreasing trend of Z_{aw} during this time period (from 57 m AHD to 56.2 m AHD). During the second period (**B**) Z_{aw} is constantly increasing (from 56.2 m AHD to 57.1m AHD). The third period (**C**) comprises a showed a constantly decreasing Z_{aw} trend. During all the three time

periods the trend of the b_n is opposite in behaviour compared to the potentiometric surface indicating unconfined LNAPL conditions.

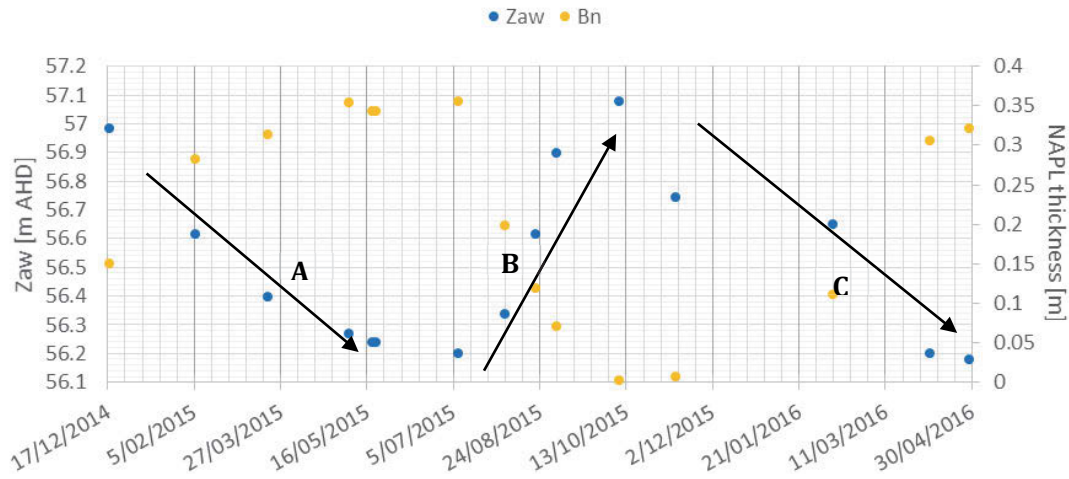


Figure 5. 1. Hydrograph plot of the potentiometric surface elevations versus gauged LNAPL thickness for well PB29 (17/12/2014 - 28/4/2016). The arrows show the general trend of Z_{aw} changes with time.

NAPL gauge thickness plots

Figure 5.2 illustrates the gauge thickness plot of the tested well PB29.

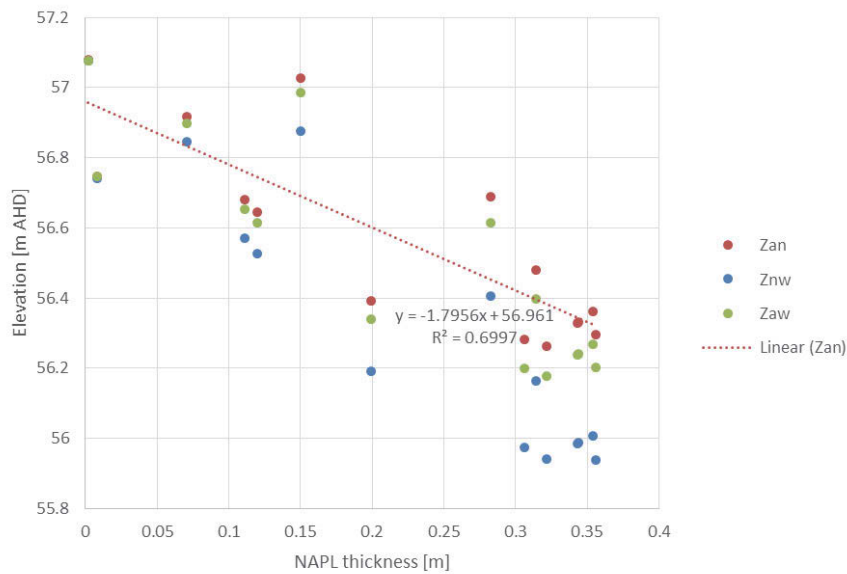


Figure 5. 2. Gauge thickness plot of the air-NAPL interface, LNAPL-water interface, and potentiometric surface elevations versus gauged LNAPL thickness for well PB29 (17/12/2014 – 28/4/2016).

It can be inferred that this graph presents unconfined LNAPL conditions depicting an increasing trend of in-well thickness as Z_{an} , Z_{nw} and Z_{aw} decrease (Kirkman, Adamski & Hawthorne 2013). The red line exhibits a relatively linear relationship between the Z_{an} and b_n . This plot depicts one period of rising and two periods of falling water table elevation (according to Figure 5.1). The presented R square statistic value of Z_{an} is 0.699, for the whole monitoring history of the specific well.

Figures 5.3 – 5.5 present gauge thickness plots for the same well after filtering the presented data in Figure 5.2 according to the different depicted Z_{aw} trends in Figure 5.1. These graphs showed R squared statistic values higher than 0.96 indicating the high correlation of the linear relationship among the data points. More specifically, Figure 5.2 was filtered according to different depicted Z_{aw} trends in Figure 5.1. Arrow “A” for instance in Figure 5.1, presents a drainage period. Thus, Figure 5.3 shows only data points of this time period. Figure 5.4 corresponds to the imbibition period “B”, and Figure 5.5 corresponds to the drainage period “C”, respectively.

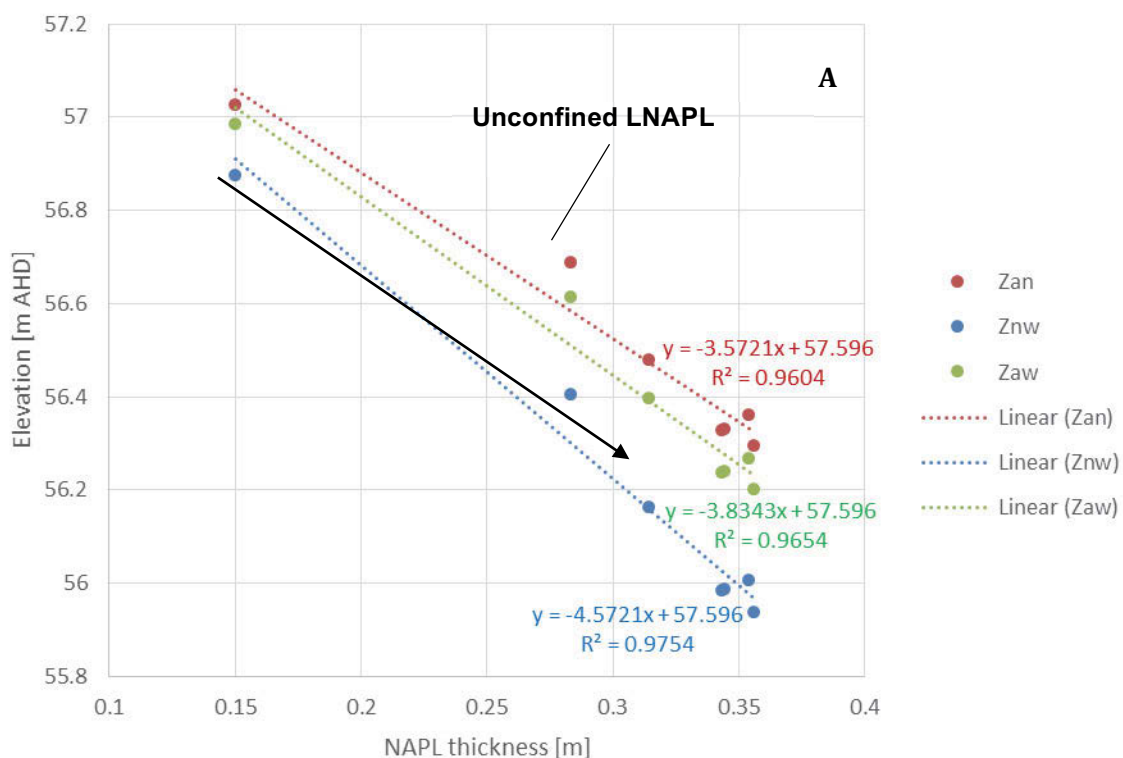


Figure 5. 3. Gauge thickness plot of the air-NAPL interface, LNAPL-water interface, and potentiometric surface elevations versus gauged LNAPL thickness for well PB29 (17/12/2014 - 7/7/2015). The arrow shows the trend of Z_{aw} with time.

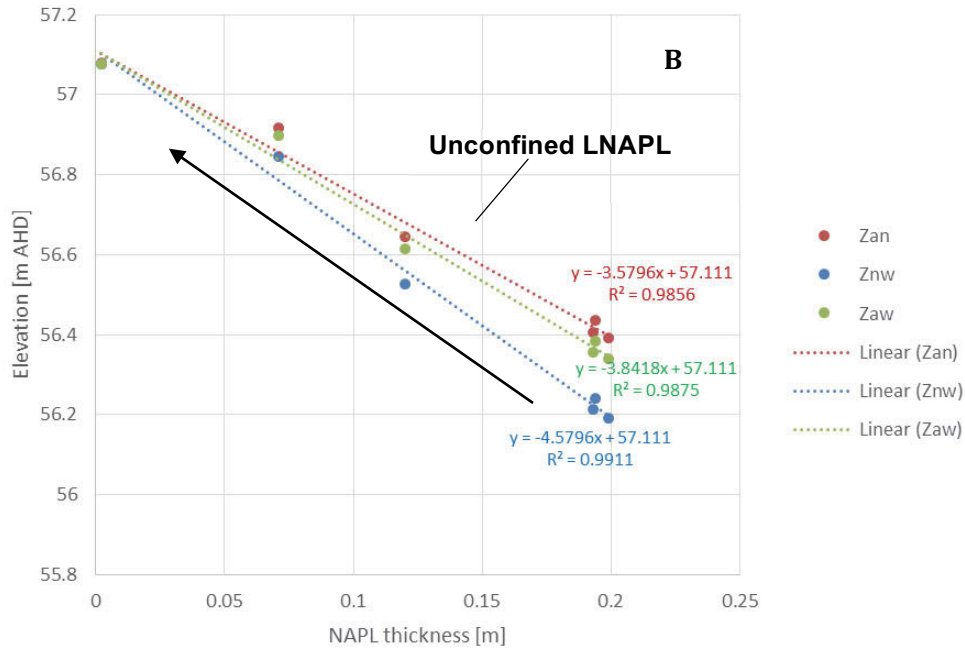


Figure 5. 4. Gauge thickness plot of the air-NAPL interface, LNAPL-water interface, and potentiometric surface elevations versus gauged LNAPL thickness for well PB29 (3/8/2014- 8/10/2015). The arrows show the trend of Z_{aw} with time.

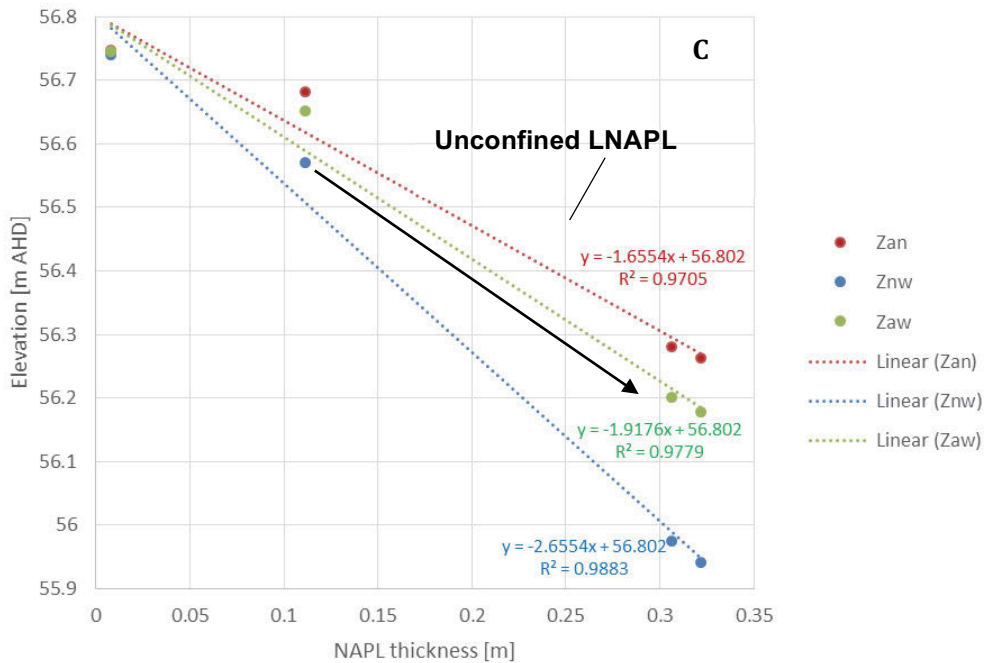


Figure 5. 5. Gauge thickness plot of the air-NAPL interface, LNAPL-water interface, and potentiometric surface elevations versus gauged LNAPL thickness for well PB29 (10/11/2015- 28/4/2016). The arrows show the trend of Z_{aw} with time.

Hydrostratigraph

Figure 5.6 shows the hydrostratigraph at well location PB29. The stratigraphic transition from sand (SP) to silty sand (SM) - silt (ML) was based on the stratigraphic core description of the well PB33 located 4 m away from PB29 (Figure B.3, Appendix B) and the HPT73 profile. According to the log description of the PB33 well, the transition point between sand (SP) and silty sand (SM) is at 56.85 m AHD and the transition from silty sand (SM) to silt (ML) takes place at 57.12 m AHD. On the other hand, the transition point at HPT73 profile between a coarse and a finer texture material (the distance between the HPT73 and PB29 is 1 meter) is located at 56.85 m AHD (Figure 5.7), with a coarser zone to be located just above it, in contrast with the transition of silty sand (SM) to silt (ML) as described at PB33 well. As a result, above elevation 56.85 m AHD, both silty sand (SM) and silt (ML) are presented, assuming the same materials with PB33 well location. The ground level elevation at PB29 well location is 61.23 m AHD, at HPT73 is 61.22 m AHD and at the location PB33 is 61.32 m AHD.

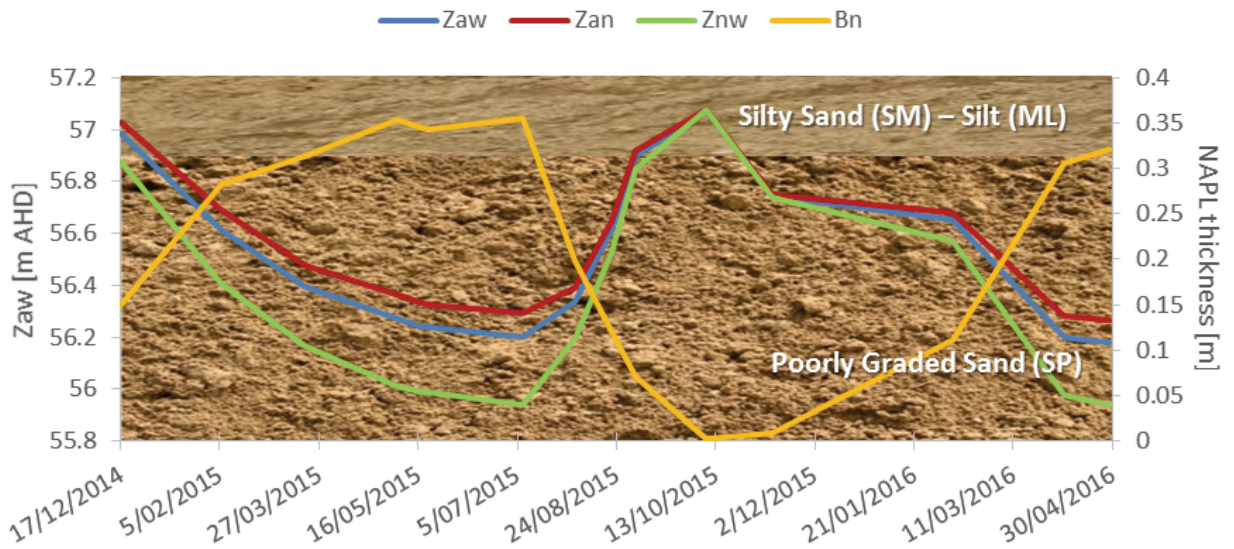


Figure 5. 6. A hydrostratigraph illustrating the in-well air-NAPL interface, LNAPL-water interface, the potentiometric surface elevation and the gauged LNAPL thickness in time including the stratigraphic description for well PB29 (17/12/2014- 28/4/2016).

NAPL saturations- HPT profile

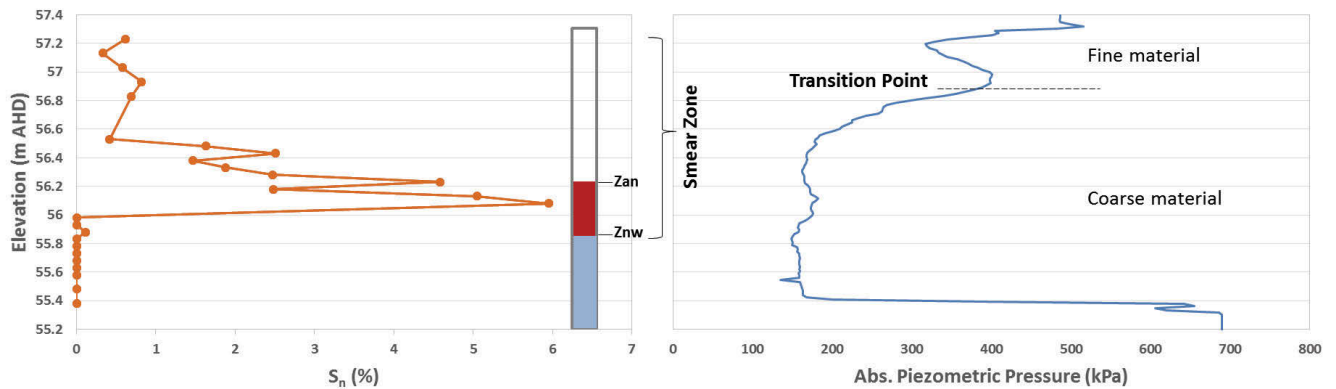


Figure 5. 7. NAPL saturations (MP50 location: 18/05/2016) along with in-well fluid elevations (well PB29: 17/05/2016) and HPT 73 (20/05/2016) profile at research area A, indicating the smear zone and the stratigraphic transition point at site of research. MP50 and HPT73 were installed 1.5 and 1.15 m respectively away from the presented well PB29.

NAPL saturations (S_n) obtained by soil coring at location MP50, are presented in Fig. 5.7. MP50 is located 1.5m away from PB29 well location. The graph depicts the smear zone (MP50 profile) and the stratigraphic transition point (HPT 73 profile). More details regarding the S_n calculations are presented at Table B.5 in Appendix B. No changes in water table elevation occurred between the periods presented in Figure 5.7 and therefore it is believed that the results are comparable.

It should be noticed that, the locations where residual and entrapped NAPL were present, are consistent with the history of fluid elevations. The transition from a coarse to a fine texture material takes place at 56.85 m AHD according to the HPT profile consistent with the stratigraphic log description and the gauge thickness plot's infection point. The highest elevation of presented NAPL saturations is at 57.20 m AHD. Also, the highest monitored Z_{an} elevation was at 57.10 m AHD (see Figure 5.6). According to the NAPL saturation profile, NAPL was detected (comprising mobile, residual and entrapped NAPL) from 55.9 to 57.20 m AHD indicating the smear zone. The lowest NAPL elevation (boundary) is consistent with the hydrostratigraph in Figure 5.6. The lowest monitored Z_{nw} elevation is 55.90 m AHD (Figure 5.6) a consistent value with Figure 5.7, explaining why (entrapped) NAPL is located down to this elevation (Newell 1995). In unconfined NAPL conditions (at equilibrium conditions), the apparent thickness is a good estimate of the mobile NAPL interval in the formation (Reyenga & Hawthorne 2011). Furthermore, the NAPL residual saturation distribution corresponds to the maximum product thickness (Charbeneau 2007b). The transition point at 56.85 m AHD

exhibits lower HPT absolute piezometric pressure values (~400 kPa) in comparison with the inflection point at PB27 well (~550 kPa) indicating a more permeable material at this elevation. This is the reason why PB29 contains consistently unconfined NAPL, due to the lower entry pressure of this material (Johnston 2010).

Interestingly, the LIF profiles in this area (Figures B. 10 – 11, Appendix B) revealed a narrow NAPL distribution (in a 12 cm interval) of high signal values. Taking into account that low NAPL saturations (soil coring) are present, the high LIF values may indicate a geological dissimilarity at this interval. In this case, this thin layer probably worked as a preferential migration pathway with coarser material and/or better connectivity restricting the NAPL vertical displacement. Interestingly, the soil description of MP50 core revealed a slightly coarser material between 56.12 and 56.27 m AHD.

Bail-down testing analysis

Figure 5.8 and illustrates an example of NAPL recovery during bail-down testing data. The analysis of the bail-down test can be seen in Appendix J. The baildown tests took place in a period of unconfined LNAPL conditions according to the diagnostic gauge plots and the presented hydrostratigraph above. More bail-down testing data can be seen in Appendix C. Baildown tests took place also during periods of high potentiometric surface elevation NAPL conditions presenting negligible recovery and as a result zero T_n values because of the NAPL entrapment phenomena (CL:AIRE 2014; Johnston 2010; Marinelli & Durnford 1996).

Figure 5.9 presents unconfined LNAPL conditions as constant NAPL discharge periods were not detected (Kirkman, Adamski & Hawthorne 2013). This outcome is consistent with the identification of unconfined conditions through the DGPs and hydrostratigraph. Regarding the bail-down test procedure, 2.85 L NAPL and 0.80 L water were removed. The initial NAPL thickness before the test was 0.322 m. The thickness after the removal of the product was 0.125m and the final thickness after 124min was 0.318 m, which is almost 100 % recovery of the initial product thickness. The recovery period (>95% recovery of apparent thickness) was ~ 23 min.

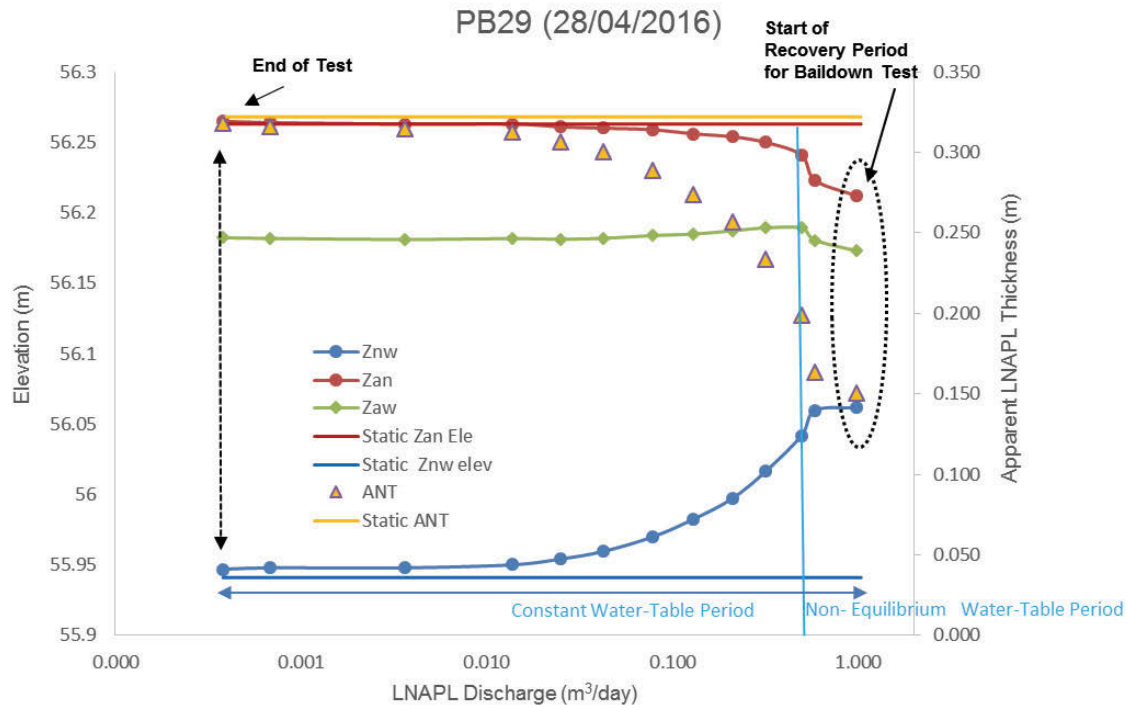


Figure 5. 8. Bailldown test results presenting the gauged referenced air-LNAPL (Z_{an}) and LNAPL-water interfaces (Z_{nw}), the potentiometric surface elevation (Z_{aw}), the apparent thickness (ANT) and the static elevations for Z_{an} , Z_{nw} and ANT vs. LNAPL discharge for well PB29.

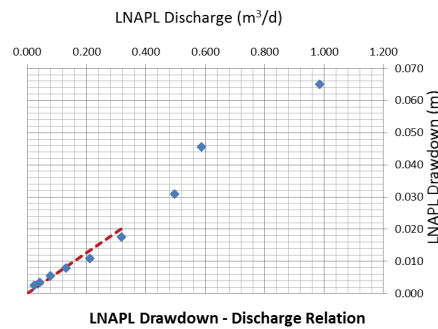


Figure 5. 9. LNAPL drawdown- discharge relation during bailldown testing.

Figure 5.9 illustrates the discharge versus drawdown relationship during the bailldown testing recovery. The plot shows that borehole recharge from the filter pack is not significant (large discharge value at the beginning of the recovery, $0.9 \text{ m}^3/\text{d}$). The formation and wellbore LNAPL fluids were initially in equilibrium thus, a drawdown correction was not applied to the data. Moreover, the figure depicts behaviour that maybe suggests unconfined LNAPL conditions because there is a continuously decreasing discharge with decreasing drawdown (API 2012; Hawthorne 2011b).

Summary of the results at area A

NAPL gauge thickness plots (Figures 5.2 - 5.5), a hydrograph (Figure 5.1), a hydrostratigraph (Figure 5.6), NAPL saturations – HPT profile (Figure 5.7), baildown testing recovery graphs and discharge versus drawdown plots (Figures 5.8 - 5.9) were presented for the identification of the LNAPL hydrogeological conditions at area A. The NAPL diagnostic plots were consistent with the all other lines of evidence presenting unconfined NAPL conditions.

5.1.2. LNAPL hydrogeological conditions in area B

NAPL gauge thickness plots

Figure 5.10 exhibits the gauge thickness plot of the tested well PB27. According to the graph, the change between the confined and unconfined NAPL layer (change between the Z_{an} slopes) is anticipated at ~ 56.8 m AHD. It should be noticed that there are data points ($b_n= 0.3$ m) that affect negatively the relationship of the tested parameters. No clear trends that may have an impact on the identification of NAPL hydrogeological conditions have been presented in the literature (Hartsock 2014; Kahraman 2013). Consequently, Figures 5.11 – 5.13 present gauge thickness plots for the same well after filtering the presented data in Figure 5.10 according to the different depicted Z_{aw} trends in Figure 5.1.

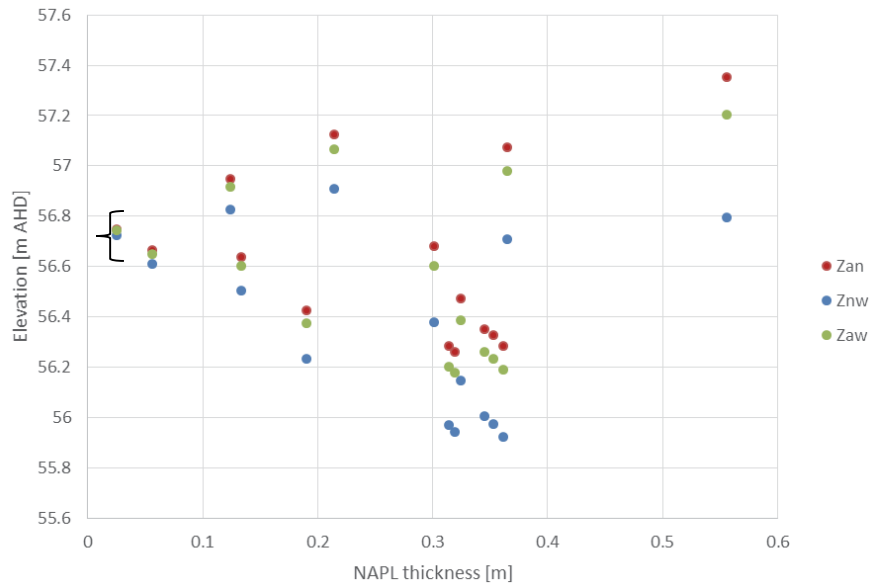


Figure 5. 10. Gauge thickness plot of the air-NAPL interface, LNAPL-water interface, and potentiometric surface elevations versus gauged LNAPL thickness for well PB27 (25/11/2014 - 24/4/2016).

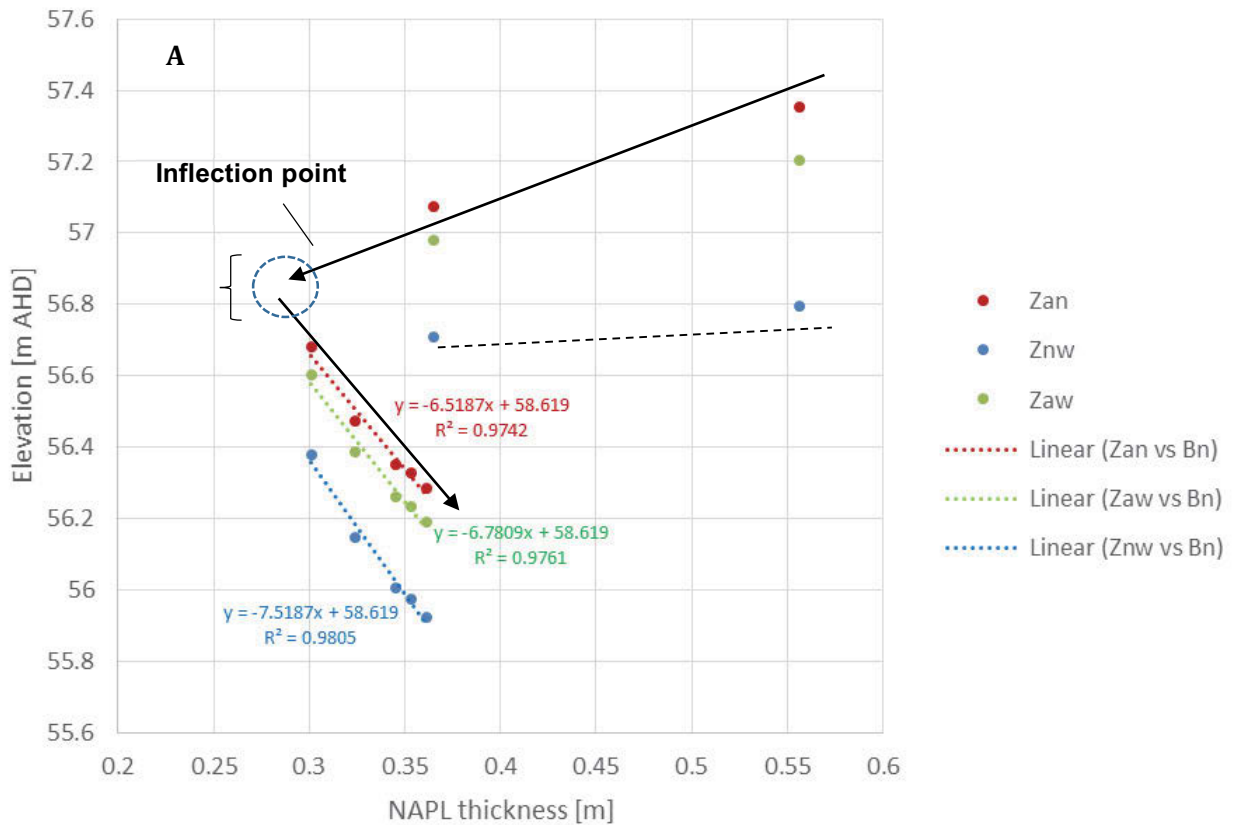


Figure 5. 11. Gauge thickness plot of the air-NAPL interface, LNAPL-water interface, and potentiometric surface elevations versus gauged LNAPL thickness for well PB27 (25/11/2014 - 14/ 7/2015). The arrows show the trend of Z_{aw} with time.

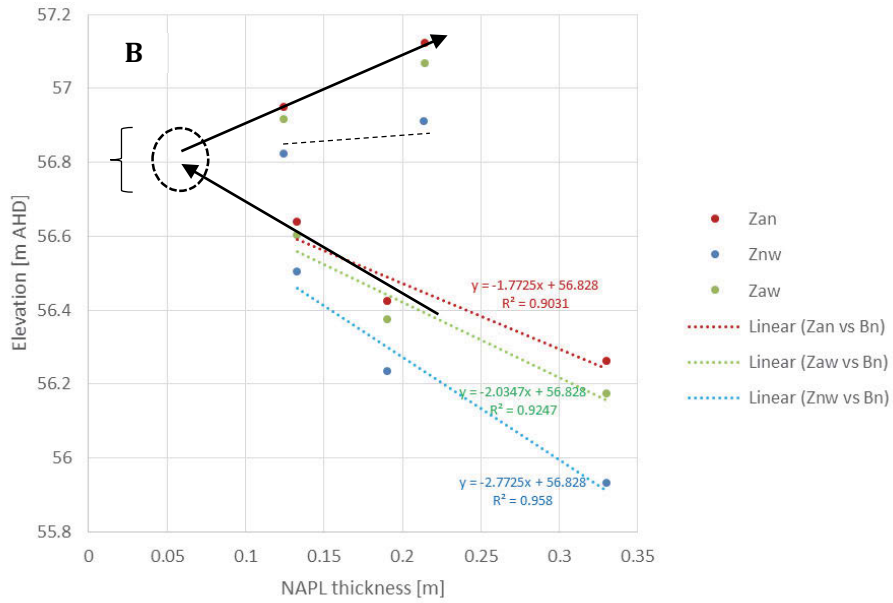


Figure 5. 12. Gauge thickness plot of the air-NAPL interface, LNAPL-water interface, and potentiometric surface elevations versus gauged LNAPL thickness for well PB27 (14/7/2015 - 8/10/2015). The arrows show the trend of Z_{aw} with time.

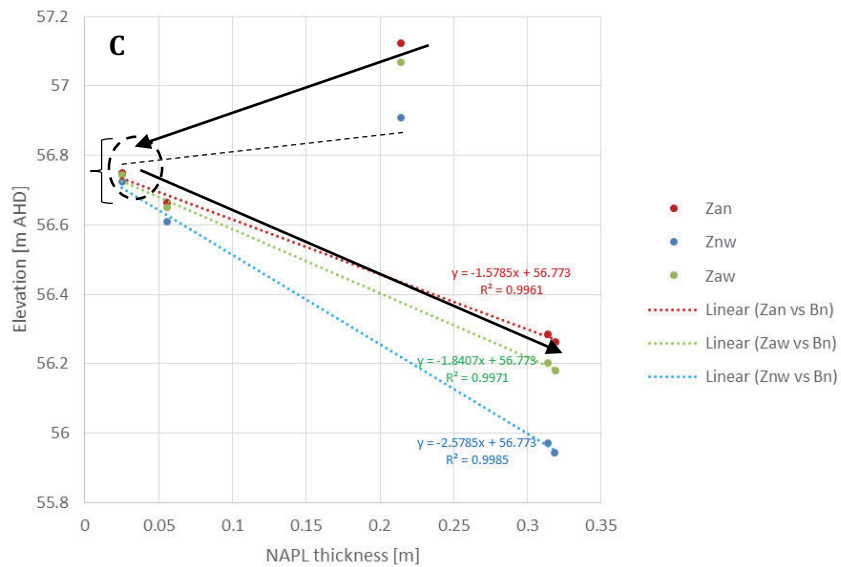


Figure 5. 13. Gauge thickness plot of the air-NAPL interface, LNAPL-water interface, and potentiometric surface elevations versus gauged LNAPL thickness for well PB27 (8/10/2015 - 28/4/2016). The arrows show the trend of Z_{aw} with time.

All the graphs indicate that there is a transition from unconfined to confined LNAPL conditions at elevations higher than 56.8 m AHD. The observation that both the potentiometric surface and the thickness in the well decrease for a stable Z_{nw} possibly indicates confined

LNAPL conditions (inflection point) (Hawthorne 2011a, 2011b; Kirkman, Adamski & Hawthorne 2013).

Hydrostratigraph

Figure 5.14 displays the hydrostratigraph at well location PB27. The stratigraphic transition from sand (SP) to clay (CH) was based on the stratigraphic core description of the well PB35 located 4 m away from PB27 due to a stratigraphic missing part in the log description of the PB27 well (Figure B.2, Appendix B). According to the log description of the PB35 well (Figure B.1, Appendix B), the transition point between sand (SW) and silt (ML) is at 56.75 m AHD. Even though, the transition (inflection) point at HPT74 profile (the distance between the HPT74 and PB27 is 1 meter) is at 56.60 m AHD (Figure 5.15), the transition elevation in Figure 5.14 is depicted at 56.75 m AHD (according to PB35 stratigraphic description) due to the fluid elevations and NAPL thickness behaviour which suggests unconfined NAPL conditions from 56.60 to 56.75 m AHD. The ground level elevation at PB27 well location is 61.15 m AHD and at the location of PB35 is 61.17 m AHD. Assuming the same stratigraphic transition at PB27 (SP material is depicted at elevations below 56.75 m AHD after core logging), the presented hydrostratigraph was designed.

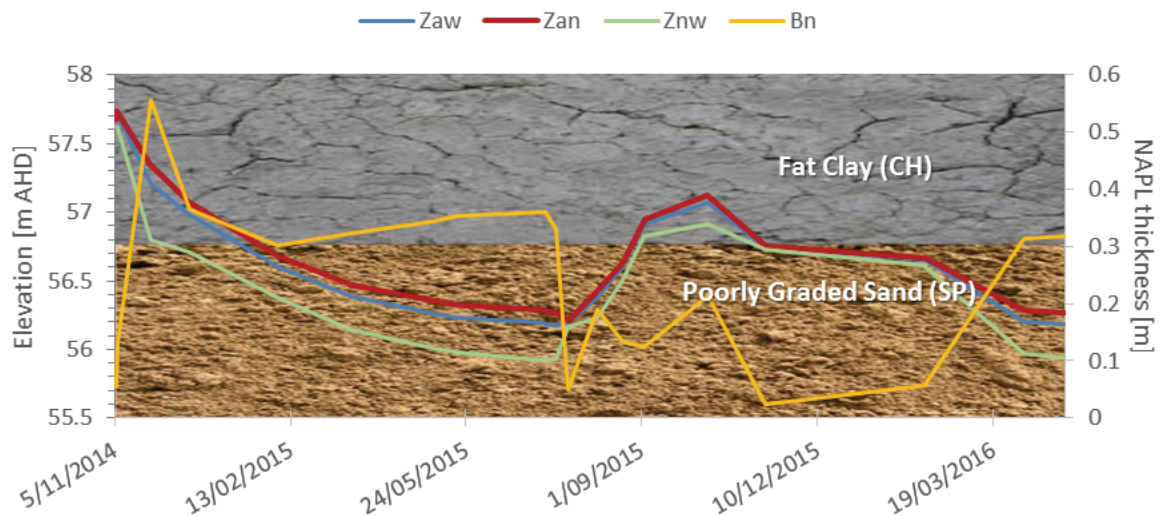


Figure 5. 14. A hydrostratigraph illustrating the in-well air-NAPL interface, LNAPL-water interface, the potentiometric surface elevation and the gauged LNAPL thickness in time including the stratigraphic description for site DK, well PB27 (5/11/2014- 28/4/2016).

Initially (11/2014- 02/2015), both the potentiometric surface and the thickness in the well are decreasing indicating confined LNAPL conditions. Moreover, the Z_{an} interface is above the confining layer showing a decreasing trend. In the next period (02/2015- 07/2015), the Z_{aw} , the Z_{nw} and the Z_{an} interfaces depicted a decreasing trend, however the apparent thickness slightly increased indicating unconfined NAPL conditions. The Z_{an} remained below the confining layer (56.8 m AHD). Between July and August 2015, two weeks skimming process took place resulting the thickness decline presented in the plot. From 8/2015 to 9/2015 Z_{aw} , Z_{nw} and Z_{an} increased. The thickness at the beginning of this period increased because of the product recovery after skimming and then decreased showing unconfined NAPL conditions. During the next illustrated time period (9/2015- 11/2015) Z_{an} interface was above the confining layer. At first stage, the potentiometric and the Z_{an} interfaces increased in parallel with the thickness in the well, while all together decreased indicating confined conditions. Finally, the period 11/2015- 4/2016 with Z_{an} being below the confining layer, the potentiometric surface, the Z_{nw} and the Z_{an} interfaces showed a decreasing trend, however the product thickness in the well increased indicating unconfined NAPL conditions (Hartsock 2014; Hawthorne 2011b; Kirkman, Adamski & Hawthorne 2013).

NAPL saturations- HPT profile

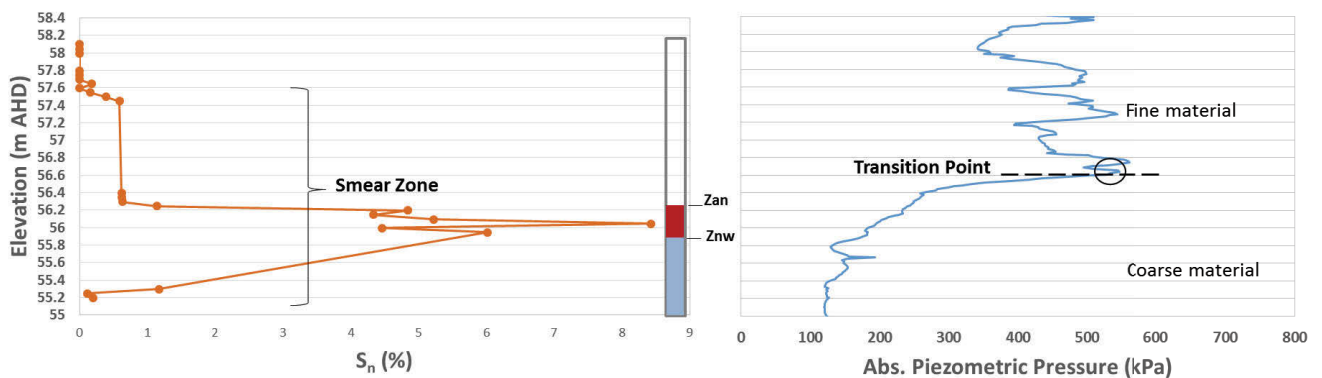


Figure 5. 15. NAPL saturations (MP58 well location: 18/05/2016) along with in-well fluid elevations (well PB27:18/05/2016) and HPT 74 (20/05/2016) profile at research area B, indicating the smear zone and the stratigraphic transition point at site of research. MP58 and HPT74 were installed 1.5 and 1.4 m respectively away from the presented well PB27.

NAPL saturations (S_n) obtained by soil coring at location MP58, are presented in Fig. 5.15. Details regarding the S_n calculations are presented at Table B.6 in Appendix B. MP58 is located 1.5m away from PB27 well location. Figure 5.15 depicts the smear zone (MP58 profile)

and the stratigraphic transition point (HPT 74 profile) close to PB27 well location. The transition from a coarse to a fine texture material takes place at 56.60 m AHD according to the HPT profile consistent with the stratigraphic log description and the gauge thickness plot's inflection point. It should be mentioned that changes in pressure depicted in HPT profiles are related qualitative to changes of intrinsic permeability. As it can be inferred from the graph, residual NAPL saturations were found until 57.63 m AHD that is consistent with the history of fluid elevations as presented in Fig. 5.14. NAPL saturations above the inflection point maybe indicate the existence of preferential pathways in the fine material (Adamski et al. 2005) or unconfined NAPL in the vicinity of the tested well. Furthermore, the presence of NAPLs at 56.60 m AHD (inflection point) is an indication of a confined NAPL period during the water table fluctuations (Hartsock 2014; Kahraman 2013; Kirkman, Adamski & Hawthorne 2013). Moreover, NAPL saturations, found until 55.23 m AHD indicate entrapped NAPL conditions. The lowest NAPL elevation (boundary) is not consistent with the hydrostratigraph in Figure 5.14. The lowest monitored Z_{nw} elevation is 55.9 m AHD. Possibly reasons can be related to the well development procedure inducing NAPL gradient during pumping water out of the well, and/or due to the existence of macropores. In the case of macropore networks, LNAPL can penetrate below the Z_{nw} , even without water table fluctuations (Adamski et al. 2005).

Bail-down testing analysis

Figures 5.16 illustrates NAPL recovery during bail-down testing data. The baildown test took place in a period of unconfined LNAPL conditions according to the diagnostic gauge plots and the presented hydrostratigraph above. More bail-down testing data regarding this well can be seen in Appendices C and J. At Z_{nw} 56.05 m AHD, a constant discharge rate is depicted (for a time period of more than 20 min) possibly because of geologic heterogeneity at this point. Constant discharge periods is an indication of potential confined NAPL conditions (API 2012; Kirkman, Adamski & Hawthorne 2013) however, Figures 5.11 – 5.13 suggest unconfined NAPL conditions for the specific time period. Moreover, the constant discharge period takes place at the end of the recovery test, at $Z_{nw} \sim 56.05$ m AHD, whereas the inflection point is located at 56.60-56.80 m AHD.

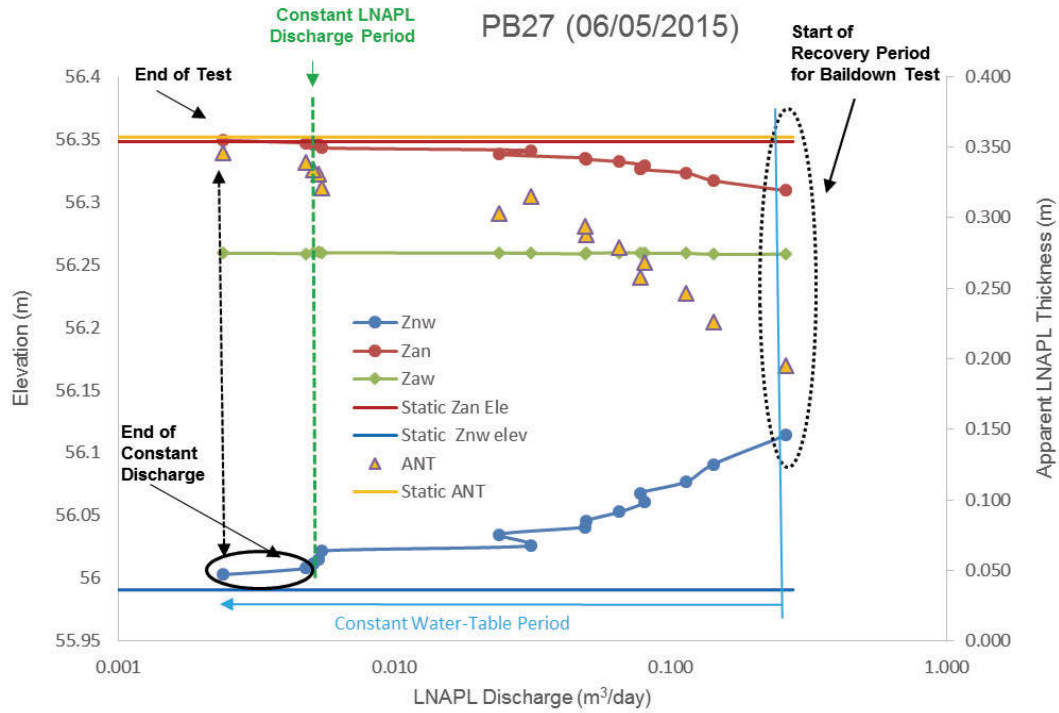


Figure 5. 16. Bardown test results presenting the gauged referenced air-LNAPL (Z_{an}) and LNAPL-water interfaces (Z_{nw}), the potentiometric surface elevation (Z_{aw}), the apparent thickness (ANT) and the static elevations for Z_{an} , Z_{nw} and ANT vs. LNAPL discharge for well PB27.

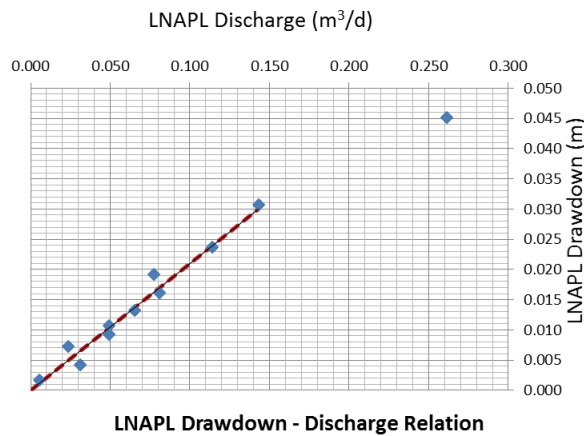


Figure 5. 17. LNAPL drawdown- discharge relation during bardown testing. After a drawdown adjustment of 0.0043 m.

Figure 5.17 illustrates the discharge versus drawdown relationship during the bardown testing recovery. The plot displays that borehole recharge from the filter pack is not significant (large discharge value at the beginning of the recovery) (API 2012). The formation and wellbore LNAPL fluids were initially in non-equilibrium thus, a drawdown correction (0.0043

m) was applied to the data. Furthermore, the figure depicts behaviour that suggests unconfined LNAPL conditions because a continuously decreasing discharge with decreasing drawdown is illustrated (API 2012; Hawthorne & Kirkman 2011; Kirkman, Adamski & Hawthorne 2013).

Summary of the results at area B

NAPL gauge thickness plots (Figures 5.10 – 5.13), a hydrostratigraph (Figure 5.14), NAPL saturations - HPT profiles (Figure 5.15), baildown testing recovery graphs and discharge versus drawdown plots (Figures 5.16 and 5.17) were presented for the identification of the LNAPL hydrogeological conditions at the tested well location PB27. According to the diagnostic gauge plots, the transition point between confined and unconfined NAPL is around 56.8 m AHD, a value consistent with the range of 56.60-56.75 m AHD (transition elevation from coarse to fine texture material) as presented by the other lines of evidence.

5.1.3. LNAPL hydrogeological conditions in area C

NAPL gauge thickness plots

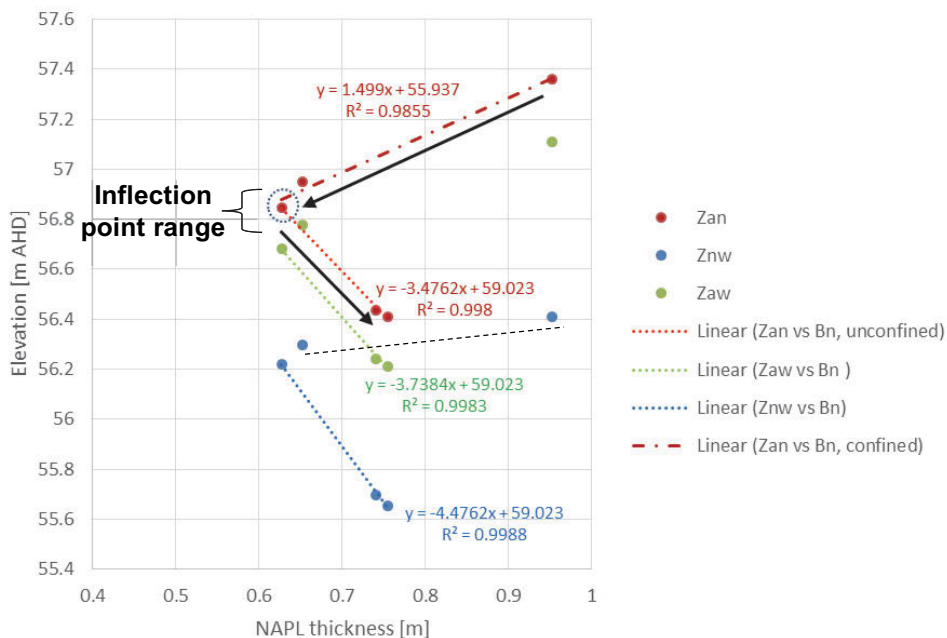


Figure 5. 18. Gauge thickness plot of the air-NAPL interface, LNAPL-water interface, and potentiometric surface elevations versus gauged LNAPL thickness for well PB40 (8/10/2015- 28/4/2016). The arrows show the Z_{aw} elevation with time.

Figure 5.18 exhibits the gauge thickness plot for the well PB40 during a drainage period. The graph presents both confined and unconfined LNAPL conditions. The transition between confined and unconfined NAPL conditions is anticipated to be at around 56.7 - 56.8 m AHD. At elevations higher than 56.7 m AHD, a positive relationship between Z_{an} and b_n (indicative of NAPL confined conditions) is presented in the hydrograph of Figure 5.19.

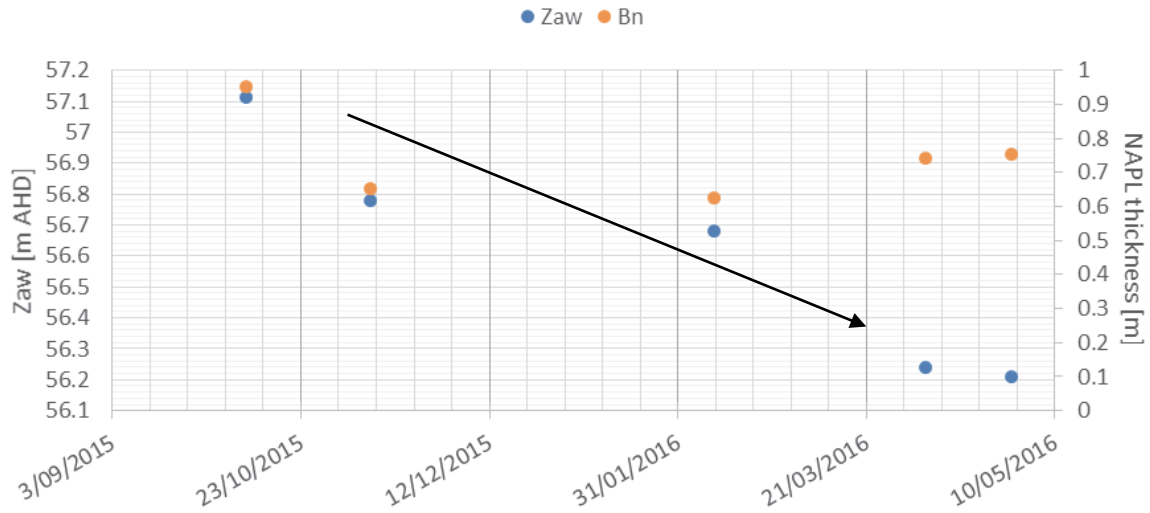


Figure 5. 19. Hydrograph plot of the potentiometric surface elevations versus gauged LNAPL thickness for well PB40 (8/10/2015-28/4/2016). The arrow shows how Z_{aw} changes with time.

Hydrostratigraph

Figure 5.20 presents the hydrostratigraph at well location PB40. The stratigraphic transition from well graded (SW) -silty sand (SM) to silt (ML) was based on the stratigraphic core description of the well PB39 located 4 m away from PB40 (Figure B.4, Appendix B) and on the HPT60, HPT62 profiles. According to the log description of the PB39 well, the transition point between well graded (SW) -silty sand (SM) and silt (ML) is at 56.70 m AHD. On the other hand, the transition point at HPT60 profile (located 2 m away from PB40) between a coarse and a finer texture material is located at 56.55 m AHD and the transition point at HPT62 profile (located 2 m away from PB40) is located at 56.80 m AHD (Figure 5.21). The remediation well PB40 is located between HPT60 and HPT62 anticipating (assuming) a transition point elevation between the transition points of these two HPT profiles. Taking also into consideration the assumption that the same materials with PB39 well exist at PB40 location, the hydrostratigraph in Figure 5.20 is plotted. The transition point is at 56.8 m AHD according the behaviour of the fluid levels under confined and unconfined NAPL periods. The ground

level elevation at PB40 well location is 61.36 m AHD, at HPT60 is 61.29 m AHD, at HPT62 is 61.31 m AHD and at the location PB39 is 61.40 m AHD.

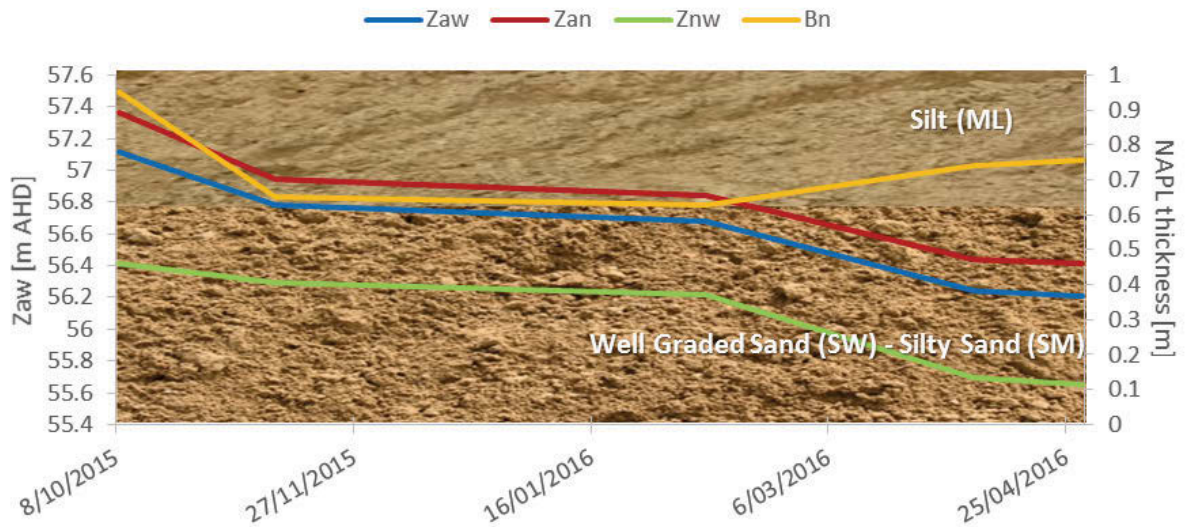


Figure 5. 20. A hydrostratigraph illustrating the air-NAPL interface, LNAPL-water interface, the potentiometric surface elevation and the gauged LNAPL thickness in time including the stratigraphic description for well PB40 (8/10/2015- 28/4/2016).

NAPL saturations- HPT profiles

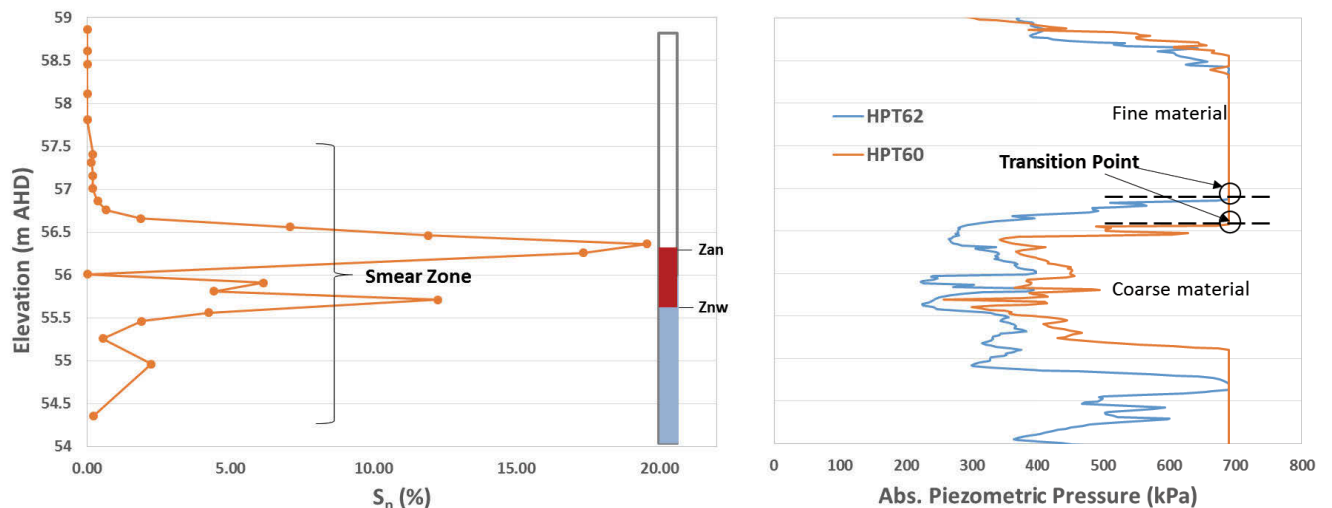


Figure 5. 21. NAPL saturations (MP44 location: 18/05/2016) along with in-well fluid elevations (well PB40: 18/05/2016) and HPT 60, HPT62 (20/05/2016) profiles at research area C, indicating the smear zone and the stratigraphic transition point at site of research. MP44, HPT60 and HPT62 were installed 1.3, 1.85 and 2.0 m respectively away from the presented well PB40.

S_n obtained by soil coring at location MP44, are presented in Fig. 5.21. Details regarding the S_n calculations are presented at Table B.7 in Appendix B. MP50 is located 1.3 m away from PB40 well location. The graph exhibits the smear zone and the stratigraphic transition points (HPT60, HPT62 profiles) close to PB40 well location. The transition from a coarse to a fine texture material takes place at 56.55 m AHD according to the HPT60 profile consistent with the stratigraphic log description and the inflection point in the diagnostic gauge plot. HPT62 revealed a transition at 56.80 m AHD, 25 cm higher than the inflection point elevation at HPT60 location. NAPL saturations were measured (comprising mobile, residual and entrapped NAPL) from 54.36 to 57.41 m AHD. The highest NAPL saturation elevation is at ~ 57.4 m AHD consistent with the highest monitored Z_{an} elevation at 57.40 m AHD (see Figure 5.20). The presence of NAPL in the unsaturated zone (from 56.50 to 57.40 m AHD) can be explained probably due to preferential macropore networks existence (Adamski et al. 2005; Totsche et al. 2003). The lowest NAPL elevation (boundary) is not consistent with the hydrostratigraph in Figure 5.20. This could be due to pumping tests conducted at this area before the soil coring procedure.

Bail-down testing analysis

Figure 5.22 illustrates a discharge versus drawdown relationship during bail-down testing (see also Appendix J) at PB40 well. The baildown test took place in periods of unconfined LNAPL conditions according to the diagnostic gauge plot and the hydrostratigraph presented above. The outcome of the next figure, that is unconfined LNAPL conditions, is consistent with the aforementioned findings of the other lines of evidence.

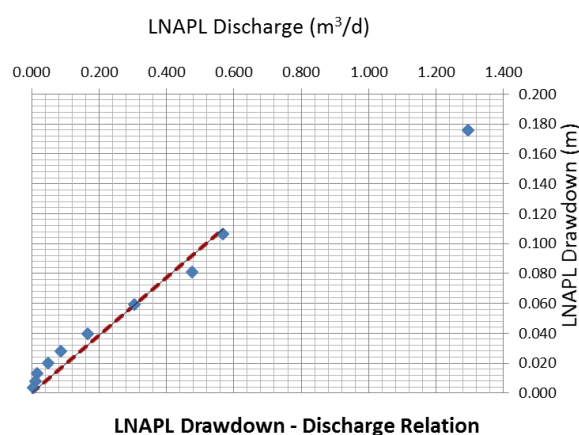


Figure 5. 22. LNAPL drawdown- discharge relation during baildown testing depicting unconfined NAPL conditions (06/04/2016).

Summary of the results at area C

A NAPL gauge thickness plot (Figure 5.18), a hydrograph (Figure 5.19), a hydrostratigraph (Figure 5.20), NAPL saturations - HPT profiles (Figure 5.21) and a discharge versus drawdown plot 5.22 were presented for the identification of the LNAPL hydrogeological conditions at the tested well location PB40. According to the diagnostic gauge plot, the transition point between confined and unconfined NAPL is at around 56.7- 56.8 m AHD, a value consistent with the range 56.55 - 56.8 m AHD as presented by the other lines of evidence.

5.2. Spatial Variability of LNAPL Saturation

NAPL saturations at well locations MP50 (Area A), MP58 (Area B) and MP44 (Area C) along with in-well thicknesses (wells: PB29, PB27 and PB40) are depicted in Figure 5.23. As it can be seen the three areas of research presented different vertical NAPL distributions and saturation values which are depended on the soil properties and the NAPL accumulation (which is unknown) at each location (Huntley, Hawk & Corley 1994; Illangasekare, Armbruster & Yates 1995; Jeong & Charbeneau 2014; Waddill & Parker 1997). The highest saturations were located in the mobile interval between the Z_{an} and Z_{nw} elevations and somewhat above the Z_{an} elevation at the top capillary fringe (Huntley & Beckett 2002).

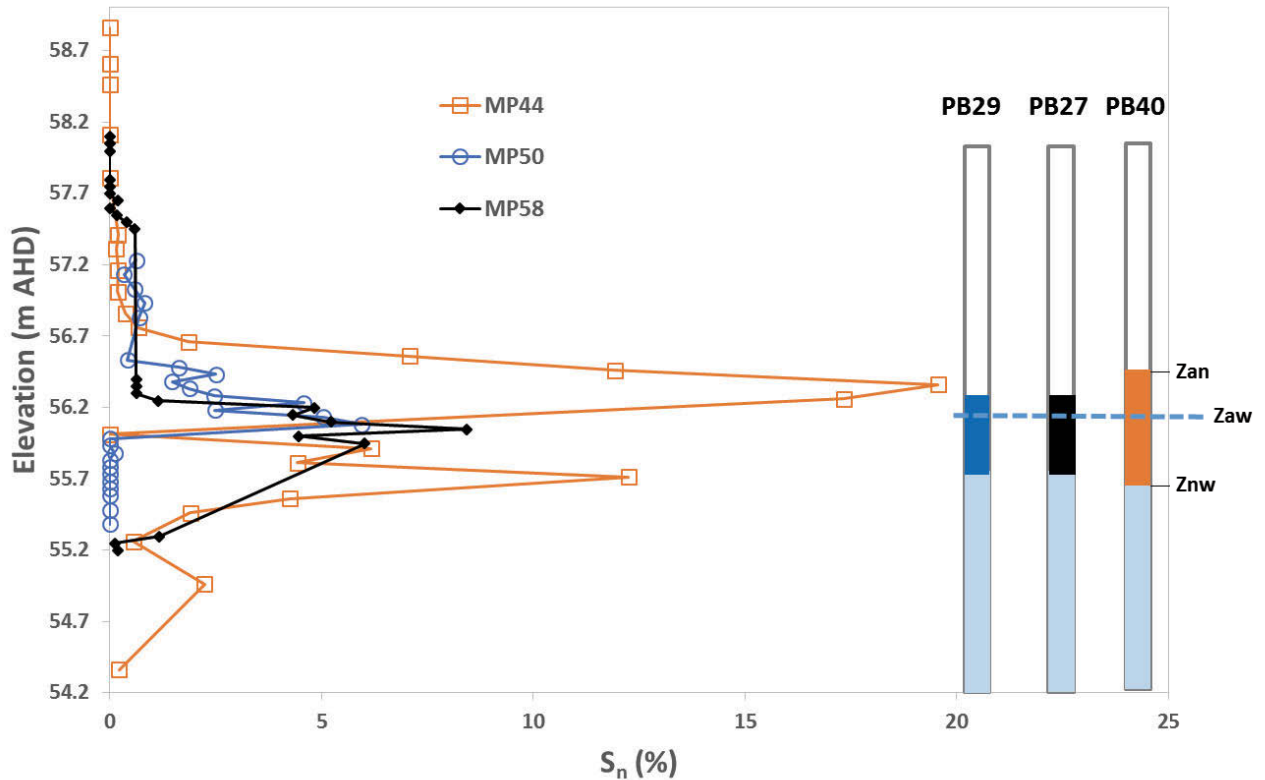


Figure 5.23. NAPL saturations at well locations MP50 (Area A), MP58 (Area B) and MP44 (Area C) along with in-well thicknesses (wells: PB29, PB27 and PB40) at the site of research (17-18/05/2016).

Vertical NAPL distribution

Figure 5.23 corresponds to unconfined NAPL conditions and low potentiometric surface elevations, in all the research areas. The MP44 well location presented a vertical NAPL distribution profile similar to the presented heterogeneous case with fine and coarse layers in the literature (Huntley, Hawk & Corley 1994). Variations in NAPL saturations were correlated qualitatively with variations in the geological material (see Figure 5.24). Intervals that presented high NAPL saturation values correspond to low piezometric pressure values in the HPT profile. This consistency between piezometric pressure values and NAPL saturation measures can be seen in the next graph. On the other hand, areas A and B (see Figures 5.7 and 5.15) illustrated vertical NAPL distributions similar to homogeneous cases that have been documented in the literature (Farr, Houghtalen & McWhorter 1990; Lenhard & Parker 1990). Consequently, in heterogeneous settings the stratigraphy may override typical smearing (redistribution) patterns related to homogeneous systems.

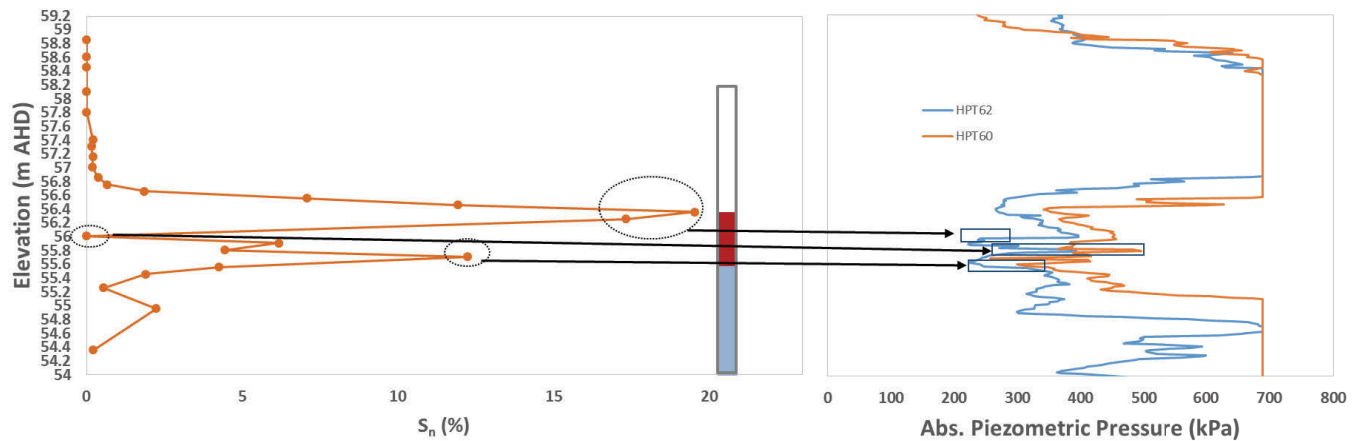


Figure 5. 24. Correlation between geological material and NAPL saturation.

Area C presented the highest NAPL saturation values (19.6%) in the mobile interval, among the other research areas (5.95% at area A and 8.43% at area B), indicating a higher NAPL accumulation. Area C presented also the highest in-well thickness the day of cores' extraction. b_n at PB40 well was 0.76 m whereas, wells PB29 and PB27 presented the same in-well thickness of 0.32 m. Furthermore, the NAPL mobile interval at area C was located in a finer texture material than in the other two areas. More specifically, the soil material at area C was well graded (SW) and silty sand (SM) with measure absolute HPT piezometric pressures of 220 - 500 kPa in the HPT profiles (see Figures 5.20 and 5.21). The soil material at area A was poorly graded sand (SP) with piezometric pressure values between 180 and 200 kPa (see Figures 5.6 and 5.7). Finally, the material at area B was the same with area A but it presented slightly higher piezometric pressure values of 180 - 250 kPa (see Figures 5.14 and 5.15).

Residual NAPL saturation

It can be inferred from Fig. 5.23 that, residual and entrapped NAPL saturations smaller than 5.95%, 8.43% and 19.6% are expected at areas A, B and C, respectively. These values are not in line with the literature (Mercer & Cohen 1990) where there is documentation of residual LNAPL saturation laboratory values ranging from 10% to 20% for the unsaturated zone and 15% to 50% for the saturated zone. It should be noted that, the usefulness of the aforementioned laboratory values have been questioned by researchers as they are much higher than the maximum LNAPL saturation values found at LNAPL contaminated sites (Adamski, Kremesec & Charbeneau 2005; Charbeneau 2007b). More specifically, in fine grained sites, maximum LNAPL saturations of only 7.6% (Adamski, Kremesec & Charbeneau 2005) and <2% (Adamski et al. 2005) have been documented. The NAPL saturation values of

this study are in agreement with the aforementioned field reported values. Thus, literature values should be used with caution as they do not capture important site specific data, such as the loading history of the LNAPL zone and the importance of large pores in the NAPL migration (Los Angeles LNAPL Working Group 2011).

Fine materials can present higher entrapped NAPL saturations than coarser materials (Charbeneau et al. 2000). MP44 well location in area C, depicts higher entrapped NAPL saturations below Z_{nw} (as well, below Z_{aw} higher NAPL entrapped saturations are expected) in comparison to the other two areas, with respect to the unknown NAPL specific volume (NAPL accumulation) at each location (Huntley, Hawk & Corley 1994). In addition, higher initial NAPL saturations result in higher entrapped saturation values (Johnston & Adamski 2005), thus higher entrapped NAPL saturations are anticipated at area C, as it depicts the higher NAPL saturation values in the mobile interval, assuming that this value was the maximum saturation value historically. Entrapped depicted NAPL saturation values at area B (2%) and C (~5%) can be related to a *f-factor* of ~0.23 that corresponds to the Safety Bay Sand (fine-to-medium sand), as it has been documented in the literature (Charbeneau 2007b; Johnston & Adamski 2005; Steffy, Barry & Johnston 1997).

NAPLs in elevations higher than the Z_{an} may be characterized as residual as they cannot move due to capillary pressure barriers. Area C presented the lowest residual NAPL saturations (above Z_{an}) due to the finer texture material at these elevations compared to the other two areas (Huntley, Hawk & Corley 1994) (see Figures 5.7, 5.15 and 5.21 where the presented piezometric pressures measured by HPT at area C were 700 kPa and at area A and B were <600 kPa). As it has been stated, the threshold NAPL entry pressure for fine texture materials is higher than in coarser materials (Adamski et al. 2005; Mercer & Cohen 1990). In addition, under equilibrium conditions, low (composition) values of C_4 - C_5 (possibly due to volatilization) above Z_{an} are maybe another evidence of residual product that is in contact with air (see Tables B.8 - 10 in Appendix B). Thus, it can be inferred that, area A may present NAPL residual saturation values in the range of 0.6 – 2.5%, area B from 0.1 to 0.16% and area C between 0.08 and 12%. Accurate saturation values of residual NAPL can be provided through capillary pressure-saturation curves. In addition, dissolved and sorbed chemical concentrations of different components presented in the NAPL mobile interval at the three research areas are presented in Tables B.11 - B.28 in Appendix B. Results indicated that dissolved and sorbed concentrations were quite low and they are a very small fraction (less than 1%) of the total TPH values measured in the cores. Thus, the error of using Equation 4 neglecting equilibrium partitioning was < 1%. One of the reasons is the low organic carbon present in the studied area (see Table B.31, Appendix B). It should also be noticed that the low-end S_n values were affected more from partitioning than the high S_n values in the mobile interval (see Tables B.16, B.19 and B. in Appendix B) as it has been documented also in the

literature (Rivett, Dearden & Wealthall, 2014). The equilibrium dissolved concentrations for benzene were in the range 2-4.5 mg/L, which is consistent with the values presented by ITRC of 1-5 mg/L as indicative of potential LNAPL presence (ITRC, 2018). Finally, extraction of cores in a close distance and LIF profiles, were used to minimize potential issues of representativeness of the analysed soil samples, as discussed in section 3.2.

5.3. LDRM Simulation and Theoretical T_n Estimation

This section presents the verification of LDRM simulation through theoretical and field based T_n estimations. LDRM model and theoretical T_n calculations were used to show the impact of geological heterogeneity on LNAPL mobility in the three research areas during unconfined LNAPL conditions. LDRM simulations and theoretical T_n calculations took place at areas A, B and C and are referred to the coring day of the monitoring wells: MP50, MP58 and MP44 on 20th of May 2016. Bail-down tests were conducted also this period of time, thus field based T_n values were calculated. Tables 5.1, 5.2 and 5.3 depict the input parameters for each research area. It should be acknowledged the uncertainty of some input parameters in the model. Best estimates from recognized databases given the limited site specific measured data were used. More specifically, the determination of input parameters was based on: 1) known input values, 2) estimated values based on soil and fluid characteristics in the API database (American Petroleum Institute 2000) and CRC CARE Technical report no. 18 (Johnston 2010).

Table 5. 1. Input parameters for area A.

Research Area A- PB29 Remediation well			
Parameter	Value	Source	Notes
Max Monitoring LNAPL Thickness (m)	0.324	Gauging data, Core saturation data, LIF	
Ground surface elevation (m)	61.087	Gauging data	
Water table elevation (m)	56.150	Gauging data	
Water vertical gradient	0.000	LDRM Default	

LNAPL density (g/cm ³)	0.740	Gauging data	
LNAPL viscosity (cp)	0.480	Gauging data	
Air/water surface tension (dyne/cm)	65.000	CRC CARE report no. 18	Average for gasoline
Air/LNAPL surface tension (dyne/cm)	20.500	CRC CARE report no. 18	Average for gasoline
LNAPL/water interfacial tension (dyne/cm)	22.900	CRC CARE report no. 18	Average for gasoline
Soil Characteristics			
Porosity	0.41	API Database	Average for SP
Hydraulic conductivity (m/d)	13	HPT	
Van Genuchten N	3.17	API Database	Average for SP
Van Genuchten α (m ⁻¹)	1.85	API Database	Average for SP
Irreducible water saturation	0.209	API Database	Average for SP
Residual LNAPL saturation	0.010	Core data, f-factor	
Permeability model	Mualem	LDRM Default	

Table 5. 2. Input parameters for area B.

Research Area B- PB27 Remediation well			
Parameter	Value	Source	Notes
Max Monitoring LNAPL Thickness (m)	0.324	Gauging data, Core saturation data, LIF	

Ground surface elevation (m)	60.993	Gauging data	
Water table elevation (m)	56.150	Gauging data	
Water vertical gradient	0.000	LDRM Default	
Elevation of soil faces interface 1 (m)	56.600	Core data	
Elevation of soil faces interface 2 (m)	56.200	Core data	
LNAPL density (g/cm ³)	0.740	Gauging data	
LNAPL viscosity (cp)	0.480	Gauging data	
Air/water surface tension (dyne/cm)	65.000	CRC CARE report no. 18	Average for gasoline
Air/LNAPL surface tension (dyne/cm)	20.500	CRC CARE report no. 18	Average for gasoline
LNAPL/water interfacial tension (dyne/cm)	22.900	CRC CARE report no. 18	Average for gasoline
Soil Characteristics for layer 1			
Porosity	0.43	API Database	Average for CL
Hydraulic conductivity (m/d)	8.00	HPT	
Van Genuchten N	2.20	API Database	Average for CL
Van Genuchten α (m ⁻¹)	0.29	API Database	Average for CL
Irreducible water saturation	0.34	API Database	Average for CL
Residual LNAPL saturation	0.010	Core data	
Permeability model	Mualem	LDRM Default	
Soil Characteristics for layer 2			
Porosity	0.38	After LDRM calibration	Average for SW-SM

Hydraulic conductivity (m/d)	8.00	HPT	
Van Genuchten N	3.55	API Database	Average for SW-SM
Van Genuchten α (m^{-1})	1.38	API Database	Average for SW-SM
Irreducible water saturation	0.19	API Database	Average for SW-SM
Residual LNAPL saturation	0.00		
Permeability model	Mualem	LDRM Default	
Soil Characteristics for layer 3			
Porosity	0.40	API Database	Average for SW (the usage of SP material showed zero T_n values)
Hydraulic conductivity (m/d)	8.00	HPT	
Van Genuchten N	1.38	API Database	Average for SW
Van Genuchten α (m^{-1})	3.55	API Database	Average for SW
Irreducible water saturation	0.34	API Database	Average for SW
Residual LNAPL saturation	0.010	Core data, f-factor	
Permeability model	Mualem	LDRM Default	

Table 5. 3. Input parameters for area C.

Research Area C- PB40 Remediation well			
Parameter	Value	Source	Notes
Max Monitoring LNAPL Thickness (m)	0.750	Gauging data, Core saturation data, LIF	
Ground surface elevation (m)	61.282	Gauging data	
Water table elevation (m)	56.155	Gauging data	

Water vertical gradient	0.000	LDRM Default	
Elevation of soil faces interface 1 (m)	56.055	Core data	
Elevation of soil faces interface 2 (m)	55.970	Core data	
LNAPL density (g/cm ³)	0.740	Gauging data	
LNAPL viscosity (cp)	0.480	Gauging data	
Air/water surface tension (dyne/cm)	65.000	CRC CARE report no. 18	Average for gasoline
Air/LNAPL surface tension (dyne/cm)	20.500	CRC CARE report no. 18	Average for gasoline
LNAPL/water interfacial tension (dyne/cm)	22.900	CRC CARE report no. 18	Average for gasoline
Soil Characteristics for layer 1			
Porosity	0.45	API Database	Average for SW
Hydraulic conductivity (m/d)	1.83	HPT	
Van Genuchten N	1.38	API Database	Average for SW
Van Genuchten α (m ⁻¹)	3.55	API Database	Average for SW
Irreducible water saturation	0.34	API Database	Average for SW
Residual LNAPL saturation	0.03	Core data	
Permeability model	Mualem	LDRM Default	
Soil Characteristics for layer 2			
Porosity	0.41	After LDRM calibration	Average for SW-SM
Hydraulic conductivity (m/d)	0.03	HPT	
Van Genuchten N	3.55	API Database	Average for SW-SM
Van Genuchten α (m ⁻¹)	1.38	API Database	Average for SW-SM

Irreducible water saturation	0.19	API Database	Average for SW-SM
Residual LNAPL saturation	0.04		
Permeability model	Mualem	LDRM Default	
Soil Characteristics for layer 3			
Porosity	0.41	API Database	Average for SW
Hydraulic conductivity (m/d)	1.83	HPT	
Van Genuchten N	1.38	API Database	Average for SW
Van Genuchten α (m^{-1})	3.55	API Database	Average for SW
Irreducible water saturation	0.34	API Database	Average for SW
Permeability model	Mualem	LDRM Default	

As maximum thickness, the b_n value the day of coring was used. Under unconfined LNAPL conditions, this value is an indication of the mobile interval assuming vertical equilibrium conditions that is when there is balance between the vertical pressure gradient and gravity (Kirkman, Adamski & Hawthorne 2013). Furthermore, it was the highest apparent thickness value under unconfined NAPL conditions at the lowest Z_{aw} . NAPL saturation values above the Z_{an} comprise product that cannot enter into the well as the capillary pressure between air-NAPL ($P_{c,an}$) is zero at Z_{an} . It should be noticed also that the van Genuchten “N” values in the API database have been derived using the Mualem expression (Charbeneau 2007a). It should be noted that, vertical equilibrium assumptions (see section 3.7) are crucial for the modelled system (Charbeneau 2007a), although they are frequently not fully met under transient conditions in the field (ASTM 2013). The time period of low and relatively constant Z_{aw} (via frequent monitoring of fluid levels) was the base to assume vertical equilibrium conditions. In addition, soil coring along with HPT-LIF profiles were used for the identification of the NAPL mobile interval. The next section presents the LDRM simulations and T_n theoretical calculations at areas B, C and A.

Area B

Area B was simulated by using three different soil layers (CL, SW - SM, SW) according to Figure 5.25. The hydraulic conductivity value was 8 m/d, as it was indicated by the HPT tool (see Fig. B.18, Appendix B). It was assumed that the hydraulic conductivity in the SW and SW-SM intervals (where the mobile interval is anticipated to be) was similar. The b_n value was 0.324 m. The van Genuchten parameters were determined as average values of the three different materials using the API database. The predicted NAPL saturation values were consistent with the field measured NAPL saturation values using the mentioned average van Genuchten parameters. The predicted T_n value was 0.32 m²/d in agreement with the field measurement of 0.5 m²/d. Fig 5.26 illustrates the saturation and NAPL relative permeability profiles after LDRM calibration.

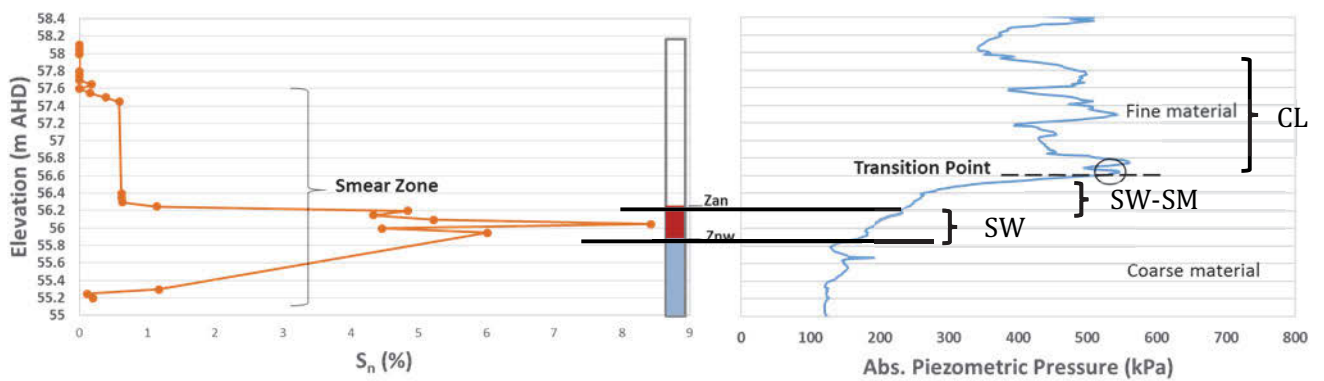


Figure 5. 25. The three simulated layers at area B.

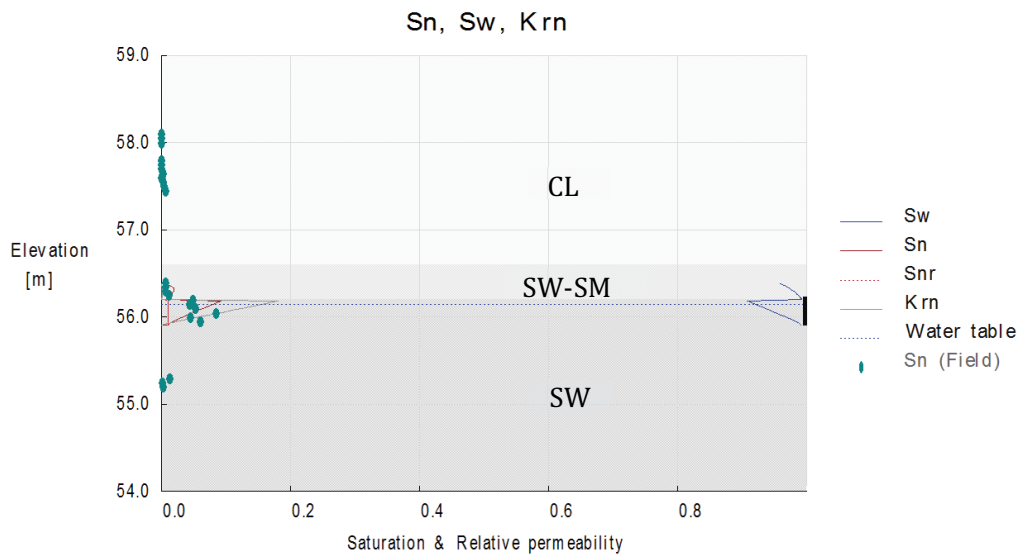


Figure 5. 26. NAPL saturation and NAPL relative permeability profiles.

Theoretical T_n estimation

Theoretical LNAPL transmissivity estimations corresponded to Fig 5.27 are presented in this section (Table 5.4). As it can be seen in the next table, the T_n theoretical estimation showed a good agreement with the field measured T_n value. T_n was estimated by using the Equation 16. The theoretical T_n estimation took place in the SW zone at elevations below 56.2 m AHD. Fig 5.27 presents 6 intervals (zones) indicating the mobile interval in the formation close to PB27 well. The last measured NAPL saturation value at core MP58 is at 55.94 m AHD and the next measured value at 55.29 m AHD. Thus, it was assumed that zone 6 is 7.4 cm as there is not other measured saturation values between 55.94 - 55.29 m AHD. In this case, it was assumed that the thickness in the well was similar to the thickness in the formation (0.324 m as the simulated periods refers to unconfined LNAPL conditions). This assumed mobile interval thickness was consistent also with the LIF 51 profile (see Figure B.13 in Appendix B). Average k_m values at every 5 cm were obtained by the LDRM simulation (see Fig. 5.26 and G.3 in Appendix G), as the NAPL saturation values were averages of 5 cm soil intervals. In addition, a hydraulic conductivity value of 8 m/d that corresponds to the HPT 74 profile was used (see Fig. B.18, Appendix B). This value corresponds to a k^* value of $9.4 \cdot 10^{-8} \text{ cm}^2$, an indication of sandy material (Lewis 1989). k^* values were calculated via Equation 5 (water was used as liquid with $\mu = 0.01 \text{ g/cm}\cdot\text{s}$, $\rho = 1 \text{ g/cm}^3$ and $g = 980 \text{ cm/s}^2$). The estimated T_n value was $0.35 \text{ m}^2/\text{d}$, a value similar to the predicted T_n value via LDRM simulation ($0.32 \text{ m}^2/\text{d}$). The values are consistent with the T_n field value of $0.5 \text{ m}^2/\text{d}$.

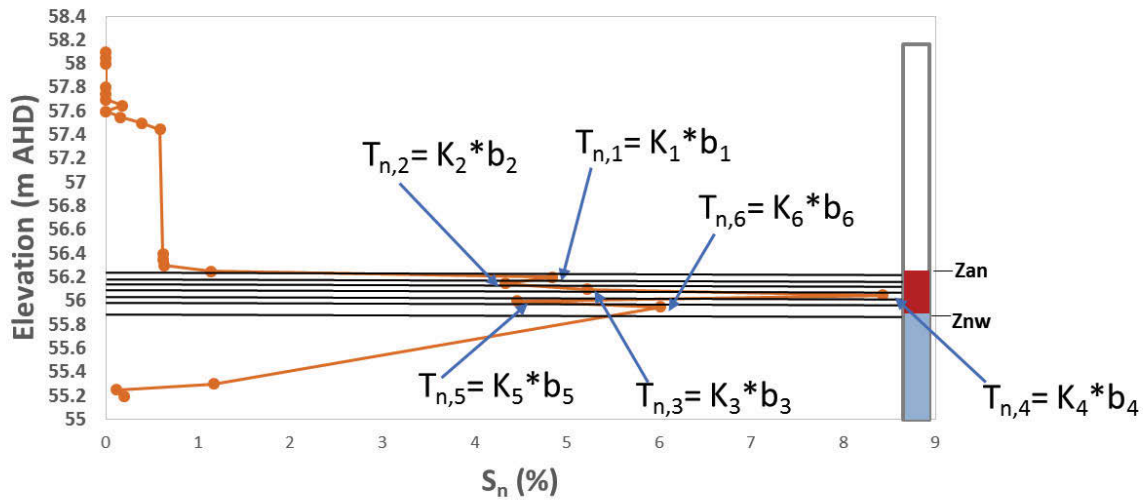


Figure 5. 27. Layers with mobile NAPL.

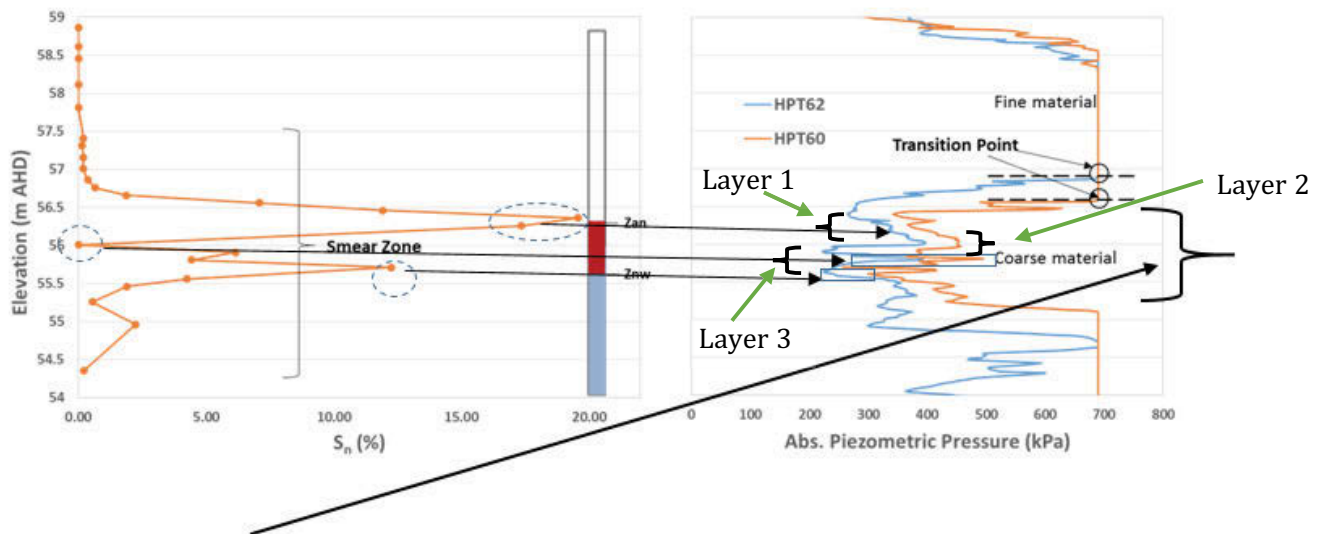
Table 5. 4. Theoretical T_n estimation.

	T_n (cm^2/s)	K_n (cm/s)	b_n (cm)	k_n	k^* (cm^2)	ρ_n (g/cm^3)	g (cm/s^2)	μ_n ($g/cm*s$)
Zone 1	0.012425	0.002485	5	0.175	0.000000094	0.74	980	0.0048
Zone 2	0.010295	0.002059	5	0.145	0.000000094	0.74	980	0.0048
Zone 3	0.00781	0.001562	5	0.11	0.000000094	0.74	980	0.0048
Zone 4	0.00568	0.001136	5	0.08	0.000000094	0.74	980	0.0048
Zone 5	0.003195	0.000639	5	0.045	0.000000094	0.74	980	0.0048
Zone 6	0.0015762	0.000213	7.4	0.015	0.000000094	0.74	980	0.0048
Sum $T_n = 0.35 m^2/d$								

Area C

Area C was simulated by using three different soil layers (SW, SW-SM, SW) according to Figure 5.28. The LDRM simulation provided a T_n value of $0.41 m^2/d$. The simulation took place including 3 layers of SW/SW-SM/SW. A consistency between piezometric pressure values and NAPL saturation measures is depicted. At the interval of 55.97 - 56.055 the HPT tool showed almost zero hydraulic conductivity (K) values and the NAPL saturation value was zero, thus at this elevation the material in the simulation changed from SW to SW-SM. As there were not measured K values for elevation higher than 56.055 m AHD, the K value at layer 1 was assumed to be similar with K value at layer 3 due to the similar Abs. piezometric

pressure values according to the HPT tool. The K value at layer 3 was an average value which equals to 1.83 m/d.



If we zoom into this area then we have in general 3 layers: SW/SW-SM/SW

Figure 5. 28. The three simulated layers at area C.

Fig 5.29 illustrates the saturation and NAPL relative permeability profiles of LDRM simulation. It can be seen that, the predicted NAPL saturation values were consistent with the field measured NAPL saturation values using the average values of van Genuchten parameters from the API database. The LDRM simulation provided a T_n value of 0.41 m²/d.

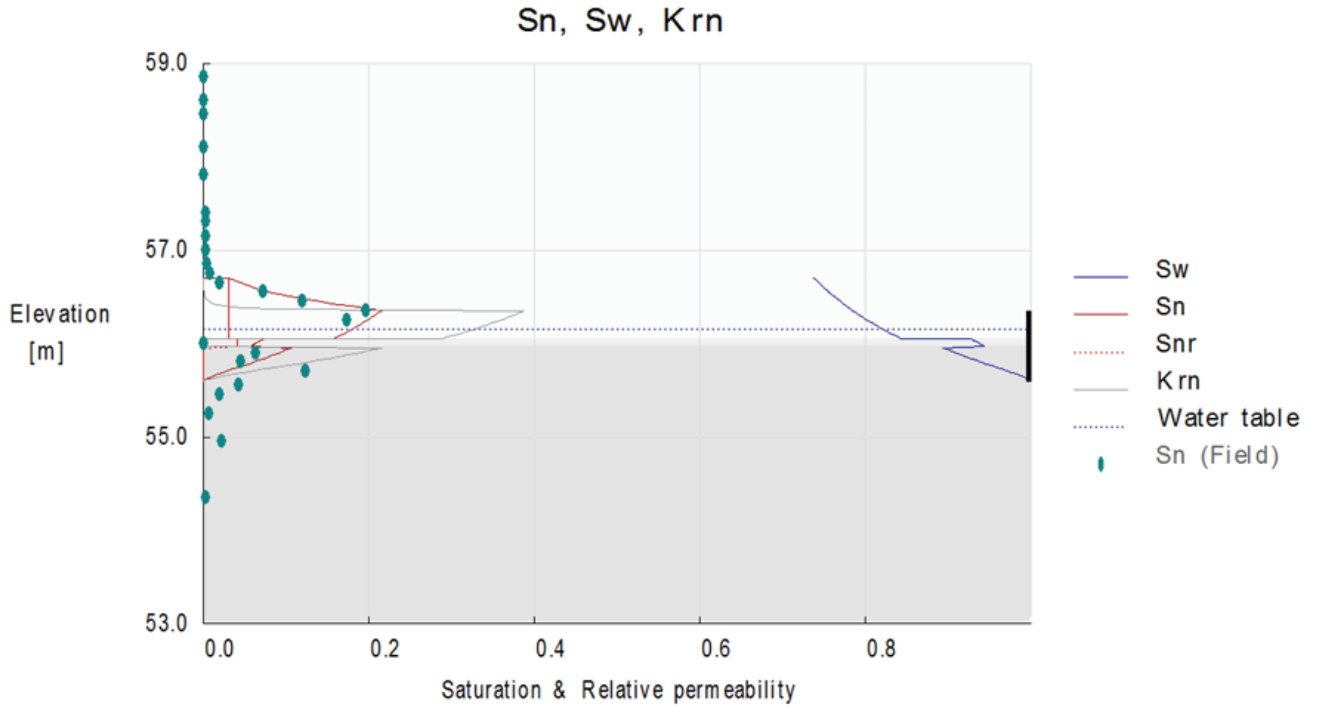


Figure 5. 29. NAPL saturation and NAPL relative permeability profiles.

Theoretical T_n estimation

Theoretical T_n estimations corresponded to Fig 5.30 are presented in Table 5.5. As it can be seen, the T_n theoretical estimation showed a good agreement with the LDRM predicted T_n value. The theoretical T_n estimation took place in the three layers presented in the LDRM simulation. Fig 5.30 presents 6 intervals consisting the mobile interval in the formation. Average k_n values for each zone were obtained by the LDRM simulation (Fig. G.4, Appendix G) and average k^* value for each zone from HPT values. At zone 1 and 2 an assumption of $K= 1.83$ m/d was used (see Fig. B.18, Appendix B). There was no BD testing on this day. On 6/4/2016 the $T_{n,BD}$ value was 0.58 m²/d and on 14/6/2016 the $T_{n,BD}$ value was 0.3 m²/d, thus a T_n value between these days is anticipated for the coring day on 20th of May. The T_n theoretical estimation of 0.436 m²/d and the LDRM predicted value of 0.41 m²/d are corresponded to the anticipated T_n of that day.

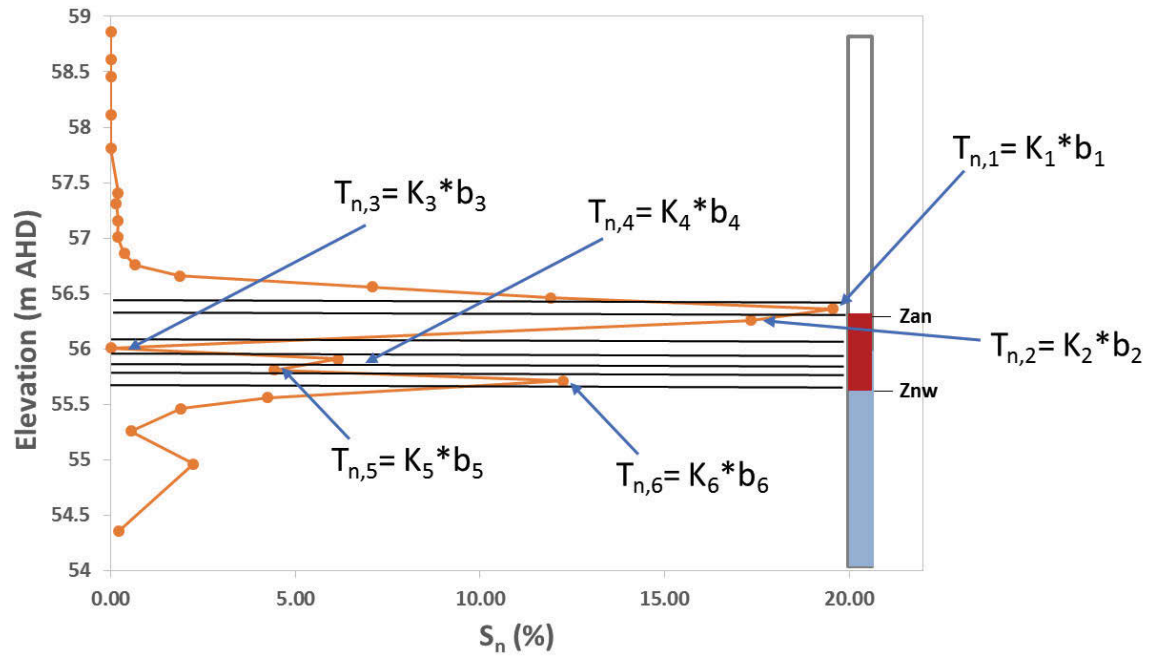


Figure 5. 30. Layers with mobile NAPL.

Table 5. 5. Theoretical T_n estimation.

	T_n (cm^2/s)	K_n (cm/s)	b_n (cm)	k_n	k^* (cm^2)	ρ_n (g/cm^3)	g (cm/s^2)	μ_n ($g/cm*s$)
Zone 1	0.0123	0.00123	10	0.37	0.000000022	0.74	980	0.0048
Zone 2	0.027	0.00108	25	0.324	0.000000022	0.74	980	0.0048
Zone 3	0.0000016	0.00000016	10	0.003	0.00000000035	0.74	980	0.0048
Zone 4	0.008	0.0008	10	0.16	0.000000033	0.74	980	0.0048
Zone 5	0.0026	0.00026	10	0.085	0.000000002	0.74	980	0.0048
Zone 6	0.00072	0.000072	10	0.025	0.000000019	0.74	980	0.0048
Sum $T_n = 0.436 m^2/d$								

Area A

Area A was simulated by using one homogeneous soil layer of SP material according to HPT and core logging descriptions (see Figures B1, B.2 and B.6 in Appendix B). The hydraulic conductivity value was 13 m/d, as it was estimated by the HPT tool. The b_n value was 0.324 m, a value similar to the maximum monitored b_n value historically (see Table 4.3 in Chapter 4). The van Genuchten parameters were determined as average values of SP material in the API database. The predicted T_n value was 0.02 m²/d inconsistent with the field measurement of 1.5 m²/d. NAPL relative permeability which is related to NAPL saturation, and intrinsic permeability are two important potential parameters that are responsible for the poor agreement between the field based and predicted T_n values. Other parameters that should be considered and are related to potential preferential pathways are: pore connectivity, pore distribution (Deb & Shukla 2012) and the existence of NAPLs (non-wetting fluid) in the large pores (Johnston 2010). Fig 5.31 illustrates the saturation and NAPL relative permeability profiles.

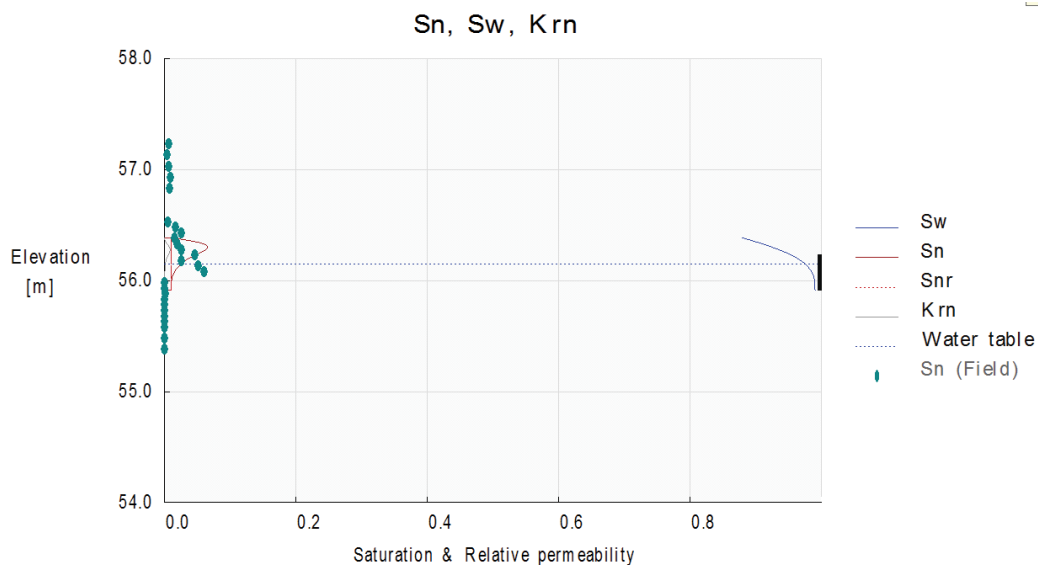


Figure 5. 31. NAPL saturation and NAPL relative permeability profiles.

The next two presented scenarios (A and B) consider the impact of k_m and k^* in the T_n estimations, respectively.

Scenario A

Scenario A is referred to the case that the field NAPL saturation values that were used in the calibration of the model were not representative of the real field conditions potentially, resulting in the calculation of inaccurate NAPL relative permeability values. Poorly

representative saturation values can be related to errors in the coring process and/or the existence of other higher NAPL saturated areas in the vicinity of the tested well that are mainly responsible for the high $T_{n,BD}$ value at this well location. The second reason has an impact on the assumption of the uniform radial distribution of LNAPL. Table 5.6 presents the input parameters for scenario A. An increase of the van Genuchten parameter α is related to higher NAPL saturation and relative permeability values (see Fig 5.32) and it is an indication of a coarser material (Charbeneau 2007b). The new van Genuchten α value is still in the range of sandy materials (Carsel & Parrish 1988). The predicted T_n value of this scenario was 1.5 m²/d and the average NAPL permeability value was 0.24 (see Figure G.1, Appendix G). It should be noticed that in this scenario the calibration of the model took place via using the average vG “N” parameter obtained by the API database for SP material, minimizing in parallel the vG “ α ” parameter (Charbeneau 2007a).

Table 5. 6. Input parameters for scenario A.

Research Area A- PB29 Remediation well			
Parameter	Value	Source	Notes
Max Monitoring LNAPL Thickness (m)	0.324	Gauging data	
Soil Characteristics			
Porosity	0.41	API Database	Average for SP
Hydraulic conductivity (m/d)	13	HPT	
Van Genuchten N	3.17	API Database	Average for SP
Van Genuchten α (m ⁻¹)	6.4	After LDRM calibration	
Irreducible water saturation	0.209	API Database	Average for SP
Permeability model	Mualem	LDRM Default	

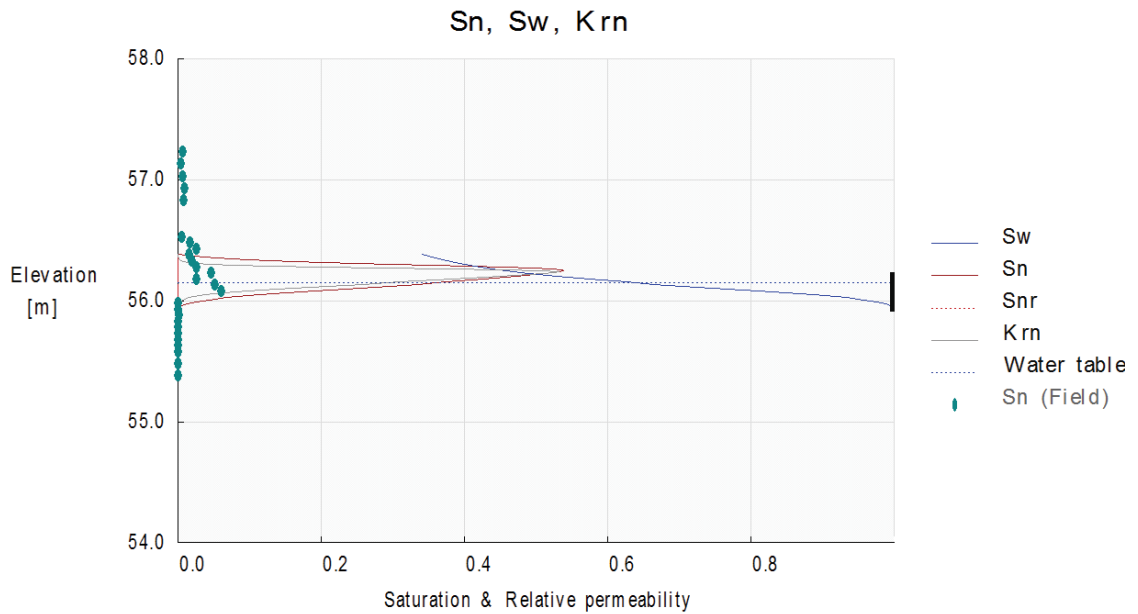


Figure 5. 32. NAPL saturation and NAPL relative permeability profiles.

Sensitivity analysis

Figure 5.33 depicts how sensitive is the T_n parameter to van Genuchten “ α ” ($vG\alpha$) parameter using the Mualem model. Different values of $vG\alpha$ (in accordance to API database) were used for a constant van Genuchten “ N ” (vGN) parameter. These points are presented in the “ N ” data series. The median vGN value of 3.17 was used obtained by the API database (SP material). Furthermore, additional vGN values were used. vGN changes of ± 20 and 40% can be seen. N_{min} (limit value) corresponds to the lowest N value ($N=1.0001$) that can be used with the Mualem model and N_{max} (upper limit value= 6) is the N median value plus 2 times the standard deviation (API database) value that corresponds to a 95% confidence level (Kendall & Stuart 1973).

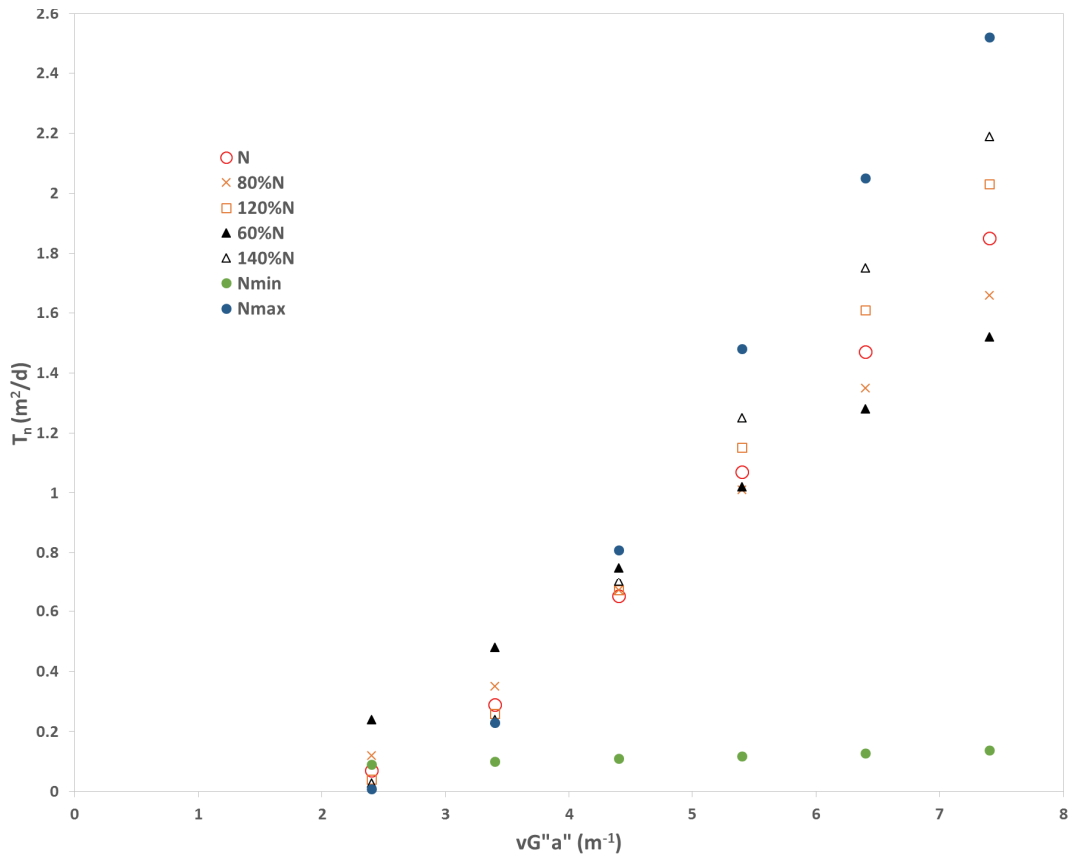


Figure 5.33. Profile of T_n along with $vG\alpha$ for different vGN values.

As it can be seen in this graph, changes in vGN values have an impact on the slope of the tested parameters. Using the Mualem model, infinite values of $vG\alpha$ and vGN can result in a T_n value of $1.5 \text{ m}^2/\text{d}$. It should be noticed that there is a critical point for $vG\alpha = 4.5 \text{ m}^{-1}$. A slightly linear relationship between T_n and $vG\alpha$ parameters is depicted in Figure 5.33 for $vG\alpha$ values higher than this point. For lower $vG\alpha$ values there is no linear relationship. In addition, above the critical point, lower vGN values result in lower slope values.

Figure 5.34 illustrates the sensitivity between T_n and van Genuchten “N” parameters using the Mualem model. This scenario corresponds to a different pore distribution thus different vGN values are used. Different values of vGN (in accordance to API database) were used for a constant van Genuchten “ α ” parameter. These points are presented in the “ α ” data series. The median $vG\alpha$ value of 1.85 was used obtained by the API database (SP material). Furthermore, additional $vG\alpha$ values were used. $vG\alpha$ changes of ± 20 and -40% can be seen. Fig. 5.34 depicts an exponential relationship between $vG\alpha$ and T_n . For vGN values close to 1 (values between 1.1 and 1), the behaviour changes. It should be noticed that higher vGN values have a negative impact on T_n , while higher $vG\alpha$ values affected T_n positively. The different behaviour in Figures 5.33 and 5.34 is related to the Equation 10.

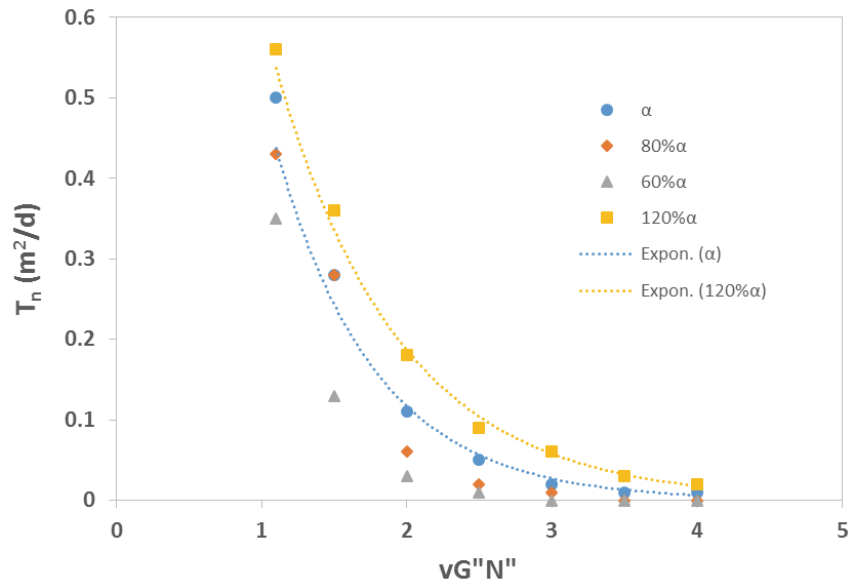


Figure 5. 34. Profile of T_n along with vGN for different $vG\alpha$ values.

Scenario B

Scenario B (Figure 5.35) simulates the existence of a preferential pathway (high NAPL transmissive zone). Specifically, this scenario refers to a coarse material with higher hydraulic conductivity values and as a result intrinsic permeability values than 13 m/d. Area A was simulated by using three soil layers SP (layer 1) - SP or coarser material (layer 2) - SP (layer 3, same material with layer 1). Core saturation (MP50 well), HPT and LIF data was used for the determination of the input parameters. Soil description of MP50 core showed that the material is similar (SP) but coarser between 56.12 and 56.27 m AHD. The van Genuchten parameters were obtained by the API database. Average values for SP material in layers 1 and 3 were used. The layer 2 was calibrated by using capillary values that most closely match the observed peak field LNAPL saturation (Charbeneau 2007a). The LIF 43 and 47 profiles (see Fig. B.10 and B.11, Appendix B) revealed a high signal response at 56.2 m AHD in an interval of 12 - 15 cm. This high response signal can be related to either high NAPL saturation values and/or a coarse soil material (Germain 2014). The b_n value of 0.2 m was used for the needs of the LDRM simulation, according to the 4 intervals of 5cm each (see Fig 5.36). Table 5.7 depicts the determined input parameters for this investigated scenario.

Table 5. 7. Input parameters for scenario B.

Research Area A- PB29 Remediation well			
Parameter	Value	Source	Notes
Max Monitoring LNAPL Thickness (m)	0.200	Gauging data, Core saturation data, LIF	
Ground surface elevation (m)	61.087	Gauging data	
Water table elevation (m)	56.150	Gauging data	
Water vertical gradient	0.000	LDRM Default	
Elevation of soil faces interface 1 (m)	56.270	Core data	
Elevation of soil faces interface 2 (m)	56.070	Core data	
LNAPL density (g/cm ³)	0.740	Gauging data	
LNAPL viscosity (cp)	0.480	Gauging data	
Air/water surface tension (dyne/cm)	65.000	CRC CARE report no. 18	Average for gasoline
Air/LNAPL surface tension (dyne/cm)	20.500	CRC CARE report no. 18	Average for gasoline
LNAPL/water interfacial tension (dyne/cm)	22.900	CRC CARE report no. 18	Average for gasoline
Soil Characteristics for layer 1			
Porosity	0.41	API Database	Average for SP
Hydraulic conductivity (m/d)	13	HPT	
Van Genuchten N	3.17	API Database	Average for SP
Van Genuchten α (m ⁻¹)	1.85	API Database	Average for SP

Irreducible water saturation	0.209	API Database	Average for SP
Permeability model	Mualem	LDRM Default	
Soil Characteristics for layer 2			
Porosity	0.40	After LDRM calibration	Unknown soil material
Hydraulic conductivity (m/d)	700	After LDRM calibration	
Van Genuchten N	2.150	After LDRM calibration	
Van Genuchten α (m^{-1})	2.300	After LDRM calibration	
Irreducible water saturation	0.210	After LDRM calibration	
Residual LNAPL saturation	0.010	Core data, f-factor	
Permeability model	Mualem	LDRM Default	
Soil Characteristics for layer 3			
Porosity	0.41	API Database	Average for SP
Hydraulic conductivity (m/d)	13	HPT	
Van Genuchten N	3.17	API Database	Average for SP
Van Genuchten α (m^{-1})	1.85	API Database	Average for SP
Irreducible water saturation	0.209	API Database	Average for SP
Residual LNAPL saturation	0.010	Core data, f-factor	
Permeability model	Mualem	LDRM Default	

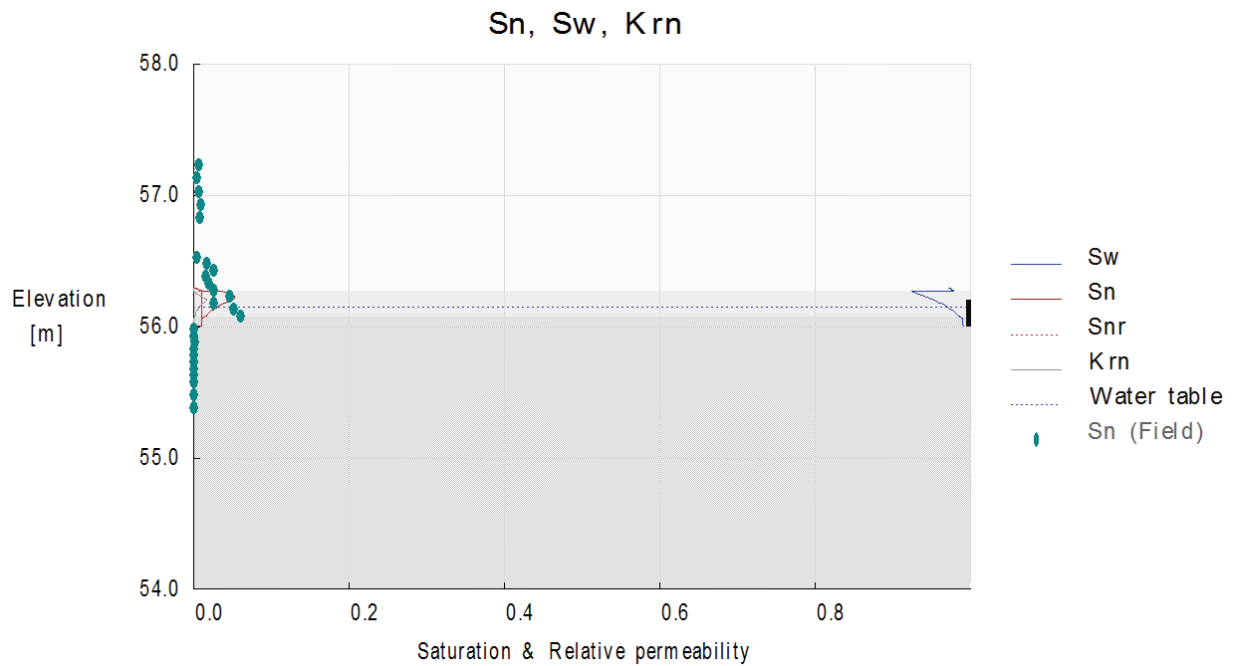


Figure 5. 35. NAPL saturation and NAPL relative permeability profiles.

This simulated scenario resulted in a T_n value of $1.5 \text{ m}^2/\text{d}$ using a very high value for hydraulic conductivity of 700 m/d and an average NAPL relative permeability value of 0.008 (see Figure G.2, Appendix G). This high hydraulic conductivity value corresponds to a very coarse sand or gravel material (Lewis 1989). Even though, this value looks unrealistic, as the soil description did not reveal such a coarse material in this specific elevation, a preferential pathway (macropore channel) due to a high pore connectivity (Deb & Shukla 2012) could explain the high T_n and low NAPL saturation values in this area.

Theoretical T_n estimation

Theoretical LNAPL transmissivity estimations corresponded to Fig 5.36 are presented in this section (Tables 5.8 and 5.9). As it can be seen in the next tables, the T_n theoretical estimations showed a good agreement with the field measured T_n value. T_n was estimated by using the Equation 16. Fig 5.36 presents 4 intervals (zones) part of the mobile interval in the formation, which contribute to the T_n value at well PB29. Each interval consists of an average NAPL saturation value and a thickness (b) value of 5 cm . k_m values (average values in 5 cm intervals) were obtained by the presented LDRM simulations (scenario A and B) (see Figures G.1-2, Appendix G). In scenario A, a hydraulic conductivity value of 13 m/d was used (HPT data, see Fig. B.18, Appendix B), whereas scenario B includes a K value of 700 m/d .

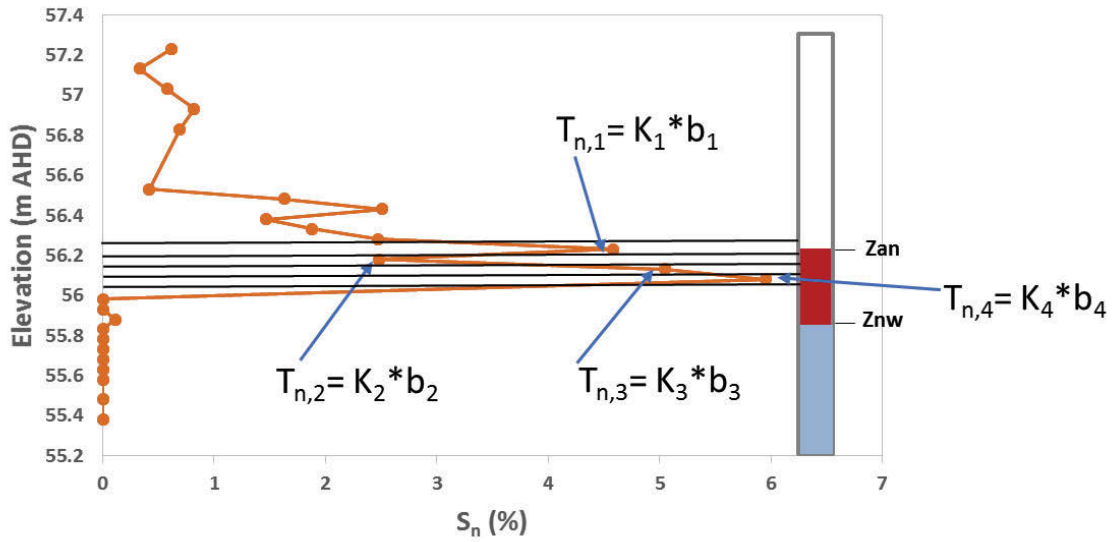


Figure 5. 36. Layers with mobile NAPL.

Table 5. 8. Theoretical T_n estimation for scenario A.

	T_n (cm^2/s)	K_n (cm/s)	b (cm)	k_n	k^* (cm^2)	ρ_n (g/cm^3)	g (cm/s^2)	μ_n ($g/cm*s$)
Zone 1	0.057	0.0114	5	0.505	0.00000015	0.74	980	0.0048
Zone 2	0.045	0.0090	5	0.400	0.00000015	0.74	980	0.0048
Zone 3	0.028	0.0056	5	0.250	0.00000015	0.74	980	0.0048
Zone 4	0.0125	0.0025	5	0.110	0.00000015	0.74	980	0.0048
Sum $T_n = 1.24 m^2/d$								

Table 5. 9. Theoretical T_n estimation for scenario B.

	T_n (cm^2/s)	K_n (cm/s)	b (cm)	k_n	k^* (cm^2)	ρ_n (g/cm^3)	g (cm/s^2)	μ_n ($g/cm*s$)
Zone 1	0.0762	0.01524	5	0.0123	0.0000083	0.74	980	0.0048
Zone 2	0.08775	0.01755	5	0.014	0.0000083	0.74	980	0.0048
Zone 3	0.02715	0.00543	5	0.0045	0.0000083	0.74	980	0.0048
Zone 4	0.0113	0.00226	5	0.0018	0.0000083	0.74	980	0.0048
Sum $T_n = 1.76 m^2/d$								

Discussion of the results in chapter 5.3

This subchapter presented the verification of LDRM simulation through theoretical and field based T_n estimations. It was studied, if the input of up to 3 layers in LDRM simulation (homogeneous layers with average K values) can predict T_n estimates similar to the field based and theoretical T_n values that are related to a higher degree of heterogeneity. It should be noticed the high importance of the field measured T_n values to the calibration of the model (Cho, M. Adamski & A. Kirkman 2010). Areas B and C were simulated well using K values obtained by the HPT tool, and provided T_n values similar to the field based measurements. The calibration of area A with a homogenous sandy material was unsuccessful, as it provided a zero T_n value, thus potential scenarios related to soil heterogeneity and/or higher NAPL saturations were examined. Finally, it should be noted that

5.4. Conclusions

In the present chapter, the LNAPL distribution and hydrogeological conditions in the three areas of research were investigated. Results indicated that the hydrogeological conditions were related to the Z_{aw} behavior and both confined and unconfined LNAPL conditions can be found in the same well seasonally (for instance PB27 and PB40 wells in areas B and C). Vertical NAPL distribution was related to the history of fluid levels in most of the cases, however entrapped and residual LNAPL saturations inconsistent with the history of fluid elevations (for instance NAPL saturation up to 0.7 m below the lowest Z_{nw}) can be related to water table drawdown events and potential macropore networks existed in the fine materials.

Diagnostic gauge plots were found to be reliable tools for the identification of NAPL conditions revealing geological transition points in the range of 56.6 to 56.8 m AHD (although more frequent fluid levels measurements could improve this estimate). The findings were consistent with other lines of evidence such as: hydrostratigraphs, core descriptions, bail-down testing data, HPT and NAPL saturation profiles. In addition, the presented transition points were consistent during different drainage-imbibition periods (Figures 5.11 - 5.13). Using stratigraphic data (as lines of evidence) from monitoring wells in areas that present strong spatial variability (Figures 5.21 and B.7 in Appendix B), may lead to uncertainty in the identification of geological transition points in the tested well. In these scenarios, DGPs can be used successfully to estimate the elevation of the confining contact at this specific location, overcoming these kind of complexities.

In contrast to other related works (Hartsock 2014; Kahraman 2013), more lines of evidence were used for the validation of the DGPs outcomes in this research. Moreover, both

confined and unconfined NAPL conditions were presented in the same well seasonally. A detailed analysis through filtered DGPs took place based on different Z_{aw} trends, presenting more accurate and clear outcomes. This kind of analysis is recommended in sites affected by water table fluctuations, where fluid levels corresponds to different drainage-imbibition periods.

In heterogeneous settings the stratigraphy may override typical smearing (redistribution) patterns related to homogeneous systems. The vertical NAPL distributions in areas A and B were similar to homogeneous cases. In contrast, area C presented a vertical NAPL distribution profile similar to heterogeneous cases due to the existing fine and coarse layers. Variations in NAPL saturations were correlated qualitatively with variations in the soil material at this area. Area C presented the highest NAPL saturation and in-well thickness values among the other research areas. In addition, this area showed the highest entrapped (5%) and residual (up to 12%) NAPL saturation estimates. Low maximum saturation values at areas A and B are in line with other documented field based studies in fine materials (Adamski, Kremesec & Charbeneau 2005; Adamski et al. 2005).

A good agreement between the estimated T_n values through LDRM simulation and theoretical calculations was found in areas B and C. At these areas, hydraulic conductivity values estimated by HPT profiles and average van Genuchten parameters obtained by the API database resulted in estimated T_n values similar to the T_n field-based values after bail-down testing. On the other hand, the simulation of area A with a homogenous sandy material (as it was indicated by the HPT profile) was unsuccessful, as it provided a zero T_n value in contrast with the field measured value of $1.5 \text{ m}^2/\text{d}$, thus potential scenarios related to soil heterogeneity and/or higher NAPL saturations were examined. A sensitivity analysis of the van Genuchten parameters showed that higher vGN values have a negative impact on T_n , while higher $vG\alpha$ values affected T_n positively.

6. Assessment of LNAPL Mobility and Recoverability

In chapter 6 of the thesis, LNAPL mobility is assessed in terms of NAPL transmissivity (T_n), in a heterogeneous aquifer under the effect of fluctuating water table conditions. The effects of lithology and NAPL distribution are elucidated. Different hydraulic methods were used for the identification of T_n accounting for the variability between the applied methods. Furthermore, the impact of mass recovery technologies (such as skimming processes enhanced by vacuum and water table drawdown), of physical properties (density and viscosity) and chemical compositions on T_n , is investigated. In the time periods of the mass recovery trials, LNAPL was under unconfined conditions in the three research areas according to multiple lines of evidence such as diagnostic gauge plots, hydrostratigraphs, LIF and HPT profiles, baildown testing analysis and LNAPL drawdown-discharge relations during the baildown tests (Kirkman, Adamski & Hawthorne 2013). The outcomes of the conducted research are presented and discussed in the sections 6.1 – 6.11.

6.1. Spatial Variability of LNAPL Transmissivity

Figure 6.1 depicts LNAPL bail-down tests which were carried out throughout the period of the research (5/2015 - 6/2016) excluding periods of remediation trials. Details of the conducted bail-down tests are presented at Table C.1 in Appendix C. Twenty five bail-down tests took place in eight wells. The individual well analyses can be seen in Appendix J.

Results indicated a range of $T_{n,BD}$ values from practically 0.03 m²/day to 2.13 m²/day across the site, as it can be seen in Figure 6.1, during unconfined LNAPL conditions. T_n exhibited strong spatial variability. For instance no NAPL was present in wells located at less than 2 m away from others with the highest T_n values. In addition, as it can be inferred from Figure 6.2, T_n showed no clear correlation with distance from the original spill source at the underground storage tank (UST) area. A good correlation would be expected in homogeneous systems with recent contaminant releases where higher NAPL saturations and T_n values could be found in the vicinity of the UST area.

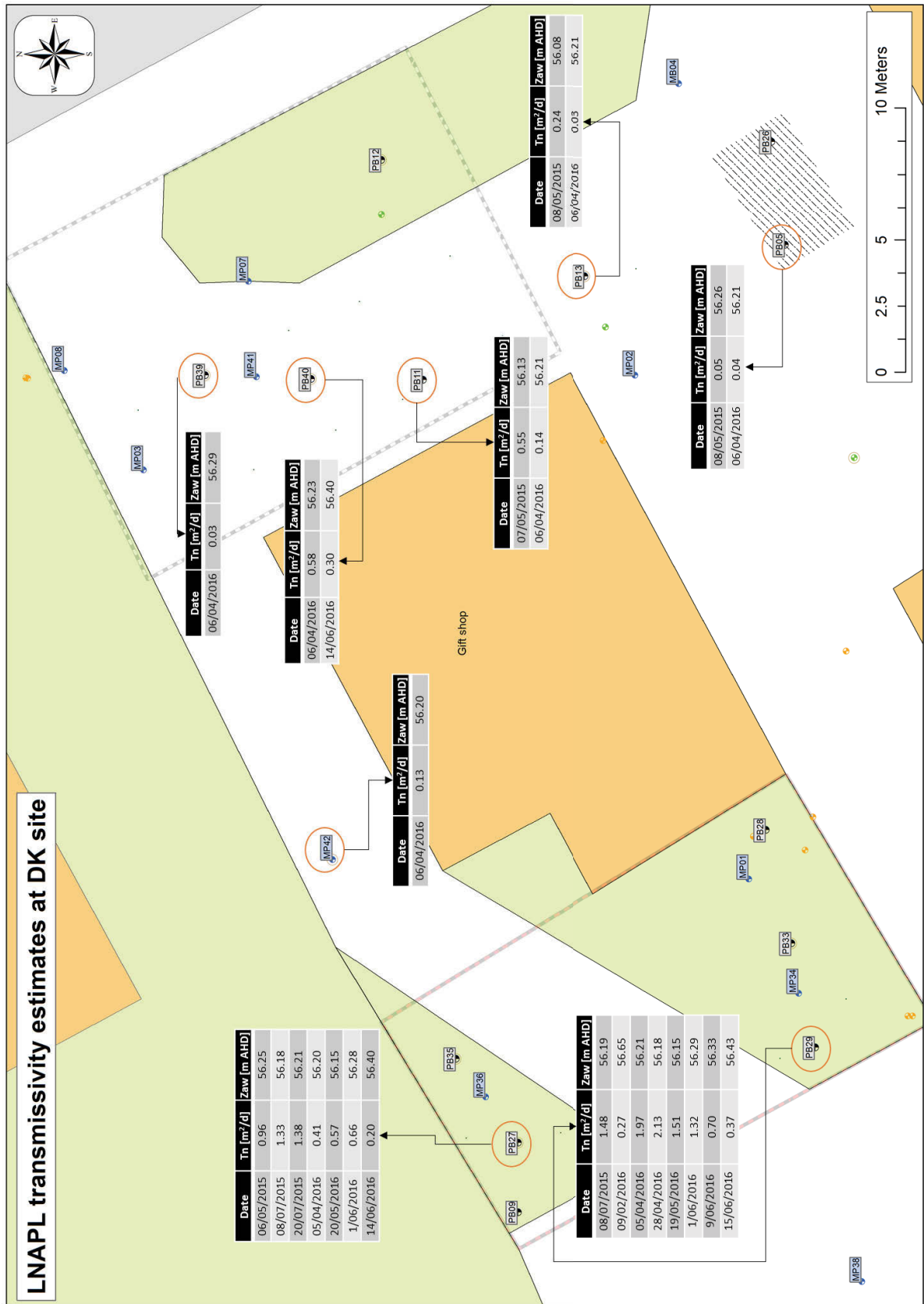


Figure 6. 1. Spatial variability of LNAPL transmissivity at the site of research.

Area A presented higher T_n values (0.26 – 2.13 m²/day) than area B (0.20 – 1.38 m²/day) and C (0.03 – 0.58 m²/day) under unconfined NAPL conditions (see Figure 6.1), even though it contained lower NAPL saturations (see Figure 5.23) and b_n values than area C, as well lower NAPL saturations and similar b_n values with area B. T_n is given by the summed product of NAPL conductivity, K_n and NAPL thickness, b_n (see Equations 15 and 16). Low NAPL saturation leads to a low value of NAPL relative permeability, as well more permeable soils and less viscous NAPLs affect positively the T_n values (Ahmed 2014; Essaid, Bekins & Cozzarelli 2015; Jeong & Charbeneau 2014). Some key parameters that may had an impact on this study were the variability in NAPL distribution (see Figures B.15 -17 in Appendix B) due to the spatial heterogeneity (see Figures B.7 – B.9 in Appendix B) as well as the finer material at NAPL mobile zone interval (SW - SM material) compared to the other two areas of research (SW, SP).

Discussion

Taking into account that there are no significant differences in density (PB29 well: 0.72 g/mL, PB27 well: 0.73 g/mL and PB40 well: 0.73 g/mL) and small measurable differences in viscosity values (PB29 well: 0.48 cP, PB27 well: 0.42 cP and PB40 well: 0.41 cP), the differences in intrinsic permeability and the NAPL saturations are responsible for the different NAPL conductivity values at the three areas of research. The high importance of porosity and maximum b_n value on the LNAPL specific volume has been acknowledged in the literature (Jeong & Charbeneau 2014). LNAPL recovery and distribution are highly affected by the soil properties. Fine grained systems present low LNAPL mobility even at high NAPL saturations (Beckett & Huntley 1998; Jeong & Charbeneau 2014). Area C presented the lowest T_n values for the highest b_n values, thus lower NAPL conductivities compared to the other areas were developed. Moreover, in area C higher NAPL saturation values were presented among the other areas, thus the low intrinsic permeability is the important parameter for the low T_n values. Area A presented the highest T_n values due to the less viscous product at PB29 well (12% lower than the other two areas) and the highest intrinsic permeability values (Huntley & Beckett 2002). Area B and C have presented not significant differences in T_n taking into consideration that area B has lower b_n and NAPL saturation values, but it contained a coarser material.

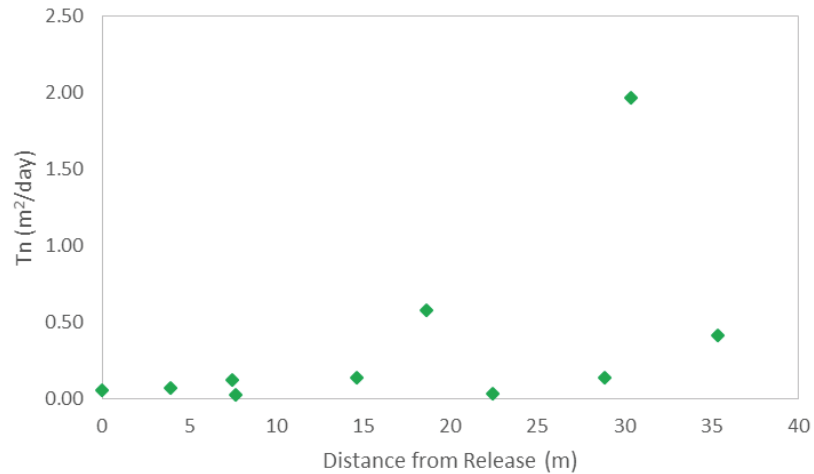


Figure 6. 2. Illustration of T_n -distance from release relationship (date 5-6/4/2016, $Z_{aw} = 56.20$ m AHD).

6.2. In-Well Thickness: An Indicator of LNAPL Transmissivity

In well thickness has been documented as a poor metric of potential NAPL recovery in the literature as high b_n values may not indicate the ability for high product recovery (Beckett & Huntley 2015; ITRC 2009a). Figure 6.3 presents the $T_n, BD - b_n$ relationship for the whole research site. This graph includes data from 8 monitoring and recovery wells (PB05, PB11, PB13, PB27, PB29, PB39, PB40, and MP42). The highest monitored b_n was 0.8 m and the lowest 0.12 m. As it can be seen, many high b_n values presented low T_n values. As it can be inferred from this figure, in well thicknesses in the range of 0.6 - 0.8 and 0.2 - 0.4m depicted T_n values between 0 and 0.8 m^2/day and from 0 to 2.13 m^2/day , respectively. This behavior suggests that b_n was not a good indicator of T_n regarding the whole site analysis. This lack of correlation between the two parameters was not unexpected since it has been also documented in the literature (Palmier, Dodt & Atteia 2016). The different types of geological setting and heterogeneity played a crucial role in the presented figure as T_n is not only related to b_n but also to soil properties assuming no changes in the physical fluid properties of LNAPL (ASTM 2013). In homogeneous cases a good correlation between T_n and b_n is anticipated.

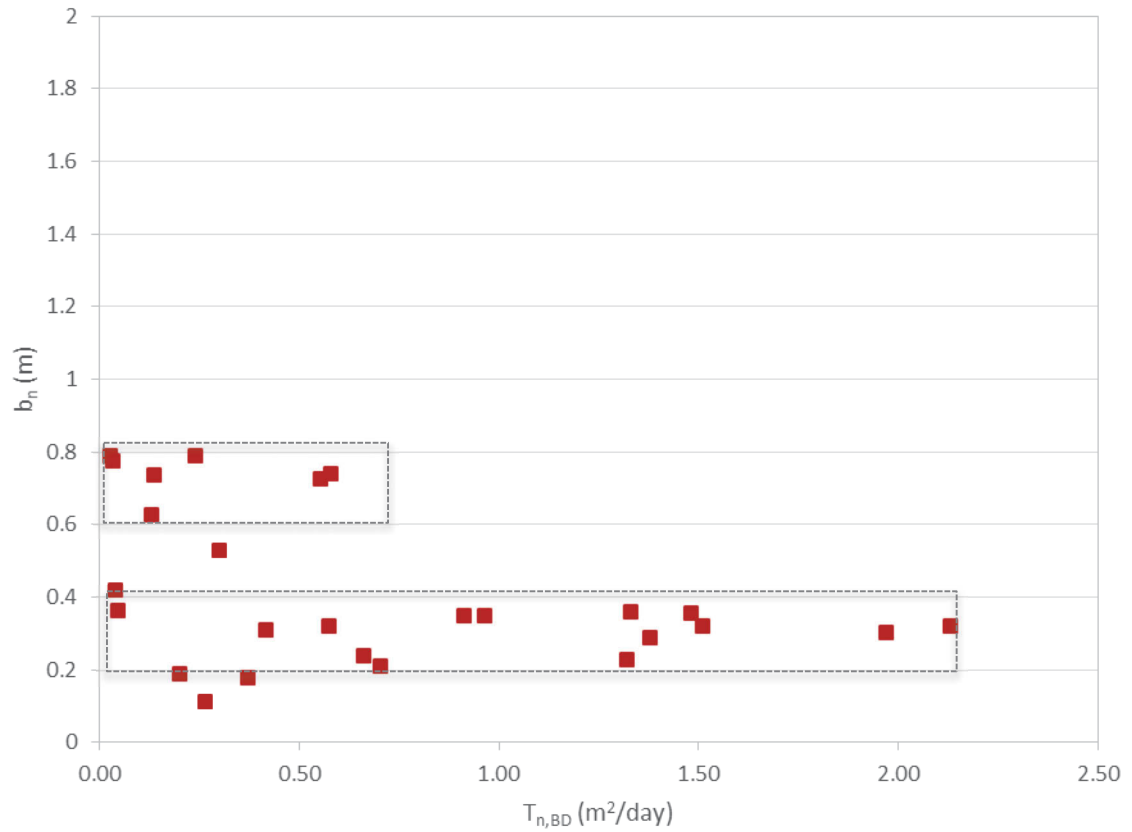


Figure 6. 3. T_n versus in-well thickness profile in the whole contaminated site.

Figures 6.4 and 6.5 illustrate $b_n - T_n$ relationships at the tested wells PB29 (area A) and PB27 (area B). Both wells showed positive relationships between the tested parameters during unconfined NAPL conditions consistent with the multiphase theory (Lenhard, Rayner & Davis 2017). A positive relationship is depicted in Figure 6.4 with $R^2= 0.76$ and in Figure 6.5 with $R^2= 0.35$. As it was mentioned above, a good correlation is expected in homogenous systems. Area A presented a better correlation maybe to the lower degree of heterogeneity compared to area B (see abs. piezometric pressures in Figures 5.7 and 5.15).

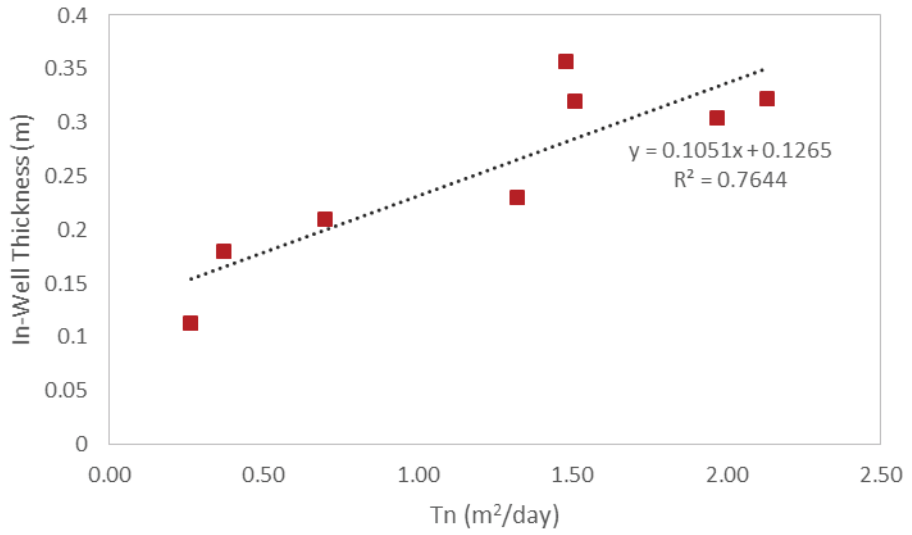


Figure 6. 4. T_n versus in-well thickness profile at PB29 well.

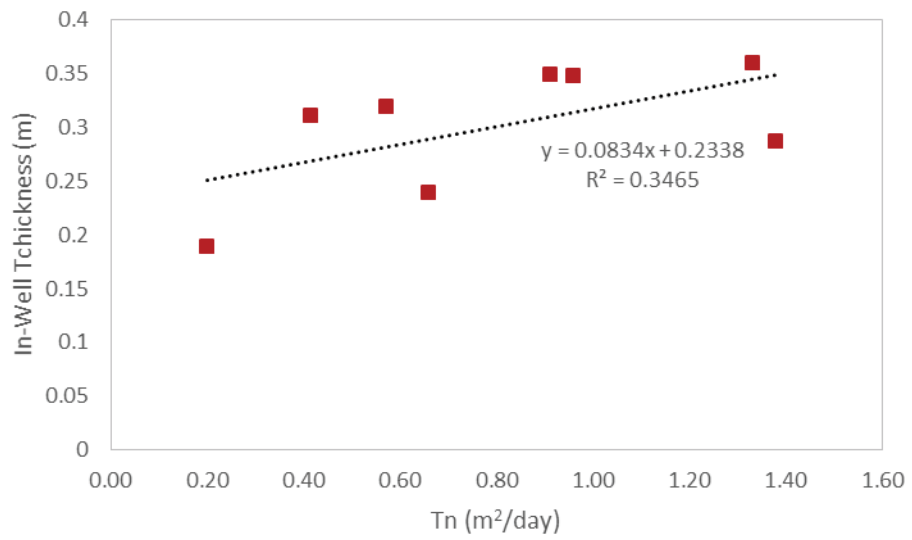


Figure 6. 5. T_n versus in-well thickness profile at PB27 well.

6.3. Variability in LNAPL Transmissivity under Natural Water Table Fluctuations

Between 2014 and 2016, during periods of unconfined LNAPL conditions, $T_{n,BD}$ followed an inverse relationship with Z_{aw} as depicted in Fig. 6.6. This graph does not include mass recovery periods. It can be inferred that, during low water table conditions, LNAPLs may more easily spread laterally. The T_n reduction during rising water table conditions was observed across the whole contaminated site and not only in the three areas studied. This behavior was related to two different processes: (i) less mobile LNAPL results because of LNAPL entrapment by water and (ii) the upward NAPL displacement was into porous media with a lower intrinsic permeability. This was more pronounced at research areas B and C where the T_n showed the lowest values just before reaching the overlying aquitard at 56.7-56.8 m AHD. Another observation (Figure 6.7) supporting the strong impact of Z_{aw} on T_n was that an increase of 25 cm in Z_{aw} resulted in a $T_{n,BD}$ decrease from 2.13 to 0.37 m²/d in area A (which exhibited the lowest NAPL mobile intervals according to LIF and core logs). These changes in T_n could explain the differences up to one order of magnitude found in comparisons between initial bail-down testing values and long-term methods such as tracer tests (Pennington et al. 2016). It should be remarked that the redistribution of the product (fresh gasoline) was favored by its relatively low density and viscosity.

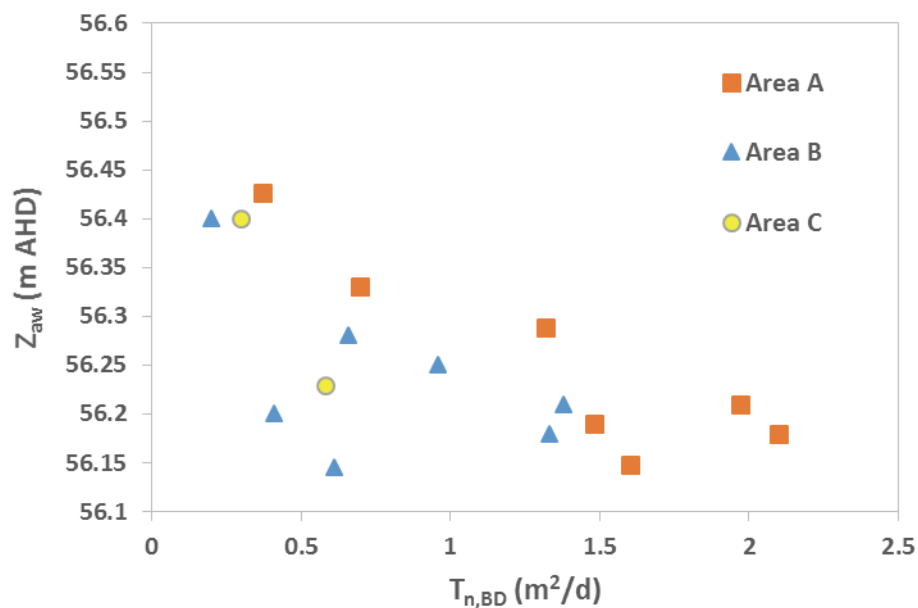


Figure 6. 6. Correlation between the T_n and Z_{aw} at the three areas of research (years: 2015-2016).

Figure 6.7 illustrates the contaminated site hydrograph during the research period. The maximum potentiometric surface elevation was 0.6 m higher in 2014 than in 2015 (57.7 m AHD in November 2014 versus 57.1 m AHD in October 2015), while the lowest elevation remained similar (approximately 56.2 m AHD) at the end of the drainage periods of 2015 and 2016. Differences in $T_{n,BD}$ at similar Z_{aw} values in 2015 compared to 2016 (54% $T_{n,BD}$ decrease at research area B) may reflect hysteresis, natural LNAPL depletion or mass migration within the LNAPL body. Hysteresis has been acknowledged as a crucial reason for a 20% T_n difference during imbibition and drainage periods in homogeneous porous media (Palmier, Cazals & Atteia 2017).

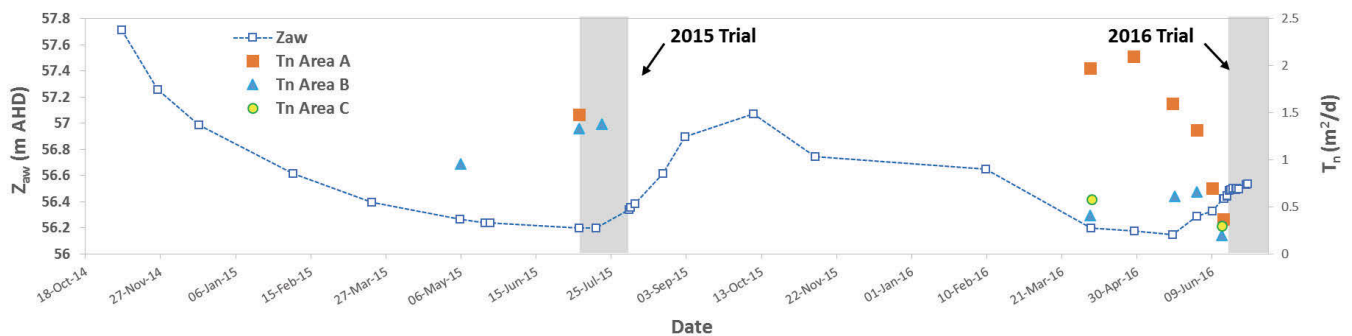


Figure 6. 7. Contaminated site hydrograph along with bail-down T_n values at the three research areas. Gray columns indicate the time periods of recovery applications in 2015 and 2016.

6.4. Estimation of LNAPL Drawdown during Mass Recovery Trials

The estimation of LNAPL drawdown (s_n) is crucial for the calculation of NAPL transmissivity during mass recovery trials. The importance of s_n can be seen at Table 6.4 in the sensitivity analysis section. For the calculation of s_n , the equilibrium levels of NAPL in the formation should be known, especially the Z_{an} of the mobile interval. Monitoring wells in the vicinity of the remediation wells were chosen. The specific monitoring wells presented the same NAPL hydrogeological conditions with the tested wells, as well a good correlation of Z_{an} elevations with $R^2 > 0.99$. Both recovery and monitoring wells presented unconfined conditions during the experiments periods of skimming processes.

2015 Mass recovery trial

During the 2015 mass recovery trial, the formation equilibrium levels at area A (constant Z_{aw}) were validated by monitoring the fluid levels in periods of mass recovery cessation.

At area B, the monitoring well PB09 was used for the estimation of Z_{an} during a rising water table. Figure 6.8 illustrates the DTP correlation between the wells PB27-PB09 (see also Table D.1 in Appendix D). The equation $y = 1.0276x + 0.0125$ is referred to unconfined LNAPL periods in both wells and it was used for the estimation of DTP at PB27 well during the skimming processes.

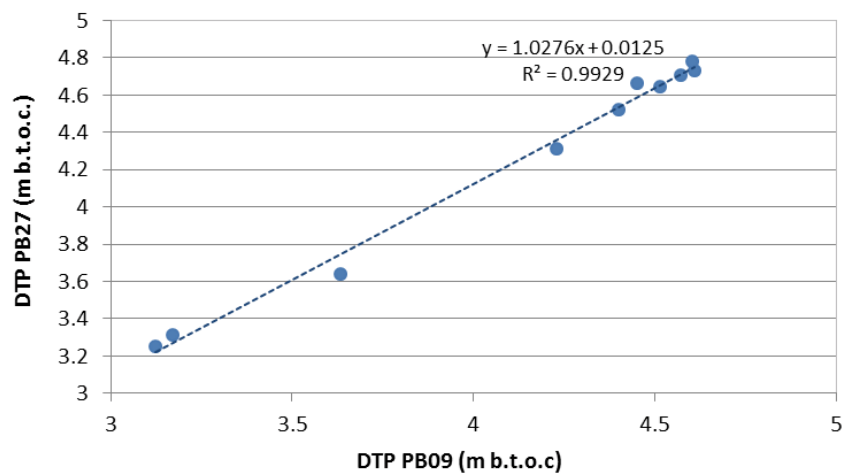


Figure 6. 8. DTP correlation between the wells PB27 - PB09 (monitoring period: 5/11/2014-21/07/2015).

2016 Mass recovery trial

Figure 6.9 presents the potentiometric surface elevation correlation between the wells PB27 and PB09 for the needs of NAPL drawdown calculation during the 2016 mass recovery trial. Two trend lines are depicted in this graph. The blue color contains data since 2015 and is related to unconfined NAPL condition periods (see Table D.2 in Appendix D). The orange color includes data only during the year 2016 under rising water table conditions. Both equations were tested with Z_{an} values of PB09 well just before the start of trial. The equation: $y = 0.976x + 1.353$ (blue color line) gave more precise results (< 1 mm difference) for the Z_{an} at PB27 compared to the equation: $y = 1.0093x + 0.5226$ (orange color line), thus the first equation was used. The difference between the two equations was in the range of 2 - 5 mm.

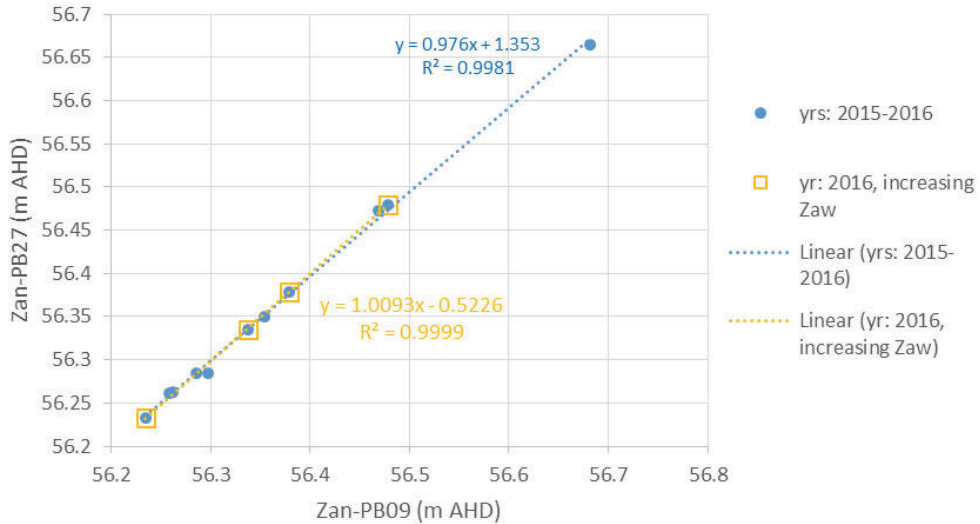


Figure 6. 9. Z_{an} correlation between the wells PB27-PB09 (monitoring period: 19/03/2015-15/06/2016).

Figure 6.10 depicts the Z_{an} correlation between the recovery well PB29 and the monitoring well MP50. The presented data points are referred to unconfined NAPL conditions. The equation: $y=0.9927x+0.4063$ for the estimation of Z_{an} at PB29 well during the hydraulic testing processes in 2016, was used. The monitoring data can be seen at Table D.3 in Appendix D.

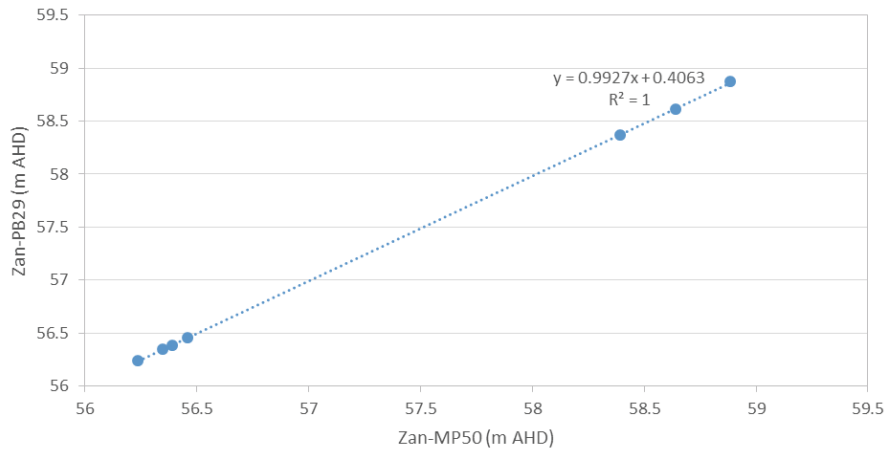


Figure 6. 10. Z_{an} correlation between the wells PB29-MP50 (monitoring period: 20/05/2016-5/10/2016).

Figure 6.11 illustrates the Z_{an} correlation between the remediation well PB40 and the monitoring well PB11. The data points are comprised in an unconfined NAPL period before the trial in 2016, during rising water table conditions (see Table 4 and Figure D.1 in Appendix D). The used equation is: $y=0.9775x+0.1308$.

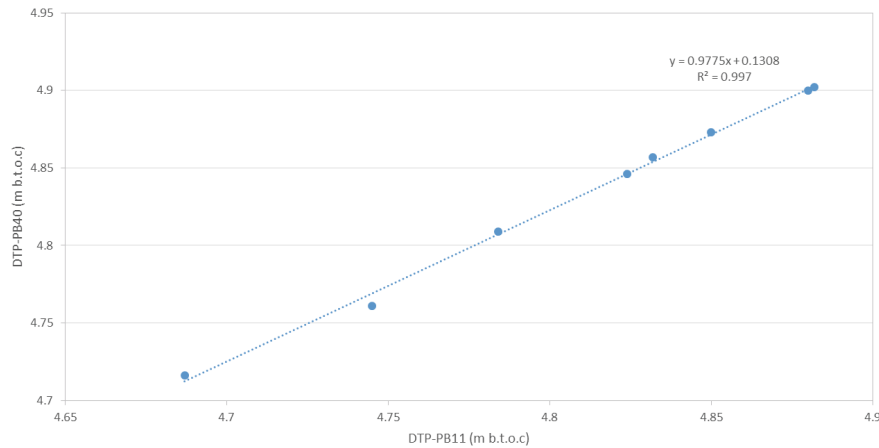


Figure 6. 11. DTP correlation between the wells PB40-PB11 (monitoring period: 5/04/2016-14/06/2016).

Summary of section 6.4

Results indicated that there was a good correlation between Z_{an} values obtained by the monitoring points MP50, PB09 and PB11 and the remediation wells PB29, PB27 and PB40 respectively. It should be noticed that, the estimation of precise s_n estimates under rising Z_{aw} during the mass recovery trials, is significant for all the presented T_n values in the next sections of the Thesis. Monitoring points that present same hydrogeological conditions with the remediation wells should be chosen, as errors especially during confined LNAPL conditions may arise.

6.5. Variability in LNAPL Transmissivity during Skimming

Table 6.1 presents the hydrogeological conditions during the conducted mass recovery experiments in 2015 and 2016. All the mass recovery tests were conducted under unconfined LNAPL conditions, according to the transition point elevation (see also Appendix K).

Table 6. 1. LNAPL hydrogeological conditions during the pilot-scale trials.

Well	Date	Transition point (m AHD)	NAPL conditions	Z_{aw} (m AHD)	$Z_{an, max}$ (m AHD)	Lithology
PB29	8/7/15-20/7/15	-	unconfined	56.18-56.20	56.29	sand
PB27	20/7/15-3/8/15	56.8	unconfined	56.20-56.30	56.33	sand with few silt

PB29	15/6/16-6/7/16	-	unconfined	56.40-56.53	56.55	sand
PB27	16/6/16-7/7/16	56.8	unconfined	56.40-56.53	56.58	sand with few silt
PB40	15/6/16-7/7/16	56.7-56.8	unconfined	56.40-56.53	56.65	sand-silty sand

Figure 6.12 shows the three chosen areas for research at the contaminated site. The three areas were chosen for experimental processes to account for spatial variability and the site heterogeneity. The areas of interest showed almost similar initial $T_{n,BD}$ values in 2015 ($1.4 \text{ m}^2/\text{day}$) and in 2016 ($0.2 - 0.37 \text{ m}^2/\text{d}$), however differences in the vertical NAPL distribution and the stratigraphic profile in the three areas, exist. The T_n calculations are presented in the Appendix E (Tables E.3 - 17).

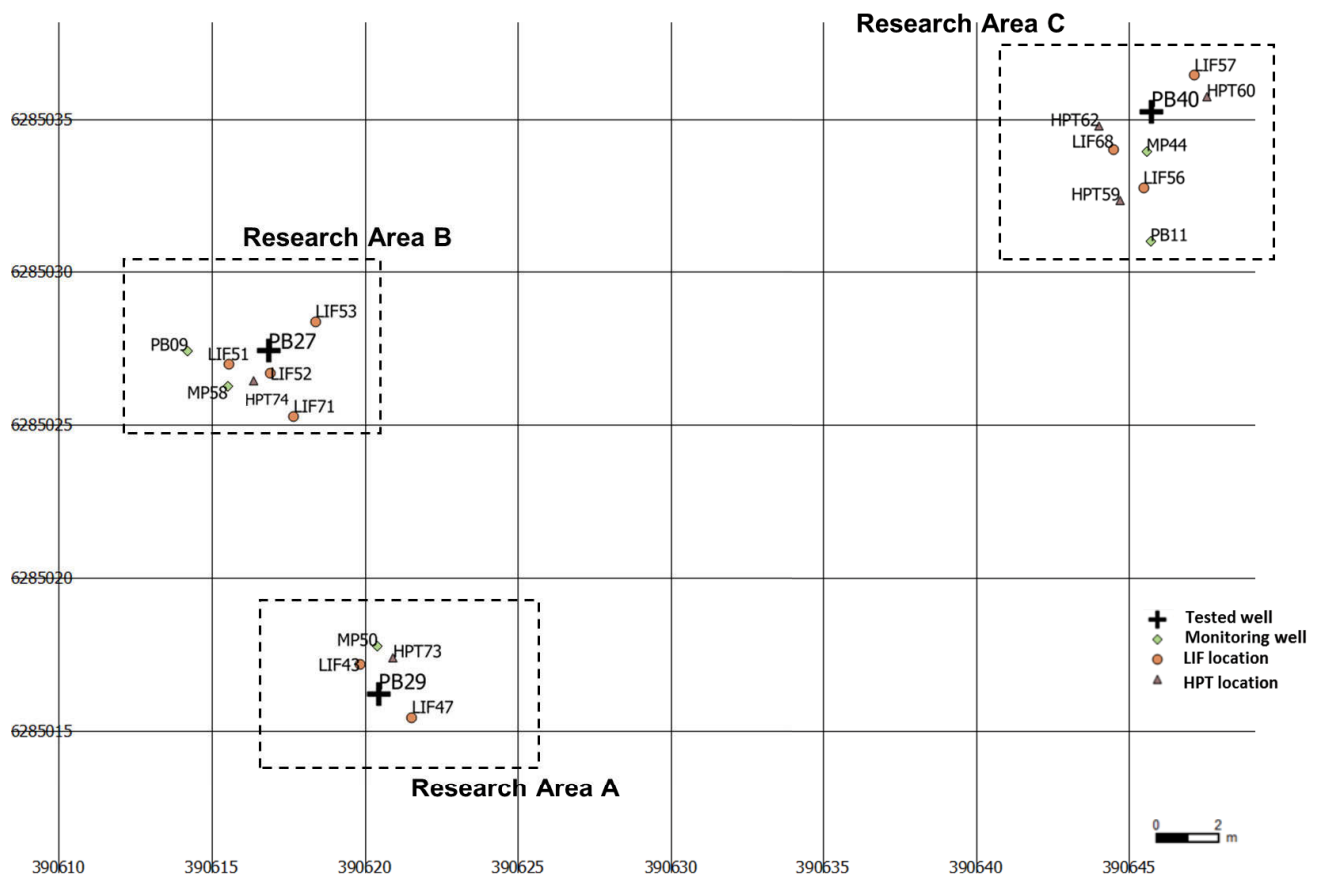


Figure 6. 12. Site layout showing the three research areas A, B and C. Tested and monitoring wells, LIF and HPT points are illustrated.

LNAPL saturations obtained from extracted cores before the 2016 mass recovery trial, as well as HPT and LIF logs from surrounding direct-push locations, are presented in Figures 6.13 - 6.15. The highest NAPL saturations were found at area C, where the material was finer.

During the skimming trials, soil coring, HPT and LIF profiles suggested that the mobile NAPL interval was mainly located in silty sands at area C. There were also greater differences between the HPT logs obtained at area C compared to the other areas. This can be seen through the three different HPT logs corresponding to this area in Fig. 6.15. In areas A and B, the mobile NAPL interval was located in sandy material. Area B (Figure 6.14) presented similarities with area A regarding the geological material. A notable measurement at area A was the distinct and very high LIF signals (compared to areas B and C, Figures B.10 – 17 in Appendix B) within an interval of just 12 cm, where a slightly coarser material was identified. Therefore, the highest LIF signals were present in the area with the lowest NAPL saturation values. Because the LIF signal depends on both the NAPL saturation and the geology, it was an interesting tool to delineate transmissive intervals, although with some limitations. This thin layer probably worked as a preferential migration pathway constraining the NAPL vertical displacement due to the capillary contrasts.

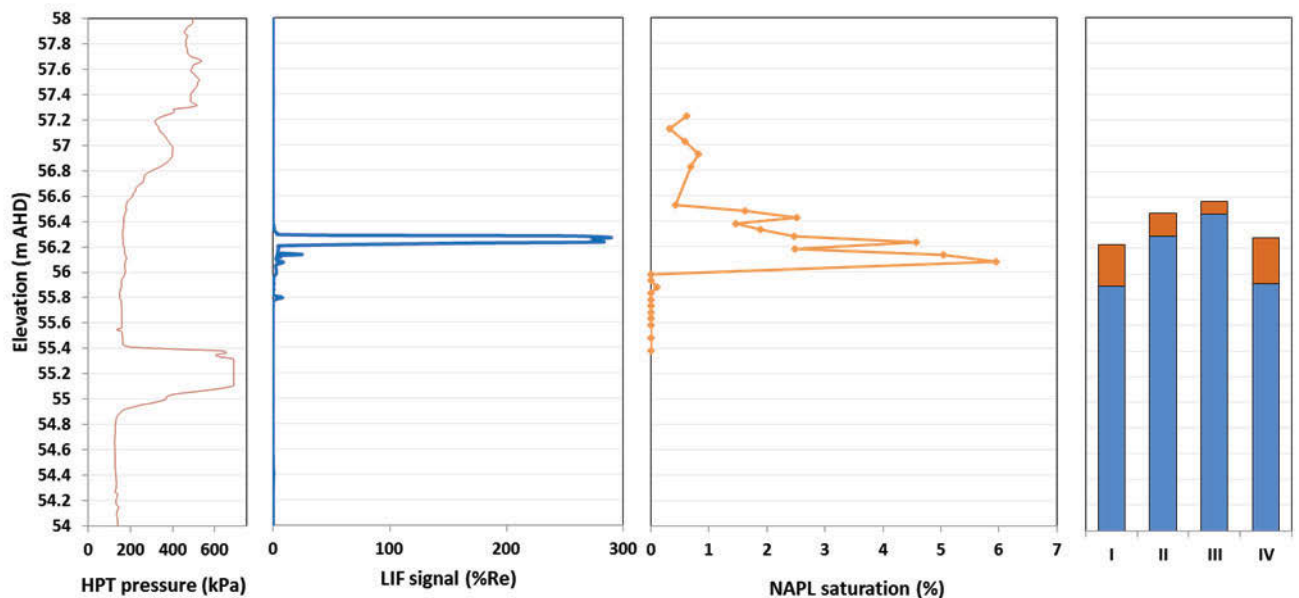


Figure 6. 13. HPT73 – LIF43 profiles along with NAPL saturations (MP50) and in-well thicknesses, b_n (PB29 well), at research area A. Four different fluid elevations are illustrated: I refers to fluid levels the day of core sampling (late May 2016), II shows the fluid levels the day before the 4-week sequential free recovery trial (mid-June 2016), III presents fluid levels just after the end of the recovery trial (early July 2016) and, finally, IV refers to the fluid levels just before the 2015 trial (early July 2015).

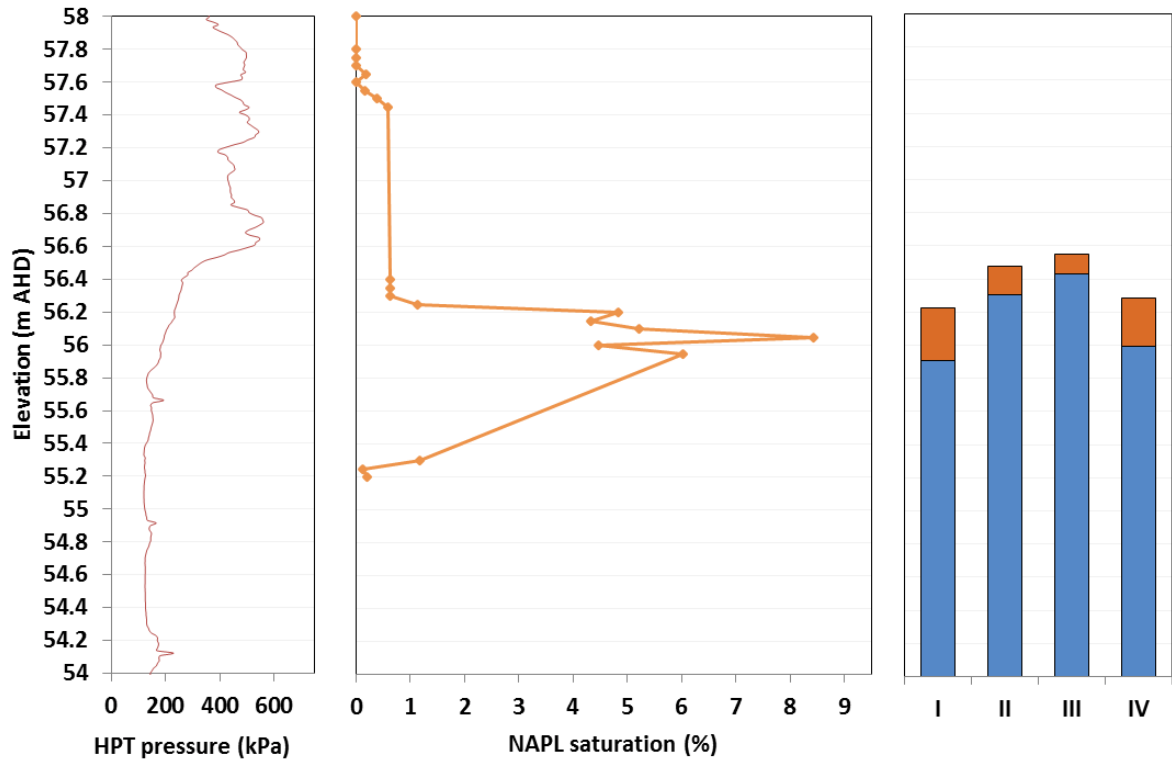


Figure 6. 14. HPT74 profile along with NAPL saturations (MP58) and in-well thicknesses, b_n (PB27 well) at research area B. Four different fluid elevations are illustrated: **I** refers to fluid levels the day of core sampling (late May 2016), **II** shows the fluid levels the day before the 4-week sequential free recovery trial (mid-June 2016), **III** presents fluid levels just after the end of the recovery trial (early July 2016) and, finally, **IV** refers to the fluid levels just before the 2015 trial (early July 2015).

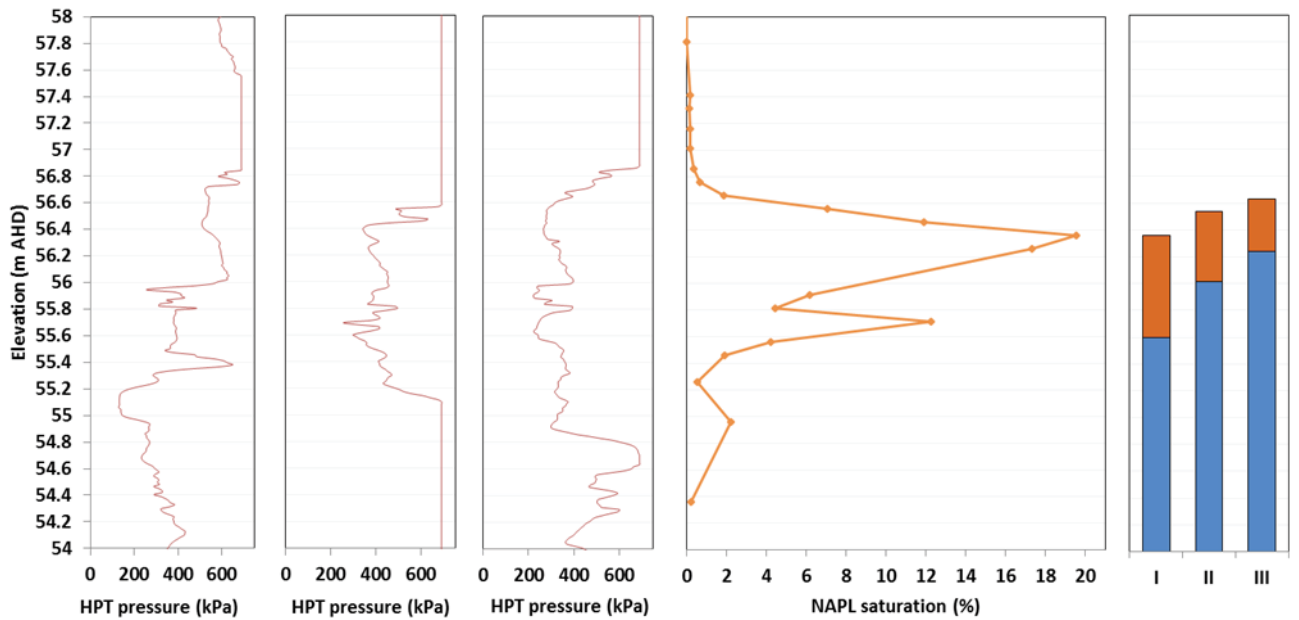


Figure 6. 15. HPT59, HPT60 HPT62 profiles along with NAPL saturations (MP44) and in-well thicknesses, b_n (PB40 well), at research area C. Three different fluid elevations are illustrated: **I** refers to fluid levels the day of core

sampling (late May 2016), **II** shows the fluid levels the day before the 4-week sequential free recovery trial (mid-June 2016) and **III** presents fluid levels just after the end of the recovery trial (early July 2016).

In addition, Figures 6.13 – 6.15 present four sets of fluid levels (**I**, **II**, **III**, **IV**) corresponding to different time periods through the research. **I** refers to fluid levels the day of core sampling (late May 2016), **II** shows the fluid levels the day before the 4-week sequential free recovery trial (mid-June 2016), **III** presents fluid levels just after the end of the recovery trial (early July 2016) and, finally, **IV** refers to the fluid levels just before the 2015 trial (early July 2015). Both **I** and **IV** refer to the lowest monitored Z_{aw} during the years 2015-2016 with small differences in Z_{an} and Z_{nw} . The NAPL saturation profiles correspond to the case **I**. A different NAPL distribution, exhibiting lower NAPL saturation values is expected at case **II**, as it has been documented in the case of a gasoline contaminated sandy aquifer with a rising potentiometric surface (Steffy, Johnston & Barry 1995). At the beginning of the mass recovery trials, higher values of $T_{n,BD}$ were measured in July 2015 (1.48 m²/d) compared to June 2016 (0.37 m²/d). In 2015, the research took place under low water table conditions, whereas in 2016 the water table was 20 - 25 cm higher. It should be remarked that the NAPL recovery was negligible in all the research areas at the end of the 2016 trial.

2015 Mass recovery trials

Figures 6.16 and 6.17 illustrate time series of T_n during bail-down ($T_{n,BD}$) and skimming ($T_{n,SK}$) testing along with Z_{aw} at areas A and B (see Tables 3 and 4, in Appendix E). The 2015 trials were conducted sequentially in areas A and B under relatively constant water table conditions in the case of area A (water table elevation increased at a rate of +1 cm/week) and a rising potentiometric surface in the case of area B (water table elevation increased at a rate of +5 cm/week). Before steady state conditions were reached, relatively high recovery rates (Q_n) occurred during startup of skimmers in many occasions, due to the amount of product stored in the well's filter pack (Johnston et al. 2002; Lundy, Li & Katyal 2002). At area A, the mass recovery trial was conducted under seasonally low water table conditions when b_n presented the highest values. Further analysis of these graphs is presented in section 6.7.

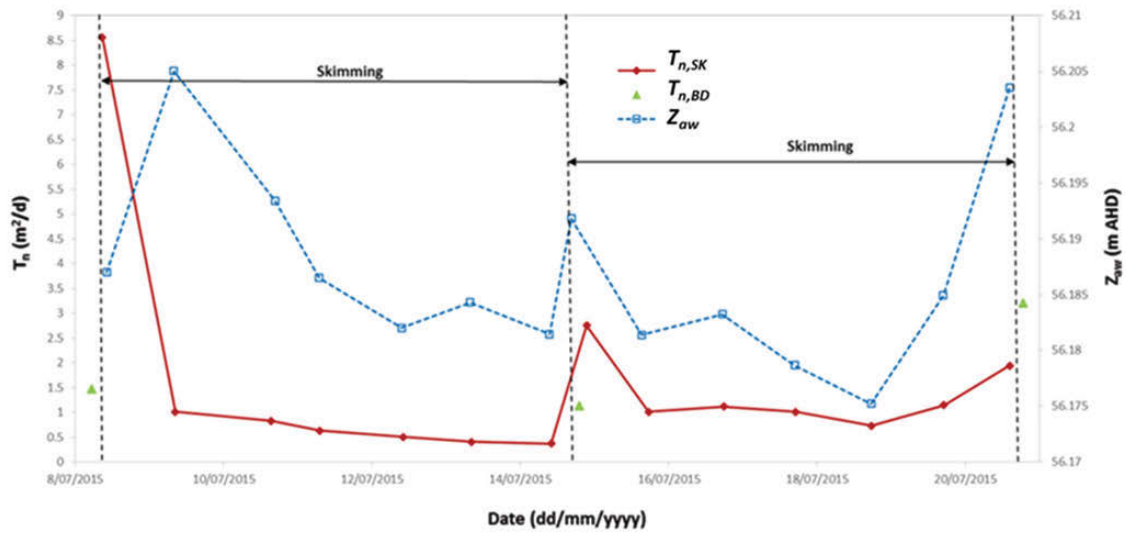


Figure 6. 16. Time series of LNAPL transmissivity and potentiometric surface elevation during bail-down testing and skimming processes, at research area A, well PB29, in 2015.

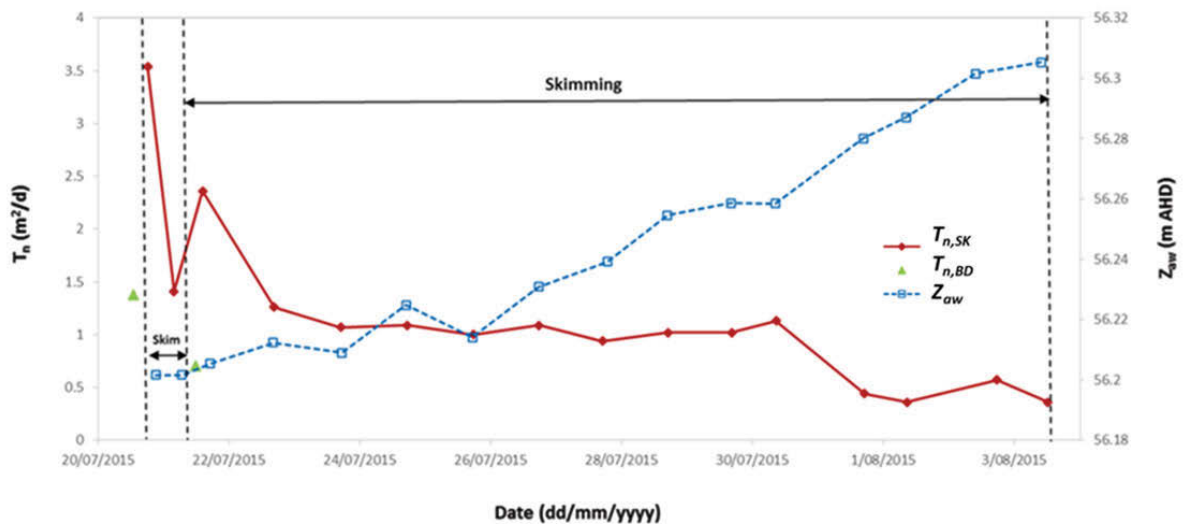


Figure 6. 17. Time series of LNAPL transmissivity and potentiometric surface elevation during bail-down testing and skimming processes, at research area B, well PB27, in 2015.

2016 Mass recovery trials

Figures 6.18 - 6.20 depict changes in T_n and Z_{avg} during the mass recovery trial in 2016 including skimming, water-enhanced skimming, vacuum- enhanced skimming and water- and vacuum-enhanced skimming. The trial was conducted under rising water table conditions (water table elevation increased at a rate of +7.5 cm/week at the beginning of the trial).

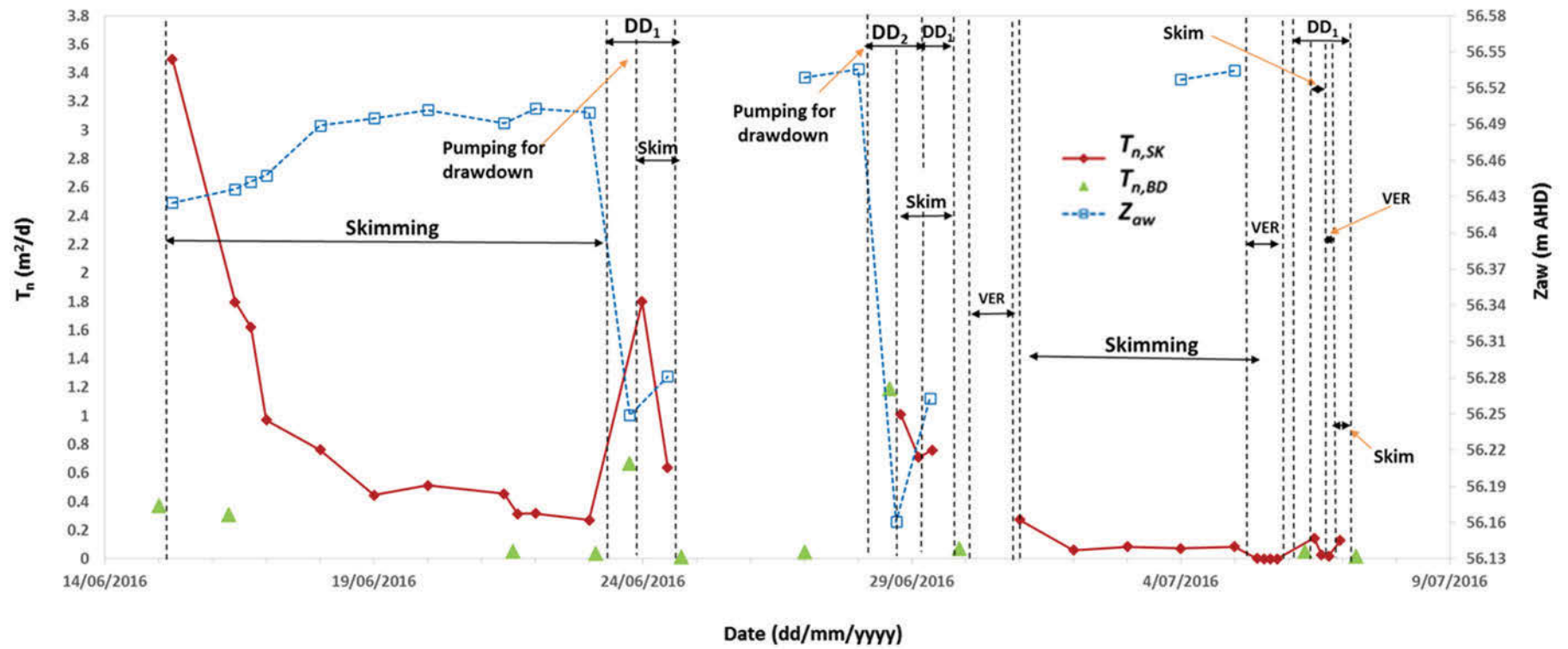


Figure 6. 18. Profiles of T_n and Z_{aw} during bail-down testing and hydraulic free recovery processes, at research area A, well PB29.

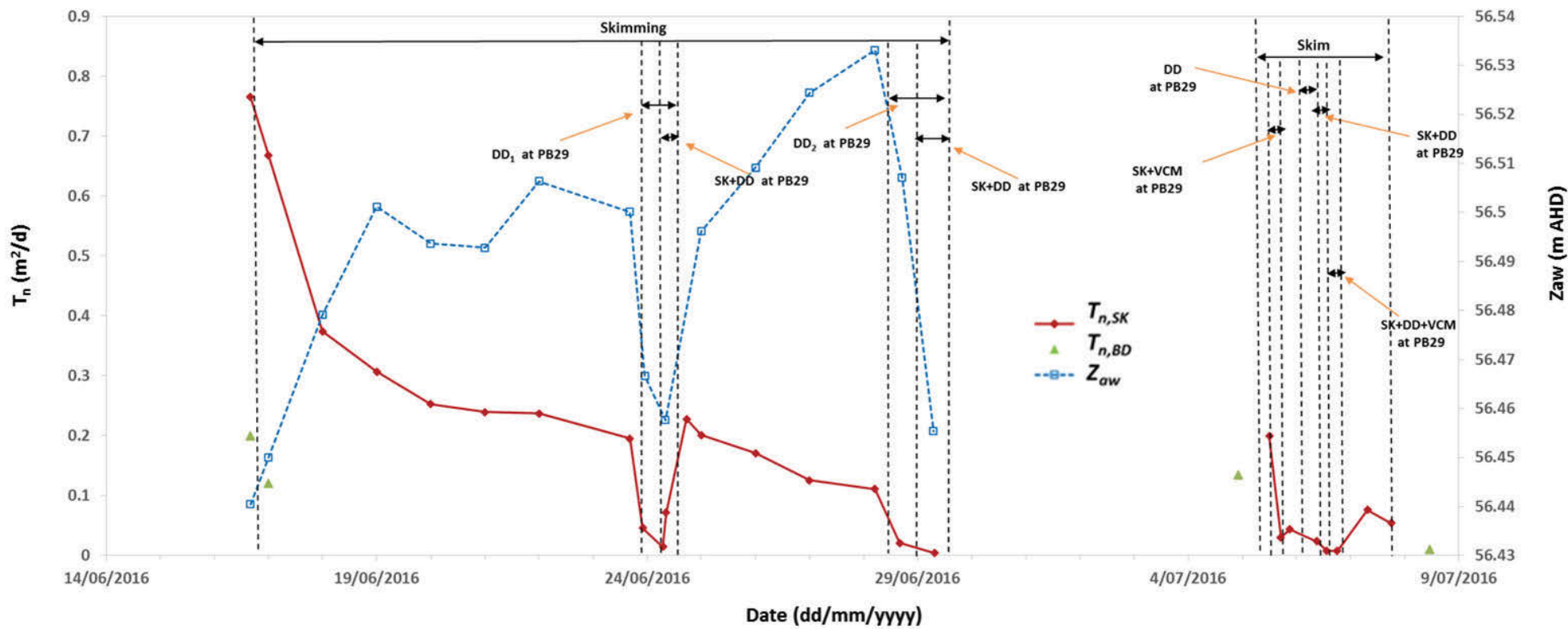


Figure 6. 19. Profiles of T_n and Z_{aw} during bail-down testing and hydraulic free recovery processes, at research area B, well PB27.

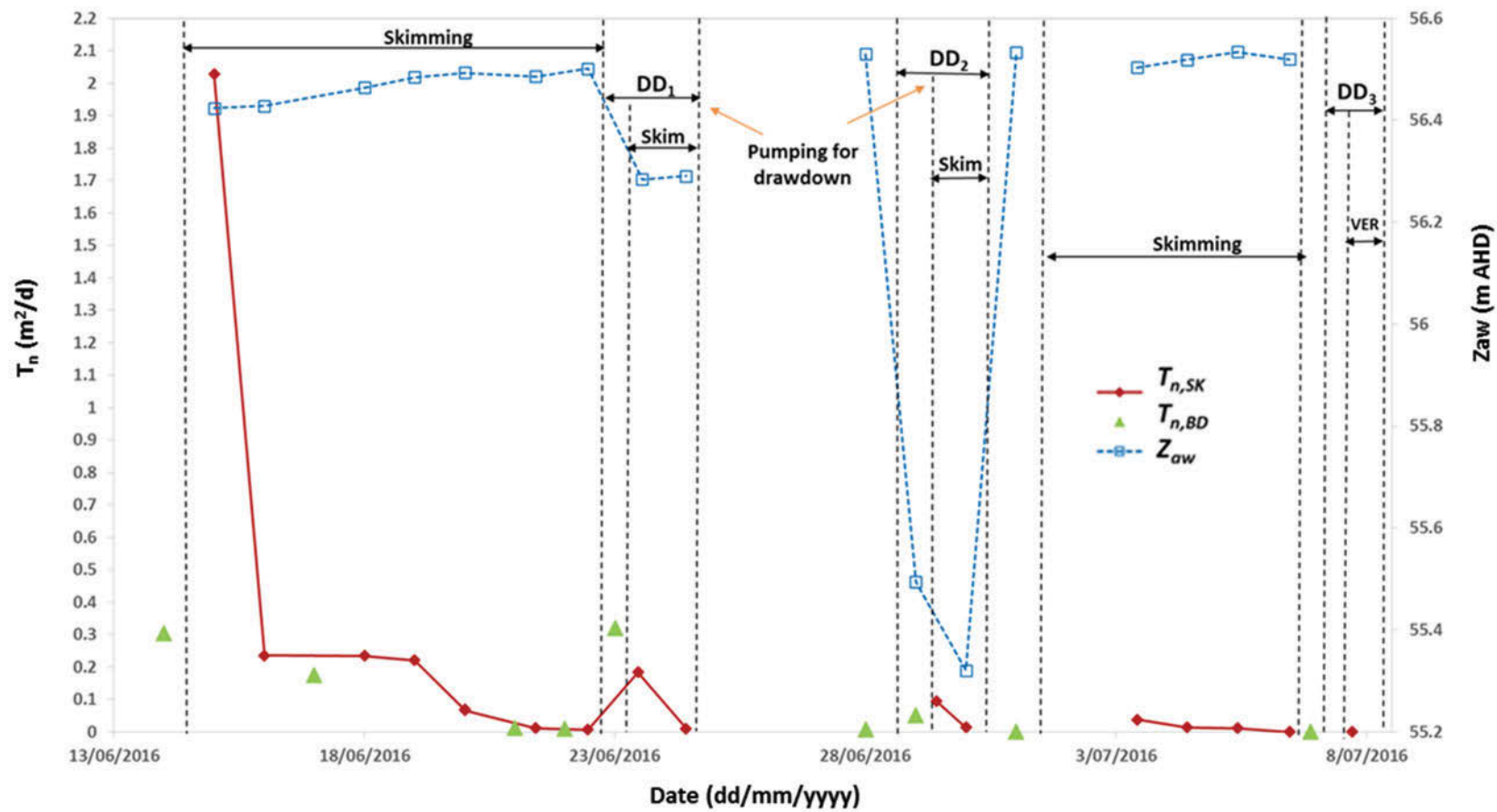


Figure 6. 20. Profiles of T_n and Z_{aw} during bail-down testing and hydraulic free recovery processes, at research area C, well PB40.

Figure 6.21 illustrates changes in $T_{n,SK}$ with Z_{aw} during the first week of the skimming trial in 2016. As it can be inferred from this graph, during the first 5-cm rise in Z_{aw} , the LNAPL recoverability was less affected at research area C than in the other areas. One important factor was that the NAPL saturations were higher. How the NAPL saturation is affected by Z_{aw} changes depends on the capillary pressure-saturation relationship. Moreover, the NAPL mobile interval was larger at this area. In relation to this, the in-well thickness (4.5 times larger at area C than at area A) was reduced by 7% at area C, but it decreased by 15% at area A during this period of time. Thus, entrapment phenomena and vertical displacement had a higher impact at area A at this stage. It should also be noticed that the lowest NAPL recovery rates were measured at area C. Later measurements showed $T_{n,SK}$ approaching zero under constant water table conditions at area C due to product depletion through skimming in the surrounding subsurface. Low $T_{n,BD}$ measured values in surrounding wells was another indication of the low LNAPL mobility at this area.

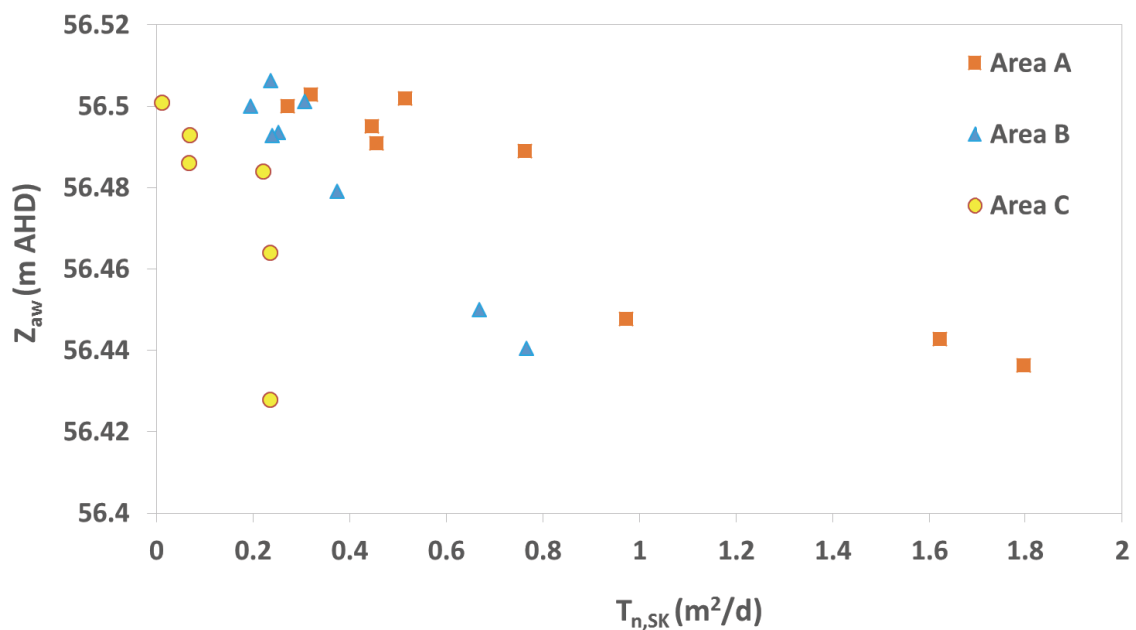


Figure 6. 21. Profiles of $T_{n,SK}$ and Z_{aw} at areas A, B, and C during the first week of the 2016 skimming trials.

Figure 6.22 presents changes in $T_{n,BD}$ before and during the skimming trial at area A in 2016. From this figure, it can be inferred that T_n was quite sensitive to water table changes, while the impact of the skimming operations was not so clear. Consequently, LNAPL entrapment and vertical displacement may have played a greater role on the temporal reduction of T_n than the mass recovery method. This is supported by relatively constant T_n during periods of stable water table conditions. Further, T_n did not change under constant Z_{aw}

at area A during the 2015 trial either, whereas the effect of a rising Z_{aw} had a negative impact on T_n at area B. The behaviour shown in Fig. 6.22 indicated that the assessment of the performance of a remediation system through T_n could be misleading. For instance, other authors acknowledged the effectiveness of a LNAPL recovery system after observing a T_n decrease of 47% in 18 months of recovery operation (Palmier, Dodt & Atteia 2016). However, Fig. 6.7 shows a 54% $T_{n,BD}$ reduction under natural conditions without remediation operations at area B between 2015 and 2016

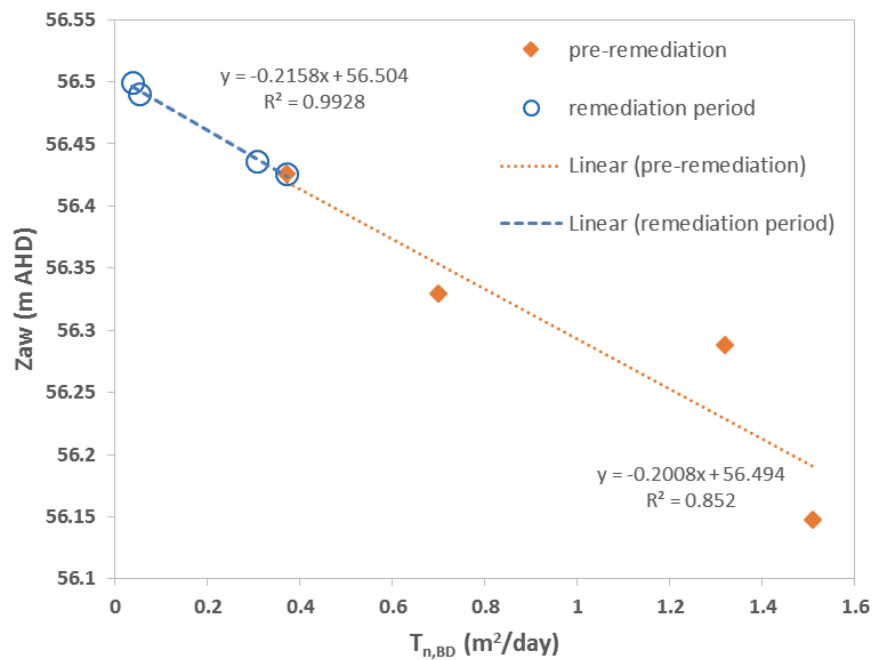


Figure 6. 22. $T_{n,BD}$ values before and during the 2016 skimming trial at area A.

6.6. Variability in LNAPL Transmissivity during Induced Water Table Drawdown

Figures 6.23 – 6.25 show T_n changes at areas A, B and C during the recovery trials in both years 2015 and 2016. This graph depicts T_n values obtained by bail-down testing, skimming and water-enhanced skimming operations. A comparison between the applied methods is discussed in detail in section 6.7.

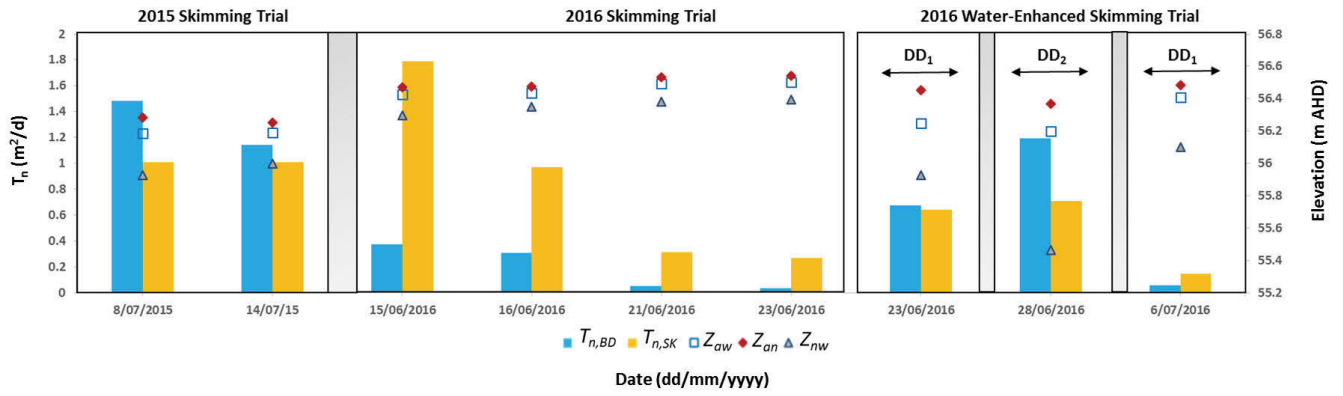


Figure 6. 23. Comparison of T_n values between bail-down testing, skimming and water enhanced skimming along with fluid elevations at area A (2015 and 2016 trials).

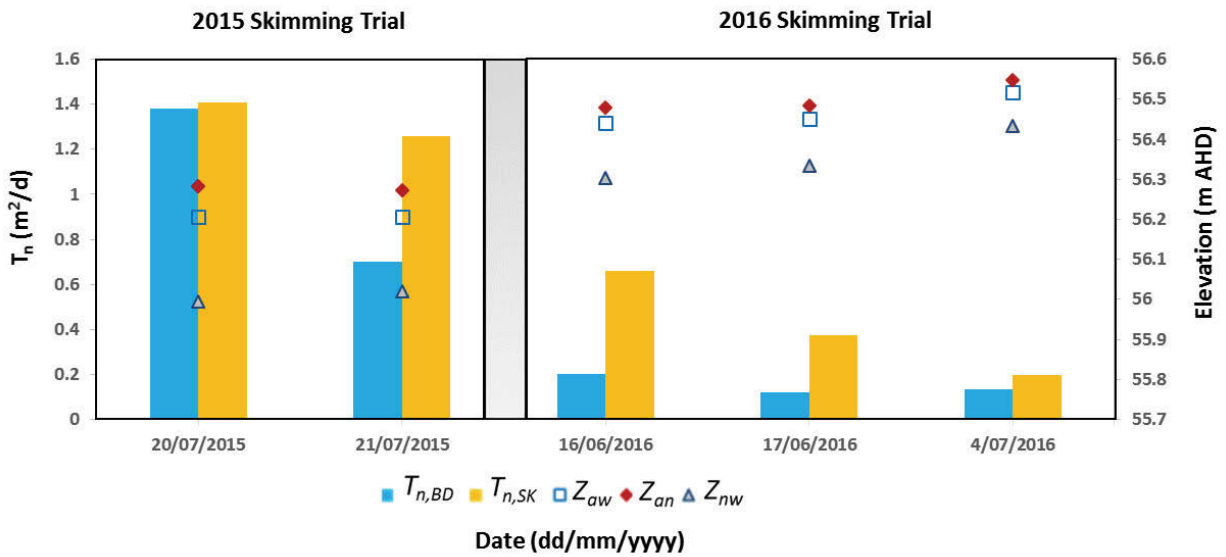


Figure 6. 24. Comparison of T_n values between bail-down testing, skimming and water enhanced skimming along with fluid elevations at area B (2015 and 2016 trials).

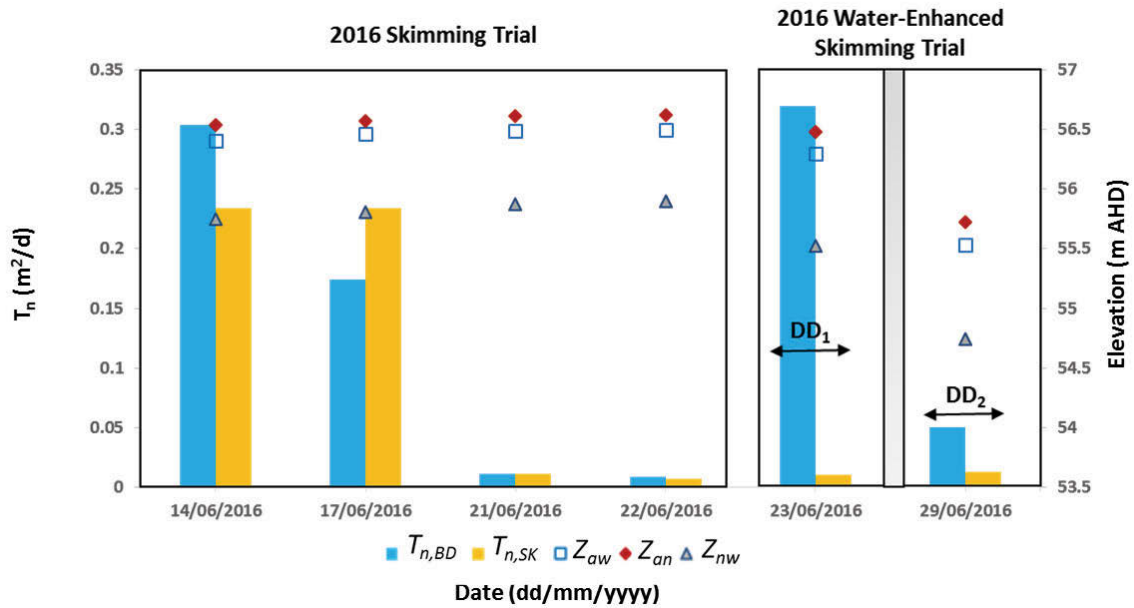


Figure 6. 25. Comparison of T_n values between bail-down testing, skimming and water enhanced skimming along with fluid elevations at area C (2015 and 2016 trials).

As concerns area A (see Fig. 6.23), T_n values were found to be higher than those obtained without altering the Z_{aw} . The applied DD_2 resulted in higher T_n values and in-well thicknesses compared to DD_1 . Afterwards, DD_1 was imposed again at area A, presenting lower T_n values compared to the first application of DD_1 . This behavior was influenced by the redistribution and entrapment of NAPL after DD_2 as well as the product depletion.

As regards area C, the main difference was that T_n was higher only during the first hours after inducing water table drawdown. Afterwards, $T_{n,SK}$ was close to zero due to the low intrinsic permeability (see HPT logs in Fig. 6.15) and the depletion of accumulated product in the vicinity of the well. Once that this NAPL was extracted, the applied drawdown and the generated gradient was not enough to induce the migration of NAPL located further away, referring to the short timeframe of the conducted experiments. Consequently, experiments of inducing water table drawdown should last long enough to remove these artifacts and assess NAPL recoverability in the long-term. The application of DD_2 did not favor a T_n increase, taking into consideration that Z_{nw} was 54.7 m AHD and, according to Fig. 6.15, low entrapped NAPL saturations in a clayey material existed from 54.7 to 55.3 m AHD, not contributing significantly to the NAPL recovered volume.

6.7. Comparison between LNAPL Transmissivity Estimated from Bail-down and Mass Recovery Methods

A comparison of T_n values estimated through the different applied testing methods is shown in Figures 6.23 - 6.25 (see also Appendix K). The presented values of $T_{n,SK}$ refer to steady state conditions. In general, there was a relatively close agreement between $T_{n,BD}$ and $T_{n,SK}$ in most of the cases, with differences within a factor of 2. This magnitude is considered reasonable (ASTM 2013) and consistent with what has been documented in the literature (Nagaiah, Law & Ueland 2015). More specifically, the differences between $T_{n,BD}$ and $T_{n,SK}$ were relatively small under stable water table conditions. However, larger differences by a factor up to 7.3 were found at area A and up to 3.2 at area B during the 2016 mass recovery trial under rising water table conditions.

Fig. 6.26 presents the changes of $T_{n,SK} / T_{n,BD}$ ratio with different potentiometric surface elevations at areas A, B and C. The figure contains periods when skimming and water-enhanced skimming recovery methods were applied. As the $T_{n,SK} / T_{n,BD}$ ratio approaches the unity, bail-down testing estimations could be considered as good predictors of T_n and recoverability for mass recovery applications. Before inducing a gradient in the potentiometric surface, it could be inferred that there was a better agreement between $T_{n,SK}$ and $T_{n,BD}$ at area C, where the material was finer compared to areas A and B. One main factor was the radius of capture.

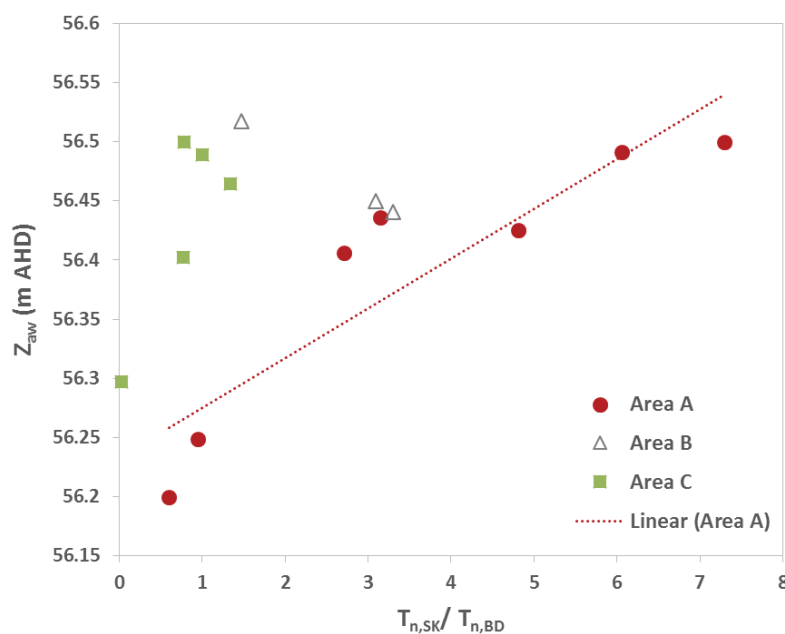


Figure 6. 26. Profile of Z_{aw} values along with $T_{n,SK} / T_{n,BD}$ ratio values at areas A, B and C during the skimming and water-enhanced skimming trials in 2016.

Figure 6.26 also showed that the difference between both applied methods may be a function of Z_{aw} among other factors. Thus, it was observed that the aforementioned difference by a factor of 7.3 corresponded to the highest Z_{aw} . As depicted in Fig. 6.13, the LNAPL distribution at area A was mainly present within a short interval and not significantly smeared across the lithological profile, whereas a wider LNAPL vertical distribution with higher saturations existed at area C. Therefore, the remarkably high $T_{n,SK} / T_{n,BD}$ ratio at high Z_{aw} was likely due to the coupled effect of the differences in the radius of capture between the two estimation methods and the low LNAPL saturations predominantly constrained to a thin layer. Apparently, bail-down testing was more sensitive to the rising water table than the skimming system, as it can be inferred from the decreasing $T_{n,SK}$ with an increasing $T_{n,SK} / T_{n,BD}$ ratio. Thus, the accuracy of $T_{n,BD}$ as a predictor of $T_{n,SK}$ may be compromised when significant water table fluctuations exist. Area B presented also a narrow NAPL distribution and similar b_n and NAPL saturation values to area A at the beginning of the trial. This period, similar $T_{n,SK} / T_{n,BD}$ ratio values of 3 at both areas can be seen in the graph above. Thus, it could be said that the evolution of the discrepancies between both applied methods can be different at areas with similar NAPL distribution and saturations due to dissimilar geological layering.

Regarding the water-enhanced skimming experiments (Figures 6.23 and 6.25), the estimated values of $T_{n,BD}$ compared well with $T_{n,SK}$ at research area A (factors 1.7- 2.7), while the difference was higher at research area C (factors 3.8 – 32). At this area, NAPL recovery diminished rapidly, being the NAPL flow towards the well negligible due to the low intrinsic permeability of the silty sand material. As a consequence the bail-down test performed at the start of the experiment was not a good predictor of the $T_{n,SK}$ evolution.

6.8. Effect of Induced Vacuum on LNAPL transmissivity

Table 6.2 presents only $T_{n,SK}$ results at area A as the applied vacuum at area C resulted in no product recovery (see Tables E.9, 10 and 16 in Appendix E). As it was presented above, the water table drawdown showed already zero $T_{n,SK}$ values at area C and the applied vacuum during potentiometric surface drawdown did not favor the product recovery.

Table 6. 2. Effect of applied vacuum on T_n at PB29 well, area A.

Date	Remediation Technique	Applied Vacuum (kPa)	Water Removal Rate (L/min)	T_n (m²/day)
05/07/2016	SK+VCM	-1	-	0.0034
05/07/2016	SK+VCM	-2	-	0.0020
05/07/2016	SK+VCM	-3	-	0.0015
05/07/2016	SK+VCM	-4	-	0.0012
06/07/2016	SK+VCM+DD	-1.5	4	0.028
06/07/2016	SK+VCM+DD	-2.5	4	0.019

Where: SK+VCM is vacuum enhanced skimming processes and SK+VCM+DD is water and vacuum enhanced skimming applications.

The applied vacuum in area A presented lower $T_{n,SK}$ values during SK+VCM and SK+VCM+DD experiments. As it can be inferred from this table, there is an inverse relationship between applied vacuum and T_n values during SK+VCM and SK+VCM+DD. The T_n estimation was based on Equations 29 and 30. Higher applied vacuum pressure increases the air flow which enhances the volatilization of NAPL, thus higher Q_a values affected negatively the T_n . Furthermore, water and vacuum enhanced trials depicted 10 times higher T_n values than the vacuum enhanced processes for the same applied vacuum values.

The mass recovery testing at area C presented lower liquid and gas phase extraction rates than area A (see performance assessment in Appendix H). Vacuum enhanced recovery has been documented as more suitable in permeable soils (Halmemies 2003). Travel times of gases to vapor extraction wells are influenced as well by permeability anisotropy (Shan, Falta & Javandel 1992) and spatial variability of permeability has a negative impact on vapor recovery times (Massmann, Shock & Johannesen 2000).

It should be mentioned that, during the application of vacuum more than 99.5% of the total NAPL recovery at both areas was in gas phase. Related works in the literature have also documented cases where NAPL extraction took place mainly in gas phase during the application of vacuum (Halmemies et al. 2003; Li et al. 2002). The high volatility of gasoline and the fine textured material at the top of the aquifer which allows the application of an effective vacuum (Heffron, Blanchard & Dogrul 2003) and acts also as a barrier for the upward migration of vapours (high accumulated VOCs masses), are two significant reasons for the high NAPL removal through gas phase. In contrast, other related research works in sandy materials (Johnston et al. 2002; Johnston et al. 2001) have documented similar contribution of liquid recovery and VOC extraction to NAPL removal. Consequently, in such heterogeneous

systems, the application of vacuum for gas phase removal is more preferable (due to the aforementioned reasons above) than the application of skimming or water-enhanced skimming that target only on liquid phase recovery, as the low intrinsic permeability and the rising water table may limit the LNAPL removal.

6.9. The Impact of Physical Properties Changes and Mobile Interval on T_n

In this section, the impact of the physical properties changes and mobile NAPL interval (linked to the intrinsic permeability) on $T_{n,BD}$ during the mass recovery trials in 2016, is presented.

Physical changes

Tables F.4-6 in Appendix F present the density and viscosity measurements during the recovery trials the year 2016 at the three research areas A, B and C. As it has already been presented in Equation 15 and 16, NAPL transmissivity is affected by changes in density and viscosity of NAPL. In this section, an evaluation of the impact of physical properties on T_n is presented. Chemical composition changes affect the density and viscosity values. BTEX and nC4-nC5 presented the highest mass percentages in the NAPL samples (see chemical composition changes section in Appendix F), as well nC4-nC5 illustrates 3-5 times lower viscosity values compared to BTEX (Lari, Johnston & Davis 2016). Figures F.1, F.2 and F.3 in Appendix F depicted changes of less than 10% on BTEX and nC4-nC5 mass percentages during the 2016 experimental procedures.

During the 2016 mass recovery trial, measurements of the physical properties showed changes of the ratio density/viscosity up to 17% in the three research areas, however $T_{n,BD}$ was decreased by more than 90% due to changes in b_n , NAPL relative permeability and intrinsic permeability as it is presented later in this section.

Mobile interval and T_n changes

The presented b_n analysis refers to the three research areas during one imbibition period in 2015 and another one imbibition period in 2016 (mass recovery periods), in contrast with section 6.2 which contains an analysis of the whole contaminated site since 2015 (natural

conditions). The conclusion of subchapter 6.2 was based on several well locations of different NAPL hydrogeological conditions and distributions indicating that, b_n was not a good indicator of T_n estimates. As it has already been presented in Equations 15 and 16, T_n depends on the thickness of the NAPL mobile interval. The mass recovery experiments took place under unconfined NAPL conditions, where in-well NAPL thickness can be used as an indication of the NAPL mobile interval in the formation (Kirkman, Adamski & Hawthorne 2013). A decrease of NAPL thickness (of the mobile interval) in the formation is related to a NAPL saturation reduction (Beckett & Huntley 1998; Lundy, Li & Katyal 2002). NAPL saturations were measured only at the beginning of the experiments in 2016, thus changes of b_n will be related with changes in NAPL relative permeability.

Figures 6.27 – 6.29 present the relationship between b_n and $T_{n,BD}$ at areas A, B and C. The blue colour line corresponds to the mass recovery trial in 2016 and the red colour line to the 2015 experimental trial. As it can be inferred from these graphs, $T_{n,BD}$ decreases as b_n illustrates lower values. Different slopes between 2015 and 2016 are depicted.

As regards area A, taking into consideration that similar values for intrinsic permeability are expected the two years of research according to the HPT profile (see Figure 5.7 and Table 6.1), the difference in in-well thickness (80% higher in 2015) is responsible for the difference in $T_{n,BD}$ values, assuming not significant changes in NAPL density and viscosity values between the two years. Higher b_n values than 0.177m are referred to water table drawdown periods during the trials, and as a result these values do not correspond to the NAPL mobile interval zone. During the induced water table drawdown periods, b_n and as a result $T_{n,BD}$ values increased due to the water table applied gradient. In contrast, area C presented almost zero $T_{n,BD}$ values for high b_n values (b_n was estimated by the monitoring point PB11) due to finer texture material at this location as was presented in the previous subchapters.

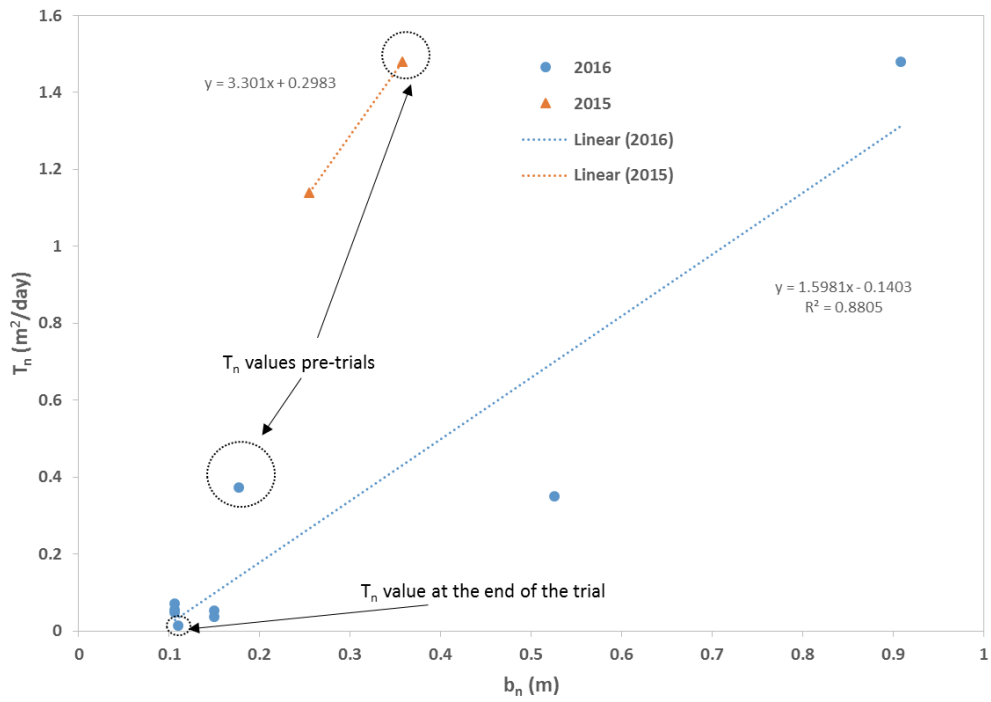


Figure 6. 27. Profile of T_n and b_n at PB29 well (yrs: 2015, 2016).

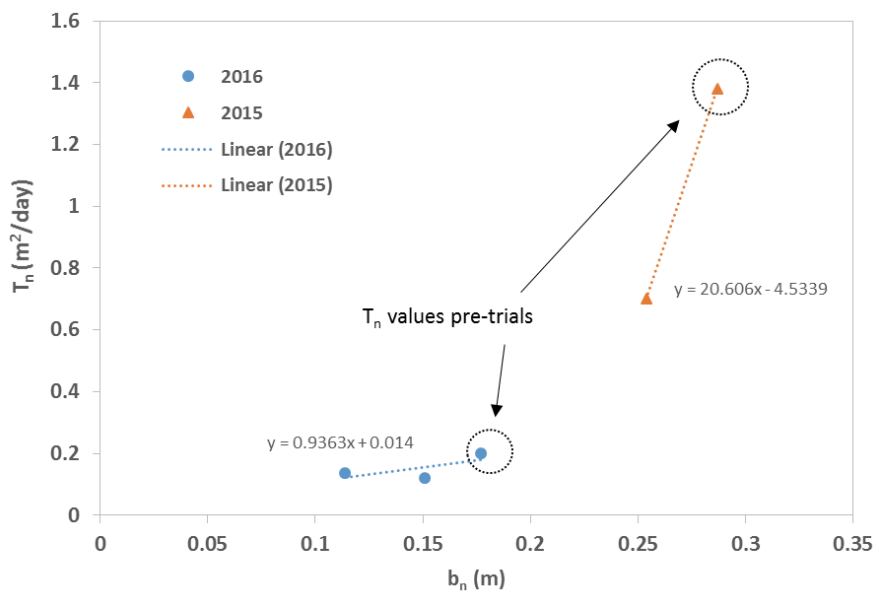


Figure 6. 28. Profile of T_n and b_n at PB27 well (yrs: 2015, 2016).

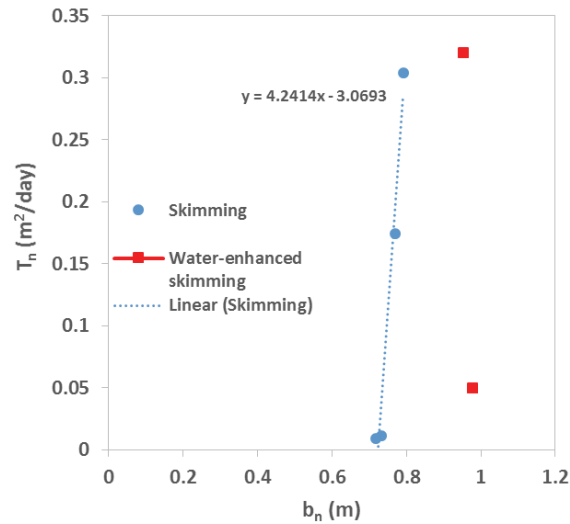


Figure 6. 29. Profile of T_n and b_n at PB40 well (yrs: 2016).

Intrinsic permeability is another crucial parameter (part of Equation 15) that needs to be evaluated for its contribution to T_n reduction during the 2016 experiments and is related to the mobile interval location. As regards area A, intrinsic permeability decreased slightly during the mass recovery experiments under rising water table conditions, taking into account the piezometric pressure values obtained by the HPT tool (see Figure 6.30). Thus, the reduction of b_n (related to NAPL saturations) and the thin vertical LNAPL distribution linked to a preferential migration pathway (where restrictions to vertical LNAPL movement were measured) were the main reasons for the decrease of T_n , taking into account the low impact of the physical changes. Figures 6.31 and 6.32 present the b_n values at the beginning and at the end of the mass recovery trials at areas B and C, respectively. At both locations, the mobile NAPL interval was found in a finer texture material at the end of the experiments compared to the formation material before the start of the testing, thus the lower intrinsic permeability should have contribute in parallel with the lower NAPL relative permeability and b_n values to the $T_{n,BD}$ reduction.

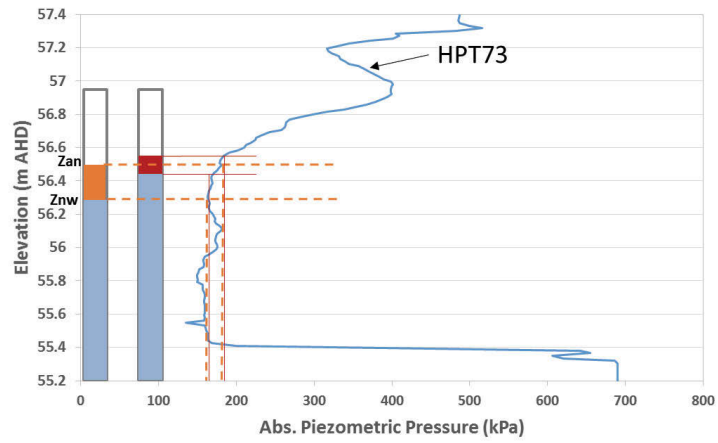


Figure 6. 30. Fluid levels along with abs. piezometric pressures at PB29 well location.

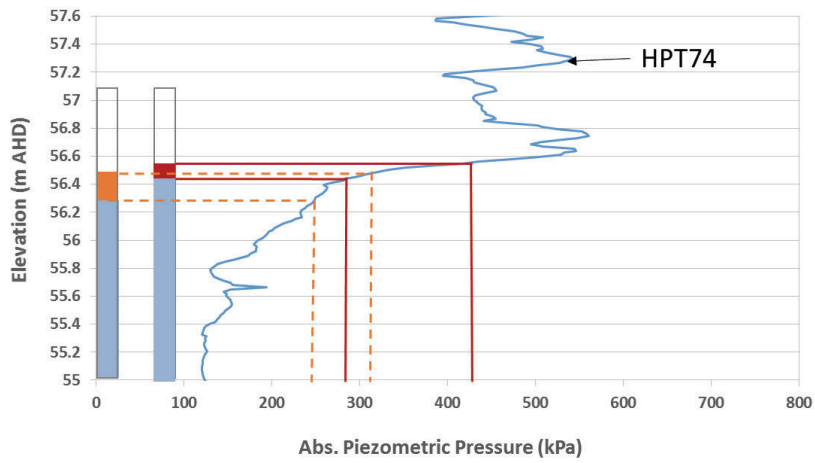


Figure 6. 31. Fluid levels along with abs. piezometric pressures at PB27 well location.

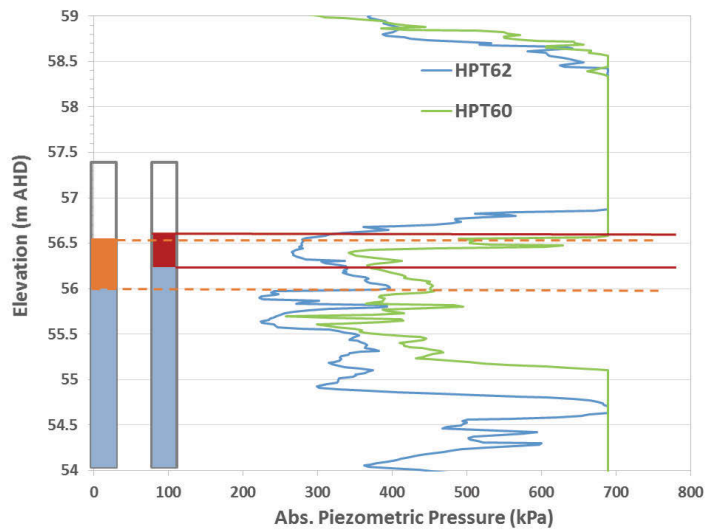


Figure 6. 32. Fluid levels along with abs. piezometric pressures at PB40 well location.

6.10. Uncertainty in Estimation of LNAPL Transmissivity

In the present subchapter, a sensitivity and error analysis is presented. Parameters that are used as input values in the API spreadsheet are tested for the PB27 well, at area B. Furthermore, two parameters that can affect the estimation of NAPL transmissivity value, are investigated as part of the sensitivity and error analysis. The first parameter is the effect of different NAPL removal amounts on the calculation of $T_{n,BD}$, as LNAPL transmissivity varies with test conditions (Beckett & Huntley 2015). Two or more different initial displacements should be used at each well during a testing period, as Butler et al (Butler, McElwee & Liu 1996) indicated regarding water displacements during slug tests. Furthermore, the test duration of a slug test is depended on the water displacement (Hyder, Butler Jr & McElwee 1993). The second tested parameter is the radius of capture during the skimming processes. The number of 4.6 was used in the present research as a value for the $\ln(R_{oi}/r_w)$, as a suggestion from ASTM (ASTM 2013). An analysis of how this parameter can affect the accuracy of T_n estimation, is presented.

6.10.1 Sensitivity and error analysis

For the needs of this analysis, NAPL recovery data that corresponds to PB27 well, was used. This section refers to bail-down testing procedures but not to remediation operations, as the direct or inverse relationship between the measured parameters and the $T_{n,BD}$ estimations can be seen in Equations 31 - 34. The bail-down test was conducted on 20/05/2016 before the start of the 4-week remediation trial. Table 6.3 presents the errors in T_n estimation if drawdown correction and cut-off time are not applied. Four different scenarios are presented. T_n standard deviation values for all the conducted bail-down tests of this research due to the Bouwer and Rice model application, are presented at Table C.1 in Appendix C.

Table 6. 3.Errors in $T_{n,BD}$ estimation if drawdown correction and cut-off time are not applied.

Parameter	Applied parameters	Applied parameters	Applied parameters	Applied parameters
Drawdown correction (m)	-0.0005	-	-0.0005	-
Cut-off time (min)	4.2	4.2	-	-
T_n (m ² /day)	0.66	0.74	0.69	0.76
Percent Change (%)	-	12	4.5	15

As it can be inferred from this table, both drawdown correction and cut-off time can affect the $T_{n,BD}$ estimation and that is the reason these parameters should be applied in the $T_{n,BD}$ analysis for more accurate results. Even though, the drawdown correction was only 0.5 mm, it had an influence of 12% change in the T_n calculation. It should be noticed that the specific outcomes are related to the specific tested well under specific testing conditions and as a result differences in other wells may arise.

Table 6.4 presents the effects of different air-NAPL interface elevation values (DTP) on T_n estimations. In chapter 3.3 it was presented that the measurer error is less than 2 mm. In chapter 6.4 it was indicated that the DTP levels at PB27 well, were estimated precisely by using the monitoring well PB11. Two equations were presented depicting a difference of 2 - 5 mm between each other, although the most accurate was used for the NAPL drawdown estimation.

Table 6. 4. Effect of DTP values to T_n estimates.

Difference from the equilibrium levels (mm)	DTP (m b.t.o.c.)	T_n (m^2/day)	Percent Change (%)
-10	4.642	0.66	0
-5	4.647	0.65	1.5
-2	4.650	0.65	1.5
0 (as used in the Bail-down T_n analysis)	4.652	0.66	-
2	4.654	0.84	27
5	4.657	0.68	3
10	4.662	0.76	15

The results indicated that $T_{n,BD}$ estimation can be quite sensitive even for 2 mm difference in DTP value. Thus the equilibrium fluid levels should be known precisely. During NAPL recovery, the DTP elevation reached the value 4.652 m *b.t.o.c.* indicating that the error in T_n estimation is low ($\leq 1.5\%$).

Table 6.5 presents the conducted sensitivity analysis at PB27 well by increasing individual parameters by 20%, while maintaining initial values of the other tested parameters. Results indicated that, the recovery time, well casing radius and J ratio revealed the highest values of percentage change. NAPL volume had no impact on $T_{n,BD}$ estimation as the DTP value did not change.

Table 6. 5. Effect of increasing initial values by 20% on T_n estimates.

Parameter	Initial value	T_n (m²/day)	Initial value increased 20%	T_n (m²/day)	Percent Change
Recovery time (min)	53	0.66	64	0.55	-17%
Well casing radius (m)	0.05	0.66	0.06	0.78	+18%
Well radius (m)	0.075	0.66	0.09	0.72	+9
Specific yield	0.175	0.66	0.21	0.68	+3%
J ratio	-0.292	0.66	-0.35	0.58	-20%
NAPL volume (L)	2	0.66	2.4	0.66	0%

Table 6.6 summarizes the relationship of the tested parameters to T_n estimates, based on the sensitivity and error analysis. Sensitivity is based on the percentage change. Parameters with values higher than 14% are considered as high sensitive. Recovery time, well casing radius, J ratio and drawdown correction depicted high sensitivity. Well radius presented moderate sensitivity and air-NAPL interface elevation exhibited high to low sensitivity. The remaining parameters showed low or no sensitivity.

Table 6. 6. Sensitivity and relationship to T_n for parameters related to bail-down testing.

Parameter	Sensitivity	Relationship to T_n
Recovery time	High	Negative
Well casing radius	High	Positive
J ratio	High	Negative
Drawdown correction	High	Positive
DTP	Low-High	Positive
Well radius	Moderate	Positive
Specific yield	Low	Positive
Cut-off time	Low	Positive
NAPL volume	None	None
LNAPL density ratio	None	None

6.10.2 Effect of product amount removal on LNAPL transmissivity estimation

Bail-down testing was used to elucidate the impact of different NAPL amount removals on the estimation of $T_{n,BD}$ value, at research areas A and B. At PB29 well location, three different experiments were conducted. At PB27 well location, the research took place including four experiments in two different dates under different water table conditions. The conditions under which the tests were conducted as well as a summary of the results of these tests are presented in Table 6.7. As it can be seen at this table, at research area A, higher NAPL removals affected negatively the T_n values, however at research area B, the T_n remained constant for different product removals under different water table conditions.

Table 6. 7. LNAPL transmissivity values and NAPL conditions for different extracted NAPL volumes at research areas A (PB29 well) and B (PB27 well) during baildown testing.

Well	Date	V_n (mL)	$Z_{an,i}$ (m AHD)	$Z_{nw,i}$ (m AHD)	Z_{aw} (m AHD)	$b_{n,1}$ (m)	$b_{n,2}$ (m)	Δt_i (min)	T_n (m ² /d)
PB29	19/5/16	2750	56.23	55.91	56.15	0.32	0.10	0.50	1.51
PB29	19/5/16	1200	56.23	55.91	56.15	0.32	0.18	0.35	2.06
PB29	19/5/16	3900	56.23	55.91	56.15	0.32	0.07	0.57	1.29
PB27	20/5/16	2400	56.23	55.91	56.14	0.32	0.09	0.20	0.57
PB27	20/5/16	1700	56.23	55.92	56.14	0.32	0.14	0.30	0.56
PB27	14/6/16	2100	56.45	56.27	56.40	0.18	0.01	0.30	0.20
PB27	14/6/16	950	56.45	56.27	56.40	0.18	0.08	0.25	0.20

where, V_n is the extracted amount of NAPL, $Z_{an,i}$ is the initial air-LNAPL interface in equilibrium before bailing, $Z_{nw,i}$ is the initial LNAPL-water interface before bailing, Z_{aw} is the potentiometric groundwater surface, $b_{n,1}$ is the initial apparent thickness before bailing, $b_{n,2}$ is the apparent thickness at first measurement after bailing, Δt_i is the time of the first stage observations and T_n the estimated LNAPL transmissivity.

Figure 6.33 illustrates the NAPL saturations at research areas A and B along with the apparent thicknesses ($b_{n,2}$) at first measurement after bailing.

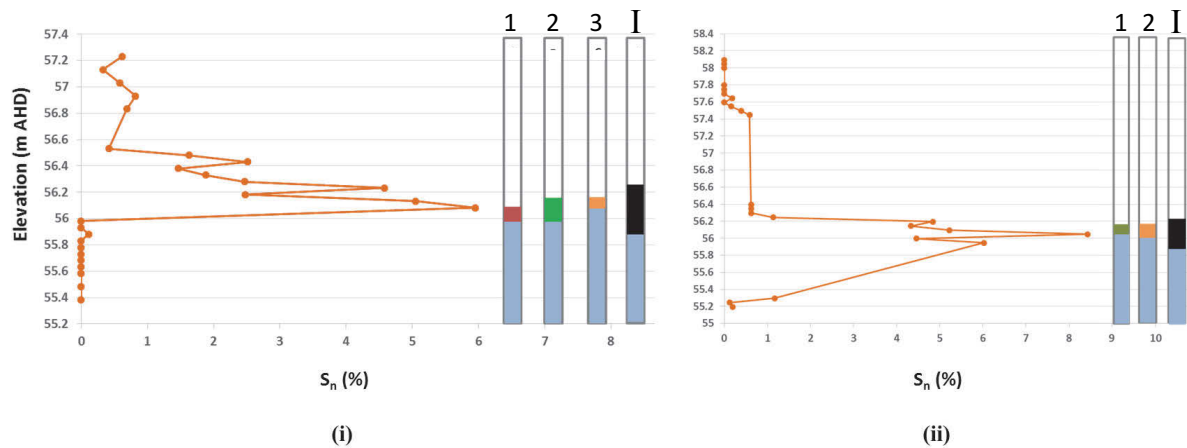


Figure 6. 33. A schematic illustrating the apparent thicknesses (cases 1 – 3) after bailing of the conducted experiments at area A (i) and B (ii) and NAPL saturations along with potentiometric surface elevations. Case I refers to the initial apparent thickness before bailing.

The graph above is referred to conducted experiments under low water table conditions, the same time period of cores' (MP50, MP58) extraction. The last two experiments presented at Table 6.7 (at area B) were taken place under higher potentiometric surface elevation, thus different NAPL saturations are expected. For this reason they are not depicted at the figure.

As it can be inferred, at research area A where a narrow NAPL distribution exists, the $T_{n,BD}$ is depended on the Z_{an} and Z_{nw} elevations just after the bailing process (see Table 6.7). In other words, $T_{n,BD}$ depends on the connectivity zone between the mobile NAPL interval in the formation and the apparent thickness in the well. Thus, the amount of bailed NAPL affected the calculated $T_{n,BD}$ value. On the other hand, at research area B, $T_{n,BD}$ (see Table 6.7) was not affected by the different product removals under the two different water table conditions. This could be explained, possibly due to the different vertical NAPL distribution (wider) at this area compared to area A, taking also into consideration that the geologic material was relatively similar in both areas. The obtained results regarding different NAPL removals can be related to slug tests procedures, testing different water displacements. Related work in the literature (McElwee, Bohling & Butler 1995) has indicated that large drawdowns should be used, as the errors are inversely proportional to the initial head. Furthermore, the estimation of hydraulic conductivity using the Bouwer and Rice method can be affected by using different water drawdowns (Hyder, Butler Jr & McElwee 1993).

6.10.3 Effect of radius of capture on T_n estimation

The radius of capture (R_{oi}) during the skimming processes is crucial for a precise estimation of $T_{n,SK}$ value. The real R_{oi} was difficult to be measured in the field site of research due to rising water table conditions. The recommended value, based on pilot scale results, $\ln(R_{oi}/r_w) = 4.6$ was used (ASTM 2013; Kirkman & Hawthorne 2013). This value corresponds to R_{oi} values of 7.5m as the r_w value of the recovery wells (PB29, PB27 and PB40) was 50mm. Figure 6.34 presents the effect of R_{oi} (range 0.1m – 20m) on $T_{n,SK} / T_{n,BD}$ ratio at the three research areas, the day before the start of the pilot-scale mass recovery experiments in 2016 (see also Table E.1 in Appendix E).

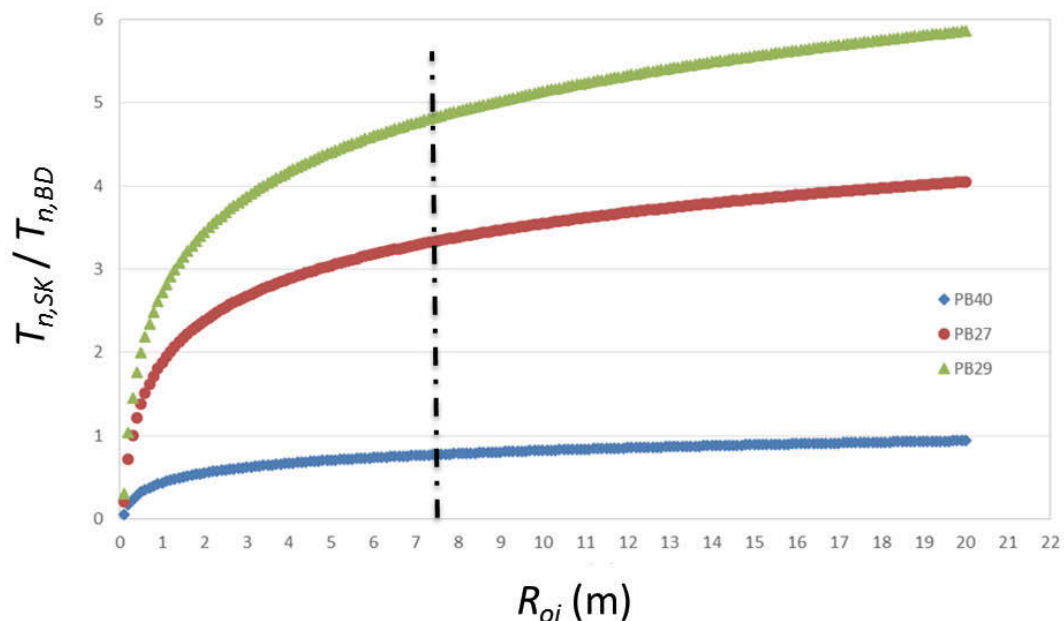


Figure 6. 34. Effect of R_{oi} on $T_{n,SK} / T_{n,BD}$ at well locations PB29, PB27 and PB40 (16-17/06/2016).

As it can be inferred from this graph, the ratio $T_{n,SK} / T_{n,BD}$ was affected less by R_{oi} changes at PB40 well location (area C) this specific day of research. Furthermore, PB40 presented lower ratio values compared to the other locations, approaching the value 1. This graph can be related to Figure 6.26. It should be noticed that, the error of using the 4.6 value is less than 20 percent based on pilot testing results as it has been documented in the literature (Kirkman & Hawthorne 2013), however in this research work, the error becomes higher for R_{oi} values less than 7.5m, especially for the well locations PB29 and PB27. It should be noted that, the real R_{oi} was difficult to be measured in the field site of research due to rising water table conditions. More specifically, measurements of b_n changes and any decrease in Z_{an} in the monitoring wells close to the recovery well locations, were taken. Changes measured in a range of $\pm 0-3$ mm (in b_n and in Z_{an}) were not helpful for the estimation of R_{oi} (possible reasons:

measurer errors and influence of a rising Z_{aw}). The rising potentiometric surface instead resulted in an increase of Z_{an} values across the site. In such cases, where monitoring points are within the radius of capture and NAPL drawdown is affected by the rising water table conditions, other methods such as the injection of tracers in the monitoring network should be used. During relatively static water table conditions, again the calculation of R_{oi} was unsuccessful. More monitoring points are needed in the vicinity of the recovery wells because the shape of R_{oi} is unknown and maybe not radial.

6.11. Conclusions

In the present chapter, LNAPL mobility was assessed in terms of NAPL transmissivity (T_n) in a gasoline contaminated heterogeneous aquifer under the effect of fluctuating water table conditions. The effects of lithology, NAPL in-well thickness and NAPL distribution were investigated. Different hydraulic methods were used for the identification of T_n accounting for the variability between the applied methods. Furthermore, the impact of mass recovery technologies such: (i) skimming; (ii) water-enhanced skimming; (iii) vacuum-enhanced skimming and (iv) water- and vacuum-enhanced skimming on T_n , physical properties (density and viscosity) and chemical compositions, was investigated.

Three research areas (A, B and C) were tested. The three areas of research presented differences in NAPL distributions, geological material and $T_{n,BD}$ values, although they were located in a close distance. During the mass recovery trials in 2015 and 2016, LNAPL was under unconfined conditions. These periods of time, the mobile NAPL interval at area A was located in a poorly graded sandy (SP) material, at area B, in a well graded sandy material (SW) and at area C, in a silty sand (SM) geological setting.

A range of $T_{n,BD}$ values from practically 0.03 m²/day to 2.13 m²/day was found at the field site during unconfined LNAPL conditions. T_n exhibited a strong spatial variability. T_n and in-well thickness exhibited a positive relationship in the tested areas under unconfined LNAPL conditions. Research area C presented the lowest $T_{n,BD}$ values (0.03 – 0.58 m²/day) among the three research areas since 2015 (maximum values of 2.13 m²/day at research area A and 1.38 m²/day at research area B), although it showed higher NAPL saturations and in-well thicknesses. Thus, the low intrinsic permeability at area C was a key factor for the lower T_n values, besides of the differences in NAPL distribution.

b_n was not a good indicator of $T_{n,BD}$ regarding the whole site analysis, as monitoring wells with the highest measured b_n values (for instance PB40 well in area C), presented relatively low $T_{n,BD}$ values. However, specific well tests analyses at the wells, PB29, PB27 and

PB40, revealed positive relationships between the b_n and $T_{n,BD}$ during unconfined NAPL conditions.

$T_{n,BD}$ showed variability with water table fluctuations under natural conditions. An inverse relationship was found between $T_{n,BD}$ and the potentiometric surface elevation. NAPL mobility was affected as vertical displacement and entrapment processes cause the mobile interval to become narrower and to be found at elevations with different geological conditions.

As regards the skimming trials, a relatively close agreement with similar trends was found between $T_{n,BD}$ and $T_{n,SK}$ in most of the cases, with the relative differences not exceeding a factor of 2. This magnitude is considered reasonable (ASTM 2013) and consistent with what has been documented in the literature (Nagaiah, Law & Ueland 2015). More specifically, the differences between $T_{n,BD}$ and $T_{n,SK}$ were relatively small under stable water table conditions in 2015 and during some periods in 2016. However, discrepancies between both methods by a factor up to 7.3 were found at area A and up to 3.2 at area B during the 2016 skimming trial under rising water table conditions. The discrepancies between both applied methods increased with Z_{aw} only at area A. This was probably due to the coupled effect of the differences in the radius of capture between the two applied methods and the low NAPL saturations predominantly linked to a thin layer. Bail-down testing was more sensitive to the rising water table than the skimming system at this area.

Regarding the water-enhanced skimming experiments, the estimated values of $T_{n,BD}$ compared well with $T_{n,SK}$ at research area A (factors 1.7- 2.7), while the difference was higher at research area C (factors 3.8 – 32). At this area, NAPL recovery diminished rapidly, being the NAPL flow towards the well negligible due to the low intrinsic permeability of the silty sand material. As a consequence the bail-down test performed at the start of the experiment was not a good predictor of the $T_{n,SK}$ evolution.

During the 2016 mass recovery trial, the mobile NAPL interval at area A was located mainly in the same geological setting (the intrinsic permeability decreased slightly), thus, the reduction of b_n (related to NAPL saturations) was the main reason for the decrease of T_n taking into account the low impact of the physical changes. At areas B and C, the mobile NAPL interval was found in a finer texture material at the end of the experiments compared to the formation material before the start of the testing, thus the lower intrinsic permeability should have contribute in parallel with the lower NAPL relative permeability and b_n values to the $T_{n,BD}$ reduction.

The $T_{n,BD}$ sensitivity analysis showed that recovery time, well casing radius, J ratio and drawdown correction may have a high impact on $T_{n,BD}$ estimation. Different NAPL volume removals during bail-down testing at research area A showed that the $T_{n,BD}$ was depended on the Z_{an} and Z_{nw} elevations just after the bailing process, that is the connectivity zone between the mobile NAPL interval in the formation with the apparent thickness in the well. On the other

hand, at research area B, $T_{n,BD}$ was not affected by the different product removals, due to the different vertical NAPL distribution compared to area A, taking into consideration that the geologic material was similar in both tested areas.

Conceptual Understanding of the Site

The integrated findings of Chapters 5 and 6 along with the Site and NAPLs characteristics in Chapter 4, constitute the initial conceptual site model of the study area. Figure 6.35 presents an updated version of the contaminated site hydrograph along with $T_{n,BD}$ values at the three research areas.

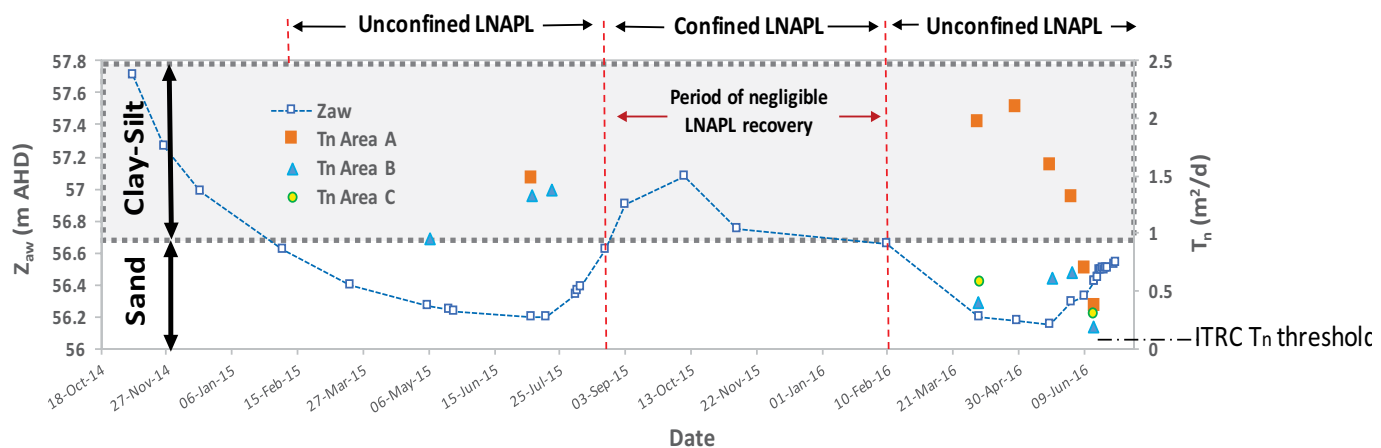


Figure 6. 35. Conceptual understanding of the research site.

From a contamination and remediation viewpoint, the integrated findings indicate that:

- The study area presents both confined and unconfined LNAPL conditions due to Z_{aw} changes.
- The transition point between the sandy and clayey/silty material is at ~56.7 m AHD.
- LNAPL distribution and mobility are highly affected by Z_{aw} changes.
- LNAPL was practical immobile in elevations higher than 56.6 m AHD. This behaviour was related to two different processes: (i) less mobile LNAPL because of LNAPL entrapment by water and (ii) upward LNAPL displacement into porous media with a lower intrinsic permeability. The potential disconnection between the LNAPL in the well and the formation under these conditions (confined or near-confined LNAPL) could be an additional reason behind this behavior.

- Under low Z_{aw} , T_n was higher than the suggested T_n endpoint value (0.07 m²/d) by ITRC.
- Zero values of $T_{n,BD}$ during high Z_{aw} should not be used as endpoints of hydraulic recovery because T_n changes in a cyclic basis under natural conditions.
- Remediation through mass recovery techniques should take place under low water table conditions (56.2 – 56.5 m AHD).
- All tested mass recovery technologies (i- Skimming, ii- Water enhanced skimming, iii- Vacuum enhanced skimming, iv-Vacuum and water enhanced skimming) in area A were effective, resulting in both liquid and vapour phase LNAPL recovery.
- In area C, where the material is finer, the liquid phase recovery was negligible.
- Two main reasons for the high NAPL removal in gas phase in the research site are: (i) the high volatility of gasoline and (ii) the fine grained material at the top of the aquifer which allows the application of an effective vacuum and acts also as a barrier for the upward migration of vapours.

7. Conclusions and Recommendations

7.1. Summary of Research

The focus of this thesis is to examine LNAPL distribution and mobility in a heterogeneous gasoline contaminated site under water table fluctuations. There are major deficiencies to predicting the fate of LNAPL in heterogeneous and dynamic subsurface environments during variable water table conditions. The aim of this research was to evaluate: (i) the impact of water table fluctuations on LNAPL distribution and hydrogeological conditions within the heterogeneous subsurface and (ii) the impact of the nexus between water table fluctuations, geological heterogeneity and different NAPL distributions on LNAPL transmissivity.

The conducted research was field-based using a gasoline contaminated site in Western Australia. A unique feature of the research site was the very recent nature of the spill, the 2 - 3 m seasonal water table fluctuations and the heterogeneous subsurface material. These challenging conditions required a broad suite of tools to gain insight into the research objectives. LNAPL distribution and hydrogeological conditions were evaluated using diagnostic gauge plots, hydrostratigraphs, contaminant concentrations in cores, high resolution characterization methods, LDRM simulations and baildown testing. LNAPL mobility was assessed in terms of NAPL transmissivity (T_n). T_n was evaluated using bail-down testing during both seasonal water table fluctuations and during induced hydraulic conditions (skimming, water-enhanced skimming, vacuum-enhanced skimming and water- and vacuum-enhanced skimming). Collectively these tools and approaches have given useful insight into NAPL distribution and mobility under both natural and induced hydraulic conditions during seasonal changes and mass recovery applications

7.2. Conclusions

In this section, (generalizable) conclusions which may have a wider generic relevance over and above the local site scenario are marked with an asterisk (*).

As regards the the impact of water table fluctuations on LNAPL distribution and hydrogeological conditions within the heterogeneous subsurface (**1st research objective**), the specific findings from Chapter 5 indicated that:

- NAPL hydrogeological conditions were related to the Z_{aw} behaviour and both confined and unconfined LNAPL conditions can be found in the same well seasonally (remediation wells in areas B and C) (*).
- Diagnostic gauge plots (DGPs) were found to be reliable tools for the identification of NAPL conditions (*). The findings were consistent with other lines of evidence such as: hydrostratigraphs, core descriptions, bail-down testing data, HPT and NAPL saturation profiles. In addition, the presented geological transition points were consistent during different drainage - imbibition periods.
- A detailed analysis through filtered DGPs took place based on different Z_{aw} trends, presenting more accurate and clear outcomes. This kind of analysis is recommended in sites affected by water table fluctuations, where fluid levels corresponds to different drainage - imbibition periods (*).
- Vertical NAPL distribution was related to the history of fluid levels in most of the cases, however entrapped and residual NAPL saturations inconsistent with the history of fluid elevations can be related to water table drawdown events and potential macropore networks existed in the fine materials.
- In heterogeneous settings the stratigraphy may override typical smearing patterns related to homogeneous systems. The vertical NAPL distributions in areas A and B were similar to homogeneous cases. In contrast, area C presented a vertical NAPL distribution profile similar to heterogeneous cases due to the existing fine and coarse layers. Variations in NAPL saturations were correlated qualitatively with variations in the soil material at this area.
- Area C presented the highest NAPL saturation and in-well thickness values among the other research areas. In addition, this area exhibited the highest entrapped (5%) and residual (up to 12%) NAPL saturation estimates. Low maximum saturation values at areas A and B are in line with other documented field based studies in the literature (Adamski, Kremesec & Charbeneau 2005; Adamski et al. 2005).

As regards the the impact of the nexus between water table fluctuations and geological heterogeneity on T_n (**2nd research objective**), the specific findings from Chapter 6 were as follows:

- An inverse relationship between the Z_{aw} and T_n was found under natural conditions.

- During unconfined LNAPL conditions $T_{n,BD}$ ranged from 0.03 m²/day to 2.13 m²/day exhibiting a strong spatial variability.
- Areas with high b_n and NAPL saturation values (such as Area C) may exhibit lower T_n than areas (such as A and B) presenting lower b_n and saturation values. Intrinsic permeability is a significant factor in these cases (*).
- b_n was not a good indicator of $T_{n,BD}$ regarding the whole site analysis, as monitoring wells with the highest measured b_n values (for instance PB40 well in area C), presented low $T_{n,BD}$ values. However, specific well tests analyses at the wells, PB29, PB27 and PB40, revealed positive relationships between the b_n and $T_{n,BD}$ during unconfined NAPL conditions
- Water table fluctuations played a crucial role on the behavior of T_n and should always be taken into consideration by remediation practitioners, researchers and regulators (*).
- Under constant water table conditions, T_n was found to be a relatively reliable metric for the management of saturation-based risks in LNAPL contaminated sites, although exhibiting a strong spatial dependency. $T_{n,BD}$ and $T_{n,SK}$ were usually in a close agreement. Consequently, $T_{n,BD}$ is helpful in order to decide the appropriateness of establishing a new mass recovery system. In addition, the stable T_n behavior favors the suitability of T_n as a leading metric (*).
- In contrast, variable water table conditions may affect the evolution of T_n in such a way that its applicability as a metric may be questionable without a deep knowledge of the site conditions (*). Examples supporting the aforementioned statement were presented throughout the results of this research:
 - i. it was observed that T_n may change in a cyclic basis under natural conditions. Thus, regulatory limits like the endpoint criterion proposed by ITRC (ITRC 2009a) should be applied with caution and preferably under low water table conditions in most of the cases (still depending on the relative importance of entrapment and the implications of vertical displacement). The results of this study encourage the application of periodic bail-down testing as part of a broader adaptive management strategy (*);
 - ii. it was documented that $T_{n,BD}$ may potentially be more sensitive to water table changes than to the product depletion through skimming. As a consequence, T_n is not necessarily representing the remediation performance of the mass recovery system only. It also comprises the coupled effects produced by the variable water table as well as the potential migration and natural losses occurring within the

NAPL body. For instance, in this research the decrease in $T_{n,BD}$ due to natural conditions without remediation operations was similar to that presented in the literature after 18 months of LNAPL recovery (Palmier, Dodt & Atteia 2016). Consequently, the understanding of these effects is essential in order to select the most adequate remediation technology, for instance in cases where mass recovery techniques should be replaced by monitored natural attenuation strategies;

- iii. the effect of the water table fluctuations is linked to the geological setting and the NAPL distribution. Accordingly, areas with similar initial $T_{n,BD}$ values may exhibit a clearly different evolution with time. During this research study, T_n was found to be less sensitive to Z_{aw} when wider NAPL distributions and higher saturations were present. As a consequence, the application of T_n as a leading metric is compromised without a deep knowledge of the conditions in the subsurface (*). Being aware of the depositional environment and existing vertical heterogeneity may help to understand the influence of LNAPL vertical displacement and entrapment phenomena on T_n . Furthermore, evidence that Z_{aw} may affect the discrepancy between $T_{n,SK}$ and $T_{n,BD}$ was presented. The magnitude of this difference may be related to the geological setting and LNAPL distribution, in particular when there are relevant preferential migration pathways with coarser material and/or better connectivity. For this reason, some errors may arise from the usage of $T_{n,BD}$ as a start-up metric under these conditions.
- In conclusion, the findings of this research encourage the use of T_n as a metric for the management of LNAPL contaminated sites, always accompanied by an adequate understanding of the conceptual site model. Both the geological setting and the NAPL distribution may have an effect on the behavior of T_n , magnified in the case of variable water table conditions. Thus, a proper characterization of the area surrounding the remediation well makes T_n gain reliability as a metric. On the other hand, periodic bail-down testing assists in the assessment of the T_n variability with time. Periodic measurements of $T_{n,BD}$ would also provide further insight in the comparisons between bail-down and long-term testing methods like those already documented in the literature (Pennington et al. 2016).

7.3. Recommendations for Future Work

T_n may show a strong spatial variability and diminish in just a few meters, since preferential pathways and other forms of heterogeneity and anisotropy always exist. The

delineation of NAPL distributions and such heterogeneities through high-resolution characterization methods remain an ongoing research issue. It should be noticed that, the estimation of the radius of capture under field conditions is not straightforward because of the complex nature of the NAPL distribution and the effects of the water table fluctuations. Assumptions regarding radial flow towards the well and little induced error with a $\ln (R_{oi}/r_w)$ value of 4.6 are usually taken, although further research is necessary to elucidate their validity, particularly for fine-grained systems and anisotropic conditions. The development of new analytical solutions could help to achieve a better description of the field complexity in T_n estimations.

When compared to the water table effects, mass recovery technologies may be inefficient in reducing NAPL mobility, so the potentiometric surface behavior must be taken into consideration in order to design an efficient remediation strategy. Further research is recommended for different degrees of LNAPL saturation and additional distributions of geological and contaminant properties.

The estimation procedure also has an impact on the calculated T_n value to a certain extent. Further research under controlled environments is suggested to keep elucidating the complex interrelation between T_n , NAPL properties, NAPL distribution, geological setting and temporal effects (including variable Z_{aw} , natural source zone depletion, NAPL migration and product depletion through mass recovery methods).

Estimates of LNAPL residual saturation must consider the nature of the LNAPL release and the maximum LNAPL saturation values that exist under field conditions. Capillary pressure –saturation, and relative permeability-saturation relationships can determine further the impact of water table fluctuations to residual saturation and NAPL transmissivity in the different areas of this research. Phenomena of hysteresis may elucidate differences of measured T_n between different years at the same well location. Laboratory scale experiments incorporating obtained soil cores by the research site, are recommended.

8. References

- Abdul, A.S. 1992, 'A New Pumping Strategy for Petroleum Product Recovery from Contaminated Hydrogeologic Systems: Laboratory and Field Evaluations', *Ground Water Monitoring & Remediation*, vol. 12, no. 1, pp. 105-14.
- Adamski, M., Kremesec, V. & Charbeneau, R.J. 2005, 'Residual saturation: What is it? How is it measured? How should we use it? Ground Water Management - Petroleum Hydrocarbons and Organic Chemicals in Ground Water: Prevention, Assessment, and Remediation Conference, 2005, 243-256.'
- Adamski, M., Kremesec, V., Kolhatkar, R., Pearson, C. & Rowan, B. 2005, 'LNAPL in fine-grained soils: Conceptualization of saturation, distribution, recovery, and their modeling', *Ground Water Monitoring and Remediation*, vol. 25, no. 1, pp. 100-12.
- Ahmed, W. 2014, 'Three Phase (Water, Air and NAPL) Modeling of Bail-Down Test (Master's Thesis). Stuttgart, 2014.'
- Air Force Center for Environmental Excellence 2000, *Source Reduction Effectiveness at Fuel Contaminated Sites Technical Summary Report*.
- Alexandra, R., Gerhard, J.I. & Kueper, B.H. 2012, 'Hydraulic Displacement of Dense Nonaqueous Phase Liquids for Source Zone Stabilization', *Ground Water*, vol. 50, no. 5, pp. 765-74.
- American Petroleum Institute 2000, 'API LNAPL Parameters Database, Version 2.0'.
- Andrews, M. 2000, 'LNAPL Recovery by Water-motive Multiphase Extraction', Interactive Hydrology; Proceedings. Barton, A.C.T.: Institution of Engineers, Australia, pp. 522-6.
- API 2012, *LNAPL transmissivity workbook: A tool for baildown test analysis*, American Petroleum Institute (API), Washington, 2012.
- Aral, M.M. & Liao, B. 2000, 'LNAPL Thickness Interpretation Based on Bail-Down Tests', *Ground Water*, vol. 38, no. 5, pp. 696-701.
- ASTM 2009, *D2488-09a. Standard Practice for Description and Identification of Soils (Visual-Manual Procedure)*, ASTM International, West Conshohocken, PA.
- ASTM 2013, *E2856-13, Standard Guide for Estimation of LNAPL Transmissivity*, ASTM International, West Conshohocken, PA.
- ASTM 2014, *E2531-06 (2014), Standard Guide for Development of Conceptual Site Models and Remediation Strategies for Light Nonaqueous-Phase Liquids Released to the Subsurface*.
- Awar, Z.R.A. 2008, 'Adapting, Optimizing, and Evaluating a Model for the Remediation of LNAPL in Heterogeneous Soil Environments', The University of Texas at Austin.
- Baker, R. & Bierschenk, J. 1995, 'Vacuum-enhanced recovery of water and NAPL: Concept and field test', *Soil & sediment contamination*, vol. 4, no. 1, pp. 57-76.

- Batu, V. 2012, 'An Assessment of the Huntley (2000) Baildown Tests Data Analysis Method', *Groundwater*, vol. 50, no. 4, pp. 500-3.
- Beckett, G.D. & Huntley, D. 1998, 'Soil properties and design factors influencing free-phase hydrocarbon cleanup', *Environmental Science and Technology*, vol. 32, no. 2, pp. 287-93.
- Beckett, G.D. & Huntley, D. 2015, 'LNAPL Transmissivity: A Twisted Parameter', *Groundwater Monitoring & Remediation*, vol. 35, no. 3, pp. 20-4.
- Beckett, G.D. & Lyverse, M.A. 2002, 'A protocol for performing field tasks and follow-up analytical evaluation for LNAPL transmissivity using well baildown procedures. (Chevron Texaco Energy Research Technology Company)'.
- Bouwer, H. & Rice, R.C. 1976, 'A slug test for determining hydraulic conductivity of unconfined aquifers with completely or partially penetrating wells', *Water Resources Research*, vol. 12, no. 3, pp. 423-8.
- Brooks, R.H, Corey, A.T., 1964, *Hydraulic properties of porous media*, Colorado State University Hydrology Paper no. 3, Fort Collins.
- Brost, J. E., DeVaul, E. G. 2000. Non-Aqueous Phase Liquid (NAPL) Mobility Limits in Soil. Soil and Groundwater Research Bulletin No. 9, June 2000, American Petroleum Institute, 10 p.
- Bujewski, G. & Rutherford, B. 1997, *The rapid optical screening tool (ROST) laser-induced fluorescence (LIF) system for screening of petroleum hydrocarbons in subsurface soils. Innovative Technology Verification Report EPA/600/R-97/020 (Feb. 1997).*
- Burdine, N.T. 1953, 'Relative permeability calculations from pore size distribution data. Journal of Petroleum Technology, 5(3), 71-78'.
- Butler, J.J. & Healey, J.M. 1998, 'Relationship Between Pumping-Test and Slug-Test Parameters: Scale Effect or Artifact?', *Ground Water*, vol. 36, no. 2, pp. 305-12.
- Butler, J.J., McElwee, C.D. & Liu, W. 1996, 'Improving the Quality of Parameter Estimates Obtained from Slug Tests', *Ground Water*, vol. 34, no. 3, pp. 480-90.
- Carsel, R.F. & Parrish, R.S. 1988, 'Developing joint probability distributions of soil water retention characteristics', *Water Resources Research*, vol. 24, no. 5, pp. 755-69.
- Charbeneau, R., Kirkman, A. & Adamski, M. 2013, "An Assessment of the Huntley (2000) Baildown Test Data Analysis Method," *Groundwater*, vol. 51, no. 5, pp. 657-9.
- Charbeneau, R.J. 2007a, *Charbeneau, R.J. 2007, LNAPL Distribution and Recovery Model (LDRM). Volume 2: User and Parameter Selection Guide: API Publ. No. 4760. American Petroleum Institute. Washington, D.C.*

- Charbeneau, R.J. 2007b, *LNAPL Distribution and Recovery Model (LDRM). Volume 1: 754 Distribution and Recovery of Petroleum Hydrocarbon Liquids in Porous Media. API Publ. No. 755 4760. American Petroleum Institute. Washington, D.C.*
- Charbeneau, R.J. & Chiang, C.Y. 1995, 'Estimation of Free-Hydrocarbon Recovery from Dual-Pump Systems', *Ground Water*, vol. 33, no. 4, pp. 627-34.
- Charbeneau, R.J., Johns, R.T., Lake, L.W. & McAdams, M.J. 2000, 'Free-Product Recovery of Petroleum Hydrocarbon Liquids', *Ground Water Monitoring & Remediation*, vol. 20, no. 3, pp. 147-58.
- Charbeneau, R.J., Kirkman, A.J. & Muthu, R. 2012, *API LNAPL Transmissivity Workbook: A Tool for Baildown Test Analysis.*
- Chatzis, I., Morrow, N.R. & Lim, H.T. 1983, 'Magnitude and Detailed Structure of Residual Oil Saturation'.
- Cho, P., M. Adamski & A. Kirkman 2010, 'LNAPL Transmissivity as a Metric: The Future in Tracking LNAPL Recovery Progress. Presented at ASTSWMO Conference, June 8-9 2010, San Diego'.
- Chompusri, S., Rivett, M.O. & Mackay, R. 2002, 'LNAPL redistribution on a fluctuating water table: column experiments. Groundwater Quality: Natural and Enhanced Restoration of Groundwater Pollution (Proceedings of the Groundwater Quality Conference held at Sheffield. UK. June 2001). IAHS Publ. no. 275, 225-231.'
- CL:AIRE 2010, *A Framework for Assessing the Sustainability of Soil and Groundwater Remediation, Contaminated Land: Applications in Real Environments (CL:AIRE), London, UK.*
- CL:AIRE 2014, *An illustrated handbook of LNAPL transport and fate in the subsurface. CL:AIRE, London. ISBN 978-1-905046-24-9.*
- Cooper, H.H., Bredehoeft, J.D. & Papadopoulos, I.S. 1967, 'Response of a finite-diameter well to an instantaneous charge of water', *Water Resources Research*, vol. 3, no. 1, pp. 263-9.
- Corapcioglu, M.Y. & Baehr, A.L. 1987, 'A compositional multiphase model for groundwater contamination by petroleum products: 1. Theoretical considerations', *Water Resources Research*, vol. 23, no. 1, pp. 191-200.
- CRC CARE 2015, *A practitioner's guide for the analysis, management and remediation of LNAPL, CRC CARE Technical Report no. 34, CRC for Contamination Assessment and Remediation of the Environment, Adelaide, Australia.*
- Davis, E.L. & Lien, B.K. 1993, *Laboratory study on the use of hot water to recover light oily wastes from sands, EPA/600/R-93/021, U.S.EPA, R.S. Kerr Environ. Res. Lab., Ada, OK, 59 pp.*

- Deb, S.K. & Shukla, M.K. 2012, 'Variability of hydraulic conductivity due to multiple factors', *American Journal of Environmental Science*, vol. 8, no. 5, pp. 489-502.
- Delin, G.N. & Herkelrath, W.N. 2014, 'Effects of a Dual-Pump Crude-Oil Recovery System, Bemidji, Minnesota, USA', *Groundwater Monitoring & Remediation*, vol. 34, no. 1, pp. 57-67.
- Demond, A.H. & Roberts, P.V. 1991, 'Effect of interfacial forces on two-phase capillary pressure—saturation relationships', *Water Resources Research*, vol. 27, no. 3, pp. 423-37.
- Dillard, L.A., Essaid, H.I. & Herkelrath, W.N. 1997, 'Multiphase flow modeling of a crude-oil spill site with a bimodal permeability distribution', *Water Resources Research*, vol. 33, no. 7, pp. 1617-32.
- Dobson, R., Schroth, M.H. & Zeyer, J. 2007, 'Effect of water-table fluctuation on dissolution and biodegradation of a multi-component, light nonaqueous-phase liquid', *Journal of Contaminant Hydrology*, vol. 94, no. 3–4, pp. 235-48.
- Drake, S.S., O'Carroll, D.M. & Gerhard, J.I. 2013, 'Wettability contrasts between fresh and weathered diesel fuels', *Journal of Contaminant Hydrology*, vol. 144, no. 1, pp. 46-57.
- EPA 1996, *How to Effectively Recover Free Product at Leaking Underground Storage Tank Sites: A Guide for State Regulators. Office of Underground Storage Tanks. EPA 510-R-96-001.*
- EPA SA 2009, *Site Assessment: Guidelines for the Assessment and Remediation of Groundwater Contamination, Environmental Protection Authority South Australia, Adelaide.*
- EPA Victoria 2002, *The Clean Up and Management of Contaminated Groundwater, Publication 840, EPA Victoria, Melbourne.*
- Essaid, H.I., Bekins, B.A. & Cozzarelli, I.M. 2015, 'Organic contaminant transport and fate in the subsurface: Evolution of knowledge and understanding', *Water Resources Research*, vol. 51, no. 7, pp. 4861-902.
- Essaid, H.I., Herkelrath, W.N. & Hess, K.M. 1993, 'Simulation of fluid distributions observed at a crude oil spill site incorporating hysteresis, oil entrapment, and spatial variability of hydraulic properties', *Water Resources Research*, vol. 29, no. 6, pp. 1753-70.
- Farr, A.M., Houghtalen, R.J. & McWhorter, D.B. 1990, 'Volume Estimation of Light Nonaqueous Phase Liquids in Porous Media', *Ground Water*, vol. 28, no. 1, pp. 48-56.
- Ferrand, L.A., Milly, P.C.D. & Pinder, G.F. 1989, 'Experimental determination of three-fluid saturation profiles in porous media', *Journal of Contaminant Hydrology*, vol. 4, no. 4, pp. 373-95.

- Gabr, M.A., Sharmin, N. & Quaranta, J.D. 2013, 'Multiphase Extraction of Light Non-aqueous Phase Liquid (LNAPL) Using Prefabricated Vertical Wells', *Geotechnical and Geological Engineering*, vol. 31, no. 1, pp. 103-18.
- Gavrilescu, M. 2006, 'Overview of In Situ Remediation Technologies for Sites and Groundwater', *Environmental Engineering & Management Journal*, vol. 5, no. 1, pp. 79-114.
- Germain, R. 2014, 'Laser-Induced Fluorescence, Theory and Data Interpretation. Dakota Technologies. Montana DEQ Group'.
- Germain, R.W.S., Einarson, M.D., Fure, A., Chapman, S. & Parker, B. 2014, 'Dye based laser-induced fluorescence sensing of chlorinated solvent DNAPLs', paper presented to the *3rd International Symposium on Cone Penetration Testing :: May 12-14, 2014 - Las Vegas, Nevada*.
- Gidakos, E. & Aivalioti, M. 2007, 'Large scale and long term application of bioslurping: The case of a Greek petroleum refinery site', *Journal of Hazardous Materials*, vol. 149, no. 3, pp. 574-81.
- Halmemies, S. 2003, 'Development of a Vacuum-Extraction Based Emergency Response Method and Equipment for Recovering Fuel Spills from Underground. PhD Thesis. Tampere University of Technology, Publications 411.'
- Halmemies, S., Gröndahl, S., Arffman, M., Nenonen, K. & Tuhkanen, T. 2003, 'Vacuum extraction based response equipment for recovery of fresh fuel spills from soil', *Journal of Hazardous Materials*, vol. 97, no. 1, pp. 127-43.
- Hampton, D.R. 2003, 'Improving Bail-Down Testing of Free Product Wells, in Proc. of 2003 Petroleum Hydrocarbons and Organic Chemicals in Ground Water, Prevention, Detection, and Remediation Conference and Exposition, Aug. 19-22, 2003, Costa Mesa, CA, National Ground Water Association, 16-30.'
- Hartsock, J. 2014, 'Evaluating the Effectiveness of Pre-remedial LNAPL Recovery Modeling using the 'LNAPL Distribution and Recovery Model' at Two Active Remediation Sites [M.Sc. Thesis]: Emporia State University'.
- Hawthorne, J.M. 2010, 'LNAPL Transmissivity Tn Remediation Design, Progress and Endpoints - PowerPoint PPT Presentation. <http://www.slideserve.com/misty/lnapl-transmissivity-tn-remediation-design-progress-and-endpoints>'.
- Hawthorne, J.M. 2011a, 'Confined LNAPL, Applied NAPL Science Review (Volume 1, Issue 5), May 2011'.
- Hawthorne, J.M. 2011b, 'Diagnostic Gauge Plots, Applied NAPL Science Review (Volume 1, Issue 2), February 2011.'
- Hawthorne, J.M. 2011c, 'Perched LNAPL, Applied NAPL Science Review (Volume 1, Issue 6), June 2011'.

- Hawthorne, J.M. 2014a, 'Calculating NAPL Drawdown', *Applied NAPL Science Review*, vol. 4, no. 3.
- Hawthorne, J.M. 2014b, 'Site Wide Analysis of LNAPL Distribution and Hydrogeologic Conditions Using Plume Scale Diagnostic Gauge Plots, *Applied NAPL Science Review* (Volume 4, Issue 1), January 2014'.
- Hawthorne, J.M. & Kirkman, A.J. 2011, ' Discharge vs. Drawdown Graphs, *Applied NAPL Science Review* (Volume 1, Issue 4), April 2011.'.
- Heffron, M., Blanchard, B. & Dogrul, H. 2003, 'Evaluation of Vacuum-Enhanced Skimming For the Remediation of a Large LNAPL Plume', *Proceedings of 2003 Petroleum Hydrocarbons and Organic Chemicals in Ground Water: Prevention, Assessment, and Remediation, 20th Conference and Exposition, Costa Mesa, California, August 19-22*, NGWA, pp. 78-91.
- Hernández-Espriú, A., Martínez-Santos, P., Sánchez-León, E. & Marín, L.E. 2012, 'Free-product plume distribution and recovery modeling prediction in a diesel-contaminated volcanic aquifer', *Physics and Chemistry of the Earth, Parts A/B/C*, vol. 37–39, pp. 43-51.
- Hinchee, R.E. & Reisinger, H.J. 1987, 'A Practical Application of Multiphase Transport Theory to Ground Water Contamination Problems', *Ground Water Monitoring & Remediation*, vol. 7, no. 1, pp. 84-92.
- Hoeppel, R. & Place, M. 1998, *Application guide for bioslurping. Volume I, Summary of the principles and practises of bioslurping. Technical Memorandum TM-2300-ENV. NAVAL Facilities Engineering Service Center Port Hueneme, California 93043-4370.*
- Huling, S.G. & Weaver, J.W. 1991, *Ground water issue: dense nonaqueous phase liquids. EPA/540/4-91-002.*
- Huntley, D. 2000, 'Analytic Determination of Hydrocarbon Transmissivity from Baildown Tests', *Ground Water*, vol. 38, no. 1, pp. 46-52.
- Huntley, D. & Beckett, G.D. 2002, 'Persistence of LNAPL sources: relationship between risk reduction and LNAPL recovery', *Journal of Contaminant Hydrology*, vol. 59, no. 1–2, pp. 3-26.
- Huntley, D., Hawk, R.N. & Corley, H.P. 1994, 'Nonaqueous Phase Hydrocarbon in a Fine-Grained Sandstone: 1. Comparison Between Measured and Predicted Saturations and Mobility', *Ground Water*, vol. 32, no. 4, pp. 626-34.
- Hyder, Z. & Butler, J.J. 1995, 'Slug Tests in Unconfined Formations: An Assessment of the Bouwer and Rice Technique', *Ground Water*, vol. 33, no. 1, pp. 16-22.
- Hyder, Z., Butler Jr, J.J. & McElwee, C.D. 1993, *An Approximate Technique for Analysis of Slug Tests in Wells. Open file report 93-44. Prepared for presentation at The American Geophysical Union, 1993 Fall Meeting, San Fransisco, Ca.*

- Illangasekare, T.H., Armbruster, E.J. & Yates, D.N. 1995, 'Non-Aqueous-Phase Fluids in Heterogeneous Aquifers'—Experimental Study', *Journal of Environmental Engineering*, vol. 121, no. 8, pp. 571-9.
- Illangasekare, T.H., Ramsey Jr, J.L., Jensen, K.H. & Butts, M.B. 1995, 'Experimental study of movement and distribution of dense organic contaminants in heterogeneous aquifers', *Journal of Contaminant Hydrology*, vol. 20, no. 1–2, pp. 1-25.
- ITRC 2009a, 'Evaluating LNAPL Remedial Technologies for Achieving Project Goals'.
- ITRC 2009b, 'Part 1, An improved understanding of LNAPL behavior in the subsurface-state of science vs. state of practise. Internet-Based Training 1 (IBT-1), LNAPLs Team'.
- ITRC 2018, 'LNAPL-3: LNAPL Site Management: LCSM Evolution, Decision Process, and Remedial Technologies'.
- Jeong, J. & Charbeneau, R.J. 2014, 'An analytical model for predicting LNAPL distribution and recovery from multi-layered soils', *Journal of Contaminant Hydrology*, vol. 156, pp. 52-61.
- Johns, R.T., Lake, L.W., Obigbesan, A.B., Bermudez, L., Hassan, M.R. & Charbeneau, R.J. 2003, 'Analytical Solutions for Free-Hydrocarbon Recovery Using Skimmer and Dual-Pump wells', *Ground Water Monitoring & Remediation*, vol. 23, no. 1, pp. 97-106.
- Johnston, C., Fisher, S., Innes NL & JL, R. 2005, 'Field evidence for biodegradation of petroleum hydrocarbons during multi-phase extraction', in N Kalogerakis (ed.), *Proceedings of the 3rd European Bioremediation Conference, Chania, 4-7 July, P019*.'
- Johnston, C., Fisher, S. & Rayner, J. 2002, 'Removal of petroleum hydrocarbons from the vadose zone during multi-phase extraction at a contaminated industrial site', in *Groundwater Quality: Natural and Enhanced Restoration of Groundwater Contamination (Proceedings of the Groundwater Quality 2001 Conference)*, Sheffield, UK, June, IAHS Publ. No. 275, pp. 287-293.'
- Johnston, C., Innes N, Fisher, S. & Rayner, J. 2002, *Evaluation of NAPL Recovery Methods: Field Trial at the BP Kwinana Refinery, 2001. A consultancy report to BP*.
- Johnston, C., Rayner, J., Fisher, S., Trefry, M., Briegel, D. & Innes N 2001, *Evaluation of NAPL Recovery Methods: Field Trial at the BP Kwinana Refinery, 2000. A consultancy report to BP*.
- Johnston, C.D. 2010, 'CRC CARE Tech. Report 18- Selecting and assessing strategies for remediating LNAPL in soils and aquifers'.
- Johnston, C.D. & Adamski, M. 2005, 'Relationship between initial and residual LNAPL saturation for different soil types, in *Proceedings of the 2005 Petroleum Hydrocarbons and Organic Chemicals in Groundwater: Prevention, Assessment, and Remediation Conference, Costa Mesa, 17-19 August, pp. 29-42*'.

- Johnston, C.D. & Trefry, M.G. 2009, 'Characteristics of light nonaqueous phase liquid recovery in the presence of fine-scale soil layering', *Water Resources Research*, vol. 45, no. 5, pp. n/a-n/a.
- Kahraman, I. 2013, 'Analysis of a LNAPL Recovery System Using LDRM in a South Texas Facility [M.Sc. Thesis]: Austin, The University of Texas'.
- Kaluarachchi, J.J. 1996, 'Effect of subsurface heterogeneity on free-product recovery from unconfined aquifers', *Journal of Contaminant Hydrology*, vol. 22, no. 1, pp. 19-37.
- Kemblowski, M.W. & Chiang, C.Y. 1990, 'Hydrocarbon Thickness Fluctuations in Monitoring Wells', *Ground Water*, vol. 28, no. 2, pp. 244-52.
- Kendall, M.G. & Stuart, D.G. 1973, *The Advanced Theory of Statistics. Vol 2: Inference and Relationship*, Griffin, London. .
- Khan, F.I., Husain, T. & Hejazi, R. 2004, 'An overview and analysis of site remediation technologies', *Journal of Environmental Management*, vol. 71, no. 2, pp. 95-122.
- Kirkman, A. & Hawthorne, J.M. 2013, 'Manual Kimming Testing to Measure LNAPL Transmissivity. Applied NAPL Science Review, Volume 3, Issue 1, March 2013'.
- Kirkman, A., J.; & Hawthorne, J.M. 2014, 'Transmissivity—the Emerging Metric for LNAPL Recoverability—Part 2 A Tangible Perspective on the Hydraulic Recovery Endpoint. http://www.neiwpc.org/lustline/lustline_pdf/lustline_76.pdf, pp. 15-20.
- Kirkman, A.J. 2013, 'Refinement of Bouwer-Rice Baildown Test Analysis', *Groundwater Monitoring & Remediation*, vol. 33, no. 1, pp. 105-10.
- Kirkman, A.J., Adamski, M. & Hawthorne, J.M. 2013, 'Identification and Assessment of Confined and Perched LNAPL Conditions', *Groundwater Monitoring & Remediation*, vol. 33, no. 1, pp. 75-86.
- Kirshner, M., Pressly, N.C. & Roth, R.J. 1996, 'In Situ Remediation of Jet A in Soil and Ground Water by High Vacuum, Dual Phase Extraction', *Ground Water Monitoring & Remediation*, vol. 16, no. 1, pp. 73-9.
- Kittel, J.A., Leeson, A., Hinchee, R.E., Miller, R.E. & Haas, P.E. 1994, *Results of a Multi-site Field Treatability Test for Bioslurping: A Comparison of LNAPL Rates Using Vacuum-enhanced Recovery (bioslurping), Passive Skimming, and Pump Drawdown Recovery Techniques. BATTELLE MEMORIAL INST COLUMBUS OH., Battelle Memorial Institute, Air Force Center for Environmental Excellence. Technology Transfer Division. Battelle Press, 1994.*
- Kittel, J.A., R.E. Hinchee, R. Hoeppel & Miller, R. 1994, *Bioslurping - Vacuum-Enhanced Free-Product Recovery Coupled With Bioventing: A Case Study. Petroleum Hydrocarbons and Organic Chemicals in Ground Water: Prevention, Detection, and Remediation. Conference, Nov. 2-4, 1994, Houston, Texas, pp. 255-270.*

- Kolhatkar, R., V. Kremesec, S. Rubin, C. Yukawa & Senn, R. 1999, 'Application of Field and Analytical Techniques to Evaluate Recoverability of Subsurface Free Phase Hydrocarbons, Proc. 1999 Petroleum Hydrocarbons and Organic Chemicals in Ground Water, NGWA, Nov. 17-19, 1999, Houston, TX, 5-15.'
- Koll, C.S., Palmerton, D.L.J. & Kunzel, R.G. 1994, 'Comparison of a wellpoint vacuum pump system to dual pump recovery system effectiveness for the extraction of light non-aqueous phase liquids', *Ground Water*, vol. 32, no. 5, p. 853.
- Kramer, J., Lesson, A., Headington, G., Walton, S. & Eastep, J. 1997, *Free recovery testing at the sites 27 & 28, Nellis AFB, Nevada. Report by Battelle to US Airforce Center for Environmental Excellence, Brooks AFB, Contract no. F41624-94-c-8012, Texas, Nov 1997, 87 pp.*
- Kueper, B.H., Redman, D., Starr, R.C., Reitsma, S. & Mah, M. 1993, 'A Field Experiment to Study the Behavior of Tetrachloroethylene Below the Water Table: Spatial Distribution of Residual and Pooled DNAPL', *Ground Water*, vol. 31, no. 5, pp. 756-66.
- Kuo, T., Chen, Y., Lin, C. & Chen, J. 2016, 'Oil recovery from a fluctuating water table', *Petroleum Science and Technology*, vol. 34, no. 17-18, pp. 1562-7.
- Lari, K.S., Johnston, C.D. & Davis, G.B. 2016, 'Gasoline Multiphase and Multicomponent Partitioning in the Vadose Zone: Dynamics and Risk Longevity', *Vadose Zone Journal*, vol. 15, no. 3.
- Lekmine, G., Bastow, T.P., Johnston, C.D. & Davis, G.B. 2014, 'Dissolution of multi-component LNAPL gasolines: The effects of weathering and composition', *Journal of Contaminant Hydrology*, vol. 160, pp. 1-11.
- Lenhard, R.J., Dane, J.H., Parker, J.C. & Kaluarachchi, J.J. 1988, 'Measurement and simulation of one-dimensional transient three-phase flow for monotonic liquid drainage', *Water Resources Research*, vol. 24, no. 6, pp. 853-63.
- Lenhard, R.J., Johnson, T.G. & Parker, J.C. 1993, 'Experimental observations of nonaqueous-phase liquid subsurface movement', *Journal of Contaminant Hydrology*, vol. 12, no. 1, pp. 79-101.
- Lenhard, R.J. & Parker, J.C. 1990, 'Estimation of Free Hydrocarbon Volume from Fluid Levels in Monitoring Wells', *Ground Water*, vol. 28, no. 1, pp. 57-67.
- Lenhard, R.J., Rayner, J.L. & Davis, G.B. 2017, 'A practical tool for estimating subsurface LNAPL distributions and transmissivity using current and historical fluid levels in groundwater wells: Effects of entrapped and residual LNAPL', *Journal of Contaminant Hydrology*, vol. 205, no. Supplement C, pp. 1-11.
- Lenhard, R. J., Sookhak Lari, K., Rayner, J. L., & Davis, G. B., 2018. Evaluating an analytical model to predict subsurface LNAPL distributions and transmissivity from current and

historic fluid levels in groundwater wells: Comparing results to numerical simulations. Groundwater Monitoring & Remediation.

- Lesson, A., Cumming, L., Wheeler, M. & Headington, G. 1997, *Free recovery testing at the 290 fuel Yard and North Tank Area, Tinker AFB, Oklahoma. Report by Battelle to US Airforce Center for Environmental Excellence, Brooks AFB, Contract no. F41624-94-c-8012, Texas, May 1997, 149 pp.*
- Lewis, M.A. 1989, *Water in Earth Science Mapping for planning, development and conservation. McCall, J and Marker, B; Graham and Trotman (editors).*
- Li, J.B., Huang, G.H., Chakma, A. & Zeng, G.M. 2002, 'Numerical Simulation of Dual Phase Vacuum Extraction for the Removal of Nonaqueous Phase Liquids in Subsurface: A Canadian Case Study', 2002/1/1/.
- Los Angeles LNAPL Working Group 2011, 'Light Non-Aqueous Phase Liquids (LNAPL) Literature Review Version 1.0, Western States Petroleum Association, Torrance, California.'
- Lundy, D.A., Li, D.W. & Katyal, A. 2002, 'Assessment of Upconing During Vacuum-Enhanced Skimming, A Case Study of Free-Phase Jet Fuel Recovery from Alluvium', *Proceedings of the 2002 Petroleum Hydrocarbons and Organic Chemicals in Ground Water: Prevention, Detection, and Remediation, November 5-8, , NGWA, Atlanta, Georgia, pp. P333-44.*
- Lundy, D.A. & Zimmerman, L.M. 1996, 'Assessing recoverability of LNAPL plumes for recovery system conceptual design. In Proceedings of the 10th National Outdoor Action Conference and Expo, May 13–15, 1996. Las Vegas, Nevada: National Groundwater Association, 19–33.'
- Mackay, D.M., Roberts, P.V. & Cherry, J.A. 1985, 'Transport of organic contaminants in groundwater', *Environmental Science & Technology*, vol. 19, no. 5, pp. 384-92.
- Marinelli, F. & Durnford, D.S. 1996, 'LNAPL Thickness in Monitoring Wells Considering Hysteresis and Entrapment', *Ground Water*, vol. 34, no. 3, pp. 405-14.
- Massmann, J., Shock, S. & Johannesen, L. 2000, 'Uncertainties in cleanup times for soil vapor extraction', *Water Resources Research*, vol. 36, no. 3, pp. 679-92.
- McCall, W. 2011, *Application of the Geoprobe HPT Logging System for Geo-Environmental Investigations. Geoprobe Technical Bulletin No. MK3184.*
- McElroy, W.J., Drinkwater, L.A. & Kanzler, B.A. 1992, 'Impact of Water Table Fluctuations on Remediation of Non-Aqueous Phase Liquids Issues, October 13-15, 1992, Boston MAarriott, Newton, Massachusetts (Ground Water Management Book 13); P95-109'.

- McElwee, C.D., Bohling, G.C. & Butler, J.J. 1995, 'Sensitivity analysis of slug tests. Part 1. The slugged well', *Journal of Hydrology*, vol. 164, no. 1, pp. 53-67.
- Mercer, J.W. & Cohen, R.M. 1990, 'A review of immiscible fluids in the subsurface: Properties, models, characterization, and remediation, *J. Contam. Hydrol.*, 6: 107-163.'
- Mualem, Y. 1976, 'A new model for predicting the hydraulic conductivity of unsaturated porous media. *Water resources research*, 12(3), 513-522'.
- Nagaiah, M., Law, D.R. & Ueland, S. 2015, 'Transmissivity as a Primary Metric for LNAPL Recovery—Case Study Comparison of Short-Term vs. Long-Term Methods', *Remediation Journal*, vol. 26, no. 1, pp. 43-55.
- Newell, C., Acree, S, Ross, R & Huling, S 1995, *Light nonaqueous phase liquids, Ground Water Issue, US EPA/540/S-95-500, United States Environmental Protection Agency, Washington, DC.*
- NRC 1997, *Innovations in Ground Water and Soil Cleanup: From Concept to Commercialization, National Academy Press, Washington.*
- Oostrom, M., Falta, R.W., Mayer, A.S., Javandel, I. & Hassanizadeh, S.M. 2005, 'Remediation', *Soil and Groundwater Contamination: Nonaqueous Phase Liquids—Principles and Observations*, American Geophysical Union, pp. 141-89.
- Oostrom, M., Hofstee, C. & Wietsma, T.W. 2006, 'Behavior of a Viscous LNAPL Under Variable Water Table Conditions', *Soil and Sediment Contamination: An International Journal*, vol. 15, no. 6, pp. 543-64.
- Palmier, C., Cazals, F. & Atteia, O. 2017, 'Bail-Down Test Simulation at Laboratory Scale. ', *Transp. Porous Med.* , vol. 116, no. 2, pp. 567-83.
- Palmier, C., Dodt, M. & Atteia, O. 2016, 'Comparison of Oil Transmissivity Methods Using Bail-Down Test Data', *Groundwater Monitoring & Remediation*, vol. 36, no. 3, pp. 73-83.
- Park, J.H., Johnston, C.D. & Davis, G.B. 2015, *Three-phase Modelling of LNAPL recovery options for a petroleum hydrocarbon mixture in a sand aquifer. Report EP 149975. CSIRO, Australia, pp.53.*
- Parker, J.C., Lenhard, R.J. & Koppusamy, T. 1987, 'A parametric model for constitutive properties governing multiphase flow in porous media', *Water Resources Research*, vol. 23, no. 4, pp. 618-24.
- Parker, J.C., Waddill, D.W. & Johnson, J.A. 1994, 'UST Corrective Action Technologies: Engineering Design of Free Product Recovery Systems, US EPA. Risk Reduction Engineering Laboratory, Edison, N.J., 27-28.'
- Peargin, T.R. & Wickland, D.C. 1999, 'Evaluation of short term multi-phase extraction effectiveness for removal of non-aqueous phase liquids from groundwater monitoring wells', *API - National Ground Water Association Petroleum Hydrocarbons and Organic*

- Chemicals in Ground Water: Prevention, Detection and Remediation Joint Conference Proceedings*, vol. 1, pp. 16-25.
- Pennington, A., Smith, J., Koons, B. & Divine, C.E. 2016, 'Comparative Evaluation of Single-Well LNAPL Tracer Testing at Five Sites', *Groundwater Monitoring & Remediation*, vol. 36, no. 2, pp. 45-58.
- Ponsin, V., Maier, J., Guelorget, Y., Hunkeler, D., Bouchard, D., Villavicencio, H. & Höhener, P. 2015, 'Documentation of time-scales for onset of natural attenuation in an aquifer treated by a crude-oil recovery system', *Science of The Total Environment*, vol. 512–513, no. 0, pp. 62-73.
- Prince-Larson, N. & Markley, D.E. 1994, 'Recovery of Light Nonaqueous-phase Liquids Without Groundwater Pumping ', *Proceedings of the Eighth National Outdoor Action Conference and Exposition on Aquifer Remediation, Ground Water Monitoring, and Geophysical Methods, May 23-25*, NGWA, Minneapolis Convention Center, Minneapolis, Minnesota, pp. 119-28.
- Purtill, J. 1998, 'The Use of a Water-motive, Multiphase Extraction System for the Removal of Hydrocarbons from a Clayey Aquifer ', *2nd Queensland Environmental Conference: Environmental Solutions for the Real World*, ed. A. Goonetilleke, Barton, A.C.T.: Institution of Engineers, Australia, pp. 33-9.
- Qin, X.S., Huang, G.H., Zeng, G.M. & Chakma, A. 2008, 'Simulation-based optimization of dual-phase vacuum extraction to remove nonaqueous phase liquids in subsurface', *Water Resources Research*, vol. 44, no. 4, pp. n/a-n/a.
- Rao, P.S.C., Jawitz, J.W., Enfield, C.G., Falta Jr, R.W., Annable, M.D. & Wood, A.L. 2002, 'Technology integration for contaminated site remediation: clean-up goals and performance criteria. Groundwater quality Conference, Sheffield, UK, 2001: Natural and enhanced restoration of groundwater pollution, no 275, 571-578.'
- Rivett, O.M, Wealthall, G.P, Dearden, R.A, McAlary, T.A. 2011. Review of unsaturated-zone transport and attenuation of volatile organic compound (VOC) plumes leached from shallow source zones. *Journal of Contaminant Hydrology*, vol.123, pp 130-156.
- Reyenga, L. & Hawthorne, J.M. 2011, 'The mobile NAPL interval, Part 2: Confined and Perched NAPL, December 2015'.
- Ryan, R.G. & Dhir, V.K. 1996, 'The effect of interfacial tension on hydrocarbon entrapment and mobilization near a dynamic water table', *Journal of Soil Contamination*, vol. 5, no. 1, pp. 9-34.
- Sale, T., Taylor, G.R., Iltis, G. & Lyverse, M. 2007, 'Measurement of LNAPL Flow Using Single-Well Tracer Dilution Techniques', *Ground Water*, vol. 45, no. 5, pp. 569-78.

- Shan, C., Falta, R.W. & Javandel, I. 1992, 'Analytical solutions for steady state gas flow to a soil vapor extraction well', *Water Resources Research*, vol. 28, no. 4, pp. 1105-20.
- Simon, J.A. 2012, 'Editor's perspective—LNAPL transmissivity: Mobility is the new state-of-the-art cleanup metric', *Remediation Journal*, vol. 22, no. 3, pp. 1-8.
- Skibitzke, H.E. 1958, *An equation for potential distribution about well being bailed*, Report, 58-96.
- Sleep, B.E., Sehayek, L. & Chien, C.C. 2000, 'A Modeling and experimental study of light nonaqueous phase liquid (LNAPL) accumulation in wells and LNAPL recovery from wells', *Water Resources Research*, vol. 36, no. 12, pp. 3535-45.
- Soga, K., Page, J.W.E. & Illangasekare, T.H. 2004, 'A review of NAPL source zone remediation efficiency and the mass flux approach', *Journal of Hazardous Materials*, vol. 110, no. 1–3, pp. 13-27.
- Sookhak Lari, K., Davis, G.B. & Johnston, C.D. 2016, 'Incorporating hysteresis in a multi-phase multi-component NAPL modelling framework; a multi-component LNAPL gasoline example', *Advances in Water Resources*, vol. 96, pp. 190-201.
- Steffy, D.A., Barry, D.A. & Johnston, C.D. 1997, 'Influence of antecedent moisture content on residual LNAPL Saturation', *Journal of Soil Contamination*, vol. 6, no. 2, pp. 113-47.
- Steffy, D.A., Johnston, C.D. & Barry, A. 1998, 'Numerical simulations and long-column tests of LNAPL displacement and trapping by a fluctuating water table', *Journal of Soil Contamination*, vol. 7, no. 3.
- Steffy, D.A., Johnston, C.D. & Barry, D.A. 1995, 'A field study of the vertical immiscible displacement of LNAPL associated with a fluctuating water table. Groundwater Quality: Remediation and Protection. IAHS Publ. no. 225, 49-57.'
- TCEQ 2008, *TCEQ Regulatory Guidance: Risk-Based NAPL Management, TCEQ Guidance Document RG-366/TRRP-32*.
- Teramoto, E.H. & Chang, H.K. 2017, 'Field data and numerical simulation of btex concentration trends under water table fluctuations: Example of a jet fuel-contaminated site in Brazil', *J Contam Hydrol*, vol. 198, pp. 37-47.
- Testa, S.M. & Paczkowski, M.T. 1989, 'Volume Determination and Recoverability of Free Hydrocarbon', *Ground Water Monitoring & Remediation*, vol. 9, no. 1, pp. 120-8.
- Totsche, K.U., Kögel-Knabner, I., Haas, B., Geisen, S. & Scheibke, R. 2003, 'Preferential flow and aging of NAPL in the unsaturated soil zone of a hazardous waste site: implications for contaminant transport', *Journal of Plant Nutrition and Soil Science*, vol. 166, no. 1, pp. 102-10.
- U.S. Department of Energy 2006, *JV TASK 47- Demonstration of Vacuum Enhanced Recovery and Feasibility of Permeable Treatment Barriers for Site Remediation at Hazen*, 2006-EERC-09-09.

- U.S. Department of Energy 2007, *JV TASK 59 - Demonstration of Accelerated In Situ Contaminant Nutrient Distribution Degradation by Vacuum-Enhanced*, 2007-E E RC-04-08.
- U.S. EPA 1990, *Laboratory Investigation of Residual Liquid Organics from Spills, Leaks, and Disposal of Hazardous Wastes in Groundwater*, EPA/600/6-90/004.
- US EPA 2005, *A Decision-making Framework for Cleanup of Sites Impacted with Light Non-Aqueous Phase Liquids (LNAPL)*, EPA 542-R-04-011.
- USACE 1999, *Multi-Phase Extraction*, EM 1110-1-4010.
- USEPA 1997, *Presumptive Remedy: Supplemental Bulletin Multi-Phase Extraction (MPE) Technology for VOCs in Soil and Groundwater*, EPA 540-F-97-004.
- USEPA 2005, *Cost and Performance Report for LNAPL Characterization and Remediation: Multi-Phase Extraction and Dual-Pump Recovery of LNAPL at the BP Former Amoco Refinery, Sugar Creek, MO*.
- Van Geel, P.J. & Sykes, J.F. 1997, 'The importance of fluid entrapment, saturation hysteresis and residual saturations on the distribution of a lighter-than-water non-aqueous phase liquid in a variably saturated sand medium', *Journal of Contaminant Hydrology*, vol. 25, no. 3, pp. 249-70.
- Van Genuchten, M.T. 1980, 'A closed-form equation for predicting the hydraulic conductivity of unsaturated soils. Soil Science Society of America Journal, 44(5), 892-898'.
- Waddill, D.W. & Parker, J.C. 1997, 'Simulated Recovery of Light, Nonaqueous Phase Liquid from Unconfined Heterogeneous Aquifers', *Ground Water*, vol. 35, no. 6, pp. 938-47.
- Wang, W., Kuo, T., Chen, Y., Fan, K., Liang, H. & Chen, J. 2014, 'Effect of precipitation on LNAPL recovery performance: An integration of laboratory and field results', *Journal of Petroleum Science and Engineering*, vol. 116, pp. 1-7.
- Westerby, G. 1992, 'Remediation of subsurface gasoline losses at two retail outlets in Southern Ontario. ', *Subsurface Contamination by Immiscible Fluids*, no. Edited by Weyer. Balkema, Rotterdam, , pp. 551-62.
- White, M.D., Ostrom, M. & Lenhard, R.J. 2004, 'A Practical Model for Mobile, Residual, and Entrapped NAPL in Water-Wet Porous Media', *Ground Water*, vol. 42, no. 5, pp. 734-46.
- Wilson, J.L., Conrad, S.H., Mason, W.R., Peplinski, W. & Hagan, W. 1990, *Laboratory investigation of residual liquid organics from spills, leaks and the disposal of hazardous wastes in groundwater*, EPA/600/6-90/004, Washington, DC, US Environmental Protection Agency.
- Xitech 1999, 'Free-Product Recovery System- Technical Notes. '.

- Yimsiri, S., Euaapiwatch, S., Flores, G., Katsumi, T. & Likitlersuang, S. 2016, 'Effects of water table fluctuation on diesel fuel migration in one-dimensional laboratory study', *European Journal of Environmental and Civil Engineering*, pp. 1-27.
- Zhu, J.L., Parker, J.C., Lundy, D.A. & Zimmerman, L.M. 1993, 'Estimation of soil properties and free product volume from baildown tests. In Proc. Petroleum Hydrocarbons and Organic Chemical in Ground Water, National Water Well Association, Dublin Ohio, 99-111.'
- Zilliox, L., Razakarisoa, O. & Rinck, G. 1992, ' Case history: A kerosene spill at Strasbourg-Entzheim international airport, France.', *Subsurface Contamination by Immiscible Fluids*, no. Edited by Weyer. Balkema, Rotterdam, pp. 503-10.

Appendices

Appendix A. Materials and Methods

Table A.1. Monitoring network details.

Installation	Well Type	Date Installed	Reference Elevation* (m AHD)	Max Depth (m)
MB1	GW well	10/06/2013	61.322	8.5
MB2	GW well	10/06/2013	61.422	8
MB3	GW well	10/06/2013	60.975	8
MB4	GW well	11/06/2013	61.457	8.5
MP01	GW well	1/04/2014	61.211	9.5
MP02	GW well	4/04/2014	61.497	9.2
MP03	GW well	4/04/2014	61.316	7.5
MP04	GW well	4/04/2014	61.202	9.5
PB05	GW well	4/04/2014	61.327	9.5
MP06	GW well	4/04/2014	61.124	9
MP07	GW well	4/04/2014	61.228	6.75
MP08	GW well	4/04/2014	61.299	6.75
MP10	GW well	5/08/2014	61.184	8.25
PB11	GW well	5/08/2014	61.237	9
PB12	GW well	6/08/2014	61.257	9
PB13	GW well	7/08/2014	61.236	9.75
PB26	GW well	4/11/2014	61.333	9.5
PB27	GW well	5/11/2014	60.993	9
PB28	GW well	5/11/2014	61.304	9
PB29	GW well	5/11/2014	61.087	9
MP30	GW well	6/11/2014	59.366	9
MP31	GW well	6/11/2014	60.638	9.2
PB33	GW well	3/08/2015	61.214	9
MP34	GW well	3/08/2015	61.052	9
PB35	GW well	4/08/2015	61.105	9
MP36	GW well	4/08/2015	61.088	9.2
MP37	GW well	4/08/2015	60.884	9.2
MP38	GW well	4/08/2015	60.989	9.2
PB39	GW well	5/08/2015	61.402	9.1
PB40	GW well	5/08/2015	61.282	9.1
MP41	GW well	5/08/2015	61.315	9.1
MP42	GW well	6/08/2015	61.278	9.2
PB09	GW well	unknown	60.868	5.5
MP44	GW well	17/5/2016	61.269	
MP50	GW well	18/5/2016	61.134	
MP58	GW well	19/5/2016	60.978	
MP76	GW well	08/2016	61.002	
MP77	GW well	08/2016	61.144	
MP78	GW well	08/2016	61.227	
ML14	multilev	7/08/2014	61.258	9.75
ML15	multilev	7/08/2014	61.397	8.5
ML16	multilev	8/08/2014	61.243	9.75
ML17	multilev	8/08/2014	61.42	9.75
ML32	multilev	6/11/2014	60.917	8.5
VP18D	SV well	17/10/2014	61.219	1
VP18S	SV well	17/10/2014	61.219	0.5
VP19D	SV well	17/10/2014	61.2	1
VP19S	SV well	17/10/2014	61.2	0.5
VP20D	SV well	17/10/2014	61.2	1
VP20S	SV well	17/10/2014	61.2	0.5
VP22D	SV well	17/10/2014	61.411	1
VP22S	SV well	17/10/2014	61.411	0.5
VP23D	SV well	17/10/2014	61.11	1
VP23S	SV well	17/10/2014	61.11	0.5
VP24D	SV well	17/10/2014	61.2	1
VP24S	SV well	17/10/2014	61.2	0.5
VP25D	SV well	17/10/2014	61.4	1
VP25S	SV well	17/10/2014	61.4	0.5
VP21D	SV well	25/11/2014	60.8	1
VP21S	SV well	25/11/2014	60.8	0.5

Where*: Top of casing (m AHD)

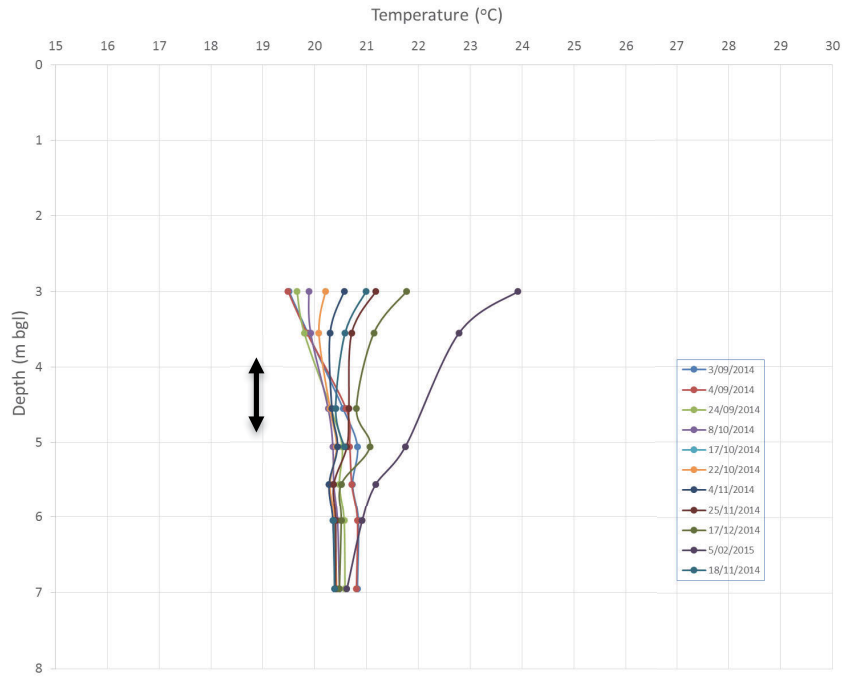


Figure A.1. Temperature profile along with depth at well ML15, at UST area.

Table A.2. HPT - LIF network details (profiles were measured in the research site between 17th and 20th of May 2016).

Site location	Reference Elevation* (m AHD)
HPT59	61.298
HPT60	61.292
HPT61	61.277
HPT62	61.312
HPT63	61.329
HPT64	61.336
HPT72	61.078
HPT73	61.221
HPT74	61.138

HPT75	61.387
LIF43	61.211
LIF45	61.392
LIF46	61.322
LIF47	61.21
LIF48	61.099
LIF49	61.085
LIF51	61.117
LIF52	61.124
LIF53	61.165
LIF54	61.246
LIF55	61.12
LIF56	61.224
LIF57	61.305
LIF65	61.35
LIF66	61.332
LIF67	61.229
LIF68	61.294
LIF69	61.283
LIF70	61.073
LIF71	61.118

Where *: Ground level elevation (m AHD)

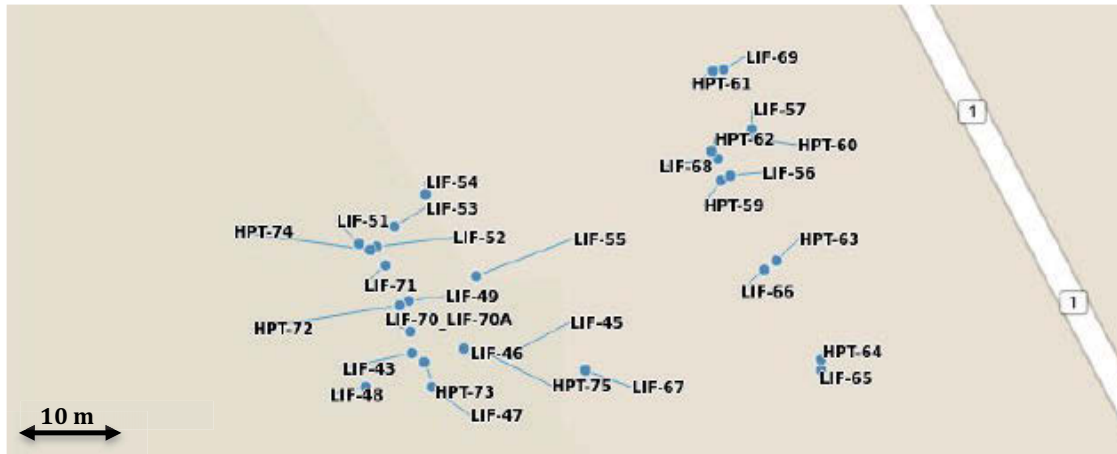


Figure A.2. HPT - LIF network at research site (17-20/5/2016).

Table A.3. Chronology of events during field trial of NAPL recovery at PB29 well

Date	Time	Activity
08/07/15	07:39	Bail-down test
08/07/15	08:20	Skimmer on
14/07/15	12:35	Skimmer off
14/07/15	14:43	Bail-down test
14/07/15	15:45	Skimmer on
20/07/15	14:40	Skimmer off
21/07/15	09:04	Bail-down test
15/06/16	13:30	Bail-down test
15/06/16	18:45	Skimmer on
16/06/16	12:02	Skimmer off
16/06/16	13:35	Bail-down test
16/06/16	16:40	Skimmer on
17/06/16	03:00	Skimmer off
17/06/16	10:22	Skimmer on
21/06/16	09:47	Skimmer off
21/06/16	11:47	Bail-down test
21/06/16	17:16	Skimmer on
23/06/16	09:17	Skimmer off
23/06/16	11:15	Bail-down test
23/06/16	16:20	Water pump on
23/06/16	19:57	Bail-down test
23/06/16	22:37	Skimmer on
24/06/16	12:18	Skimmer off, water pump off
24/06/16	16:00	Bail-down test
27/06/16	16:50	Bail-down test
28/06/16	11:30	Water pump on
28/06/16	17:05	Bail-down test

28/06/16	22:00	Skimmer on
29/06/16	09:33	Skimmer off, water pump off
29/06/16	14:17	Bail-down test
30/06/16	15:17	Skimmer on, vacuum on
30/06/16	17:36	Skimmer off, vacuum off
01/07/16	11:40-12:00	Well development
01/07/16	15:05	Skimmer on
04/07/16	15:05	Skimmer off
05/07/16	12:20	Skimmer on
05/07/16	14:16	Vacuum on
05/07/16	17:00	Vacuum off
05/07/16	18:34	Skimmer off
05/07/16	21:51	Water pump on
06/07/16	10:14	Bail-down test
06/07/16	12:15	Skimmer on
06/07/16	13:40	Vacuum on
06/07/16	18:00	Vacuum off
06/07/16	19:04	Skimmer off, water pump off
07/07/16	14:21	Bail-down test

Table A.4. Chronology of events during field trial of NAPL recovery at PB27 well

Date	Time	Activity
20/07/15	15:48	Bail-down test
20/07/15	17:40	Skimmer on
21/07/15	09:45	Skimmer off
21/07/15	12:54	Bail-down test
21/07/15	14:00	Skimmer on
03/08/15	14:00	Skimmer off
16/06/16	08:27	Bail-down test
16/06/16	15:50	Skimmer on
17/06/16	03:00	Skimmer off
17/06/16	10:00	Bail-down test
17/06/16	16:08	Skimmer on
22/06/16	15:03	Skimmer off
22/06/16	19:33	Skimmer on
30/06/16	11:11	Skimmer off
04/07/16	17:50	Bail-down test
05/07/16	08:51	Skimmer on
07/07/16	18:36	Skimmer off
08/07/16	10:47	Bail-down test
08/07/16	14:36	Skimmer on

Table A.5. Chronology of events during field trial of NAPL recovery at PB40 well.

Date	Time	Activity
14/06/16	16:03	Bail-down test
15/06/16	21:54	Skimmer on
17/06/16	02:00	Skimmer off
17/06/16	08:35	Bail-down test
17/06/16	16:40	Skimmer on
21/06/16	09:27	Skimmer off
21/06/16	11:00	Bail-down test
21/06/16	17:48	Skimmer on
22/06/16	10:08	Skimmer off
22/06/16	11:00	Bail-down test
23/06/16	11:40	Water pump on
23/06/16	16:58	Bail-down test
23/06/16	21:34	Skimmer on
24/06/16	12:46	Skimmer off, water pump off
28/06/16	09:02	Bail-down test
28/06/16	16:05	Water pump on
29/06/16	11:00	Bail-down test
29/06/16	15:48	Skimmer on
30/06/16	21:42	Skimmer off, water pump off
01/07/16	10:13	Bail-down test
01/07/16	15:04	Skimmer on
05/07/16	14:43	Skimmer off
05/07/16	22:03	Skimmer on
06/07/16	14:28	Skimmer off
06/07/16	15:30	Bail-down test
06/07/16	21:50	Water pump on
07/07/16	15:28	Skimmer on
07/07/16	16:02	Vacuum on
07/07/16	23:21	Skimmer off, water pump off, vacuum off
08/07/16	14:15	Skimmer on

Table A.6. Chronology of NAPL and vapour sampling at recovery wells PB29, PB27 and PB40, in 2016.

Well	Date	Time	Sampling
PB29	15/06/16	18:52	NAPL sample #1
PB29	23/06/16	08:57	NAPL sample #2
PB29	24/06/16	12:03	NAPL sample #3
PB29	27/06/16	15:02	NAPL sample #4
PB29	29/06/16	07:45	NAPL sample #5
PB29	04/07/16	15:03	NAPL sample #6

PB29	05/07/16	14:16-17:00	Vapour samples
PB29	05/07/16	21:16	NAPL sample #7
PB29	06/07/16	13:25	NAPL sample #8
PB29	06/07/16	13:40-18:00	Vapour samples
PB29	06/07/16	19:03	NAPL sample #9
PB29	08/07/16	18:00	NAPL sample #10
PB27	16/06/16	16:35	NAPL sample #1
PB27	23/06/16	08:53	NAPL sample #2
PB27	24/06/16	09:49	NAPL sample #3
PB27	29/06/16	18:13	NAPL sample #4
PB27	05/07/16	10:26	NAPL sample #5
PB27	07/07/16	18:35	NAPL sample #6
PB27	08/07/16	10:47	NAPL sample #7
PB40	15/06/16	22:50	NAPL sample #1
PB40	22/06/16	16:17	NAPL sample #2
PB40	23/06/16	22:05	NAPL sample #3
PB40	24/06/16	12:39	NAPL sample #4
PB40	27/06/16	15:22	NAPL sample #5
PB40	29/06/16	21:15	NAPL sample #6
PB40	01/07/16	14:45	NAPL sample #7
PB40	06/07/16	10:30	NAPL sample #8
PB40	06/07/16	15:29	NAPL sample #9
PB40	07/07/16	16:05-23:20	Vapour samples
PB40	08/07/16	12:24	NAPL sample #10

Appendix B. Site Characterization

Elevation (m AHD)	UCSC	Graphic Log & ID	Description & Bottom Boundary S = sharp, <5 mm A = abrupt, 5-20 mm C = clear, 20-50 mm G = gradual, 50-100 mm D = diffuse, >100 mm	Munsell Colour	Average grain size & (maximum)
61.17					
60.17	(CH)fs	1	Reddish at the top	7.5 YR 5/8, Bright brown	
59.17	s(CL)	2	G	7.5 YR 5/6, Bright brown	
	60% (CH)fs, 40% s(CL)	3&4	red and white	7.5 YR 5/8, Bright brown	
	40% s(CL), 60% (CL)fs	5&6	40% Perhaps sandier than above; white; 60% Same as 3, reddish at the top	2.5 Y 6/1, Yellowish grey	
58.17	40% (CH)fs, 60% (CH)fs	7&8	40% Same as 4 (white); Organic matter, roots; 60% The last 40 cm are very fat; Same as 3(reddish)		
	(ML)s	9	Same 2 colours		(380-800 µm)
57.17	(ML)s	10	Classification same as above; 70% white, 30% red; The white is sandier than the red		
	SW-SM	11	Still 2 colours, the white looks sandier	10 Y/R 6/6, Bright yellowish brown	190-380 µm
56.17	(SW)fm	12	The red is siltier; grey	10 Y/R 6/2, Greyish yellow brown	190-380 µm
	(SW)fm	13	Last 5 cm are coarser 4.5; Same colour as above with 5.63-5.88 m being reddish		190-380 µm
55.17	(SW)fm	14		10 Y/R 5/6, Yellowish brown	380-800 µm
	SW/SM	15	It's mud; Same colour as above		(380-800 µm)
	(SW)tm	16		10 Y/R 8/4, Light yellow orange	0.6-1.4 mm
	SW-SM	17	Same as 15		(380-800 µm)
	(SW)fm	18	Same as 14		(380-800 µm)
54.17		19	Lost core, mud, maybe SM		(380-800 µm)
	GP	20		10 Y/R 6/4, Dull yellow orange	
	SW-SM	21		2.5 Y 5/1, Yellowish grey	0.6-1.4 mm (0.8-2 mm)
		22	C "Lost" core, maybe (SW)-SM		
	(SW)tm	23	grey		
53.17	GW	24	Last 10 cm are coarser; Same colour as above	2.5 Y 5/3, Yellowish brown	0.6-1.4 mm (0.8-2 mm)

Figure B.1. Stratigraphic log description, PB35 well, area B. Where, CL: lean clay, CH: fat clay, ML: silt, SP: poorly graded sand, SW: well graded sand, SM: silty sand, SC: clayey sand, GP: poorly graded gravel.

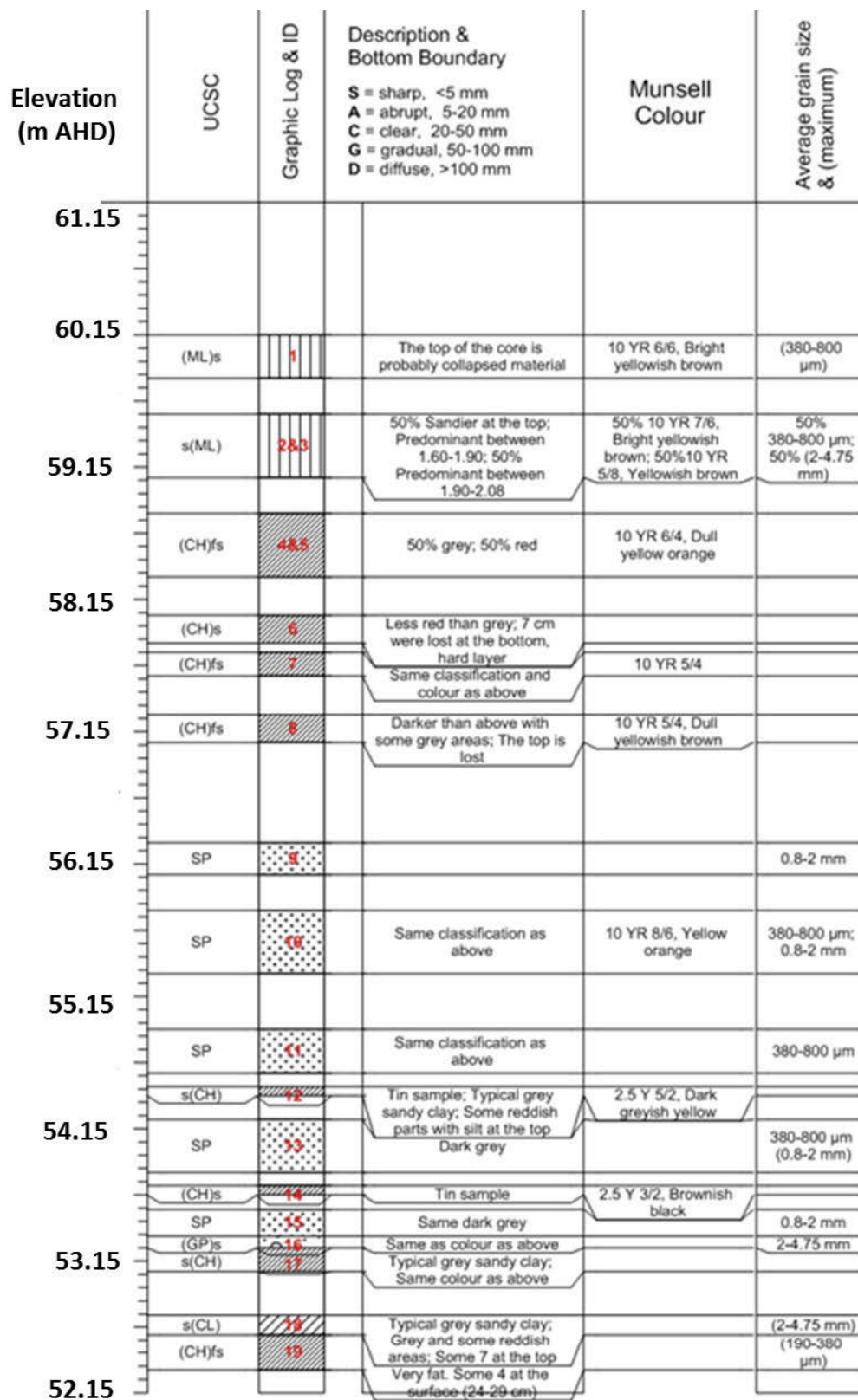


Figure B.2. Stratigraphic log description, PB27 well, area B.

Elevation (m AHD)	UCSC	Graphic Log & ID	Description & Bottom Boundary	Munsell Colour	Average grain size & (maximum)
61.32					
60.32	(CL)slm	1	Fatter at the bottom	7.5 YR 5/6, Bright brown	
59.32	s(CL)	2	Sandier at the top; Some reddish areas at the bottom	7.5 YR 5/8, Bright brown	190-380 µm
58.32	80% (CL)sfm, 20% s(CL)	3,4	80% red; 20 % white with mica	80% 5 YR 5/6, Bright reddish brown; 20% 10 YR 6/4, Dull yellow orange	70-110 µm
58.32	80% (CL)sfm, 20% s(CL)	5,6	80% Same as above; 20% Perhaps sandier than above (SC?)	80% 5 YR 5/6, Bright reddish brown; 20% 10 YR 6/4, Dull yellow orange	
57.32	CH	7	Same 2 colour, but the red is fat; Colour same as above		
57.32	s(ML)	8	Colour same as above (50%-50%)		70-110 (150-190 µm)
57.32	SM	9	Well graded	10 YR 8/2, Light grey	190-380 µm (0.8-2 mm)
56.32	SP	10	Coarser at the bottom, maximum 5, D boundary; Colour similar as above	10 YR 7/4, Dull yellow orange	190-380 µm
56.32	SP	11	G	10 YR 6/8, Bright yellowish brown	
55.32	SP	12	Same as above	10 YR 6/8, Bright yellowish brown	0.8-2 mm
55.32	(SP)tg	13	Colour same as above	10 YR 7/8, Yellow orange	2-4.75 mm
55.32	(SP)gic	14	Grey	2.5 Y 5/3, Yellowish brown	190-380 µm
55.32	(SP-SC)fm	15		10 YR 5/6, Yellowish brown	190-380 µm
55.32	(CH)s	16		5 Y 5/1, Grey	
54.32	(SP)g	17	The "top" of the core is lost	Grey	0.8-2 mm
54.32	GP	18		Grey	2-4.75 mm
54.32	(SW)fmg	19		5 Y 4/2, Greyish olive	
53.32	(SW)fmg	20	Same classification as above	2.5 Y 6/4, Dull yellow	
53.32	(SW)fmg	21	Same classification as above		
52.32					

Figure B.3. Stratigraphic log description, PB33 well, area A.

Elevation (m AHD)	UCSC	Graphic Log & ID	Description & Bottom Boundary	Munsell Colour	Average grain size & (maximum)
61.40					
	(CL)fs	1	Soil horizon	7.5 YR 3/4, Dark brown	
60.40	(CL)fs	2	D Same classification as above. A lot of organic matter	5 YR 4/8, Reddish brown	
	(CL)fs	3	Same classification as above	10 YR 5/6, Yellowish brown	
	80% (CL)fs; 20% s(ML)	4&5	80% Same as above (red); 20% grey	80% 10 YR 5/6; 20% 2.5 Y 7/3(Light yellow)	
59.40	(CH)ts	6	Same classification as 4 but with red stains; grey areas are a bit sandier 4	5 YR 3/6, Dark reddish brown	
	(CH)ts	7&8	70% Similar classification as above; 30% as above. A lot of organic matter	70% Yellowish brown	
58.40	(CH)ts	9&10			
	(CH)ts	11	2 colours as above but they are darker now	10 YR 4/2, Greyish yellow brown	
57.40	(ML)sfc	12	Grey areas	2.5 Y 5/4, Yellowish brown	70-110 µm
	(ML)sfc	13	CL?: Same as above	2.5 Y 5/4	
	s(ML)c	14	CL?	5 Y 5/2, Greyish olive	
56.40	SW-SM	15		2.5 Y 5/4, Yellowish brown	150-190 µm (0.8-2 mm)
		16	Lost core		
	SW-SM	17		2.5 Y 4/4, Olive brown	(380-800 µm)
	SW	18		5 Y 6/1, Grey	380-800 µm
55.40	SW	19		5 Y 6/1, Grey	0.8-2 mm (0.8-2 mm)
	GP	20		2.5 Y 7/3, Light yellow	2-4.75 mm
54.40	(SW)tg	21	C The colour of the whole core is quite similar, light brown	2.5 Y 6/4, Dull yellow	0.8-2 mm
	SW-SM	22	G Black stain in the last 4 cm	5 Y 5/2, Greyish olive	
	(SW)tg	23		5 Y 6/2, Greyish olive	2-4.75 mm
	(SW)tmg	24		5 Y 7/2, Light grey	380-800 µm (0.8-2 mm)
	(SW)tg	25		5 Y 6/2, Greyish olive	0.8-2 mm
53.40	(SW-SM)tg	26		5 Y 6/3, Olive yellow	0.8-2 mm
	(CH)ts	27	Very fat; Dark	5 Y 4/1, Grey	
	CH	28	Very fat; Reddish areas	N 4/0, Grey	
52.40					

Figure B.4. Stratigraphic log description, PB39 well, area C.

The HPT profiles were measured in the research site between 17th and 20th of May 2016

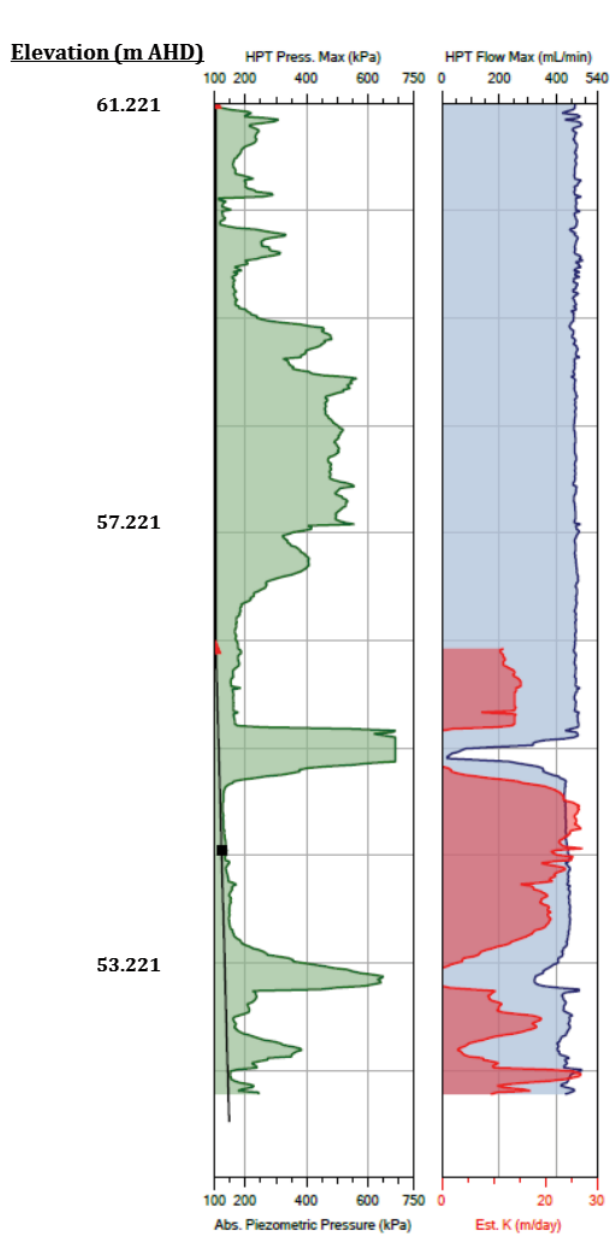


Figure B.5. HPT 73 profile, area A.

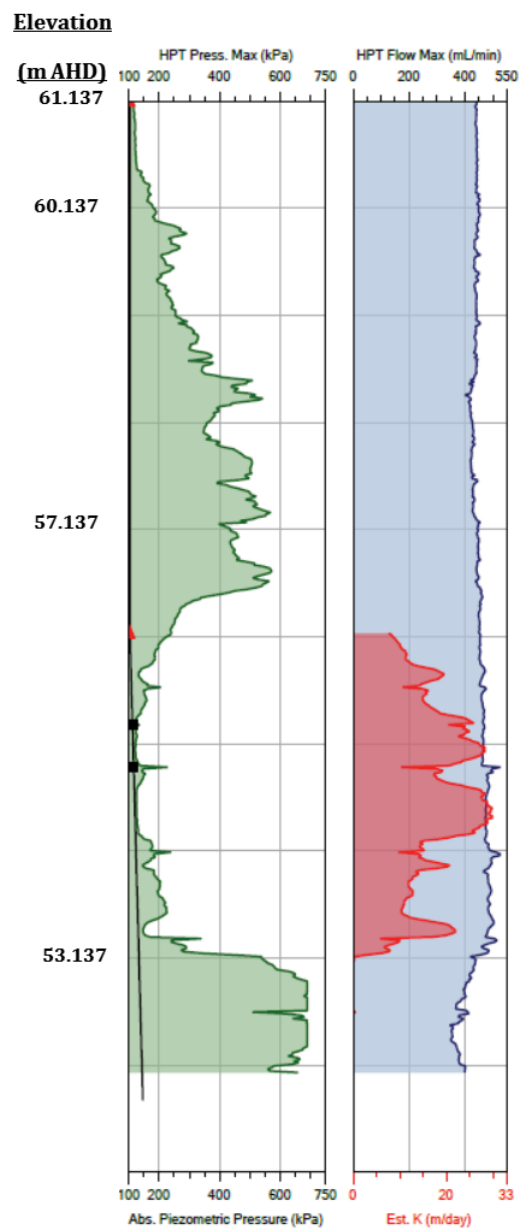


Figure B.6. HPT 74 profile, area B.

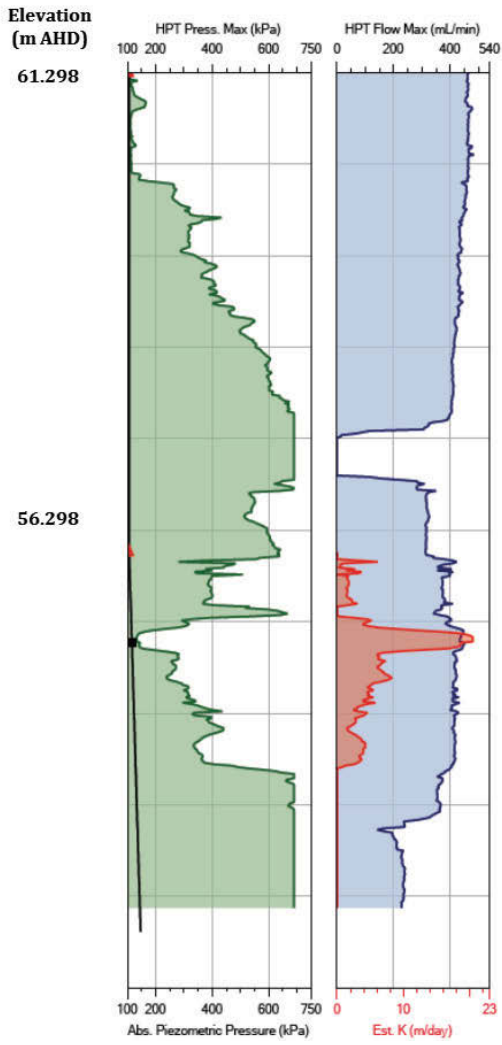


Figure B.7. HPT 59 profile, area C.

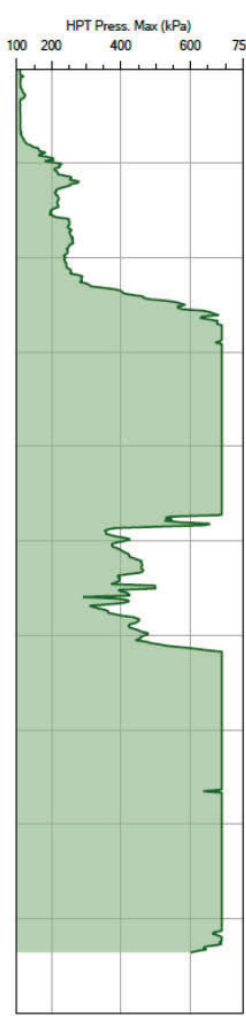


Figure B.8. HPT 60 profile.

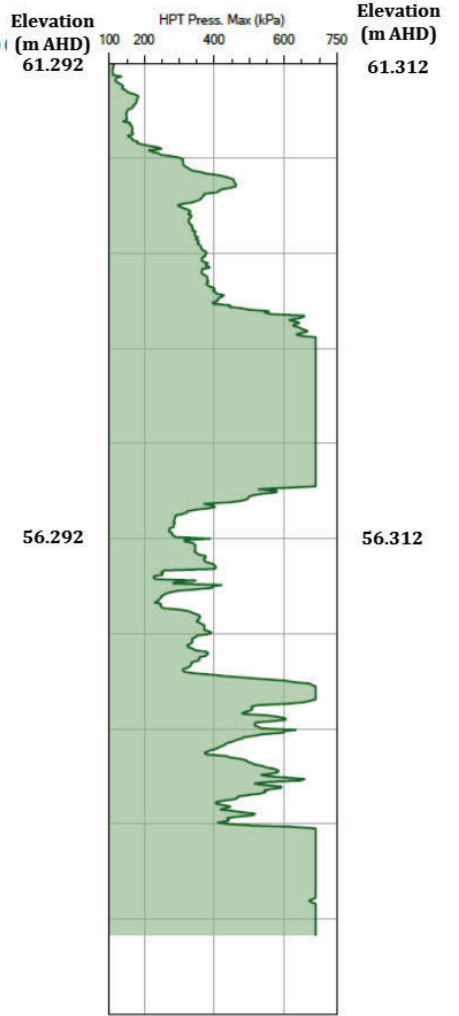


Figure B.9. HPT 62.

Laboratory studies shows that the gasoline product measured density is between 0.73 and 0.80 g/cm³. The average density value of the contaminated site is 0.739 g/cm³. Product was collected and tested more than one times in some wells for better evaluation of this physical property.

Table B.1. Measured product densities across the research site.

Well ID	Density Average (g/cm³)
MP02	0.734
MP03	0.738
MP05	0.731
MP07	0.742
MP01	0.732
MP07	0.741
MP03	0.744
MP01	0.725
PB11	0.729
MP02	0.732
PB13	0.725
MP05	0.726
MP01	0.726
MP02	0.733
MP03	0.747
MP05	0.743
MP07	0.734
MP08	0.736
MP09	0.760
PB11	0.743
PB12	0.805
PB13	0.739

The LIF profiles were measured in the research site between 17th and 20th of May 2016

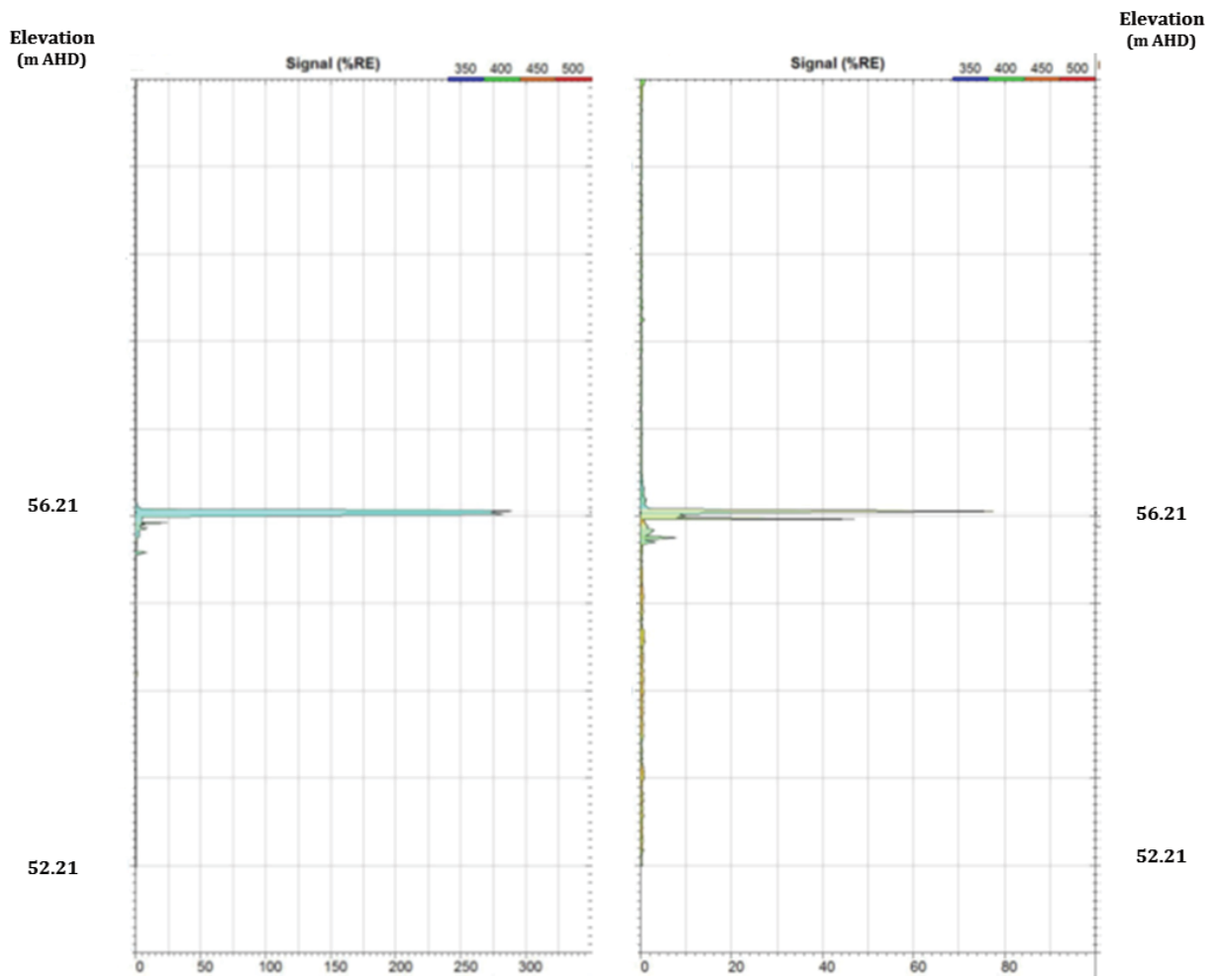


Figure B.10. LIF43 profile, area A.

Figure B.11. LIF47 profile, area A.

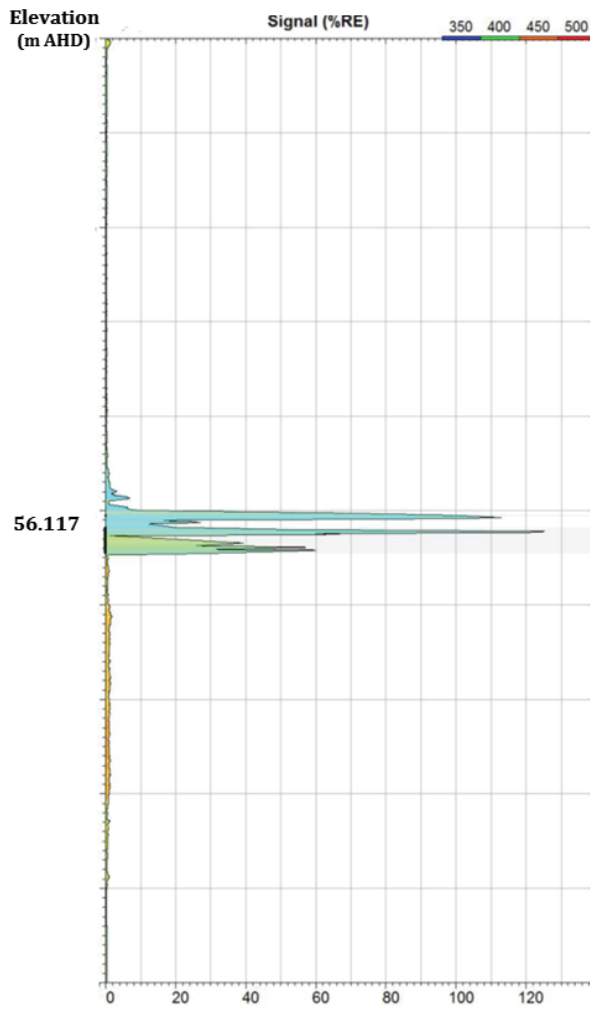


Figure B.12. LIF51 profile, area B.

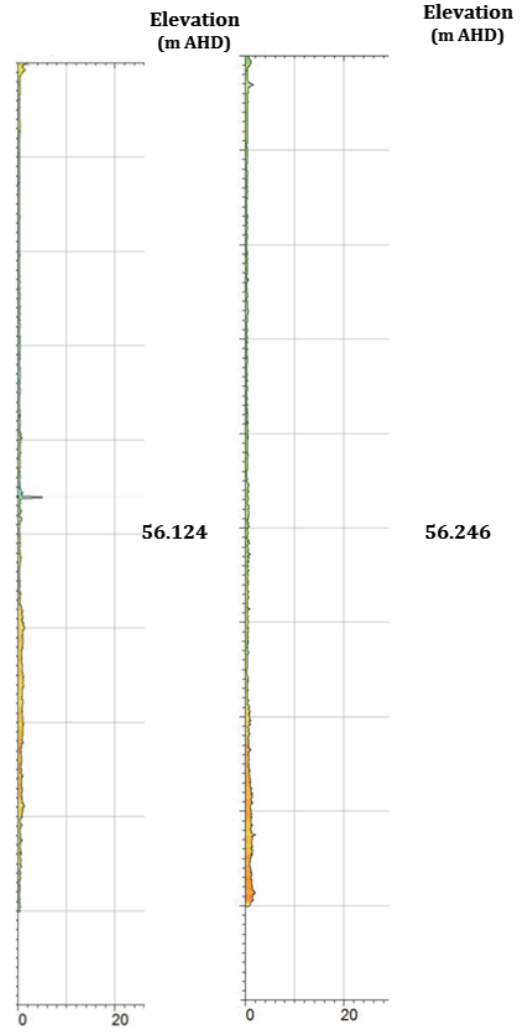


Figure B.13. LIF52 profile

Figure B.14. LIF54

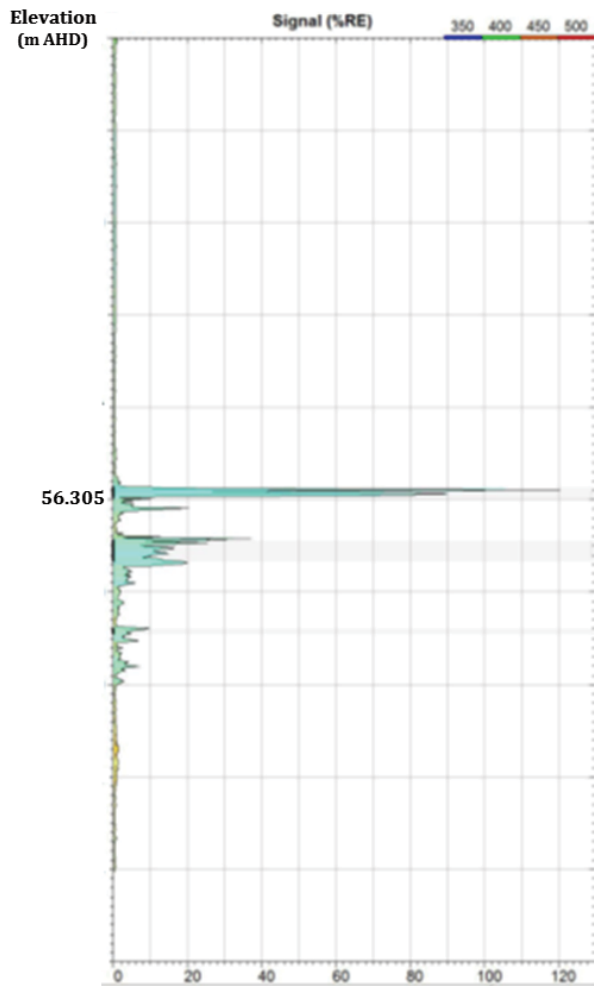


Figure B.15. LIF57 profile, area C.

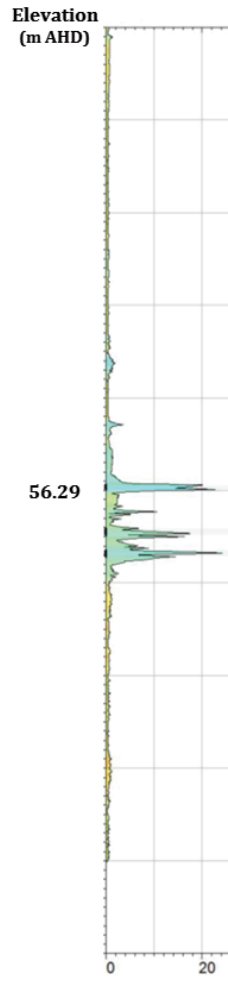


Figure II.16. LIF68 profile

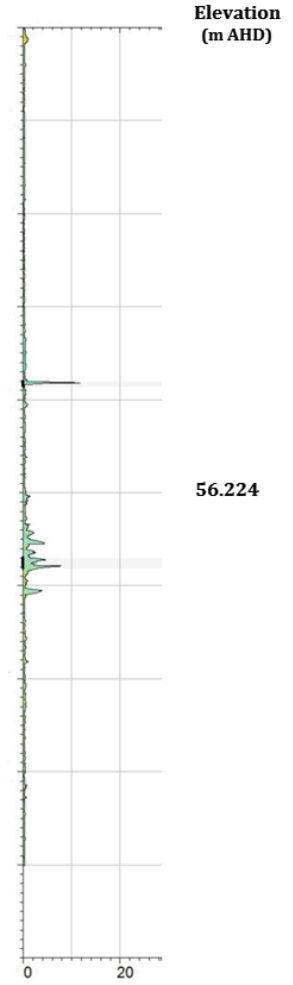


Figure B.17. LIF56

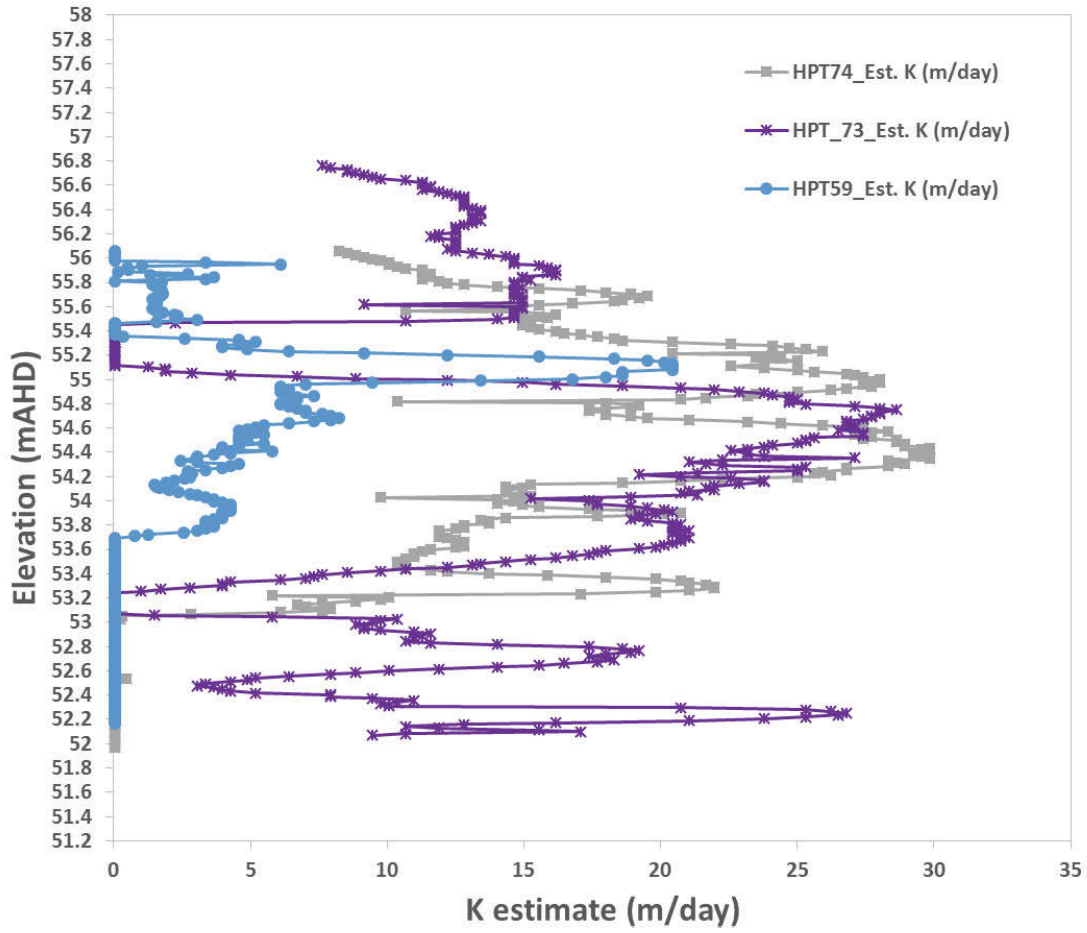


Figure B.18. K estimates at the three research areas; area A (HPT73), area B (HPT74) and area C (HPT59).

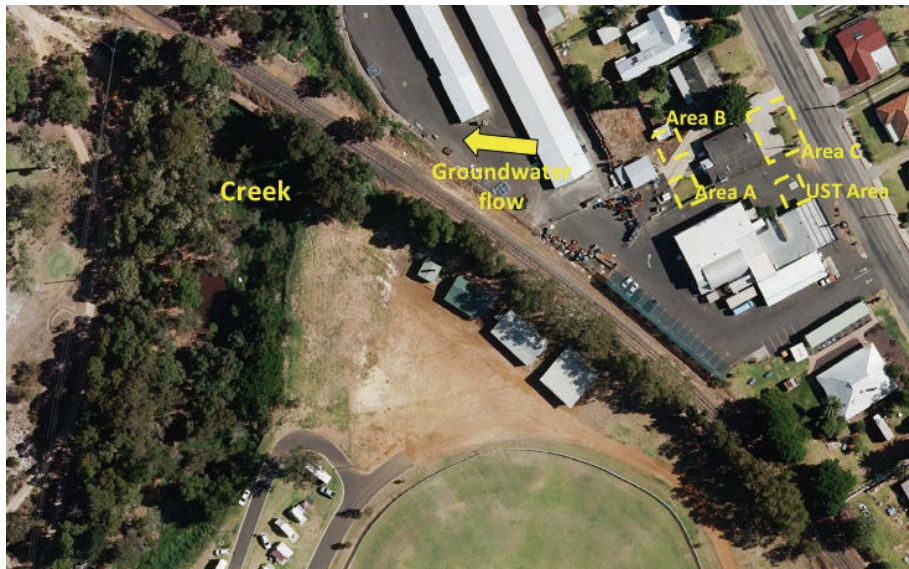


Figure B.19. Groundwater flow direction.

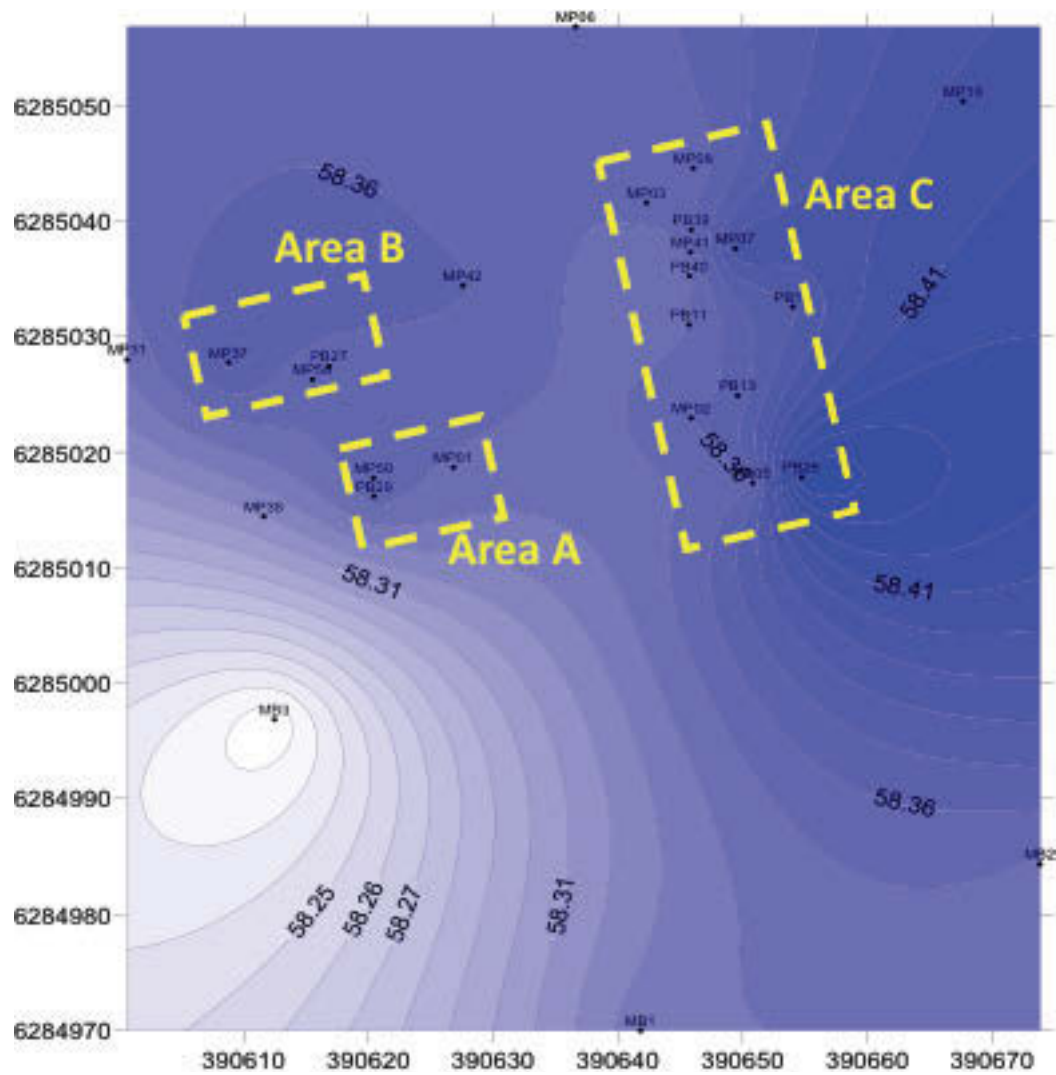


Figure B.20. Contours of Z_{aw} in meters on 26/07/2016. The contour interval is 1cm.



Figure B.21. Expected extension of LNAPL plume according to fluid levels in the monitoring network. Question marks indicate areas with no installed monitoring points.

Table B.2. NAPL compositions in MP50 core, area A.

Elevation (m AHD)	TPH C4-C15 (mg/kg)	Benzene	Toluene	EthylBenzene	m/p-Xylene	o-Xylene	BTEX (mg/kg)	Naphthalene	2-MN	1-MN	Phenanthrene	PAHs (mg/kg)
57.231	1215	19	277	40	148	57	541	2	0	0	0	2
57.131	647	7	93	14	50	19	183	1	0	0	0	1
57.031	1150	13	218	34	123	46	434	2	0	0	0	2
56.931	1500	18	299	45	171	65	598	3	0	0	0	3
56.831	1275	12	248	40	153	58	511	3	0	0	0	3
56.531	1743	11	272	49	184	73	588	3	0	0	0	4
56.481	3688	39	749	117	433	164	1503	7	1	1	0	8
56.431	5222	47	840	131	481	190	1689	8	1	1	0	10
56.381	3263	38	682	106	403	151	1379	6	1	1	0	8
56.331	4120	50	841	135	476	185	1686	8	1	1	0	10
56.281	5455	40	719	111	411	156	1437	6	0	1	0	7
56.231	9689	103	1611	256	899	357	3225	15	3	2	0	20
56.181	5192	58	880	137	492	193	1760	8	1	1	0	11
56.131	8941	114	1604	244	866	339	3167	14	2	3	0	19
56.081	8702	156	2364	327	1158	466	4471	19	4	3	0	26
55.981	172	5	37	4	15	6	66	0	0	0	0	0
55.931	127	3	13	1	4	2	24	0	0	0	0	0
55.881	201	3	11	1	2	1	18	0	0	0	0	0
55.831	43	3	13	1	2	1	20	0	0	0	0	0
55.781	63	3	11	0	2	1	17	0	0	0	0	0
55.731	80	3	11	0	2	1	16	0	0	0	0	0
55.681	66	3	9	1	1	0	14	0	0	0	0	0
55.631	71	2	7	0	1	0	11	0	0	0	0	0
55.581	102	2	5	0	1	0	8	0	0	0	0	0
55.481	92	1	0	0	0	0	2	0	0	0	0	0
55.381	80	0	1	0	0	0	2	0	0	0	0	0

Table B.3. NAPL compositions in MP58 core, area B.

Elevation (m AHD)	TPH C4-C15 (mg/kg)	Benzene	Toluene	EthylBenzene	m/p-Xylene	o-Xylene	BTEX (mg/kg)	Naphthalene	2-MN	1-MN	Phenanthrene	PAHs (mg/kg)
58.096	42	0	0	0	0	0	1	0	0	0	0	0
58.046	64	0	1	0	1	0	2	0	0	0	0	0
57.996	117	0	0	0	0	0	1	0	0	0	0	0
57.796	78	1	3	0	1	0	5	0	0	0	0	0
57.746	182	1	17	4	16	5	43	0	0	0	0	0
57.696	128	1	8	1	5	2	18	0	0	0	0	0
57.646	259	1	34	7	27	10	78	0	0	0	0	0
57.596	128	1	21	5	20	7	53	0	0	0	0	0
57.546	284	2	53	10	45	17	127	1	0	0	0	1
57.496	698	4	116	22	91	33	267	1	0	0	0	2
57.446	1031	4	146	35	130	48	362	3	0	0	0	3
56.396	1942	6	206	46	175	66	499	3	1	1	0	5
56.346	1726	8	229	45	169	65	516	3	1	1	0	4
56.296	1704	10	278	53	206	77	624	4	0	1	0	5
56.246	2863	12	303	52	200	74	641	3	0	0	0	4
56.196	11680	61	1175	193	703	277	2409	11	2	2	0	15
56.146	9362	55	1118	187	667	260	2286	10	2	2	0	14
56.096	9910	64	1366	224	806	313	2774	12	3	2	0	17
56.046	16655	122	2480	397	1362	545	4906	21	5	4	0	31
55.996	9657	82	1457	237	836	331	2943	13	3	2	0	18
55.946	9392	62	1083	169	610	237	2161	9	1	2	0	12
55.296	3763	45	732	112	401	158	1449	6	1	1	0	7
55.246	247	6	61	8	28	10	113	0	0	0	0	0
55.196	246	4	38	5	17	7	71	0	0	0	0	0

Table B.4. NAPL compositions in MP44 core, area C.

Elevation (m AHD)	TPH C4-C15 (mg/kg)	Benzene	Toluene	EthylBenzene	m/p-Xylene	o-Xylene	BTEX (mg/kg)	Naphthalene	2-MN	1-MN	Phenanthrene	PAHs (mg/kg)
58.861	89	1	4	0	1	0	7	0	0	0	0	0
58.611	74	0	5	1	4	1	12	0	0	0	0	0
58.461	74	0	8	1	6	2	18	0	0	0	0	0
58.111	74	0	3	1	5	2	12	0	0	0	0	0
57.811	160	1	16	4	17	7	44	0	0	0	0	0
57.411	348	2	52	12	49	19	134	1	0	0	0	2
57.311	247	2	60	10	38	15	126	1	0	0	0	1
57.161	616	2	91	20	76	30	219	2	0	0	0	2
57.011	744	4	115	24	92	35	269	2	0	0	0	2
56.861	1055	6	160	35	135	51	387	2	1	0	0	3
56.761	1370	12	242	43	164	63	524	3	1	0	0	4
56.661	3882	30	493	79	294	116	1012	4	1	1	0	6
56.561	15046	162	1992	321	1130	459	4063	17	5	4	0	25
56.461	20537	231	2908	415	1449	585	5587	21	6	5	0	33
56.361	33017	412	5476	767	2570	1078	10303	39	13	9	0	62
56.261	28600	312	3985	617	2051	871	7836	33	10	8	0	51
56.011	14882	299	4080	611	2022	864	7877	36	11	8	0	55
55.911	12331	167	2242	327	1144	466	4346	21	5	4	0	31
55.811	7167	74	1000	148	546	214	1982	10	2	1	0	13
55.711	22300	230	3115	462	1585	653	6045	31	8	5	0	44
55.561	6320	86	1139	175	625	249	2274	10	2	2	0	14
55.461	3556	50	709	107	407	161	1433	7	1	1	0	9
55.261	994	12	141	19	70	27	270	1	0	0	0	2
54.961	3984	46	663	89	340	129	1268	6	1	1	0	8
54.361	445	4	48	7	23	9	90	0	0	0	0	0

Table B.5. Calculation parameters for NAPL saturations in MP50 core, area A.

Elevation	Thetag	Bulkdensity	thetaV	mg_per_kg	TPH_mLperkg_dry	TPH_vol%	Sat%
57.231	0.19	1.44	0.27	1441.92	1.95	0.28%	0.62
57.131	0.16	1.46	0.23	749.57	1.01	0.15%	0.33
57.031	0.16	1.45	0.23	1333.43	1.8	0.26%	0.58
56.931	0.15	1.51	0.22	1722.53	2.33	0.35%	0.82
56.831	0.14	1.51	0.22	1459.17	1.97	0.30%	0.69
56.531	0.15	0.98	0.14	1998.76	2.7	0.27%	0.42
56.481	0.13	1.38	0.18	4181.48	5.65	0.78%	1.63
56.431	0.05	1.49	0.08	5498.14	7.43	1.10%	2.51
56.381	0.11	1.41	0.15	3619.06	4.89	0.69%	1.47
56.331	0.11	1.41	0.16	4589.73	6.2	0.88%	1.88
56.281	0.11	1.41	0.15	6052.56	8.18	1.15%	2.47
56.231	0.13	1.43	0.19	10968.26	14.82	2.12%	4.58
56.181	0.15	1.42	0.21	5957.3	8.05	1.15%	2.48
56.131	0.19	1.51	0.28	10612.25	14.34	2.17%	5.05
56.081	0.20	1.63	0.33	10457.98	14.13	2.30%	5.95
55.981	0.26	1.44	0.37	< 200			0
55.931	0.24	1.43	0.34	< 200			0
55.881	0.24	1.48	0.35	248.27	0.34	0.05%	0.11
55.831	0.23	1.49	0.35	< 200			0
55.781	0.22	1.55	0.34	< 200			0
55.731	0.22	1.54	0.34	< 200			0
55.681	0.22	1.56	0.35	< 200			0
55.631	0.20	1.65	0.34	< 200			0
55.581	0.16	1.84	0.30	< 200			0
55.481	0.18	1.82	0.33	< 200			0
55.381	0.19	1.78	0.33	< 200			0

Table B.6. Calculation parameters for NAPL saturations in MP58 core, area B.

Elevation	Thetag	Bulkdensity	thetaV	TPH_mg_per_kg_dry	H_mLperkg	TPH_vol%	Sat%
58.096	0.18	1.63	0.29	< 200			0
58.046	0.19	1.57	0.30	< 200			0
57.996	0.19	1.56	0.29	< 200			0
57.796	0.23	1.28	0.30	< 200			0
57.746	0.25	1.33	0.33	< 200			0
57.696	0.24	1.36	0.33	< 200			0
57.646	0.13	1.67	0.22	293.81	0.4	0.07%	0.18
57.596	0.10	1.65	0.17	< 200			0
57.546	0.12	1.55	0.18	317.98	0.43	0.07%	0.16
57.496	0.13	1.53	0.19	785.94	1.06	0.16%	0.39
57.446	0.11	1.56	0.16	1138.91	1.54	0.24%	0.59
56.396	0.08	1.19	0.10	2106.7	2.85	0.34%	0.62
56.346	0.07	1.28	0.09	1854.38	2.51	0.32%	0.62
56.296	0.07	1.30	0.09	1821.52	2.46	0.32%	0.63
56.246	0.07	1.35	0.10	3073.93	4.15	0.56%	1.14
56.196	0.09	1.37	0.12	12674.27	17.13	2.34%	4.84
56.146	0.10	1.43	0.14	10303.4	13.92	1.99%	4.33
56.096	0.08	1.53	0.13	10724.13	14.49	2.21%	5.22
56.046	0.14	1.47	0.20	18929.91	25.58	3.76%	8.43
55.996	0.16	1.40	0.22	11189.37	15.12	2.11%	4.46
55.946	0.20	1.59	0.32	11264.5	15.22	2.41%	6.02
55.296	0.28	1.07	0.30	4798.88	6.48	0.70%	1.17
55.246	0.23	1.39	0.32	303.82	0.41	0.06%	0.12
55.196	0.23	1.71	0.39	301.91	0.41	0.07%	0.2

Table B.7. Calculation parameters for NAPL saturations in MP44 core, area C.

Elevation	Thetag	Bulkdensity	thetaV	TPH_mg_per_kg_dry	TPH_mLperkg_dry	TPH_vol%	Sat%
58.86	0.22	1.42	0.31	< 200			0.00
58.61	0.20	1.45	0.29	< 200			0.00
58.46	0.15	1.53	0.22	< 200			0.00
58.11	0.12	1.11	0.14	< 200			0.00
57.81	0.19	1.07	0.20	< 200			0.00
57.41	0.18	1.51	0.28	411.97	0.56	0.08%	0.20
57.31	0.17	1.55	0.26	288.25	0.39	0.06%	0.15
57.16	0.18	1.15	0.20	724.96	0.98	0.11%	0.20
57.01	0.17	1.00	0.17	867.02	1.17	0.12%	0.19
56.86	0.15	1.22	0.18	1212.98	1.64	0.20%	0.37
56.76	0.12	1.46	0.18	1538.6	2.08	0.30%	0.67
56.66	0.11	1.45	0.15	4291.16	5.8	0.84%	1.86
56.56	0.13	1.42	0.19	17077.39	23.08	3.28%	7.08
56.46	0.17	1.54	0.27	24129.76	32.61	5.01%	11.92
56.36	0.21	1.53	0.32	40020.42	54.08	8.27%	19.55
56.26	0.21	1.55	0.32	34467.05	46.58	7.21%	17.33
56.01							0.00
55.91	0.21	1.42	0.30	14937.28	20.19	2.86%	6.17
55.81	0.22	1.55	0.35	8771.28	11.85	1.84%	4.43
55.71	0.24	1.46	0.35	27675.27	37.4	5.48%	12.25
55.56	0.23	1.60	0.36	7745.71	10.47	1.68%	4.24
55.46	0.21	1.46	0.31	4304.22	5.82	0.85%	1.90
55.26	0.26	1.46	0.37	1248.41	1.69	0.25%	0.55
54.96	0.21	1.50	0.31	4811.95	6.5	0.97%	2.24
54.36	0.22	1.42	0.31	541.31	0.73	0.10%	0.22

Table B.8. TPH and C₄-C₅ values along with elevations in MP50 core, area A.

Elevation	TPH	C₄C₅
(m AHD)	(mg/kg)	(mg/kg)
57.231	1442	35
57.131	750	25
57.031	1333	<10
56.931	1723	36
56.831	1459	19
56.531	1999	37
56.481	4181	<10
56.431	5498	342
56.381	3619	56
56.331	4590	74
56.281	6053	806
56.231	10968	1399
56.181	5957	141
56.131	10612	1273
56.081	10458	570
55.981	<200	<10
55.931	<200	<10

Table B.9. TPH and C₄-C₅ values along with elevations in MP58 core, area B.

Elevation	TPH	C₄C₅
(m AHD)	(mg/kg)	(mg/kg)
57.546	317	< 10
57.496	785	< 10
57.446	1138	< 10
56.396	2106	624
56.346	1854	159
56.296	1821	< 10
56.246	3073	1072
56.196	12674	2280
56.146	10303	1380
56.096	10724	1320
56.046	18929	2228
55.996	11189	1375
55.946	11264	1212
55.296	4798	289
55.246	303	< 10
55.196	301	14

Table B.10. TPH and C₄-C₅ values along with elevations in MP44 core, area C.

Elevation	TPH	C₄C₅
(m AHD)	(mg/kg)	(mg/kg)
58.111	< 200	< 10
57.811	< 200	< 10
57.411	411	21
57.311	288	17
57.161	724	72
57.011	867	19
56.861	1212	61
56.761	1538	< 10
56.661	4291	549
56.561	17077	1594
56.461	24129	2735
56.361	40020	5023
56.261	34467	2991
55.911	14937	1890
55.811	8771	1178
55.711	27675	3760
55.561	7745	1030
55.461	4304	472
55.261	1248	125
54.961	4811	407
54.361	541	100

Chemical concentrations of gasoline components in NAPL, dissolved and sorbed phase

In this section total TPH concentrations obtained from extracted cores (MP50, MP58 and MP44) in the three areas of research are used to calculate expected TPH concentrations in the aqueous, solid and NAPL phases assuming equilibrium partitioning conditions. Equilibrium TPH concentrations present as NAPL are compared to the total TPH values to evaluate the errors derived from neglecting mass transfer phenomena in the estimation of LNAPL saturation values calculated by simply using equation 4. It has to be noted that there are always errors and uncertainty associated to the sampling procedure, since some compounds could volatilise at some extent.

These calculations were made for representative samples from two intervals in the saturated zone: (i) the mobile interval with the highest TPH values and (ii) the entrapped LNAPL zone presenting low-end TPH values.

In the saturated zone the mathematical form for the $C_{sat,i}$ calculation of the component i in the mixture is (Brost & De Vaull, 2000):

$$C_{sat,i} = \frac{S_{w,i} * X_i}{\rho_{fb}} * (\theta_w + K_{s,i} * \rho_{fb}) \quad [Equation 23]$$

where:

$C_{sat,i}$: chemical concentration of the component i in soil at which sorption limits of soil particles and solubility limits of soil pore water have been reached;

$S_{w,i}$: water solubility of i compound;

X_i : mole fraction of component i in mixture;

ρ_{fb} : soil bulk density;

θ_w : volumetric water content;

$K_{s,i}$: soil-water partition coefficient of component i .

The chemical concentration of component i in dissolved and sorbed phase is calculated by the next equations respectively (Brost & De Vaull, 2000):

$$C_{dissolved,i} = \frac{S_{w,i} * X_i}{\rho_{fb}} * \theta_w \quad [Equation 24]$$

$$C_{sorbed,i} = S_{w,i} * X_i * K_{s,i} \quad [Equation 25]$$

The mathematical form for the $K_{s,i}$ calculation is:

$$K_{s,i} = f_{oc} * K_{oc} \quad [Equation 26]$$

where:

f_{oc} : fraction organic carbon;

K_{oc} : organic matter-water partition coefficient.

All presented parameters were measured in the laboratory except from S_w and K_{oc} . Values for these two parameters were obtained by the RAIS database (rais.ornl.gov). θ_w was assumed to be equal to a measured porosity value of 0.4. Using the total porosity is a conservative approach since the pore space is variably occupied by LNAPL under field conditions.

MP50 (Area A)

The estimated average of TPH concentration in the mobile interval is 7016 mg/Kg. This value is referred as Total TPH including TPHs in NAPL, sorbed and dissolved phase. Tables B.11 and B.12 present the input parameters for the calculation of dissolved and sorbed concentrations of each measured component. Aromatics and Aliphatics are presented respectively.

Table B.11. Input parameters for the calculation of chemical concentrations of Aromatics in dissolved and sorbed phase.

Components	$S_{w,i}$ (mg/L)	X_i (-)	ρ_{fb} (Kg/L)	θ_w (-)	$K_{s,i}$ (L/Kg)	f_{oc} (-)	K_{oc} (L/Kg)	Dissolved conc. (mg/Kg)	Sorbed conc. (mg/Kg)
Benzene	1790	0.007	1.4	0.4	0.146	0.001	146	3.58	1.83
Toluene	526	0.130	1.4	0.4	0.234	0.001	234	19.54	16.00
EthylBenzene	169	0.029	1.4	0.4	0.446	0.001	446	1.41	2.21
m/p-Xylene	161	0.104	1.4	0.4	0.375	0.001	375	4.78	6.27
o-Xylene	178	0.041	1.4	0.4	0.383	0.001	383	2.08	2.79
135-TMB	48.2	0.014	1.4	0.4	0.602	0.001	602	0.19	0.40
124-TMB	57	0.048	1.4	0.4	0.614	0.001	614	0.78	1.67
123-TMB	75.2	0.011	1.4	0.4	0.627	0.001	627	0.23	0.50
Naphthalene	31	0.002	1.4	0.4	1.54	0.001	1540	0.01	0.08

Table B.12. Input parameters for the calculation of chemical concentrations of Aliphatics in dissolved and sorbed phase.

Chemical Groups	$S_{w,i}$ (mg/L)	X_i (-)	ρ_{fb} (Kg/L)	θ_w (-)	$K_{s,i}$ (L/Kg)	f_{oc} (-)	K_{oc} (L/Kg)	Dissolved conc. (mg/Kg)	Sorbed conc. (mg/Kg)
C5-C6	28	0.186	1.4	0.4	0.794	0.001	794	1.495	4.155
C7-C8	4.2	0.193	1.4	0.4	3.98	0.001	3980	0.232	3.232
C9-C10	0.33	0.102	1.4	0.4	31.6	0.001	31600	0.010	1.070
C11-C12	0.026	0.106	1.4	0.4	251	0.001	251000	0.001	0.696
C13-C15	0.00059	0.008	1.4	0.4	5010	0.001	5010000	0.000	0.026

Table B.13. Difference between total TPH and TPH as NAPLs.

Total TPH (mg/Kg)	Dissolved + Sorbed (mg/Kg)	TPH in NAPL phase (mg/Kg)	Difference (%)
7016	75.28	6941	1.07

Table B.14 presents the maximum dissolved and sorbed concentrations of the individual components that are related with the maximum X_i values measured in the mobile interval.

Components	Max X_i (-)	Max Dissolved conc. (mg/Kg)	Max Sorbed conc. (mg/Kg)
Benzene	0.009	4.50	2.30
Toluene	0.147	22.09	18.09
EthylBenzene	0.032	1.55	2.41
m/p-Xylene	0.133	6.12	8.03
o-Xylene	0.054	2.75	3.68
135-TMB	0.018	0.25	0.52
124-TMB	0.063	1.03	2.20
123-TMB	0.015	0.32	0.71
Naphthalene	0.002	0.02	0.10
C5-C6	0.219	1.75	4.87
C7-C8	0.217	0.26	3.63
C9-C10	0.110	0.01	1.15
C11-C12	0.124	0.00	0.81
C13-C15	0.011	0.00	0.03

MP58 (Area B)

The estimated average of TPH concentration in the mobile interval is 8696 mg/Kg. Tables B.15 and B.16 present the input parameters for the calculation of dissolved and sorbed concentrations of each measured component. Aromatics and Aliphatics are presented respectively.

Mobile interval:

Table B.15. Input parameters for the calculation of chemical concentrations of Aromatics in dissolved and sorbed phase.

Components	$S_{w,i}$ (mg/L)	X_i (-)	ρ_{fb} (Kg/L)	θ_w (-)	$K_{s,i}$ (L/Kg)	f_{oc} (-)	K_{oc} (L/Kg)	Dissolved conc. (mg/Kg)	Sorbed conc. (mg/Kg)
Benzene	1790	0.004	1.4	0.4	0.146	0.001	146	2.03	1.04
Toluene	526	0.102	1.4	0.4	0.234	0.001	234	15.45	12.66
EthylBenzene	169	0.022	1.4	0.4	0.446	0.001	446	1.07	1.66
m/p-Xylene	161	0.081	1.4	0.4	0.375	0.001	375	3.72	4.88
o-Xylene	178	0.031	1.4	0.4	0.383	0.001	383	1.59	2.13
135-TMB	48.2	0.005	1.4	0.4	0.602	0.001	602	0.07	0.14
124-TMB	57	0.016	1.4	0.4	0.614	0.001	614	0.27	0.58
123-TMB	75.2	0.004	1.4	0.4	0.627	0.001	627	0.08	0.18
Naphthalene	31	0.001	1.4	0.4	1.54	0.001	1540	0.01	0.05

Table B.16. Input parameters for the calculation of chemical concentrations of Aliphatics in dissolved and sorbed phase.

Chemical Groups	$S_{w,i}$ (mg/L)	X_i (-)	ρ_{fb} (Kg/L)	θ_w (-)	$K_{s,i}$ (L/Kg)	f_{oc} (-)	K_{oc} (L/Kg)	Dissolved conc. (mg/Kg)	Sorbed conc. (mg/Kg)
C5-C6	28	0.240	1.4	0.4	0.794	0.001	794	1.93	5.35
C7-C8	4.2	0.204	1.4	0.4	3.98	0.001	3980	0.24	3.41
C9-C10	0.33	0.100	1.4	0.4	31.6	0.001	31600	0.01	1.05
C11-C12	0.026	0.107	1.4	0.4	251	0.001	251000	0.00	0.70
C13-C15	0.00059	0.009	1.4	0.4	5010	0.001	5010000	0.00	0.03

Table B.17. Difference between total TPH and TPH as NAPLs.

Total TPH (mg/Kg)	Dissolved + Sorbed (mg/Kg)	TPH in NAPL phase (mg/Kg)	Difference (%)
8696	60.30	8635	0.69

Table B.18 presents the maximum dissolved and sorbed concentrations of the individual components that are related with the maximum X_i values measured in the mobile interval.

Components	Max X_i (-)	Max Dissolved conc. (mg/Kg)	Max Sorbed conc. (mg/Kg)
Benzene	0.005	2.76	1.41
Toluene	0.110	16.53	13.54
EthylBenzene	0.031	1.50	2.34
m/p-Xylene	0.121	5.57	7.31
o-Xylene	0.045	2.29	3.07
135-TMB	0.010	0.14	0.29
124-TMB	0.030	0.49	1.05
123-TMB	0.008	0.17	0.38
Naphthalene	0.002	0.02	0.10
C5-C6	0.325	2.60	7.23
C7-C8	0.219	0.26	3.66
C9-C10	0.145	0.01	1.51
C11-C12	0.147	0.00	0.96
C13-C15	0.020	0.00	0.06

Low-end S_n :

The TPH concentration at 55.29 m AHD is 4799 mg/Kg. Tables B.19 and B.20 present the input parameters for the calculation of dissolved and sorbed concentrations of each measured component at this elevation. Aromatics and Aliphatics are presented respectively.

Table B.19. Input parameters for the calculation of chemical concentrations of Aromatics in dissolved and sorbed phase.

Components	$S_{w,i}$ (mg/L)	X_i (-)	ρ_{fb} (Kg/L)	θ_w (-)	$K_{s,i}$ (L/Kg)	f_{oc} (-)	K_{oc} (L/Kg)	Dissolved conc. (mg/Kg)	Sorbed conc. (mg/Kg)
Benzene	1790	0.006	1.4	0.4	0.146	0.001	146	3.01	1.54
Toluene	526	0.129	1.4	0.4	0.234	0.001	234	19.36	15.86
EthylBenzene	169	0.024	1.4	0.4	0.446	0.001	446	1.15	1.79
m/p-Xylene	161	0.085	1.4	0.4	0.375	0.001	375	3.91	5.14
o-Xylene	178	0.033	1.4	0.4	0.383	0.001	383	1.70	2.28
135-TMB	48.2	0.005	1.4	0.4	0.602	0.001	602	0.07	0.15
124-TMB	57	0.018	1.4	0.4	0.614	0.001	614	0.30	0.64
123-TMB	75.2	0.004	1.4	0.4	0.627	0.001	627	0.09	0.19
Naphthalene	31	0.001	1.4	0.4	1.54	0.001	1540	0.01	0.05

Table B.20. Input parameters for the calculation of chemical concentrations of Aliphatics in dissolved and sorbed phase.

Chemical Groups	$S_{w,i}$ (mg/L)	X_i (-)	ρ_{fb} (Kg/L)	θ_w (-)	$K_{s,i}$ (L/Kg)	f_{oc} (-)	K_{oc} (L/Kg)	Dissolved conc. (mg/Kg)	Sorbed conc. (mg/Kg)
C5-C6	28	0.154	1.4	0.4	0.794	0.001	794	1.23	3.42
C7-C8	4.2	0.211	1.4	0.4	3.98	0.001	3980	0.25	3.53
C9-C10	0.33	0.110	1.4	0.4	31.6	0.001	31600	0.01	1.15
C11-C12	0.026	0.113	1.4	0.4	251	0.001	251000	0.00	0.74
C13-C15	0.00059	0.017	1.4	0.4	5010	0.001	5010000	0.00	0.05

Table B.21. Difference between total TPH and TPH as NAPLs.

Total TPH (mg/Kg)	Dissolved + Sorbed (mg/Kg)	TPH in NAPL phase (mg/Kg)	Difference (%)
4799	67.61	4731	1.41

MP44 (Area C)

The estimated average of TPH concentration in the mobile interval is 19716 mg/Kg. Tables B.22 and B.23 present the input parameters for the calculation of dissolved and sorbed concentrations of each measured component. Aromatics and Aliphatics are presented respectively.

Mobile interval:**Table B.22. Input parameters for the calculation of chemical concentrations of Aromatics in dissolved and sorbed phase.**

Components	$S_{w,i}$ (mg/L)	X_i (-)	ρ_{fb} (Kg/L)	θ_w (-)	$K_{s,i}$ (L/Kg)	f_{oc} (-)	K_{oc} (L/Kg)	Dissolved conc. (mg/Kg)	Sorbed conc. (mg/Kg)
Benzene	1790	8.9E-03	1.4	0.4	0.146	0.001	146	4.55	2.32
Toluene	526	0.127	1.4	0.4	0.234	0.001	234	19.14	15.68
EthylBenzene	169	0.026	1.4	0.4	0.446	0.001	446	1.27	1.99
m/p-Xylene	161	0.090	1.4	0.4	0.375	0.001	375	4.15	5.45
o-Xylene	178	0.037	1.4	0.4	0.383	0.001	383	1.91	2.55
135-TMB	48.2	4.9E-05	1.4	0.4	0.602	0.001	602	0.00	0.00
124-TMB	57	1.6 E-04	1.4	0.4	0.614	0.001	614	0.00	0.01
123-TMB	75.2	3.8E-05	1.4	0.4	0.627	0.001	627	0.00	0.00
Naphthalene	31	1.1E-05	1.4	0.4	1.54	0.001	1540	0.00	0.00

Table B.23. Input parameters for the calculation of chemical concentrations of Aliphatics in dissolved and sorbed phase.

Chemical Groups	S_{w,i} (mg/L)	X_i (-)	ρ_{fb} (Kg/L)	θ_w (-)	K_{s,i} (L/Kg)	f_{oc} (-)	K_{oc} (L/Kg)	Dissolved conc. (mg/Kg)	Sorbed conc. (mg/Kg)
C5-C6	28	0.243	1.4	0.4	0.794	0.001	794	1.95	5.41
C7-C8	4.2	0.193	1.4	0.4	3.98	0.001	3980	0.23	3.23
C9-C10	0.33	0.085	1.4	0.4	31.6	0.001	31600	0.01	0.89
C11-C12	0.026	0.092	1.4	0.4	251	0.001	251000	0.00	0.60
C13-C15	0.00059	0.006	1.4	0.4	5010	0.001	5010000	0.00	0.02

Table B.24. Difference between total TPH and TPH as NAPLs.

Total TPH (mg/Kg)	Dissolved + Sorbed (mg/Kg)	TPH in NAPL phase (mg/Kg)	Difference (%)
19716	71.36	19645	0.36

Table B.25 presents the maximum dissolved and sorbed concentrations of the individual components that are related with the maximum X_i values measured in the mobile interval.

Components	Max X_i (-)	Max Dissolved conc. (mg/Kg)	Max Sorbed conc. (mg/Kg)
Benzene	0.010	5.11	2.61
Toluene	0.146	21.94	17.97
EthylBenzene	0.04	1.93	3.01
m/p-Xylene	0.135	6.21	8.15
o-Xylene	0.05	2.54	3.41
135-TMB	7.7E-05	0.00	0.00
124-TMB	2.5 E-04	0.00	0.01
123-TMB	5.9E-05	0.00	0.00
Naphthalene	1.5E-05	0.00	0.00
C5-C6	0.284	2.27	6.31
C7-C8	0.203	0.24	3.39
C9-C10	0.095	0.01	0.99
C11-C12	0.122	0.00	0.80
C13-C15	0.009	0.00	0.03

Low-end S_n :

The TPH concentration at 54.96 m AHD is 4812 mg/Kg. Tables B.26 and B.27 present the input parameters for the calculation of dissolved and sorbed concentrations of each measured component at this elevation. Aromatics and Aliphatics are presented respectively.

Table B.26. Input parameters for the calculation of chemical concentrations of Aromatics in dissolved and sorbed phase.

Components	$S_{w,i}$ (mg/L)	X_i (-)	ρ_{fb} (Kg/L)	θ_w (-)	$K_{s,i}$ (L/Kg)	f_{oc} (-)	K_{oc} (L/Kg)	Dissolved conc. (mg/Kg)	Sorbed conc. (mg/Kg)
Benzene	1790	0.007	1.4	0.4	0.146	0.001	146	3.81	1.95
Toluene	526	0.131	1.4	0.4	0.234	0.001	234	19.73	16.16
EthylBenzene	169	0.008	1.4	0.4	0.446	0.001	446	0.41	0.64
m/p-Xylene	161	0.031	1.4	0.4	0.375	0.001	375	1.44	1.89
o-Xylene	178	0.012	1.4	0.4	0.383	0.001	383	0.61	0.82
135-TMB	48.2	4 E-06	1.4	0.4	0.602	0.001	602	0.00	0.00
124-TMB	57	1.4 E-05	1.4	0.4	0.614	0.001	614	0.00	0.00
123-TMB	75.2	3 E-06	1.4	0.4	0.627	0.001	627	0.00	0.00
Naphthalene	31	1 E-06	1.4	0.4	1.54	0.001	1540	0.00	0.00

Table B.27. Input parameters for the calculation of chemical concentrations of Aliphatics in dissolved and sorbed phase.

Chemical Groups	$S_{w,i}$ (mg/L)	X_i (-)	ρ_{fb} (Kg/L)	θ_w (-)	$K_{s,i}$ (L/Kg)	f_{oc} (-)	K_{oc} (L/Kg)	Dissolved conc. (mg/Kg)	Sorbed conc. (mg/Kg)
C5-C6	28	0.235	1.4	0.4	0.794	0.001	794	1.89	5.24
C7-C8	4.2	0.214	1.4	0.4	3.98	0.001	3980	0.26	3.58
C9-C10	0.33	0.082	1.4	0.4	31.6	0.001	31600	0.01	0.86
C11-C12	0.026	0.092	1.4	0.4	251	0.001	251000	0.00	0.60
C13-C15	0.00059	0.009	1.4	0.4	5010	0.001	5010000	0.00	0.03

Table B.28. Difference between total TPH and TPH as NAPLs.

Total TPH (mg/Kg)	Dissolved + Sorbed (mg/Kg)	TPH in NAPL phase (mg/Kg)	Difference (%)
4812	59.92	4752	1.25

Sensitivity analysis

Tables B.29 and B.30 present a sensitivity analysis of f_{oc} and ρ_{fb} parameters in the mobile interval at area C. f_{oc} was measured in the range of 0.001 - 0.002. ρ_{fb} was measured in the range of 1.00 - 1.60.

Table B.29. Sensitivity analysis for f_{oc} .

	f_{oc} values	Total TPH (mg/Kg)	Dissolved + Sorbed (mg/Kg)	TPH in NAPL phase (mg/Kg)	Difference (%)
Initial f_{oc} value	0.001	19716	71.36	19645	0.36
In. value increased by 50%	0.0015	19716	90.4	19626	0.46
In. value increased by 100%	0.002	19716	109.5	19607	0.55
In. value increased by 500%	0.005	19716	224	19492	1.13
In. value increased by 1000%	0.01	19716	414	19301	2.10

Table B.29 shows that the difference between total TPH and TPH in NAPL phase is sensitive to f_{oc} changes. Higher f_{oc} values were responsible for higher concentration values in sorbed phase.

Table B.30. Sensitivity analysis for ρ_{fb} different values.

	ρ_{fb} values	Total TPH (mg/Kg)	Dissolved + Sorbed (mg/Kg)	TPH in NAPL phase (mg/Kg)	Difference (%)
Initial ρ_{fb} value	1.4	19716	71.36	19645	0.36
Lowest measured value	1.0	19716	84	19631	0.43
Highest measured value	1.6	19716	67.2	19649	0.34

Table B.30 shows that the difference between total TPH and TPH in NAPL phase is not greatly affected by ρ_{fb} changes. Higher ρ_{fb} values were responsible for slightly lower concentration values in dissolved phase. Table B.31 presents the measured f_{oc} values across the research site.

Table B.31. f_{oc} values at the three research areas.

Well id	Elevation (m AHD)	f_{oc}
PB27	54.54	0.001
PB27	52.99	0.001
MP50	55.60 - 55.55	0.001
MP50	55.13 - 55.03	0.001
MP50	53.93 - 53.63	0.001
MP44	57.09 - 57.04	0.001
MP44	56.69 - 56.64	0.001
MP44	55.69 - 55.64	0.002
MP44	55.09 - 55.04	0.001
MP44	53.89 - 53.84	0.001
PB39	57.05	0.001
PB39	56.40	0.001
PB39	54.60	0.001

Appendix C. Bail-down Testing

Appendix C comprises baildown test data presenting unconfined conditions at the well locations PB29 and PB27, at research site, 2015 - 2016. The depicted baildown test in Figure C.1. took place on 5/4/2016. 2.75 L NAPL and 0.00 L water were removed. The initial NAPL thickness before the test was 0.304 m. The thickness after the removal of the product was 0.177m and the final thickness after 86min was 0.302 m, which is almost 100 % recovery of the initial product thickness. The recovery period (>95%) was ~ 40 min.

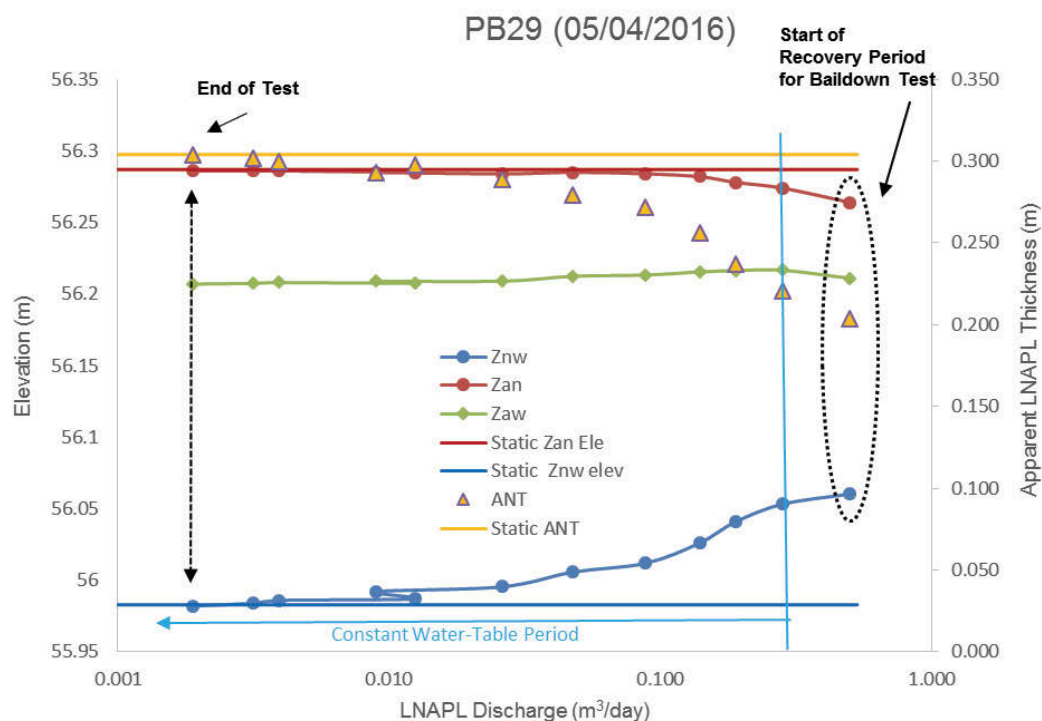


Figure C.1. Baildown test results presenting the gauged referenced air-LNAPL (Z_{an}) and LNAPL-water interfaces (Z_{nw}), the potentiometric surface elevation (Z_{aw}), the apparent thickness (ANT) and the static elevations for Z_{an} , Z_{nw} and ANT vs. LNAPL discharge for well PB29.

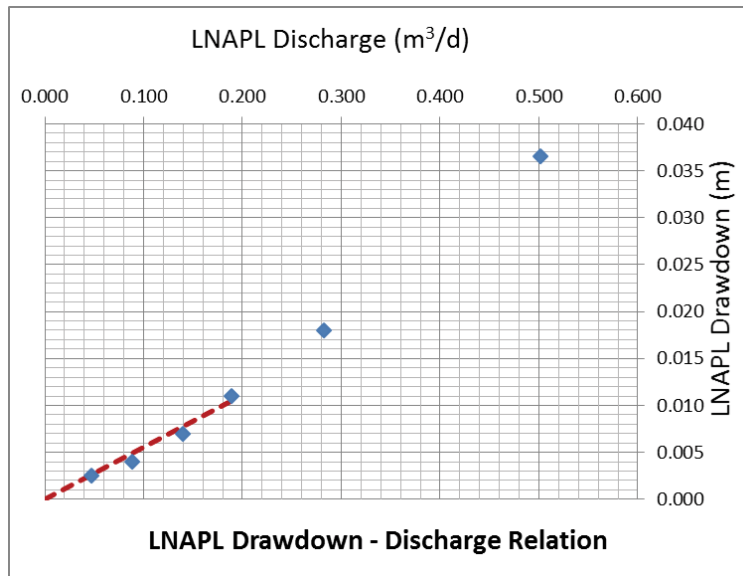


Figure C.2. LNAPL drawdown- discharge relation during baildown testing.

Figure C.2. presents the discharge versus drawdown relationship during the baildown testing recovery. The graph illustrates that borehole recharge from the filter pack maybe is not significant (large discharge value at the beginning of the recovery, 0.5 m³/d). The formation and wellbore LNAPL fluids were initially in equilibrium thus, a drawdown correction was not applied to the data. Moreover, the plot depicts behaviour that maybe suggests unconfined LNAPL conditions because there is a continuously decreasing discharge with decreasing drawdown.

Figure C.3 depicts a baildown test that took place on 20/7/2015, during an unconfined NAPL period according to Figures 5.19 and 5.21. During the test 1.75L NAPL and 0.05L water were removed. The initial NAPL thickness before the test was 0.29 m. The thickness after the removal of the product was 0.14m and the final thickness after 63min was 0.28 m, which is almost 100 % recovery of the initial product thickness. The recovery period was ~ 63 min. No constant discharge rates appeared during the recovery of the test indicating unconfined LNAPL conditions (Kirkman, Adamski & Hawthorne 2013).

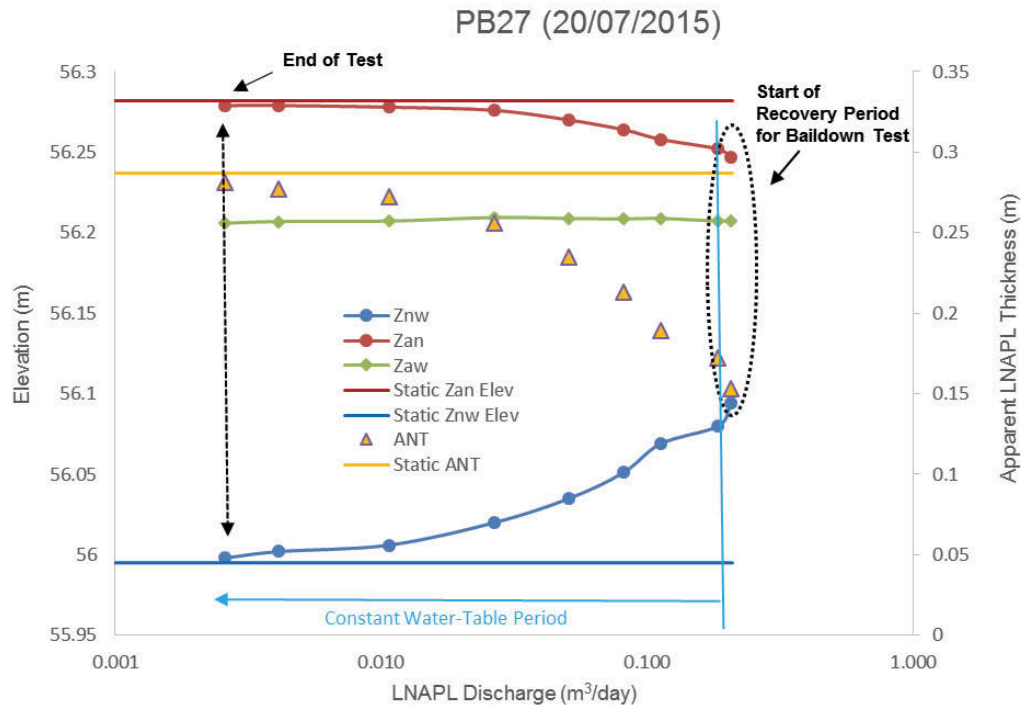


Figure C.3. Baidown test results presenting the gauged referenced air-LNAPL (Z_{an}) and LNAPL-water interfaces (Z_{nw}), the potentiometric surface elevation (Z_{aw}), the apparent thickness (ANT) and the static elevations for Z_{an} , Z_{nw} and ANT vs. LNAPL discharge for well PB27.

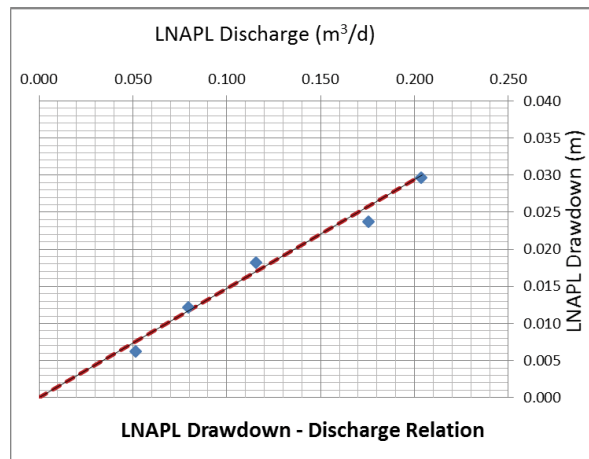


Figure C.4. LNAPL drawdown- discharge relation during baildown testing. After a drawdown adjustment of 0.0088m.

Figure C.4 depicts the discharge versus drawdown relationship during the baildown testing recovery. The graphs reveals that borehole recharge from the filter pack is not significant (large discharge value at the beginning of the recovery) (API 2012). The formation and wellbore LNAPL fluids were initially in non-equilibrium thus, a drawdown correction was

applied to the data. Moreover, the plot illustrates behaviour suggesting unconfined LNAPL conditions because a continuously decreasing discharge with decreasing drawdown is presented (Hawthorne & Kirkman 2011).

Figure C.5 illustrates a baildown test that took place on 5/04/2016, during an unconfined NAPL period according to Figures 5.20 and 5.21. During the test 2.23L NAPL and 0.37L water were removed. The initial NAPL thickness before the test was 0.31 m. The thickness after the removal of the product was 0.07m and the final thickness after 205min was 0.31 m, which is 100 % recovery of the initial product thickness. The recovery period (>95%) was ~ 110 min. The same findings with the conducted test on 6/05/2015 were found. More specifically, at $Z_{nw} \sim 56.05$ m AHD a constant discharge rate is presented during a time period of 8 minutes (higher LNAPL discharge value found compared to the previous test) in parallel with an increasing apparent thickness trend, possibly revealing geological heterogeneity at this point. The NAPL diagnostic plots, the hydrostratigraph, the same finding on 6/05/2015 (as has been discussed, unconfined NAPL and at 56.05 m AHD a possible soil heterogeneity presented) and the few measurements of constant discharge rate, dictate unconfined NAPL conditions this period of time.

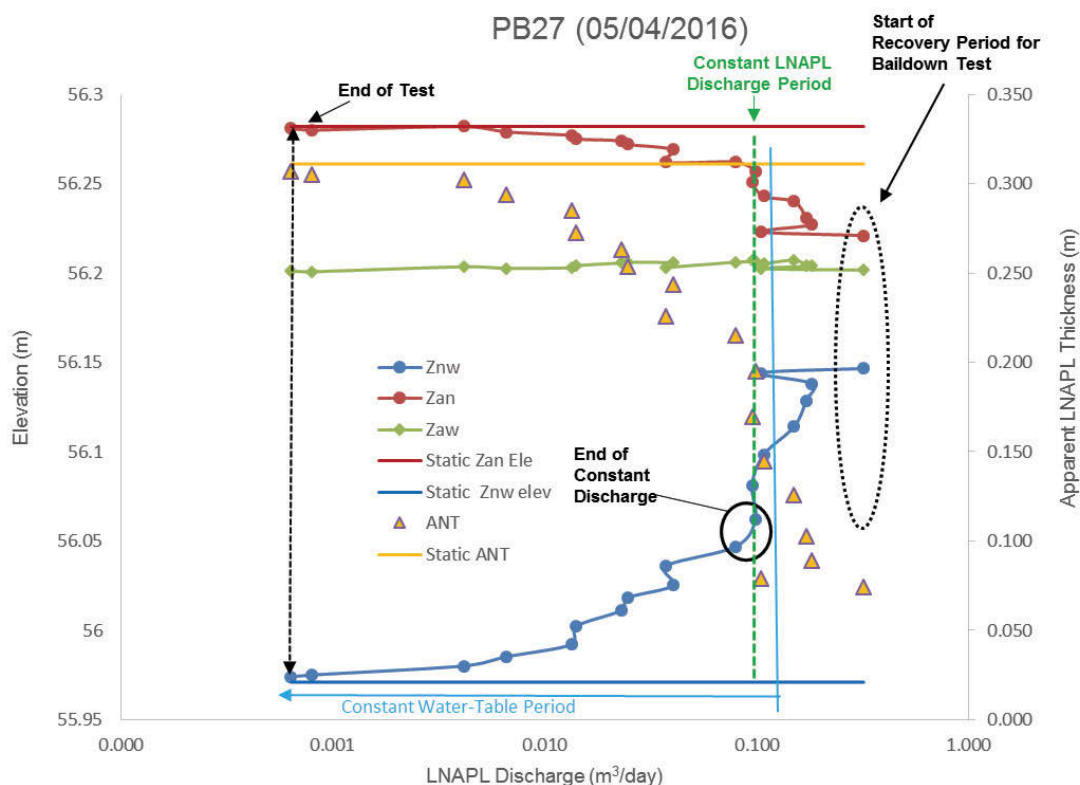


Figure C.5. Baildown test results presenting the gauged referenced air-LNAPL (Z_{an}) and LNAPL-water interfaces (Z_{nw}), the potentiometric surface elevation (Z_{aw}), the apparent thickness (ANT) and the static elevations for Z_{an} , Z_{nw} and ANT vs. LNAPL discharge for well PB27.

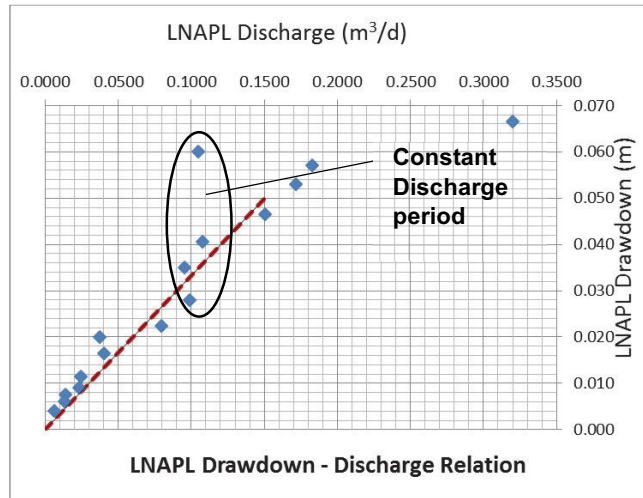


Figure C.6. LNAPL drawdown- discharge relation during baildown testing.

Figure C.6 shows the discharge versus drawdown relationship during the baildown testing recovery. The graphs reveals that borehole recharge from the filter pack is not significant (one high discharge value at the beginning of the recovery, $0.32 \text{ m}^3/\text{d}$). Moreover, the figure depicts behaviour that suggests unconfined LNAPL conditions because there is a continuously decreasing discharge with decreasing drawdown, even though few constant discharge rates are presented (not a clear indication).

Table C.1. Details of LNAPL bail-down tests and calculated T_n values.

Well ID	Date	LNAPL Vol. removed (L)	Water Vol. removed (L)	Cut off time (min)	J ratio	LNAPL Conditions	Z_{an} (m AHD)	Z_{nw} (m AHD)	Z_{aw} (m AHD)	T_n (m ² /d)
PB29	8/7/2015	1.400	0.050	0.8	-0.65	unconfined	56.285	55.927	56.191	1.480 (±0.135)
PB29	9/2/2016	0.780	0.470	3.0	-0.625	unconfined	56.683	56.57	56.653	0.265 (±0.032)
PB29	5/04/2016	2.750	0.000	2.3	-0.2	unconfined	56.287	55.983	56.207	1.969 (±0.47)
PB29	28/04/2016	2.850	0.800	2.23	-0.138	unconfined	56.263	55.941	56.179	2.133 (±0.204)
PB29	19/05/2016	2.750	1.050	1.95	-0.25	unconfined	56.232	55.908	56.147	1.510 (±0.093)
PB29	1/06/2016	3.850	2.250	1.6	-0.324	unconfined	56.348	56.116	56.287	1.323 (±0.076)
PB29	9/06/2016	4.100	0.900	2.34	-0.5	unconfined	56.385	56.172	56.329	0.699 (±0.097)
PB29	15/06/2016	7.700	1.500	6	-0.329	unconfined	56.472	56.295	56.425	0.372 (±0.015)
PB27 a	6/5/2015	0.710	0.000	1.7	-0.237	unconfined	56.341	55.991	56.250	0.910 (±0.111)
PB27 b	6/5/2015	1.600	0.370	2.1	-0.285	unconfined	56.341	55.991	56.250	0.960 (±0.021)
PB27	8/7/2015	1.700	0.050	3	-0.247	unconfined	56.279	55.919	56.185	1.330 (±0.063)
PB27	20/7/2015	1.375	0.050	0	-0.286	unconfined	56.282	55.995	56.207	1.380 (±0.046)
PB27	5/04/2016	2.230	0.370	1.6	-0.256	unconfined	56.282	55.971	56.201	0.414 (±0.023)
PB27	20/05/2016	2.400	0.900	11	-0.256	unconfined	56.228	55.908	56.144	0.572 (±0.011)
PB27	1/06/2016	2.000	1.250	4.2	-0.292	unconfined	56.341	56.105	56.279	0.664 (±0.022)
PB27	14/06/2016	2.100	0.350	1.57	-0.26	unconfined	56.448	56.263	56.399	0.204 (±0.006)
PB05	8/5/2015	1.690	0.230	5.5	-0.769	unconfined	56.357	55.995	56.262	0.046 (±0.002)
PB05	6/4/2016	3.300	0.740	2.3	-0.213	unconfined	56.322	55.904	56.213	0.039 (±0.012)
PB11	7/5/2015	2.710	0.000	11.0	-0.25	unconfined	56.319	55.594	56.130	0.550 (±0.021)

PB11	6/4/2016	5.780	0.700	8.0	-0.25	unconfined	56.405	55.669	56.213	0.136 (±0.002)
PB13	8/5/2015	2.730	0.000	7.0	-3.182	unconfined	56.290	55.499	56.084	0.240 (±0.015)
PB13	6/4/2016	6.780	0.380	20.0	-16.8	unconfined	56.420	55.63	56.214	0.027 (±0.002)
PB39	06/04/2016	8.440	0.620	10.0	-0.20	unconfined	56.491	55.715	56.289	0.034 (±0.003)
PB40	6/04/2016	5.340	1.100	4.2	-0.258	unconfined	56.425	55.685	56.232	0.577 (±0.025)
PB40	14/06/2016	19.500	0.000	0.7	-0.256	unconfined	56.566	56.038	56.428	0.304 (±0.008)
MP42	6/04/2016	1.310	0.070	9.5	-0.350	unconfined	56.363	55.736	56.199	0.130 (±0.022)

Appendix D. Formation Fluid Levels

Table D.1. DTP values of tested wells PB27 and PB09.

Date	DTP- PB09 (m b.t.o.c.)	DTP- PB27 (m b.t.o.c.)
5/11/2014	3.17	3.315
6/11/2014	3.124	3.253
25/11/2014	3.632	3.642
5/02/2015	4.23	4.311
19/03/2015	4.399	4.52
5/05/2015	4.514	4.643
18/05/2015	4.452	4.665
7/07/2015	4.571	4.708
14/07/2015	4.61	4.731
21/07/2015	4.603	4.782

Table D.2. Fluid elevations of tested wells PB27 and PB09.

Date	Z_{an} (PB09) (m AHD)	Z_{nw} (PB09) (m AHD)	b_n (PB09) (m AHD)	Z_{an} (PB27) (m AHD)	Z_{nw} (PB27) (m AHD)	b_n (PB27) (m AHD)
5/10/2016	58.635	58.532	0.103	59.193	56.955	2.238
26/07/2016	58.403	58.261	0.142	58.513	57.899	0.614
16/06/2016	56.478	56.299	0.179	56.479	56.302	0.177
9/06/2016	56.379	56.162	0.217	56.379	56.164	0.215
1/06/2016	56.337	56.103	0.234	56.335	56.098	0.237
20/05/2016	56.234	55.92	0.314	56.233	55.924	0.309
28/04/2016	56.262	55.94	0.322	56.263	55.944	0.319
5/04/2016	56.286	55.97	0.316	56.285	55.971	0.314

9/02/2016	56.682	56.556	0.126	56.665	56.609	0.056
14/07/2015	56.258	55.931	0.327	56.262	55.932	0.33
7/07/2015	56.297	55.929	0.368	56.285	55.924	0.361
5/05/2015	56.354	56.001	0.353	56.35	56.005	0.345
19/03/2015	56.469	56.134	0.335	56.473	56.149	0.324
5/02/2015	56.638	56.498	0.14	56.682	56.381	0.301
25/11/2014	57.236	57.094	0.142	57.351	56.795	0.556
6/11/2014	57.744	57.594	0.15	57.74	57.612	0.128
5/11/2014	57.698	57.548	0.15	57.678	57.623	0.055

Where: yellow colour elevations depict confined NAPL conditions at PB27 well, and are not included in Figure 6.12. Blue colour contains data of unconfined LNAPL conditions since 2015. Orange colour refers to unconfined NAPL conditions during a rising water table in 2016.

Table D.3. Fluid elevations of tested wells PB29 and MP50.

Date	Z_{an} - MP50 (m AHD)	Z_{an} - PB29 (m AHD)
5/10/2016	58.639	58.614
16/08/2016	58.885	58.872
26/07/2016	58.393	58.371
14/06/2016	56.46	56.457
9/06/2016	56.393	56.385
1/06/2016	56.348	56.348
20/05/2016	56.239	56.239

Table D.4. DTP values of tested wells PB40 and PB11.

Date	DTP- PB11 (m b.t.o.c.)	DTP- PB40 (m b.t.o.c.)
16/08/2016	1.699	2.297
26/07/2016	2.522	2.837
14/06/2016	4.687	4.716
9/06/2016	4.745	4.761
1/06/2016	4.784	4.809
20/05/2016	4.88	4.9
16/05/2016	4.882	4.902
28/04/2016	4.85	4.873
6/04/2016	4.832	4.857
5/04/2016	4.824	4.846

Where: yellow colour values depict confined NAPL conditions at both PB40 and PB11 wells, and are not taken into account in Figure 6.14.

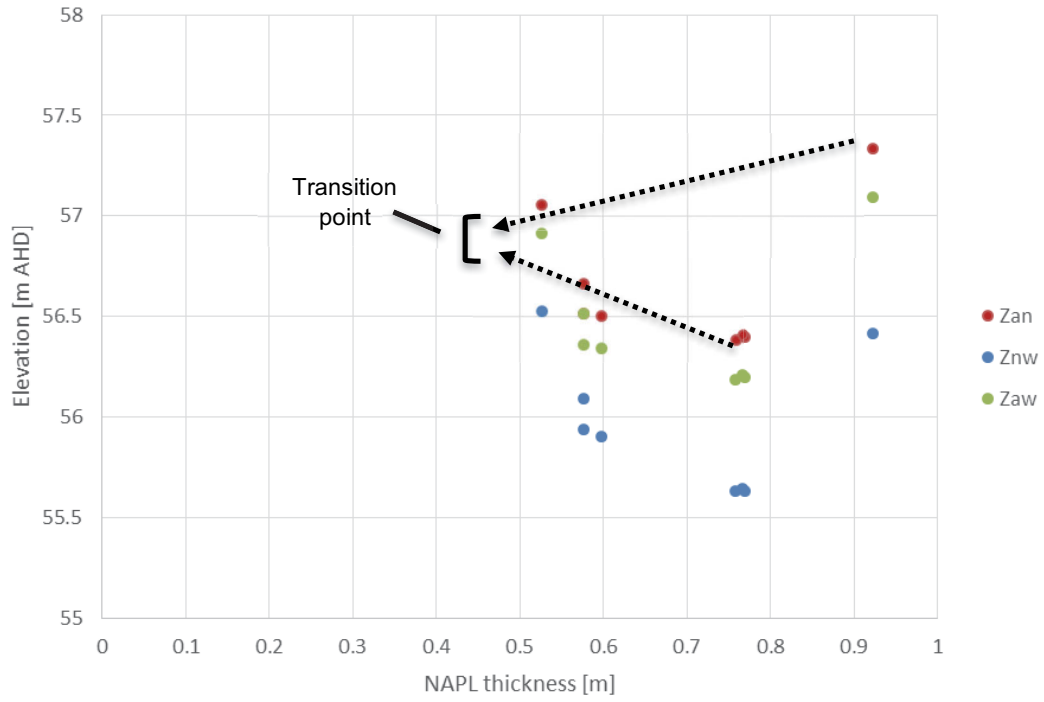


Figure D.1. Transition between confined and unconfined LNAPL conditions at PB11 well, area C.

Appendix E. T_n Estimations During Applied Mass Recovery Techniques

Table E.1. $T_{n,SK}/T_{n,BD}$ values at three well locations for R_{oi} values 0.1-3m (Figure 6.34 presents results for R_{oi} values 0.1-10 m).

	Well: PB40		Well: PB27		Well: PB29	
	Q (L/hr)		Q (L/hr)		Q (L/hr)	
	1.63		1.4049		3.936	
	S (m)		S (m)		S (m)	
	0.122		0.037		0.0385	
	BD T_n (14/6/16)		BD T_n (16/6/16)		bd (15/6/16)	
	0.304		0.2		0.372	
radius step	T_n skim (16/6/16)	SK T_n /BD T_n	T_n skim (17/6/16)	SK T_n /BD T_n	T_n skim (16/6/16)	SK T_n /BD T_n
0.1	0.014688998	0.048319072	0.041745348	0.20872674	0.112398045	0.302145282
0.2	0.050080976	0.164740052	0.142327459	0.711637296	0.383212237	1.030140421
0.3	0.070783956	0.232841959	0.201164223	1.005821113	0.541628383	1.455990278
0.4	0.085472954	0.281161031	0.24290957	1.214547852	0.654026428	1.75813556
0.5	0.096866626	0.318640216	0.275289778	1.37644889	0.741209125	1.992497648
0.6	0.106175933	0.349262939	0.301746334	1.508731669	0.812442575	2.183985417
0.7	0.114046841	0.375154082	0.324115033	1.620575165	0.872669599	2.345886018
0.8	0.120864931	0.397582011	0.343491682	1.717458409	0.92484062	2.486130699
0.9	0.126878913	0.417364846	0.360583097	1.802915486	0.970858722	2.609835274
1	0.132258603	0.435061195	0.375871889	1.879359446	1.012023317	2.720492787
1.1	0.137125125	0.45106949	0.389702284	1.94851142	1.049261222	2.820594684
1.2	0.141567911	0.465683918	0.402328445	2.011642225	1.083256767	2.911980556
1.3	0.145654878	0.479127889	0.413943387	2.069716937	1.114529636	2.996047409
1.4	0.149438819	0.491575062	0.424697144	2.123485722	1.143483791	3.073881157
1.5	0.152961583	0.503163102	0.434708653	2.173543263	1.170439464	3.146342644
1.6	0.156256909	0.514002991	0.444073793	2.220368965	1.195654812	3.214125838
1.7	0.159352392	0.5241855	0.45287099	2.264354951	1.21934099	3.277798361
1.8	0.162270891	0.533785826	0.461165208	2.305826042	1.241672914	3.337830413
1.9	0.165031554	0.542866954	0.469010866	2.345054329	1.262797101	3.394615862
2	0.167650581	0.551482175	0.476454	2.382270002	1.282837508	3.448487926
2.1	0.170141799	0.559676969	0.483533908	2.417669538	1.301899937	3.499731014
2.2	0.172517103	0.56749047	0.490284395	2.451421976	1.320075414	3.548589823
2.3	0.174786802	0.574956586	0.49673476	2.4836738	1.33744282	3.595276397
2.4	0.176959889	0.582104898	0.502910556	2.514552782	1.354070958	3.639975695
2.5	0.179044253	0.588961359	0.508834208	2.54417104	1.370020205	3.682850014
2.6	0.181046856	0.595548869	0.514525499	2.572627493	1.385343828	3.724042548
2.7	0.182973871	0.601887733	0.520001972	2.600009859	1.40008906	3.76368027
2.8	0.184830797	0.607996041	0.525279256	2.626396278	1.414297982	3.801876296
2.9	0.186622553	0.613889978	0.530371333	2.651856665	1.428008241	3.838731831
3	0.188353561	0.619584082	0.535290764	2.676453819	1.441253655	3.874337783

Table E.2. $T_{n,BD}$ values before and during skimming processes at well locations PB29, PB27 and PB40.

Well	T_n (m²/day)	Z_{aw} (m AHD)
PB29	1.51	56.148
PB29	1.32	56.288
PB29	0.699	56.33
PB29	0.372	56.426
PB29	0.308	56.436
PB29	0.052	56.49
PB29	0.037	56.5
PB27	0.61	56.15
PB27	0.2	56.4
PB27	0.121	56.448
PB40	0.58	56.23
PB40	0.304	56.4
PB40	0.174	56.45
PB40	0.011	56.48
PB40	0.009	56.5

Where yellow colour indicates the pre-remediation periods in 2016. These periods include data points during rising water table conditions with respect to unconfined NAPL behaviour (b_n decreases as Z_{aw} increases). The remediation periods contain only skimming data until the start of the water table drawdown.

Table E.3. Calculation of T_n during skimming processes at PB29 well in 2015.

Date	Q_n	s_n	T_n	Z_{aw}
	(L/hr)	(m)	(m²/d)	(m AHD)
08/07//2015	10.23	0.021	8.56	56.187
09/07//2015	10.28	0.179	1.01	56.205
10//07//2015	10.08	0.214	0.83	56.193
01/07//2015	8.80	0.247	0.63	56.186
12/07//2015	7.20	0.246	0.51	56.182
13/07//2015	5.70	0.247	0.41	56.184
14/07//2015	5.30	0.252	0.37	56.181
14/07//2015	9.40	0.060	2.75	56.191
15/07//2015	5.76	0.100	1.01	56.181
16/07//2015	5.73	0.090	1.12	56.183
17/07//2015	5.65	0.090	1.01	56.178
18/07//2015	4.13	0.100	0.73	56.175
19/07//2015	5.65	0.086	1.15	56.184
20/07//2015	8.36	0.076	1.94	56.203

Table E.4. Calculation of T_n trough bail-down testing at PB29 well in 2015.

Date	T_n
	(m²/d)
08/07//2015	1.48
14/07//2015	1.14
21/07//2015	3.20

where: green colour indicates the T_n value before the start of the skimming processes.

Table E.5. Calculation of T_n during skimming processes at PB27 well in 2015.

Date	Q_n (L/hr)	s_n (m)	T_n (m²/d)	Z_{aw} (m AHD)
20/07//2015	7.22	0.038	3.54	56.201
21/07//2015	3.05	0.038	1.41	56.201
21/07//2015	5.50	0.041	2.36	56.205
22//07//2015	3.00	0.042	1.26	56.212
23/07//2015	2.80	0.046	1.07	56.200
24/07//2015	2.85	0.050	1.09	56.224
25/07//2015	2.83	0.043	1.00	56.214
26/07//2015	2.66	0.046	1.09	56.230
27/07//2015	2.45	0.035	0.94	56.239
28/07//2015	2.05	0.034	1.02	56.254
29/07//2015	1.98	0.031	1.02	56.258
30/07//2015	2.00	0.029	1.13	56.258
31/07//2015	0.72	0.029	0.44	56.280
01/08//2015	0.60	0.029	0.36	56.287
02/08//2015	0.93	0.029	0.57	56.301
03/08//2015	0.60	0.029	0.36	56.305

Table E.6. Calculation of T_n trough bail-down testing at PB27 well in 2015.

Date	T_n (m²/d)
20/07//2015	1.38
21/07//2015	0.70

where: green colour indicates the T_n value before the start of the skimming processes.

Table E.7. Calculation of T_n during skimming processes at PB29 well in 2016.

Date	Q_n	s_n	T_n	Z_{aw}
	(L/hr)	(m)	(m²/d)	(m AHD)
15/06/2016	7.000	0.0352	3.49	56.425
16/06/2016	3.930	0.0385	1.79	56.436
16/06/2016	3.550	0.0385	1.62	56.442
17/06/2016	2.130	0.0385	0.97	56.447
18/06/2016	1.670	0.0385	0.76	56.489
19/06/2016	0.710	0.0385	0.44	56.495
20/06/2016	0.700	0.0280	0.51	56.501
21/06/2016	0.700	0.0270	0.45	56.491
21/06/2016	0.514	0.0300	0.31	56.491
22/06/2016	0.544	0.0300	0.31	56.502
23/06/2016	0.541	0.0300	0.27	56.499
1/07/2016	0.375	0.0350	0.27	NA
2/07/2016	0.085	0.0240	0.06	NA
3/07/2016	0.118	0.0240	0.08	NA
4/07/2016	0.100	0.0240	0.07	56.527
5/07/2016	0.118	0.0240	0.08	56.534

where: NA is not measured

Table E.8. Calculation of T_n during water enhanced skimming processes at PB29 well in 2016.

Date	b_n	s_{skim}	s_w	Q_n	Q_w	T_n
	(m)	(m)	(m)	(m³/day)	(m³/day)	(m²/d)
23/06/2016	0.152	0.0395	0.710	0.294	6.624	1.800
24/06/2016	0.152	0.0395	0.258	0.108	6.634	0.640
28/06/2016	0.143	0.0372	0.587	0.307	11.520	1.010

29/06/2016	0.143	0.0372	0.321	0.212	11.520	0.710
29/06/2016	0.143	0.0372	0.243	0.139	6.912	0.760
06/07/2016	0.120	0.0312	0.145	0.023	5.760	0.146
06/07/2016	0.120	0.0312	0.145	0.020	5.760	0.128

The b_n at PB29 well was calculated from the presented equation at Figure E.1. The graph shows the relationship of b_n at wells PB29 and MP50 (dates: 01-14/06/2016). The T_w was estimated from the HPT73 profile (see Figure II.5) as 57.2 m²/day. The equation $T_w = K \times b$ was used, where K is the hydraulic conductivity of the aquifer and b the thickness of the aquifer. K was estimated as 17.88 m/day.

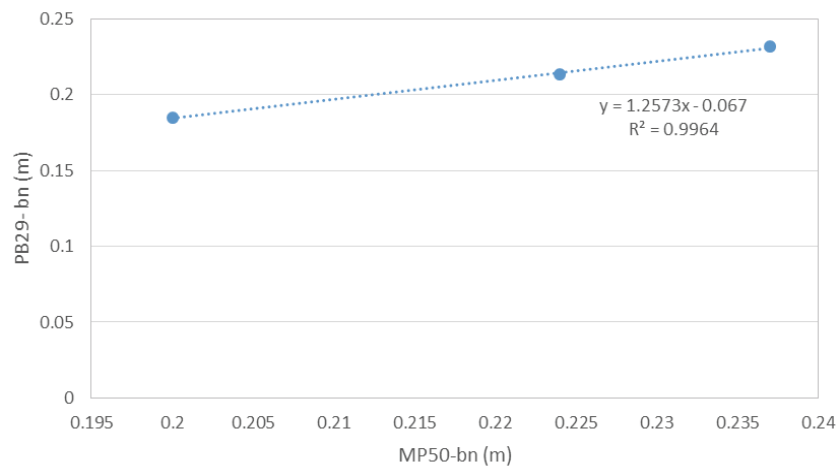


Figure E.1. Correlation of b_n at wells PB29 and MP50.

Table E.9. Calculation of T_n during vacuum enhanced skimming processes at PB29 well in 2016.

Date	Vacuum (kPa)	Q_n (m ³ /day)	Q_a (m ³ /day)	T_n (m ² /d)
05/07/2016	-1	0.0031	216	0.0034
05/07/2016	-2	0.0032	381	0.0020
05/07/2016	-3	0.0031	480	0.0015
05/07/2016	-4	0.0029	552	0.0012

Q_a was calculated as $Q_a = \text{Area of inlet pipe (m}^2) \times \text{Air velocity (m/s)}$. The inner diameter of the PVC pipe was 40mm. The value of 2.5m was used as b_a and the K_w (above the Z_{an} in the vadose zone) was estimated as 2.54 m/d using the HPT73 profile.

Table E.10. Calculation of T_n during vacuum and water enhanced skimming processes at PB29 well in 2016.

Date	Vacuum (kPa)	Q_n (m ³ /day)	Q_a (m ³ /day)	Q_w (m ³ /day)	T_n (m ² /d)
05/07/2016	-1.5	0.05088	401	5.76	0.028
05/07/2016	-2.5	0.04700	552	5.76	0.019

Table E.11. Calculation of T_n via bail-down testing at PB29 well in 2016.

Date	T_n (m ² /d)
15/06/2016	0.372
16/06/2016	0.308
21/06/2016	0.052
23/06/2016	0.037
23/06/2016	0.674
24/06/2016	0.013
27/06/2016	0.047
28/06/2016	1.199
29/06/2016	0.007
06/07/2016	0.054
07/07/2016	0.018

where: green colour indicates the T_n value before the start of the skimming processes.

Table E.12. Calculation of T_n during skimming processes at PB27 well in 2016.

Date	Q_n	s_n	T_n	Z_{aw}
	(L/hr)	(m)	(m²/d)	(m AHD)
16/06/2016	1.61	0.037	0.764	56.440
17/06/2016	1.40	0.037	0.667	56.450
18/06/2016	0.79	0.022	0.374	56.479
19/06/2016	0.65	0.023	0.307	56.501
20/06/2016	0.53	0.037	0.252	56.493
21/06/2016	0.49	0.036	0.239	56.4928
22/06/2016	0.46	0.034	0.236	56.5063
23/06/2016	0.38	0.034	0.195	56.500
23/06/2016	0.20	0.075	0.046	56.467
24/06/2016	0.07	0.081	0.014	56.457
24/06/2016	0.33	0.081	0.071	56.457
24/06/2016	0.43	0.033	0.228	56.457
25/06/2016	0.38	0.033	0.201	56.4961
26/06/2016	0.32	0.033	0.171	56.5091
27/06/2016	0.23	0.032	0.125	56.524
28/06/2016	0.21	0.033	0.111	56.533
28/06/2016	0.12	0.100	0.021	56.507
29/06/2016	0.03	0.120	0.004	56.455
5/07/2016	0.40	0.035	0.199	NA
5/07/2016	0.06	0.035	0.030	NA
5/07/2016	0.09	0.035	0.040	NA
6/07/2016	0.08	0.060	0.024	NA
6/07/2016	0.03	0.065	0.008	NA
6/07/2016	0.03	0.065	0.007	NA

7/07/2016	0.15	0.035	0.076	NA
7/07/2016	0.11	0.035	0.054	NA

Different time periods during the day are depicted in the Table 12, presenting the effects of remediation processes at PB29 well.

Table E.13. Calculation of T_n via bail-down testing at PB27 well in 2016.

Date	T_n
	(m²/d)
16/06/2016	0.2
17/06/2016	0.121
04/07/2016	0.135
08/07/2016	0.01

where: green colour indicates the T_n value before the start of the skimming processes.

Table E.14. Calculation of T_n during skimming processes at PB40 well in 2016.

Date	Q_n	s_n	T_n	Z_{aw}
	(L/hr)	(m)	(m²/d)	(m AHD)
15/06/2016	6.000	0.052	2.030	56.424
16/06/2016	1.630	0.122	0.235	56.428
18/06/2016	1.560	0.117	0.234	56.464
19/06/2016	1.470	0.117	0.221	56.484
20/06/2016	0.425	0.109	0.068	56.493
20/06/2016	0.414	0.11	0.066	56.493
21/06/2016	0.070	0.11	0.011	56.486

22/06/2016	0.042	0.107	0.007	56.501
3/07/2016	0.198	0.092	0.038	56.503
4/07/2016	0.070	0.092	0.013	56.519
5/07/2016	0.050	0.082	0.011	56.534
6/07/2016	0.000		0.000	56.519

Table E.15. Calculation of T_n during water enhanced skimming processes at PB40 well in 2016.

Date	b_n (m)	s_{skim} (m)	s_w (m)	Q_n (m ³ /day)	Q_w (m ³ /day)	T_n (m ² /d)
23/06/2016	0.452	0.1175	0.180	0.0820	3.744	0.1840
24/06/2016	0.452	0.1175	0.199	0.0042	3.744	0.0097
29/06/2016	0.404	0.1050	1.038	0.0700	8.640	0.0940
30/06/2016	0.404	0.1050	1.296	0.0100	9.120	0.0130

The b_n at PB40 well was calculated from the presented equation at Figure E.2. The graph shows the relationship of b_n at wells PB40 and PB11 (dates: 05/04/2016 -14/06/2016). The K and as a result T_w was estimated from the HPT59 profile (see Figure B.7) as 16.84 m²/day.

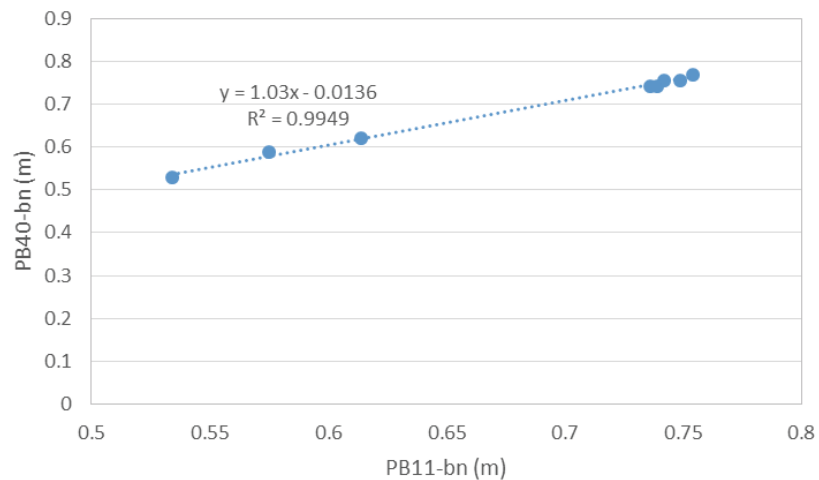


Figure E.2. Correlation of b_n at wells PB40 and PB11.

Table E.16. Calculation of T_n during vacuum enhanced skimming processes at PB40 well in 2016.

Date	Vacuum (kPa)	Q_n (m ³ /day)	Q_a (m ³ /day)	Q_w (L/min)	T_n (m ² /d)
07/07/2016	-1	0.0		4.0	0.0
07/07/2016	-3	0.0		4.0	0.0
07/07/2016	-4	0.0		4.0	0.0
07/07/2016	-2	0.0		4.0	0.0

The value of 1.73m was used as b_a and the K_w (above the Z_{an} in the vadose zone) was estimated as 1.00 m/d using the HPT59 profile.

Table E.17. Calculation of T_n via bail-down testing at PB40 well in 2016.

Date	T_n (m ² /d)
14/06/2016	0.304
17/06/2016	0.174
21/06/2016	0.011
22/06/2016	0.008
23/06/2016	0.320
28/06/2016	0.007
29/06/2016	0.055
1/07/2016	0.001
6/07/2016	0.000

where: green colour indicates the T_n value before the start of the skimming processes.

Appendix F. Physicochemical Properties

Table F.1. Mass percentage (%w/w) of six chemical compound groups in NAPL phase, at PB29 well in 2016.

Well	Date	Sample #	nC4-nC5	nC6-nC9	Tol	m/p-Xyl	BENZ/EB/o-XYL	1,3,5-TMBenz*/124-TMB/1,2,3-TMbenz*
PB29	15/06/2016	1	5.89	4.72	10.72	5.22	4.24	3.45
PB29	23/06/2016	2	5.91	4.49	10.65	5.22	4.17	3.43
PB29	24/06/2016	3	5.85	4.57	10.68	5.23	4.26	3.49
PB29	27/06/2016	4	6.22	4.67	10.90	5.25	4.27	3.41
PB29	29/06/2016	5	6.81	4.26	10.19	4.85	4.24	3.11
PB29	4/07/2016	6	5.65	4.60	10.46	5.09	4.16	3.35
PB29	5/07/2016	7	4.96	4.69	11.09	5.57	4.45	3.83
PB29	6/07/2016	8	5.82	4.59	10.42	5.17	4.22	3.49
PB29	6/07/2016	9	5.57	4.65	10.85	5.29	4.32	3.49
PB29	8/07/2016	10	5.23	4.75	11.00	5.39	4.34	3.56

Table F.2. Mass percentage (%w/w) of six chemical compound groups in NAPL phase, at PB27 well in 2016.

Well	Date	Sample #	nC4-Nc5	nC6-nC9	Tol	m/p-Xyl	BENZ/EB/o-XYL	1,3,5 TMBenz*/124-TMB/1,2,3 TMBenz*
PB27	16/06/16	1	5.81	4.65	10.23	5.28	4.14	3.47
PB27	23/06/16	2	6.22	4.36	9.88	4.94	3.96	3.21
PB27	24/06/2016	3	6.03	4.61	10.31	5.23	4.12	3.53
PB27	29/06/2016	4	4.77	4.84	11.11	5.72	4.45	3.83
PB27	05/07/16	5	5.13	4.67	10.72	5.45	4.27	3.62
PB27	7/07/2016	6	4.79	4.93	11.17	5.75	4.45	3.80
PB27	8/07/2016	7	5.09	4.72	11.31	5.65	4.63	3.65

Table F.3. Mass percentage (%w/w) of six chemical compound groups in NAPL phase, at PB40 well in 2016.

Well	Date	Sample #	nC4-nC5	nC6-nC9	Tol	m/p-Xyl	BENZ/EB/o-XYL	1,3,5 TMBenz*/124-TMB/1,2,3 TMBenz*
PB40	15/06/2016	1	6.42	4.29	10.87	5.46	4.40	3.32
PB40	22/06/2016	2	6.21	4.43	11.01	5.60	4.48	3.49
PB40	23/06/2016	3	6.15	4.41	11.02	5.59	4.47	3.43
PB40	24/06/2016	4	6.06	4.55	11.06	5.57	4.48	3.43
PB40	27/06/2016	5	6.15	4.52	11.16	5.67	4.56	3.53
PB40	29/06/2016	6	6.08	4.46	11.20	5.69	4.54	3.41
PB40	01/07/2016	7	5.27	4.50	11.49	5.85	4.65	3.58
PB40	06/07/2016	8	6.10	4.46	11.10	5.59	4.50	3.41

PB40	06/07/2016	9	5.90	4.42	11.17	5.71	4.56	3.41
PB40	08/07/2016	10	5.03	4.67	11.49	5.96	4.74	3.69

Table F.4. Density and viscosity measurements of NAPL samples, at PB29 well, in 2016 trial.

NAPL Sample #	Density (g/cm ³)	Viscosity (cP)	Ratio of Dens/Visc
1	0.72395	0.48	1.50823
2	0.72332	0.42	1.72219
3	0.72448	0.46	1.57496
4	0.73675	0.41	1.79695
5	0.72566	0.43	1.68758
6	0.72778	0.43	1.69251
7	0.73444	0.43	1.70800
8	0.72315	0.41	1.76378
9	0.72056	0.43	1.67572
10	0.73080	0.45	1.62400

Table F.5. Density and viscosity measurements of NAPL samples, at PB27 well, in 2016 trial.

NAPL Sample #	Density (g/cm ³)	Viscosity (cP)	Ratio of Dens/Visc
1	0.73290	0.42	1.74500
2	0.72115	0.45	1.60250
3	0.72090	0.41	1.75829
4	0.73988	0.45	1.64417
5	0.72869	0.48	1.51810
6	0.73765	0.42	1.75630
7	0.73812	0.46	1.60460

Table F.6. Density and viscosity measurements of NAPL samples, at PB40 well, in 2016 trial.

NAPL Sample #	Density (g/cm³)	Viscosity (cP)	Ratio of Dens/Visc
1	0.73241	0.41	1.786365
2	0.72762	0.4	1.81905
3	0.72259	0.4	1.80647
4	0.71717	0.4	1.79292
5	0.7126	0.41	1.73804
6	0.69253	0.42	1.64888
7	0.71155	0.45	1.58122
8	0.7304	0.44	1.66000
9	0.72001	0.41	1.75612
10	0.73589	0.43	1.71137

Table F.7. LNAPL removal rate (Q_n), VOC extraction rate (Q_{n,gas phase}) and BD-T_n values during the sequential application of different techniques at PB29 well, in 2016.

Applied Technology	Date	Q_n	Q_{n,gas}	T_n (Bail-down)
		(mL/sec)	(mL/sec)	(m²/day)
Sk	23/06/2016	0.150	-	0.037
Sk+DD1	24/06/2016	1.244	-	0.013
Sk+DD2	29/06/2016	2.442	-	-
Sk+DD1	29/06/2016	1.608	-	0.07
Sk	5/07/2016	0.032	-	-
VER -1 kPa	5/07/2016	0.035	112.333	-
VER -2 kPa	5/07/2016	0.037	199.118	-
VER -3 kPa	5/07/2016	0.035	288.316	-

VER -4 kPa	5/07/2016	0.033	297.590	-
Sk+DD1	6/07/2016	0.266	-	-
VER -1.5 kPa + DD1	6/07/2016	0.588	300.002	-
VER -2.5 kPa + DD1	6/07/2016	0.543	341.231	-
Sk+DD1	6/07/2016	1.481	-	0.018

Table F.8. LNAPL removal rate (Qn), VOC extraction rate (Qn,gas phase) and BD-T_n values during the sequential application of different techniques at PB40 well, in 2016.

Applied Technology	Date	Qn (mL/sec)	Qn,gas (mL/sec)
Sk	22/06/2016	0.012	-
Sk+DD1	24/06/2016	0.049	-
Sk+DD2	30/06/2016	0.112	-
Sk	6/07/2016	0	-
VER -1 kPa + DD3	7/07/2016	0	35.873
VER -2 kPa + DD3	7/07/2016	0	56.517
VER -3 kPa + DD3	7/07/2016	0	52.992
VER -4 kPa + DD3	7/07/2016	0	NA
VER -5 kPa + DD3	7/07/2016	0	NA

Chemical composition changes

Figure F.1 illustrates the mass percentage changes of chemical compounds in NAPL phase (extracted liquid phase) in response to different mass recovery applications the year 2016, at PB29 well location. Ten NAPL samples were analysed (see Table A.6 in Appendix A and Tables F.1-3 in Appendix F). Six of the main group compounds in gasoline mixtures are presented (Lekmine et al. 2014): i) nC4-nC5, ii) nC6-nC9, iii) Toluene, iv) m/p-Xylene, v) Benzene/E.Benzene/o-Xylene and vi) 1,3,5 TMB/1,2,4 TMB/1,2,3 TMB.

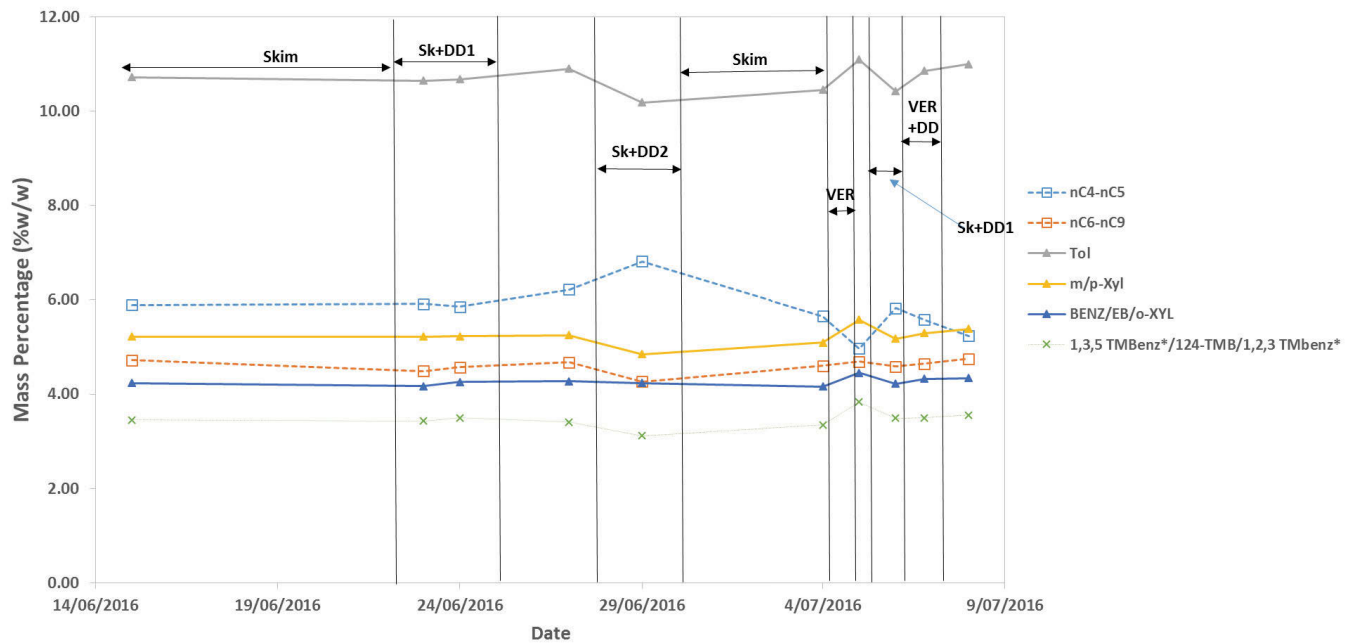


Figure F.1. Time series of chemical compounds mass percentage at PB29 well. Where: (i) Skim = skimming applications, (ii) Sk+DD = water-enhanced skimming, (iii) VER = vacuum-enhanced skimming and (iv) VER+DD = the water- and vacuum-enhanced skimming.

As it can be inferred from this graph, Toluene and nC4-nC5 presented the highest mass percentages. The mass percentage of nC4-nC5 was increased by 9% during the skimming plus water table draw-down (DD₂) and was decreased by 7% after the vacuum-enhanced skimming application. The mass percentage of BTEX and TMBs showed an opposite trend than the trend of nC4-nC5. Furthermore, no changes in the mass percentage of nC6-nC9 were found.

Graph F.2 (see also Table F.2, Appendix F) depicts the mass percentage changes of chemical compounds in NAPL phase during skimming applications the year 2016, at PB27 well location. As it can be seen in this figure, chemical changes took place after the water table drawdown applications at well location PB29. The mass percentage of toluene was increased

by 12% and nC4-nC5 was decreased by 23% during the water enhanced skimming experiments at PB29.

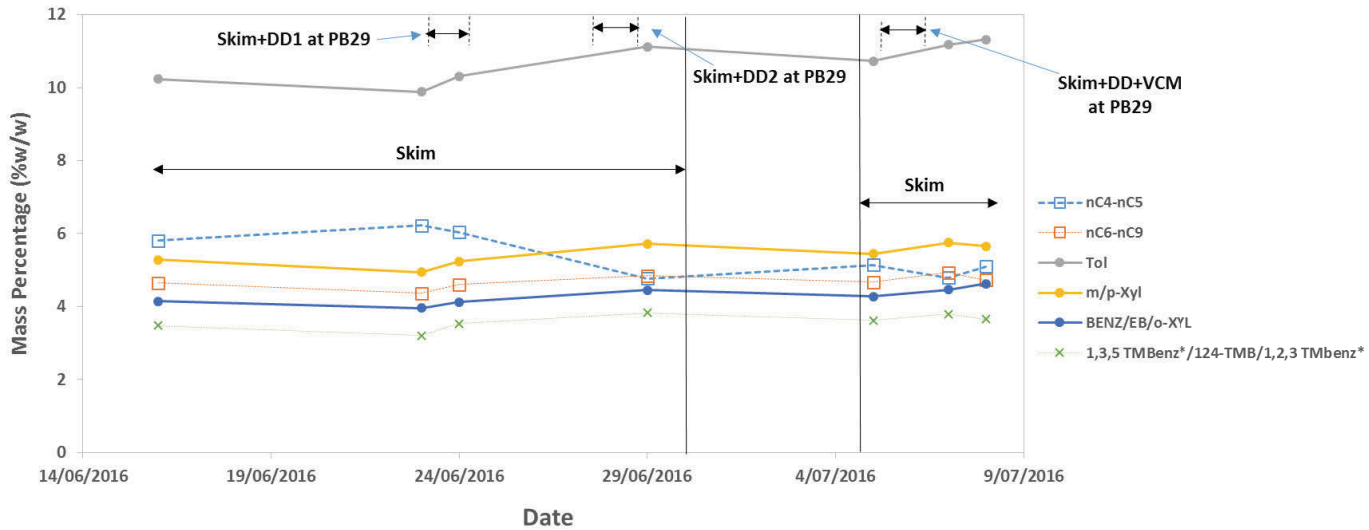


Figure F.2 Time series of chemical compounds mass percentage at PB27 well.

Figure F.3 (see also Table F.3, Appendix F) illustrates the mass percentage changes of chemical compounds in NAPL phase during different mass recovery pilot-scale applications the year 2016, at PB40 well location. As it can be seen, nC4-nC5 presented the highest changes in mass percentage after the second water table drawdown application and the vacuum and water enhance recovery.

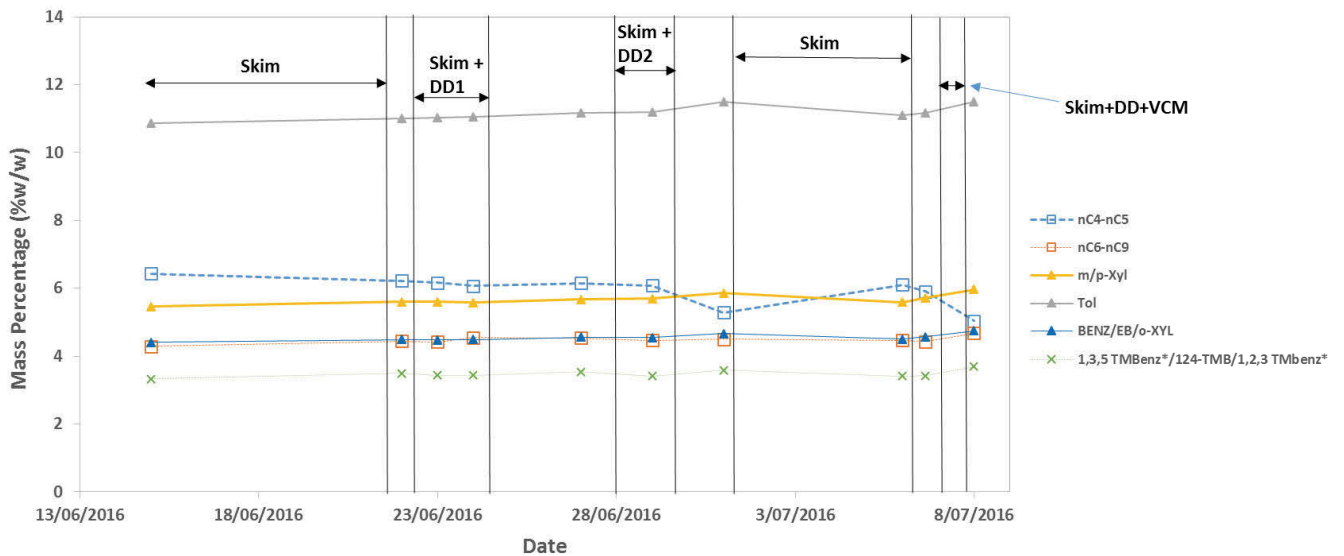


Figure F.3 Time series of chemical compounds mass percentage at PB40 well.

Appendix G. LDRM Simulation

Elevation [m]	Sn	Snr	Sw	krn
56.383	0.000	0.000	0.340	0.0000
56.375	0.010	0.000	0.345	0.0000
56.368	0.022	0.000	0.349	0.0000
56.361	0.036	0.000	0.354	0.0001
56.353	0.053	0.000	0.359	0.0003
56.346	0.074	0.000	0.364	0.0007
56.338	0.099	0.000	0.369	0.0016
56.331	0.128	0.000	0.375	0.0033
56.323	0.162	0.000	0.381	0.0068
56.316	0.202	0.000	0.387	0.0132
56.309	0.248	0.000	0.393	0.0248
56.301	0.299	0.000	0.400	0.0451
56.294	0.353	0.000	0.407	0.0784
56.286	0.406	0.000	0.414	0.1290
56.279	0.455	0.000	0.422	0.1989
56.271	0.495	0.000	0.430	0.2841
56.264	0.522	0.000	0.439	0.3738
56.257	0.536	0.000	0.448	0.4527
56.249	0.538	0.000	0.457	0.5077
56.242	0.533	0.000	0.467	0.5319
56.234	0.523	0.000	0.477	0.5271
56.218	0.498	0.000	0.502	0.4901
56.202	0.471	0.000	0.529	0.4496
56.186	0.442	0.000	0.558	0.4056
56.169	0.409	0.000	0.591	0.3585
56.153	0.374	0.000	0.626	0.3091
56.137	0.336	0.000	0.664	0.2585
56.121	0.296	0.000	0.704	0.2082
56.105	0.254	0.000	0.746	0.1602
56.088	0.212	0.000	0.788	0.1167
56.072	0.171	0.000	0.829	0.0795
56.056	0.132	0.000	0.868	0.0500
56.040	0.097	0.000	0.903	0.0285
56.024	0.067	0.000	0.933	0.0144
56.007	0.043	0.000	0.957	0.0063
55.991	0.025	0.000	0.975	0.0023
55.975	0.012	0.000	0.988	0.0006
55.959	0.005	0.000	0.995	0.0001
55.943	0.001	0.000	0.999	0.0000
55.926	0.000	0.000	1.000	0.0000
55.910	0.000	0.000	1.000	0.0000
55.910	0.000	0.000	1.000	0.0000
55.910	0.000	0.000	1.000	0.0000
55.910	0.000	0.000	1.000	0.0000
55.910	0.000	0.000	1.000	0.0000
55.910	0.000	0.000	1.000	0.0000
55.910	0.000	0.000	1.000	0.0000
55.910	0.000	0.000	1.000	0.0000

Figure G.1. LDRM results of scenario A at research area A.

Elevation [m]	Sn	Snr	Sw	krn
56.278	0.008	0.000	0.976	0.0001
56.277	0.008	0.000	0.977	0.0001
56.276	0.009	0.000	0.977	0.0001
56.275	0.009	0.000	0.977	0.0001
56.274	0.009	0.000	0.978	0.0001
56.272	0.010	0.000	0.978	0.0001
56.271	0.010	0.000	0.978	0.0001
56.270	0.010	0.000	0.978	0.0002
56.267	0.036	0.010	0.924	0.0013
56.263	0.038	0.010	0.926	0.0017
56.260	0.040	0.010	0.927	0.0022
56.256	0.043	0.010	0.929	0.0028
56.253	0.045	0.010	0.931	0.0034
56.250	0.046	0.010	0.932	0.0041
56.246	0.048	0.010	0.934	0.0049
56.243	0.049	0.010	0.935	0.0057
56.239	0.050	0.010	0.937	0.0066
56.236	0.051	0.010	0.938	0.0075
56.233	0.052	0.010	0.940	0.0085
56.229	0.052	0.010	0.941	0.0095
56.226	0.053	0.010	0.942	0.0106
56.222	0.053	0.010	0.944	0.0116
56.219	0.052	0.010	0.945	0.0126
56.216	0.052	0.010	0.947	0.0136
56.212	0.051	0.010	0.948	0.0146
56.209	0.050	0.010	0.949	0.0154
56.205	0.049	0.010	0.951	0.0161
56.202	0.048	0.010	0.952	0.0165
56.195	0.046	0.010	0.954	0.0150
56.189	0.043	0.010	0.957	0.0136
56.182	0.041	0.010	0.959	0.0122
56.176	0.039	0.010	0.961	0.0110
56.169	0.036	0.010	0.964	0.0098
56.162	0.034	0.010	0.966	0.0087
56.156	0.032	0.010	0.968	0.0077
56.149	0.030	0.010	0.970	0.0068
56.143	0.029	0.010	0.971	0.0060
56.136	0.027	0.010	0.973	0.0052
56.129	0.025	0.010	0.975	0.0045
56.123	0.023	0.010	0.977	0.0039
56.116	0.022	0.010	0.978	0.0033
56.110	0.021	0.010	0.979	0.0028
56.103	0.019	0.010	0.981	0.0023
56.096	0.018	0.010	0.982	0.0019
56.090	0.017	0.010	0.983	0.0016
56.083	0.016	0.010	0.984	0.0013
56.077	0.015	0.010	0.985	0.0010
56.070	0.014	0.010	0.986	0.0008
56.067	0.010	0.010	0.990	0.0000
56.063	0.010	0.010	0.990	0.0000
56.060	0.010	0.010	0.990	0.0000
56.056	0.010	0.010	0.990	0.0000

Figure. G.2. LDRM results of scenario B at research area A.

Elevation [m]	Sn	<u>Snr</u>	Sw	<u>k_{rn}</u>
56.383	0.000	0.000	0.959	0.0000
56.375	0.004	0.000	0.961	0.0000
56.368	0.008	0.000	0.963	0.0000
56.361	0.011	0.000	0.965	0.0001
56.353	0.014	0.000	0.967	0.0002
56.346	0.016	0.000	0.969	0.0003
56.338	0.017	0.000	0.971	0.0004
56.331	0.018	0.000	0.972	0.0005
56.323	0.019	0.000	0.974	0.0006
56.316	0.019	0.000	0.976	0.0006
56.309	0.019	0.000	0.977	0.0007
56.301	0.019	0.000	0.979	0.0007
56.294	0.018	0.000	0.980	0.0007
56.286	0.018	0.000	0.981	0.0007
56.279	0.017	0.000	0.983	0.0007
56.271	0.016	0.000	0.984	0.0007
56.264	0.015	0.000	0.985	0.0006
56.257	0.014	0.000	0.986	0.0005
56.249	0.013	0.000	0.987	0.0005
56.242	0.012	0.000	0.988	0.0004
56.234	0.011	0.000	0.989	0.0004
56.233	0.011	0.000	0.989	0.0003
56.231	0.011	0.000	0.989	0.0003
56.229	0.011	0.000	0.989	0.0003
56.227	0.010	0.000	0.990	0.0003
56.226	0.010	0.000	0.990	0.0003
56.224	0.010	0.000	0.990	0.0003
56.222	0.010	0.000	0.990	0.0003
56.221	0.010	0.000	0.990	0.0003
56.219	0.009	0.000	0.991	0.0003
56.217	0.009	0.000	0.991	0.0002
56.215	0.009	0.000	0.991	0.0002
56.214	0.009	0.000	0.991	0.0002
56.212	0.009	0.000	0.991	0.0002
56.210	0.009	0.000	0.991	0.0002
56.209	0.008	0.000	0.992	0.0002
56.207	0.008	0.000	0.992	0.0002
56.205	0.008	0.000	0.992	0.0002
56.203	0.008	0.000	0.992	0.0002
56.202	0.008	0.000	0.992	0.0002
56.200	0.008	0.000	0.992	0.0002
56.186	0.092	0.010	0.908	0.1808
56.171	0.088	0.010	0.912	0.1720
56.157	0.084	0.010	0.916	0.1629
56.142	0.079	0.010	0.921	0.1537
56.128	0.074	0.010	0.926	0.1442
56.113	0.070	0.010	0.930	0.1346
56.099	0.065	0.010	0.935	0.1248
56.084	0.060	0.010	0.940	0.1148
56.070	0.055	0.010	0.945	0.1048
56.055	0.050	0.010	0.950	0.0946
56.041	0.046	0.010	0.954	0.0844
56.026	0.041	0.010	0.959	0.0741
56.012	0.036	0.010	0.964	0.0639
55.997	0.031	0.010	0.969	0.0539
55.983	0.027	0.010	0.973	0.0441
55.968	0.023	0.010	0.977	0.0346
55.954	0.019	0.010	0.981	0.0255
55.939	0.015	0.010	0.985	0.0170
55.925	0.012	0.010	0.988	0.0090
55.910	0.010	0.010	0.990	0.0000

Figure. G.3. LDRM results of research area B.

Elevation [m]	Sn	Snr	Sw	krrn
56.474	0.123	0.030	0.766	0.0034
56.456	0.135	0.030	0.769	0.0054
56.439	0.149	0.030	0.771	0.0088
56.421	0.163	0.030	0.774	0.0147
56.403	0.178	0.030	0.776	0.0251
56.385	0.193	0.030	0.779	0.0452
56.368	0.207	0.030	0.782	0.0896
56.350	0.215	0.030	0.785	0.3864
56.335	0.213	0.030	0.787	0.3826
56.320	0.210	0.030	0.790	0.3787
56.306	0.208	0.030	0.792	0.3747
56.291	0.205	0.030	0.795	0.3706
56.276	0.203	0.030	0.797	0.3664
56.261	0.200	0.030	0.800	0.3620
56.247	0.197	0.030	0.803	0.3576
56.232	0.195	0.030	0.805	0.3531
56.217	0.192	0.030	0.808	0.3485
56.202	0.189	0.030	0.811	0.3437
56.188	0.186	0.030	0.814	0.3388
56.173	0.183	0.030	0.817	0.3338
56.158	0.180	0.030	0.820	0.3287
56.144	0.177	0.030	0.823	0.3234
56.129	0.174	0.030	0.826	0.3180
56.114	0.171	0.030	0.829	0.3124
56.099	0.168	0.030	0.832	0.3067
56.084	0.164	0.030	0.836	0.3008
56.070	0.161	0.030	0.839	0.2947
56.055	0.158	0.030	0.842	0.2885
56.051	0.073	0.040	0.927	0.0047
56.047	0.072	0.040	0.928	0.0044
56.042	0.071	0.040	0.929	0.0042
56.038	0.070	0.040	0.930	0.0040
56.034	0.069	0.040	0.931	0.0038
56.029	0.068	0.040	0.932	0.0036
56.025	0.067	0.040	0.933	0.0034
56.021	0.066	0.040	0.934	0.0032
56.017	0.065	0.040	0.935	0.0030
56.013	0.064	0.040	0.936	0.0029
56.008	0.064	0.040	0.936	0.0027
56.004	0.063	0.040	0.937	0.0025
56.000	0.062	0.040	0.938	0.0024
55.996	0.061	0.040	0.939	0.0023
55.991	0.060	0.040	0.940	0.0021
55.987	0.060	0.040	0.940	0.0020
55.983	0.059	0.040	0.941	0.0019
55.979	0.058	0.040	0.942	0.0018
55.974	0.058	0.040	0.942	0.0017
55.970	0.057	0.040	0.943	0.0016
55.951	0.106	0.000	0.894	0.2155
55.933	0.101	0.000	0.899	0.2055
55.915	0.096	0.000	0.904	0.1952
55.896	0.090	0.000	0.910	0.1845
55.878	0.084	0.000	0.916	0.1734
55.859	0.079	0.000	0.921	0.1621
55.840	0.073	0.000	0.927	0.1503
55.822	0.067	0.000	0.933	0.1383
55.804	0.061	0.000	0.939	0.1260
55.785	0.055	0.000	0.945	0.1134
55.766	0.048	0.000	0.952	0.1005
55.748	0.042	0.000	0.958	0.0875
55.729	0.036	0.000	0.964	0.0745
55.711	0.030	0.000	0.970	0.0615
55.693	0.024	0.000	0.976	0.0486
55.674	0.018	0.000	0.982	0.0362
55.655	0.012	0.000	0.988	0.0245
55.637	0.007	0.000	0.993	0.0140
55.618	0.003	0.000	0.997	0.0052
55.600	0.000	0.000	1.000	0.0000

Figure. G.4. LDRM results of research area C.

Appendix H. Performance Assessment of Selected Mass Recovery Technologies

In this section, a performance assessment of pilot-scale applied mass recovery techniques for the removal of LNAPLs in heterogeneous environments, is presented. The assessment took place via measured NAPL recovery rates in liquid and gas phase. The research took place at areas A and C, at well locations PB29 and PB40 respectively. The tested technologies included sequential trials between skimming (Sk), water-enhanced (water table drawdown) skimming (Sk+DD), vacuum-enhanced skimming (VER) and water- and vacuum- enhanced recovery applications (VER+DD). The research took place in 2016, in parallel at area A and C under a rising water table. Figures H.1 and H.2 (see also Tables D.9 and D.10 in Appendix D) illustrate the comparison of the pumped LNAPL recovery rates (Q_n) and the VOC extraction rates ($Q_{n,g}$) during pilot-testing. Skimming (Sk) and bail-down testing were repeated as controls through the pilot-testing due to the extended duration of the research and the varying water table elevation.

Figure H.1 presents the summary of the recovery rate and source of NAPL removal. As it can be seen in the graph, the water table drawdown skimming gave 8-16 times higher LNAPL recovery rates than skimming alone. Furthermore, the second applied water table drawdown (DD₂) enhanced further the NAPL recovery (by 96%). VER did not favour the liquid recovery, however the VOC extraction rates were increased for higher applied pressure values as the hydraulic gradients are larger (Halmemies 2003). An increase in applied vacuum pressure increases the air flow which enhances the volatilization of NAPL. Similar applied pressure values by Johnston et al (Johnston et al. 2002), resulted in 2.5-10 times higher recovery rates than the rate for skimming, however their research took place in a sandy aquifer, under low water table elevation with maximum NAPL saturation values of 60%, that is a 10 times higher value compared to the maximum NAPL saturation value at this research area (see Figure 6.13). VER+DD produced as much as 16-18 times the rate of skimming. Interestingly, during the application of vacuum > 99.5% of the total NAPL recovery was in gas phase. Finally, the application of vacuum during the water table drawdown affected positively the liquid recovery rate of the last applied technology (Sk+DD) by 450%.

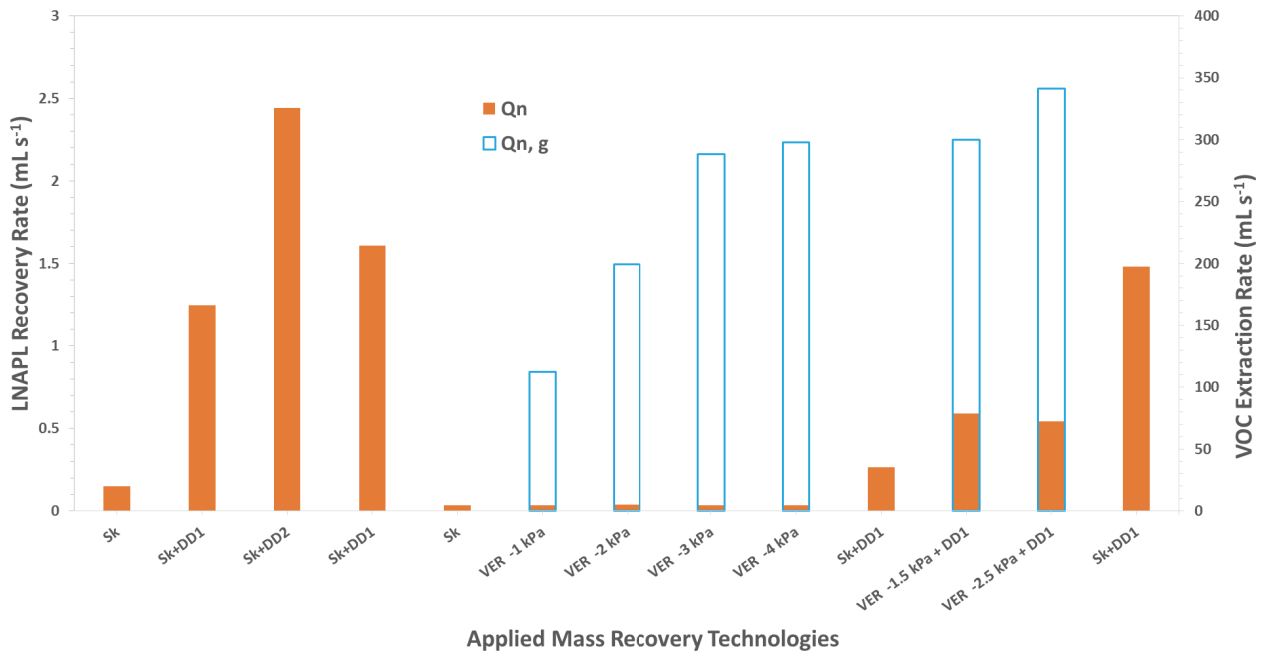


Figure H.1 Comparison of the pumped LNAPL recovery rates during pilot testing and contribution of VOC extraction to removal at PB29 well in 2016.

Figure H.2 depicts the relative efficiency of the pilot-scale applications at PB40 well in area C. Water enhanced skimming applications presented 4.5-10.5 times higher NAPL recovery values than skimming alone. Sk+DD₂ enhanced the NAPL recovery of Sk+DD₁ by 140%. The application of VER+DD did not favor the liquid recovery taking into account that the recovery through skimming (control) was zero. The recovery was 100% in gas phase. Other researches (Halmemies et al. 2003; Li et al. 2002) have documented also cases where NAPL extraction took place mainly through gas phase during the application of vacuum in fine and coarse materials. As is has been presented, the low intrinsic permeability, the NAPL entrapment and the depletion of product in the vicinity of the tested well are the main factors of the presented liquid recovery behavior.

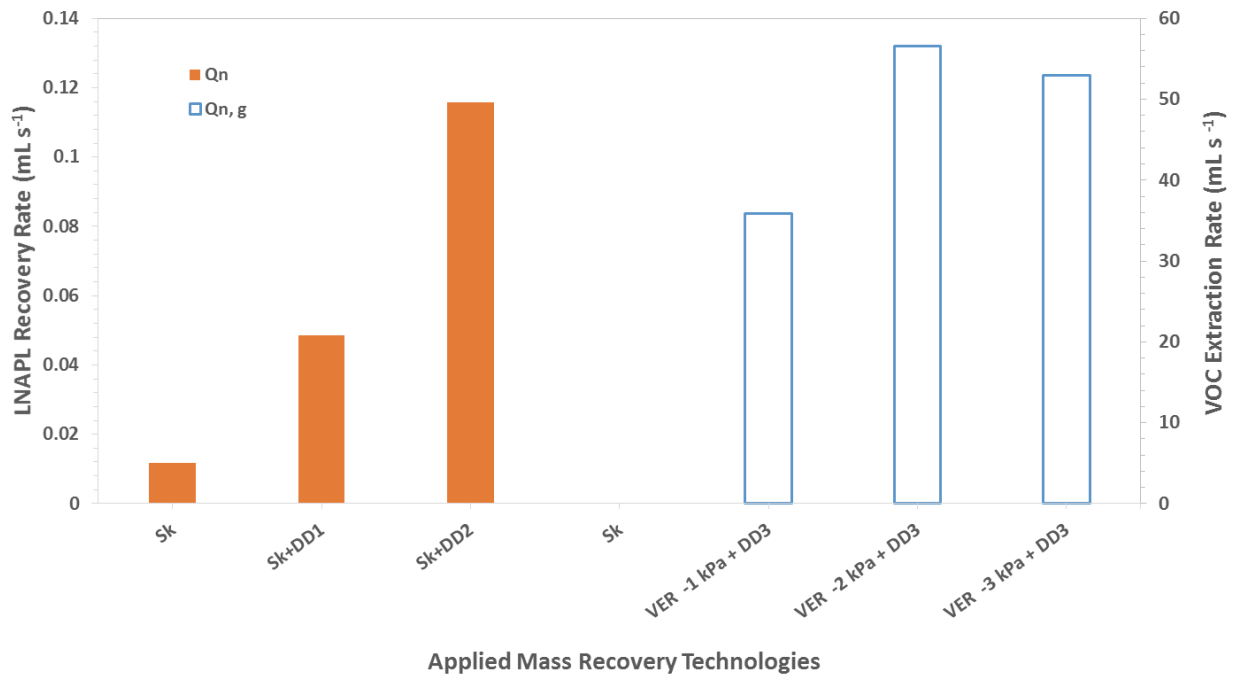


Figure H.2 Comparison of the pumped LNAPL recovery rates during pilot testing and contribution of VOC extraction to removal at PB40 well in 2016.

The pilot-testing at area C (PB40 well) presented lower liquid and gas phase extraction rates than area A (PB29 well). More specifically, skimming in PB40 well gave 10 times lower LNAPL recovery rates than skimming in PB29 well. As already has been documented (Beckett & Huntley 1998), skimming has less chance of success in fine grained settings. In addition, 6-12 times lower VOC extraction rates can be seen in PB40 well compared to PB29 well, during the application of VER+DD. In general, the NAPL recovery was less efficient in PB40 well, even though area C presented higher values of in-well thicknesses and NAPL saturations. Possible reasons of the lower NAPL (liquid phase) recoverability at area C are the lower intrinsic permeability values (Beckett & Huntley 1998; Jeong & Charbeneau 2014) (see section 6.10), the heterogeneity (Essaid, Bekins & Cozzarelli 2015; Johnston & Trefry 2009; Kaluarachchi 1996; Qin et al. 2008) and the anisotropy of NAPL relative permeability (NAPL saturation differences) and intrinsic permeability (Kaluarachchi 1996) (see Figures 5.7, 5.21, 6.30, 6.32 and Figures B.10-11 and B.15-17 in Appendix B). Vacuum enhanced recovery has been documented as more suitable in permeable soils (Halmemies 2003). Travel times of gases to vapor extraction wells are influenced as well by permeability anisotropy (Shan, Falta & Javandel 1992) and spatial variability of permeability has a negative impact on vapor recovery times (Massmann, Shock & Johannesen 2000).

The vacuum-enhanced recovery plus water table drawdown gave the greatest NAPL recovery rates (liquid and gas phase) at both areas A and C. On the other hand, skimming plus water table drawdown presented the highest NAPL removal rates in liquid phase. As a

result, the most appropriate remedial technique which minimizes the risk to receptors can be chosen in heterogeneous media. The applied vacuum did not enhance the liquid removal at these specific tested vacuum pressures. Higher vacuum pressures could not be tested as they brought mud and water-NAPL emulsion (Xitech 1999) towards the testing wells. The upconing of fluid elevations (Lundy, Li & Katyal 2002) forcing the mobile NAPL to move in an area of lower intrinsic permeability is possibly one of the reasons that VER did not enhance the liquid recovery at PB29 well. On the other hand, VER applications were efficient removing VOCs in high rates. Threshold vacuum pressure values for achieving the greater VOC recovery can be seen in PB29 (-3kPa) and PB40 wells (-2 kPa). The high volatility of gasoline and the fine grained material at the top of the aquifer which allows the application of an effective vacuum (Heffron, Blanchard & Dogrul 2003) and acts also as a barrier for the upward migration of vapours (high accumulated VOCs masses), are two of the reasons for the high NAPL removal in gas phase. In contrast, other related research works in sandy materials (Johnston et al. 2002; Johnston et al. 2001) have documented similar contribution of liquid recovery and VOC extraction to NAPL removal. The VOC extraction was lower compared to the present study possibly because of the low volatility NAPL type (weathered gasoline/kerosene). Additionally, Halmemies and Halmemies et al (Halmemies 2003; Halmemies et al. 2003) documented that gasoline is recovered easier than diesel as it is more volatile and less viscous. In conclusion, in such heterogeneous systems, the application of vacuum for gas phase removal is more preferable (mainly due to the high volatility of gasoline) than the application of skimming or water enhanced skimming that target only on liquid phase recovery, as the low intrinsic permeability and the rising water table limit the LNAPL removal in liquid phase.

Comparison with literature data

Table H.1 sums up the results of other related works for the removal of LNAPLs via mass recovery technologies. The results include only values for the techniques which were studied in the present study. It is noteworthy that maximum NAPL saturations reported in other studies are higher than the presented values of this work. In addition, the majority of the literature data reports studies that have dealt with low volatility NAPLs. Finally, the majority of the listed conducted researches have been taken place in coarser environments (sandy).

Similarities of other works compared to the present research involve the following: a) higher NAPL recovery rates have been documented under low water table conditions (Johnston et al. 2002; Johnston et al. 2001) b) VER+DD presented the highest product removal rates in liquid and gas phase, at area A and the highest VOC extraction rates in area C (Hernández-Espriú et al. 2012; Johnston et al. 2002; Johnston et al. 2001; Park, Johnston

& Davis 2015), c) skimming was the least efficient technology in terms of NAPL recovery in all the presented studies and d) during applied vacuum applications the NAPL recovery took place mainly through gas phase (Halmemies et al. 2003; Li et al. 2002).

In contrast with previously studies and other documented works (Halmemies 2003; Heffron, Blanchard & Dogrul 2003; Hernández-Espriú et al. 2012; Hoeppel & Place 1998; Johnston et al. 2002; Johnston et al. 2001; Kittel, Leeson, et al. 1994; Park, Johnston & Davis 2015), vacuum did not enhance the NAPL recovery in liquid phase. Instead, higher product recoveries were found during the water table drawdown skimming applications. During the VER application maybe a threshold was reached as regards the liquid recovery at area A (Halmemies 2003) or the applied vacuum pressures were not efficient for inducing a hydraulic gradient in this short time frame of testing. Unfortunately higher vacuum pressures could not be applied due to water-NAPL emulsion. The low intrinsic permeability is another important parameter that should be taken into consideration. Due to high volatility of the fresh gasoline and the type of material, the removal of NAPLs in gas phase was much higher compared to the liquid extraction rate in contrast to other works (Johnston et al. 2002; Johnston et al. 2001) in sandy aquifers contaminated by lower volatility NAPLs, where liquid removal was higher.

Table H.1. LNAPL removal efficiency reported in literature data.

	Type of Research	NAPL Type	Soil Material	Water Table Conditions	Maximum NAPL saturation	Applied Techn.	Results											
(Johnston et al, 2001)	Field-based	Weathered gasoline/ kerosene	Sand	High	40%	Sk Sk+DD VER VER+DD	<ul style="list-style-type: none"> ▪ The NAPL recovery rates were higher under the lower water table conditions. ▪ VER+DD gave the greatest NAPL recovery rates (4-16 times skimming alone) while VER recovery on its own produced as much as 2.5-10 times the rate for skimming. ▪ The rates for vacuum- enhanced recovery were better than those for Sk+DD ▪ NAPL removal in liquid phase was higher than the extraction in vapour phase 											
(Johnston et al, 2002)				Low	60%			(Park et al, 2015)	Modeling	Weathered gasoline/ kerosene	Sand	Not taken into account	20%	Sk Sk+DD VER VER+DD	(Hernández-Espriú et al, 2012)	Modeling	Diesel	Fine sand
(Park et al, 2015)	Modeling	Weathered gasoline/ kerosene	Sand	Not taken into account	20%	Sk Sk+DD VER VER+DD												
(Hernández-Espriú et al, 2012)	Modeling	Diesel	Fine sand	NA	70%	Sk Sk+DD VER+DD		<ul style="list-style-type: none"> ▪ Recovery efficiencies in liquid phase were 27% for Sk, 65% for Sk+DD and 67% for VER+DD 										

Present study	Field-based	Fresh gasoline	Sand-Silty sand	Rising	20%	Sk Sk+DD VER VER+DD	<ul style="list-style-type: none"> ▪ VER+DD gave the greatest NAPL recovery rates (liquid and gas phase) ▪ Sk+DD presented the highest NAPL removal rates in liquid phase ▪ Sk+DD gave 4.5-16 times higher LNAPL recovery rates than Sk ▪ VER did not favour the liquid recovery, however the VOC extraction rates were increased for higher applied pressure values ▪ VER+DD produced as much as 16-18 times the rate of skimming (sandy material) ▪ VER+DD did not enhance the liquid recovery in the silty sand material ▪ During the application of vacuum > 99.5% of the total NAPL recovery was in gas phase
----------------------	-------------	----------------	-----------------	--------	-----	------------------------------	--

Appendix I. Publications

- **Evangelos Gatsios**, Jonas Garcia-Rincon, John Rayner, Robert McLaughlan, Greg Davis, 2018. LNAPL transmissivity as a remediation metric in complex sites under water table fluctuations. *Journal of Environmental Management* vol. 215, pp 40-48.
- **Evangelos Gatsios**, Jonas Garcia-Rincon, John Rayner, Robert McLaughlan, 2018. Evaluation of Diagnostic Gauge Plots as Tools for the Identification of LNAPL Hydrogeological Conditions in Heterogeneous Porous Media. It will be presented as conference paper, in the proceedings of the 6th International Conference on Industrial and Hazardous Waste Management "CRETE2018", September 2018, At Chania, Crete, Greece.
- **Evangelos Gatsios**, Colin Johnston, John Rayner, Robert McLaughlan, 2015. Using hydraulic testing to evaluate LNAPL recovery in fine grained systems, in Clean Up Conference proceedings, Poster Presentation, Melbourne Vic 2015.
- **Evangelos Gatsios**, John Rayner, Robert McLaughlan, 2016. Use of LNAPL Transmissivity to Evaluate LNAPL Recoverability in a Fine Grained Aquifer in Western Australia. Conference paper, in the proceedings of the 5th International Conference on Industrial and Hazardous Waste Management "CRETE2016", September 2016, At Chania, Crete, Greece.
- **Evangelos Gatsios**, Colin Johnston, Robert McLaughlan, 2014. Evaluating the performance and endpoints of LNAPL remediation technologies. Poster presentation in the CRC CARE communication conference, 2014, Adelaide, Australia.

Appendix J. NAPL Baildown Testing at the Donnybrook Site (W.A.), 2015 – 2016

This Appendix has been attached as electronic file.

Appendix K. Manuscript entitled “LNAPL transmissivity as a remediation metric in complex sites under water table fluctuations”

This Appendix has been attached as electronic file.

Appendix J

NAPL Baildown Testing at the Donnybrook Site (WA), 2015 - 2016

by

Evangelos Gatsios

at

University of Technology Sydney

and

CSIRO Land & Water

November 2017

Contents

1. ABSTRACT	3
2. METHODS.....	3
3. RESULTS.....	6
3.1 Spatial Variability of LNAPL Transmissivity	6
3.2. Individual Well Test Analysis	8
PB29 8/07/2015	8
PB29 9/02/2016	12
PB29 5/04/2016	15
PB29 28/04/2016.....	19
PB29 19/05/2016.....	22
PB29 1/06/2016	25
PB29 09/06/2016.....	29
PB29 15/06/2016.....	32
PB27a 6/05/2015.....	35
PB27b 6/05/2015.....	39
PB27 8/07/2015	43
PB27 20/07/2015.....	47
PB27 5/04/2016	51
PB27 20/05/2016.....	54
PB27 01/06/2016.....	57
PB27 14/06/2016.....	60
PB05 8/05/2015	64
PB05 6/04/2016	67
PB11 7/05/2015	71
PB11 6/04/2016	74
PB13 8/05/2015	78
PB13 6/04/2016	81
PB39 06/04/2016.....	85
PB40 06/04/2016.....	87
PB40 14/06/2016.....	90
MP42 06/04/2016.....	93
4. REFERENCES.....	97

1. ABSTRACT

LNAPL bail-down tests were carried out throughout the period of the research (5/2015 - 6/2016) excluding periods of mass recovery trials. The tests were conducted in 50 and 100 mm diameter wells. The spatial variability of LNAPL Transmissivity (T_n) is presented at Table 1. For the calculations of Transmissivity the Bower & Rice method was used, presented in detail at API LNAPL transmissivity workbook. Twenty six bail-down tests took place in eight wells. The calculated values varied from 0.03 to 2.13 m²/d. The highest LNAPL transmissivity values found to be at the well locations PB29, PB27 and PB40 and that is the reason these wells have been chosen to be the remediation wells of the field trials. Moreover, all the conducted tests showed unconfined LNAPL conditions. Also, borehole recharge from the filter pack was not a significant issue for all the wells. According to ITRC guide for LNAPL technology selection, for hydraulic recovery the LNAPL transmissivity endpoint ranges from 0.1 to 0.8 ft² /day (0.009 to 0.07 m²/d).

2. METHODS

- Testing involved removing a slug of LNAPL using either three bailers tied together or a single bailer depending on the well diameter. A single bailer was used in the monitoring wells of 50 mm diameter. The volume of recovered fluids, usually LNAPL and water, was measured and the fluid levels monitored in the well to assess recovery. The field procedures entailed the instantaneous/rapid removal of LNAPL using bailers while minimising the removal of water from the well. Measurements of fluid levels in the well were made manually with an interface probe, initially every 30 seconds to 1 minute, with the interval between measurements subsequently increasing as the rate of recovery in the well decreased.
- The Bail-down test data was analysed using the API LNAPL Transmissivity Workbook (API 2012). For the estimation of LNAPL Transmissivity the Bouwer & Rice (Bouwer & Rice 1976) approach was used.
- According to API LNAPL Transmissivity Workbook's Flowchart, continuously decreasing discharge with decreasing drawdown indicates unconfined conditions, whereas constant discharge periods indicate confined or perched LNAPL (API 2012; Kirkman, Adamski & Hawthorne 2013).
- The B&R method assumes that the water table elevation remains constant.
- Cut off time and J ratio (Kirkman 2013) values are presented at Table 1 below.

- Data has been filtered to obtain consistent trends for the calculation of T_n .
- When the formation and wellbore LNAPL fluids were not initially in equilibrium, a drawdown correction was applied to the data before LNAPL transmissivity analysis.

Figure 3.7 shows three different distinct areas noted A, B and C. Section A refers to early stage collected data that represents the filter pack drainage. Section B corresponds to the NAPL flow from the adjacent formation and section C represents the end of the test (return to pre-testing conditions). Thus, section B is used for the calculation of T_n (fitting the straight line). It should be also noticed that, in this document, negative and negligible NAPL discharge values in the section B were excluded from the T_n analysis.

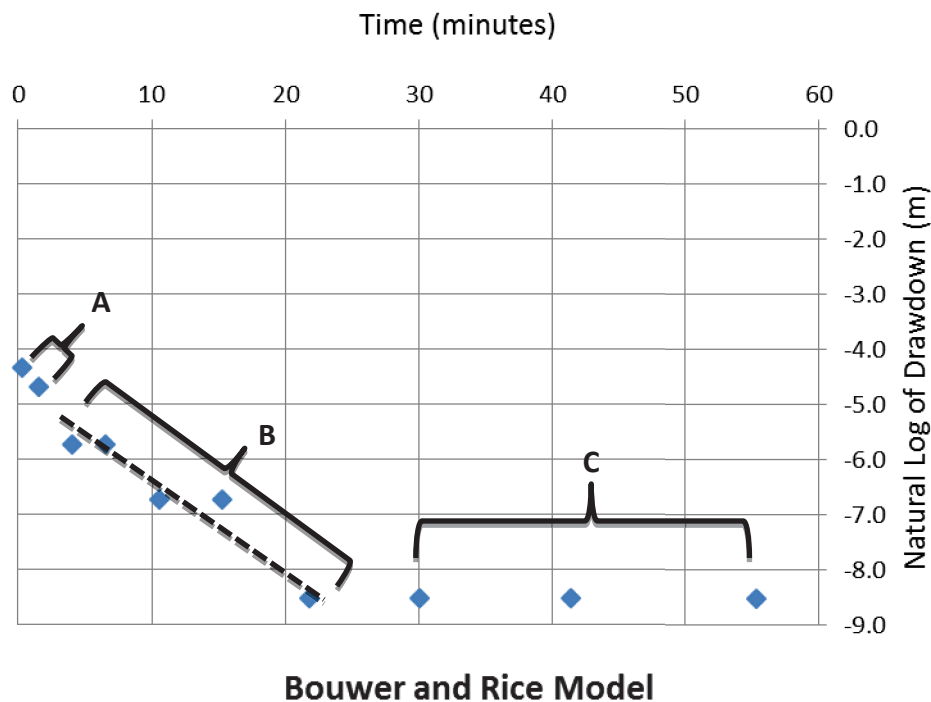


Figure 1. Example of the bail-down test data analysis using Bouwer and Rice method.

The Bouwer and Rice (Bouwer & Rice 1976) method for slug test analysis combines a simple representation for flow to the well from the Thiem equation and continuity of fluids within the well. The flow equation is:

$$Q_n = \frac{2\pi T_n s_n}{\ln(R/r_w)} \quad \text{[Equation 1]}$$

With the effective well radius determined and with use of the Kirkman J-ratio, the generalized Bouwer and Rice formula for determining the LNAPL transmissivity takes the form:

$$T_n = \frac{r_e^2 \ln(R / r_w) \ln(s_n(0) / s_n(t))}{2(-J)t} \quad \text{[Equation 2]}$$

Where:

Q_n LNAPL discharge

T_n LNAPL transmissivity

R radius of influence

r_w well borehole radius

r_e effective well radius

s_n LNAPL drawdown

J Kirkman J-ratio

t time epoch

The Field Site of Research

The study area of this research comprises the facilities of a petrol station in Western Australia, in an area of 2750 m² which is located within a residential-commercial zone. The site has operated as a fruit shop and petrol station since 1985. The local hydrology consists of a multi-layered aquifer consisting of discontinuous interbedded sandstones, siltstones and shales in the general proportion of 50% sandstone to 50% siltstone plus shale. In general, the subsurface geology seems to present 3 layer sets. Clayey and silty layer set from 0 to approximately 4.5m below ground, sandy layer (fine and coarse sand with tracers of silt and clay) set approximately from 4.5m to 8m and heavy clayey layer set approximately from 8m and below.

3. RESULTS

3.1 Spatial Variability of LNAPL Transmissivity

Table 1. Details of LNAPL bail-down tests and calculated LNAPL T_n values.

Well ID	Date	LNAPL Vol. removed (L)	Water Vol. removed (L)	Cut off time (min)	J ratio	LNAPL Conditions	Z_{an} (m AHD)	Z_{nw} (m AHD)	Z_{aw} (m AHD)	T_n (m ² /d)
PB29	8/7/2015	1.400	0.050	0.8	-0.65	unconfined	56.285	55.927	56.191	1.480 (±0.135)
PB29	9/2/2016	0.780	0.470	3.0	-0.625	unconfined	56.683	56.57	56.653	0.265 (±0.032)
PB29	5/04/2016	2.750	0.000	2.3	-0.2	unconfined	56.287	55.983	56.207	1.969 (±0.47)
PB29	28/04/2016	2.850	0.800	2.23	-0.138	unconfined	56.263	55.941	56.179	2.133 (±0.204)
PB29	19/05/2016	2.750	1.050	1.95	-0.25	unconfined	56.232	55.908	56.147	1.510 (±0.093)
PB29	1/06/2016	3.850	2.250	1.6	-0.324	unconfined	56.348	56.116	56.287	1.323 (±0.076)
PB29	9/06/2016	4.100	0.900	2.34	-0.5	unconfined	56.385	56.172	56.329	0.699 (±0.097)
PB29	15/06/2016	7.700	1.500	6	-0.329	unconfined	56.472	56.295	56.425	0.372 (±0.015)
PB27 _a	6/5/2015	0.710	0.000	1.7	-0.237	unconfined	56.341	55.991	56.250	0.910 (±0.111)
PB27 _b	6/5/2015	1.600	0.370	2.1	-0.285	unconfined	56.341	55.991	56.250	0.960 (±0.021)
PB27	8/7/2015	1.700	0.050	3	-0.247	unconfined	56.279	55.919	56.185	1.330 (±0.063)
PB27	20/7/2015	1.375	0.050	0	-0.286	unconfined	56.282	55.995	56.207	1.380 (±0.046)
PB27	5/04/2016	2.230	0.370	1.6	-0.256	unconfined	56.282	55.971	56.201	0.414 (±0.023)
PB27	20/05/2016	2.400	0.900	11	-0.256	unconfined	56.228	55.908	56.144	0.572 (±0.011)
PB27	1/06/2016	2.000	1.250	4.2	-0.292	unconfined	56.341	56.105	56.279	0.664 (±0.022)
PB27	14/06/2016	2.100	0.350	1.57	-0.26	unconfined	56.448	56.263	56.399	0.204 (±0.006)
PB05	8/5/2015	1.690	0.230	5.5	-0.769	unconfined	56.357	55.995	56.262	0.046

										(±0.002)
PB05	6/4/2016	3.300	0.740	2.3	-0.213	unconfined	56.322	55.904	56.213	0.039 (±0.012)
PB11	7/5/2015	2.710	0.000	11.0	-0.25	unconfined	56.319	55.594	56.130	0.550 (±0.021)
PB11	6/4/2016	5.780	0.700	8.0	-0.25	unconfined	56.405	55.669	56.213	0.136 (±0.002)
PB13	8/5/2015	2.730	0.000	7.0	-3.182	unconfined	56.290	55.499	56.084	0.240 (±0.015)
PB13	6/4/2016	6.780	0.380	20.0	-16.8	unconfined	56.420	55.63	56.214	0.027 (±0.002)
PB39	06/04/2016	8.440	0.620	10.0	-0.20	unconfined	56.491	55.715	56.289	0.034 (±0.003)
PB40	6/04/2016	5.340	1.100	4.2	-0.258	unconfined	56.425	55.685	56.232	0.577 (±0.025)
PB40	14/06/2016	19.500	0.000	0.7	-0.256	unconfined	56.566	56.038	56.428	0.304 (±0.008)
MP42	6/04/2016	1.310	0.070	9.5	-0.350	unconfined	56.363	55.736	56.199	0.130 (±0.022)

3.2. Individual Well Test Analysis

Note: the top and the bottom of screen that are presented below are referred to depth below well reference point.

PB29 8/07/2015

Well casing radius (m)	0.05
Well radius (m)	0.075
Top of screen (m)	2.15
Bottom of screen (m)	8.15
LNAPL baildown vol. (litre)	1.4

The baildown test took place on 8/7/2015. 1.4 L NAPL and 0.05 L water were removed. The initial NAPL thickness before the test was 0.36 m. The thickness after the removal of the product was 0.30m and the final thickness after 10min was 0.35 m, which is almost 100 % recovery of the initial product thickness. The recovery period was ~ 10 min. The elevation of water table (corrected) is constant (after the cut off time which is 0.8 min), thus B&R method can be used. The B&R method showed 1.48 (m²/d) as Transmissivity value.

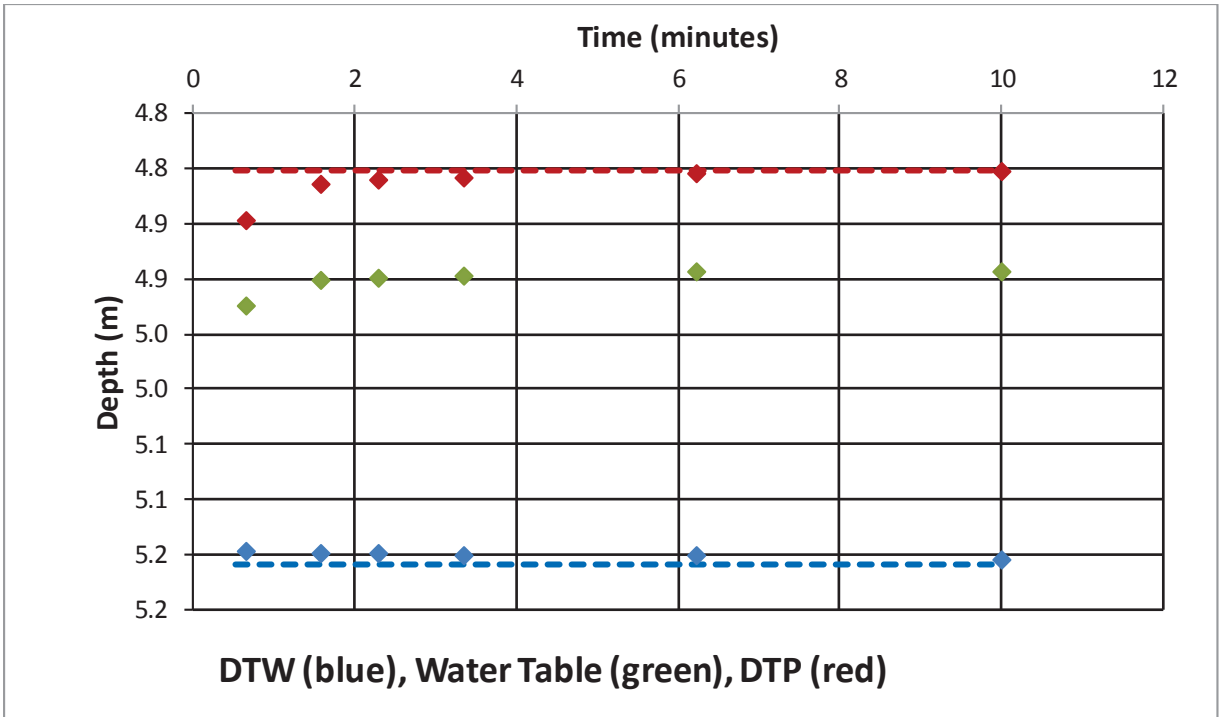


Figure 2. Time series of fluid levels during the baildown test.

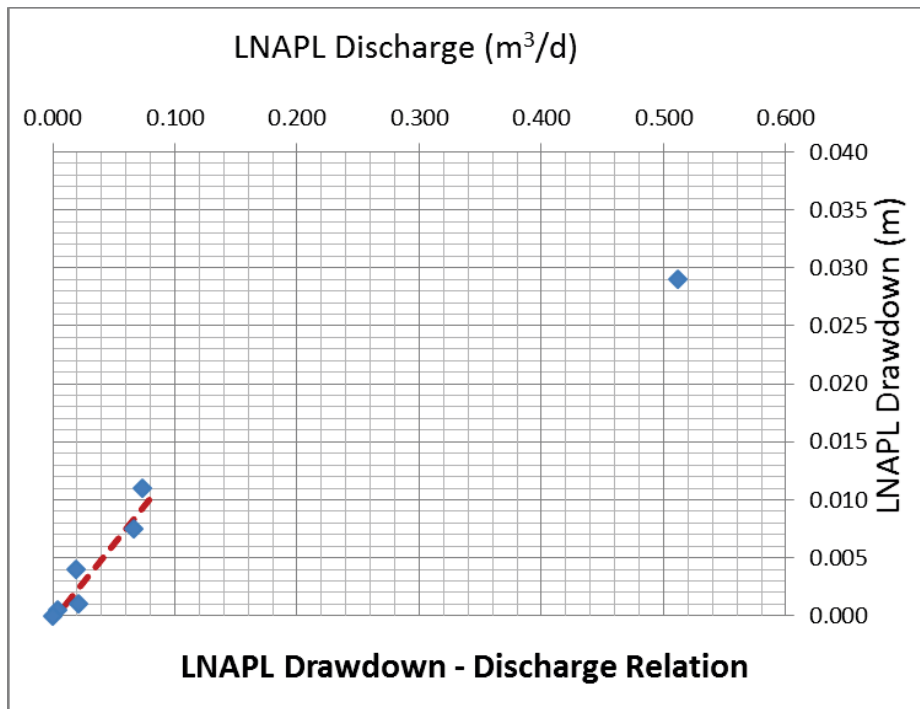


Figure 3. Pre-filtered data.

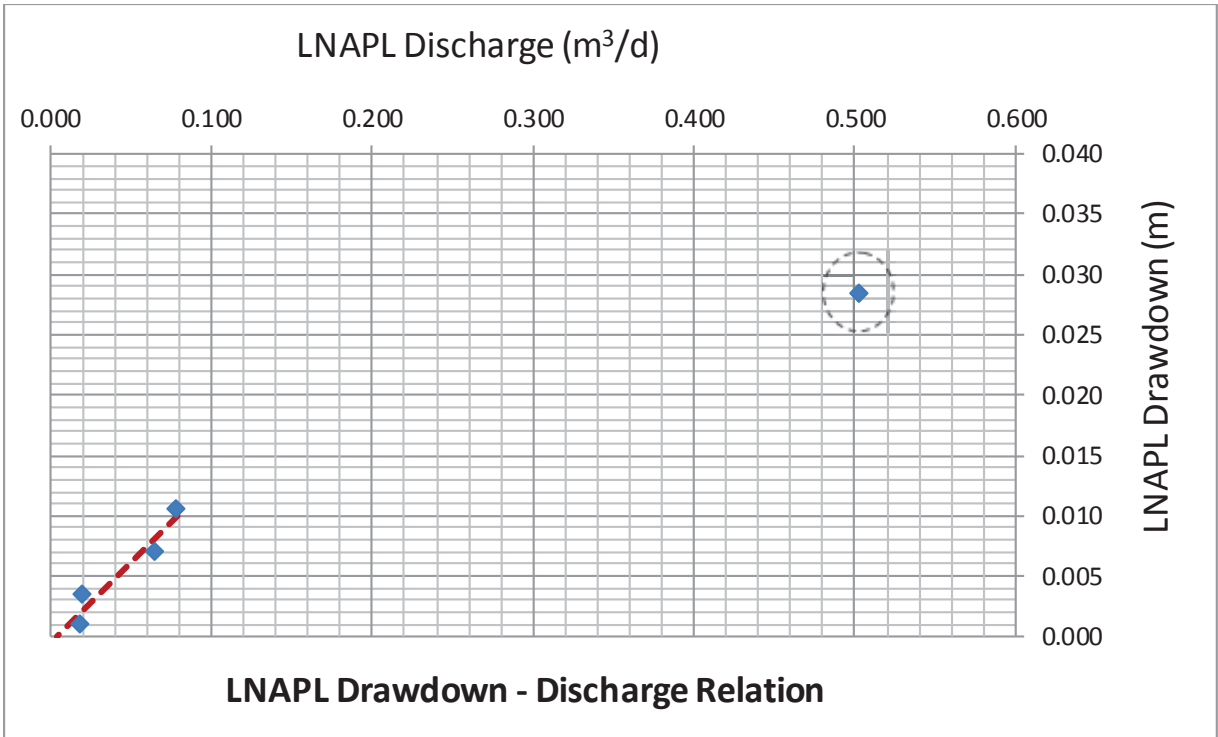


Figure 4. LNAPL drawdown- discharge relation during baildown testing (after a drawdown adjustment of 0.0002m).

The plot above shows that borehole recharge from the filter pack maybe is not significant (large discharge values at the beginning of the recovery, 0.5 m³/d). Moreover, figure depicts behaviour that suggests unconfined LNAPL conditions because we can see continuously decreasing discharge with decreasing drawdown.

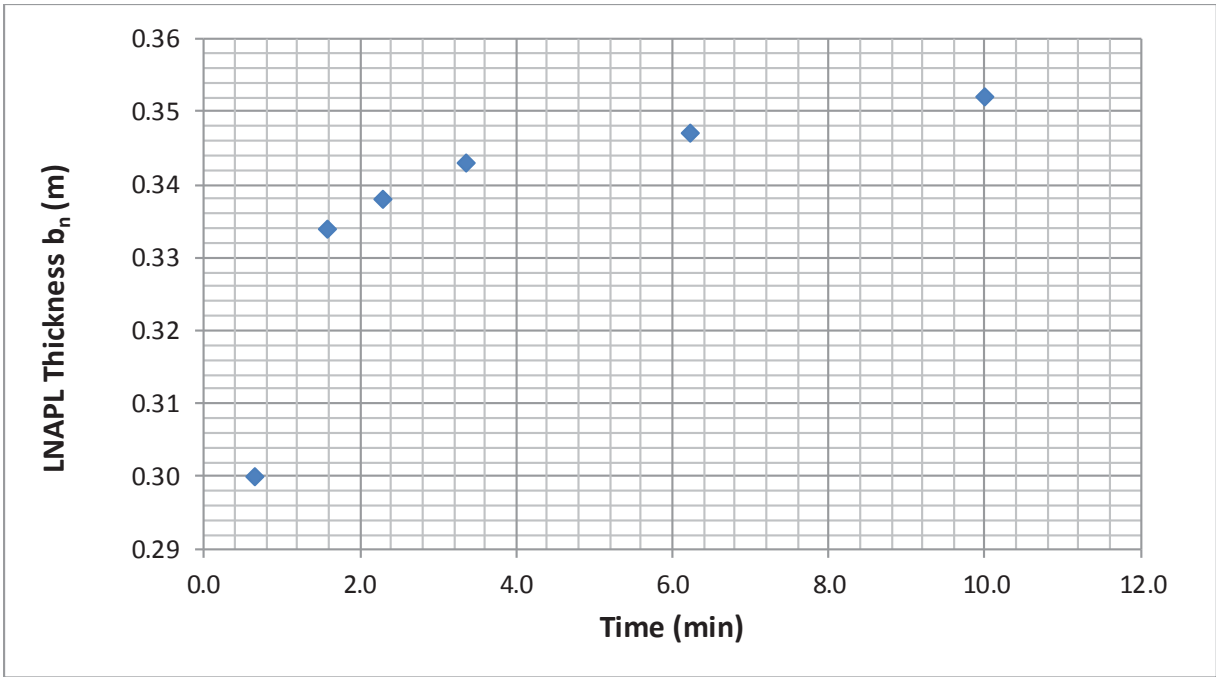


Figure 5. Time series of LNAPL thickness during baildown testing. Increasing LNAPL thickness with time.

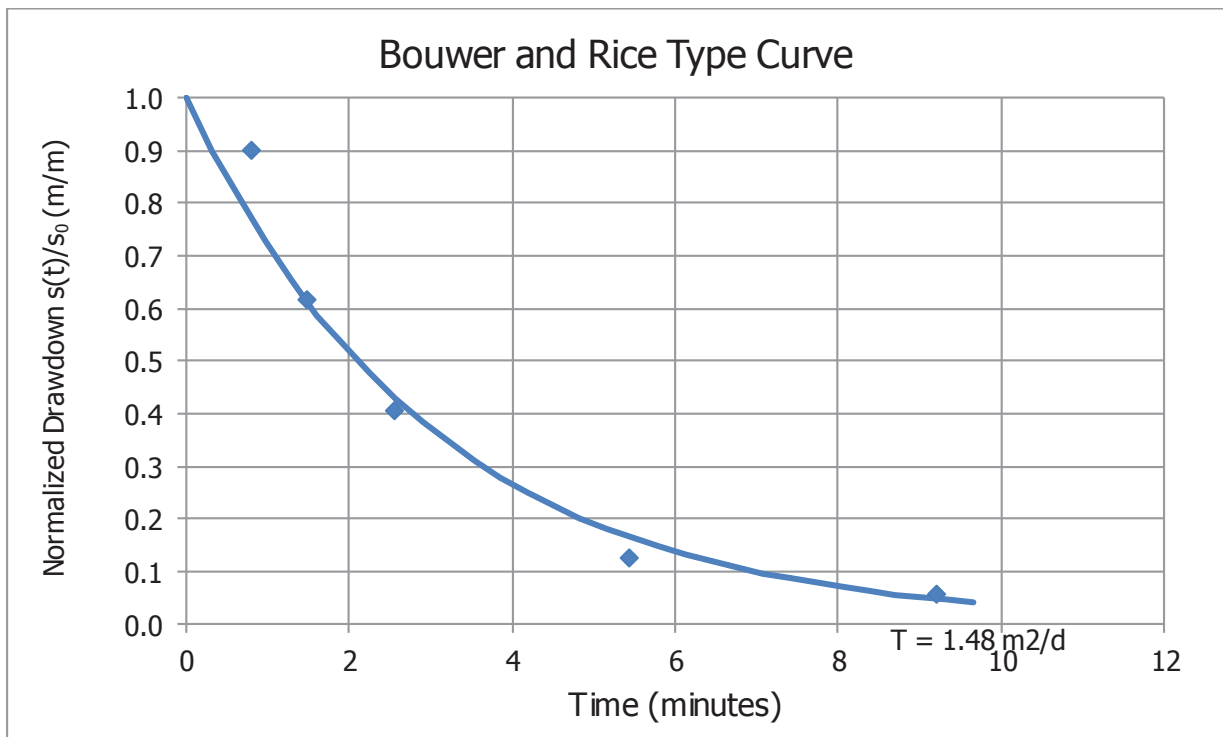


Figure 6. Bower and Rice type curve for the calculation of T_n .

PB29 9/02/2016

Well casing radius (m)	0.05
Well radius (m)	0.075
Top of screen (m)	2.15
Bottom of screen (m)	8.15
LNAPL baildown vol. (litre)	0.780

The bail-down test took place on 09/02/2016. 0.780 L NAPL and 0.470 L water were removed. The initial NAPL thickness before the test was only 0.110. The in-well thickness was 4mm higher in comparison with the conducted test on 2/9/15. The thickness after the removal of the product was 0.046m and the final thickness after 170min was 0.05 m. The elevation of water table (corrected) is constant thus, B&R method can be used. The cut off time was 3.0 min. The B&R method showed 0.265 (m²/d) as Transmissivity value.

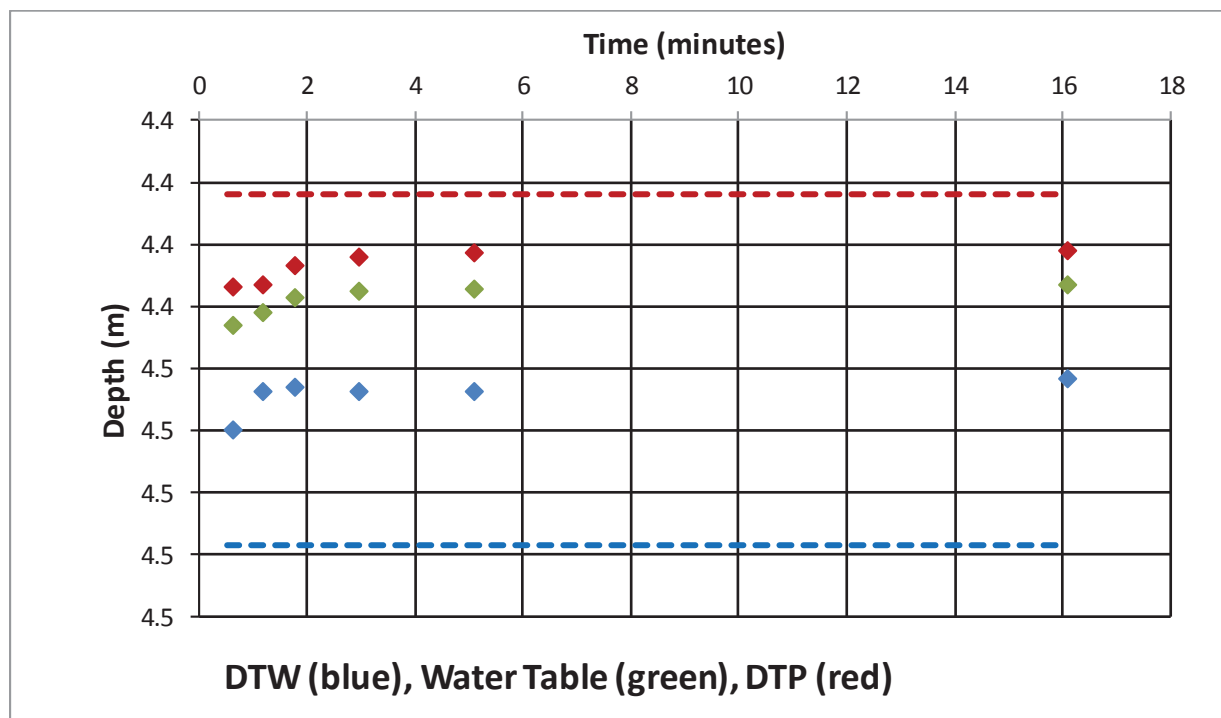


Figure 7. Time series of fluid levels during the baildown test.

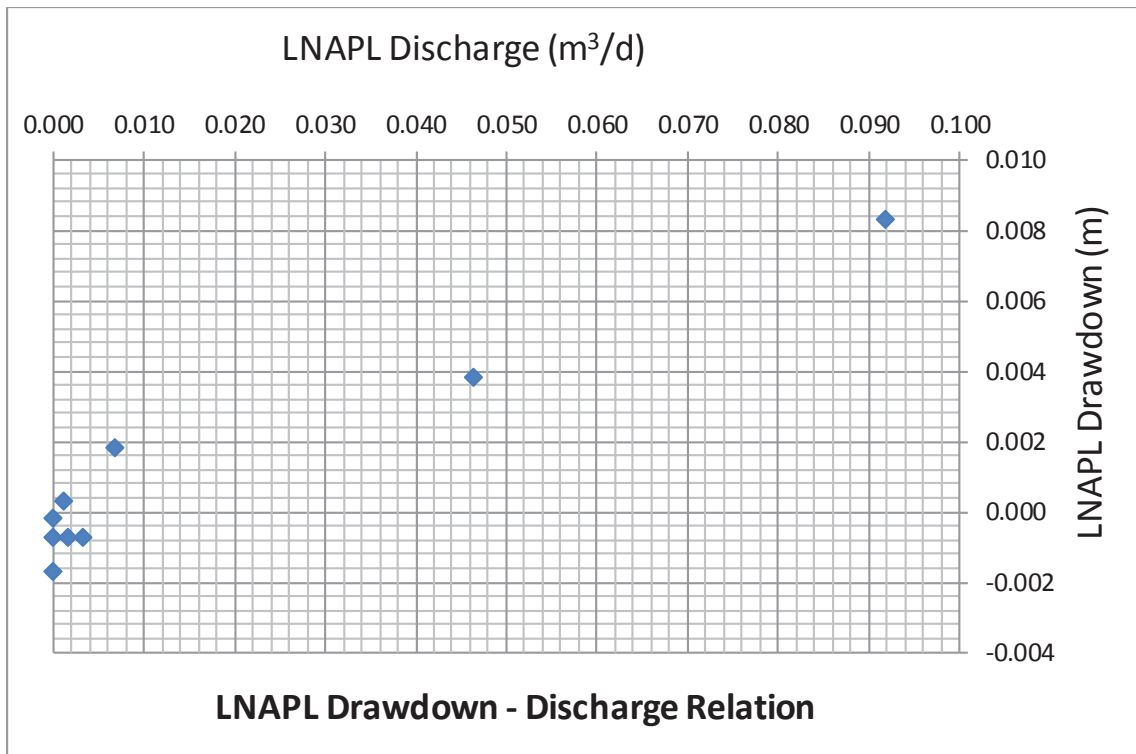


Figure 8. Pre-filtered data.

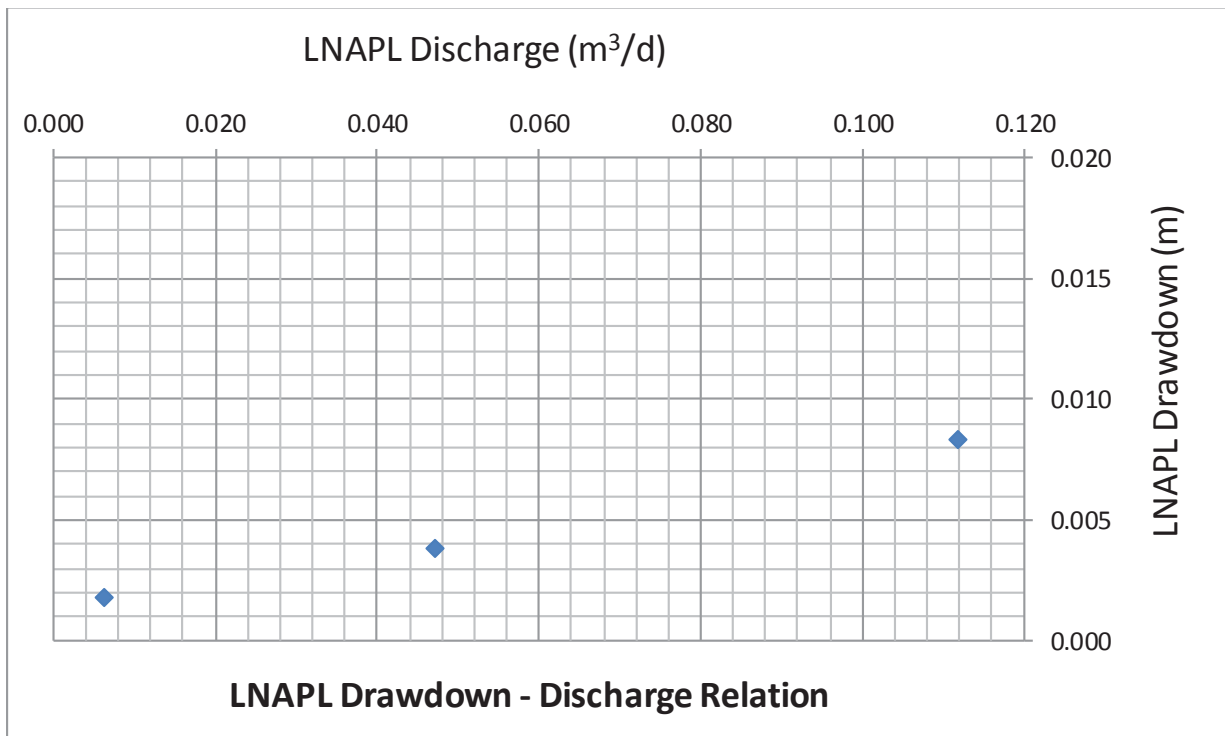


Figure 9. LNAPL drawdown- discharge relation during baildown testing (post-filtered data). After a drawdown adjustment of 0.0177m

The plot above shows that borehole recharge from the filter pack maybe is not significant (large discharge values at the beginning of the recovery, 0.11 m³/d). Moreover, figure depicts behaviour that maybe suggests unconfined LNAPL conditions because there is a continuously decreasing discharge with decreasing drawdown.

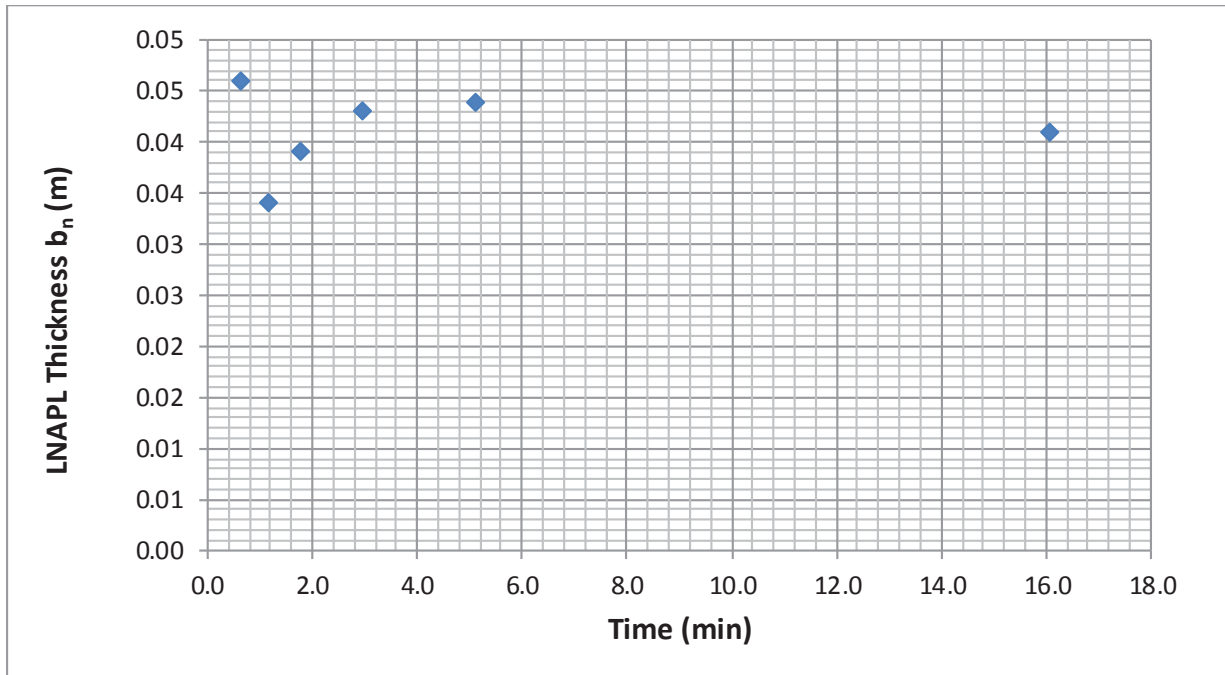


Figure 10. Time series of LNAPL thickness during baildown testing.

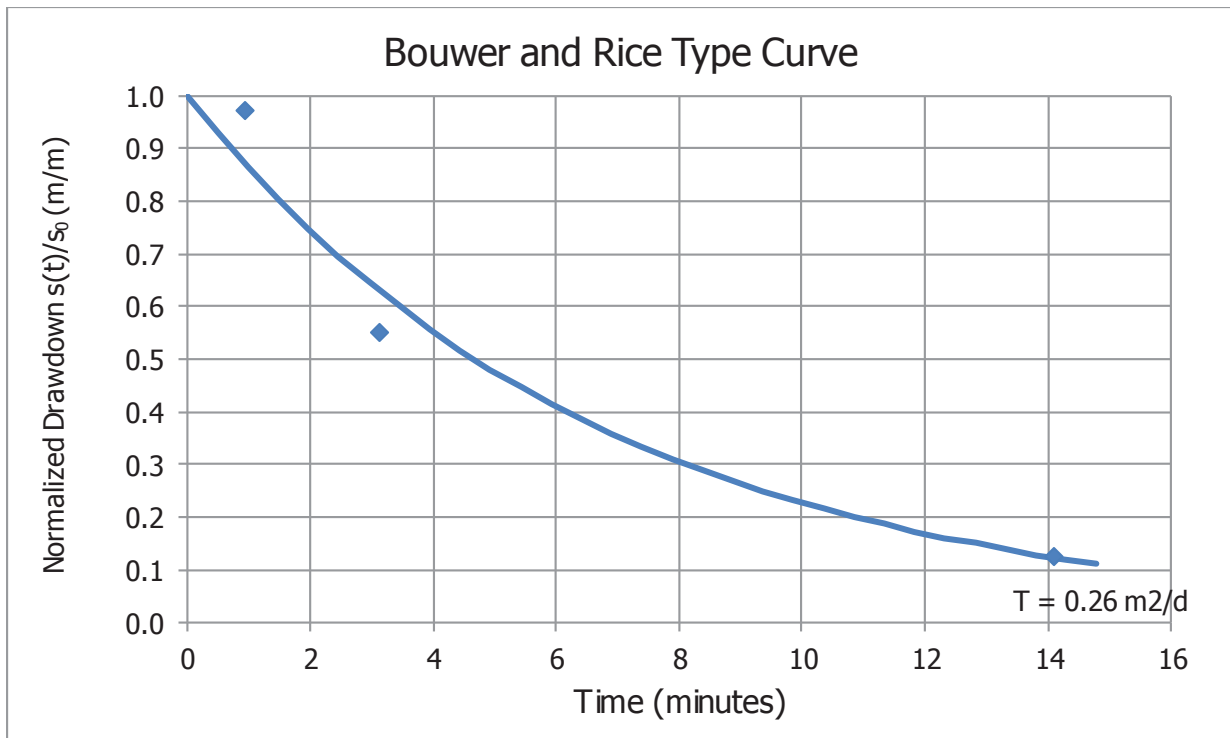


Figure 11. Bower and Rice type curve for the calculation of T_n .

PB29 5/04/2016

Well casing radius (m)	0.05
Well radius (m)	0.075
Top of screen (m)	2.15
Bottom of screen (m)	8.15
LNAPL baildown vol. (litre)	2.75

The baildown test took place on 5/4/2016. 2.75 L NAPL and 0.00 L water were removed. The initial NAPL thickness before the test was 0.304 m. The thickness after the removal of the product was 0.177m and the final thickness after 86min was 0.302 m, which is almost 100 % recovery of the initial product thickness. The recovery period (>95%) was ~ 40 min. The elevation of water table (corrected) is constant, thus B&R method can be used. The B&R method showed 1.97 (m²/d) as Transmissivity value and the cut off time was 2.3 min.

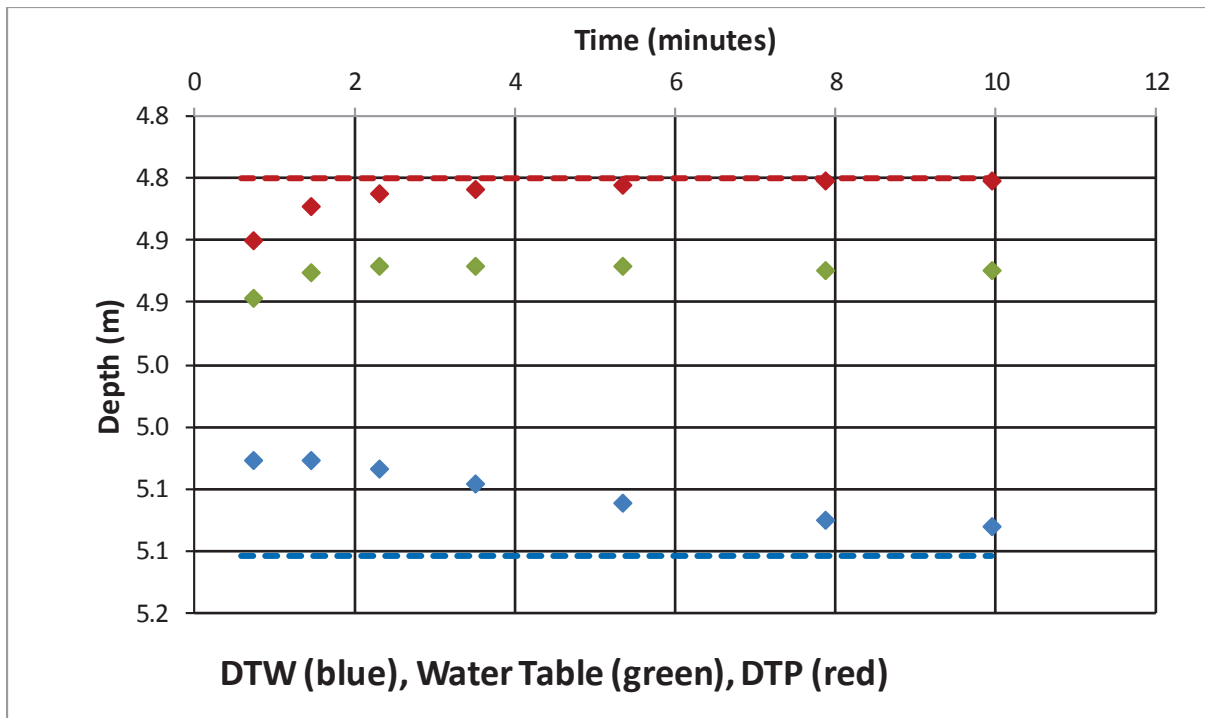


Figure 12. Time series of fluid levels during the baildown test.

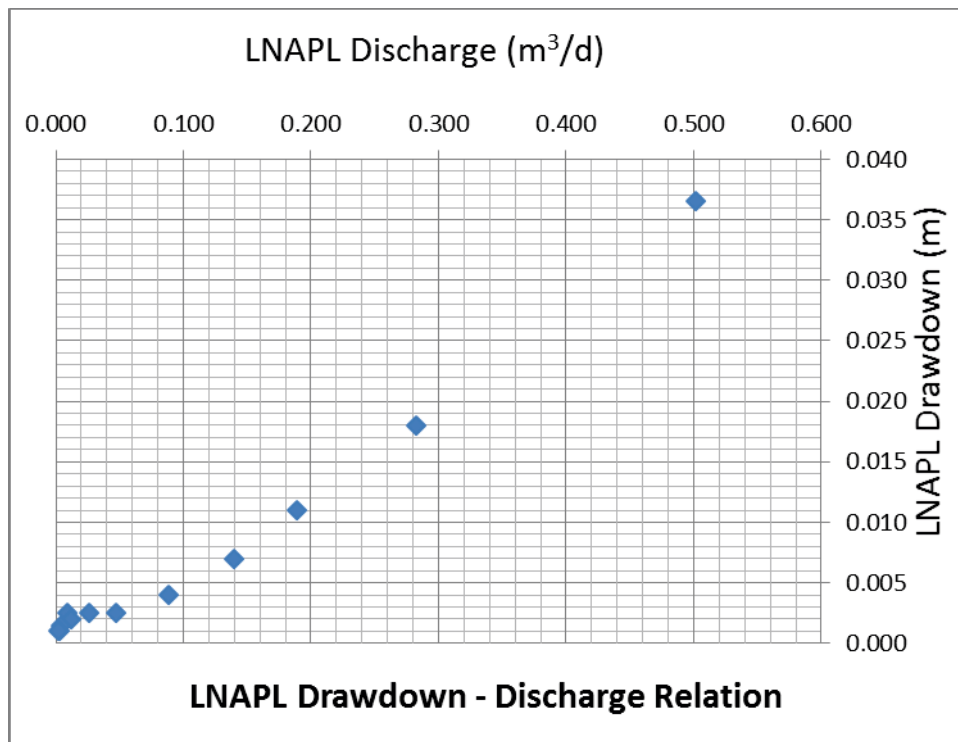


Figure 13. Pre-filtered data.

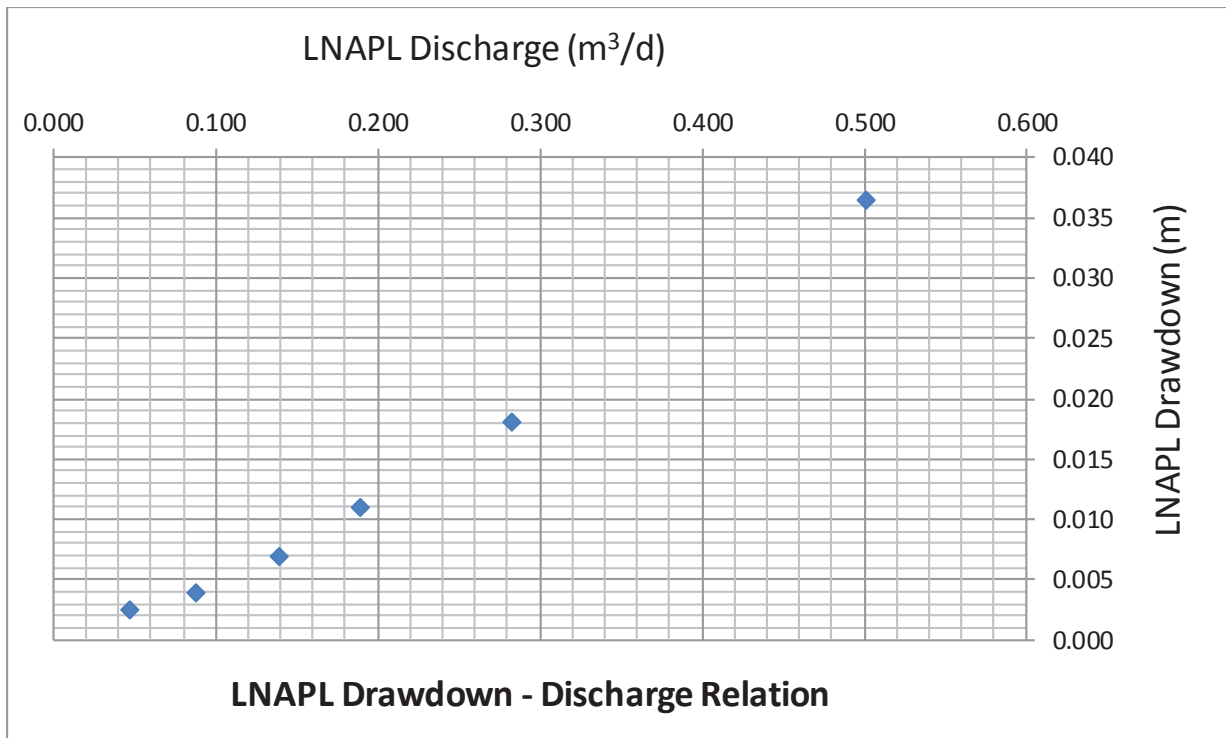


Figure 14. LNAPL drawdown- discharge relation during baildown testing (post-filtered data).

The plot above shows that borehole recharge from the filter pack maybe is not significant (large discharge value at the beginning of the recovery, 0.5 m³/d). The formation and wellbore LNAPL fluids were initially in equilibrium thus, a drawdown correction was not applied to the data. Moreover, figure depicts behaviour that maybe suggests unconfined LNAPL conditions because there is a continuously decreasing discharge with decreasing drawdown.

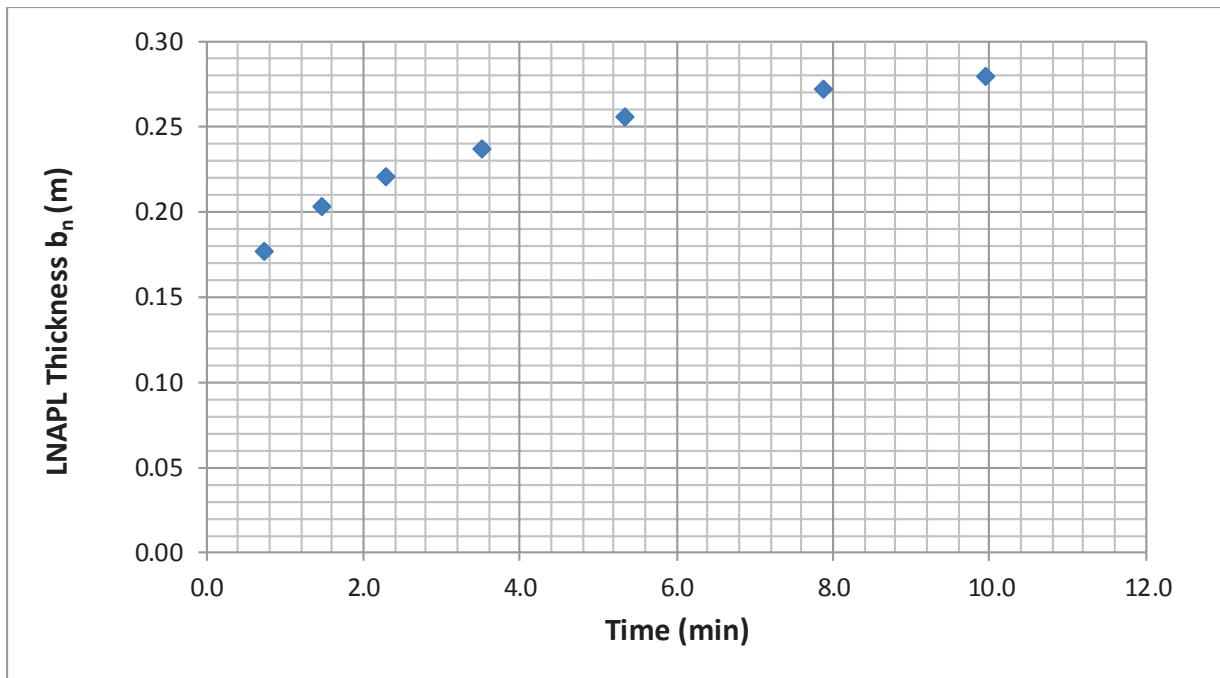


Figure 15. Time series of LNAPL thickness during baildown testing.

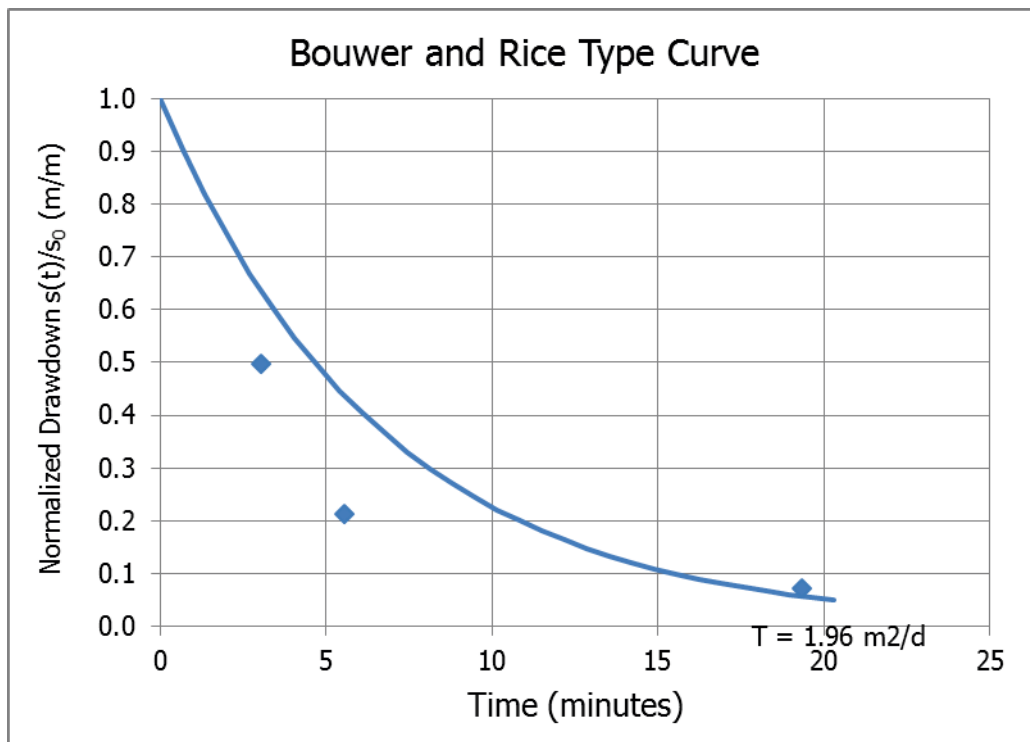


Figure 16. Bower and Rice type curve for the calculation of T_n .

PB29 28/04/2016

Well casing radius (m)	0.05
Well radius (m)	0.075
Top of screen (m)	2.15
Bottom of screen (m)	8.15
LNAPL baildown vol. (litre)	2.85

The bail-down test took place on 28/4/2016. 2.85 L NAPL and 0.80 L water were removed. The initial NAPL thickness before the test was 0.322 m. The thickness after the removal of the product was 0.125m and the final thickness after 124min was 0.318 m, which is almost 100 % recovery of the initial product thickness. The recovery period (>95%) was ~ 23 min. The elevation of water table (corrected) is constant, thus B&R method can be used. The B&R method showed 2.13 (m²/d) as Transmissivity value and the cut off time was 2.23 min.

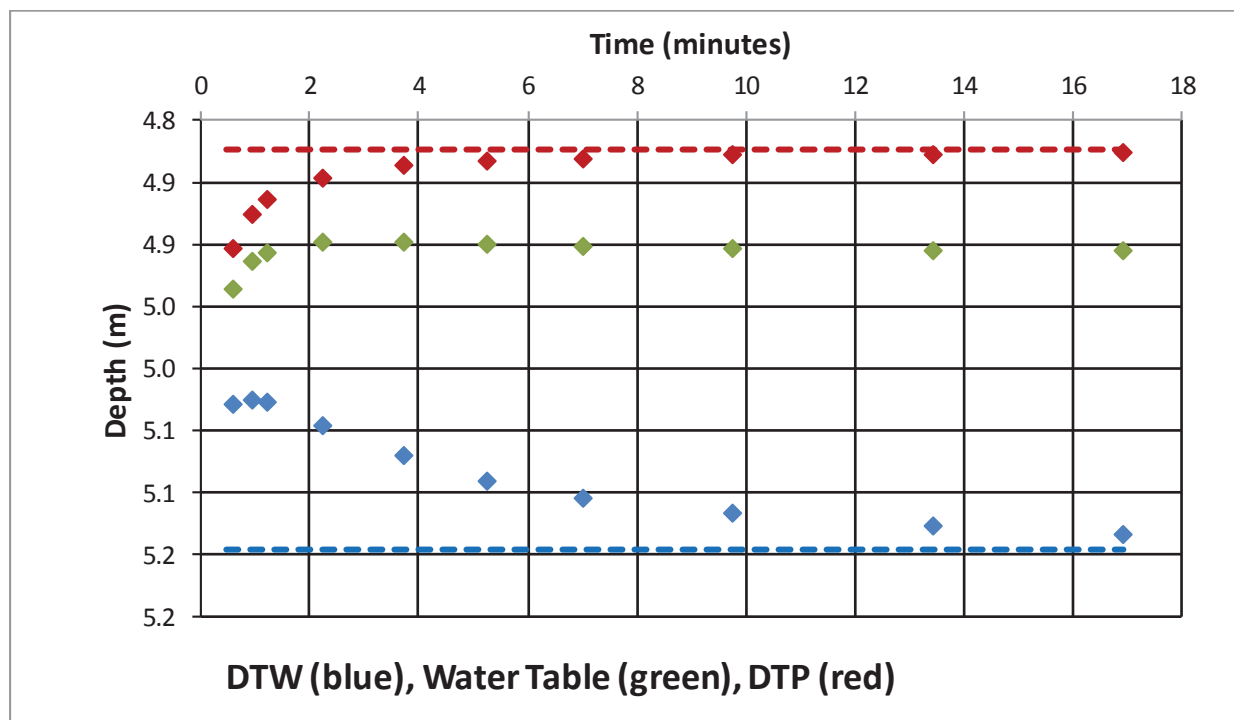


Figure 17. Time series of fluid levels during the baildown test.

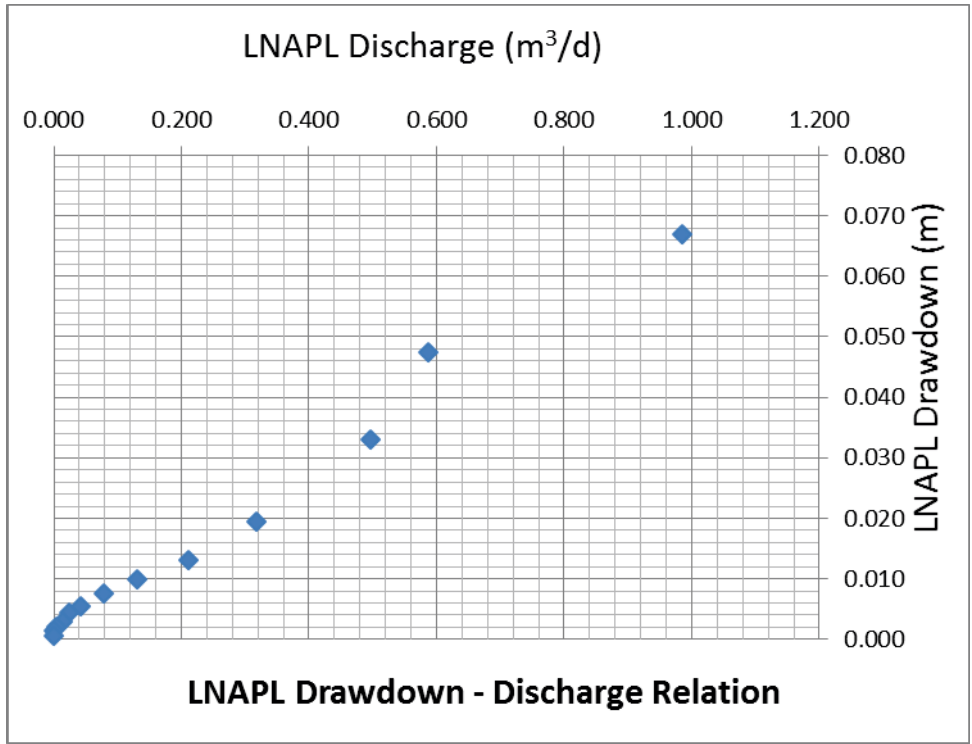


Figure 18. Pre-filtered data.

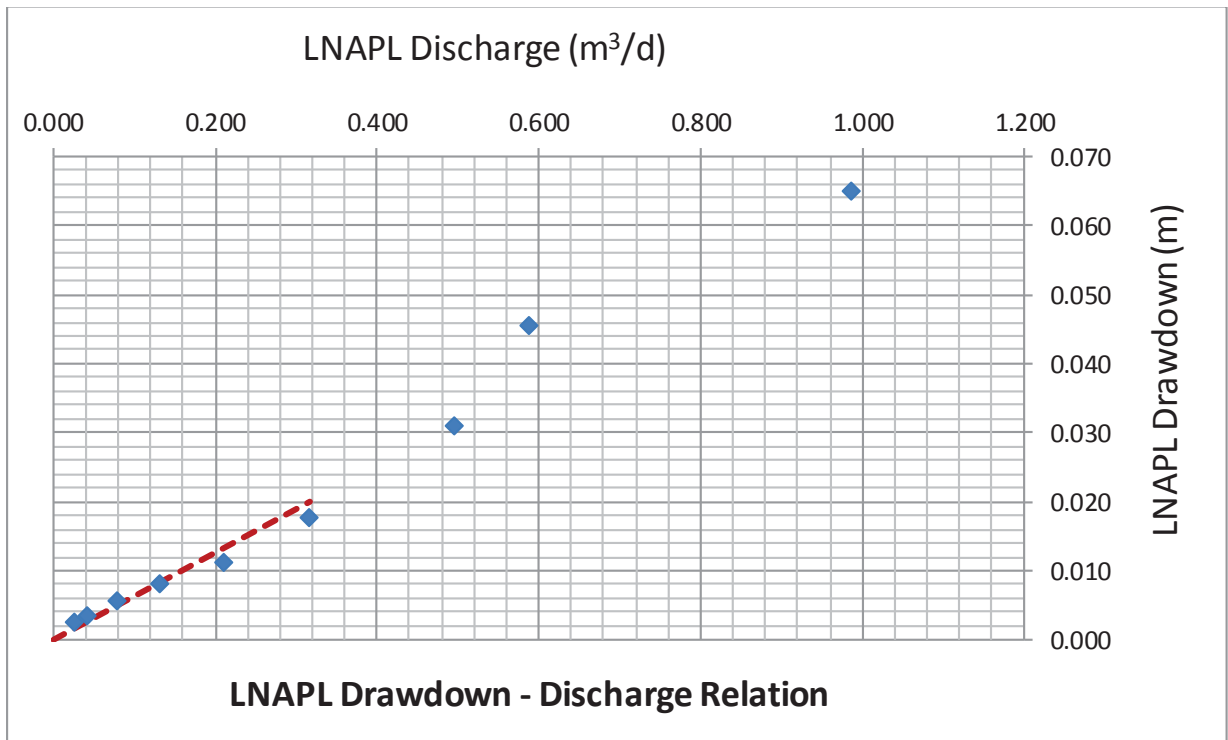


Figure 19. LNAPL drawdown- discharge relation during baildown testing (post-filtered data).

The plot above shows that borehole recharge from the filter pack maybe is not significant (large discharge value at the beginning of the recovery, 0.9 m³/d). The formation and wellbore LNAPL fluids were initially in equilibrium thus, a drawdown correction was not applied to the data. Moreover, figure depicts behaviour that maybe suggests unconfined LNAPL conditions because there is a continuously decreasing discharge with decreasing drawdown.

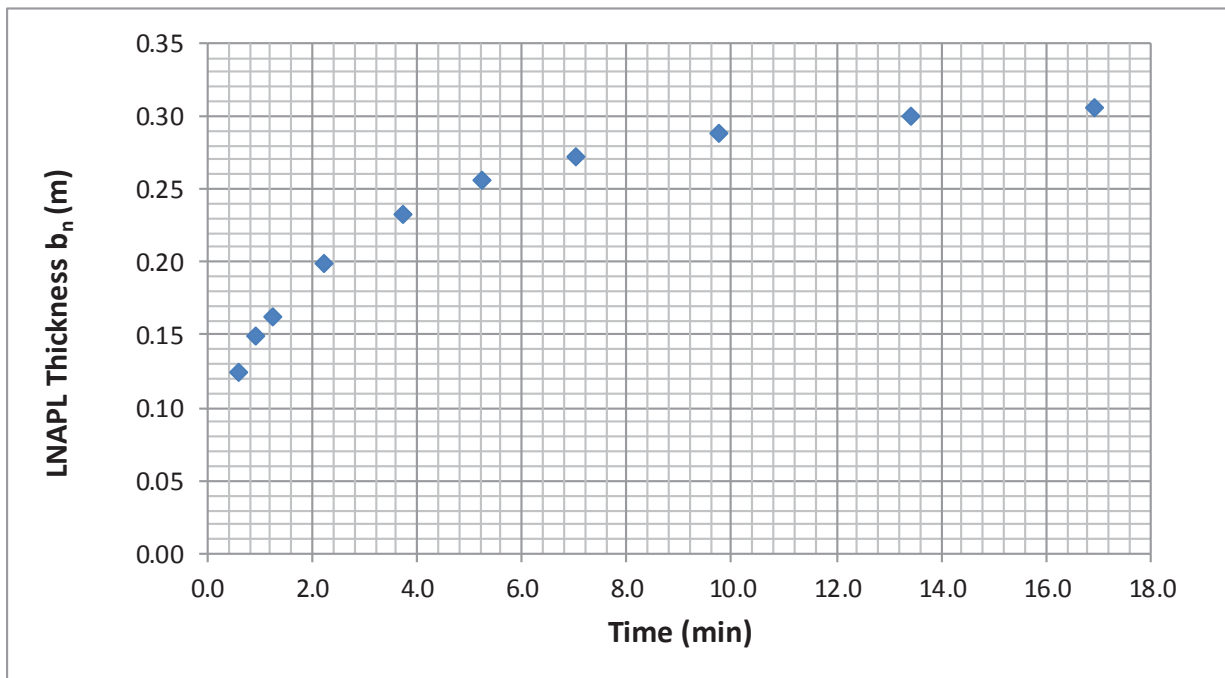


Figure 20. Time series of LNAPL thickness during baildown testing.

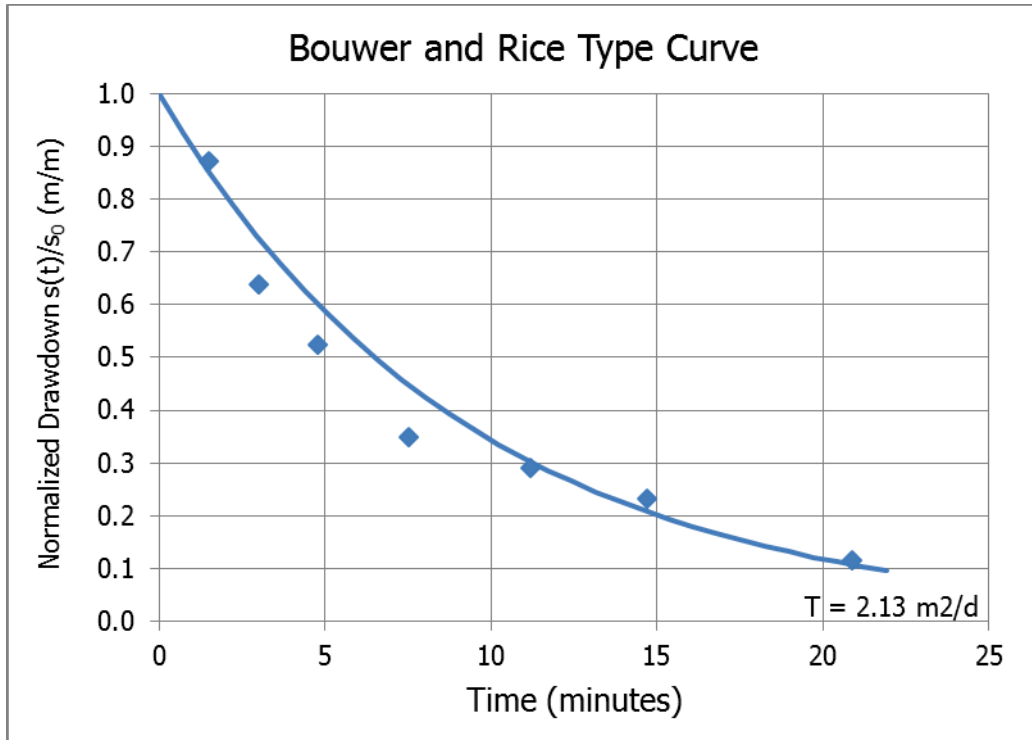


Figure 21. Bower and Rice type curve for the calculation of T_n .

PB29 19/05/2016

Well casing radius (m)	0.05
Well radius (m)	0.075
Top of screen (m)	2.15
Bottom of screen (m)	8.15
LNAPL baildown vol. (litre)	2.75

The bail-down test took place on 19/5/2016. 2.75 L NAPL and 1.05 L water were removed. The initial NAPL thickness before the test was 0.324 m. The thickness after the removal of the product was 0.10 m and the final thickness after 85 min was 0.321 m, which is almost 100 % recovery of the initial product thickness. The recovery period (>95%) was ~ 16 min. The elevation of water table (corrected) is constant, thus B&R method can be used. The B&R method showed 1.51 (m²/d) as Transmissivity value and the cut off time was 1.95 min.

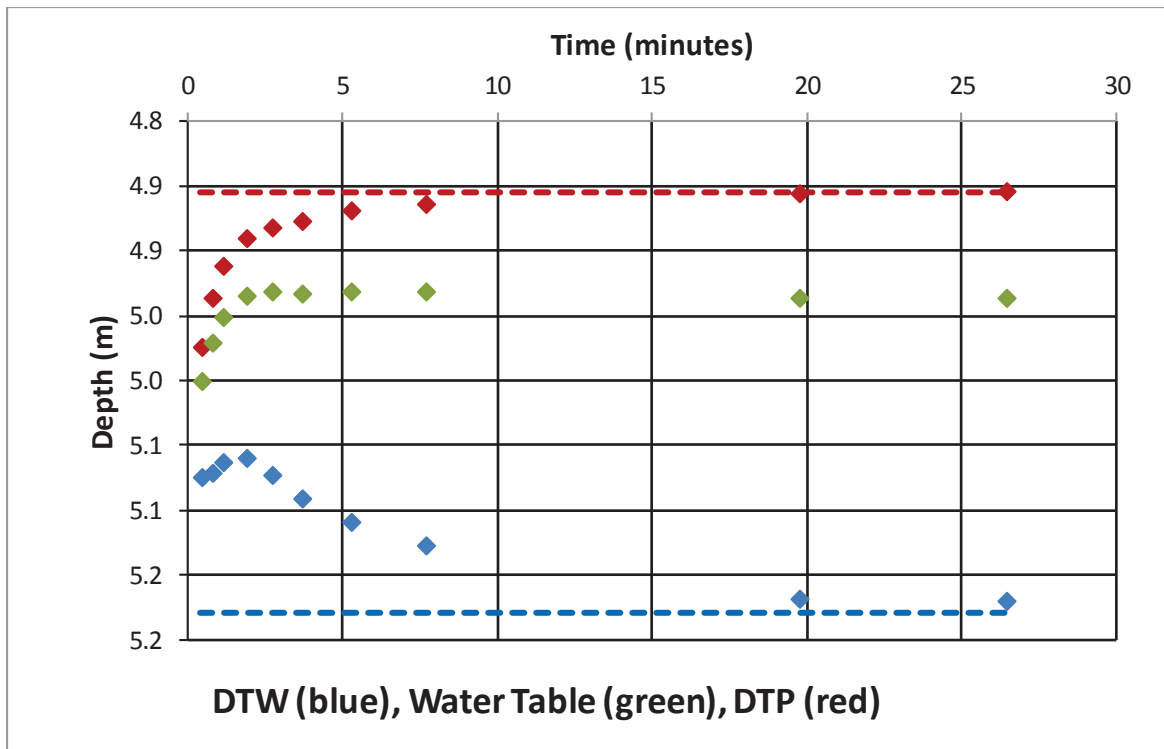


Figure 22. Time series of fluid levels during the baildown test.

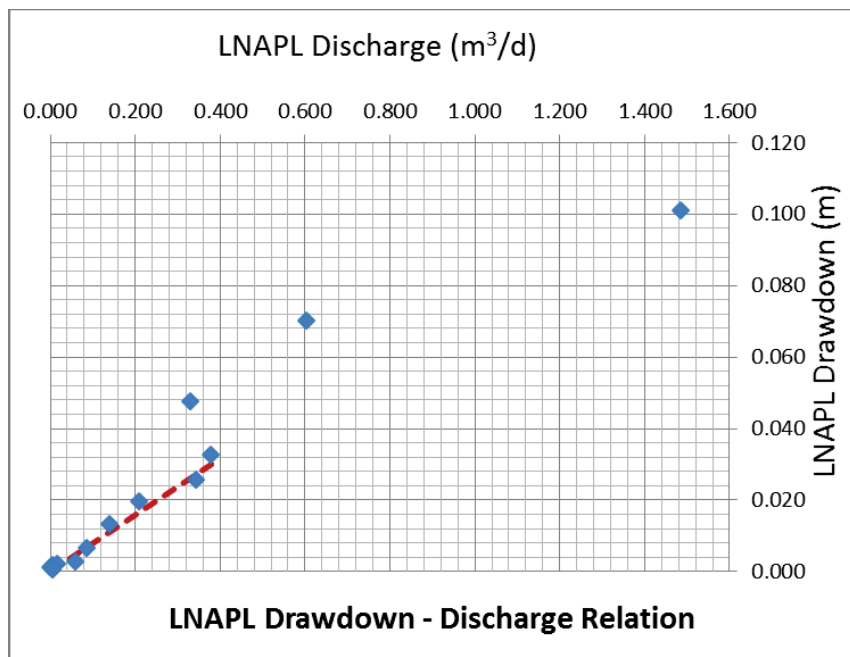


Figure 23. Pre-filtered data.

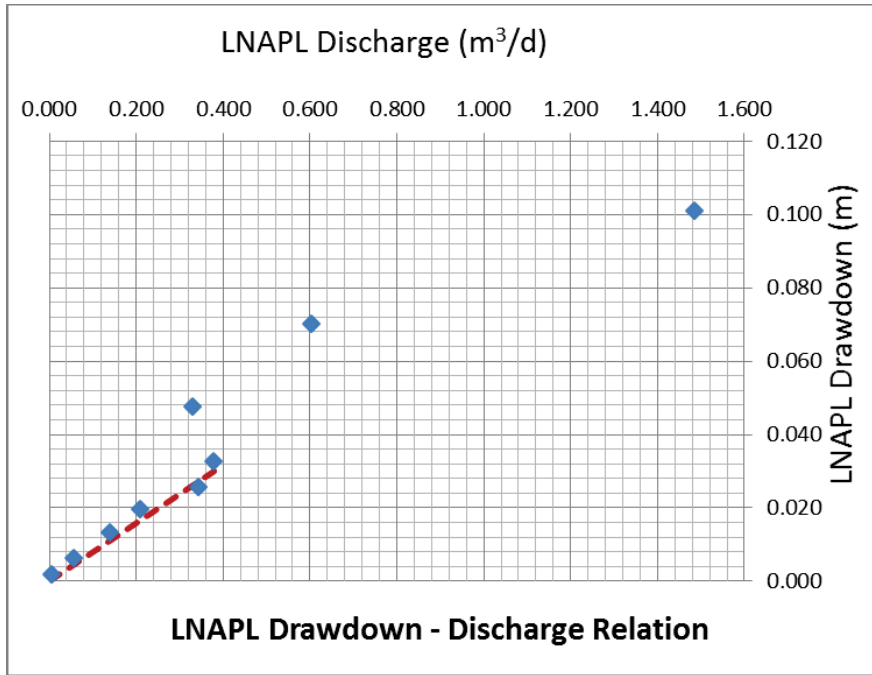


Figure 24. LNAPL drawdown-discharge relation during baildown testing (post-filtered data). After a drawdown adjustment of -0.0012 m.

The plot above shows that borehole recharge from the filter pack maybe is not significant (large discharge values at the beginning of the recovery, 1.5 m³/d). Moreover, figure depicts behaviour that maybe suggests unconfined LNAPL conditions because there is a continuously decreasing discharge with decreasing drawdown

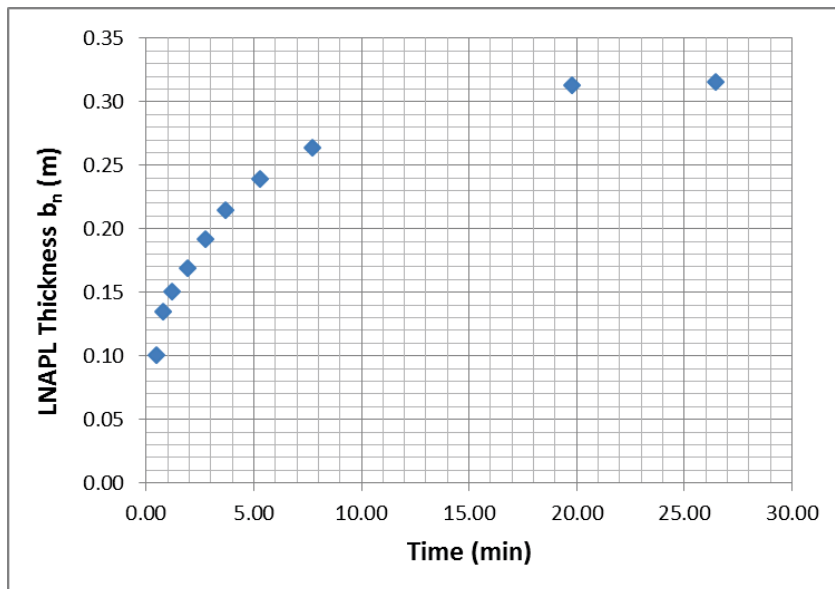


Figure 25. Time series of LNAPL thickness during baildown testing.

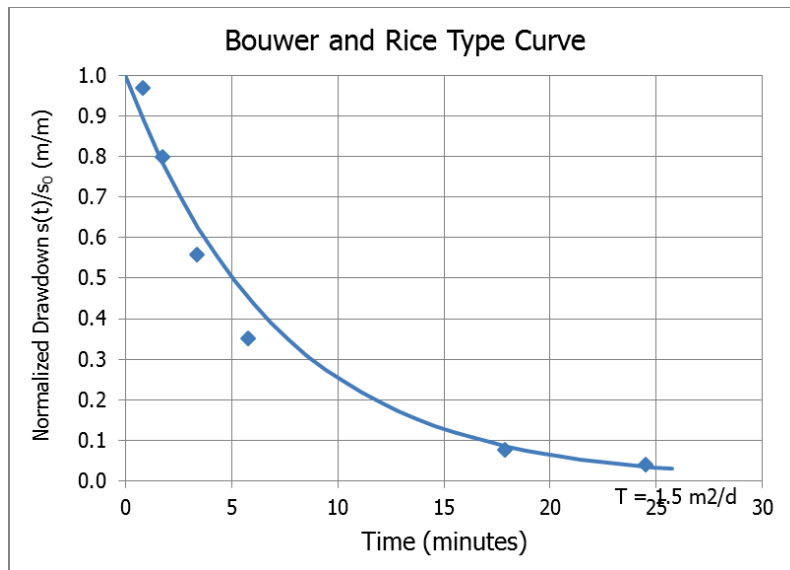


Figure 26. Bower and Rice type curve for the calculation of T_n .

PB29 1/06/2016

Well casing radius (m)	0.05
Well radius (m)	0.075
Top of screen (m)	2.15
Bottom of screen (m)	8.15
LNAPL baildown vol. (litre)	3.85

The bail-down test took place on 01/6/2016. 3.85 L NAPL and 2.25 L water were removed. The initial NAPL thickness before the test was 0.232 m. The thickness after the removal of the product was 0.162 m and the final thickness after 57 min was 0.232m, which is 100 % recovery of the initial product thickness. The elevation of water table (corrected) is constant, thus B&R method can be used. The B&R method showed 1.323 (m^2/d) as Transmissivity value and the cut off time was 1.6 min.

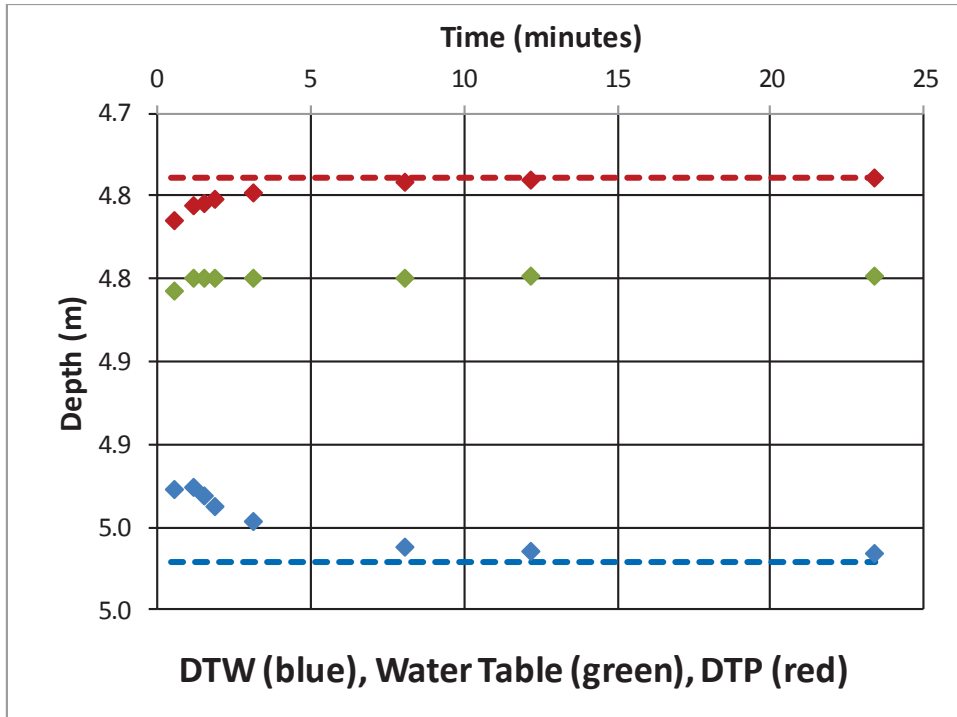


Figure 27. Time series of fluid levels during the baildown test.

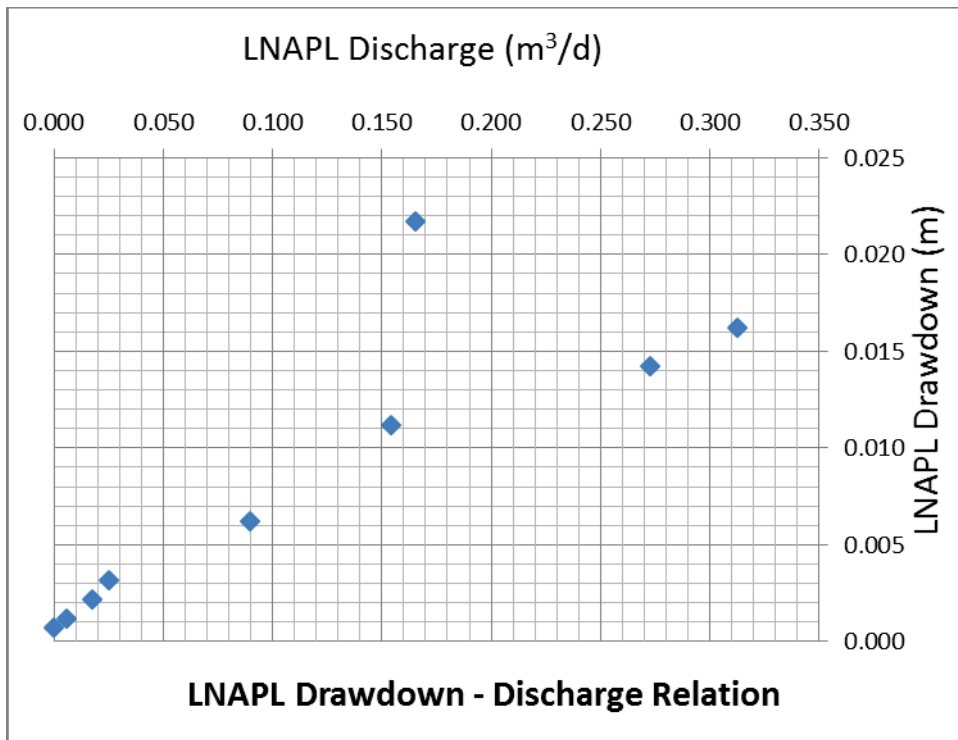


Figure 28. Pre-filtered data.

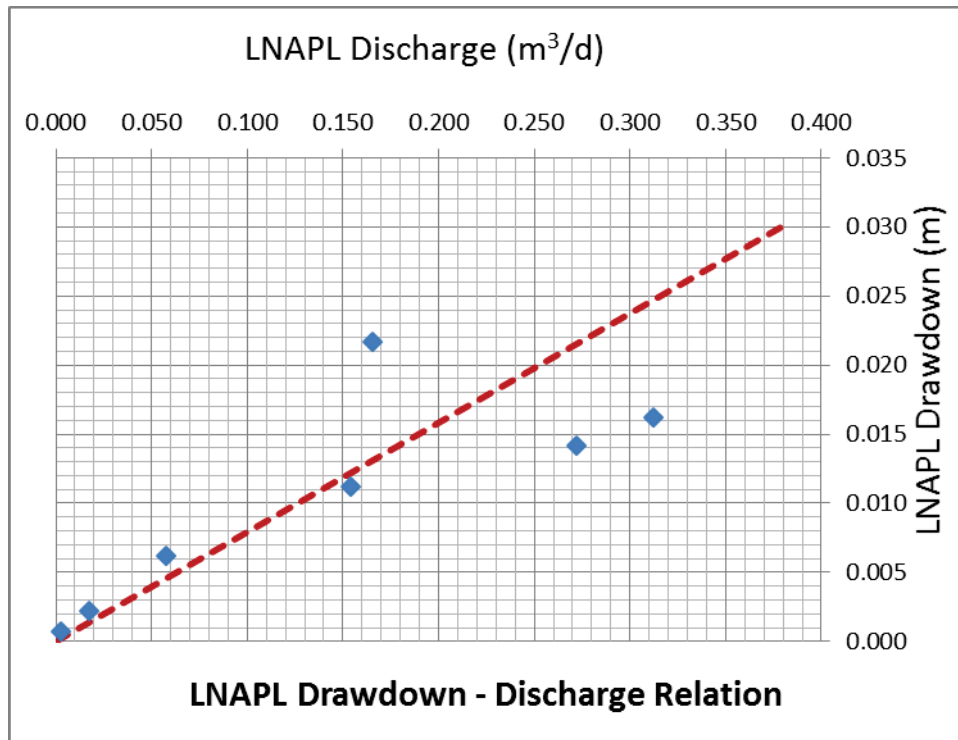


Figure 29. LNAPL drawdown- discharge relation during baildown testing (post-filtered data). After a drawdown adjustment of -0.0002 m.

The plot above shows that borehole recharge from the filter pack maybe is not significant (large discharge values at the beginning of the recovery, 0.32 m³/d). Moreover, figure depicts behaviour that maybe suggests unconfined LNAPL conditions because there is a continuously decreasing discharge with decreasing drawdown

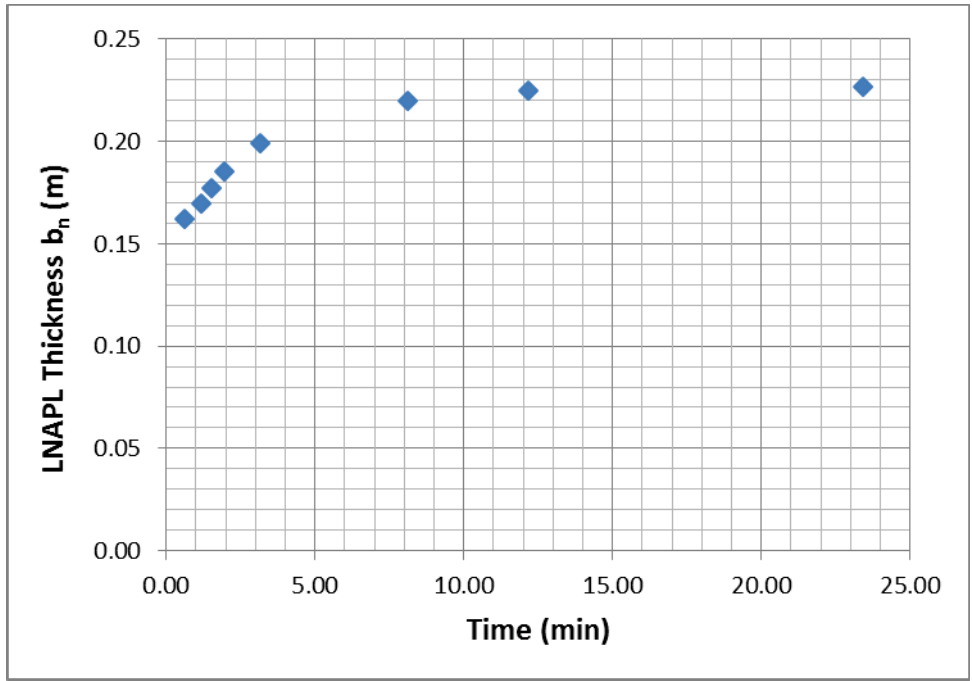


Figure 30. Time series of LNAPL thickness during baildown testing.

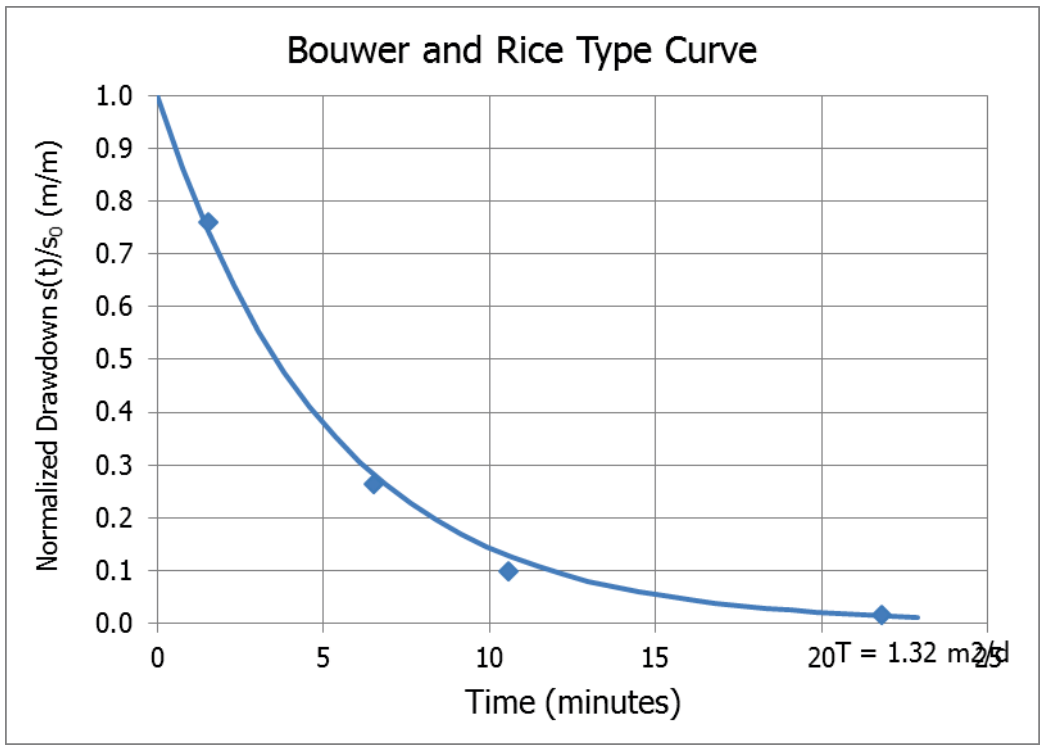


Figure 31. Bouwer and Rice type curve for the calculation of T_n .

Well casing radius (m)	0.05
Well radius (m)	0.075
Top of screen (m)	2.15
Bottom of screen (m)	8.15
LNAPL baildown vol. (litre)	4.10

The bail-down test took place on 09/6/2016. 4.1 L NAPL and 0.9 L water were removed. The initial NAPL thickness before the test was 0.213 m. The thickness after the removal of the product was 0.145 m and the final thickness after 77 min was 0.207 m, which is almost 100 % recovery of the initial product thickness. The recovery period (>95%) was ~ 14 min. The elevation of water table (corrected) is constant, thus B&R method can be used. The B&R method showed 0.699 (m²/d) as Transmissivity value and the cut off time was 2.34 min.

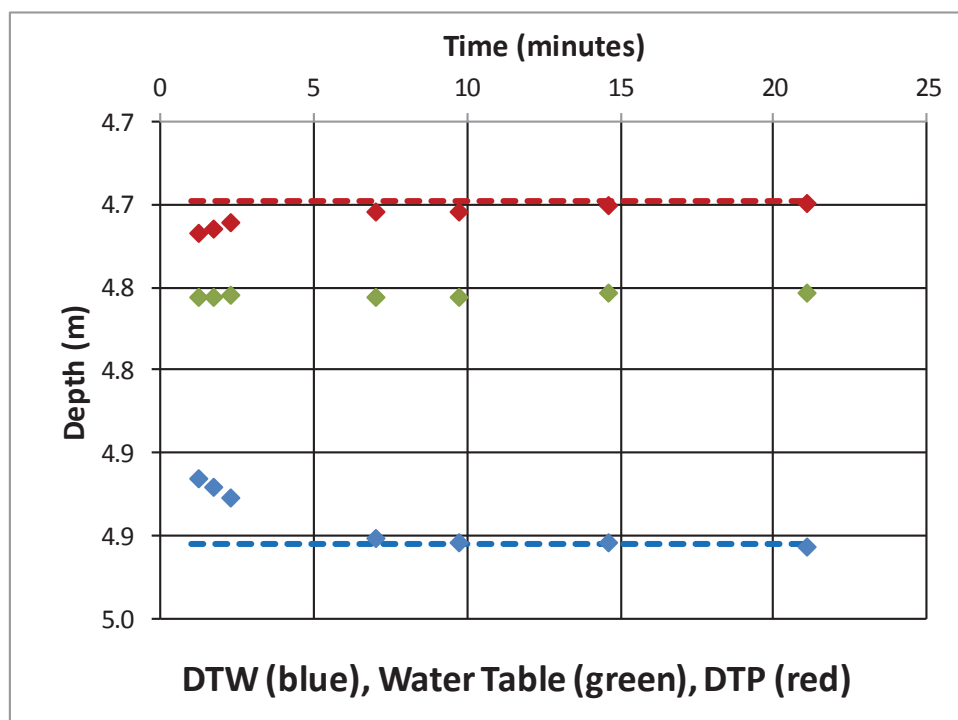


Figure 32. Time series of fluid levels during the baildown test.

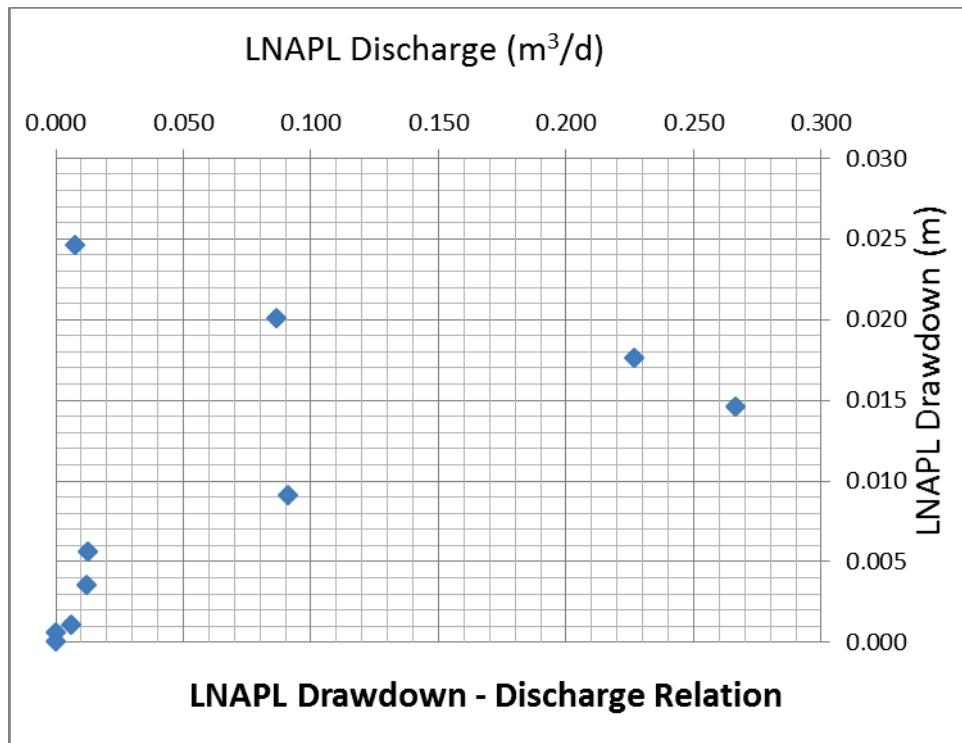


Figure 33. Pre-filtered data.

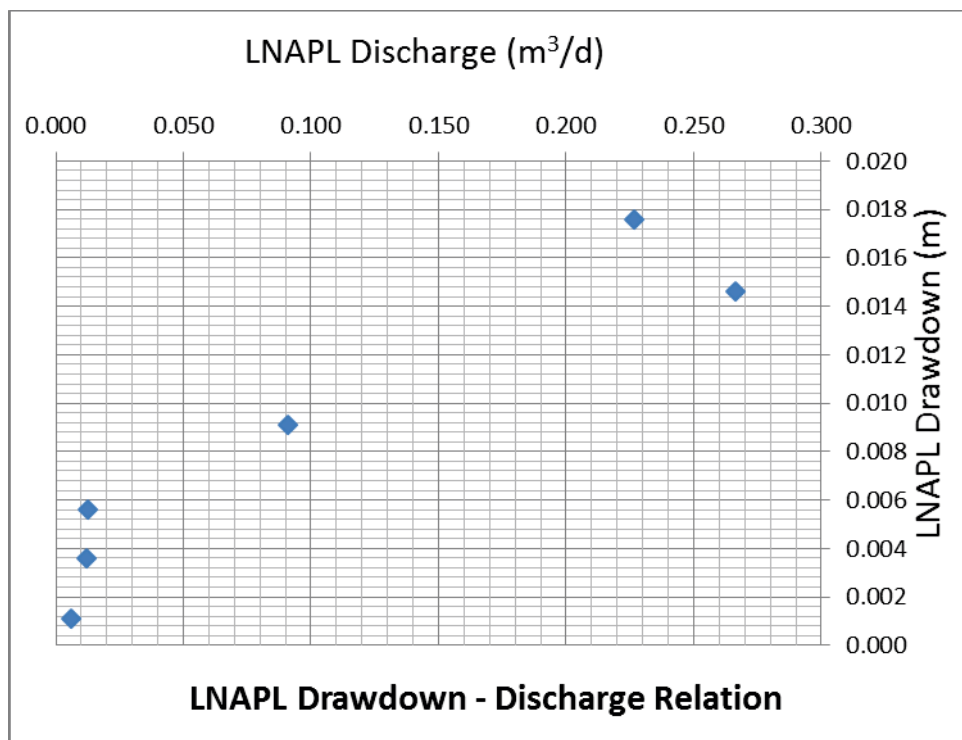


Figure 34. LNAPL drawdown- discharge relation during baildown testing (post-filtered data). After a drawdown adjustment of 0.0004 m.

The plot above shows that borehole recharge from the filter pack maybe is not significant (large discharge values at the beginning of the recovery, $0.26 \text{ m}^3/\text{d}$). Moreover, figure depicts behaviour that maybe suggests unconfined LNAPL conditions because there is a continuously decreasing discharge with decreasing drawdown.

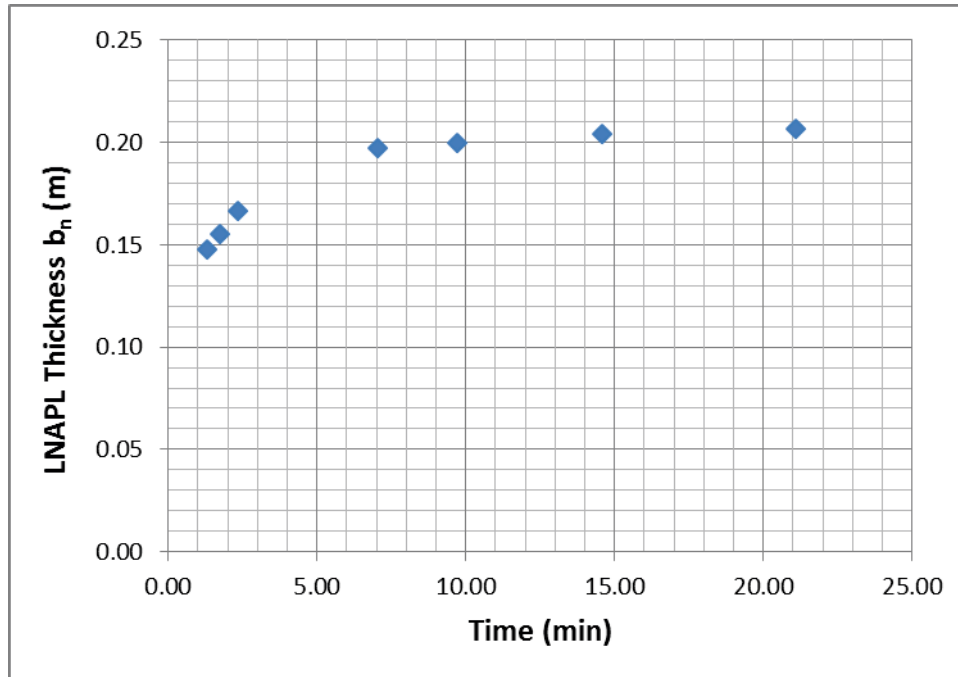


Figure 35. Time series of LNAPL thickness during baildown testing.

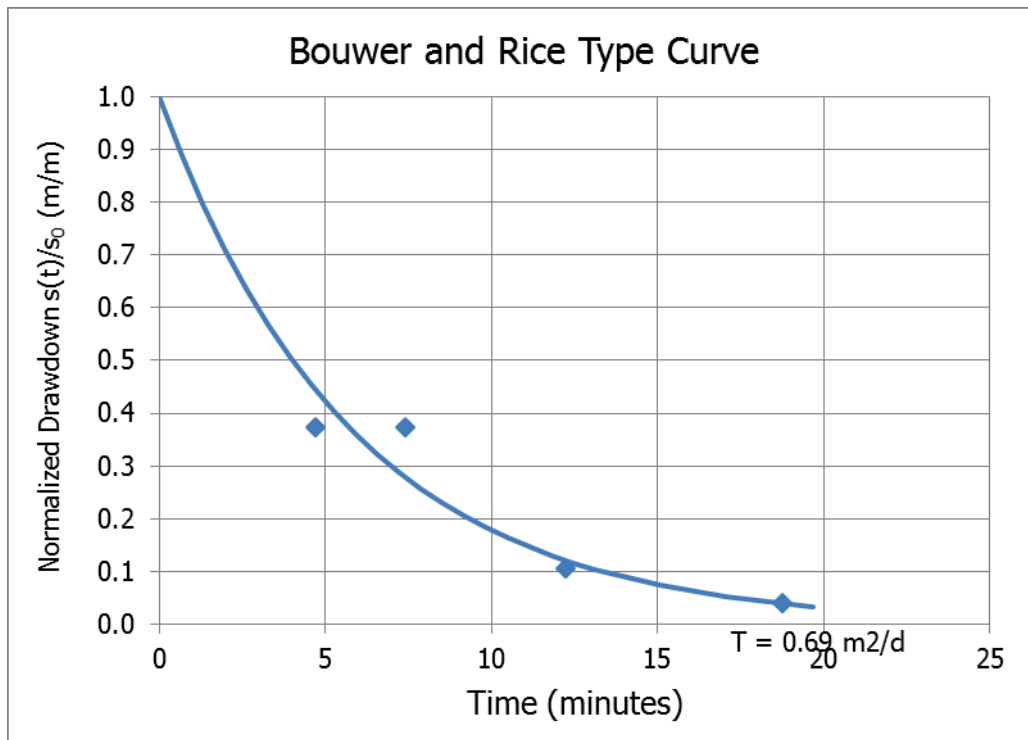


Figure 36. Bouwer and Rice type curve for the calculation of T_n .

PB29 15/06/2016

Well casing radius (m)	0.05
Well radius (m)	0.075
Top of screen (m)	2.15
Bottom of screen (m)	8.15
LNAPL baildown vol. (litre)	7.70

The bail-down test took place on 15/6/2016. 7.7 L NAPL and 1.5 L water were removed. The initial NAPL thickness before the test was 0.177 m. The thickness after the removal of the product was 0.03 m and the final thickness after 47 min was 0.161 m, which is 91 %

recovery of the initial product thickness. The elevation of water table (corrected) is constant, thus B&R method can be used. The B&R method showed 0.372 (m²/d) as Transmissivity value and the cut off time was 6 min.

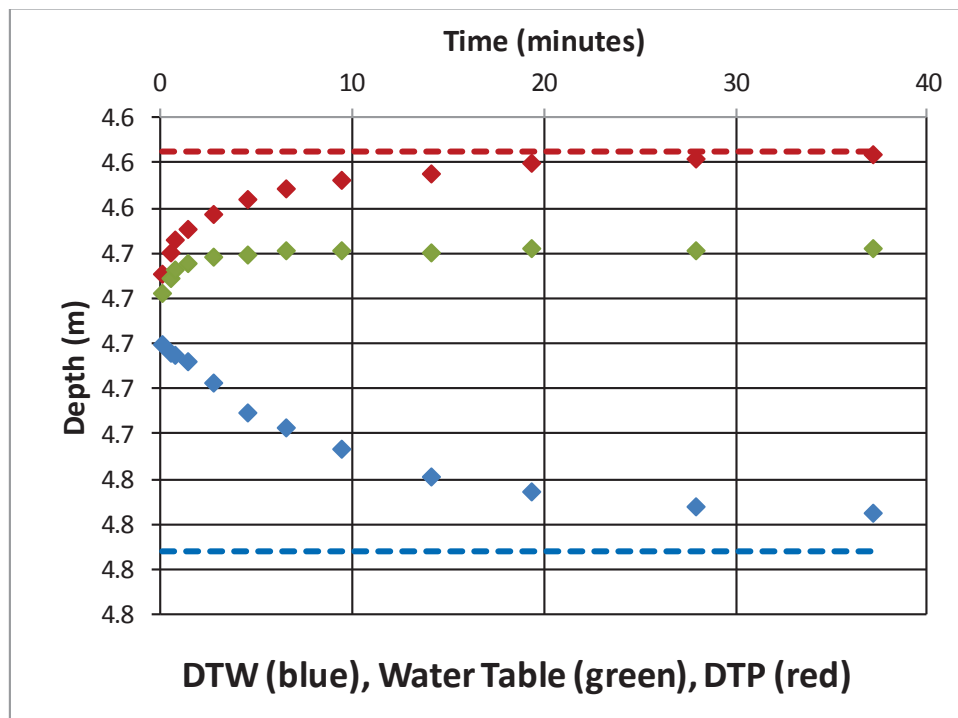


Figure 37. Time series of fluid levels during the baildown test.

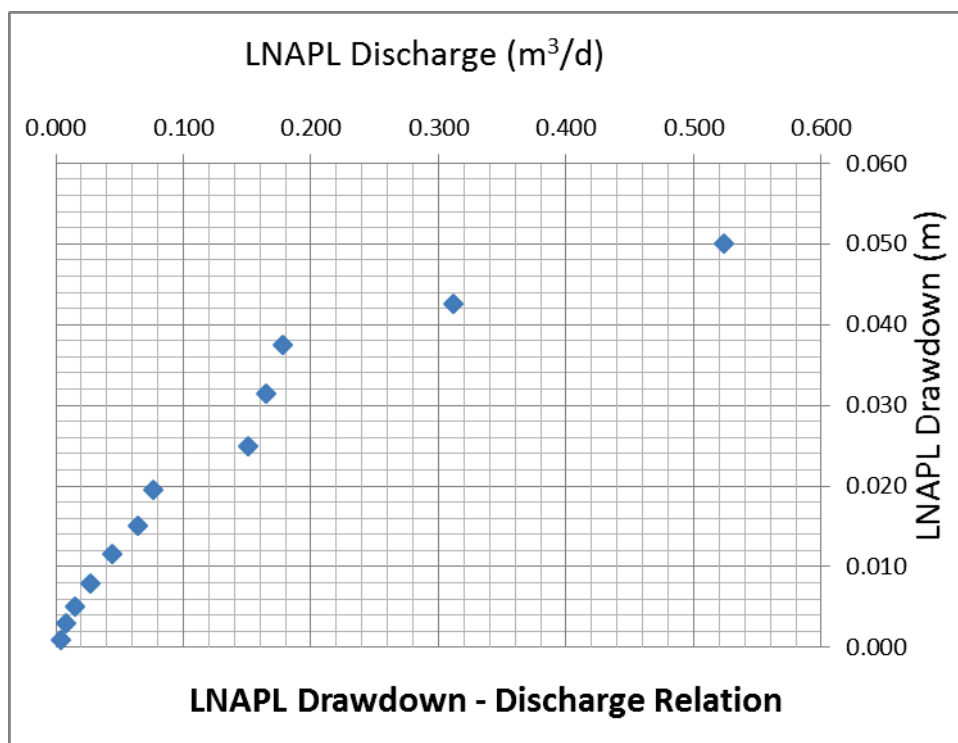


Figure 38. Pre-filtered data.

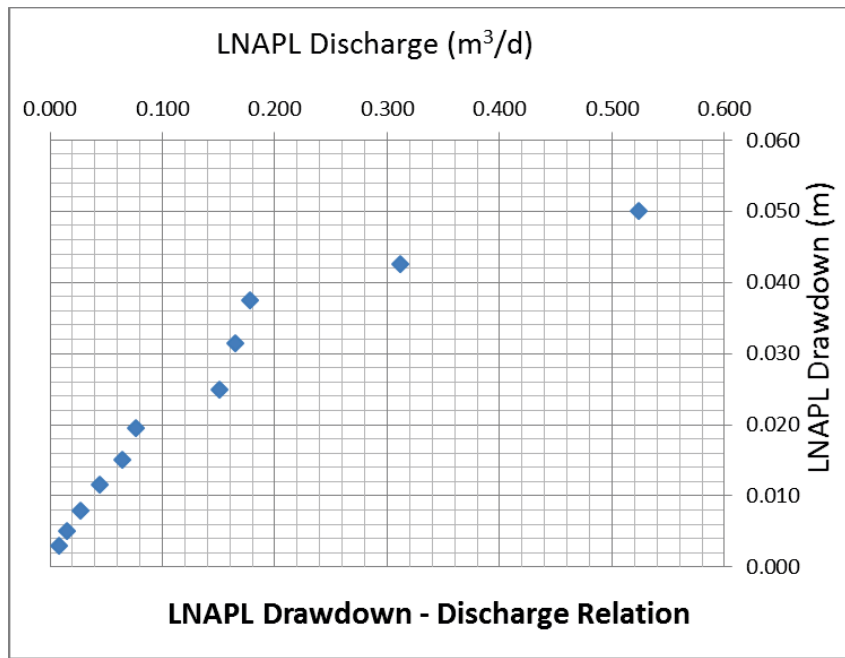


Figure 39. LNAPL drawdown- discharge relation during baildown testing (post-filtered data).

The plot above shows that borehole recharge from the filter pack maybe is not significant (large discharge values at the beginning of the recovery, 0.51 m³/d). Moreover, figure depicts behaviour that maybe suggests unconfined LNAPL conditions because there is a continuously decreasing discharge with decreasing drawdown

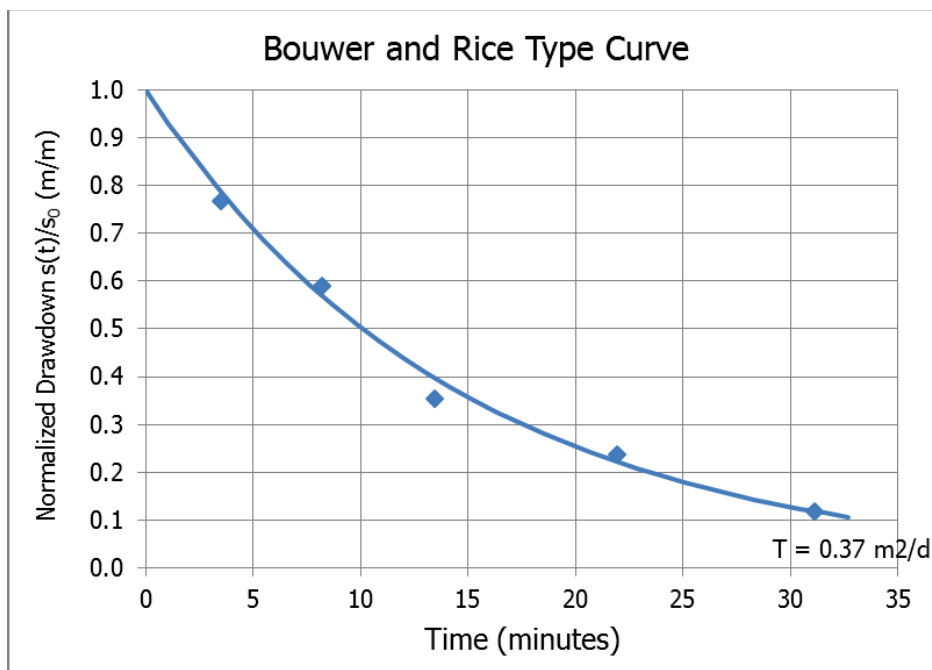


Figure 40. Bower and Rice type curve for the calculation of T_n .

PB27a 6/05/2015

Well casing radius (m)	0.05
Well radius (m)	0.075
Top of screen (m)	2
Bottom of screen (m)	7.6
LNAPL baildown vol. (litre)	0.71
Water removed (litre)	0

Two different baildown tests took place in this specific well on 6 of May 2015. During the first test 710 ml of LNAPL were removed. The initial DTP was 4.652 m whereas the final measurement of the DTP after 54 min was 4.649 that is 3 mm negative difference thus a drawdown adjustment was applied. The product thickness after 54 min was the same with the initial thus it can be assumed that the initial measurements were no under equilibrium.

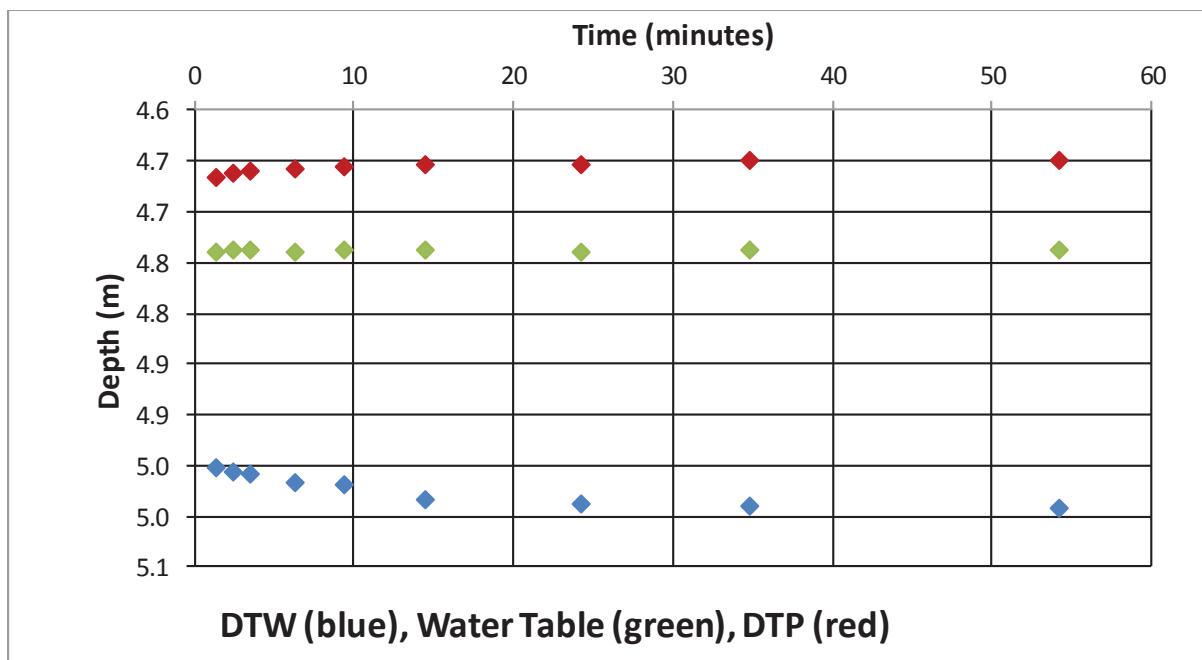


Figure 41. Time series of fluid levels during the baildown test.

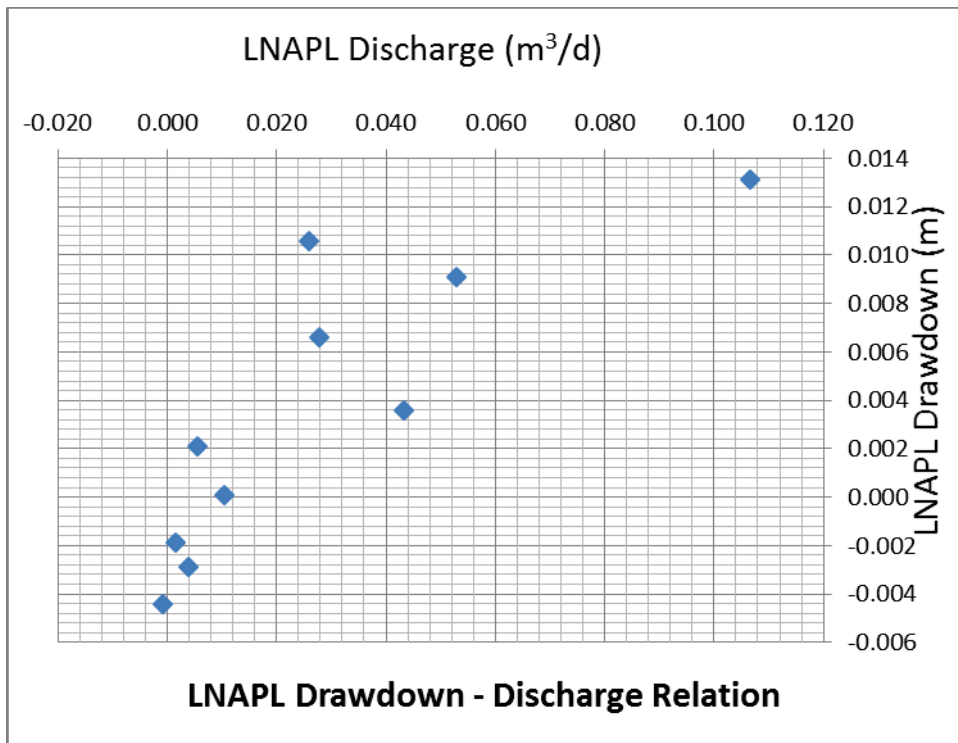


Figure 42. Pre-filtered data.

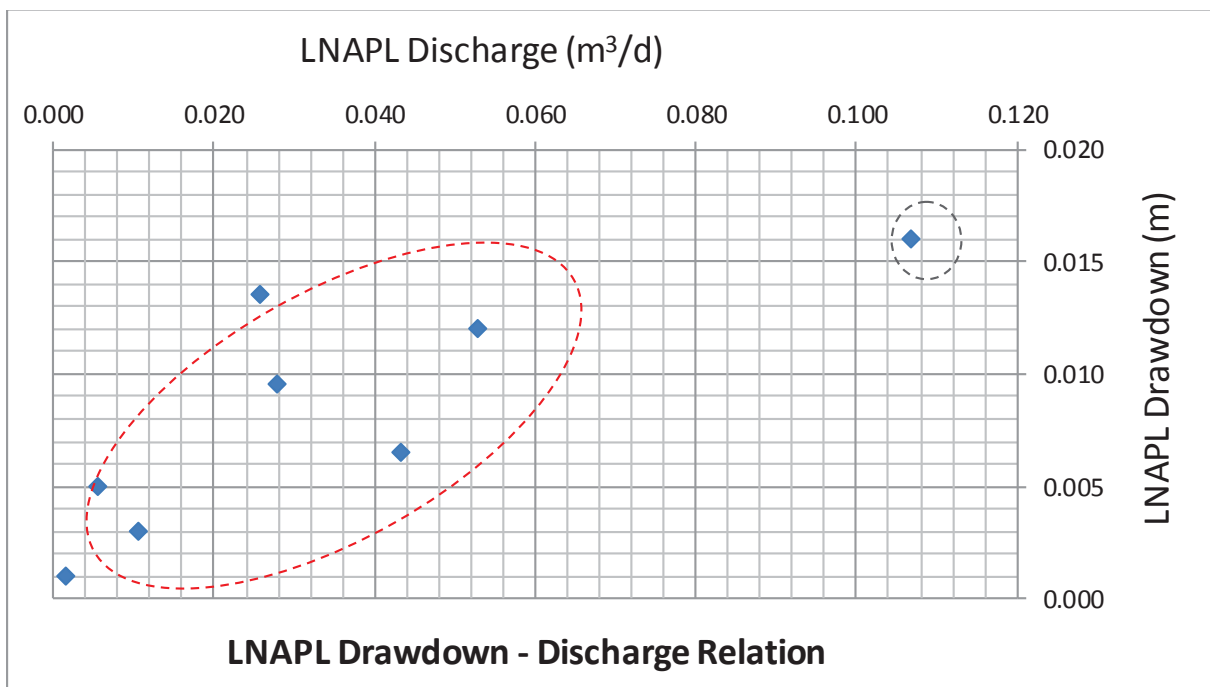


Figure 43. LNAPL drawdown-discharge relation during baildown testing (post-filtered data). After a drawdown adjustment of -0.0011 m

The figure above is after drawdown correction has been applied. This plot shows an expanded view of the data after the drawdown correction has been applied. The specific plot shows that significant borehole recharge from the filter pack is not an issue (black dashed circle). Moreover, figure depicts behaviour that suggests unconfined (red circle) LNAPL conditions because there is a decreasing LNAPL discharge with decreasing LNAPL drawdown.

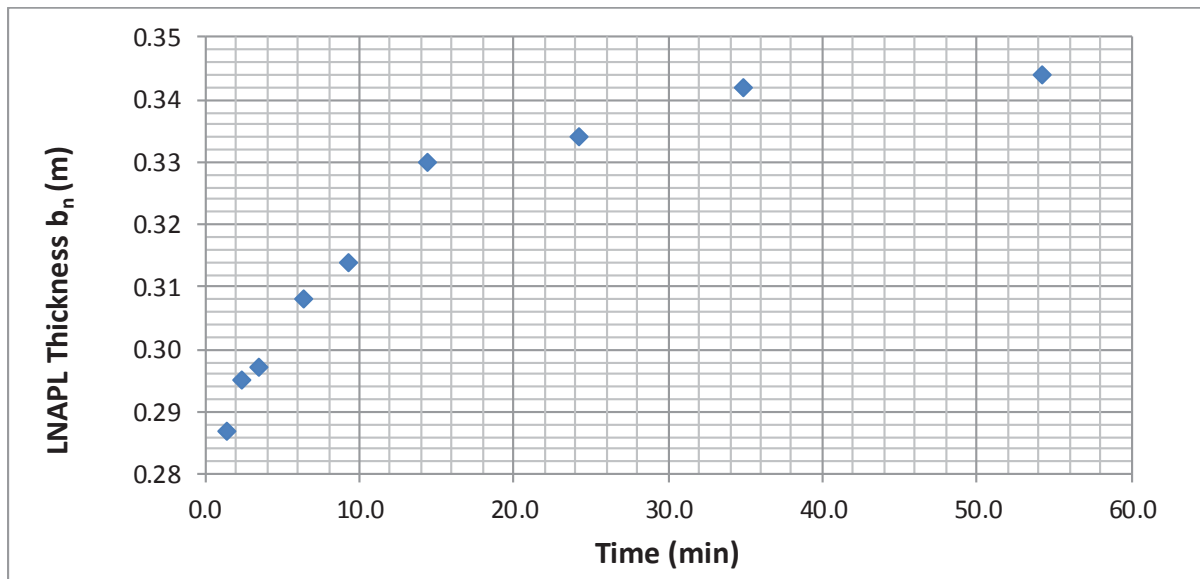


Figure 44. Time series of LNAPL thickness during baildown testing. The product thickness after 60 min of the last measurement (54th min) stayed stabilised.

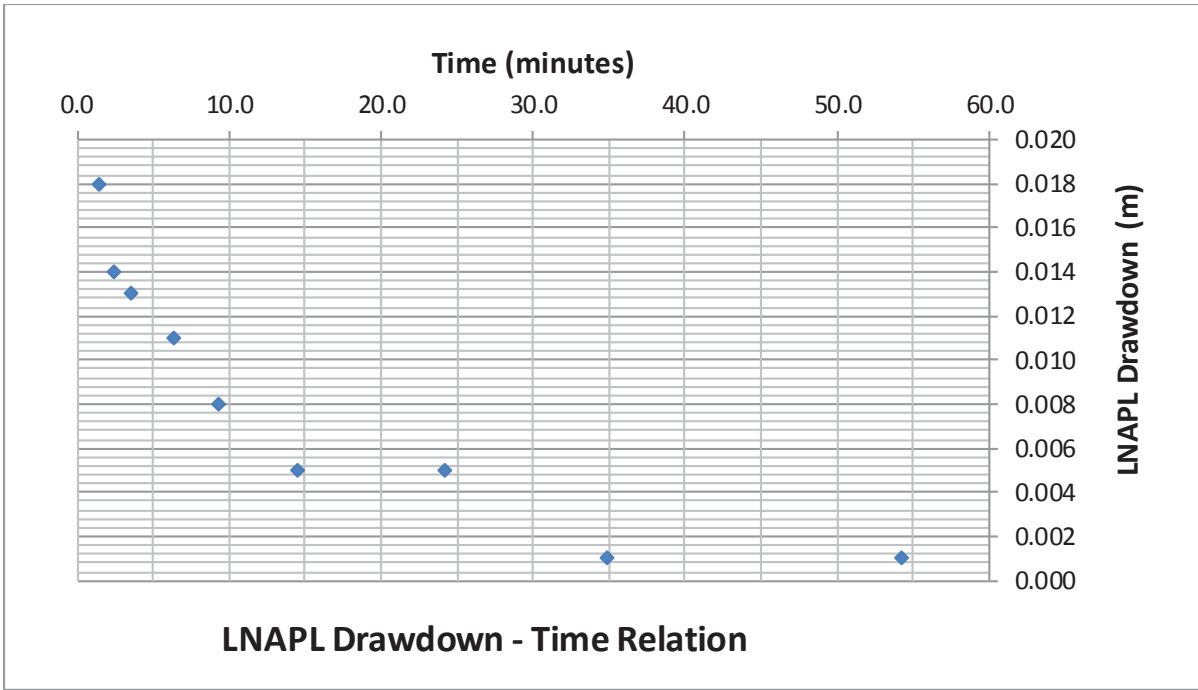


Figure 45. Time series of LNAPL drawdown during baildown testing

The figure above is after LNAPL drawdown correction has been applied and shows that the drawdown of the LNAPL is decreasing as time passes. Moreover, the elevation of water table (corrected) is constant, thus B&R method has to be used. The B&R method showed 0.91 (m^2/d) as Transmissivity value.

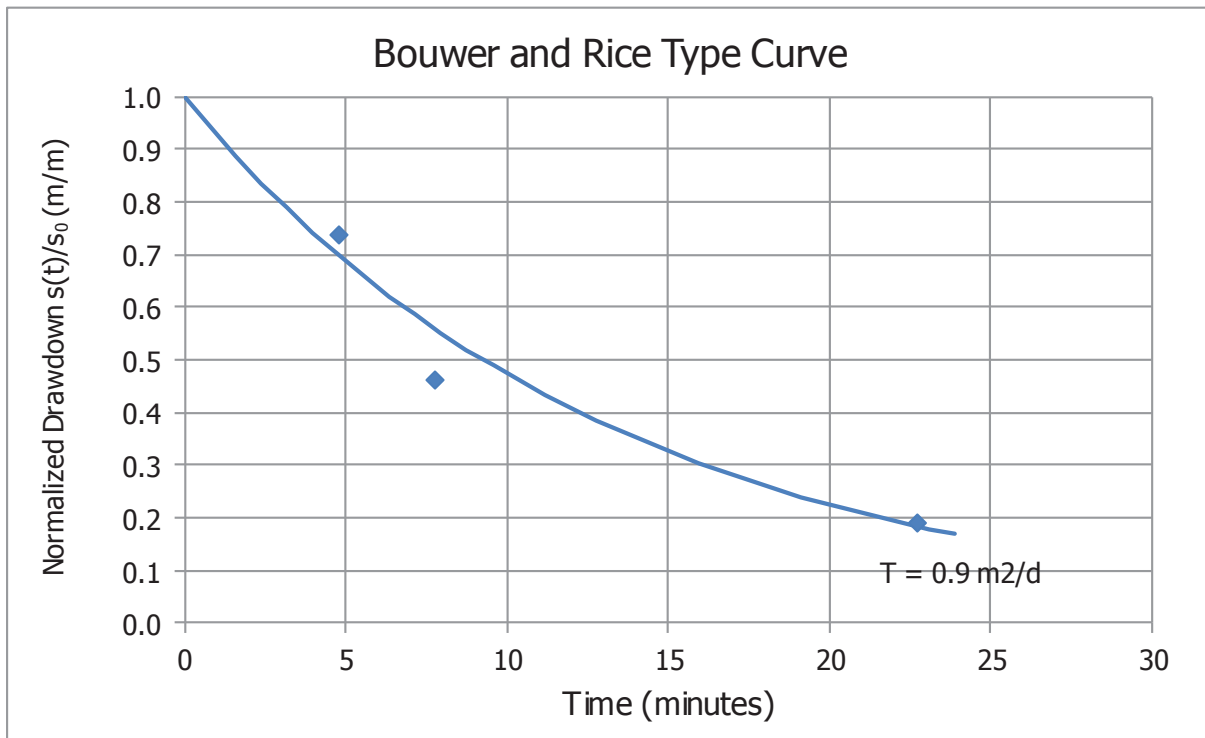


Figure 46. Bower and Rice type curve for the calculation of T_n .

PB27b 6/05/2015

Well casing radius (m)	0.05
Well radius (m)	0.075
Top of screen (m)	2
Bottom of screen (m)	7.6
LNAPL baildown vol. (litre)	1.6

The baildown test took place on 6/5/2015. 1.6 L NAPL and 0.37 L water were removed. The initial NAPL thickness was 0.35 m and the final thickness after 73 min was 0.35 m, which is 100 % recovery of the initial product thickness. The recovery period was ~ 50 min. The elevation of water table (corrected) is constant (after the cut off time which is 2.1 min), thus B&R method has to be used. The B&R method showed 0.96(m²/d) as Transmissivity value.

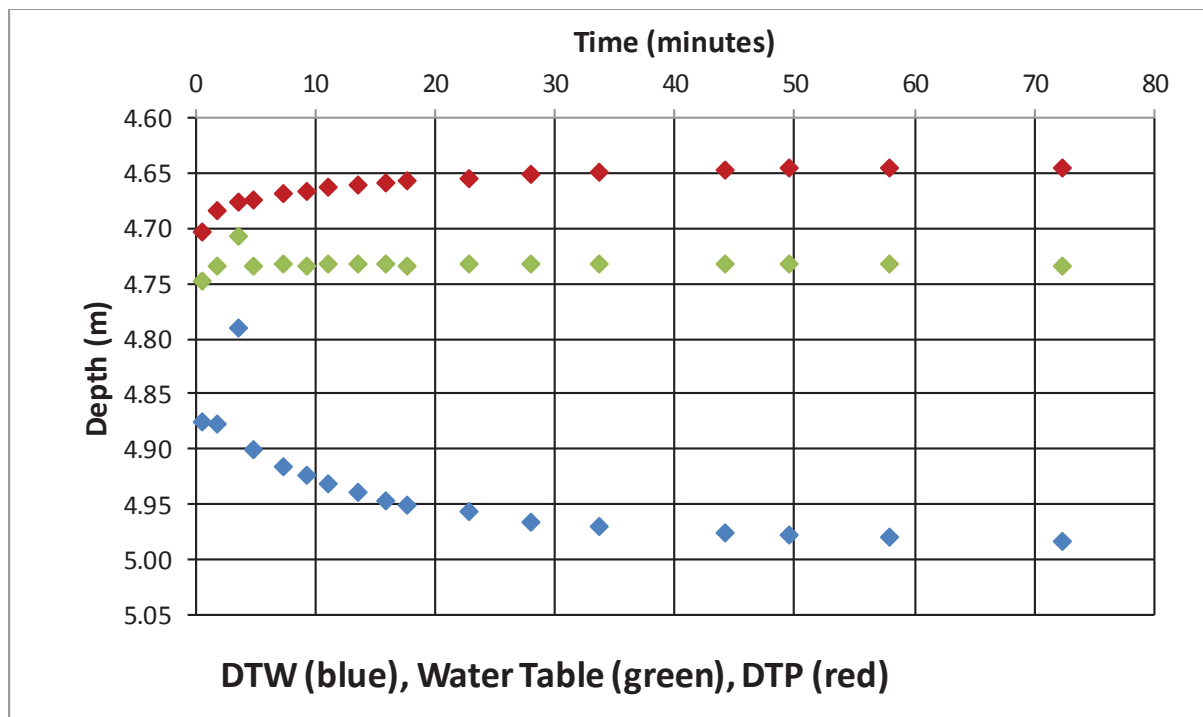


Figure 47. Time series of fluid levels during the baildown test.

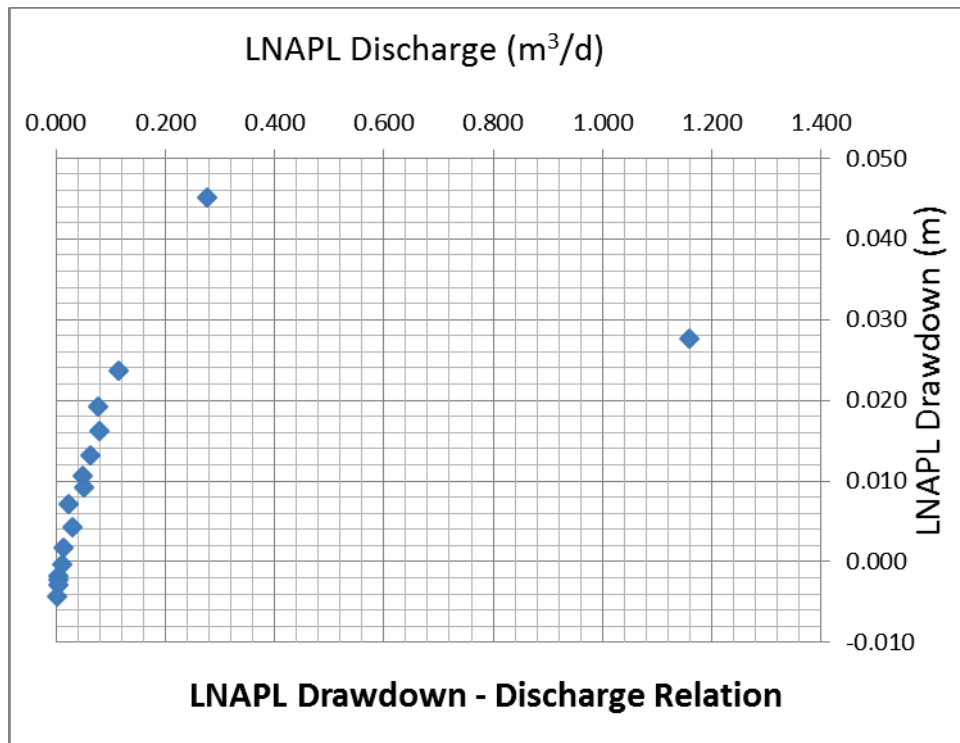


Figure 48. Pre-filtered data.

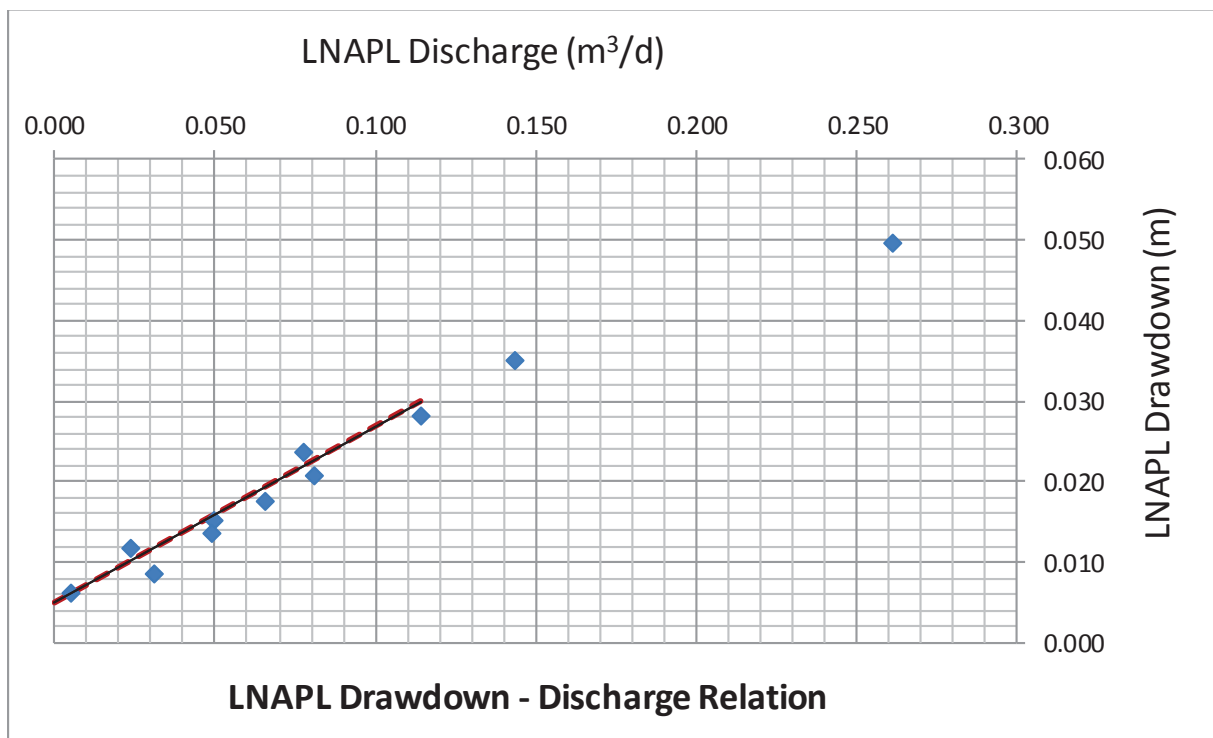


Figure 49. LNAPL drawdown- discharge relation during baildown testing. Before drawdown adjustment.

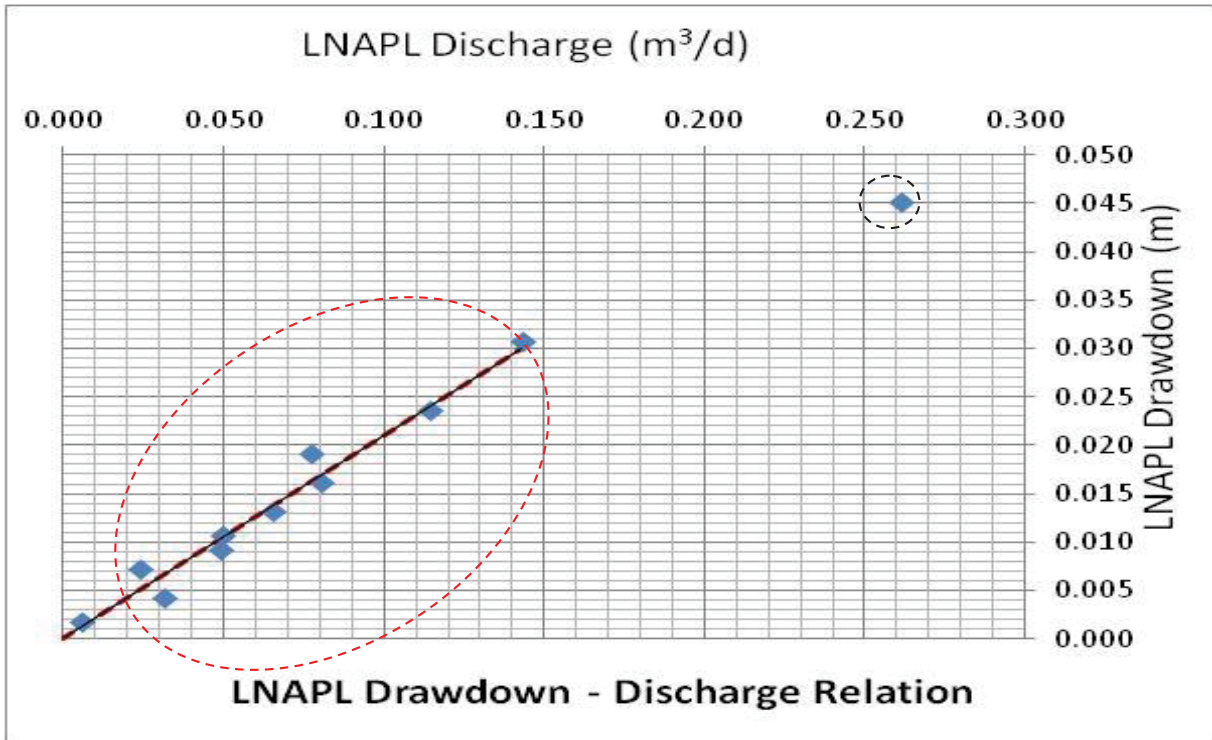


Figure 50. LNAPL drawdown-discharge relation during baildown testing (post-filtered data). After a drawdown adjustment of 0.0043 m.

The plot above shows that borehole recharge from the filter pack is not significant (large discharge values at the beginning of the recovery). Moreover, figure depicts behaviour that suggests unconfined LNAPL conditions because we can see continuously decreasing discharge with decreasing drawdown.

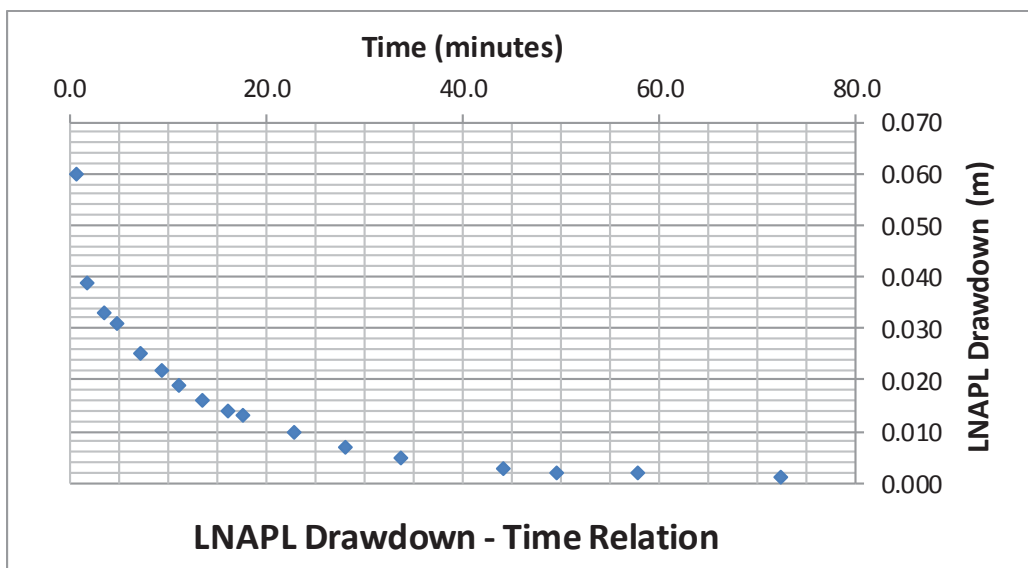


Figure 51. Time series of LNAPL drawdown during baildown testing

The figure above shows that the drawdown of the LNAPL is decreasing as time passes. The final value of the DTP was 4.646 m (where the value of discharge was also zero) and the initial value was 4.645m, which is no different. Such behaviour suggests that the formation and the wellbore LNAPL fluids were initially in equilibrium. Moreover, this final DTP value (which was equal to the initial value) is the same with the final value of the previous test which means that the first test was not under equilibrium conditions.

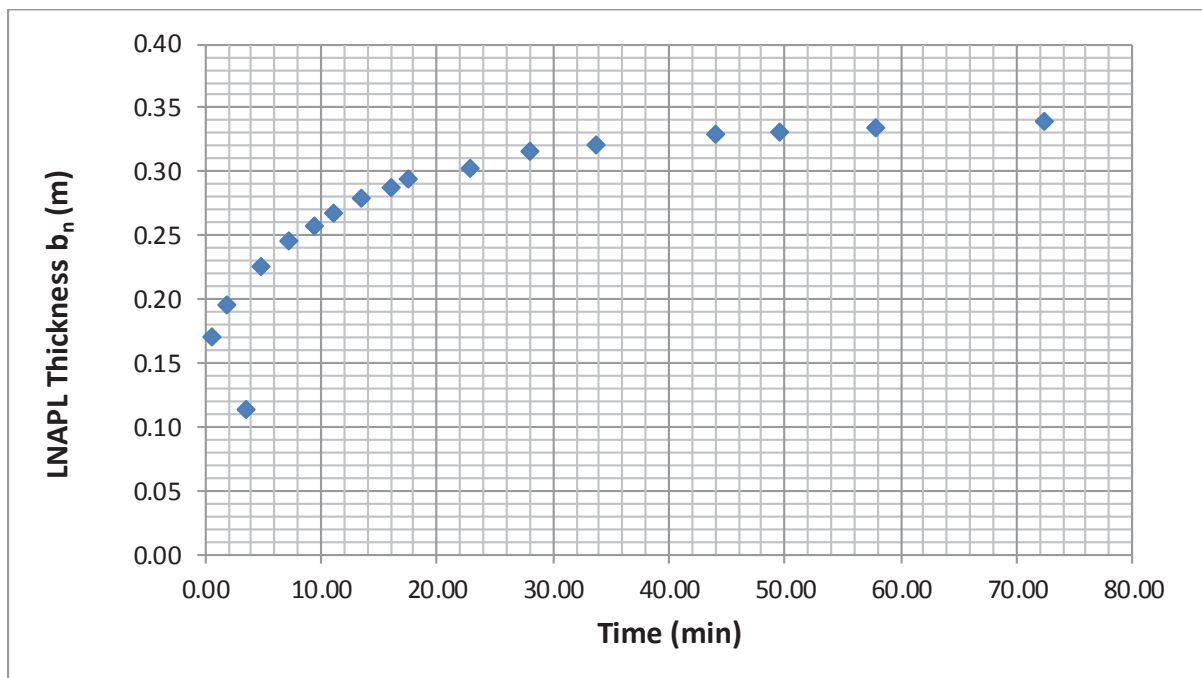


Figure 52. Time series of LNAPL thickness during baildown testing (increasing LNAPL thickness with time).

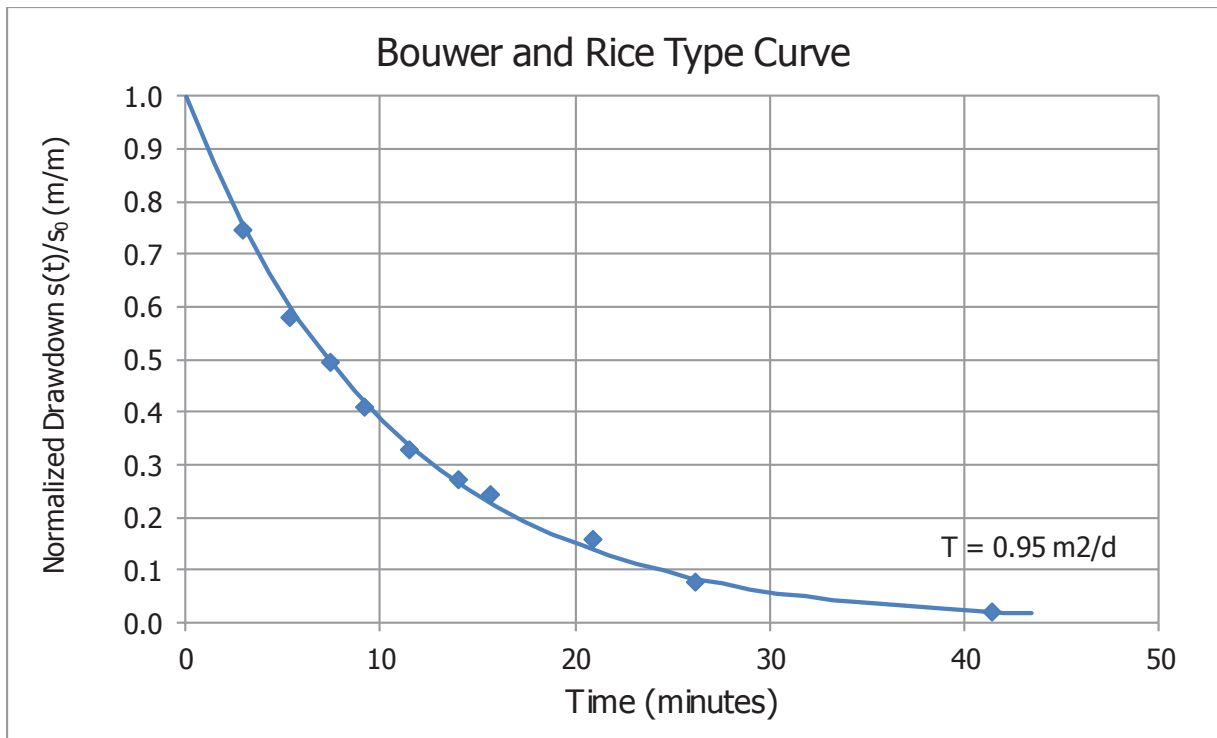


Figure 53. Bower and Rice type curve for the calculation of T_n .

PB27 8/07/2015

Well casing radius (m)	0.05
Well radius (m)	0.075
Top of screen (m)	2
Bottom of screen (m)	7.6
LNAPL baildown vol. (litre)	1.7

The baildown test took place on 8/7/2015. 1.65 L NAPL and 0.05 L water were removed. The initial NAPL thickness before the test was 0.36 m. The thickness after the removal of the product was 0.17m and the final thickness after 56min was 0.35 m, which is almost 100 % recovery of the initial product thickness. The recovery period was ~ 56 min. The elevation of water table (corrected) is constant (after the cut off time which is 3 min), thus B&R method can be used. The B&R method showed 1.33 (m^2/d) as Transmissivity value.

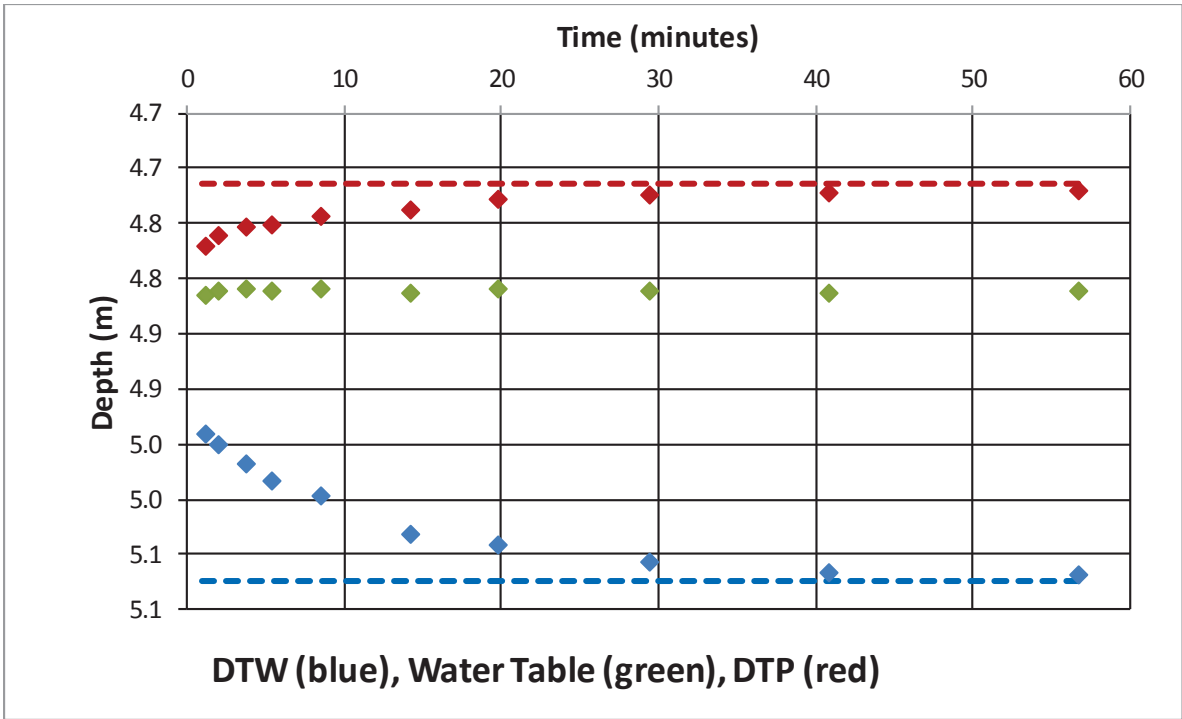


Figure 54. Time series of fluid levels during the baildown test.

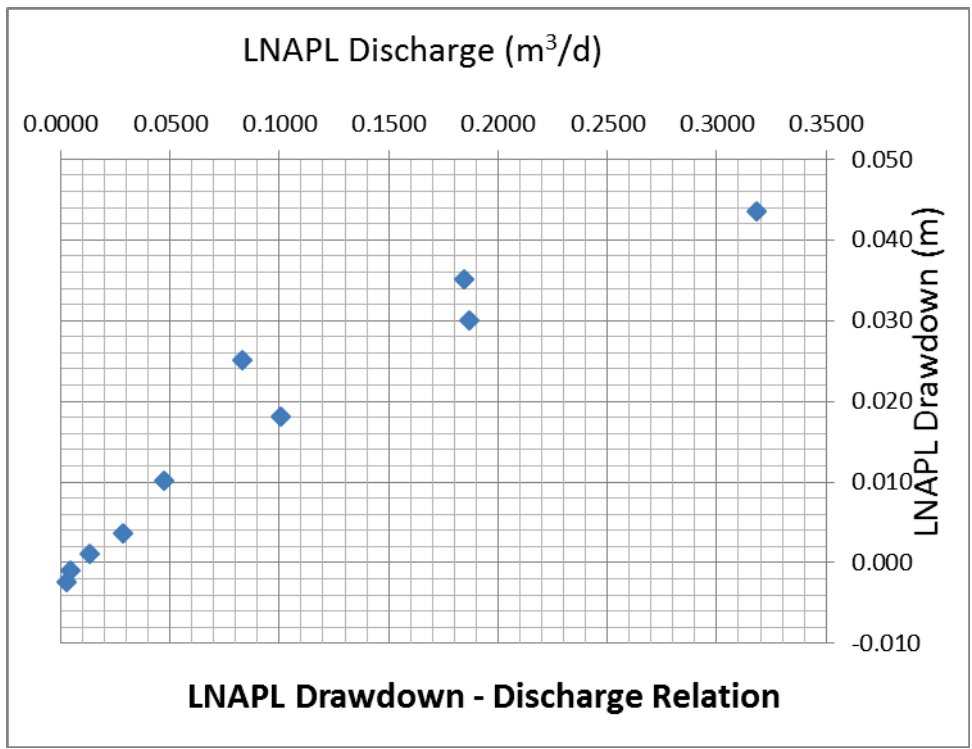


Figure 55. Pre-filtered data.

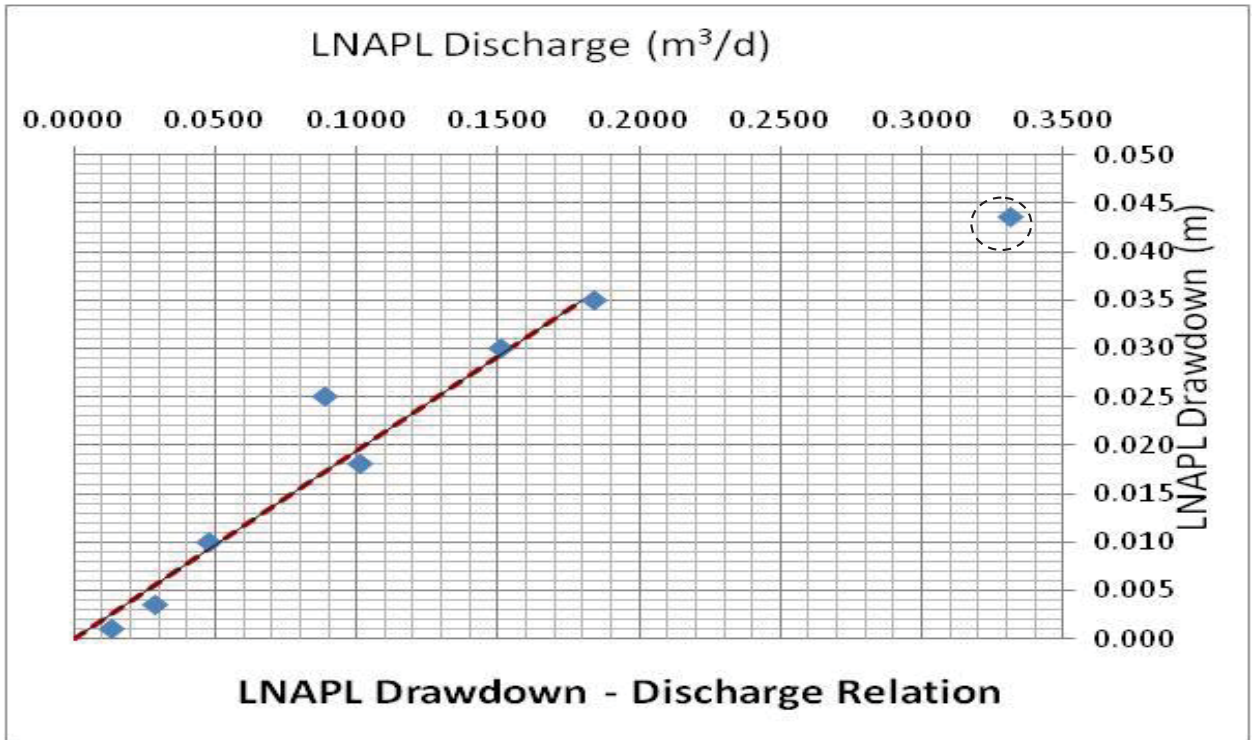


Figure 56. LNAPL drawdown- discharge relation during baildown testing (post-filtered data). After a drawdown adjustment of 0.0084 m.

The plot above shows that borehole recharge from the filter pack maybe is not significant (large discharge values at the beginning of the recovery, 0.33 m³/d). Moreover, figure depicts behaviour that suggests unconfined LNAPL conditions because we can see continuously decreasing discharge with decreasing drawdown.

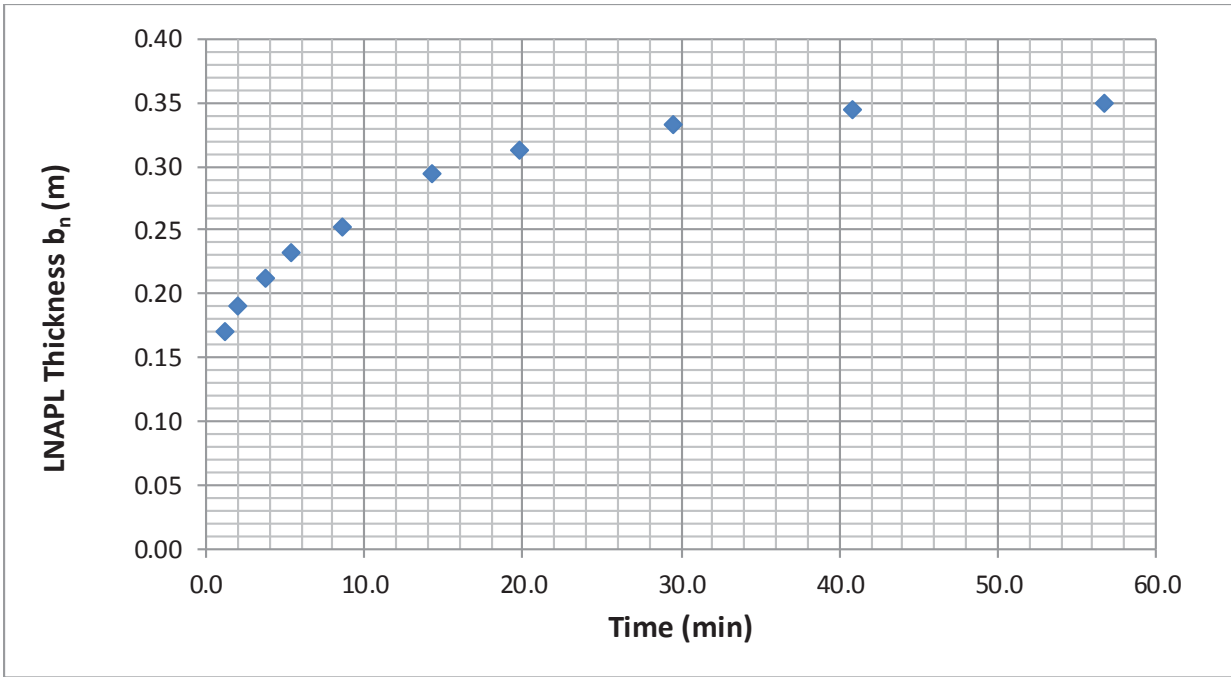


Figure 57. Time series of LNAPL thickness during baildown testing.

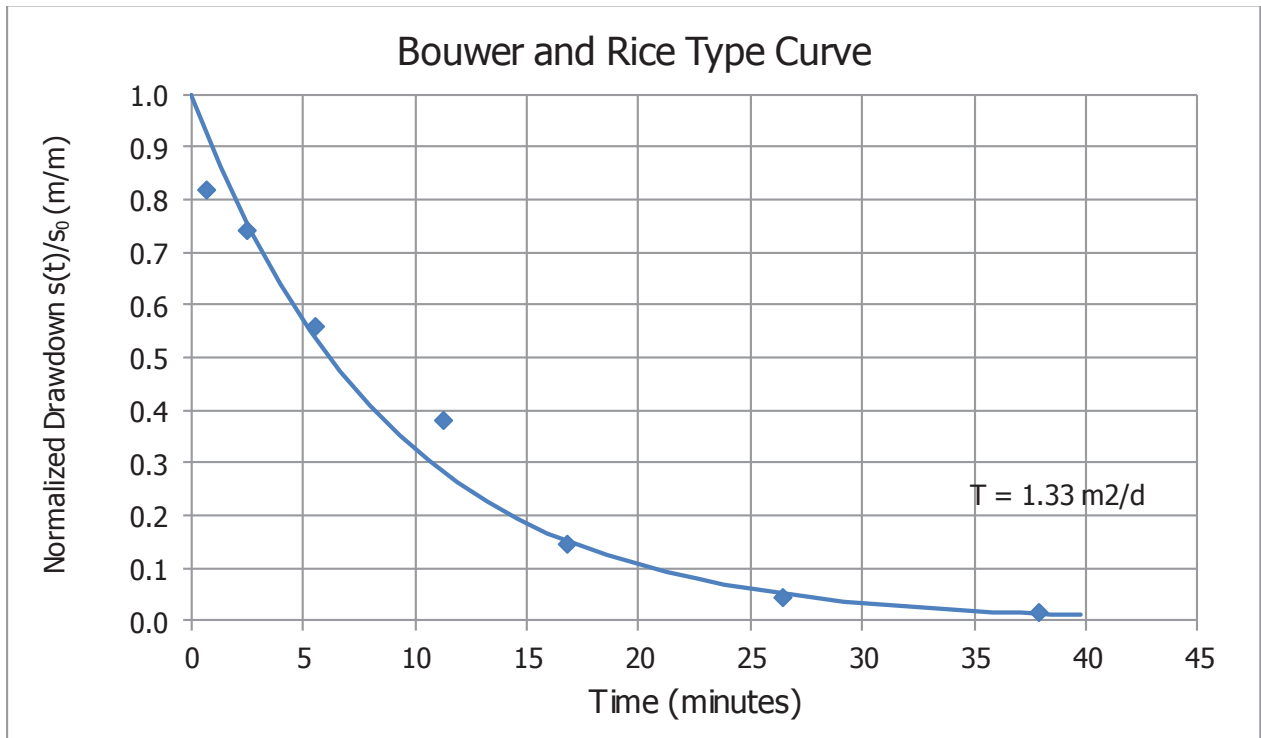


Figure 58. Bower and Rice type curve for the calculation of T_n .

Well casing radius (m)	0.05
Well radius (m)	0.075
Top of screen (m)	2
Bottom of screen (m)	7.6
LNAPL baildown vol. (litre)	1.375

The baildown test took place on 20/7/2015. 1.75 L NAPL and 0.05 L water were removed. The initial NAPL thickness before the test was 0.29 m. The thickness after the removal of the product was 0.14m and the final thickness after 63min was 0.28 m, which is almost 100 % recovery of the initial product thickness. The recovery period was ~ 63 min. The elevation of water table (corrected) is constant (cut off time is 0 min), thus B&R method has to be used. The B&R method showed 1.38 (m²/d) as Transmissivity value.

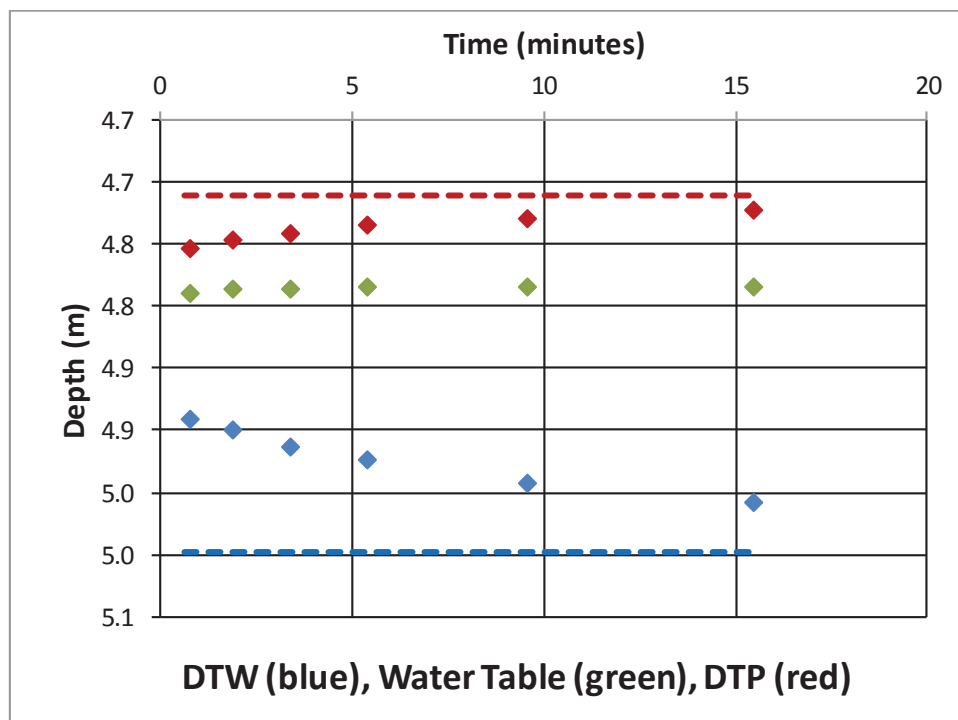


Figure 59. Time series of fluid levels during the baildown test.

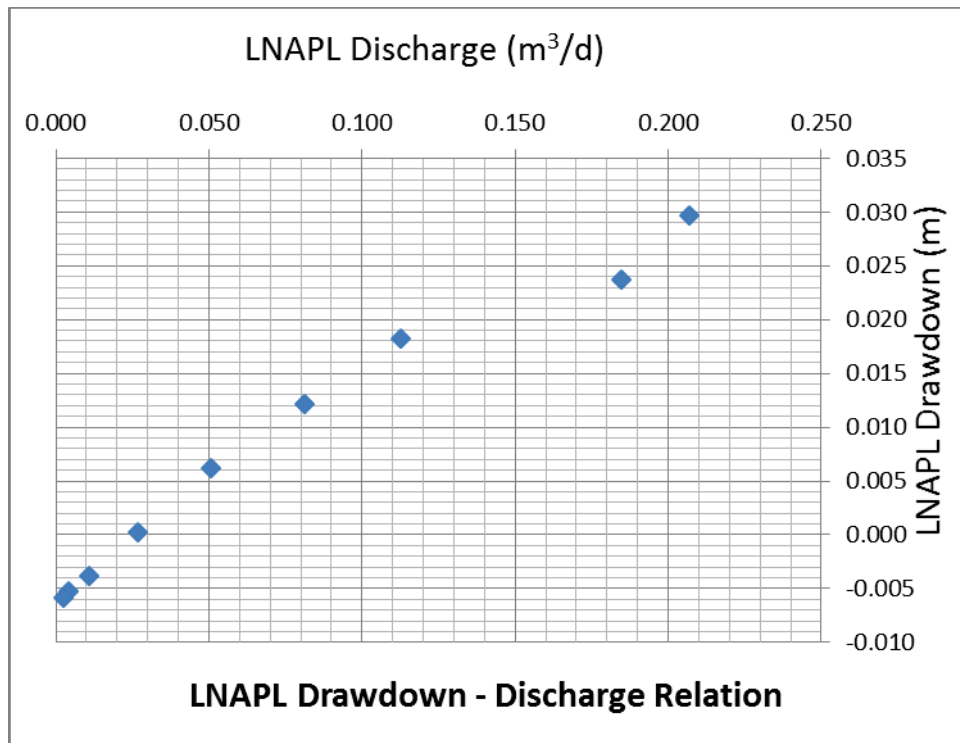


Figure 60. Pre-filtered data.

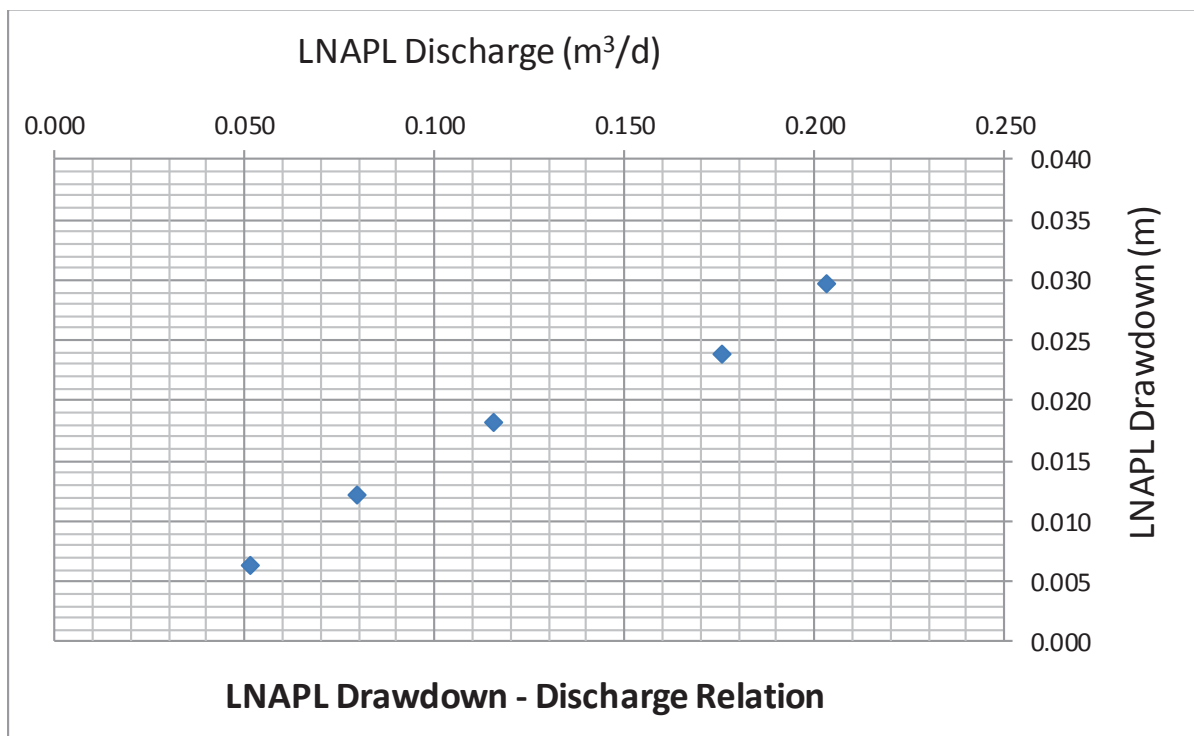


Figure 61. LNAPL drawdown- discharge relation during baildown testing after a drawdown adjustment of 0.0088m (post-filtered data).

No borehole effects at the beginning of this test because during the previous test on 8/7/2015 the first discharge value after the cut off time was close to this first value that is ~ 0.2 m³/d.

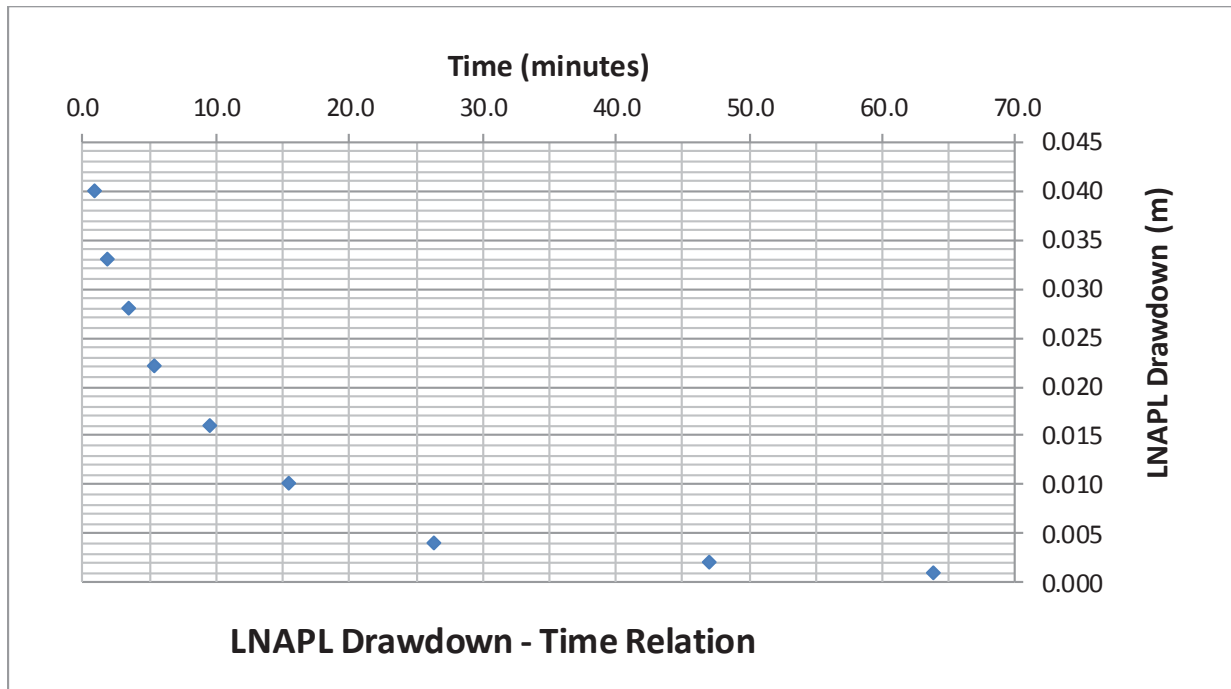


Figure 62. Time series of LNAPL drawdown during baildown testing.

The figure above shows that the drawdown of the LNAPL is decreasing as time passes until 0m drawdown. Such behaviour suggests that the formation and the wellbore LNAPL fluids were initially in equilibrium.

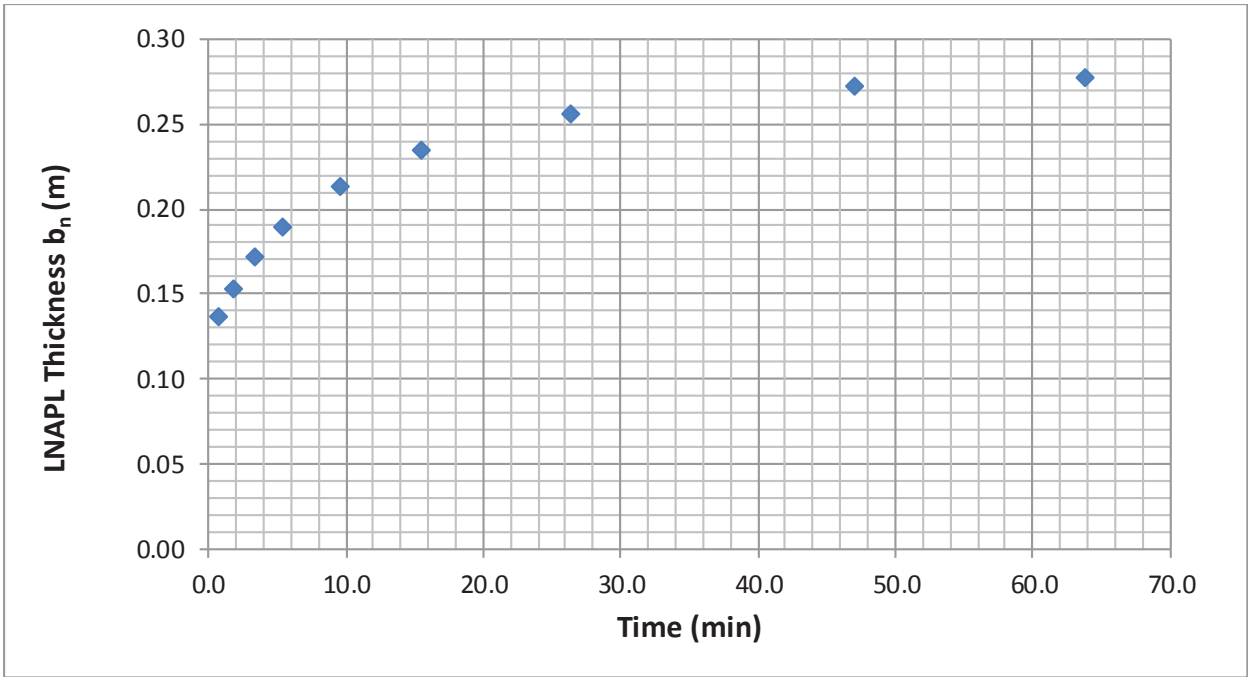


Figure 63. Time series of LNAPL thickness during baildown testing.

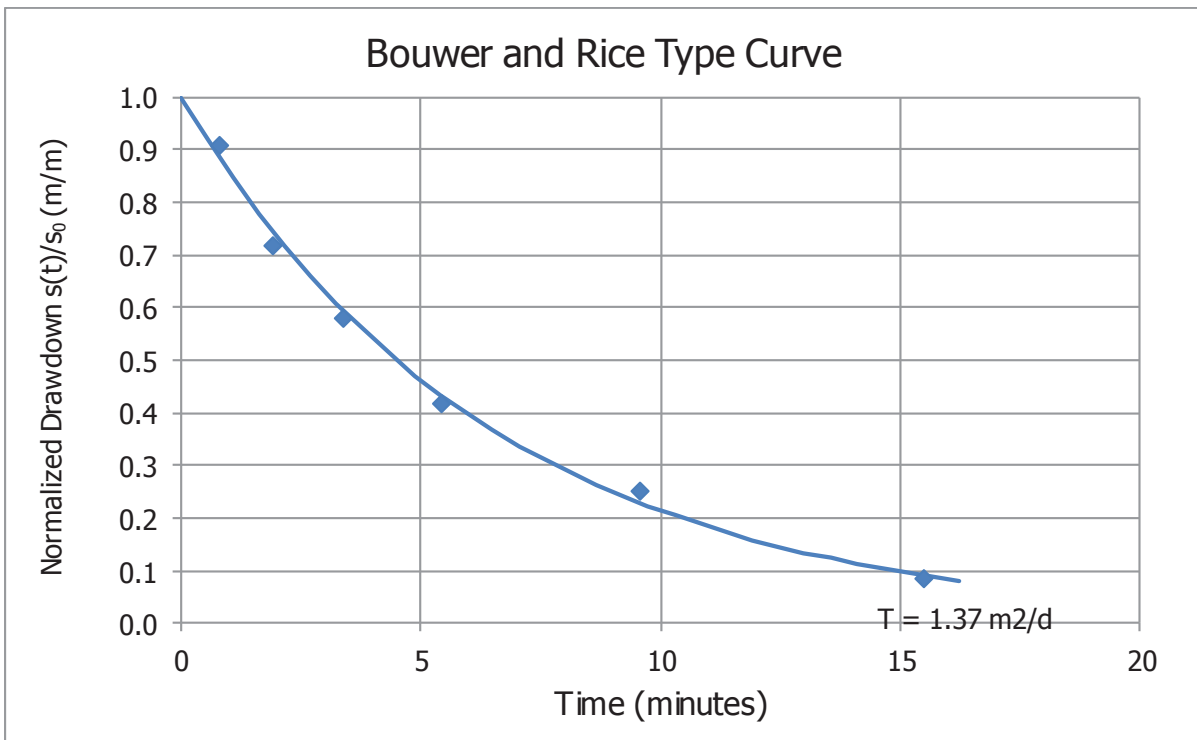


Figure 64. Bower and Rice type curve for the calculation of T_n .

Well casing radius (m)	0.05
Well radius (m)	0.075
Top of screen (m)	2
Bottom of screen (m)	7.6
LNAPL bail-down vol. (litre)	2.23

The bail-down test took place on 5/04/2016. 2.23 L NAPL and 0.37 L water were removed. The initial NAPL thickness before the test was 0.31 m. The thickness after the removal of the product was 0.07m and the final thickness after 205min was 0.31 m, which is 100 % recovery of the initial product thickness. The recovery period (>95%) was ~ 110 min. The elevation of water table (corrected) is constant thus, the B&R method can be used. The B&R method showed 0.414 (m²/d) as Transmissivity value and the cut off time was 1.6 min.

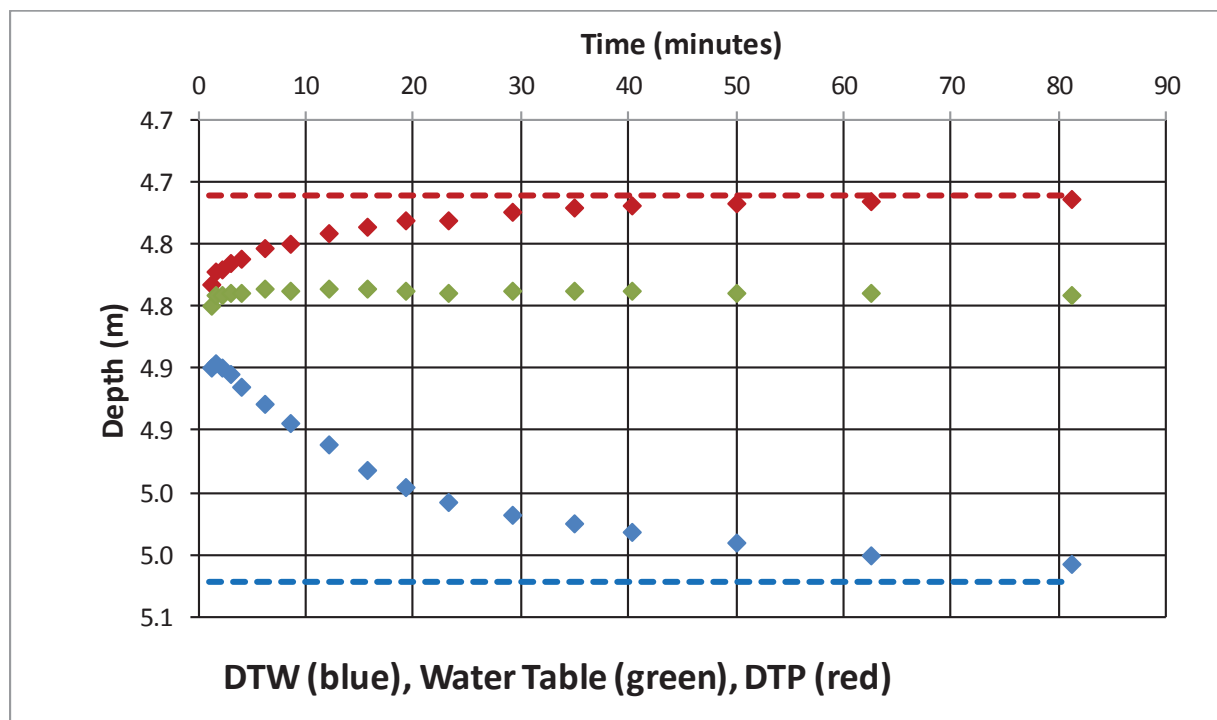


Figure 65. Time series of fluid levels during the baildown test.

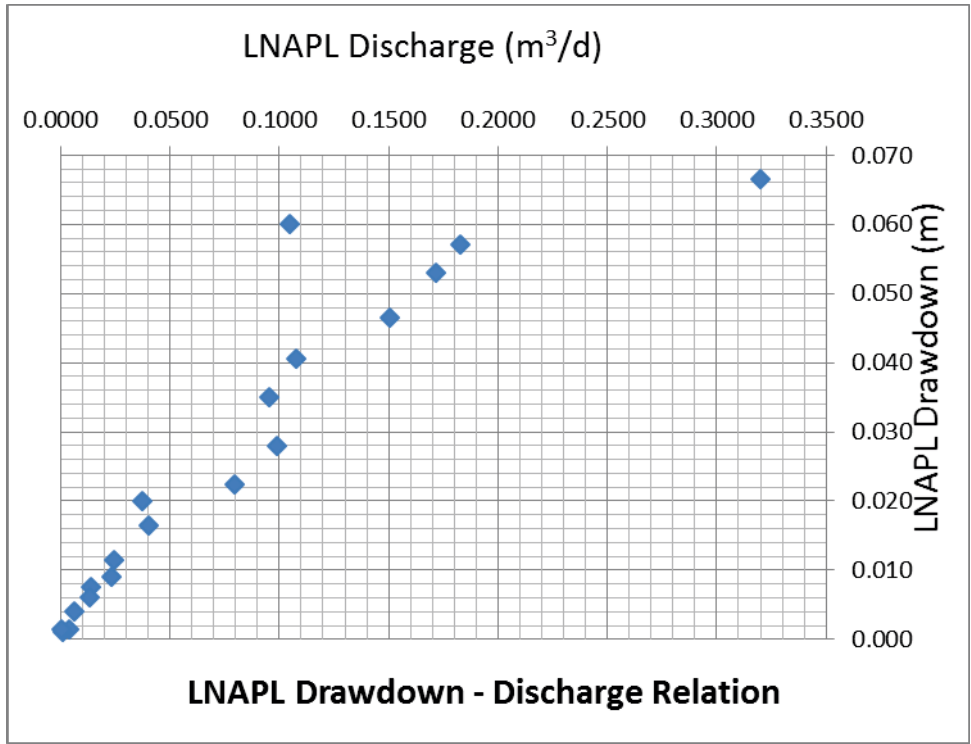


Figure 66. Pre-filtered data.

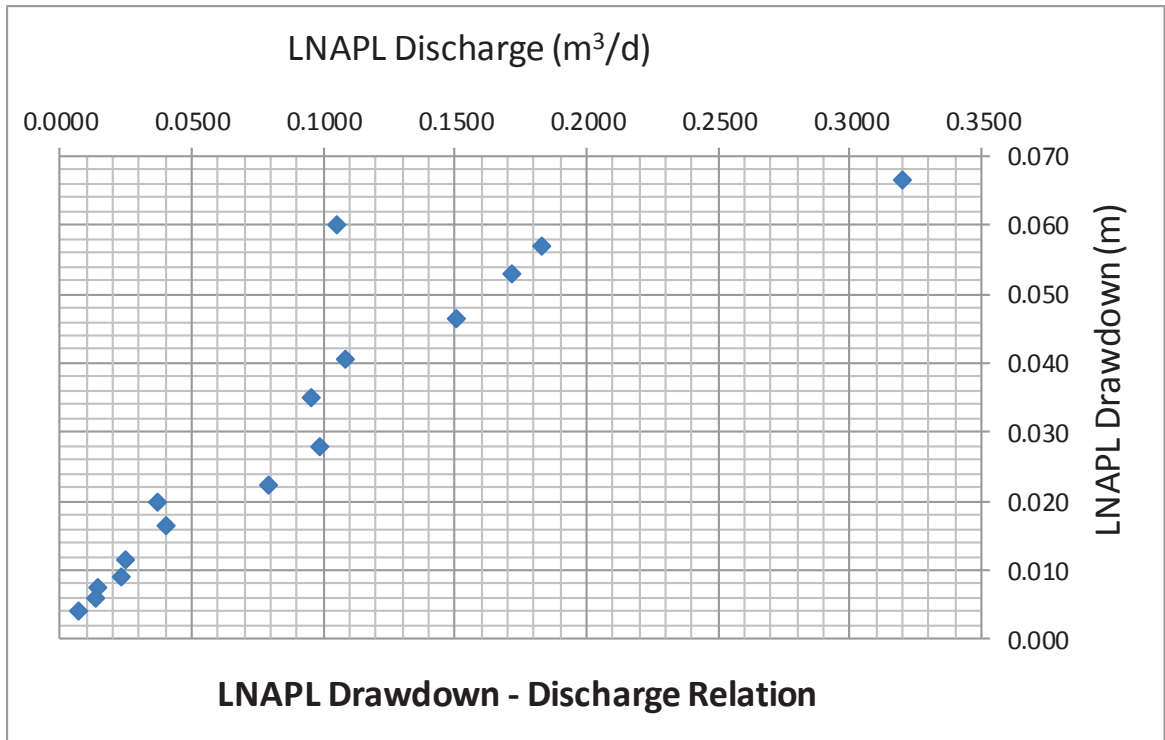


Figure 67. LNAPL drawdown- discharge relation during baildown testing (post-filtered data).

The plot above shows that borehole recharge from the filter pack maybe is not significant (large discharge values at the beginning of the recovery, $0.32 \text{ m}^3/\text{d}$). Moreover, figure depicts behaviour that suggests unconfined LNAPL conditions because there is a continuously decreasing discharge with decreasing drawdown.

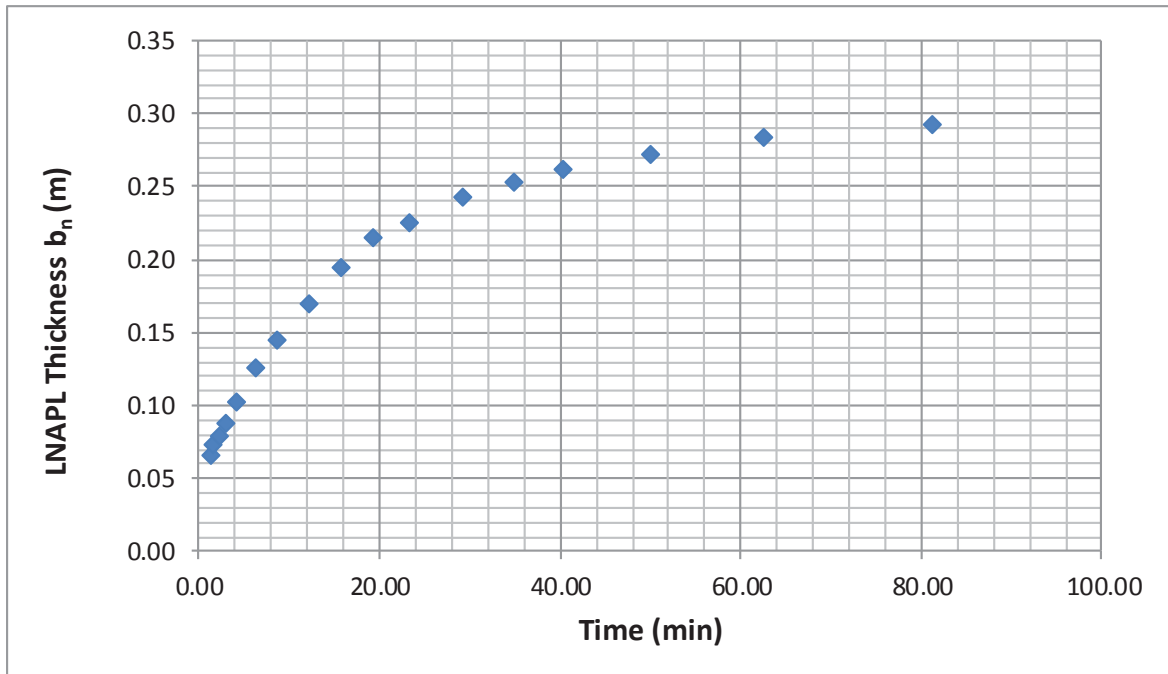


Figure 68. Time series of LNAPL thickness during baildown testing.

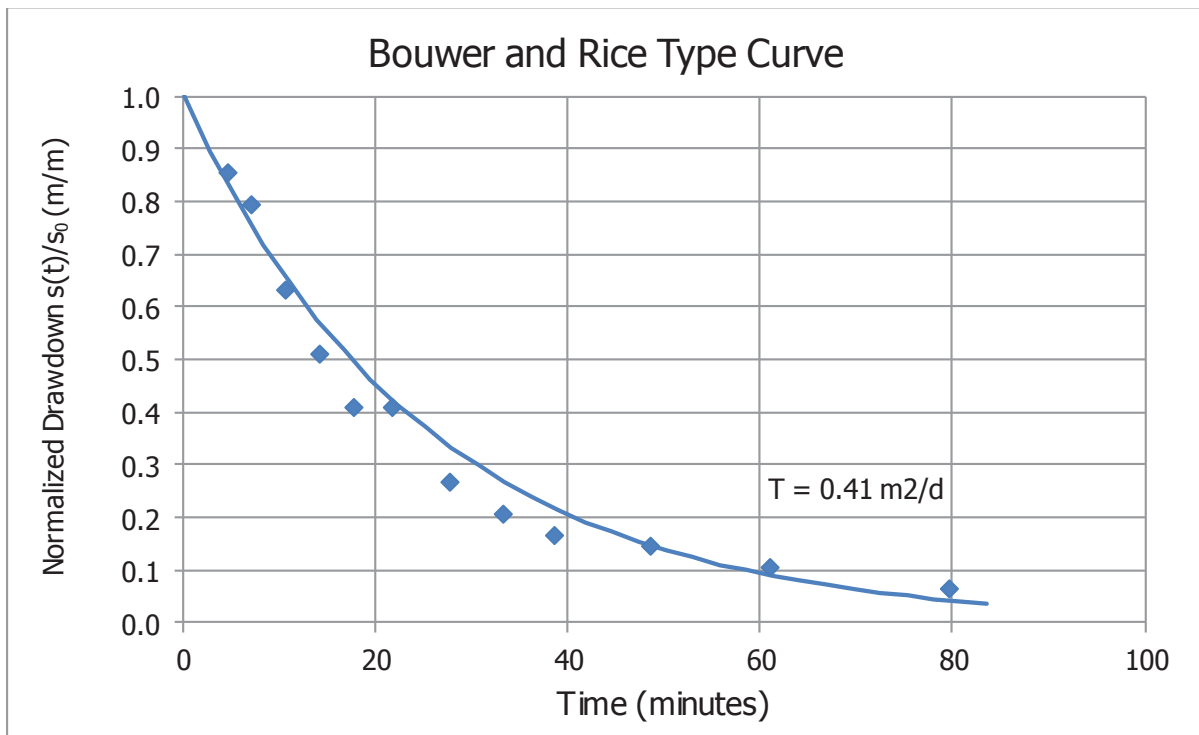


Figure 69. Bower and Rice type curve for the calculation of T_n .

PB27 20/05/2016

Well casing radius (m)	0.05
Well radius (m)	0.075
Top of screen (m)	2
Bottom of screen (m)	7.6
LNAPL bail-down vol. (litre)	2.40

The bail-down test took place on 20/05/2016. 2.40 L NAPL and 0.90 L water were removed. The initial NAPL thickness before the test was 0.32 m. The thickness after the removal of the product was 0.09m and the final thickness after 196 min was 0.308 m, which is 96% recovery of the initial product thickness. The elevation of water table (corrected) is constant thus, the B&R method can be used. The B&R method showed 0.572 (m²/d) as Transmissivity value and the cut off time was 11 min.

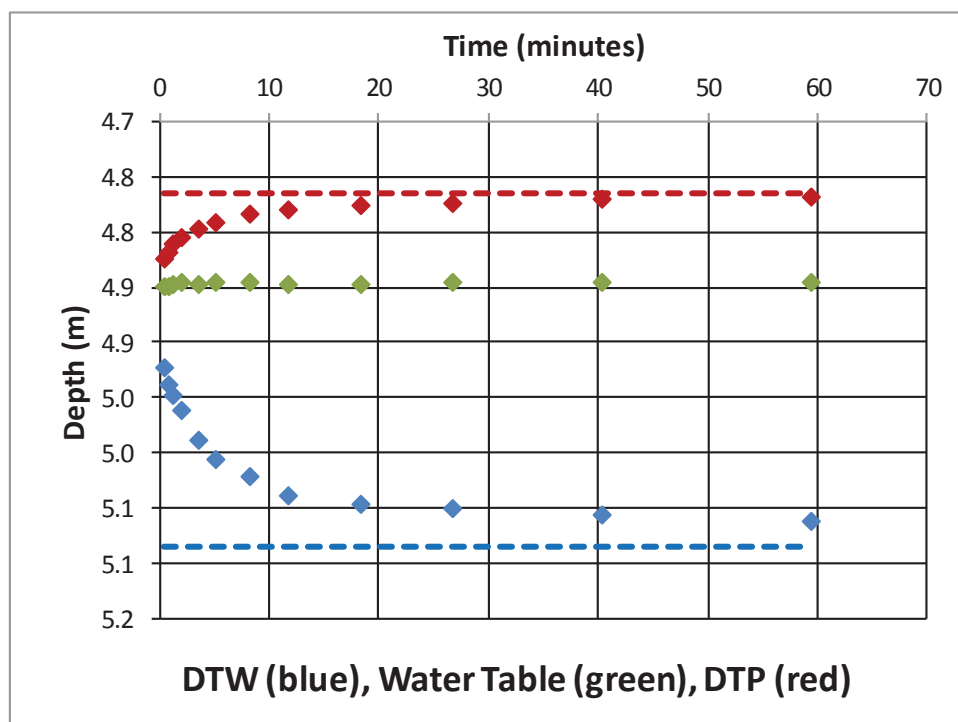


Figure 70. Time series of fluid levels during the baildown test.

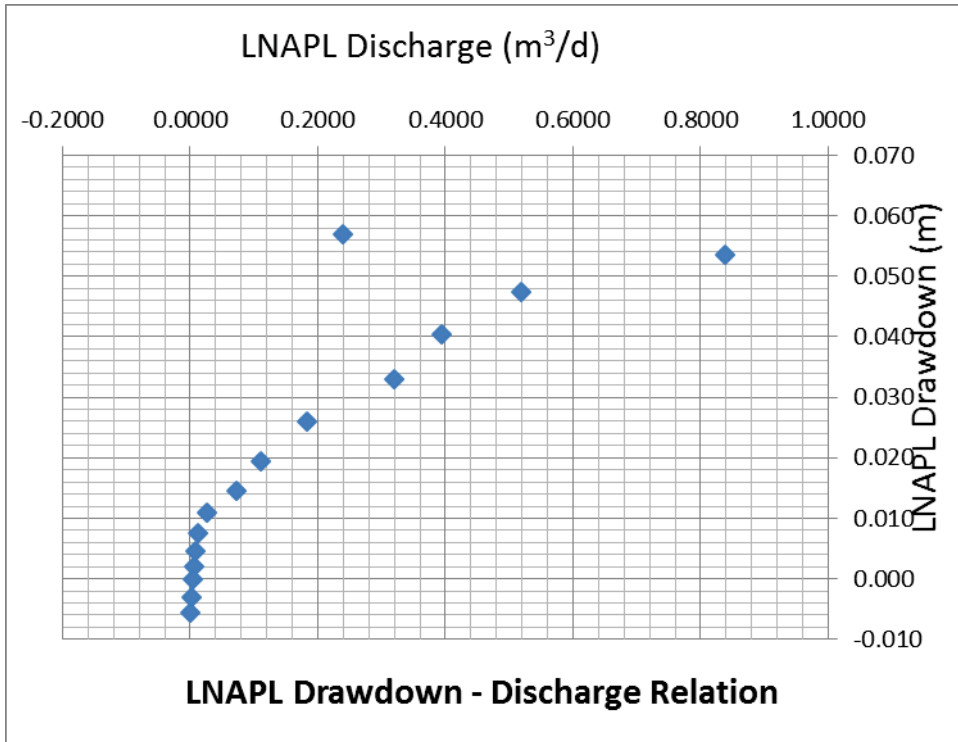


Figure 71. Pre-filtered data.

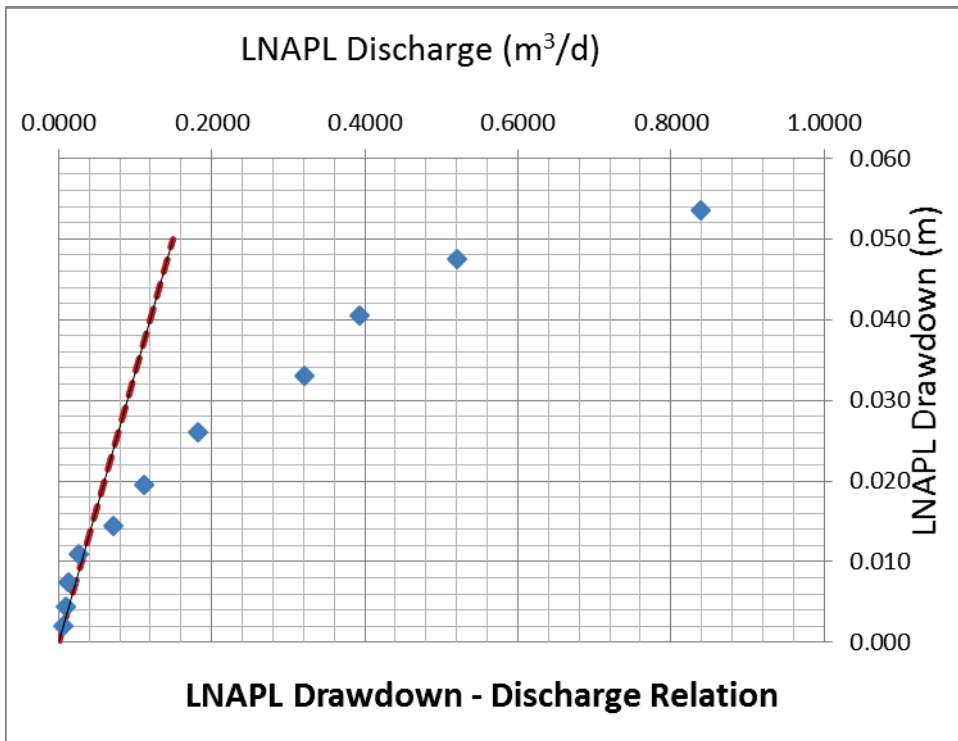


Figure 72. LNAPL drawdown- discharge relation during baildown testing after a drawdown adjustment of 0.002m (post-filtered data).

The plot above shows that borehole recharge from the filter pack maybe is not significant (large discharge values at the beginning of the recovery, 0.81 m³/d). Moreover, figure depicts behaviour that suggests unconfined LNAPL conditions because there is a continuously decreasing discharge with decreasing drawdown.

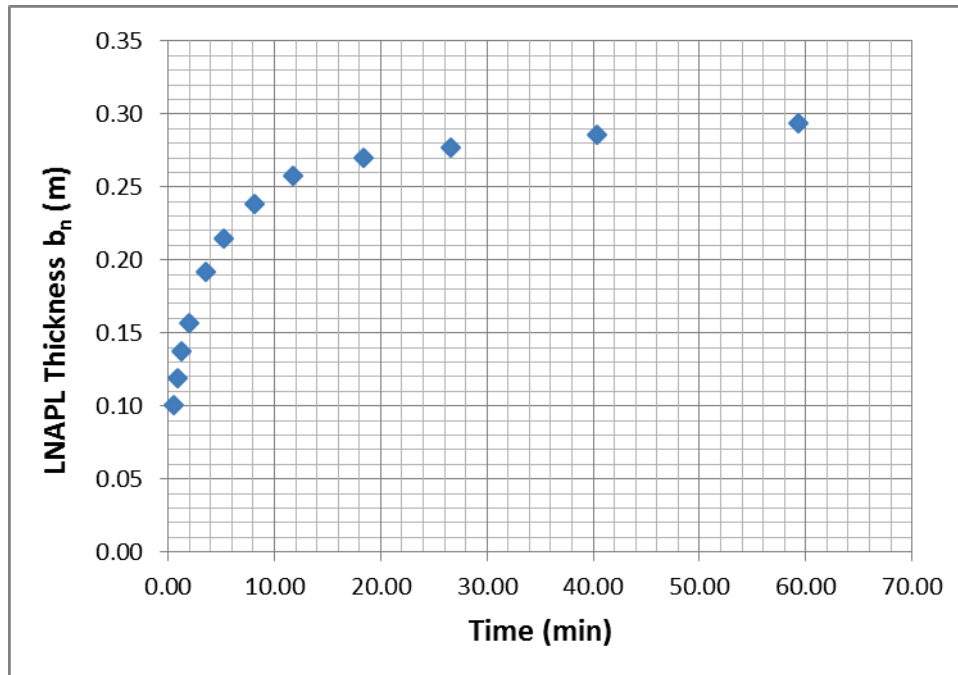


Figure 73. Time series of LNAPL thickness during baildown testing.

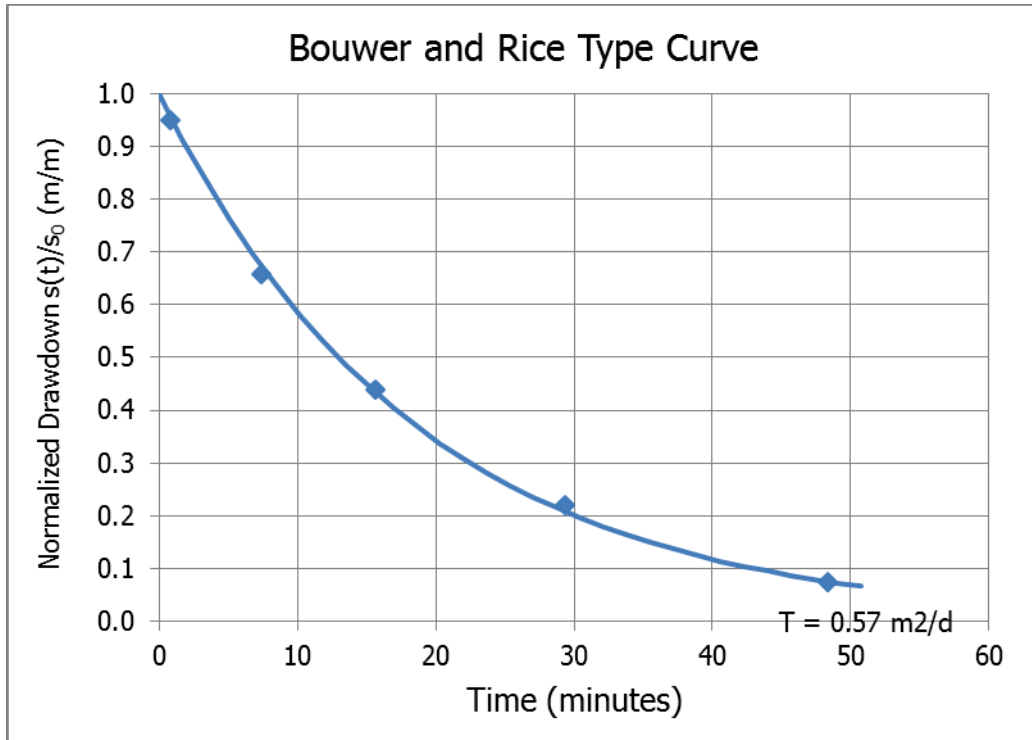


Figure 74. Bouwer and Rice type curve for the calculation of T_n .

PB27 01/06/2016

Well casing radius (m)	0.05
Well radius (m)	0.075
Top of screen (m)	2
Bottom of screen (m)	7.6
LNAPL bail-down vol. (litre)	2.00

The bail-down test took place on 01/06/2016. 2.00 L NAPL and 1.25 L water were removed. The initial NAPL thickness before the test was 0.236 m. The thickness after the removal of the product was 0.05 m and the final thickness after 157 min was 0.230 m, which is 97.5% recovery of the initial product thickness. The elevation of water table (corrected) is constant

thus, the B&R method can be used. The B&R method showed 0.664 (m²/d) as Transmissivity value and the cut off time was 4.2 min.

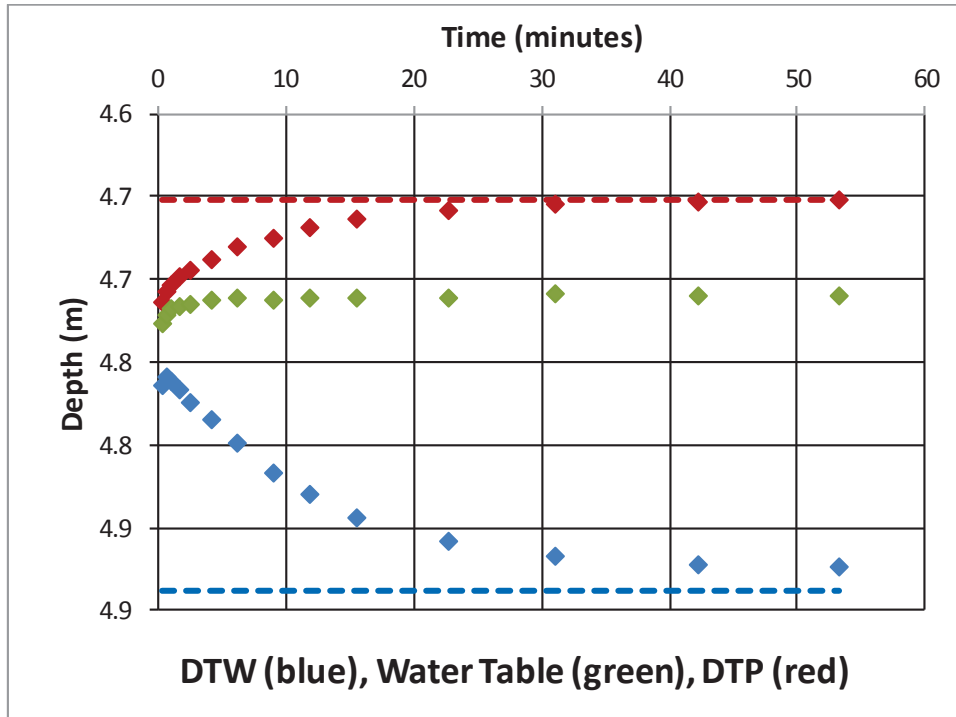


Figure 75. Time series of fluid levels during the baildown test.

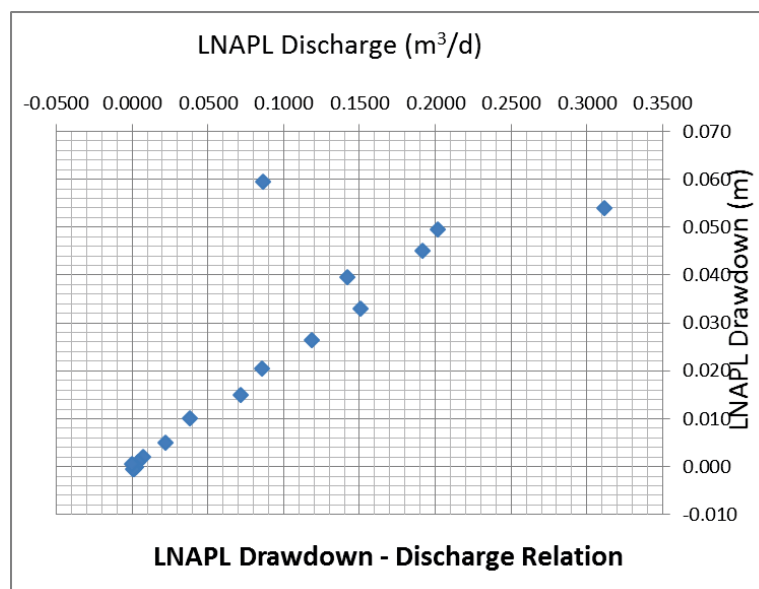


Figure 76. Pre-filtered data.

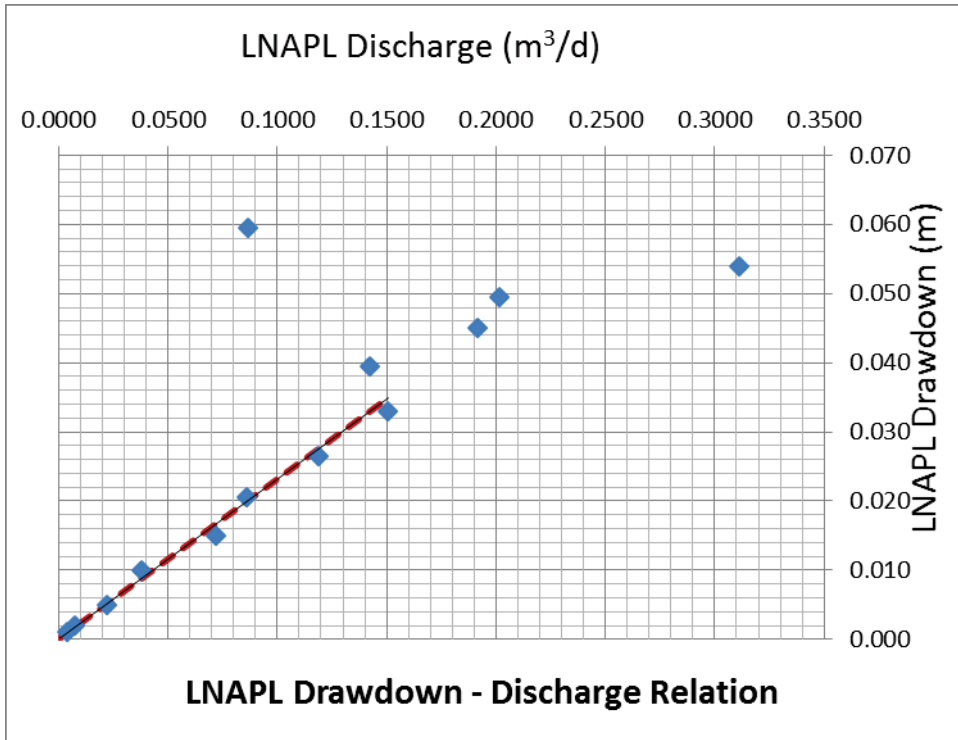


Figure 77. LNAPL drawdown- discharge relation during baildown testing after a drawdown adjustment of -0.0005 m (post-filtered data).

The plot above shows that borehole recharge from the filter pack maybe is not significant (large discharge values at the beginning of the recovery, 0.31 m³/d). Moreover, figure depicts behaviour that suggests unconfined LNAPL conditions because there is a continuously decreasing discharge with decreasing drawdown.

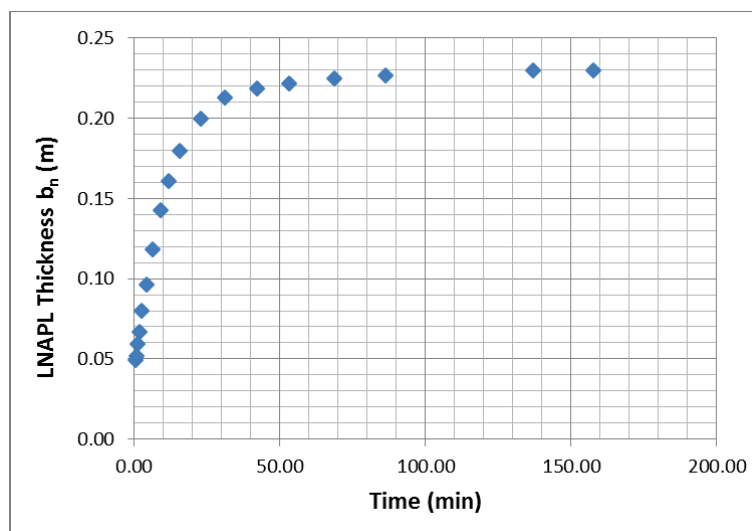


Figure 78. Time series of LNAPL thickness during baildown testing.

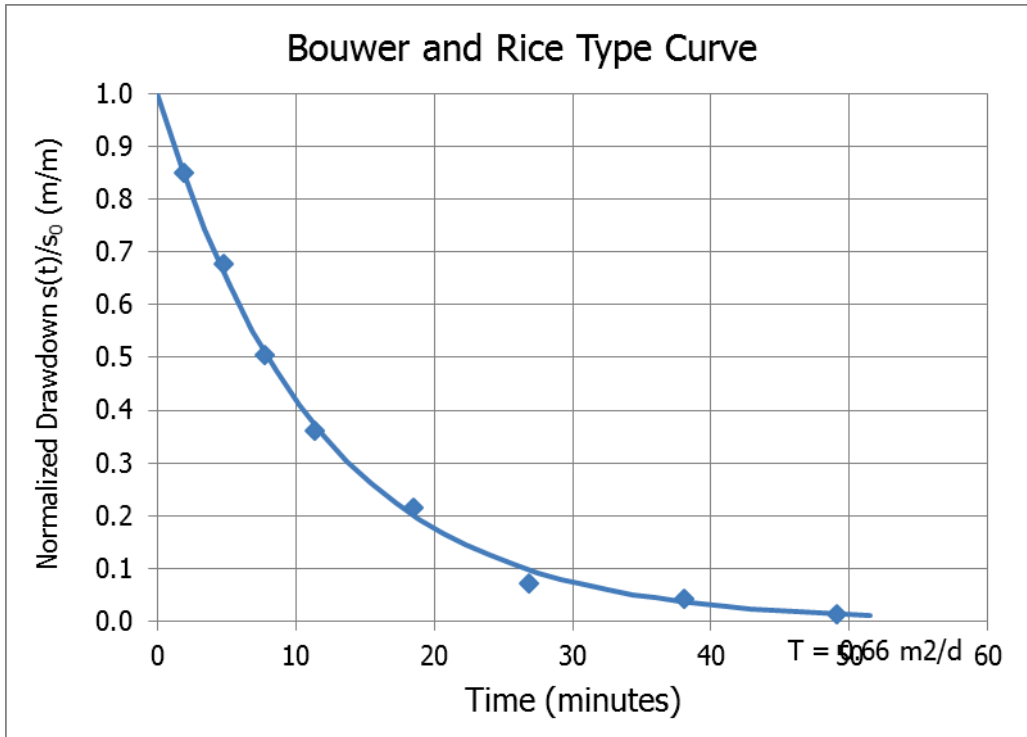


Figure 79. Bouwer and Rice type curve for the calculation of T_n .

PB27 14/06/2016

Well casing radius (m)	0.05
Well radius (m)	0.075
Top of screen (m)	2
Bottom of screen (m)	7.6
LNAPL bail-down vol. (litre)	2.10

The bail-down test took place on 14/06/2016. 2.1 L NAPL and 0.35 L water were removed. The initial NAPL thickness before the test was 0.185 m. The thickness after the removal of the product was 0.01 m and the final thickness after 145 min was 0.175 m, which is 95% recovery of the initial product thickness. The elevation of water table (corrected) is constant thus, the B&R method can be used. The B&R method showed 0.2 (m²/d) as Transmissivity value and the cut off time was 1.57 min.

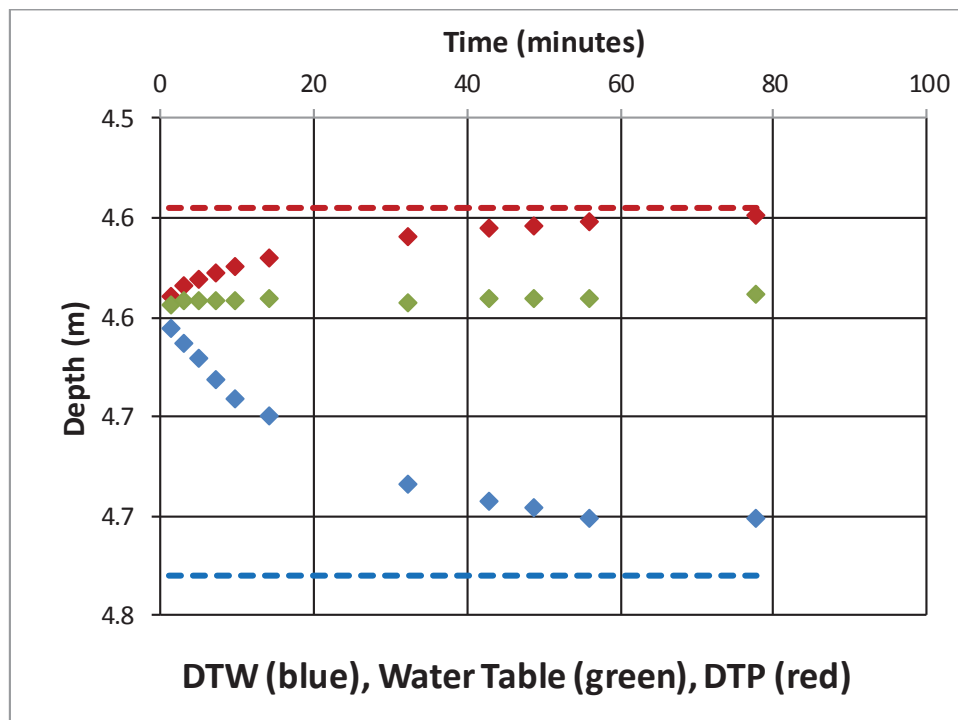


Figure 80. Time series of fluid levels during the baildown test.

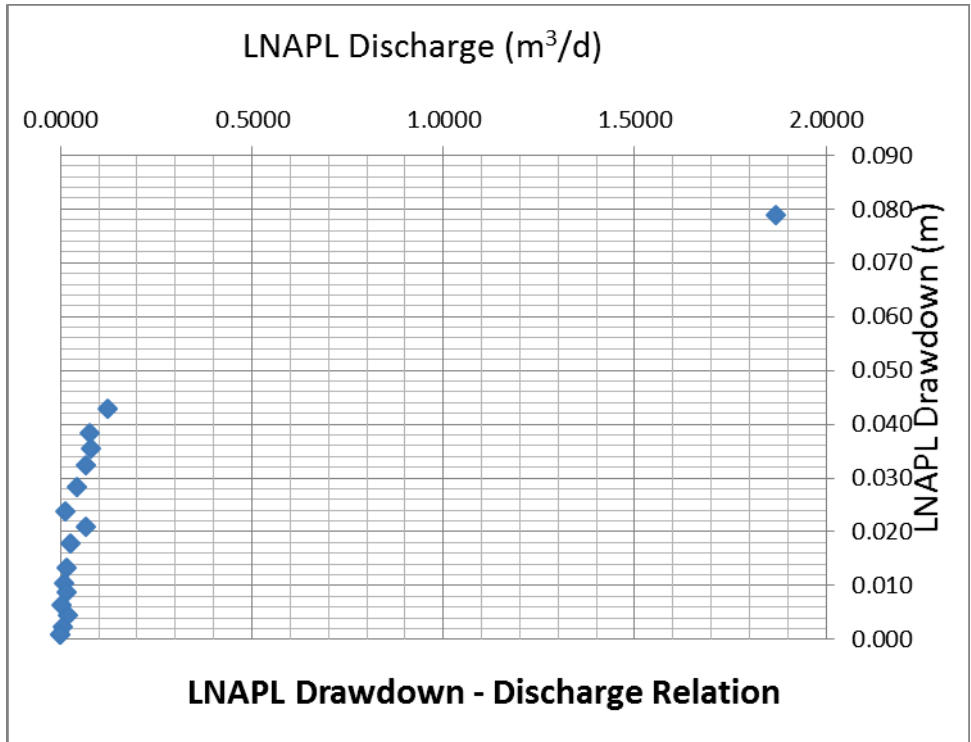


Figure 81. Pre-filtered data.

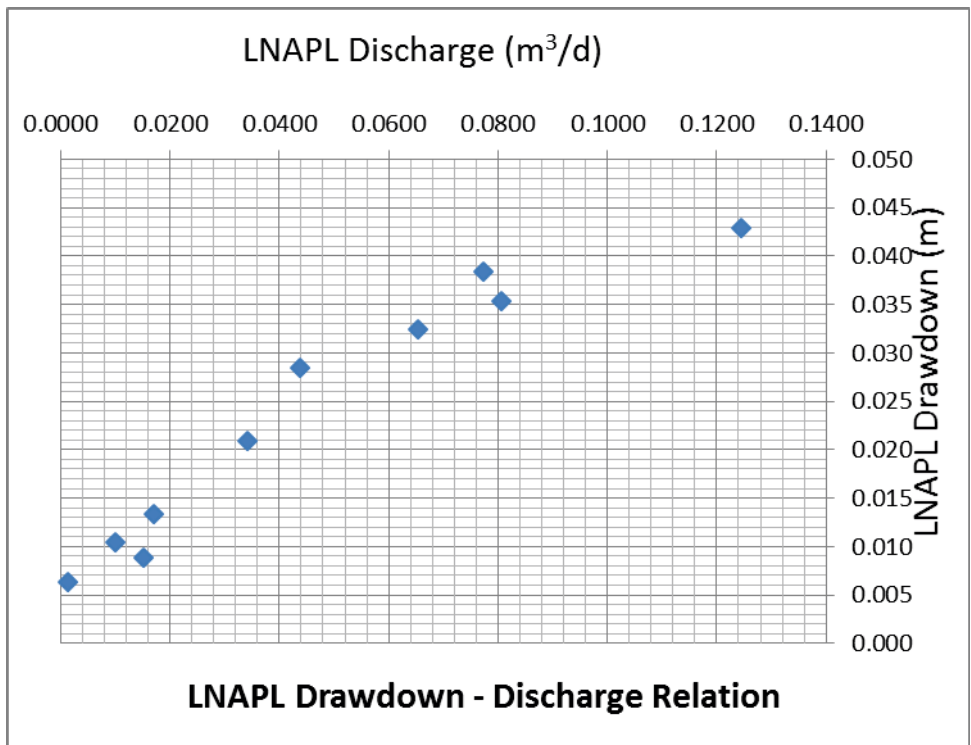


Figure 82. LNAPL drawdown- discharge relation during baildown testing after a drawdown adjustment of -0.0009 m (post-filtered data).

The plot above shows that borehole recharge from the filter pack maybe is not significant (large discharge values at the beginning of the recovery, 0.122 m³/d). Moreover, figure depicts behaviour that suggests unconfined LNAPL conditions because there is a continuously decreasing discharge with decreasing drawdown.

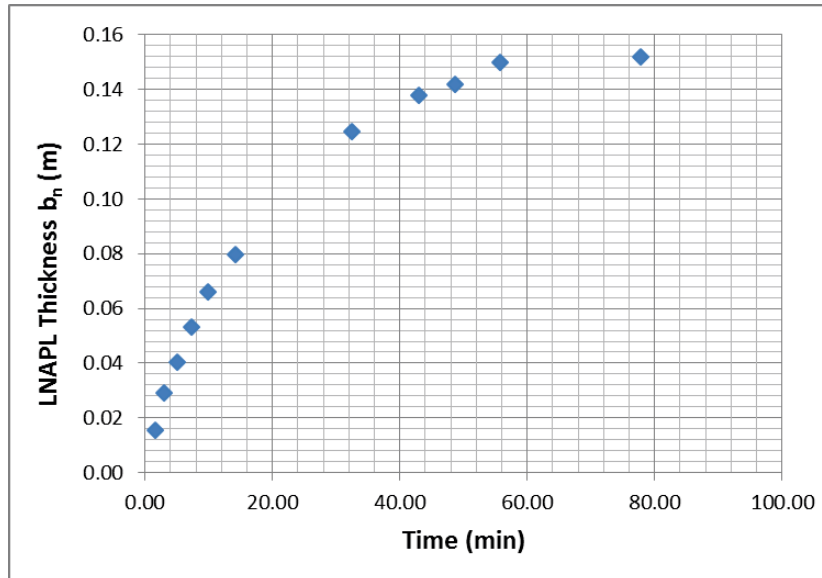


Figure 83. Time series of LNAPL thickness during baildown testing.

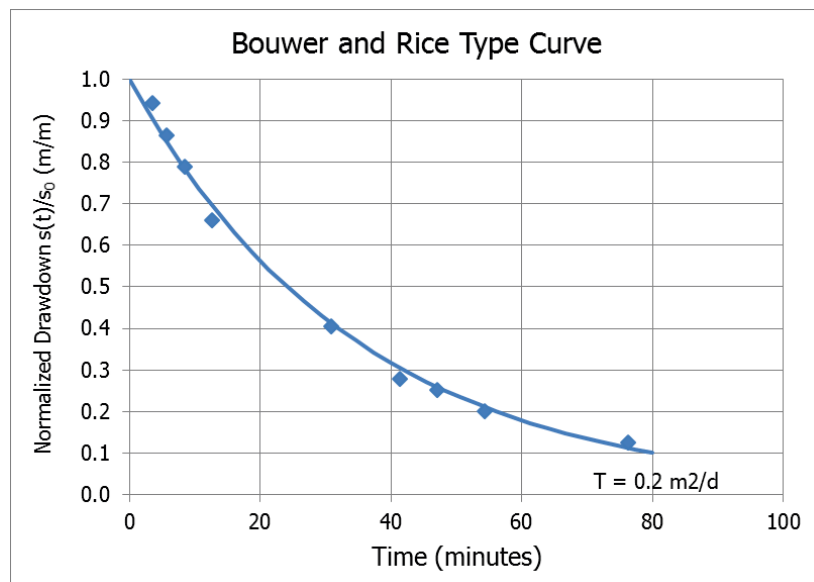


Figure 84. Bower and Rice type curve for the calculation of T_n .

PB05 8/05/2015

Well casing radius (m)	0.05
Well radius (m)	0.075
Top of screen (m)	3.5
Bottom of screen (m)	9.5
LNAPL baildown vol. (litre)	1.69

The bail-down test took place on 8/5/2015. 1.69 L NAPL and 0.23 L water were removed. The initial NAPL thickness was 0.36 m and the final thickness after 140 min was 0.23 m. The elevation of water table (corrected) is constant (after the cut off time which is 5.5 min), thus B&R method has to be used. The B&R method showed 0.046 (m²/d) as Transmissivity value.

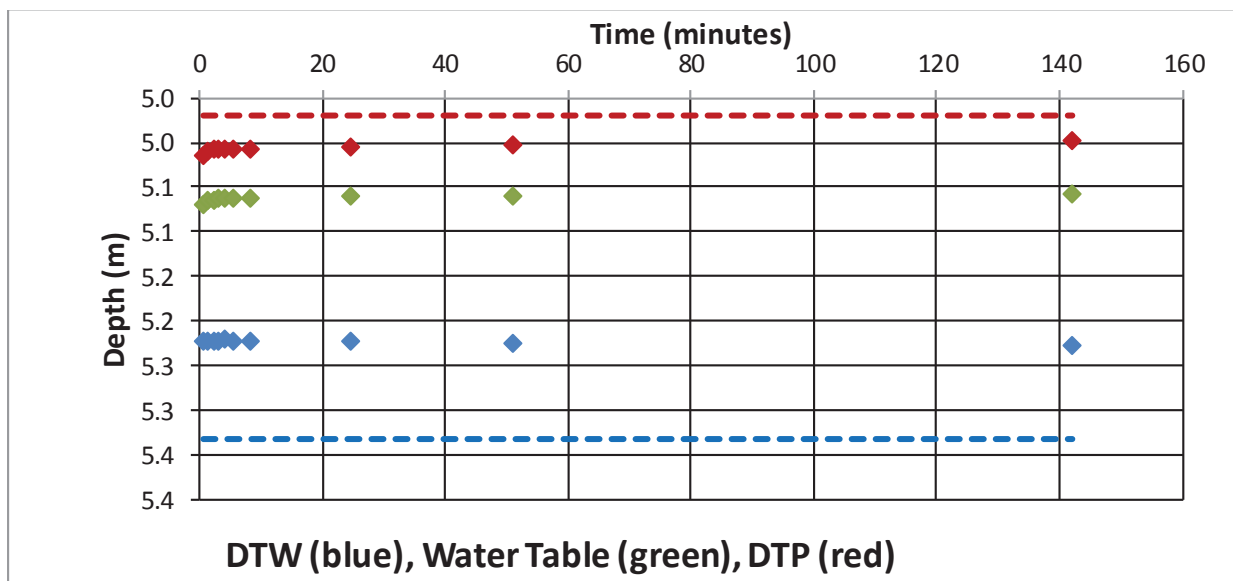


Figure 85. Time series of fluid levels during the baildown test.

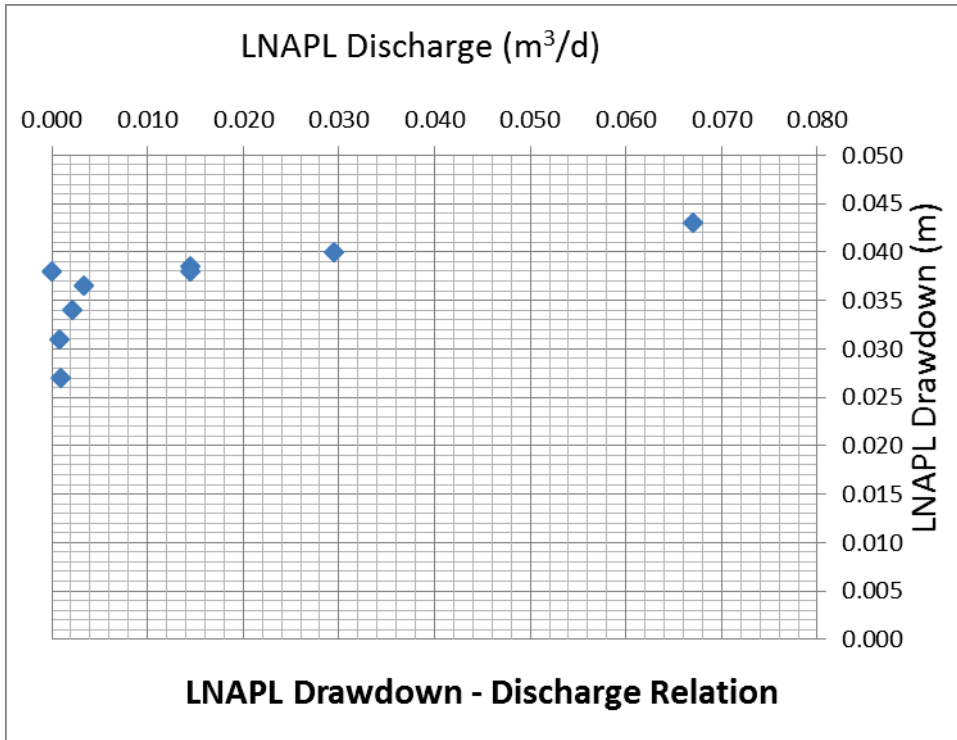


Figure 86. Pre-filtered data.

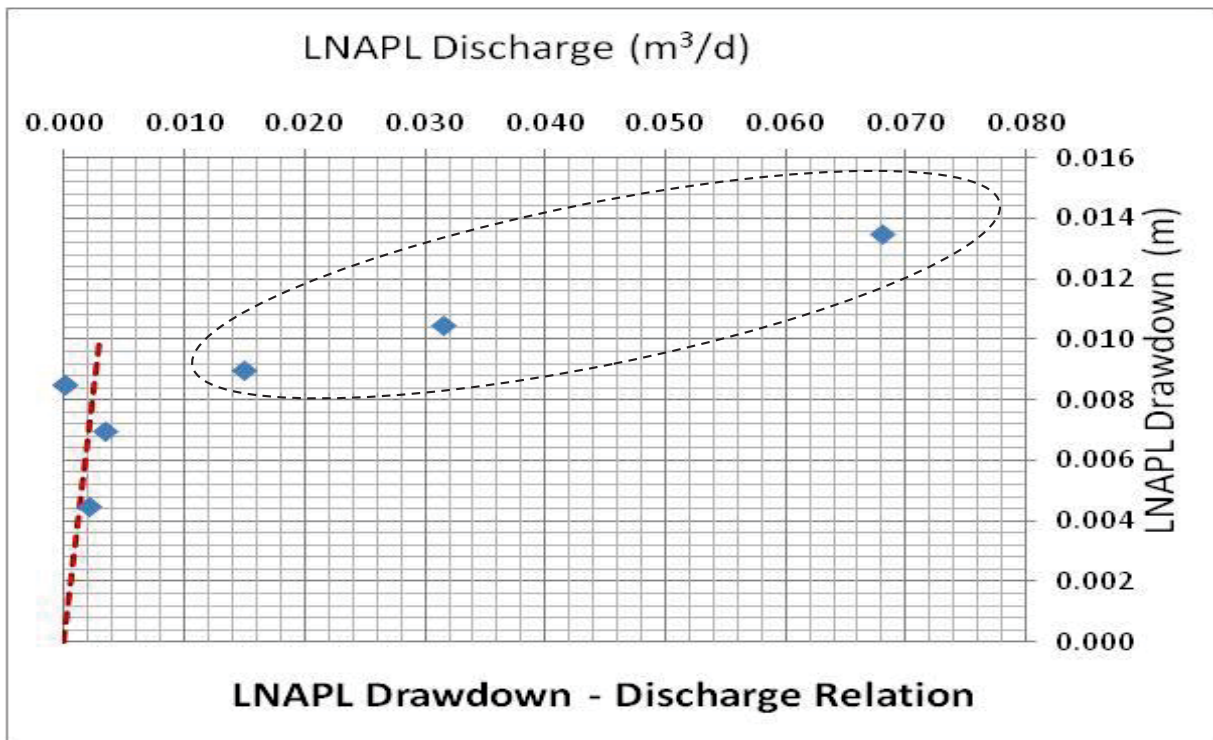


Figure 87. LNAPL drawdown- discharge relation during baildown testing. After a drawdown adjustment of 0.0269m (post-filtered data).

The figure above is after drawdown correction (0.0295m) has been applied. The specific plot shows that borehole recharge from the filter pack is significant (large discharge values at the beginning of the recovery). Moreover, figure depicts behaviour that suggests unconfined LNAPL conditions because we can see continuously decreasing discharge with decreasing drawdown.

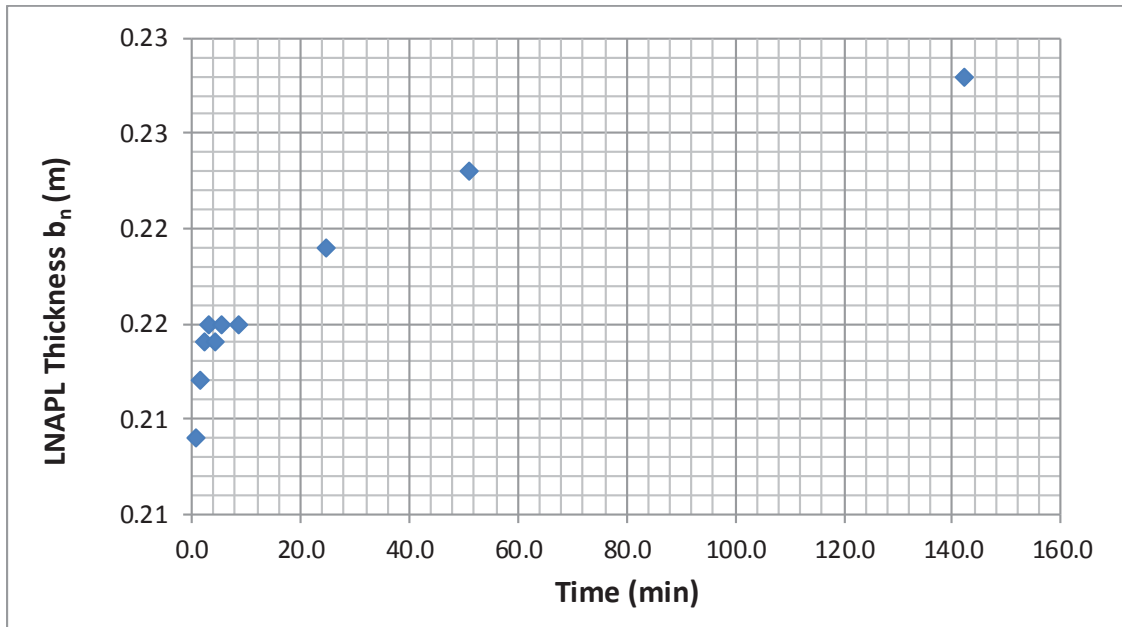


Figure 88. Time series of LNAPL thickness during baildown testing.

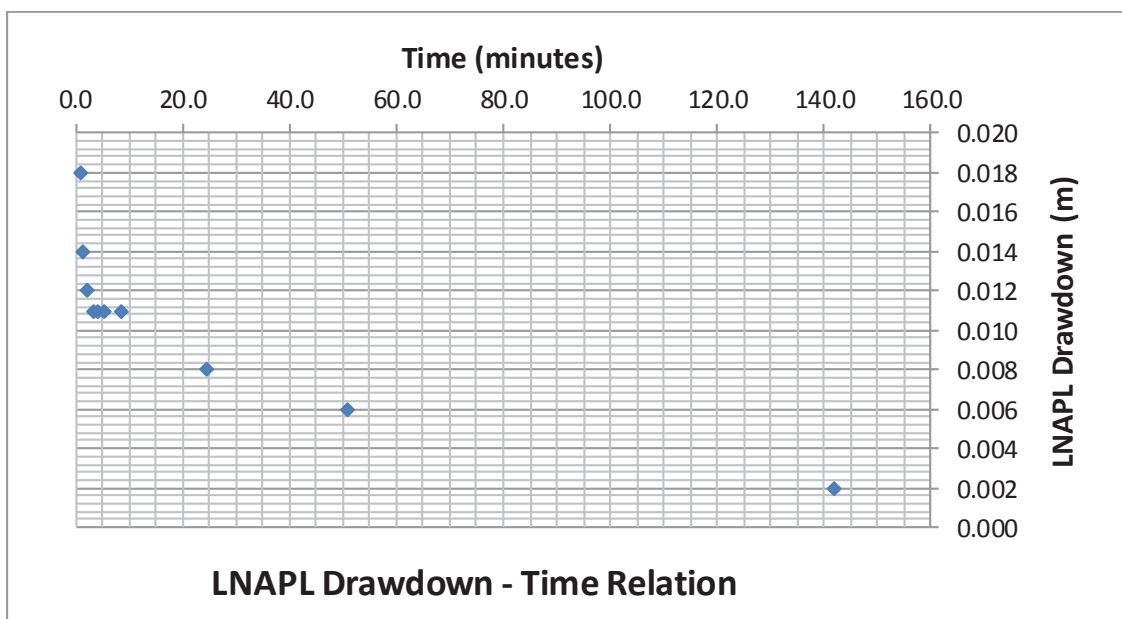


Figure 89. Time series of LNAPL drawdown during baildown testing.

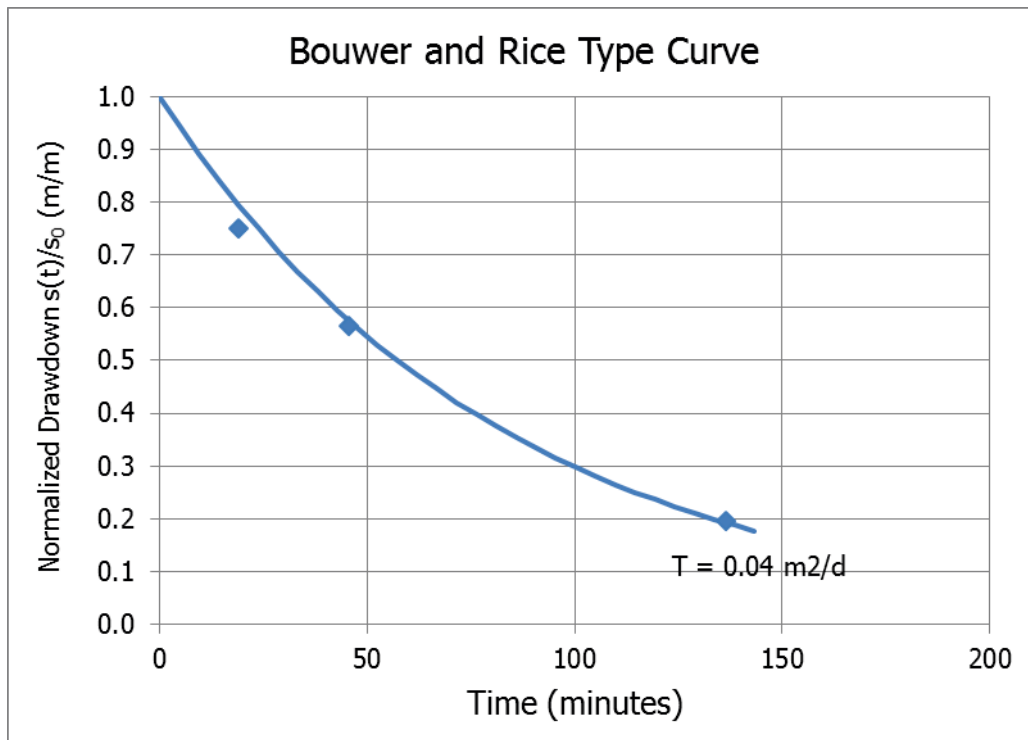


Figure 90. Bouwer and Rice type curve for the calculation of T_n .

PB05 6/04/2016

Well casing radius (m)	0.05
Well radius (m)	0.075
Top of screen (m)	3.5
Bottom of screen (m)	9.5
LNAPL bail-down vol. (litre)	3.3

The bail-down test took place on 6/04/2016. 3.30 L NAPL and 0.74 L water were removed. The initial NAPL thickness was 0.42 m and the final thickness after 940 min was 0.28 m. The elevation of water table (corrected) is constant thus, B&R method can be used. The B&R method showed 0.039 (m²/d) as Transmissivity value and the cut off time was 2.3 min.

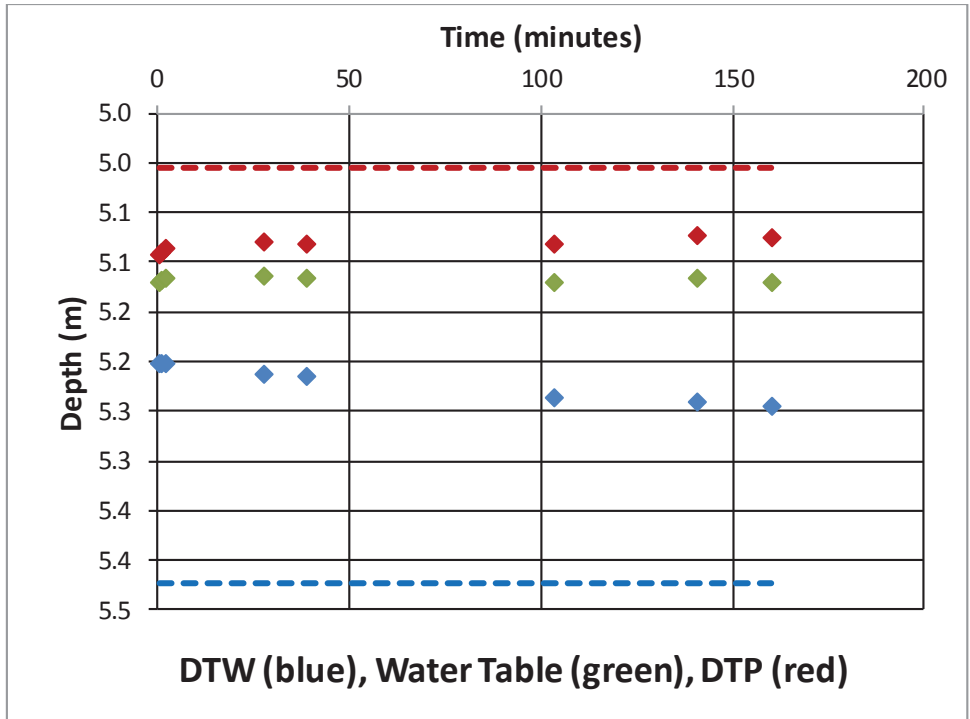


Figure 91. Time series of fluid levels during the baildown test.

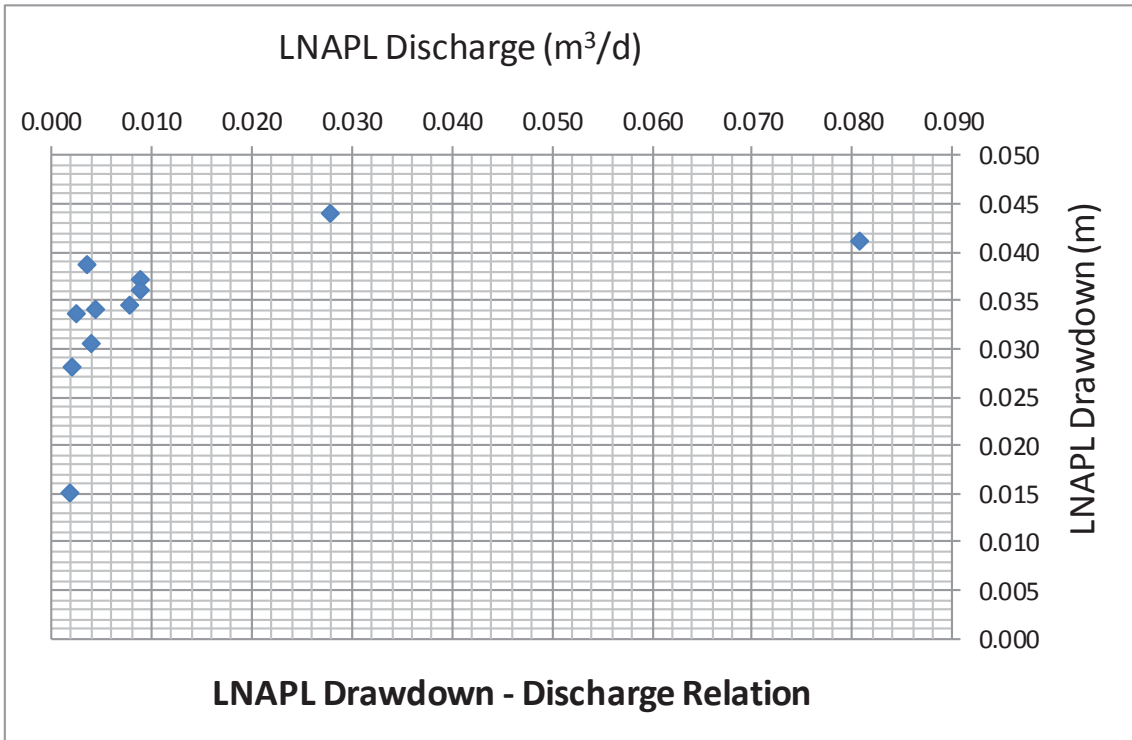


Figure 92. Pre-filtered data.

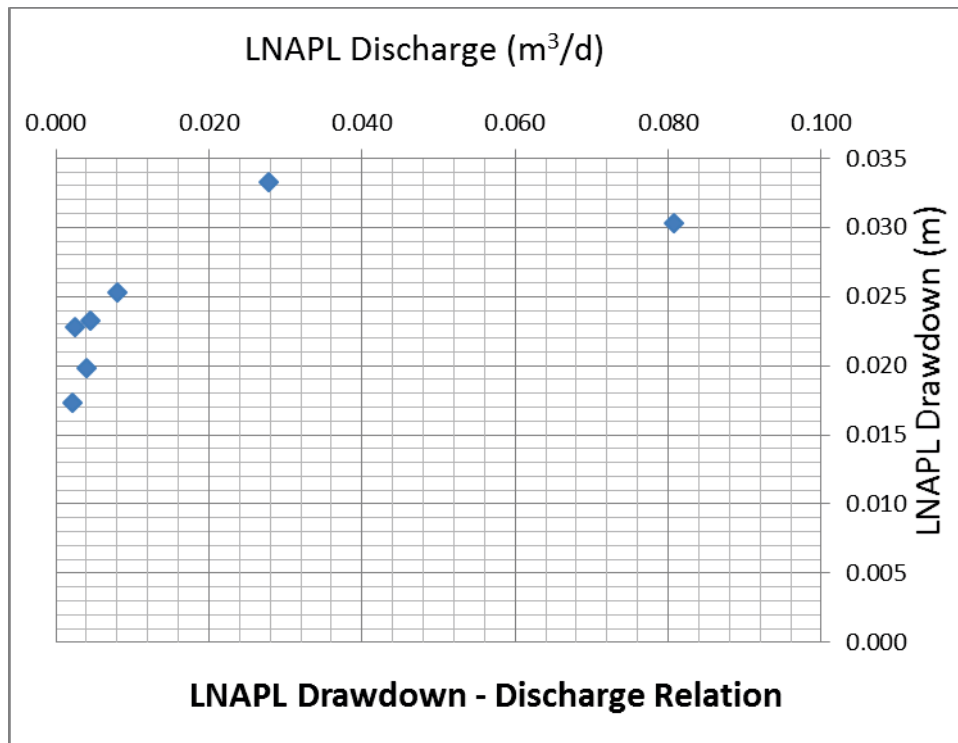


Figure 93. LNAPL drawdown- discharge relation during baildown testing. After a drawdown adjustment of 0.0527m (post-filtered data).

The figure above is after drawdown correction has been applied. The specific plot shows that borehole recharge from the filter pack is not significant. Moreover, figure depicts behaviour that suggests unconfined LNAPL conditions because we can see continuously decreasing discharge with decreasing drawdown.

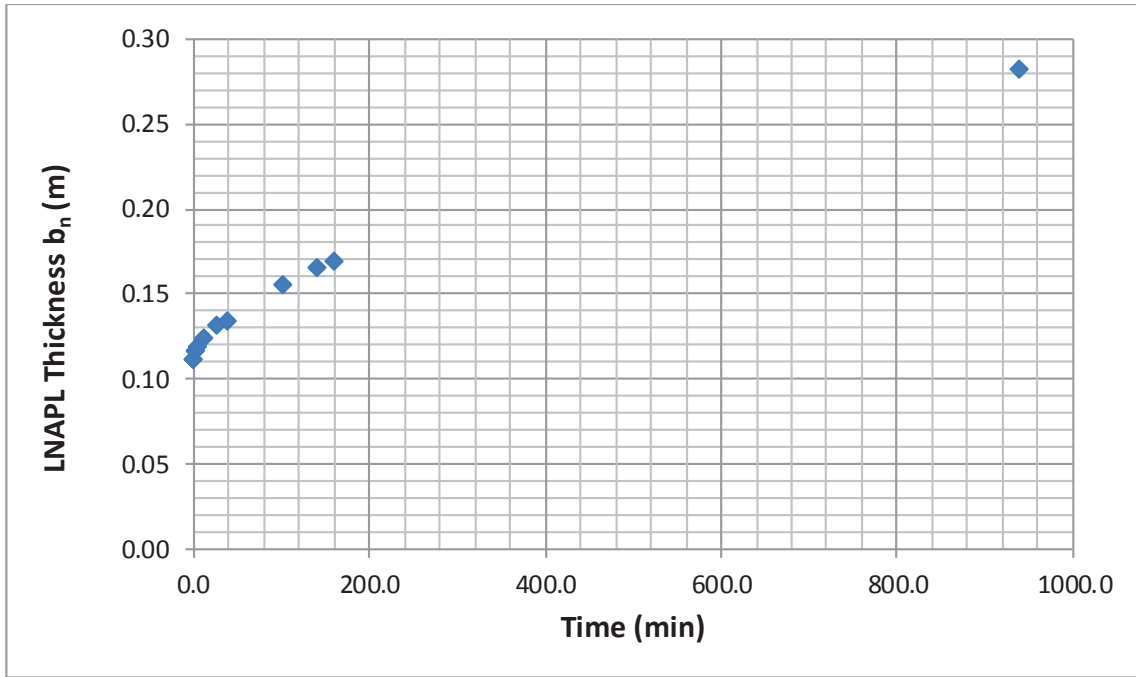


Figure 94. Time series of LNAPL thickness during baildown testing.

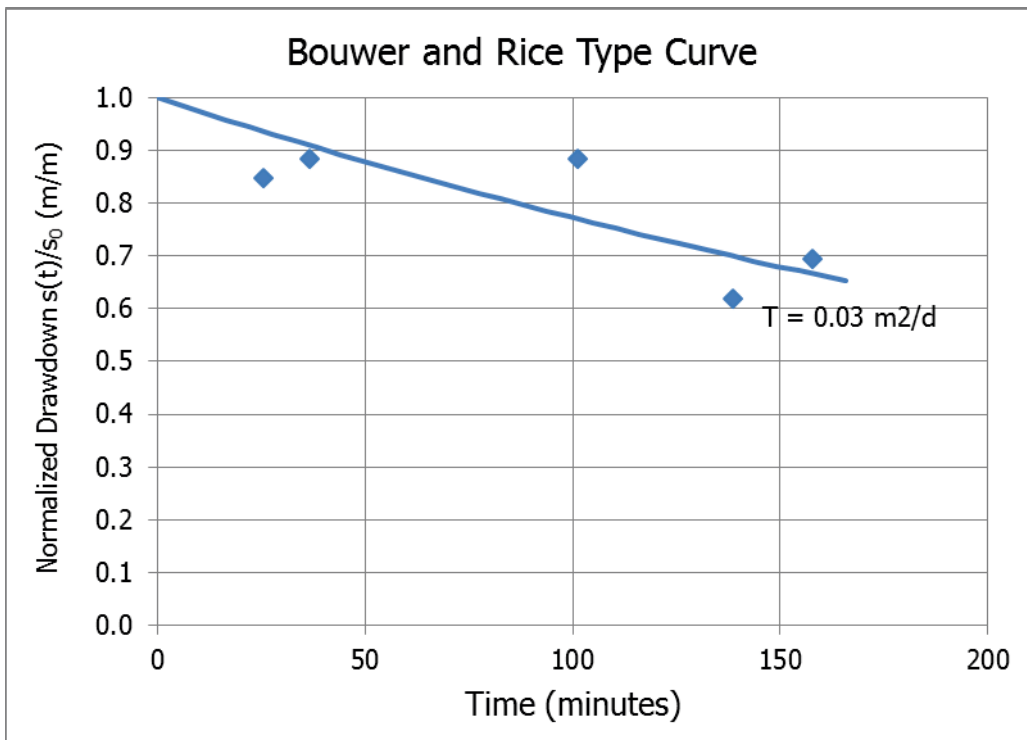


Figure 95. Bouwer and Rice type curve for the calculation of T_n .

Well casing radius (m)	0.05
Well radius (m)	0.075
Top of screen (m)	2.9
Bottom of screen (m)	8.5
LNAPL baildown vol. (litre)	2.71

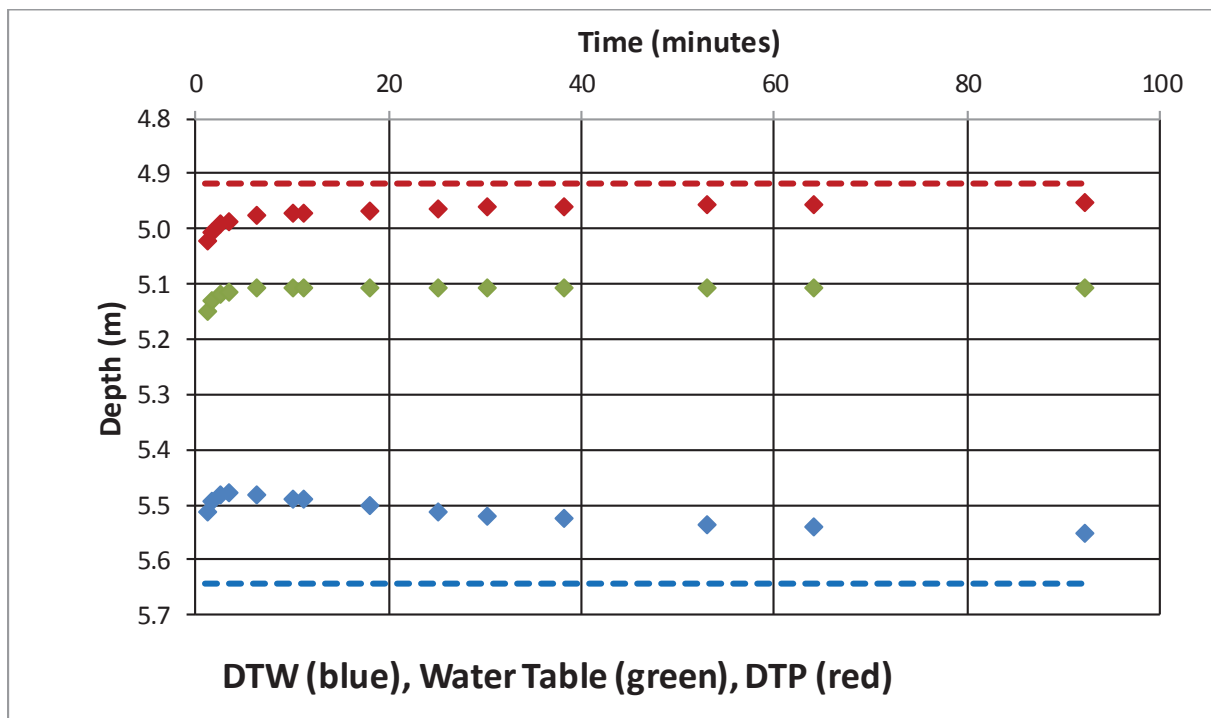


Figure 96. Time series of fluid levels during the baildown test.

The baildown test took place on 7/5/2015. 2.71 L NAPL and 0 L water were removed. The initial NAPL thickness was 0.73 m and the final thickness after 1468 min was 0.69 m. The elevation of water table (corrected) is constant (after the cut off time which is 11 min), thus B&R method has to be used. The B&R method showed 0.55 (m²/d) as Transmissivity value.

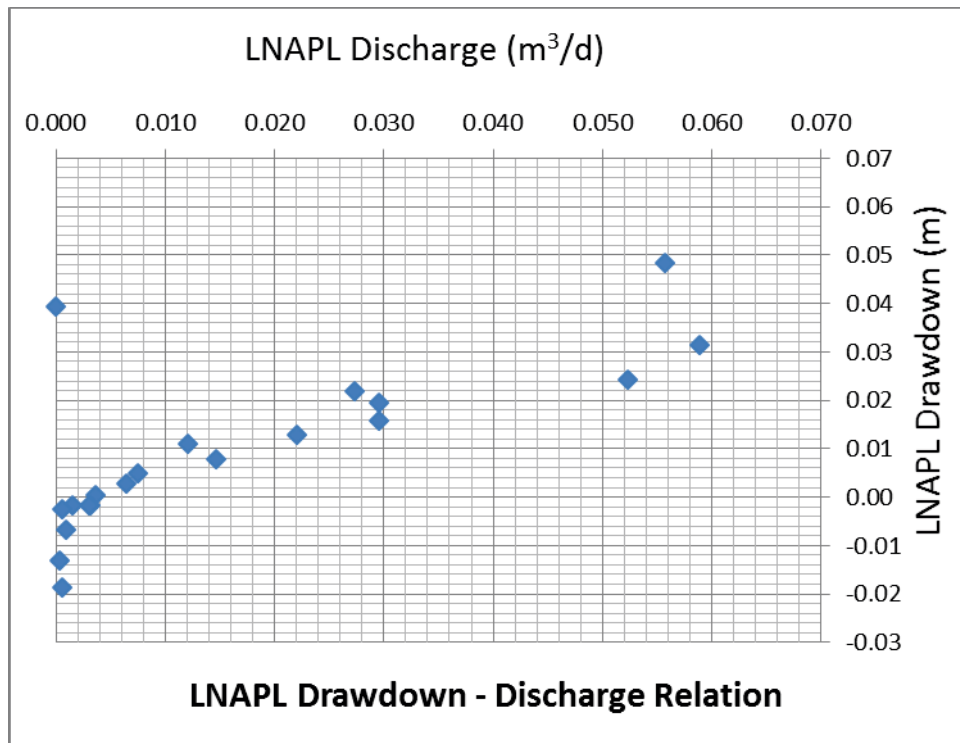


Figure 97. Pre-filtered data.

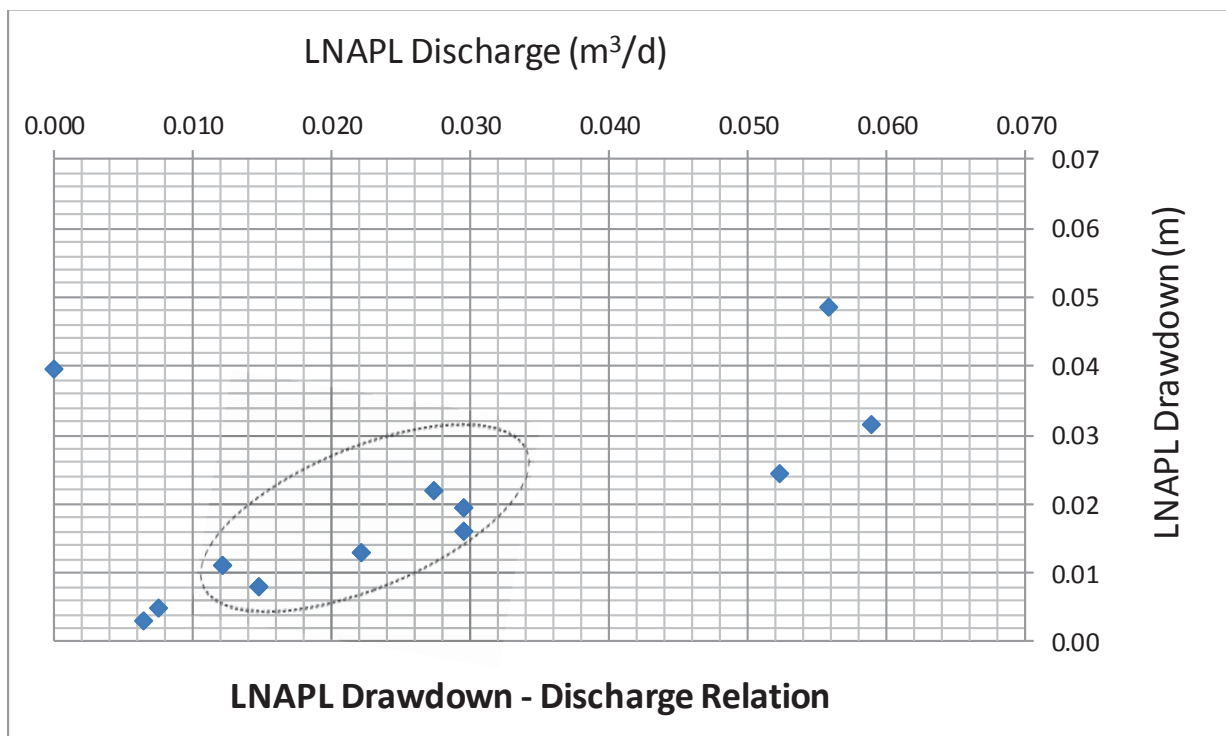


Figure 98. LNAPL drawdown- discharge relation during baildown testing. After a drawdown adjustment of 0.0326 m (post-filtered data).

The figure above is after drawdown correction (0.032m) has been applied. The specific plot shows that borehole recharge from the filter pack maybe is significant (large discharge values at the beginning of the recovery). Moreover, figure depicts behaviour that suggests unconfined LNAPL conditions because we can see continuously decreasing discharge with decreasing drawdown.

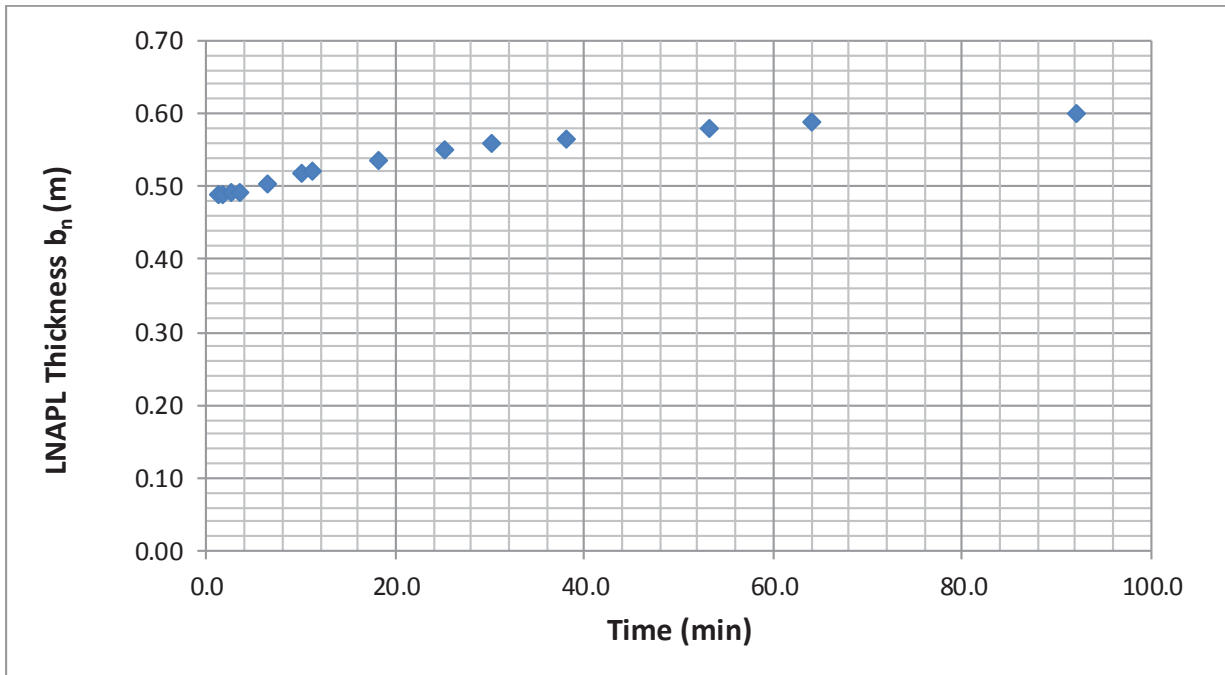


Figure 99. Time series of LNAPL thickness during baildown testing.

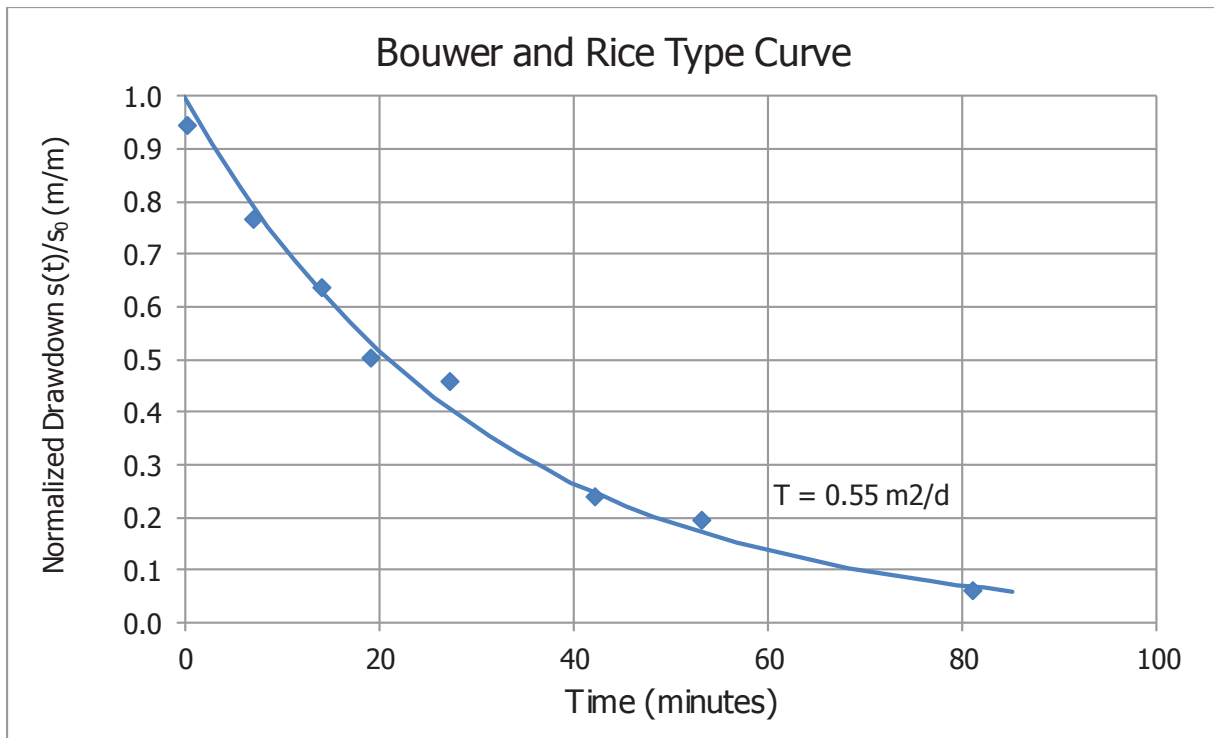


Figure 100. Bouwer and Rice type curve for the calculation of T_n .

PB11 6/04/2016

Well casing radius (m)	0.05
Well radius (m)	0.075
Top of screen (m)	2.9
Bottom of screen (m)	8.5
LNAPL bail-down vol. (litre)	5.78

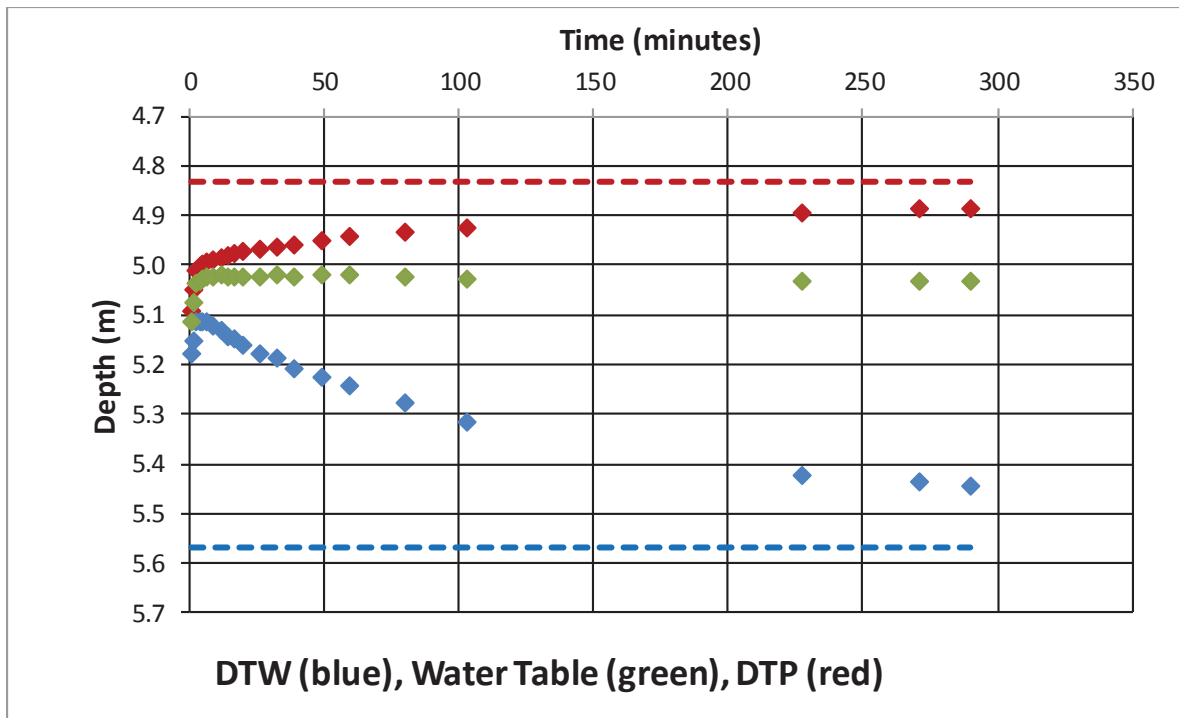


Figure 101. Time series of fluid levels during the baildown test.

The baildown test took place on 6/4/2016. 5.78 L NAPL and 0.70 L water were removed. The initial NAPL thickness was 0.74 m and the final thickness after 289 min was 0.56 m. The elevation of water table (corrected) is constant thus, B&R method has to be used. The B&R method showed 0.136 (m²/d) as Transmissivity value. The cut off time was 8 minutes.

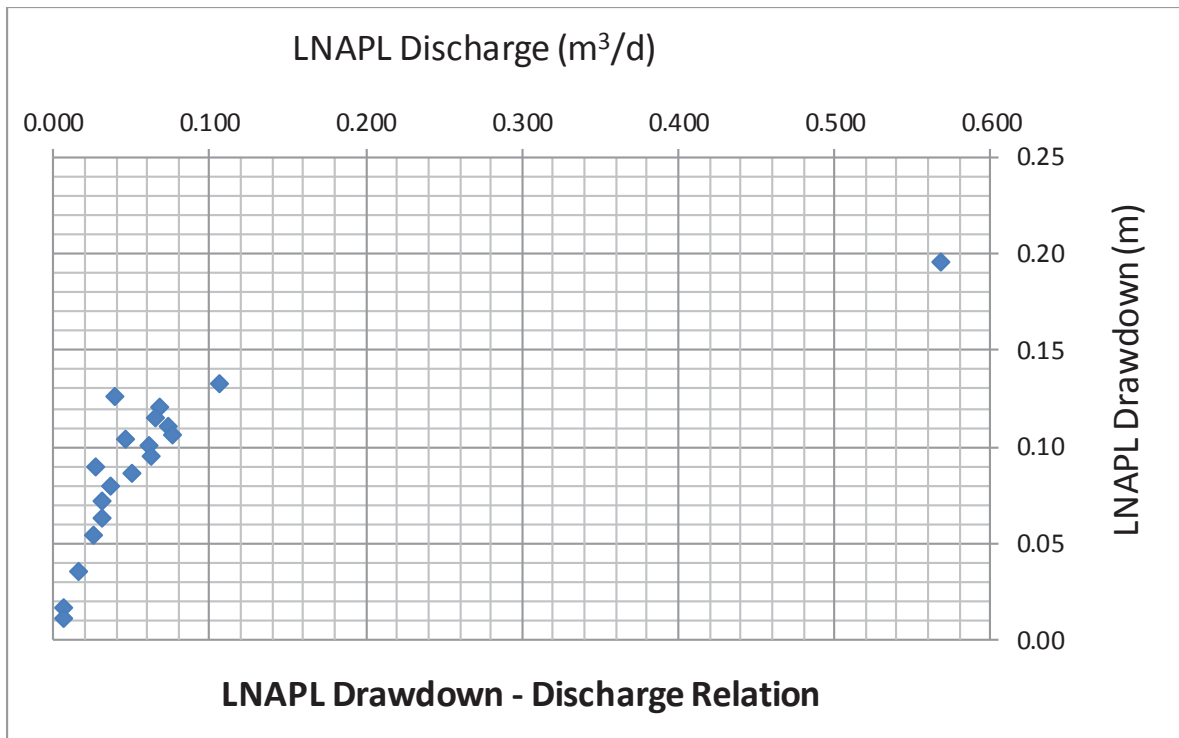


Figure 102. LNAPL drawdown- discharge relation during baildown testing. After a drawdown adjustment of 0.0428 m.

The figure above is after drawdown correction has been applied. The specific plot shows that borehole recharge from the filter pack maybe is not significant. Moreover, figure depicts behaviour that suggests unconfined LNAPL conditions because we can see continuously decreasing discharge with decreasing drawdown.

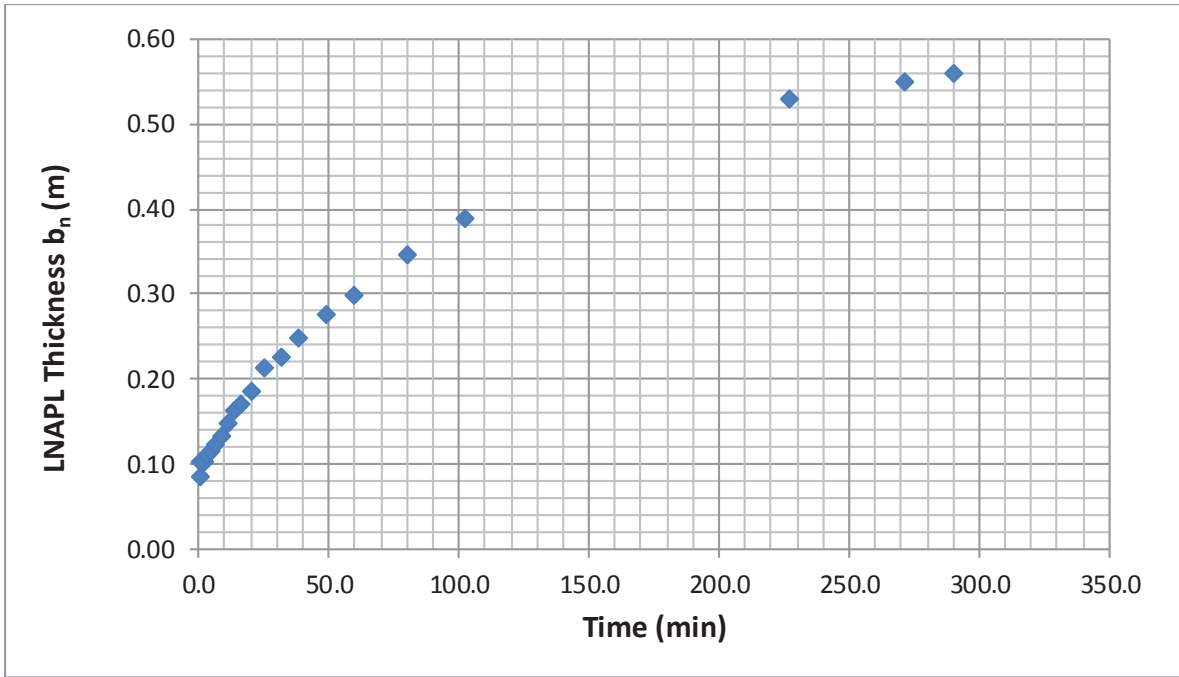


Figure 103. Time series of LNAPL thickness during baildown testing.

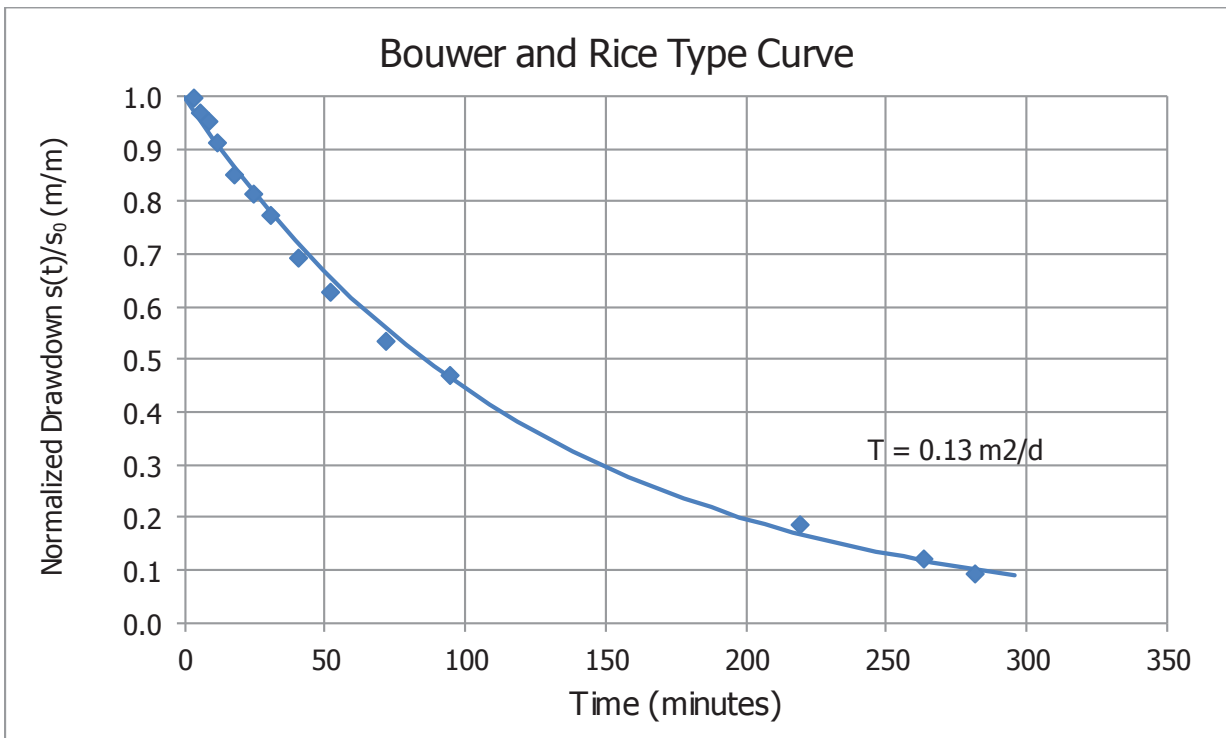


Figure 104. Bower and Rice type curve for the calculation of T_n .

Well casing radius (m)	0.05
Well radius (m)	0.075
Top of screen (m)	3.25
Bottom of screen (m)	9.25
LNAPL bail-down vol. (litre)	2.73

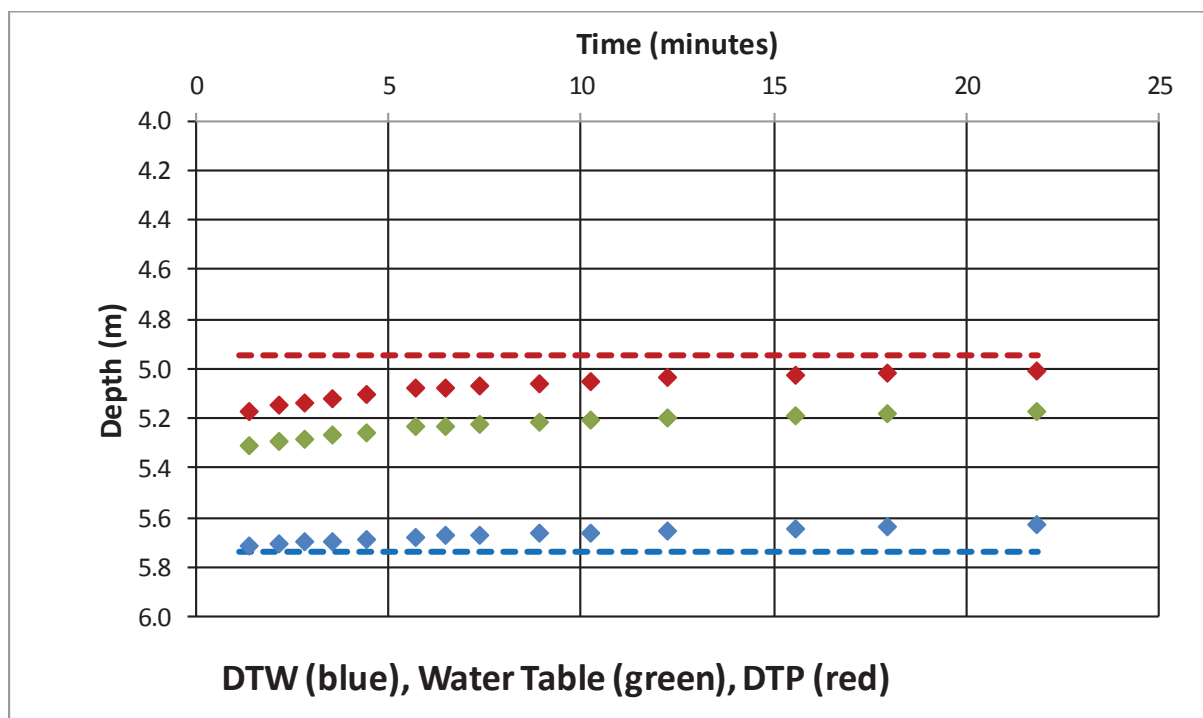


Figure 105. Time series of fluid levels during the baildown test.

The bail-down test took place on 8/5/2015. 2.73 L NAPL and 0 L water were removed. The initial NAPL thickness before the test was 0.79 m. The thickness at the beginning of the test was 0.54 m and the final thickness after 308 min was 0.62 m. The elevation of water table (corrected) is constant (after the cut off time which is 7 min), thus B&R method can be used. The B&R method showed 0.24 (m²/d) as Transmissivity value. On 28/04/16 the product thickness was 0.67m.

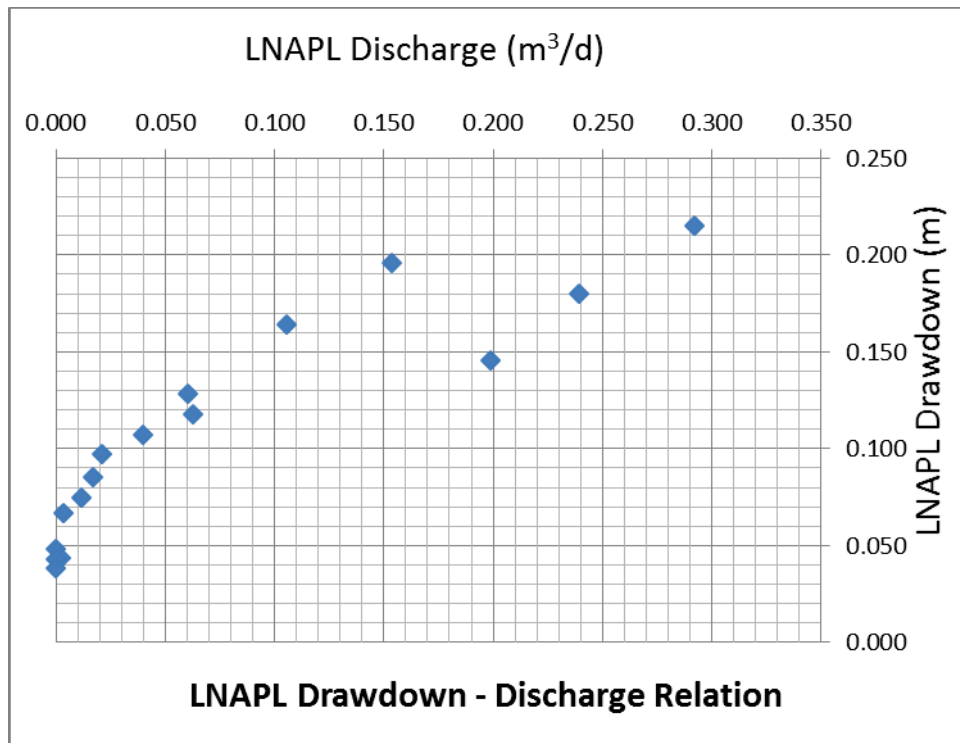


Figure 106. Pre-filtered data.

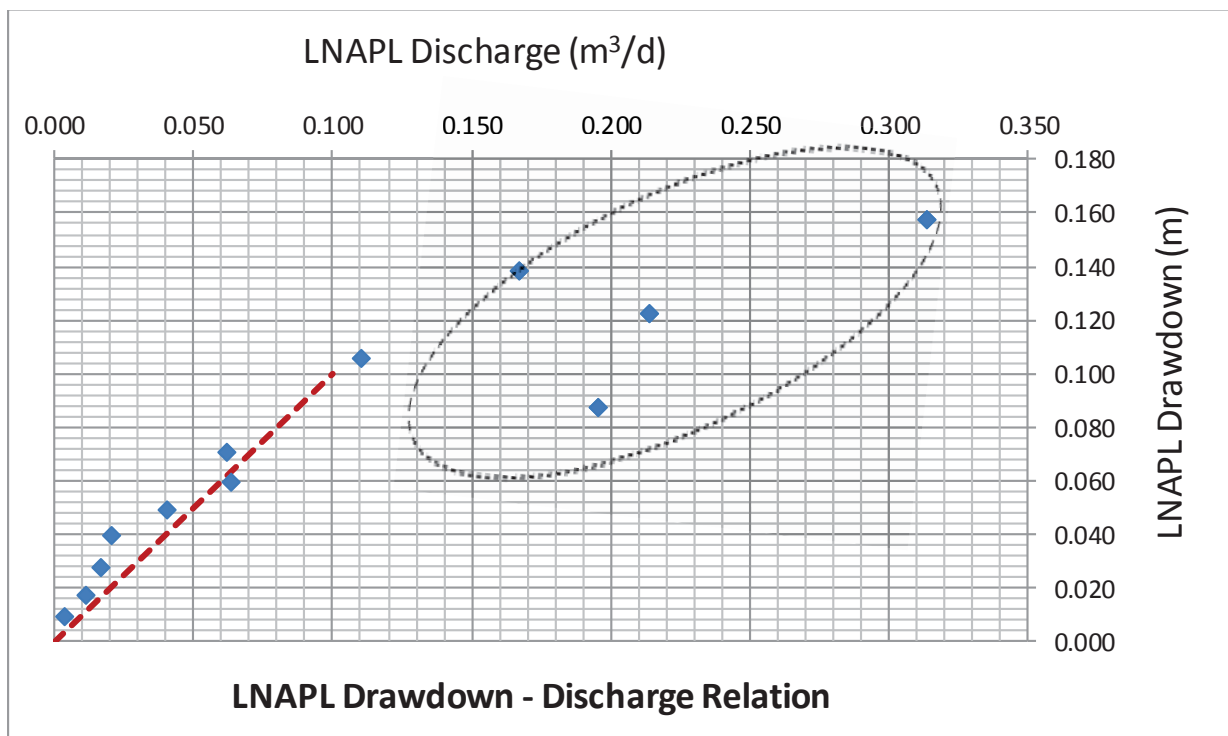


Figure 107. LNAPL drawdown- discharge relation during baildown testing. After a drawdown adjustment of 0.0582 m (post-filtered data).

The figure above is after drawdown correction (0.0582m) has been applied. The specific plot shows that borehole recharge from the filter pack is significant (large discharge values at the beginning of the recovery). Moreover, figure depicts behaviour that suggests unconfined LNAPL conditions because we can see continuously decreasing discharge with decreasing drawdown.

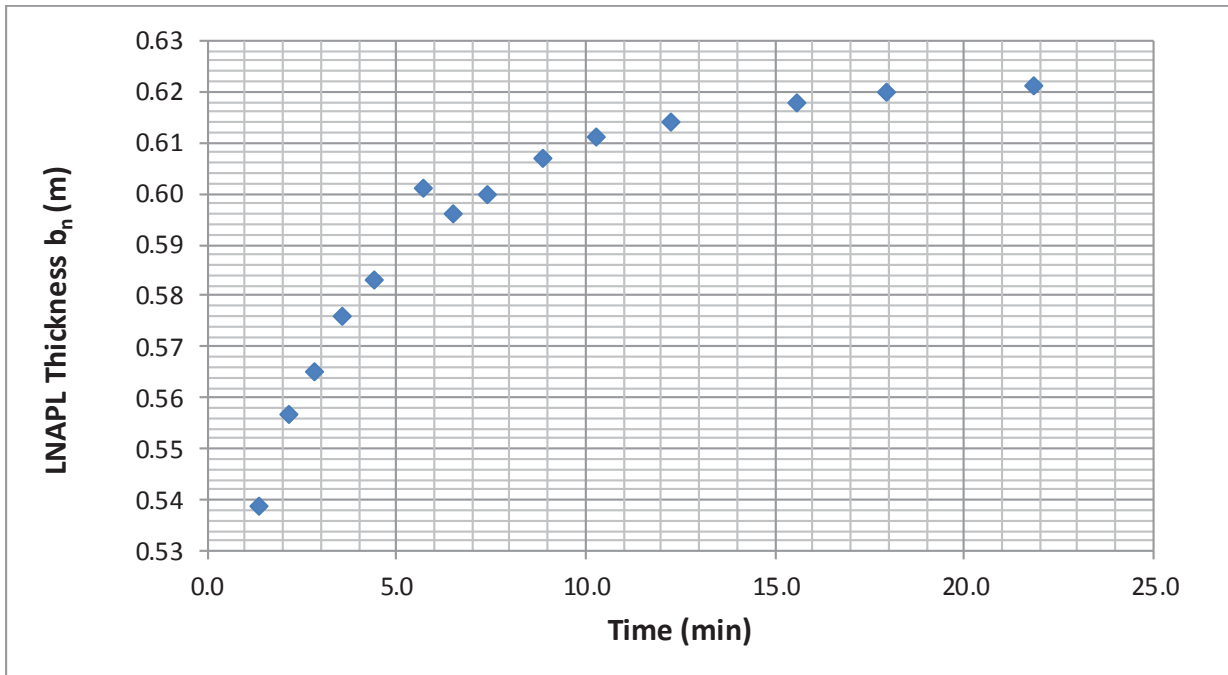


Figure 108. Time series of LNAPL thickness during baildown testing.

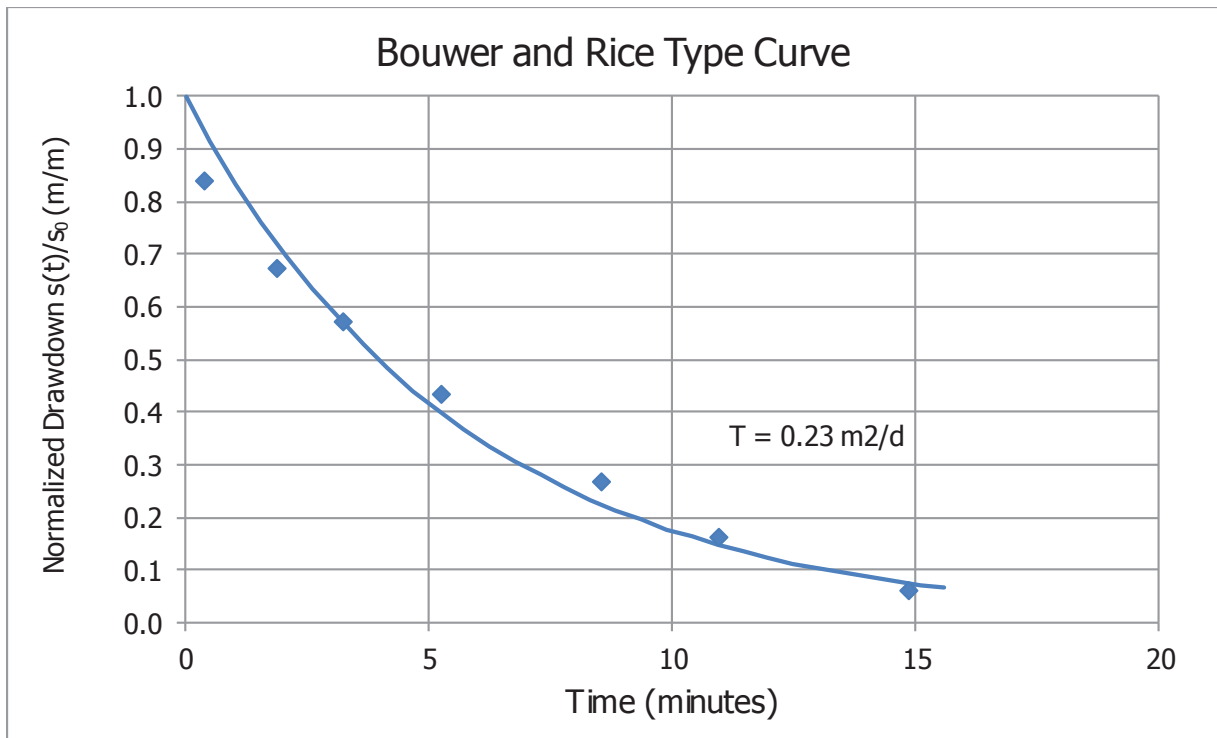


Figure 109. Bouwer and Rice type curve for the calculation of T_n .

PB13 6/04/2016

Well casing radius (m)	0.05
Well radius (m)	0.075
Top of screen (m)	3.25
Bottom of screen (m)	9.25
LNAPL bail-down vol. (litre)	2.73

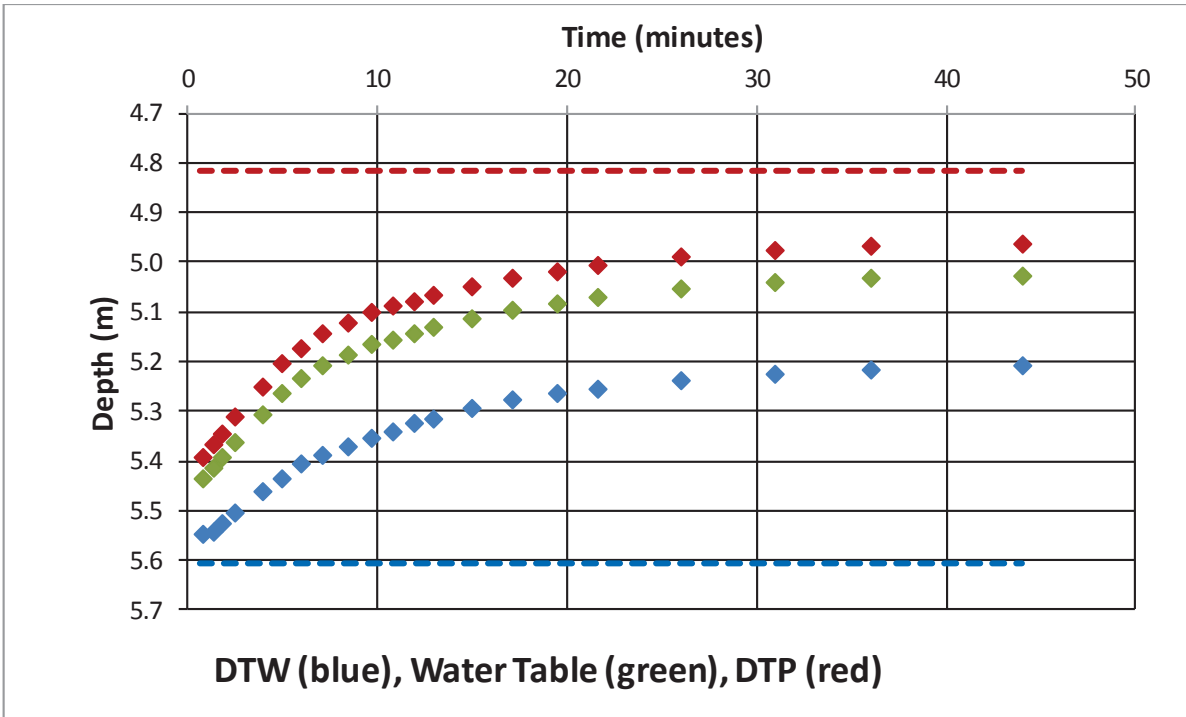


Figure 110. Time series of fluid levels during the baildown test.

The bail-down test took place on 6/4/2016. 6.78 L NAPL and 0.38 L water were removed. The initial NAPL thickness before the test was 0.79 m. The thickness at the beginning of the test was 0.15 m, after 44 minute was 0.25 m and the final thickness after 1100 min was 0.29 m. The B&R method showed 0.027 (m²/d) as Transmissivity value. The cut off time was 20 minutes.

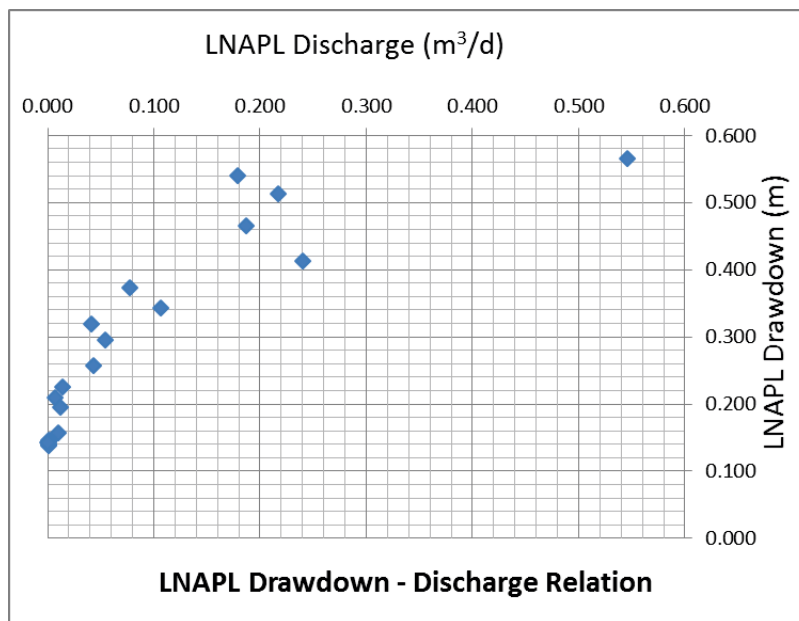


Figure 111. Pre-filtered data.

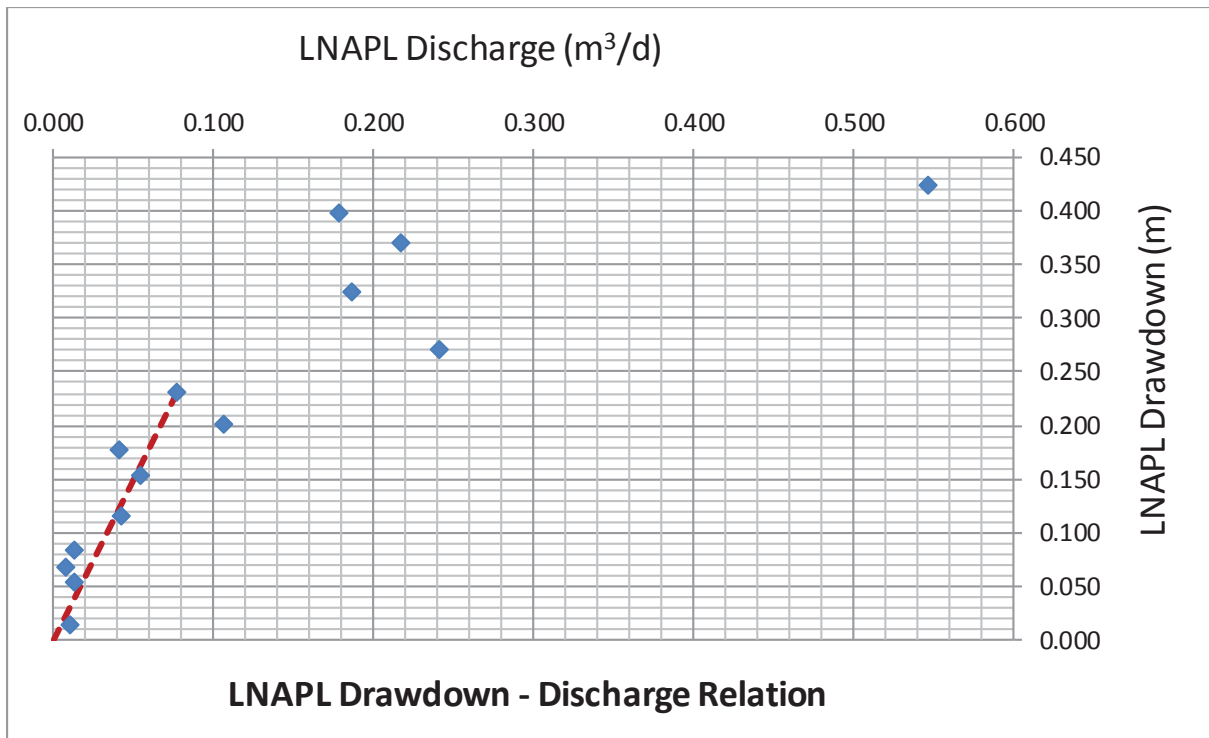


Figure 112. LNAPL drawdown- discharge relation during baildown testing. After a drawdown adjustment of 0.1421 m (post-filtered data).

The figure above is after drawdown correction (0.1421m) has been applied. The specific plot shows that borehole recharge from the filter pack is not significant. Moreover, figure depicts behaviour that suggests unconfined LNAPL conditions because we can see continuously decreasing discharge with decreasing drawdown.

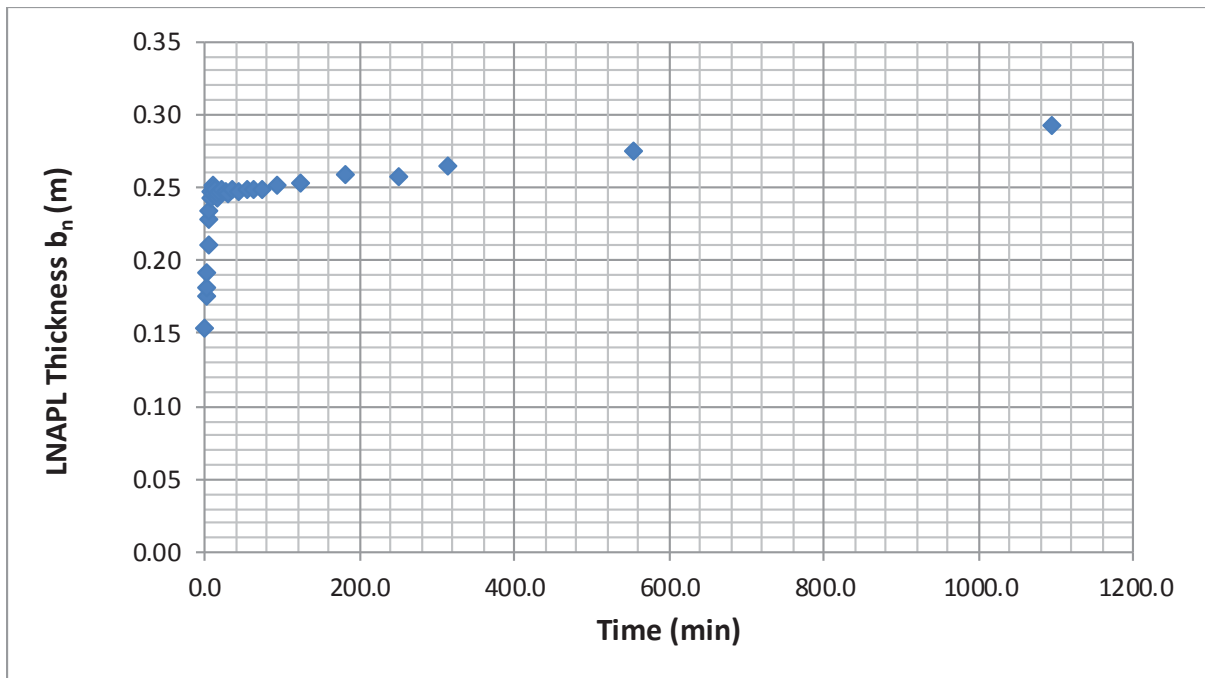


Figure 113. Time series of LNAPL thickness during baildown testing.

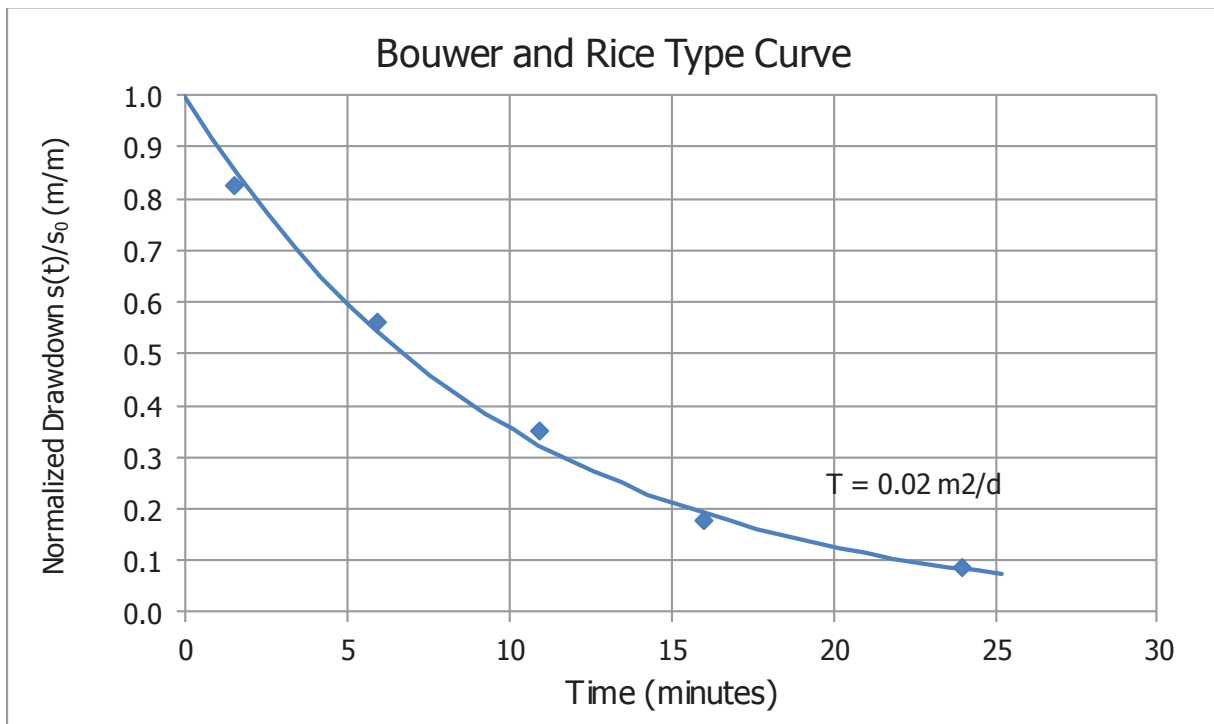


Figure 114. Bower and Rice type curve for the calculation of T_n .

Well casing radius (m)	0.05
Well radius (m)	0.075
Top of screen (m)	3.10
Bottom of screen (m)	9.10
LNAPL bail-down vol. (litre)	8.44

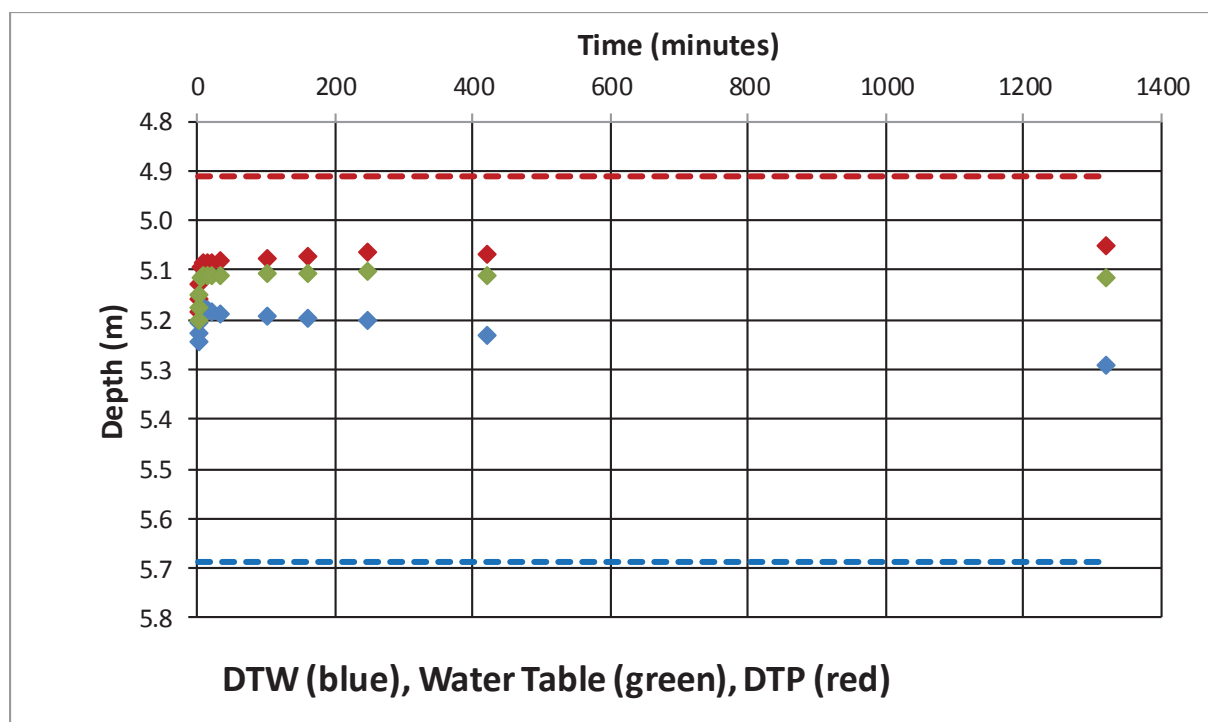


Figure 115. Time series of fluid levels during the baildown test.

The bail-down test took place on 06/04/2016. 8.44 L NAPL and 0.62 L water were removed. The initial NAPL thickness before the test was 0.78 m. The thickness after the removal of the product was 0.06m, after 400 minutes the thickness was 0.16m and the final thickness after 1320min was 0.24 m. The elevation of water table (corrected) is constant thus, B&R method can be used. The B&R method showed 0.034 (m²/d) as Transmissivity value and the cut off time was 10 min.

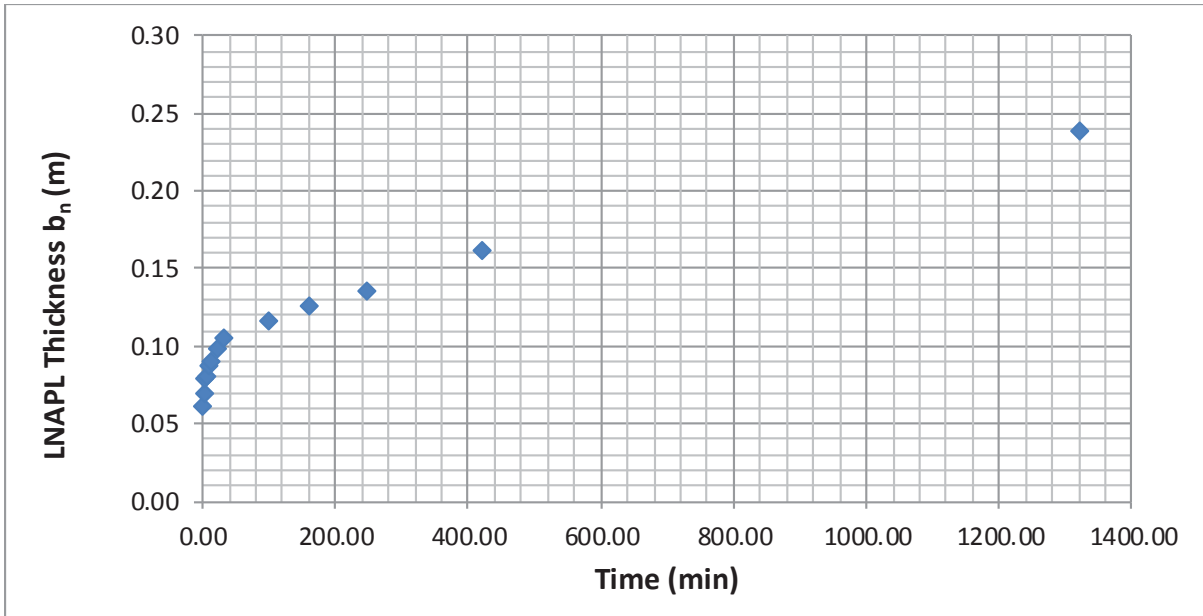


Figure 116. Time series of LNAPL thickness during baildown testing.

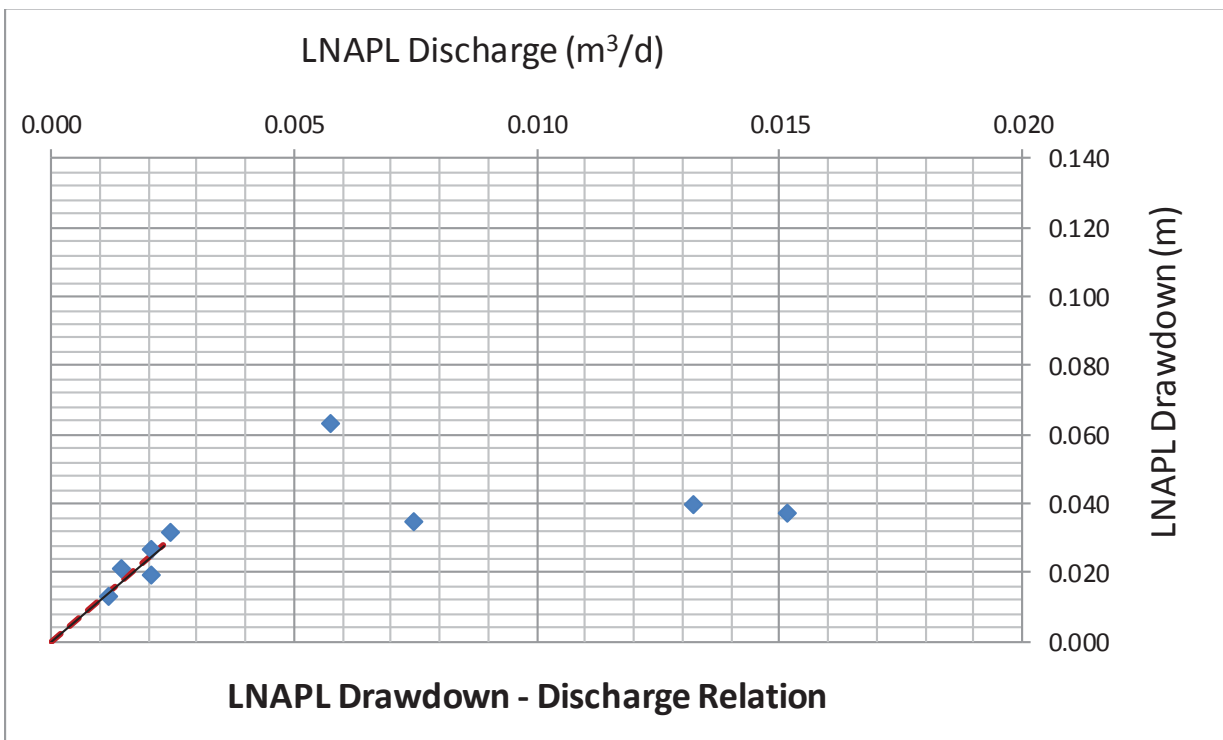


Figure 117. LNAPL drawdown- discharge relation during baildown testing. After a drawdown adjustment of 0.1368 m.

The figure above is after drawdown correction (0.1368m) has been applied. The specific plot shows that borehole recharge from the filter pack is an issue. Moreover, figure depicts

behaviour that suggests unconfined LNAPL conditions because it can be seen a continuously decreasing discharge with decreasing drawdown.

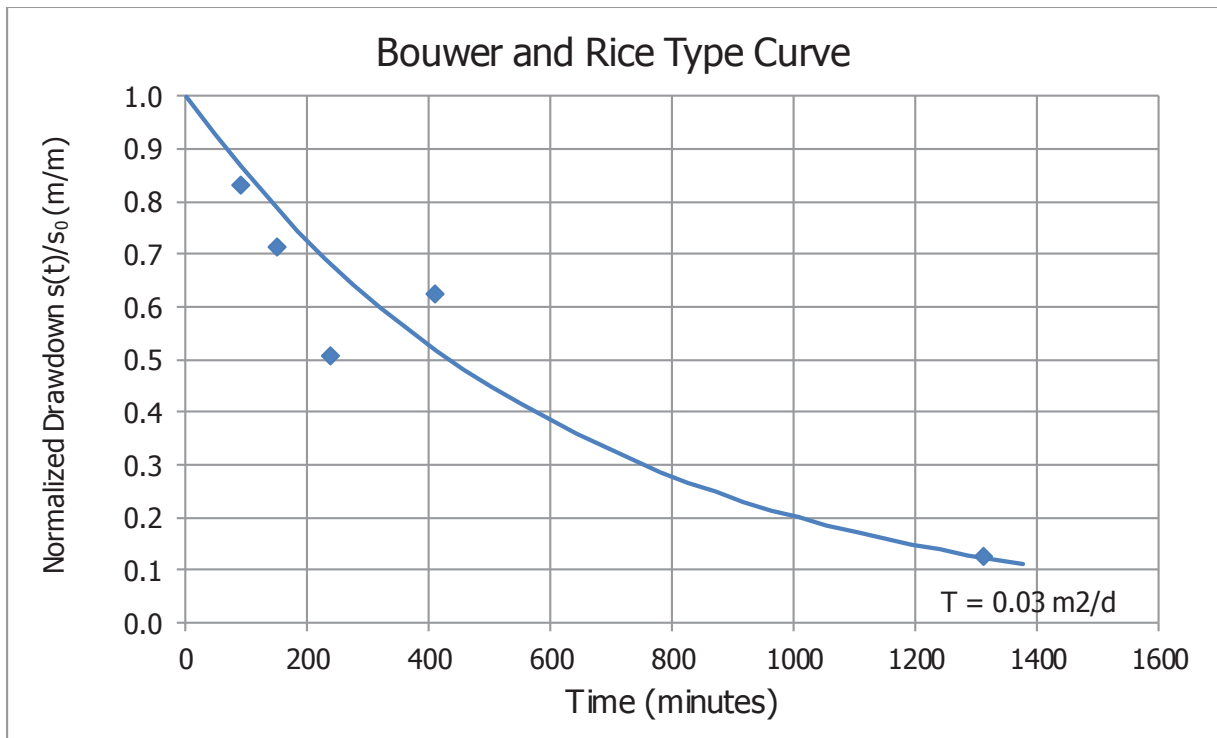


Figure 118. Bower and Rice type curve for the calculation of T_n .

PB40 06/04/2016

Well casing radius (m)	0.05
Well radius (m)	0.075
Top of screen (m)	3.10
Bottom of screen (m)	9.10
LNAPL bail-down vol. (litre)	5.34

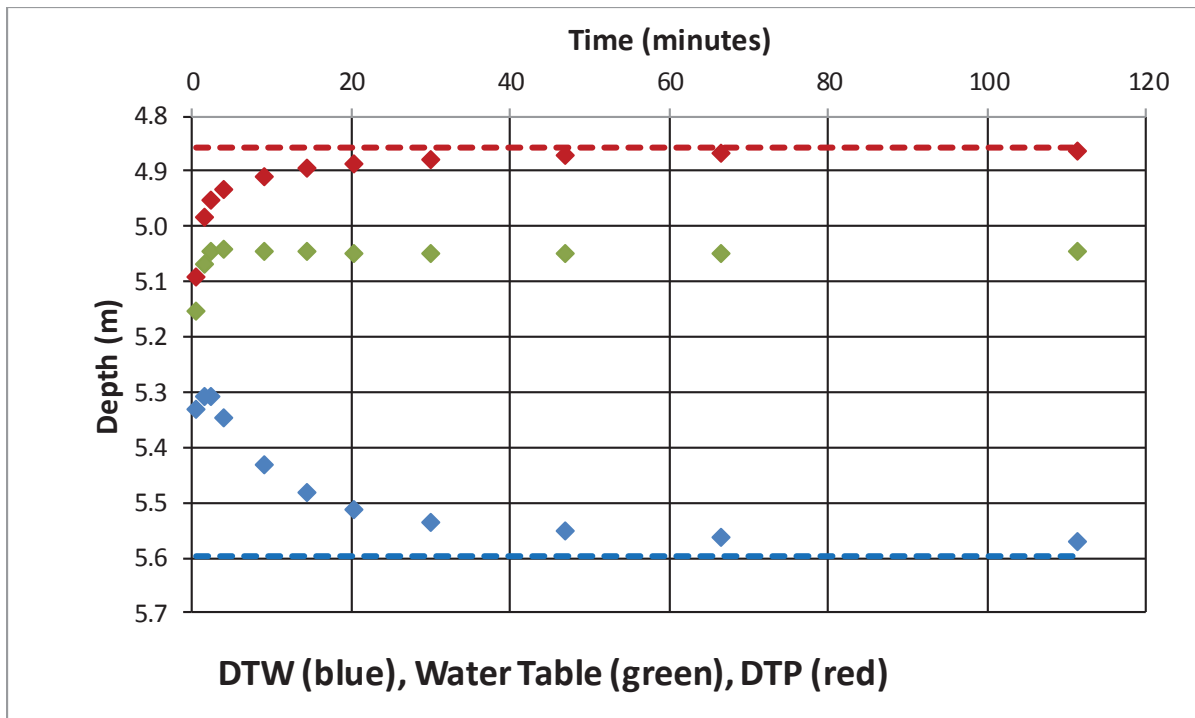


Figure 119. Time series of fluid levels during the baildown test.

The bail-down test took place on 06/04/2016. 5.34 L NAPL and 1.10 L water were removed. The initial NAPL thickness before the test was 0.74 m. The thickness after the removal of the product was 0.24m, after 111 minutes was 0.71 m and the final thickness after 430 min was 0.74 m. The elevation of water table (corrected) is constant thus, B&R method can be used. The B&R method showed 0.577 (m^2/d) as Transmissivity value and the cut off time was 4.2 min.

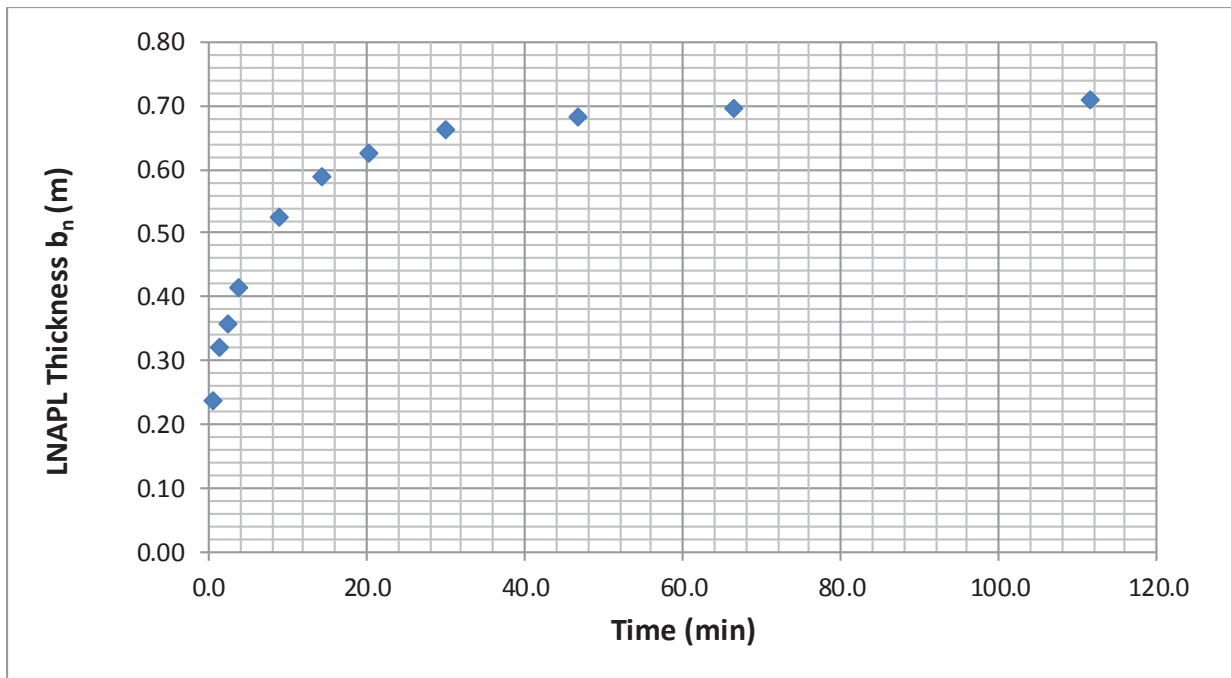


Figure 120. Time series of LNAPL thickness during baildown testing.

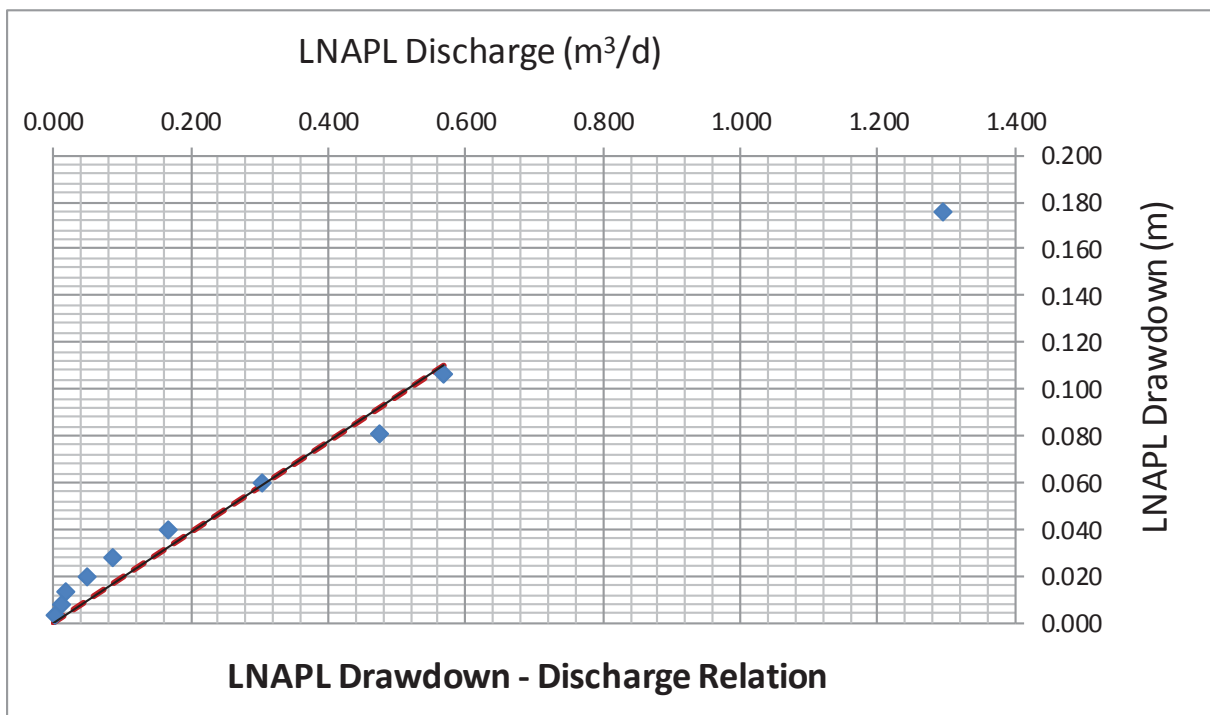


Figure 121. LNAPL drawdown- discharge relation during baildown testing. After a drawdown adjustment of 0.004 m.

The figure above is after drawdown correction (0.004m) has been applied. The specific plot shows that borehole recharge from the filter pack is not significant (one large discharge value at the beginning of the recovery). Moreover, figure depicts behaviour that suggests

unconfined LNAPL conditions because it can be seen a continuously decreasing discharge with decreasing drawdown.

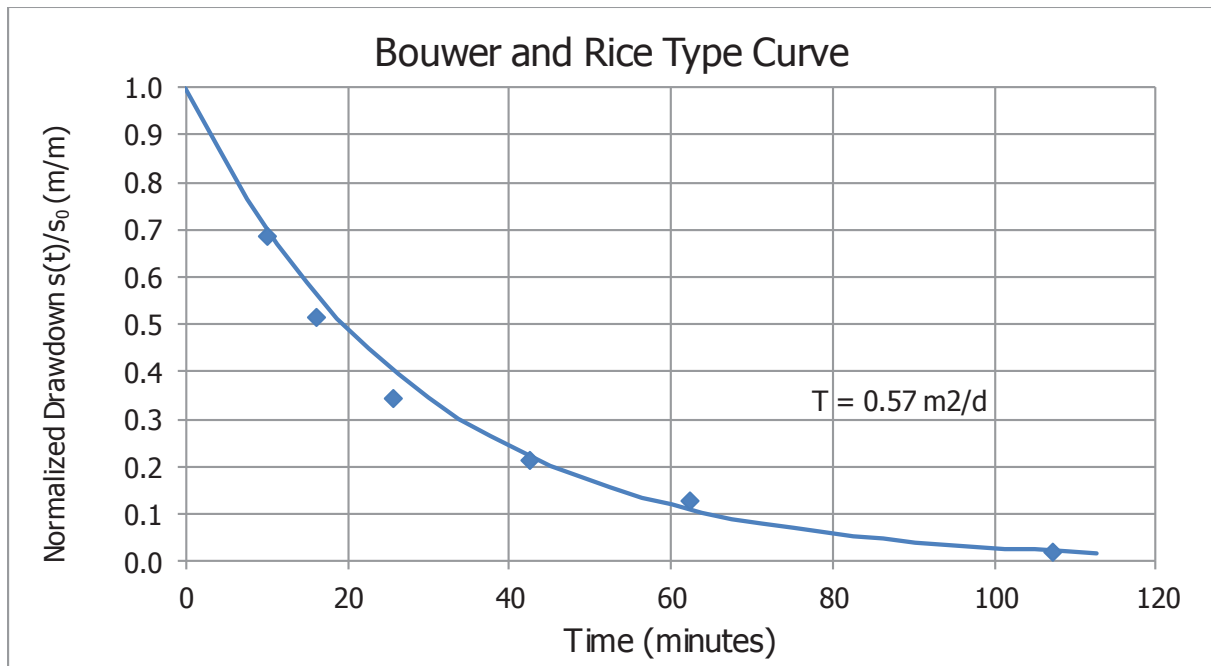


Figure 122. Bower and Rice type curve for the calculation of T_n .

PB40 14/06/2016

Well casing radius (m)	0.05
Well radius (m)	0.075
Top of screen (m)	3.10
Bottom of screen (m)	9.10
LNAPL bail-down vol. (litre)	19.5

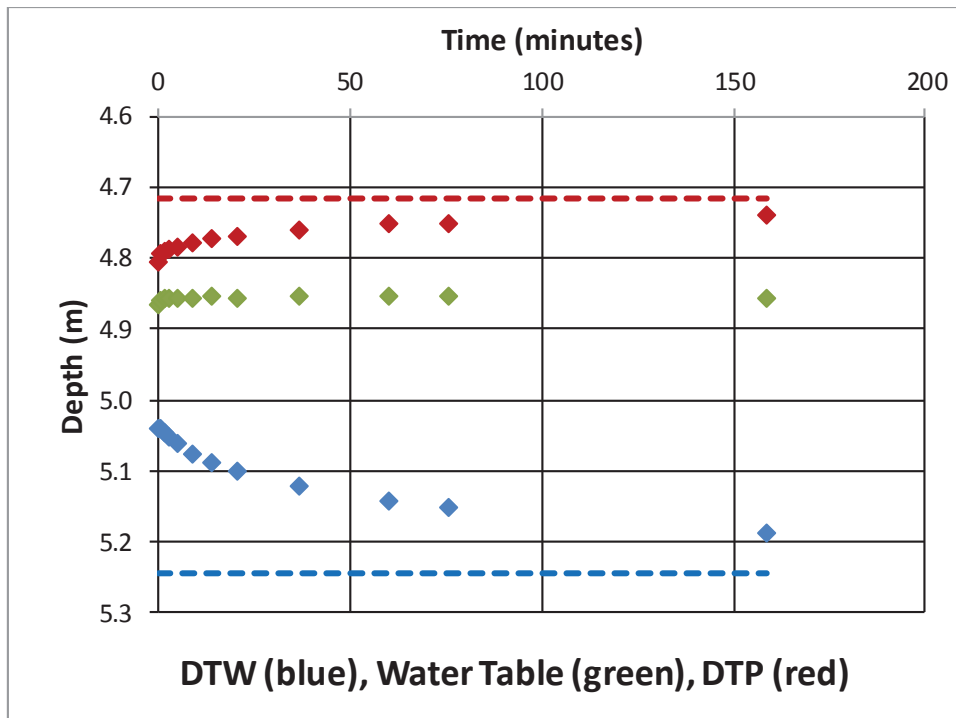


Figure 123. Time series of fluid levels during the baildown test.

The bail-down test took place on 14/06/2016. 19.5 L NAPL and 0 L water were removed. The initial NAPL thickness before the test was 0.528 m. The thickness after the removal of the product was 0.23 m, after 158 minutes was 0.45 m. The elevation of water table (corrected) is constant thus, B&R method can be used. The B&R method showed 0.304 (m²/d) as Transmissivity value and the cut off time was 0.7 min.

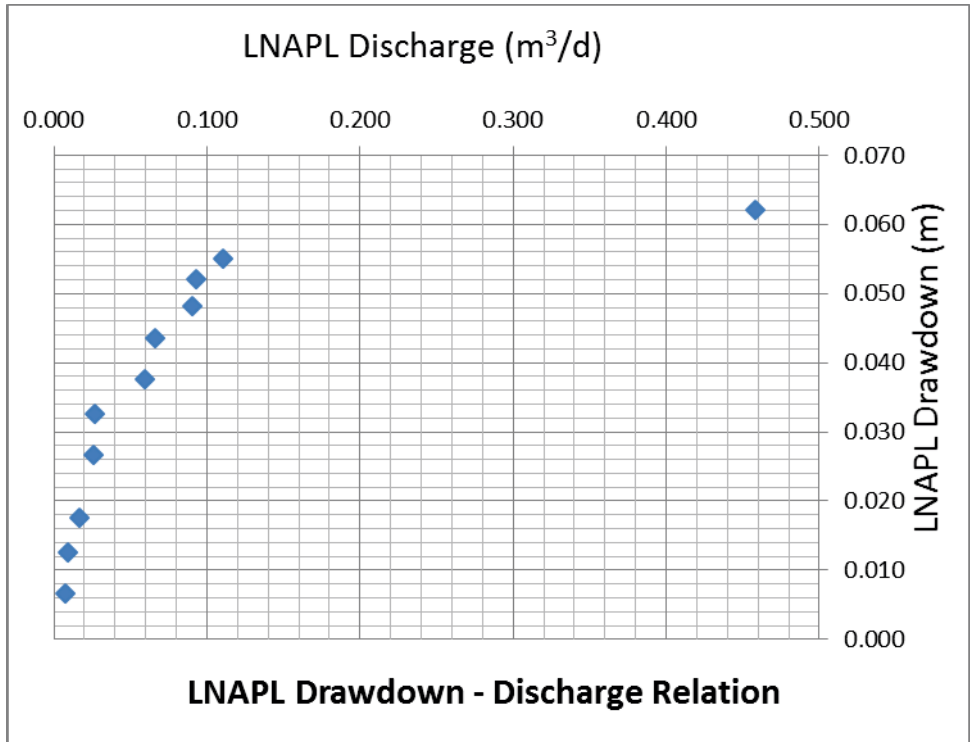


Figure 124. LNAPL drawdown- discharge relation during baildown testing. After a drawdown adjustment of 0.0224 m.

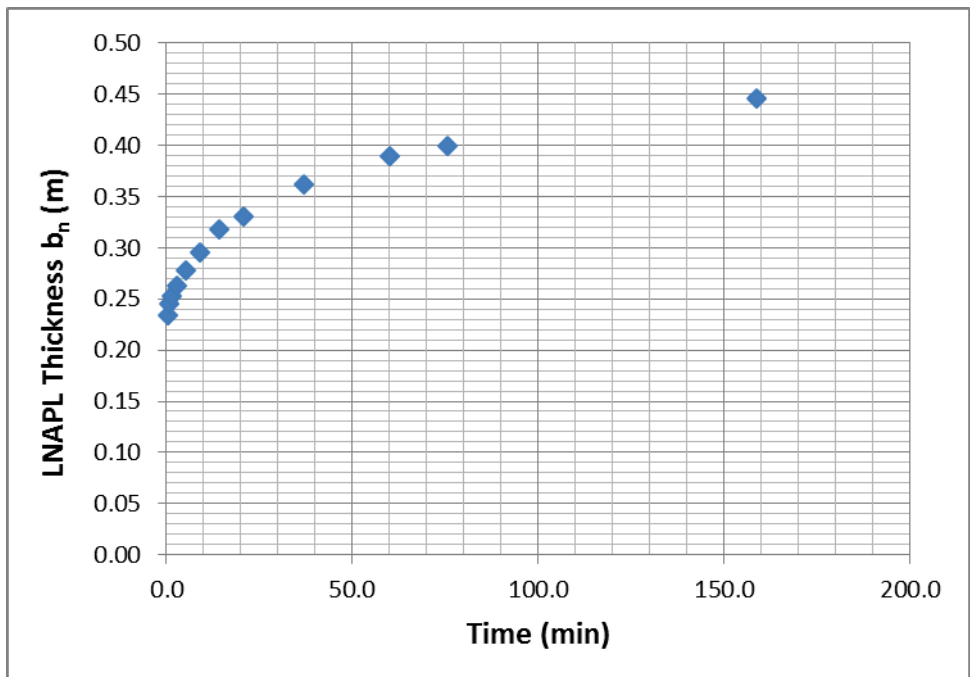


Figure 125. Time series of LNAPL thickness during baildown testing.

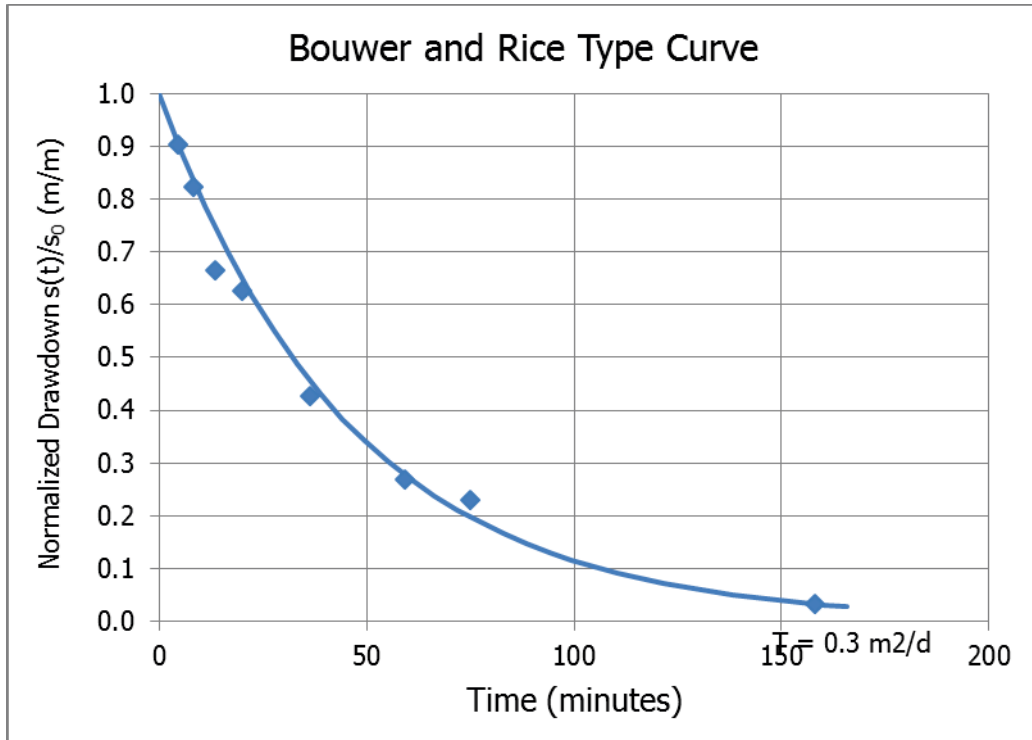


Figure 126. Bouwer and Rice type curve for the calculation of T_n .

MP42 06/04/2016

Well casing radius (m)	0.05
Well radius (m)	0.075
Top of screen (m)	3.20
Bottom of screen (m)	9.20
LNAPL bail-down vol. (litre)	1.31

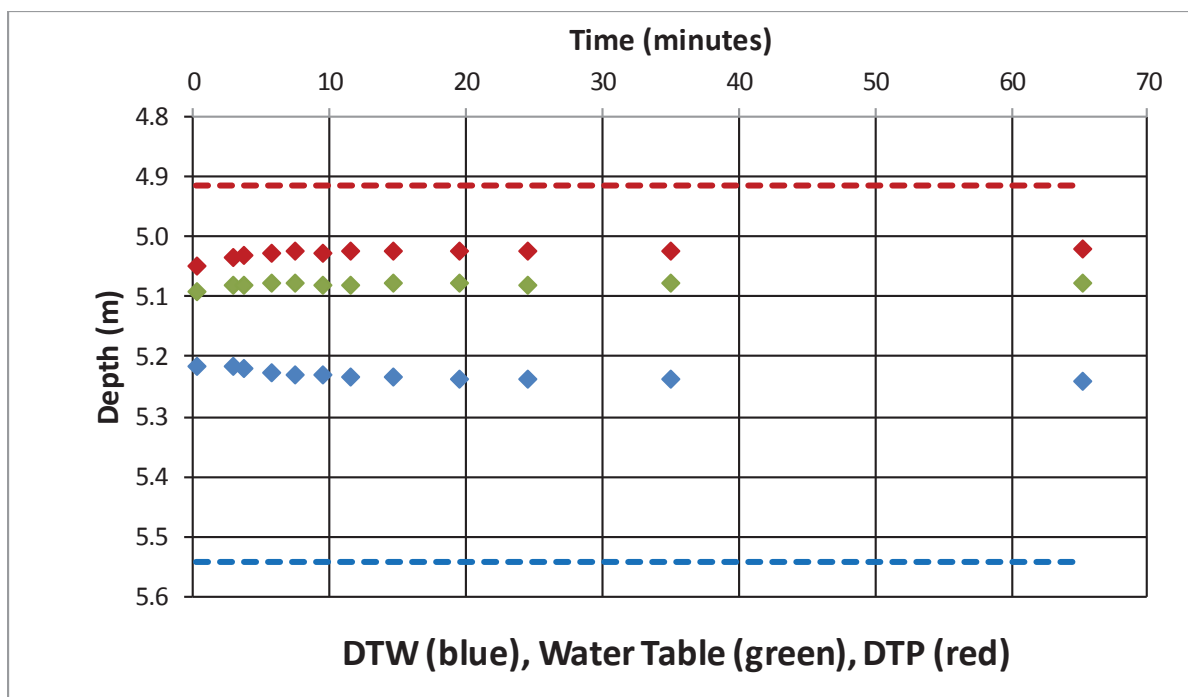


Figure 127. Time series of fluid levels during the baildown test.

The bail-down test took place on 06/04/2016. 1.31 L NAPL and 0.07 L water were removed. The initial NAPL thickness before the test was 0.63 m. The thickness after the removal of the product was 0.17m, after 65 minutes was 0.22 m and the final thickness after 1300 min was 0.225 m. The elevation of water table (corrected) is constant thus, B&R method can be used. The B&R method showed 0.139 (m^2/d) as Transmissivity value and the cut off time was 7.4 min. On 28/04/16 the product thickness was 0.04m.

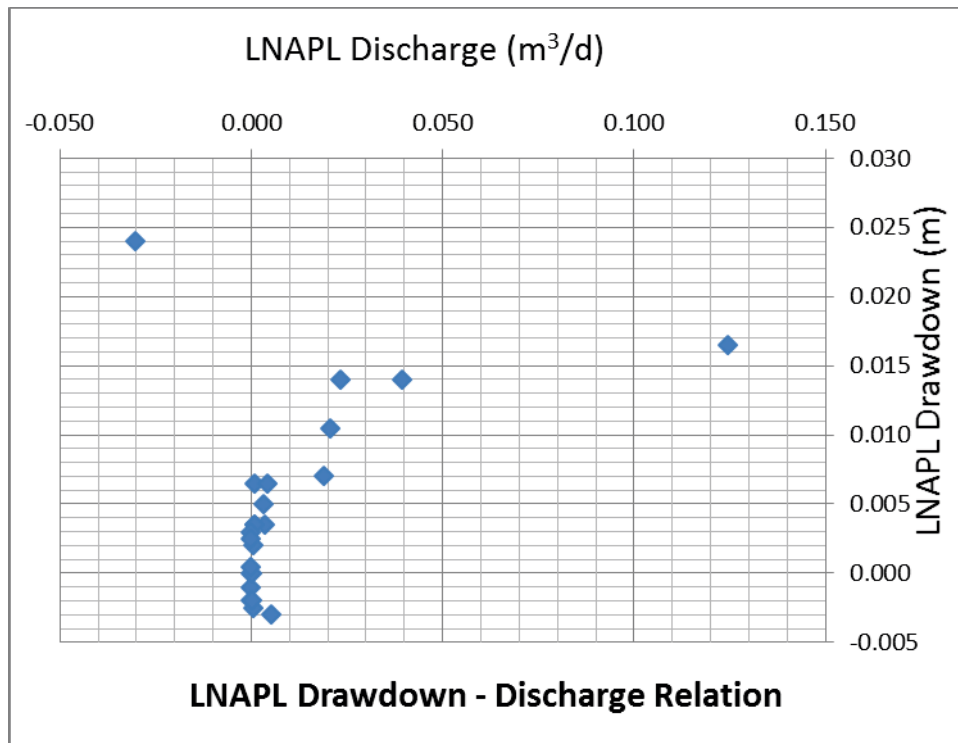


Figure 128. Pre-filtered data.

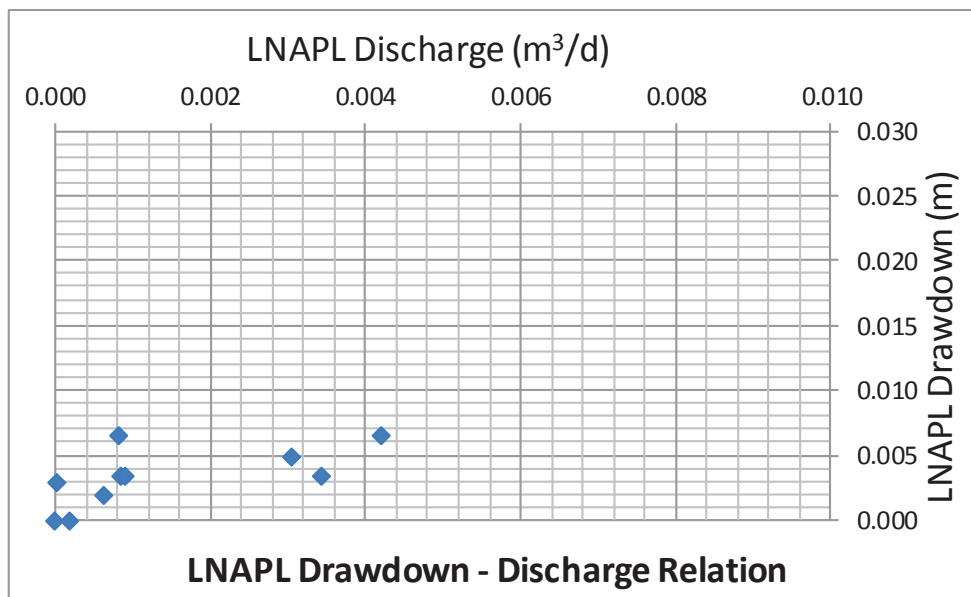


Figure 129. LNAPL drawdown- discharge relation during baildown testing. After a drawdown adjustment of 0.105m.

The figure above is after drawdown correction (0.105m) has been applied. The specific plot shows that borehole recharge from the filter pack is not significant. Moreover, figure depicts behaviour that suggests unconfined LNAPL conditions because it can be seen a continuously decreasing discharge with decreasing drawdown.

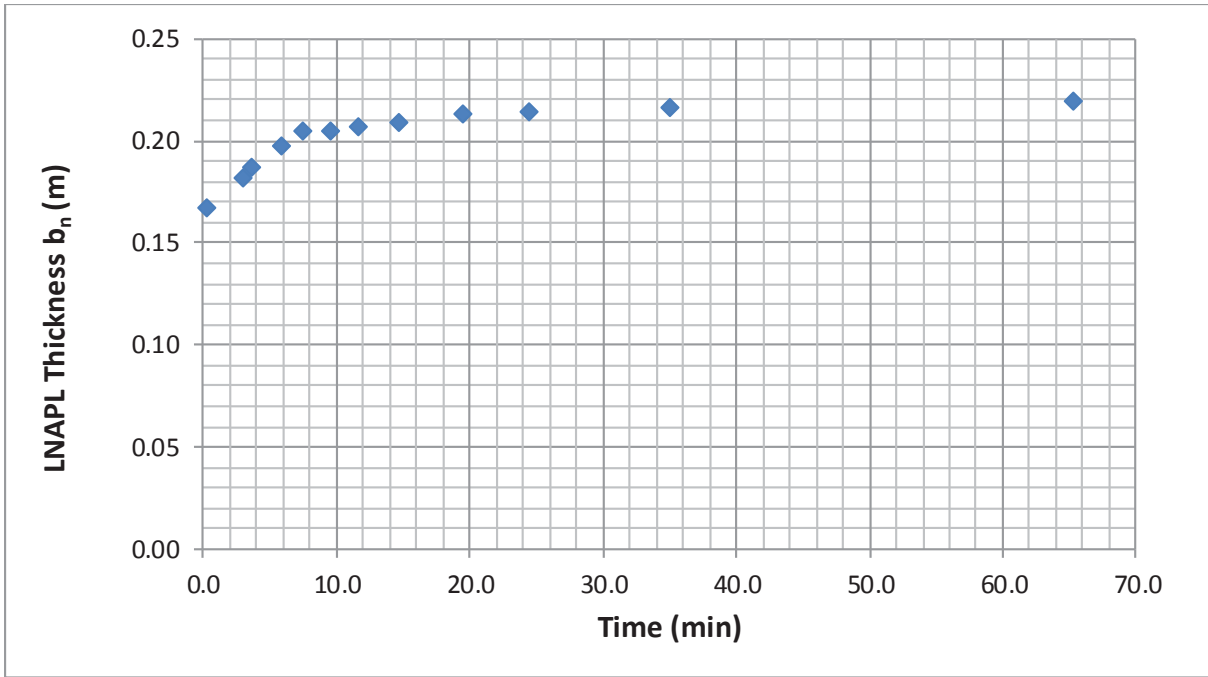


Figure 130. Time series of LNAPL thickness during baildown testing.

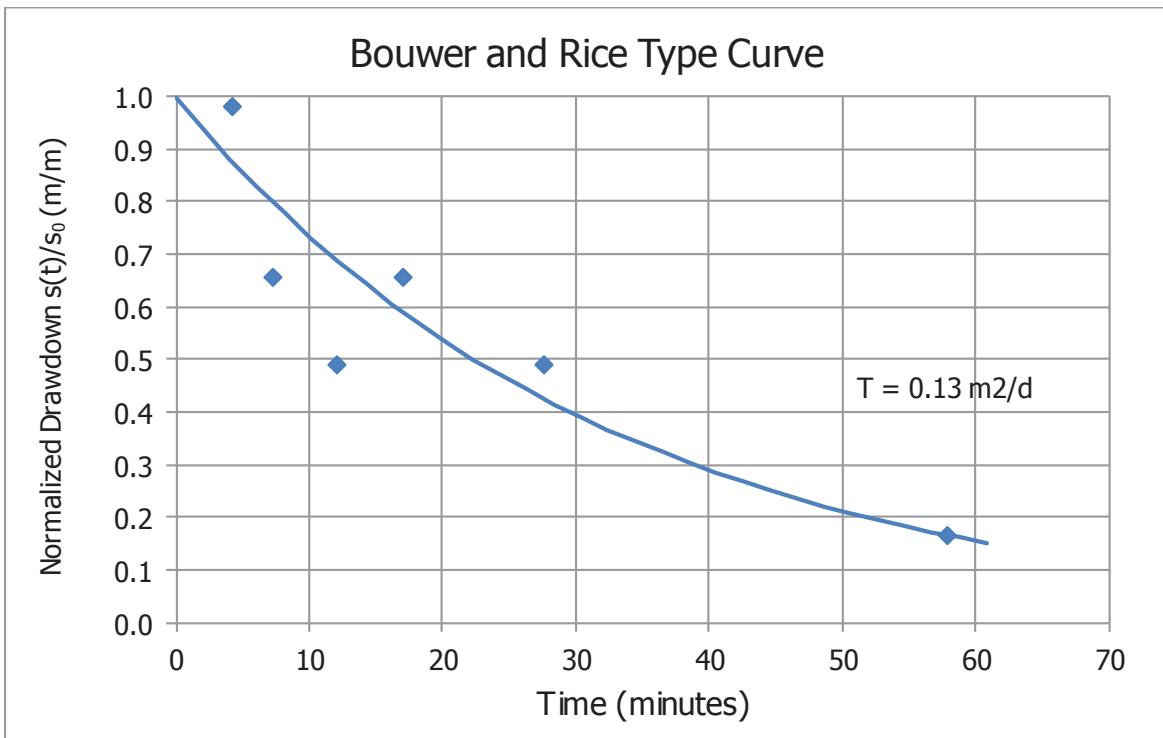


Figure 131. Bower and Rice type curve for the calculation of T_n .

4. REFERENCES

API 2012, *LNAPL transmissivity workbook: A tool for baildown test analysis*, American Petroleum Institute (API), Washington, 2012.

Bouwer, H. & Rice, R.C. 1976, 'A slug test for determining hydraulic conductivity of unconfined aquifers with completely or partially penetrating wells', *Water Resources Research*, vol. 12, no. 3, pp. 423-8.

Hawthorne, J.M. 2014, 'Filtering Baildown Test Data. Applied NAPL Science Review, Volume 4, Issue 2, March 2014'.

Kirkman, A.J. 2013, 'Refinement of Bouwer-Rice Baildown Test Analysis', *Groundwater Monitoring & Remediation*, vol. 33, no. 1, pp. 105-10.

Kirkman, A.J., Adamski, M. & Hawthorne, J.M. 2013, 'Identification and Assessment of Confined and Perched LNAPL Conditions', *Groundwater Monitoring & Remediation*, vol. 33, no. 1, pp. 75-86.

Appendix K

1
2
3
4
5
6
7
8
9
10
11
12
13
14
15
16
17
18
19
20
21
22
23
24
25
26
27
28
29
30
31
32
33
34
35
36
37
38
39
40
41
42
43
44
45
46

The presented manuscript has been approved for publication by the 1) CSIRO e-publish and 2) CRC CARE. It will be submitted to the Journal of Environmental Management.

1) CSIRO approval

Dear Evangelos Gatsios,

Manuscript ID: EP178287

Manuscript Title: LNAPL transmissivity as a remediation metric in complex sites under water table fluctuations

Authors: Evangelos Gatsios, Jonas Garcia Rincon, John Rayner, Robert G McLaughlan, and Greg Davis

I am pleased to inform you that your manuscript is now approved to be submitted for publication.

Please ensure that you return to the ePublish - Approval Module to record your interactions with the Publisher.

<https://epublish.csiro.au>

The next step is to record when you submit this manuscript to the publisher/conference organiser. You use the task 'Submit to Publisher' which now appears in your task list. At this time you can attach the version of the manuscript which is sent to the publisher/conference organiser.

After this there are two other steps:

'Publisher Decision' - whether it is Accepted or Rejected 'Confirm Published Manuscript' - when it is published

Publications will not appear in the Repository until after the Confirm Published step is completed by authors.

Yours sincerely,

Declan Page

47 2) CRC CARE approval

48

49 **Publication Approval and Collection System - status update**

50

51 Hi Evangelos,

52

53 Your Publication Approval and Collection System application with id 905 has been approved.

54 Please note that once your publication has been accepted by the publisher, you will be

55 required to login and complete the application by adding any currently missing information

56 via the 'Publication Data' link in your dashboard at

57 href='https://www.pacs.crccare.com/dashboard.php'>

58 <https://www.pacs.crccare.com/dashboard.php> .

59

60 This information will include application details not yet supplied (such as page number,

61 volume edition, place of publication etc), and publication verification information (such as f

62 inal manuscript, scans of cover pages, acknowledgement pages etc).

63

64 You will receive occasional email reminders about this.

65

66

www.crccare.com

Building X, University Boulevard,

University of South Australia

Mawson Lakes SA 5095

+61 8 8302 5038

67

68

69

70

71

72

73 **LNAPL transmissivity as a remediation metric in complex sites under water**
74 **table fluctuations**

75

76

77

78 Evangelos Gatsios ^{a, b, c*}, Jonás García-Rincón ^{a, b, c}, John L. Rayner ^{a, c}, Robert G.

79 McLaughlan ^{b, c}, Greg B. Davis ^{a, c, d}

80

81

82 ^aCSIRO Land and Water, Private Bag No. 5, Wembley, WA 6913, Australia

83 ^b Faculty of Engineering and Information Technology, University of Technology

84 Sydney, 15 Broadway, Ultimo, NSW 2007, Australia

85 ^c Cooperative Research Centre for Contamination Assessment and Remediation of the

86 Environment (CRC CARE), Australia

87 ^d School of Earth and Environment, University of Western Australia, Nedlands, WA,

88 Australia

89

90

91

92 *Corresponding author at: CSIRO Land and Water, 147 Underwood Avenue, Floreat,

93 WA 6014, Australia. Tel.: +61893336028; Tel.: +61893336756.

94

95 E-mail addresses: Evangelos.Gatsios@csiro.au (E. Gatsios),

96 Jonas.Garciarincon@csiro.au (Jonás García-Rincón), John.Rayner@csiro.au (John L.

97 Rayner), Robert.McLaughlan@uts.edu.au (Robert G. McLaughlan),

98 Greg.Davis@csiro.au (Greg B. Davis).

99

100 **Abstract**

101 LNAPL transmissivity (T_n) is being proposed as an improved metric for LNAPL
102 recoverability. In this paper, the applicability of T_n as a lagging and leading metric in
103 heterogeneous sites under variable water table conditions was investigated. Bail-down
104 and mass recovery (skimming) testing methods were compared in three areas of a
105 gasoline contaminated site in Western Australia. High-resolution characterisation
106 methods were applied in the vicinity of the measured wells to account for differences
107 in the stratigraphic profile and LNAPL distribution. The results showed a range of T_n
108 from 0.30 m²/day to 2.13 m²/day under unconfined LNAPL conditions, exhibiting a
109 strong spatial variability and an inverse relationship with the potentiometric surface
110 elevation (Z_{aw}). In addition, we found temporal reductions of T_n may be more affected
111 by Z_{aw} than by the application of mass recovery technologies. These observations
112 reflected limitations of T_n as a lagging metric and a remediation endpoint. On the
113 other hand, the consistency and accuracy of T_n as a leading metric was affected by the
114 subsurface conditions. For instance, the area with a wider LNAPL distribution and
115 higher LNAPL saturations was less sensitive to changes in Z_{aw} than the other two
116 areas during the skimming trials. In addition, the T_n values from bail-down and
117 skimming testing were generally in a close agreement (less than a factor of 2
118 difference), although higher discrepancies (by a factor up to 7.3) were found,
119 probably linked to the geological setting and Z_{aw} . Therefore, under stable Z_{aw} , T_n was
120 found to be a relatively reliable metric. In contrast, variable water table conditions
121 affected the evolution of T_n and caution should be exercised in such scenarios.
122 Consequently, remediation practitioners, researchers and regulators should account
123 for the nexus between T_n , LNAPL distribution, geological setting and temporal effects
124 for a more efficient and sustainable management of complex sites.

125

126 Keywords: complex NAPL distribution; heterogeneity, LNAPL transmissivity;
127 remediation performance metric; water table fluctuations.

128

129 **1. Introduction**

130

131 Petroleum hydrocarbons such as gasoline, diesel and jet fuel found as light
132 non-aqueous phase liquids (LNAPLs) in the subsurface pose potential risks to human
133 health and the environment because of their mobility and toxicity. Thus, saturation-
134 and composition-based risks exist (Tomlinson et al., 2017). In the past, in-well
135 LNAPL thickness (b_n) was used as a measure of potential LNAPL mobility and
136 recoverability. However, it has been widely recognised that b_n varies between
137 different geological materials, LNAPL properties and hydrogeologic conditions
138 (ASTM, 2013). Consequently, the analysis of b_n should be performed with caution
139 through the application of proper models that account for capillary pressure-saturation
140 relationships (Farr et al., 1990; Lenhard and Parker, 1990; Sleep et al., 2000) and
141 equilibrium in-well fluid levels should be representative of the fluid pressures in the
142 formation.

143 From the LNAPL remediation activities and investigations over time, LNAPL
144 transmissivity (T_n), which is a measure of potential LNAPL mobility, is being
145 proposed as an important new metric for the management of LNAPL contaminated
146 sites overcoming the aforementioned limitations of b_n (NAVFAC, 2017). T_n is defined
147 in an analogous way to groundwater transmissivity and can be estimated through bail-
148 down testing, manual skimming, mass recovery system analysis (e.g. analysis of
149 LNAPL skimming systems) or tracer tests (ASTM, 2013). Of the various techniques,

150 bail-down testing is the most commonly applied since it requires less resources than
151 the other methods.

152 However, an in depth knowledge of the site conditions and the underlying
153 multiphase physics is still essential to properly assess the system, since T_n has also
154 been recently described as a complex parameter (Beckett and Huntley, 2015). Fig. 1
155 illustrates this complexity by showing the multiple interrelated sources of variability
156 that affect T_n . The estimated T_n value depends on the applied methodology, test
157 conditions, water table fluctuations as well as fluid and geological properties. These
158 factors are usually related to T_n in a complex way, for instance hysteresis exists in the
159 relationships between relative permeability, capillary pressure and saturation,
160 determined by the geological and fluid properties. A 20% T_n difference during
161 imbibition and drainage periods in homogeneous porous media has been documented
162 (Palmier et al., 2017).

163 Water table fluctuations may play a crucial role on LNAPL redistribution, its
164 mobility and the partitioning into other phases and can affect the value of T_n by orders
165 of magnitude (Beckett and Huntley, 2015). Two main mechanisms are behind this
166 relationship between the potentiometric surface elevation (Z_{aw}) and T_n . Firstly, the
167 induced vertical displacement of LNAPL mass to zones with different intrinsic
168 permeability. Secondly, the generation of immobile LNAPL, in particular the
169 entrapment of LNAPL when Z_{aw} increases (Lenhard et al., 1993; Steffy et al., 1995;
170 Chompusri et al., 2002). Hydrographs obtained from field sites usually show that Z_{aw}
171 and T_n follow opposite trends (Beckett and Huntley, 2015), thus indicating the
172 importance of entrapment phenomena in unconsolidated porous media. Recently, a
173 model to predict subsurface LNAPL volumes and T_n after consideration of immobile

174 LNAPL resulting from water table fluctuations in homogenous scenarios was
175 presented (Lenhard et al., 2017).

176 In spite of the aforementioned complexities, T_n is applied in the design,
177 implementation and evaluation of remediation systems as both a leading and lagging
178 metric (Kirkman, 2013). A leading metric is an indicator of the potential future
179 performance of a system. For instance, T_n is used to determine the start-up of a
180 LNAPL mass recovery system or to gain insight into the expected LNAPL recovery
181 rates. On the other hand, a lagging metric is an indicator of the past and current
182 performance of a system. For instance, T_n is used to assess the progress of LNAPL
183 mass recovery techniques and it is also used as an endpoint criterion to determine the
184 shutdown of the system. A T_n value of 0.009 to 0.07 m²/day has been suggested as an
185 endpoint for hydraulic LNAPL recovery (ITRC, 2009). However, regardless of the
186 specific remediation metric, it has been remarked that is frequently convenient to
187 apply alternative endpoints in lieu of regulatory standards (Harclerode et al., 2016)
188 and adopt adaptive management strategies (Price et al., 2017) in the case of complex
189 contaminated sites.

190 The objective of this paper is to assess the impact water table fluctuations may
191 have on the applicability of T_n as a leading and lagging metric in complex sites.
192 Although it has been stated that water table fluctuations may play a crucial role on T_n
193 (Kirkman and Hawthorne, 2014; Beckett and Huntley, 2015), none of the existing
194 field-based research papers (Nagaiah et al., 2015; Palmier et al., 2016; Pennington et
195 al., 2016) has directly addressed the nexus between T_n , water table fluctuations,
196 geological heterogeneity and complex NAPL distributions. Thus, the outcomes of this
197 study could encourage further research on this nexus and have a valuable impact on

198 new regulatory frameworks and more efficient and sustainable contaminated site
199 management strategies.

200

201 **2. Materials and methods**

202

203 *2.1 Characteristics of the field site*

204 The study area comprised an operating petrol station in Western Australia
205 located within a residential-commercial zone. It occupied an area of 2750 m² where
206 the topography is relatively flat. The local hydrogeology consists of a multi-layered
207 unconsolidated aquifer system formed in a fluvial depositional environment.
208 Discontinuous interbedded sands, silts and clays are present. In general, the
209 stratigraphic profile consists of three main strata: a clayey silt layer approximately 0-
210 4.5 m below the surface; a sandy layer (fine and coarse sand with up to 30% of silt
211 and clay) approximately 4.5-8 m below the surface; and heavy clays approximately 8
212 m and deeper below the surface. A fining-upward sequence was observed in the sandy
213 unit according to core logs. The study area typically experiences annual water table
214 fluctuations of 2-3 m. The gasoline release occurred in 2013. The exact amount of
215 released product remains unknown. The LNAPL was mainly found in the sandy
216 material under different confinement conditions. The product was relatively fresh
217 with a measured mass density of 730 kg/m³ and a viscosity between 4.1x10⁻⁴ kg m⁻¹ s⁻
218 ¹ and 4.8x10⁻⁴ kg m⁻¹ s⁻¹. Between 2014-2016, 85 monitoring points were installed
219 including production (100-mm diameter) and monitoring wells (50-mm diameter),
220 multi-level strings and vapor point wells. Site characterisation included soil coring
221 and direct-push profiling methods such as HPT (Hydraulic Profiling Tool) and LIF
222 (Laser-Induced Fluorescence) at distances of less than 2 m away from installed wells.

223 Three areas (A, B and C), exhibiting differences in the vertical LNAPL
224 distribution and the stratigraphic profile, were chosen to investigate the effect of water
225 table fluctuations under different scenarios. The distance between the tested wells in
226 areas A and B was 12 m. Area C was located 30 m away from the other two areas.
227 The geological material at area C was generally finer textured than at the other two
228 areas. Area A had unconfined LNAPL conditions during all of the measurements
229 (2014-2016). Areas B and C had both confined and unconfined LNAPL conditions
230 since 2014. The transition point between confined and unconfined NAPL conditions
231 was in the range of 56.7- 56.8 m AHD (Australian Height Datum), according to
232 different lines of evidence such as diagnostic gauge plots, core logging, HPT profiles,
233 bail-down testing and hydrostratigraphs (Kirkman et al., 2013). Table 1 presents the
234 monitoring network and the LNAPL hydrogeological conditions at the three research
235 areas during the mass recovery testing periods.

236

237 2.2 Experimental procedure

238 Periodic measurements of $T_{n,BD}$ (T_n estimated through bail-down testing) were
239 obtained across the field site between 2015 and 2016. These measurements were
240 taken under natural conditions to investigate two main aspects: (i) the spatial and
241 temporal variability of T_n and (ii) the suitability of applying a single T_n value as an
242 endpoint criterion in a dynamic system (results presented in section 3.1). On the other
243 hand, LNAPL mass recovery methods were also tested to assess: (i) the applicability
244 of T_n as a lagging metric monitoring the progress of the remediation system and (ii)
245 the consistency of $T_{n,BD}$ as a leading metric in areas with similar $T_{n,BD}$ values, but
246 different LNAPL distributions and geological materials (results presented in section
247 3.2). $T_{n,BD}$ and $T_{n,SK}$ (T_n estimated through skimming) were also compared to

248 investigate the accuracy of $T_{n,BD}$ as a predictor of $T_{n,SK}$ (results presented in section
249 3.3).

250 In 2015, the LNAPL mass recovery trials were conducted sequentially in areas
251 A and B. In area A, there was relatively constant water table conditions (water table
252 elevation increased at a rate of +1 cm/week). In area B, there was a rising
253 potentiometric surface (water table elevation increased at a rate of +5 cm/week). The
254 2016 trials were conducted in parallel during rising water table conditions (water table
255 elevation increased at a rate of +7.5 cm/week at the beginning of the trial) at the three
256 research areas.

257 In 2015, the skimming operations to recover LNAPL in areas A and B lasted
258 two weeks. In 2016, the skimming operation at area B lasted four weeks. A 4-week
259 sequential mass recovery trial took place at areas A and C. Besides skimming, the
260 other applied LNAPL recovery techniques were water-enhanced recovery (dual pump
261 inducing water table drawdown), vacuum-enhanced recovery and water- and vacuum-
262 enhanced recovery, but their results are not included in this paper. LIF profiles and
263 continuous soil cores were obtained before the start of the 2016 trials (mid-May 2016)
264 to delineate the LNAPL vertical distribution. The equilibrium fluid levels used in the
265 T_n analysis were estimated from the surrounding monitoring wells.

266

267 *2.3 Measurements and calculations*

268 To measure T_n in the field by the bail-down testing procedure, initial Z_{an}
269 (elevation of the air/LNAPL interface in a well) and Z_{nw} (elevation of the
270 LNAPL/water interface in a well) measurements are conducted. LNAPL is then
271 removed from the well, which causes LNAPL to flow into the well from the
272 surrounding porous media. Both Z_{an} and Z_{nw} are measured as LNAPL flows into the

273 well. Given the properties of the existing product and the equipment that was
 274 employed, bail-down testing was apparently more reliable than the manual skimming
 275 method, even at relatively low in-well thicknesses. The data was analysed by using
 276 the modified Bouwer and Rice equation (Kirkman, 2013):

$$277 \quad T_{n,BD} = \frac{r_e^2 \ln(R_{oi} / r_e) \ln(s_{n(0)} / s_{n(t)})}{2(-J)t} \quad (1)$$

278 where:

279 R_{oi} = radius of capture (L);

280 r_e = effective well radius (L);

281 $s_{n(0)}$ = maximum induced drawdown (L);

282 $s_{n(t)}$ = LNAPL drawdown at time t (L);

283 t = elapsed time (T);

284 J = ratio of change in NAPL drawdown to change in NAPL thickness.

285 It should be noted that some of the theoretical assumptions in the Bouwer and
 286 Rice approach (Bouwer and Rice, 1976) are not necessarily met for multiphase
 287 systems and T_n analysis (Batu, 2012). However, several authors have defended this
 288 methodology claiming that is robust enough under both field and laboratory
 289 conditions (Charbeneau et al., 2013; Palmier et al., 2017), with different analytical
 290 solutions presenting a good correlation at field scale under unconfined conditions
 291 (Palmier et al., 2016).

292 As regards the mass recovery procedure, the LNAPL recovery rates were
 293 systematically measured and the corresponding LNAPL drawdowns estimated. The
 294 modified Thiem equation (Charbeneau, 2007) was used for the calculation of $T_{n,SK}$:

$$295 \quad T_{n,SK} = \frac{Q_n \ln\left(\frac{R_{oi}}{r_w}\right)}{2\pi s_n} \quad (2)$$

296 where:

297 Q_n = the time-weighted mean of the measured LNAPL recovery rates (L³/T);

298 s_n = the geometric mean of the estimated LNAPL drawdowns (L);

299 r_w = well radius (L).

300 The value of $\ln(R_{oi}/r_w)$ was assumed to be equal to 4.6 introducing little error
301 according to the literature (ASTM, 2013).

302 The estimated $T_{n,BD}$ value may not compare identically with $T_{n,SK}$ because of
303 the analysis procedure and temporal and spatial scale dissimilarities. This discrepancy
304 between different methods may be also due to poor well development or other
305 artifacts, as it has been documented in the case of comparisons between slug tests and
306 pumping tests in groundwater systems (Butler and Healey, 1998). The spatial scale of
307 the selected methods is determined by their radius of capture, typically larger for
308 coarser-grained sediments (Beckett and Huntley, 1998).

309

310 **3. Results and discussion**

311

312 *3.1 Variability in LNAPL transmissivity under natural water table fluctuations*

313 Fig. 2 depicts the distribution of the T_n and b_n values obtained through the field
314 site monitoring network during the two years of research. A range of $T_{n,BD}$ from 0.3
315 m²/day to 2.13 m²/day was found across the entire site during unconfined LNAPL
316 conditions. Area C had the lowest $T_{n,BD}$ values (0.3 – 0.58 m²/day) among the three
317 areas since 2015 (maximum values of 2.13 m²/day at research area A and 1.38 m²/day
318 at research area B), although it showed higher LNAPL saturations and b_n . Thus, the
319 low intrinsic permeability at area C is a key factor for the lower T_n values, besides of
320 the differences in LNAPL distribution. This lack of correlation between T_n and b_n was

321 consistently observed at the field site, as shown in Fig. 2. This behaviour was not
322 unexpected since it has been also documented in the literature (Palmier et al., 2016).
323 However, a positive relationship between these two parameters was found at specific
324 tested wells under unconfined LNAPL conditions, consistent with the multiphase
325 theory (Lenhard et al., 2017), although the coefficients of determination were just
326 between 0.35 and 0.76. T_n exhibited a strong spatial variability. For instance, no
327 LNAPL was present in wells located less than 2 m away from others with the highest
328 T_n values.

329 Between 2015 and 2016, T_n followed an inverse relationship with Z_{aw} as
330 depicted in Fig. 3. The T_n reduction during rising water table conditions was observed
331 across the whole contaminated site and not only in the three areas studied. This
332 behaviour was related to two different processes: (i) less mobile LNAPL results
333 because of LNAPL entrapment by water and (ii) the upward LNAPL displacement
334 was into porous media with a lower intrinsic permeability. This was more pronounced
335 at areas B and C where the T_n showed the lowest values just before reaching the
336 overlying aquitard at 56.7- 56.8 m AHD. Another observation supporting the strong
337 impact of Z_{aw} on T_n was that an increase of 25 cm in Z_{aw} resulted in a $T_{n,BD}$ decrease
338 from 2.13 to 0.37 m²/d in area A (which exhibited the lowest LNAPL mobile intervals
339 according to LIF and core logs). These changes in T_n could explain the differences up
340 to one order of magnitude found in comparisons between initial bail-down testing
341 values and long-term methods such as tracer tests (Pennington et al., 2016). It should
342 be remarked that the redistribution of the product (fresh gasoline) was favoured by its
343 relatively low density and viscosity.

344 Fig. 4 illustrates the site hydrograph during the study period. The maximum
345 potentiometric surface elevation was 0.6 m higher in 2014 than in 2015 (57.7 m AHD

346 in November 2014 versus 57.1 m AHD in October 2015), while the lowest elevation
347 was similar (approximately 56.2 m AHD) for both years. Differences in $T_{n,BD}$ at
348 similar Z_{aw} values in 2015 compared to 2016 (54% T_n decrease at area B) may reflect
349 hysteresis, natural LNAPL depletion or mass migration within the LNAPL body.

350

351 *3.2 Variability in LNAPL transmissivity during skimming*

352 LNAPL saturations obtained from extracted cores before the 2016 mass
353 recovery trial, as well as HPT and LIF logs from surrounding direct-push locations,
354 are presented in Fig. 5. The highest LNAPL saturations were found at area C, where
355 the material was finer. During the skimming trials, soil coring, HPT and LIF profiles
356 suggested that the mobile LNAPL interval was mainly located in silty sands at this
357 area. In addition, there were greater differences between the HPT logs obtained at
358 area C compared to the other areas. This can be seen from the three different HPT
359 logs corresponding to this area in Fig. 5. In areas A and B, the mobile LNAPL
360 interval was located in poorly graded sand material. Data for area B is not shown in
361 Fig. 5 because of the similarities with of geological material and T_n evolution with
362 area A. A notable measurement at area A was the distinct and very high LIF signals
363 within an interval of just 12 cm, where a slightly coarser material was identified.
364 Therefore, the highest LIF signals were present in the area with the lowest LNAPL
365 saturation values. Because the LIF signal depends on both the LNAPL saturation and
366 the geology, it was an interesting tool to delineate transmissive intervals, although
367 with some limitations. This thin layer probably worked as a preferential migration
368 pathway constraining the LNAPL vertical displacement due to the capillary contrasts.

369 In addition, Fig. 5 presents four times that fluid levels (I, II, III, IV) were
370 recorded. Times I and IV were at the lowest monitored Z_{aw} during the years 2015-

371 2016 with small differences in Z_{an} and Z_{nw} . The LNAPL saturation profiles shown in
372 Fig. 5 correspond to time I. A different LNAPL distribution, exhibiting lower NAPL
373 saturation values is expected at time II, as it has been previously documented in the
374 case of a gasoline contaminated sandy aquifer with a rising potentiometric surface
375 (Steffy et al., 1995). At the beginning of the mass recovery trials, higher values of
376 $T_{n,BD}$ were measured in July 2015 (1.48 m²/d) compared to June 2016 (0.37 m²/d). In
377 2015, measurements were taken under low water table conditions, whereas in 2016
378 the water table was 20-25 cm higher. It should be remarked that the LNAPL recovery
379 was negligible in all the research areas at the end of the 2016 trial.

380 Fig. 6 illustrates changes in $T_{n,SK}$ with Z_{aw} during the first week of the
381 skimming trial in 2016. As it can be inferred from Fig. 6, during the first 5-cm rise in
382 Z_{aw} , the LNAPL recoverability was less affected at area C than at the other areas. One
383 important factor was that the LNAPL saturations were higher. How the LNAPL
384 saturation is affected by Z_{aw} changes depends on the capillary pressure-saturation
385 relationship. Moreover, the LNAPL mobile interval was larger at this area. In relation
386 to this, the in-well thickness (4.5 times larger at area C than at area A) was reduced by
387 7% at area C, but it decreased by 15% at area A during this period of time. Thus,
388 entrapment phenomena and vertical displacement had a higher impact at area A at this
389 stage. It should also be noticed that the lowest LNAPL recovery rates were measured
390 at area C. Later measurements showed $T_{n,SK}$ approaching zero under constant water
391 table conditions at area C due to product depletion through skimming in the
392 surrounding subsurface. Low $T_{n,BD}$ measured values in surrounding wells was another
393 indication of the low LNAPL mobility at this area.

394 Fig. 7 presents changes in $T_{n,BD}$ before and during the skimming trial at area A
395 in 2016. From this figure, it can be inferred that T_n was quite sensitive to water table

396 changes, while the impact of the skimming operations was not so clear. Consequently,
397 LNAPL entrapment and vertical displacement may have played a greater role on the
398 temporal reduction of T_n than the mass recovery method. This is supported by
399 relatively constant T_n during periods of stable water table conditions. Further, T_n did
400 not change under constant Z_{aw} at area A during the 2015 trial either, whereas the
401 effect of a rising Z_{aw} had a negative impact on T_n at area B (Gatsios et al., 2016). The
402 behaviour shown in Fig. 7 indicated that the assessment of the performance of a
403 remediation system through T_n could be misleading. For instance, other authors
404 acknowledged the effectiveness of a LNAPL recovery system after observing a T_n
405 decrease of 47% in 18 months of recovery (Palmier et al., 2016). However, Fig. 4
406 shows a 54% $T_{n,BD}$ reduction under natural conditions without remediation operations
407 at area B between 2015 and 2016.

408

409 *3.3 Comparison between LNAPL transmissivity estimated through bail-down and* 410 *mass recovery testing methods*

411 A comparison of T_n values estimated through the different applied testing
412 methods at areas A and C during the recovery trials in 2015 and 2016 is shown in Fig.
413 8. In general, there was relatively close agreement between $T_{n,BD}$ and $T_{n,SK}$ with
414 differences within a factor of 2. This difference is considered reasonable (ASTM,
415 2013) and is consistent with what has been documented in the literature (Nagaiah et
416 al., 2015). More specifically, differences between $T_{n,BD}$ and $T_{n,SK}$ were relatively small
417 under stable water table conditions. However, larger differences by a factor up to 7.3
418 were found at area A during the 2016 LNAPL mass recovery trial under rising water
419 table conditions, as it can be seen in Fig. 8.

420 Fig. 9 presents the changes of the $T_{n,SK}/T_{n,BD}$ ratio with different potentiometric
421 surface elevations at areas A and C. The figure contains periods when skimming and
422 water-enhanced skimming recovery methods were employed. As the $T_{n,SK}/T_{n,BD}$ ratio
423 approaches the unity, bail-down testing estimations could be considered as good
424 predictors of T_n and recoverability for mass recovery applications. Before inducing a
425 gradient in the potentiometric surface, it could be inferred that there was a better
426 agreement between $T_{n,SK}$ and $T_{n,BD}$ at area C, where the material was finer compared to
427 area A. One main factor may be the radius of capture.

428 Fig. 9 also showed that the difference between both applied methods may be a
429 function of Z_{aw} among other factors. Thus, it was observed that the aforementioned
430 difference by a factor of 7.3 corresponded to the highest Z_{aw} . As depicted in Fig. 5a,
431 the LNAPL distribution at area A was mainly present within a short interval and not
432 significantly smeared across the lithological profile, whereas a wider LNAPL vertical
433 distribution with higher saturations existed at area C. Therefore, the remarkably high
434 $T_{n,SK}/T_{n,BD}$ ratio at high Z_{aw} was probably due to the coupled effect of the differences
435 in the radius of capture between the two applied methods and the low NAPL
436 saturations predominantly constrained to a thin layer. Apparently, bail-down testing
437 was more sensitive to the rising water table than the skimming system, as it can be
438 inferred from the decreasing $T_{n,SK}$ with an increasing $T_{n,SK}/T_{n,BD}$ ratio. Thus, the
439 accuracy of $T_{n,BD}$ as a predictor of $T_{n,SK}$ may be compromised when significant water
440 table fluctuations exist.

441

442 4. Conclusions

443

444 In the present study, the applicability of T_n as a metric in heterogeneous sites
445 impacted by water table fluctuations was investigated. Water table fluctuations played
446 a crucial role on the behaviour of T_n and should always be taken into consideration by
447 remediation practitioners, researchers and regulators. The findings of this research
448 encourage the use of T_n as a metric for the management of LNAPL contaminated sites,
449 always accompanied by an adequate understanding of the conceptual site model.

450 Under constant water table conditions, T_n was found to be a relatively reliable
451 metric for the management of saturation-based risks in LNAPL contaminated sites,
452 although exhibiting a strong spatial dependency. $T_{n,BD}$ and $T_{n,SK}$ were usually in a
453 close agreement. Consequently, $T_{n,BD}$ is helpful in order to decide the appropriateness
454 of establishing a new mass recovery system. In addition, the stable T_n behaviour
455 favours the suitability of T_n as a leading metric.

456 In contrast, variable water table conditions may affect the evolution of T_n in
457 such a way that its applicability as a metric may be questionable without a deep
458 knowledge of the site conditions. Examples supporting the aforementioned statement
459 were presented throughout the results of this research:

460 (i) it was observed that T_n may change in a cyclic basis under natural
461 conditions. Thus, regulatory limits like the endpoint criterion proposed by ITRC
462 (ITRC, 2009) should be used with caution and preferably under low water table
463 conditions (still depending on the relative importance of entrapment and the
464 implications of vertical displacement). The results of this study encourage the
465 application of periodic bail-down testing as part of a broader adaptive management
466 strategy;

467 (ii) it was documented that $T_{n,BD}$ may potentially be more sensitive to water
468 table changes than to the product depletion through skimming. As a consequence, T_n

469 is not necessarily representing the remediation performance of the mass recovery
470 system only. It also comprises the coupled effects produced by the variable water
471 table as well as the potential migration and natural losses occurring within the NAPL
472 body. For instance, in this research the decrease in $T_{n,BD}$ due to natural conditions
473 without remediation operations was similar to that presented in the literature after 18
474 months of LNAPL recovery (Palmier et al., 2016). Consequently, the understanding
475 of these effects is essential in order to select the most adequate remediation
476 technology, for instance in cases where mass recovery techniques should be replaced
477 by monitored natural attenuation strategies;

478 (iii) the effect of the water table fluctuations is linked to the geological setting
479 and the NAPL distribution. Accordingly, areas with similar initial $T_{n,BD}$ values may
480 exhibit a clearly different evolution with time. During this research study, T_n was
481 found to be less sensitive to Z_{aw} when wider LNAPL distributions and higher
482 saturations were present. As a consequence, the application of T_n as a leading metric
483 is compromised without a deep knowledge of the conditions in the subsurface. Being
484 aware of the depositional environment and existing vertical heterogeneity may help to
485 understand the influence of LNAPL vertical displacement and entrapment phenomena
486 on T_n . Furthermore, evidence that Z_{aw} may affect the discrepancy between $T_{n,SK}$ and
487 $T_{n,BD}$ was presented. The magnitude of this difference may be related to the geological
488 setting and LNAPL distribution, in particular when there are relevant preferential
489 migration pathways with coarser material and/or better connectivity. For this reason,
490 some errors may arise from the usage of $T_{n,BD}$ as a start-up metric under these
491 conditions.

492 In conclusion, both the geological setting and the LNAPL distribution have an
493 effect on the behaviour of T_n , magnified in the case of variable water table conditions.

494 Thus, a proper characterisation of the area surrounding the remediation well makes T_n
495 gain reliability as a metric. On the other hand, periodic bail-down testing assists in the
496 assessment of the T_n variability with time. Periodic measurements of $T_{n,BD}$ would also
497 provide further insight into the comparisons between bail-down and long-term testing
498 methods like those already documented in the literature (Pennington et al., 2016).
499 Further research under controlled environments is suggested to keep elucidating the
500 complex interrelation between T_n , NAPL properties, NAPL distribution, geological
501 setting and temporal effects (including variable Z_{aw} , natural source zone depletion,
502 NAPL migration and product depletion through mass recovery methods).

503

504 **Acknowledgements**

505

506 This work was supported by the Cooperative Research Centre for Contamination
507 Assessment and Remediation of the Environment (CRC CARE), whose activities are
508 funded by the Australian Government's Cooperative Research Centres Programme.
509 Author Evangelos Gatsios would like to thank the Public Benefit Foundation
510 “Alexander S. Onassis” for its financial support. We are also grateful for the
511 assistance of CSIRO Land and Water staff: Gabriel Paiva Lago and Robert Woodbury
512 in the instrumentation, characterisation and monitoring of the field site; Trevor
513 Barstow and Yasuko Geste in the chemical analysis of the samples; Elise Bekele and
514 Robert Lenhard for their many valuable comments.

515

516 **References**

517

518 ASTM International (2013). The standard guide for estimation of LNAPL
519 transmissivity (ASTM E2856-13).

520 Batu, V. (2012). An assessment of the baildown tests data analysis method.
521 *Groundwater*, 50(4), 500-503.

522 Beckett, G. D., & Huntley, D. (1998). Soil properties and design factors influencing
523 free-phase hydrocarbon cleanup. *Environmental Science & Technology*, 32(2), 287-
524 293.

525 Beckett, G. D., & Huntley, D. (2015). LNAPL transmissivity: a twisted parameter.
526 *Groundwater Monitoring & Remediation*, 35(3), 20-24.

527 Bouwer, H., & Rice, R. C. (1976). A slug test for determining hydraulic conductivity
528 of unconfined aquifers with completely or partially penetrating wells. *Water*
529 *Resources Research*, 12(3), 423-428.

530 Butler, J. J., & Healey, J. M. (1998). Relationship between pumping-test and slug-test
531 parameters: scale effect or artifact? *Groundwater*, 36(2), 305-312.

532 Charbeneau, R. J. (2007). LNAPL Distribution and Recovery Model (LDRM).
533 Volume 1: distribution and recovery of petroleum hydrocarbon liquids in porous
534 media (API Publication 4760). Washington, D.C.: American Petroleum Institute.

535 Charbeneau, R., Kirkman, A., & Adamski, M. (2013). Discussion of ‘An assessment
536 of the Huntley (2000) baildown test data analysis method’ by Vedat Batu.
537 *Groundwater*, 51(5), 657-659.

538 Chompusri, S., Rivett, M. O., & Mackay, R. (2002). LNAPL redistribution on a
539 fluctuating water table: column experiments. In S. F. Thornton & S. E. Oswald (Eds.),
540 *Groundwater Quality: Natural and Enhanced Restoration of Groundwater Pollution*.
541 Oxfordshire: IAHS Press.

542 Farr, A. M., Houghtalen, R. J., & McWhorter, D. B. (1990). Volume estimation of
543 light nonaqueous phase liquids in porous media. *Groundwater*, 28(1), 48-56.

544 Gatsios, E., Rayner, J. L., & McLaughlan, R. G. (2016). Use of LNAPL
545 transmissivity to evaluate LNAPL recoverability in a fine grained aquifer in Western
546 Australia. In *Proceedings of the 5th International Conference on Industrial and*
547 *Hazardous Waste Management, Chania, Crete.*

548 Harclerode, M. A., Macbeth, T. W., Miller, M. E., Gurr, C. J., & Myers, T. S. (2016).
549 Early decision framework for integrating sustainable risk management for complex
550 remediation sites: drivers, barriers, and performance metrics. *Journal of*
551 *Environmental Management*, 184(1), 57-66.

552 Huntley, D. (2000). Analytic determination of hydrocarbon transmissivity from
553 baildown tests. *Groundwater*, 38(1), 46-52.

554 ITRC (2009). Evaluating LNAPL remedial technologies for achieving project goals
555 (LNAPL-2). Washington, D.C.: Interstate Technology & Regulatory Council.

556 Kirkman, A. J. (2013). Refinement of Bouwer-Rice baildown test analysis.
557 *Groundwater Monitoring & Remediation*, 33(1), 105-110.

558 Kirkman, A. J., Adamski, M., & Hawthorne, J. M. (2013). Identification and
559 assessment of confined and perched LNAPL conditions. *Groundwater Monitoring &*
560 *Remediation*, 33(1), 75-86.

561 Kirkman, A., J., & Hawthorne, J. M. (2014, December). Transmissivity—the
562 emerging metric for LNAPL recoverability—Part 2 a tangible perspective on the
563 hydraulic recovery endpoint. *L.U.S.T.Line*, 15-20.

564 Lenhard, R. J., & Parker, J. C. (1990). Estimation of free hydrocarbon volume from
565 fluid levels in monitoring wells. *Groundwater*, 28(1), 57-67.

566 Lenhard, R. J., Johnson, T. G., & Parker, J. C. (1993). Experimental observations of
567 nonaqueous-phase liquid subsurface movement. *Journal of Contaminant Hydrology*,
568 12(1-2), 79-101.

569 Lenhard, R. J., Rayner, J. L., & Davis, G. B. (2017). A practical tool for estimating
570 subsurface LNAPL distributions and transmissivity using current and historical fluid
571 levels in groundwater wells: Effects of entrapped and residual LNAPL. *Journal of*
572 *Contaminant Hydrology*. 205, 1-11.

573 Nagaiah, M., Law, D. R., & Ueland, S. (2015). Transmissivity as a Primary Metric for
574 LNAPL Recovery—Case Study Comparison of Short-Term vs. Long-Term Methods.
575 *Remediation Journal*, 26(1), 43-55.

576 NAVFAC (2017). Environmental restoration: new developments in LNAPL site
577 management (ESAT N62583-11-D-0515). Naval Facilities Engineering Command.

578 Palmier, C., Dodt, M., & Atteia, O. (2016). Comparison of oil transmissivity methods
579 using bail-down test data. *Groundwater Monitoring & Remediation*, 36(3), 73-83.

580 Palmier, C., Cazals, F., & Atteia, O. (2017). Bail-down test simulation at laboratory
581 scale. *Transport in Porous Media*, 116(2), 567-583.

582 Pennington, A., Smith, J., Koons, B., & Divine, C. E. (2016). Comparative evaluation
583 of single-well LNAPL tracer testing at five sites. *Groundwater Monitoring &*
584 *Remediation*, 36(2), 45-58.

585 Price, J., Spreng, C., Hawley, E. L., & Deeb, R. (2017). Remediation management of
586 complex sites using an adaptive site management approach. *Journal of Environmental*
587 *Management*, 204(2), 738-747.

588 Sleep, B. E., Sehayek, L., & Chien, C. C. (2000). A modeling and experimental study
589 of light nonaqueous phase liquid (LNAPL) accumulation in wells and LNAPL
590 recovery from wells. *Water Resources Research*, 36(12), 3535-3545.

591 Steffy, D. A., Johnston, C. D., & Barry, D. A. (1995). A field study of the vertical
592 immiscible displacement of LNAPL associated with a fluctuating water table. In K.
593 Kovar & J. Krásný (Eds.), *Groundwater Quality: Remediation and Protection*.
594 Oxfordshire: IAHS Press.

595 Tomlinson, D. W., Rivett, M. O., Wealthall, G. P., & Sweeney, R. E. (2017).
596 Understanding complex LNAPL sites: Illustrated handbook of LNAPL transport and
597 fate in the subsurface. *Journal of Environmental Management*, 204(2), 748-756.

598

599

600

601

602

603

604

605

606

607

608

609

610

611

612

613 **List of Figures and Tables**

614

615 **Fig. 1.** Sources of variability contributing to the complex nature of T_n .

616

617 **Fig. 2.** Distribution of T_n and b_n values across the site in the years of research.

618

619 **Fig. 3.** Correlation between the T_n and Z_{aw} at the three areas of research (years: 2015-
620 2016).

621

622 **Fig. 4.** Contaminated site hydrograph along with bail-down T_n values at the three
623 research areas. Gray columns indicate the time periods of recovery applications in
624 2015 and 2016.

625

626 **Fig. 5.** a) HPT73 and LIF43 profile along with NAPL saturations (MP50) and b_n
627 (PB29 well), at area A and b) HPT59, HPT60 HPT62 profiles along with NAPL
628 saturations (MP44) and b_n (PB40 well), at area C. Four different fluid elevations are
629 illustrated: **I** refers to fluid levels the day of core sampling (late May 2016), **II** shows
630 the fluid levels the day before the 4-week sequential free recovery trial (mid-June
631 2016), **III** presents fluid levels just after the end of the recovery trial (early July 2016)
632 and, finally, **IV** refers to the fluid levels just before the 2015 trial (early July 2015).

633

634 **Fig. 6.** Profiles of $T_{n,SK}$ and Z_{aw} at areas A, B, and C during the first week of the 2016
635 skimming trials.

636

637 **Fig. 7.** $T_{n,BD}$ values before and during the 2016 skimming trial at area A.

638

639 **Fig. 8.** Comparison of T_n values between bail-down testing and skimming along with
640 fluid elevations at (a) area A (2015 and 2016 trials) and (b) area C (2016 trial).

641

642 **Fig. 9.** Profile of Z_{aw} values along with $T_{n,sk}/T_{n,BD}$ ratio values at areas A and C during
643 the skimming and water-enhanced skimming trials in 2016.

644

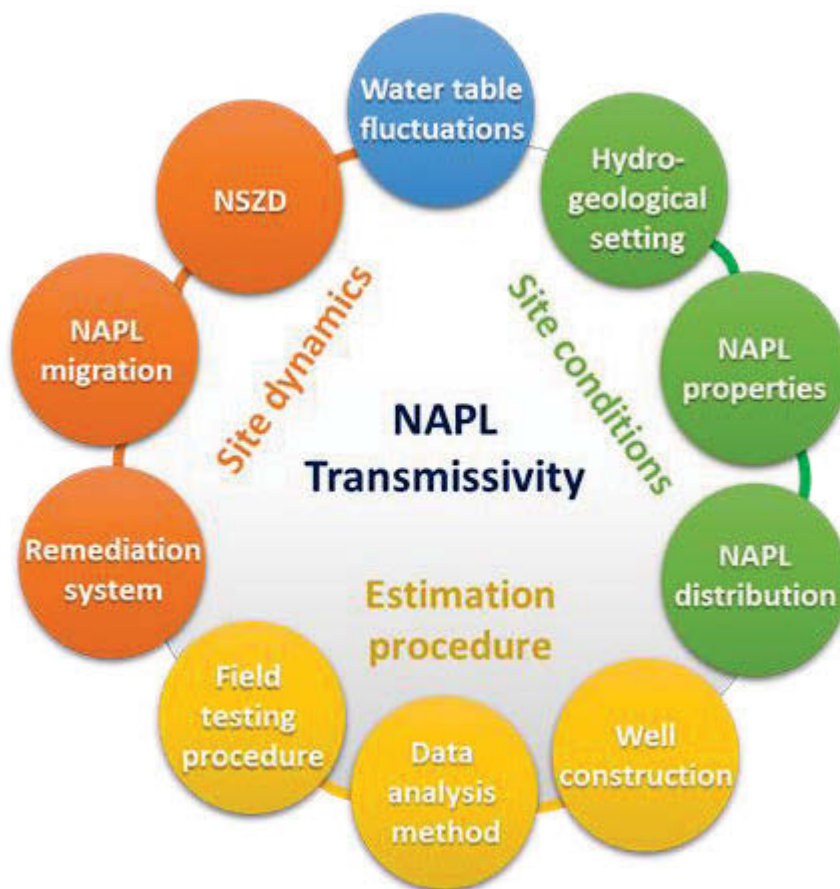
645 **Table. 1.** Monitoring network and NAPL hydrogeological conditions during the pilot-
646 scale mass recovery trials at the three research areas. Numbers in parenthesis indicate
647 distance from recovery wells.

648

649

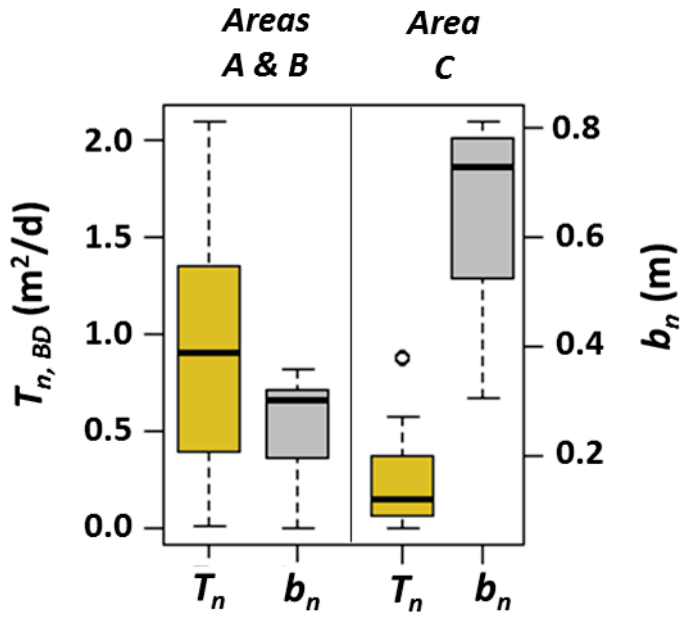
650

651



652

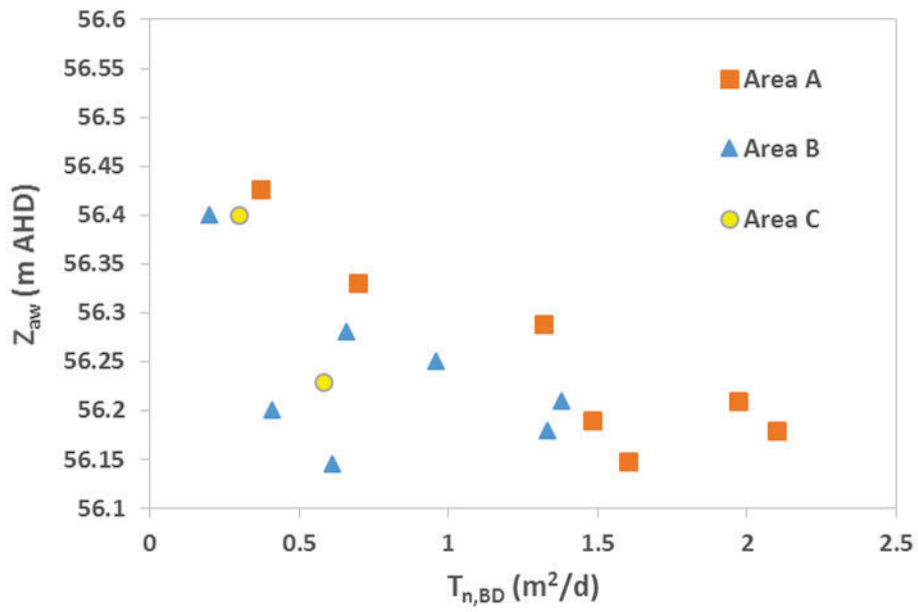
653 **Fig. 1**



654

655

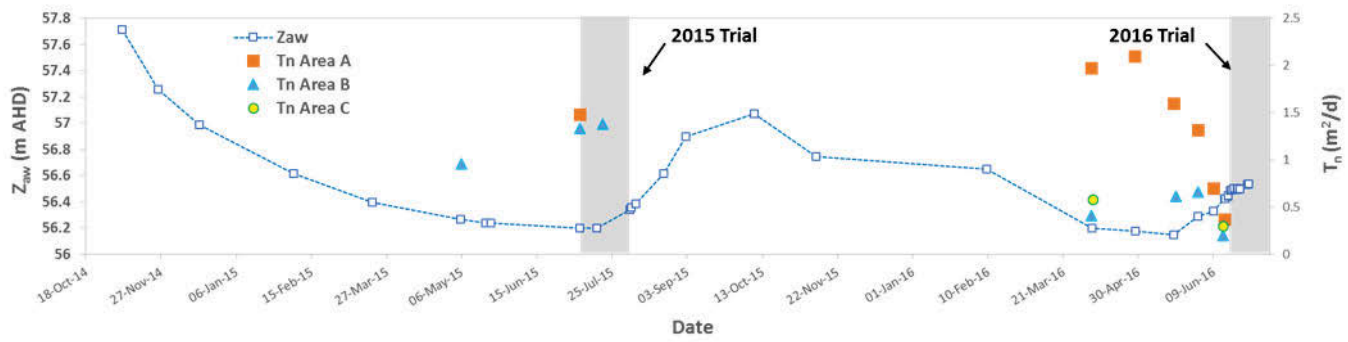
656 **Fig. 2**



657

658 **Fig. 3**

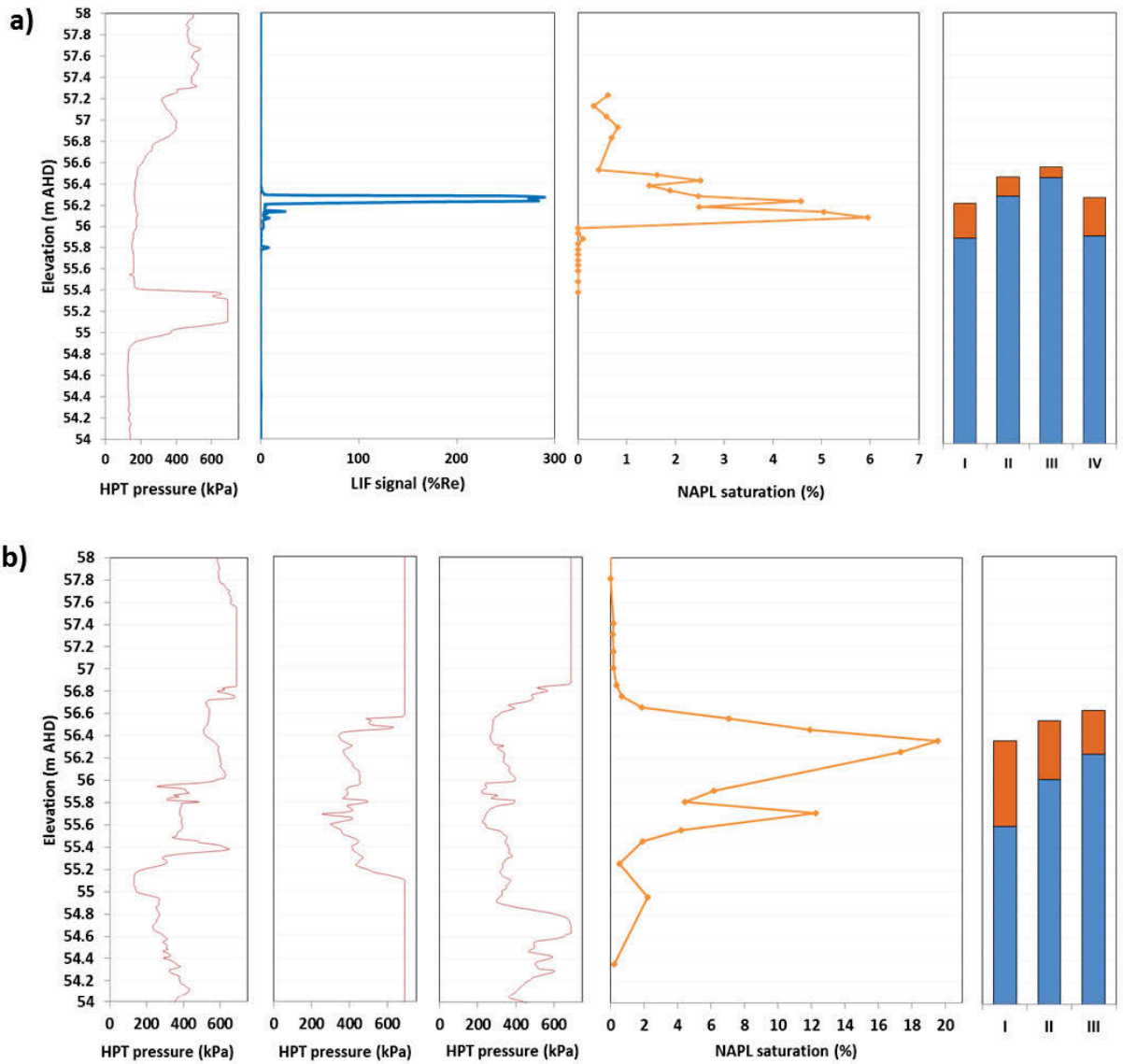
659



660

661 **Fig. 4**

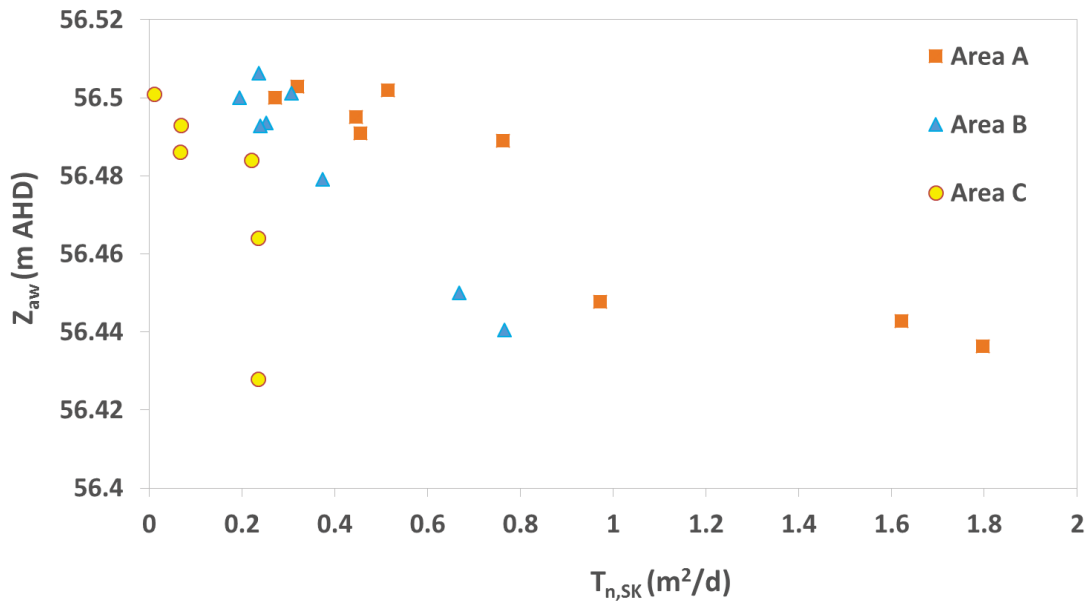
662



663

664

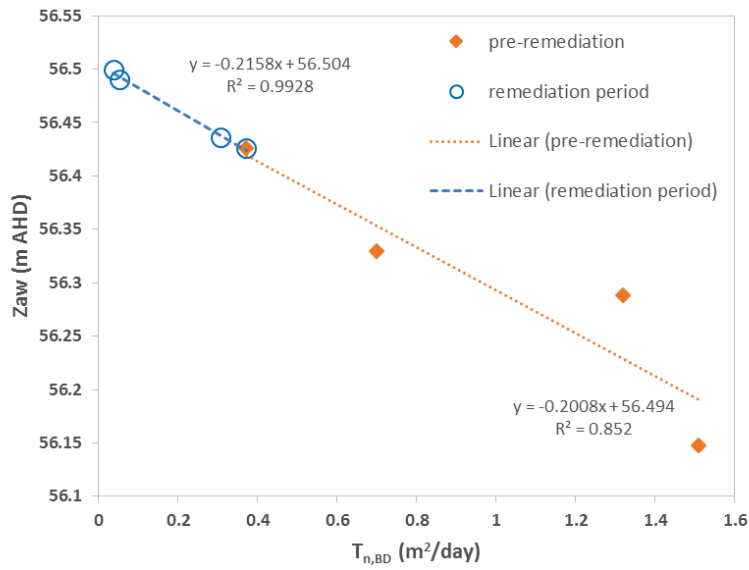
665 Fig. 5



666

667 Fig. 6

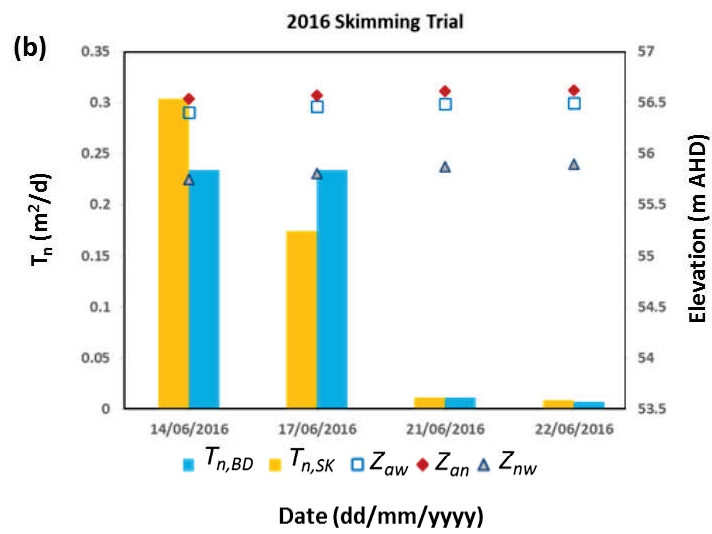
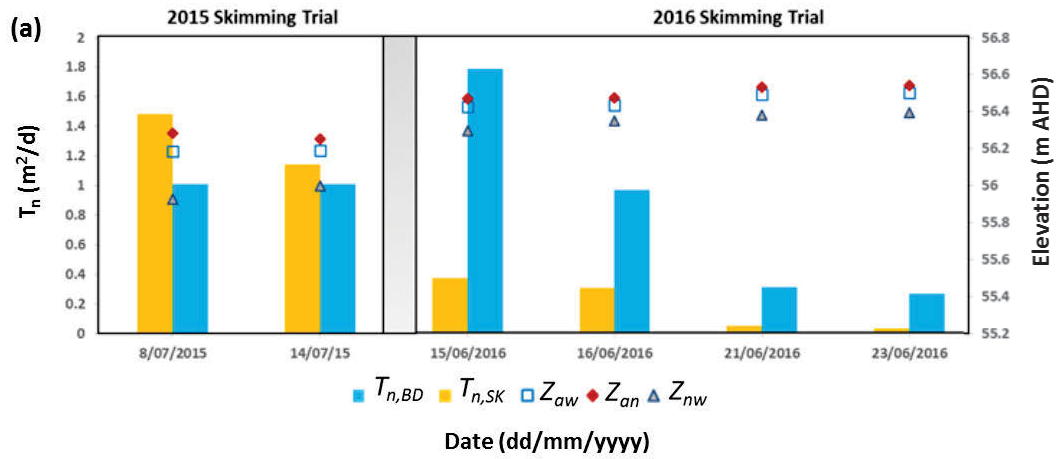
668



669

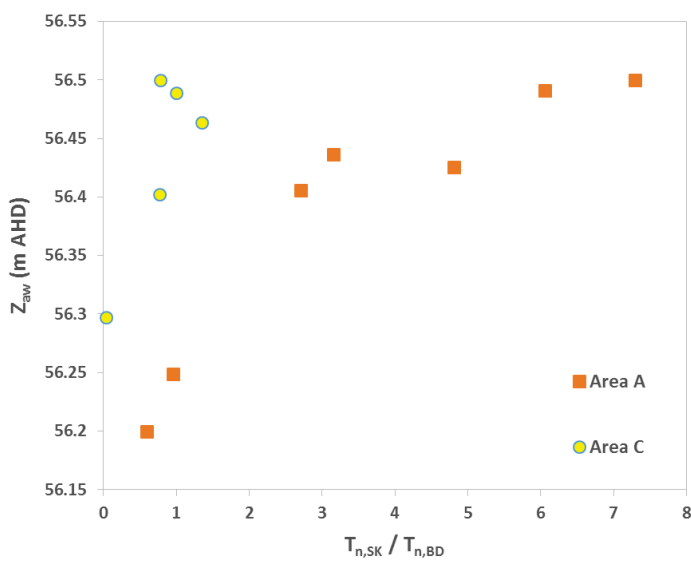
670 Fig. 7

671



672

673 Fig. 8



674

675 Fig. 9

676

677 **Table 1.**

Research Area	Recovery Well	Observation Wells	LIF Profiles	HPT Profiles	NAPL Conditions
A	PB29	MP50 (1.5 m)	LIF43 (1 m) LIF47 (1.5 m)	HPT73 (1.5 m)	Unconfined
B	PB27	PB09 (2.5 m)	LIF 51 (1.5 m) LIF52 (1 m) LIF53 (2 m)	HPT74 (1 m)	Unconfined
C	PB40	PB11 (4 m)	LIF57 (2 m) LIF68 (2 m)	HPT59 (3 m) HPT60 (2 m) HPT62 (2 m)	Unconfined

678

679

680

681

682

683